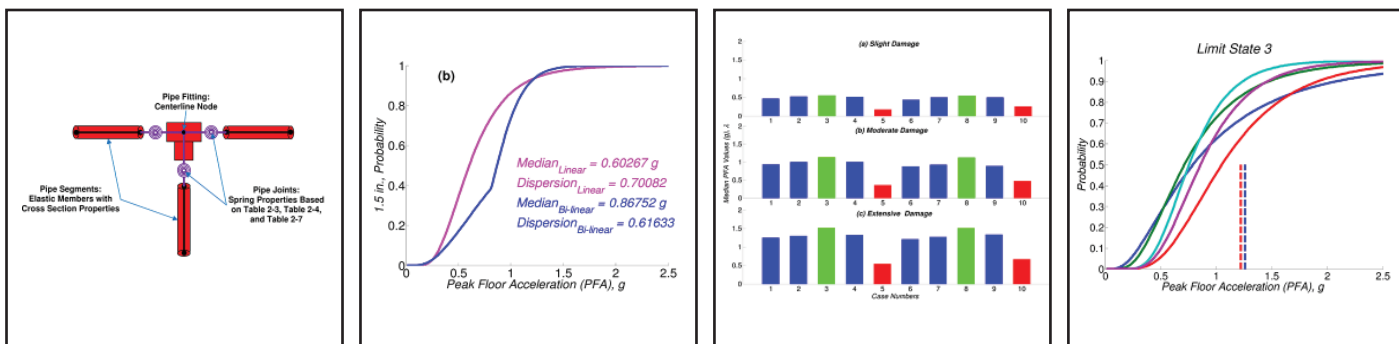


Comprehensive Analytical Seismic Fragility of Fire Sprinkler Piping Systems

by

Siavash Soroushian, Emmanuel "Manos" Maragakis, Arash E. Zaghi,
Alicia Echevarria, Yuan Tian and Andre Filiatrault



Technical Report MCEER-14-0002

August 26, 2014

Sponsored by the
National Science Foundation
NSF Grant Number CMMI-0721399

Project Title

Simulation of the Seismic Performance of Nonstructural Systems

Project Team

University of Nevada, Reno

University at Buffalo, State University of New York

Georgia Institute of Technology

Rutherford & Chekene

University of California, San Diego

Consortium of Universities for Research in Earthquake Engineering (CUREE)

Web Site

<http://www.nees-nonstructural.org>

DISCLAIMER

This report is based upon work supported by the National Science Foundation under Grant No. CMMI-0721399. Any opinions, findings, and conclusions or recommendations expressed in this material are those of the investigators and do not necessarily reflect the views of MCEER, the National Science Foundation, or other sponsors.

Comprehensive Analytical Seismic Fragility of Fire Sprinkler Piping Systems

by

Siavash Soroushian,¹ Emmanuel "Manos" Maragakis,² Arash E. Zaghi,³
Alicia Echevarria,⁴ Yuan Tian⁵ and Andre Filiatral⁶

Publication Date: August 26, 2014
Submittal Date: January 30, 2014

Technical Report MCEER-14-0002

NSF Grant Number CMMI-0721399

- 1 Postdoctoral Fellow, Department of Civil and Environmental Engineering, University of Nevada, Reno
- 2 Dean of College of Engineering, University of Nevada, Reno
- 3 Assistant Professor, Department of Civil and Environmental Engineering, University of Connecticut
- 4 Graduate Student, Department of Civil and Environmental Engineering, University of Connecticut
- 5 Technical Analyst, GE Oil & Gas; former Graduate Student, Department of Civil, Structural and Environmental Engineering, University at Buffalo, State University of New York
- 6 Professor, Department of Civil, Structural and Environmental Engineering, University at Buffalo, State University of New York

MCEER
University at Buffalo, State University of New York
212 Ketter Hall, Buffalo, NY 14260
E-mail: mceer@buffalo.edu; Website: <http://mceer.buffalo.edu>



University of Nevada, Reno



Project Overview

NEES Nonstructural: Simulation of the Seismic Performance of Nonstructural Systems

Nonstructural systems represent 75% of the loss exposure of U.S. buildings to earthquakes, and account for over 78% of the total estimated national annualized earthquake loss. A very widely used nonstructural system, which represents a significant investment, is the ceiling-piping-partition system. Past earthquakes and numerical modeling considering potential earthquake scenarios show that the damage to this system and other nonstructural components causes the preponderance of U.S. earthquake losses. Nevertheless, due to the lack of system-level research studies, its seismic response is poorly understood. Consequently, its seismic performance contributes to increased failure probabilities and damage consequences, loss of function, and potential for injuries. All these factors contribute to decreased seismic resilience of both individual buildings and entire communities.

Ceiling-piping-partition systems consist of several components, such as connections of partitions to the structure, and subsystems, namely the ceiling, piping, and partition systems. These systems have complex three-dimensional geometries and complicated boundary conditions because of their multiple attachment points to the main structure, and are spread over large areas in all directions. Their seismic response, their interaction with the structural system they are suspended from or attached to, and their failure mechanisms are not well understood. Moreover, their damage levels and fragilities are poorly defined due to the lack of system-level experimental studies and modeling capability. Their seismic behavior cannot be dependably analyzed and predicted due to a lack of numerical simulation tools. In addition, modern protective technologies, which are readily used in structural systems, are typically not applied to these systems.

This project sought to integrate multidisciplinary system-level studies to develop, for the first time, a simulation capability and implementation process to enhance the seismic performance of the ceiling-piping-partition nonstructural system. A comprehensive experimental program using both the University of Nevada, Reno (UNR) and University at Buffalo (UB) NEES Equipment Sites was developed to carry out subsystem and system-level full-scale experiments. The E-Defense facility in Japan was used to carry out a payload project in coordination with Japanese researchers. Integrated with this experimental effort was a numerical simulation program that developed experimentally verified analytical models, established system and subsystem fragility functions, and created visualization tools to provide engineering educators and practitioners with sketch-based modeling capabilities. Public policy investigations were designed to support implementation of the research results.

The systems engineering research carried out in this project will help to move the field to a new level of experimentally validated computer simulation of nonstructural systems and establish a model methodology for future systems engineering studies. A system-level multi-site experimental research plan has resulted in a large-scale tunable test-bed with adjustable

dynamic properties, which is useful for future experiments. Subsystem and system level experimental results have produced unique fragility data useful for practitioners.

A comprehensive simulation methodology is developed for fire sprinkler piping systems and is used to generate seismic fragility parameters of these systems. This model is validated using the experimental results of four different piping subsystems, which incorporates a newly developed hysteresis model for threaded and grooved tee joints. Then, the modeling methodology is used to obtain the seismic response of selected fire sprinkler piping systems of the University of California at San Francisco (UCSF) Hospital under two suites of ninety-six artificially generated tri-axial floor acceleration histories. As a result of this study, main run pipes with grooved joints, cable braces, and armover pipes are found to be more vulnerable compared to the other components. Also, by providing 3 in. and 8 in. clearance from large and small pipe diameters, respectively, the leakage failure in piping systems is more probable compared to the first pounding of the piping system with its surroundings.

Project Management Committee

Manos Maragakis, Principal Investigator, University of Nevada, Reno, Department of Civil Engineering, Reno, NV 89557; *maragaki@unr.edu*.

André Filiatral, Co-Principal Investigator, University at Buffalo, State University of New York, Department of Civil, Structural and Environmental Engineering, Buffalo, NY 14260; *af36@buffalo.edu*.

Steven French, Co-Principal Investigator, Georgia Institute of Technology, College of Architecture, P.O. Box 0695, Atlanta, GA 30332; *Steve.French@arch.gatech.edu*.

William Holmes, Rutherford & Chekene, 55 Second Street, Suite 600, San Francisco, CA 94105; *wholmes@ruthchek.com*.

Tara Hutchinson, Co-Principal Investigator, University of California, San Diego, Department of Structural Engineering, 9500 Gilman Drive, #0085, La Jolla, CA 92093; *tara@ucsd.edu*.

Robert Reitherman, Co-Principal Investigator, CUREE, 1301 S. 46th Street, Bldg. 420, Richmond, CA 94804; *reitherman@curee.org*.

ABSTRACT

For the first time, a comprehensive simulation methodology is developed for fire sprinkler piping systems and is used to generate seismic fragility parameters of these systems. The experimentally based analytical model accounts for inelastic behavior constituents of the system including: threaded joints, grooved joints, solid braces, cable braces, hangers, and restrainers. The model incorporates a newly developed hysteresis model for threaded and grooved tee joints that is validated by the experimental results of several tee subassemblies. The modeling technique at the subsystem level is validated using the experimental results of four different piping subsystems. The methodology is used to obtain the seismic response of selected fire sprinkler piping systems of University of California at San Francisco (UCSF) Hospital under two different suites of ninety-six artificially generated tri-axial floor acceleration histories. Eight classes of piping systems with variations on types of braces, weights, joints, and location of restrainers are considered in this study. After the component fragility parameters are obtained for the components of all piping cases, system level fragility parameters are defined, and a joint probabilistic seismic demand model is utilized to develop system fragility parameters. The effect of seismic performance variation on eight classes of piping systems was examined through component and system level fragility curves. These curves showed that the main run pipes with grooved type joints are more vulnerable compared to the threaded joints. Removing the water weight from the piping system reduced the failure probability in all components (especially in grooved joints). Cable braces are found to be more vulnerable compared to the solid braces. The behavior of armover pipes was improved by removing the wire restrainers from these pipes.

Finally, the probability of the impact between the pipes and their surrounding contents is studied by providing different clearances from the piping system. To do so, the displacement demands on the fire sprinkler systems are studied through two subsystem level experiments and two designed classes of the UCSF piping plan. The displacement fragility curves for large and small pipe diameters are obtained and compared with the probability of damage inside piping systems. These curves showed that, by providing 3 in and 8 in clearance from large and small pipe diameters, respectively, the leakage failure in piping systems is more probable compared to the first pounding of the piping system with its surroundings.

ACKNOWLEDGMENTS

The research presented in this study was funded by the National Science Foundation (NSF) under grant number CMMI-0721399, Simulation of the Seismic Performance of Nonstructural Systems. Any opinions, findings, conclusions or recommendations expressed in this document are those of the investigators and do not necessarily reflect the views of the sponsors. The input provided by the Practice Committee of the NEESR-GC Nonstructural Project, composed of W. Holmes (Chair), D. Allen, D. Alvarez, R. Fleming, and P. Malhotra; and its Advisory Board, composed of R. Bachman (Chair), S. Eder, R. Kirchner, E. Miranda, W. Petak, S. Rose and C. Tokas, has been crucial for the completion of this research.

The authors also acknowledge the advice received from industry and academic representatives active in the specific professional areas (alphabetically): John Anderson, Matthew S. Hoehler, Ahmad Itani, Gokhan Pekcan, Keri Ryan, and Arash E. Zaghi, who reviewed the main parts of this study and made valuable suggestions.

TABLE OF CONTENTS

SECTION	TITLE	PAGE
SECTION 1 INTRODUCTION 1		
1.1	Motivation and Background	1
1.2	Literature Review	2
1.2.1	Fire Sprinkler Piping Systems	2
1.2.2	Fragility Study	21
1.3	Objectives and Scope	29
1.4	Report Organization	30
SECTION 2 ANALYTICAL MODEL FOR PIPING TEE JOINTS 33		
2.1	Introduction	33
2.2	Tee-Joint Tests at the University at Buffalo	34
2.2.1	Test Setup	34
2.2.2	Loading Protocol	35
2.2.3	Summary of the Joint Observations	35
2.3	Development of an Analytical Model for Piping Tee Joints	38
2.3.1	Element and Material Mode	38
2.3.2	Analytical Models of Threaded Joints	39
2.3.3	Analytical Models of Grooved Joints	48
2.4	Concluding Remarks	55
SECTION 3 ANALYTICAL MODELS OF PIPING COMPONENTS 57		
3.1	Introduction	57
3.2	Pipe Hangers	57
3.2.1	Code Requirements	58
3.2.2	Pipe Hanger Tests at the University of Nevada, Reno	58
3.2.3	Analytical Model of Pipe Hangers	60
3.2.4	Calibration of Material Model for Pipe Hangers	61
3.2.5	Element Model for Pipe Hangers	62
3.3	Seismic Sway Braces	64
3.3.1	Code Requirements	65
3.3.2	Solid Sway Braces	65
3.3.3	Tension Only Sway Braces	66
3.4	Restrainers	70
3.4.1	Code Requirements	70
3.4.2	Wire Restrainer Tests at the University of Nevada, Reno	71
3.4.3	Analytical Model of Wire Restrainers	72
3.4.4	Calibration of Analytical Model for Wire Restrainers	74
3.5	Pipe Runs	75
3.5.1	Code Requirements	75
3.5.2	Analytical Model of Pipe Runs	76
3.6	Concluding Remarks	77

SECTION 4	VERIFICATION OF ANALYTICAL MODEL OF PIPING SYSTEM	
	EXPERIMENTS	79
4.1	Introduction	79
4.2	Hospital Piping Assemblies Tested at University of Nevada, Reno, I	79
4.2.1	Test Background	80
4.2.2	Instrumentation Plan	82
4.2.3	Loading Protocol	83
4.2.4	Generation of the Analytical Model	84
4.2.5	Experimental-Analytical Result Comparison	87
4.3	Hospital Piping Assemblies Tested at University of Nevada, Reno, II	90
4.3.1	Test Background	90
4.3.2	Instrumentation Plan	92
4.3.3	Loading Protocol	93
4.3.4	Generation of the Analytical Model	95
4.3.5	Experimental-Analytical Result Comparison	96
4.4	Piping Subsystem Tested at University of Buffalo	97
4.4.1	Test Background	97
4.4.2	Instrumentation Plan	99
4.4.3	Loading Protocol	99
4.4.4	Generation of the Analytical Model	100
4.4.5	Experimental-Analytical Result Comparison	102
4.5	Piping System at Full Scale 5-Story Building at E-Defense Experiment	104
4.5.1	Test Background	104
4.6	Instrumentation	109
4.6.1	Structural Instrumentation	109
4.6.2	Piping System	111
4.6.3	Excitation Plan	114
4.6.4	Generation of the Analytical Model	118
4.6.5	Experimental-Analytical Result Comparison	120
4.7	Concluding Remarks	130
SECTION 5	COMPONENT FRAGILITY STUDIES	131
5.1	Introduction	131
5.2	Fragility Analysis Methodology	132
5.2.1	Cloud Approach (Probabilistic Seismic Demand Analysis, PSDA)	132
5.2.2	Scaled Approach (Incremental Dynamic Analysis, IDA)	134
5.3	Specifications of Hospital Fire Sprinkler Piping System	135
5.4	Considered Variables in Fire Sprinkler Analytical Models	137
5.5	Generation of Analytical Models for Fire Sprinkler Systems	139
5.5.1	Real Time Element Removal Algorithm	141
5.5.2	Modal Analysis and Damping Model	143
5.6	Generation of the Input Motions	144
5.6.1	Motion Set 1: Motions with Uniform S_{DS} Distribution	147
5.6.2	Motion Set 2: Motions with Lognormal S_{DS} Distribution	149
5.6.3	Intensity Measure (IM) Selection	152
5.7	Component Demands	153
5.8	Pipe Joint Capacity Parameters	158

5.8.1	Threaded Joints	159
5.8.2	Grooved Joints	160
5.9	Damage States	160
5.9.1	Threaded Joints	161
5.9.2	Grooved Joints	162
5.9.3	Supports	163
5.10	Component Fragility Curves	164
5.11	Effect of Variations of Design, Motion, and Fragility Parameters on Component Fragility Curves	176
5.11.1	Component Demands	176
5.11.2	Joint Types	179
5.11.3	Motion Suites	181
5.11.4	Water Weight	182
5.11.5	Wire Restrainers	183
5.11.6	Bracing	184
5.12	Concluding Remarks	185
SECTION 6 SYSTEM LEVEL FRAGILITY STUDIES		189
6.1	Introduction	189
6.2	Methodology	189
6.3	System Fragility Curves	191
6.4	Effect of Variations of Design and Motion on System Fragility Curves	198
6.4.1	Joint Types	198
6.4.2	Motion Suites	200
6.4.3	Water Weight	201
6.4.4	Wire Restrainers	202
6.4.5	Bracing	203
6.5	Concluding Remarks	204
SECTION 7 DISPLACEMENT FRAGILITY ANALYSIS		207
7.1	Introduction	207
7.2	Drift Sensitive Pipe Runs	210
7.2.1	Fragility Analysis Methodology	210
7.2.2	Pipe Joint Damage States	210
7.2.3	Joint Rotation/ Story Drift Ratio	211
7.2.4	Fragility Curves	213
7.3	Displacement Demand on Large Pipe diameters	217
7.3.1	Code Requirements	217
7.3.2	Displacement Demands	217
7.3.3	Limit States	220
7.3.4	Fragility Curves	220
7.4	Displacement Demand on Small Pipe Diameters	223
7.4.1	Code Requirements	224
7.4.2	Displacement Demands	224
7.4.3	Limit States	225
7.4.4	Fragility Curves	225
7.5	Concluding Remarks	228

SECTION 8 SUMMARY AND CONCLUSIONS	229
8.1 Summary	229
8.2 Findings and Conclusions	231
8.3 Future Work and Recommendations	234
SECTION 9 REFERENCES	237
APPENDIX A HANGING, BRACING, AND RESTRAINT OF SYSTEM PIPING	249
APPENDIX B UCSF FIRE SPRINKLER PIPING PLAN	267
APPENDIX C PSDMS OF FIRE SPRINKLER PIPING SYSTEMS	283
APPENDIX D COMPONENT FRAGILITY CURVES OF PIPING SYSTEMS	305

LIST OF ILLUSTRATIONS

FIGURE	TITLE	PAGE
Figure 1-1	Schematic of a Typical Fire Sprinkler Piping System	3
Figure 1-2	(a) Pipe Pulled out from Elbow at Elmendorf AFB Warehouse (b) Close up View of Figure (a) (NRC, 1973)	9
Figure 1-3	Pipe Joint Failure (Photo by John F. Meehan)	9
Figure 1-4	(a) Leakage Caused by Pipe Damage at Joint (Photo courtesy of Degenkolb Engineers) (b) Damage to Suspended Fire Protection Piping (Photos Courtesy of Mason Industries)	10
Figure 1-5	(a) Failures of Water Sprinkler Piping Near Joints (Miranda et al. 2012). and (b) Permanent Offset of Pipe Hanger (Photo: P. Correa)	11
Figure 1-6	(a) Relationship Between Building Damage Rate and Type of Building Structure (b) Equipment Damage Factor (Mizutani et al., 2012)	12
Figure 1-7	Fire Sprinkler System Damage in the Tohoku Earthquake (a) Graph of Damaged Parts (b) Percent of Damaged Pipes that Leaked Water	13
Figure 1-8	Test Setup of Static Bending Test of Joints (Antaki and Guzy, 1998)	14
Figure 1-9	Test Setup for Dynamic Test of Grooved Coupling and Threaded Joints	15
Figure 1-10	(a) Threaded Specimen Mounted on Shake Table (b) Threads Do Not Exhibit Damage After Dynamic Test to Leak (c) Failed Mechanical Coupling During Dynamic Test (Antaki and Guzy, 1998)	15
Figure 1-11	(a) Hospital Room Elevation View (b) Plan View of Sprinkler System (Filiatrault et al., 2008)	16
Figure 1-12	Finite Element Model of the 8 inch Victaulic Test Setup (Martinez and Hodgson, 2007)	18
Figure 1-13	(a) Geometry of the Three-Story Hospital Building (b) Three Dimensional View of Fire Piping Model (Soroushian et. al, 2011)	19
Figure 1-14	RC Moment Frame Building Configurations (Ju and Gupta, 2012)	21
Figure 1-15	Seismic Event Timeline (Basoz and Kiremidjian, 1996)	23
Figure 1-16	Sample Fragility Curve	24
Figure 1-17	Sample Empirical Fragility Curves for Pipe Tee-Joint (Tian et al., 2012)	25
Figure 1-18	Sample Analytical Fragility Curves for Piping Systems (Ju and Gupta, 2012)	26
Figure 1-19	Probabilistic Seismic Demand Model (Zaghi et al., 2012)	27
Figure 2-1	Tee Joint Experimental Set-Up (Tian et al., 2012)	34
Figure 2-2	Tee Joint Experimental Loading Protocol (a) Monotonic (b) Cyclic (Tian et al., 2012)	35
Figure 2-3	Observed Damage in Threaded Tee Joints (Tian et al., 2012)	36
Figure 2-4	Moment-Rotation Hysteresis Response of Tee Joint Subassemblies with Different Diameters (Tian et al., 2012)	36
Figure 2-5	Observed Damage in Grooved Tee Joints (Tian et al., 2012)	37
Figure 2-6	Moment-Rotation Hysteresis Response of Tee Joint Subassemblies with Different Diameters (Tian et al., 2012)	37
Figure 2-7	Pinching4 Material Properties (OpenSees, 2012)	38
Figure 2-8	Analytical-Experimental Comparison of Second 3/4 in. Specimen on Left Side of Tee Joint	39

Figure 2-9	Analytical-Experimental Hysteresis Comparison of 3/4 in. Pipe Diameter	40
Figure 2-10	Analytical-Experimental Hysteresis Comparison of 1 in. Pipe Diameter	41
Figure 2-11	Analytical-Experimental Hysteresis Comparison of 2 in. Pipe Diameter	41
Figure 2-12	Analytical-Experimental Hysteresis Comparison of 4 in. Pipe Diameter	42
Figure 2-13	Analytical-Experimental Hysteresis Comparison of 6 in. Pipe Diameter	42
Figure 2-14	Average and Calibrated Backbone Curve for 6 in. Pipe Diameter	45
Figure 2-15	Sample Generic Analytical-Experimental Hysteresis Comparison of Different Pipe Diameters	46
Figure 2-16	Fitted Curves on Backbone Curve Parameters of the Generic Model	47
Figure 2-17	Proposed Hysteresis Behavior of Different Pipe Diameters	48
Figure 2-18	Analytical-Experimental Comparison of Second 2 in. Grooved Fit Specimen on Left Side of Tee Joint	49
Figure 2-19	Analytical-Experimental Hysteresis Comparison of 2 in. Pipe Diameter	50
Figure 2-20	Analytical-Experimental Hysteresis Comparison of 2 in. Pipe Diameter	51
Figure 2-21	Sample Generic Analytical-Experimental Hysteresis Comparison of Different Grooved Pipe Diameters	52
Figure 2-22	Fitted-Developed Backbone Curves of the Generic Model (Includes Moment-Rotation Equations)	54
Figure 2-23	Sample of Generic Hysteresis Curves Proposed for 2.5 in. and 5 in. Pipe Diameter	54
Figure 3-1	(a) Pipe hanger and (b) Deck Fastener (c) Hanger Clip (d) Hanger Clip and Surge Clip (e) Surge Clips	58
Figure 3-2	(a) Loading History of Rod Tensile Test (b) Rod Force/Displacement Curves (Goodwin et al., 2005)	59
Figure 3-3	Behavior of Steel Material Model (a) Backbone Curve (b) Hysteresis Loop Due to Cyclic Load	60
Figure 3-4	Accuracy of Analytical Hanger Modeling (a) Tensile Member, (b) Force-Displacement Relationship, and (c) Error in Force Between Members	62
Figure 3-5	Sample Behavior of a Bending Members (a) Bending Member, (b) Moment-Rotation Relationships, and (c) Error in Moment Between Members	63
Figure 3-6	Behavior of a Bending Member with $nc=16$, $nr=3$ (a) Bending Member, (b) Moment-Rotation Relationship, and (c) Error in Moment Between Members	63
Figure 3-7	Proposed Analytical Model of Pipe Hangers (a) Tensile Behavior, (b) Bending Behavior	64
Figure 3-8	(a) Lateral and Longitudinal Solid Braces (b) Deck Fastener(c) Longitudinal Pipe-Attachment Clip	65
Figure 3-9	(a) Photograph of Tension-Only Braces (Cables) (b) Lateral and (c) Longitudinal Bracing (Goodwin et al., 2005)	66
Figure 3-10	(a) Loading History of Cable Tensile Test (b) Cable Force/Displacement Curves (Goodwin et al., 2005)	67
Figure 3-11	Behavior of EPPG Material for Cable Bracing (a) Model without Gap (b) Model with Gap	68

Figure 3-12	Accuracy of Analytical Cable Modeling (a) Tensile Member (b) Force-Displacement Relationship (c) Error in Force between Members	69
Figure 3-13	Wire Restrainers and the Deck Connection Detail	70
Figure 3-14	Tensile Test of Wire Restrainers (a) Testing Machine (b) Extensometer (c) Testing Sample of Wires	71
Figure 3-15	(a) Loading History of Wire Tensile Test (b) Rod Force/Displacement Curves	71
Figure 3-16	Behavior of EPPG Material for Wire Restrainers (a) Model without Gap (b) Model with Gap	72
Figure 3-17	Hysteresis Behavior of EPPG Material for Wire Restrainers (a) Model without Cyclic Damage (b) Model with Cyclic Damage	73
Figure 3-18	Accuracy of Analytical Wire Modeling (a) Tensile Member (b) Force-Displacement Relationship (c) Error in Force between Members	74
Figure 3-19	Typical Pipe Runs of a Sprinkler Piping System	75
Figure 3-20	Schematic of Analytical Modeling for Pipe Runs	76
Figure 4-1	Experimental Setup a) Schematic of the Setup, b) Final Setup, (Zaghi et al., 2012).	80
Figure 4-2	Piping Assembly a) Plan View, b) Elevation View (Zaghi et al, 2012)	81
Figure 4-3	Seismic Bracing Layout (Zaghi et al, 2012)	82
Figure 4-4	Instrumentation View	83
Figure 4-5	Achieved Table Motion on 60% IM in N-S Direction	84
Figure 4-6	Models of the Piping Subassemblies (a) SAP Model (b) OpenSees Model	84
Figure 4-7	(a) First EGGP Material (b) Second EGGP Material (c) Combining Diagram (d) Combined EGGP Material for Cable Bracing	86
Figure 4-8	Magnitude of Low-Pass Butterworth Filter Transfer Function	87
Figure 4-9	The First Two Modes of Piping Subassembly (a) First mode (b) Second mode	88
Figure 4-10	Comparison of Experimental and Analytical Results: Displacement History at Locations “ Δ_1 ” through “ Δ_4 ”, 5% Damped Spectral Acceleration at locations “ Acc_1 ” and “ Acc_2 ”	89
Figure 4-11	Experimental Setup	91
Figure 4-12	Plan View of Horizontal Sliding Top Frame	91
Figure 4-13	Detail at Wheel Locations	92
Figure 4-14	Instrumentation View	92
Figure 4-15	(a) Plan View of the WC70 Structure (b) OpenSees Structural Model	93
Figure 4-16	Achieved Table-Slider Motion on 50% IM in N-S Direction	95
Figure 4-17	Comparison of Experimental and Analytical Results: Displacement History at Locations “ Δ_1 ” and “ Δ_2 ” and 5% Damped Spectral Acceleration at location “ Acc_1 ”	96
Figure 4-18	Test Set-Up for Sprinkler Piping Subsystem Testing (Tian, 2012)	98
Figure 4-19	Piping System Plan View of (a) the First Floor (b) the Second Floor (c) and the Elevation View of the Riser Pipe (Tian, 2012).	98
Figure 4-20	Sample of Achieved, Displacement, Velocity, and Acceleration Histories at Maximum Considered Earthquake (MCE) Level	100
Figure 4-21	Models of the Piping Subsystem (a) SAP Model (b) OpenSees Model	101

Figure 4-22	The First Local Mode of Piping Subsystem	102
Figure 4-23	Comparison of Experimental and Analytical Results: a) Tee Joint Rotation History at Location “a”, b) 5% Damped Spectral Acceleration at the Tip of the Branch Line Labeled “b”, c) Acceleration History at the Tip of the Branch Line Labeled “c”, d) Absolute Displacement History at the Tip of the Branch Line Labeled “d”, e), f) Axial Force in the Hanger Labeled “e”, and f) Axial Force at the Wire Restrainer Labeled “f”	103
Figure 4-24	(a) 5-Story Steel Moment Frame Specimen Set on Triple Pendulum Isolators (b) Plan View (c) Elevation View	105
Figure 4-25	Schematic of Test Building along with the Installed Nonstructural Floors	106
Figure 4-26	Overall Plan View of Piping System	106
Figure 4-27	Pipe Connections (a) Riser-Main Run Grooved Fit Connection (b) Main Run- Branch Line Grooved Fit Connection (c) Branch Line Threaded Connection	107
Figure 4-28	Pipe hanger and (b) Top Connection (c)Main Run Bottom Connection (d) Branch Line bottom Connection (e) Surge Clips	107
Figure 4-29	Sprinkler Heads and Drops: (a) 2 in. Oversized Gap Configuration, (b) No Gap Configuration, and (c) Flexible Drop	108
Figure 4-30	(a) Lateral and Longitudinal Brace Near Riser (b) Lateral Brace at the End of Main Run (c) Two Longitudinal Braces at the End of Riser on Fourth Floor	108
Figure 4-31	Wire Restrainers and the Top Connection Detail	109
Figure 4-32	Instrumentation for Measuring Story Drift	110
Figure 4-33	Layout of Displacement Transducers to Measure Story Drift in 2 nd to 5 th Stories	110
Figure 4-34	Layout of Accelerometers at the 5 th Floor	111
Figure 4-35	(a) Layout of Displacement Transducer at Piping System (b-e) Instrument Detail	112
Figure 4-36	(a) View of Accelerometers on Main Run and Branch Line Pipes (b,c) Instrument Detail	113
Figure 4-37	(a) View of Accelerometers on Sprinkler Heads (b,c) Instrument Detail	113
Figure 4-38	Models of the Piping Subsystem (a) SAP Model (b) OpenSees Model	119
Figure 4-39	Schematic of Used Accelerometers to Obtain Transfer Functions	121
Figure 4-40	Definition of Half-Power Bandwidth	121
Figure 4-41	Transfer Functions for Piping System	122
Figure 4-42	Rayleigh Damping Model	123
Figure 4-43	The First Three Local Modes of Piping System	124
Figure 4-44	Calculated Horizontal Components of Acceleration Histories at Geometric Center of 4 th Floor under 35RRS (XY-Fixed Base)	125
Figure 4-45	Calculated Horizontal Components of Acceleration Histories at Geometric Center of 4 th Floor under WSM80 (3D-Fixed Base)	125
Figure 4-46	Comparison of Experimental and Analytical Acceleration History of First Branch Line in Y Direction under 35RRS (XY-Fixed Base)	126

Figure 4-47	Comparison of Experimental and Analytical Acceleration History of First Branch Line in X Direction under 35RRS (XY-Fixed Base)	126
Figure 4-48	Comparison of Experimental and Analytical Acceleration History of Second Branch Line in Y Direction under 35RRS (XY-Fixed Base)	127
Figure 4-49	Comparison of Experimental and Analytical Acceleration History of Second Branch Line in X Direction under 35RRS (XY-Fixed Base)	127
Figure 4-50	Comparison of Experimental and Analytical Acceleration History of Third Branch Line in X-Y Directions under 35RRS (XY-Fixed Base)	128
Figure 4-51	Comparison of Experimental and Analytical Spectral Acceleration of All Branch Lines in X Direction under 35RRS (XY-Fixed Base)	128
Figure 4-52	Comparison of Experimental and Analytical Spectral Acceleration of All Branch Lines in Y Direction under 35RRS (XY-Fixed Base)	129
Figure 4-53	Comparison of Experimental and Analytical Displacement History of Third Main Run in X Direction under Fixed Base 35RRS (XY) and WSM80 (3D)	129
Figure 5-1	3-D View of UCSF Medical Center Sprinkler Piping System	136
Figure 5-2	First Forty Natural Periods of All Piping Cases (0.005 Initial Gap Strain on Wire Restrainers)	143
Figure 5-3	First Forty Natural Periods of All Piping Cases (Closed Gap Strain on Wire Restrainers)	144
Figure 5-4	Design Response Spectrum, (a) Horizontal Response Spectra, (b) Vertical Response Spectra	146
Figure 5-5	(a) Distribution of Peak Horizontal Floor Acceleration, (b) Horizontal Spectral Floor Acceleration, (c) Distribution of Peak Vertical Floor Acceleration, (d) Vertical Spectral Floor Acceleration with Uniform S_{DS} Distribution	149
Figure 5-6	Distribution of (a) S_{DS} Acceleration (b) Peak Horizontal Floor Acceleration, (c) Horizontal Spectral Floor Acceleration, (d) Distribution of Peak Vertical Floor Acceleration, (e) Vertical Spectral Floor Acceleration of Motions with Lognormal S_{DS} Distribution	151
Figure 5-7	Sample Probabilistic Seismic Demand: (a) Percentage of Failed Wires, (b) 2.5 in. Pipe Joint Rotation (rad.), Case 1	155
Figure 5-8	Sample Probabilistic Seismic Demand: (a) Percentage of Failed Wires, (b) 2.5 in. Pipe Joint Rotation (rad.), Case 2	155
Figure 5-9	Sample Probabilistic Seismic Demand: (a) Percentage of Failed Wires, (b) 2.5 in. Pipe Joint Rotation (rad.), Case 3	156
Figure 5-10	Sample Probabilistic Seismic Demand: (a) Percentage of Failed Wires, (b) 2.5 in. Pipe Joint Rotation (rad.), Case 4	156
Figure 5-11	Sample Probabilistic Seismic Demand: (a) Percentage of Failed Wires, (b) 2.5 in. Pipe Joint Rotation (rad.), Case 5	156
Figure 5-12	Sample Probabilistic Seismic Demand: (a) Percentage of Failed Wires, (b) 2.5 in. Pipe Joint Rotation (rad.), Case 6	157
Figure 5-13	Sample Probabilistic Seismic Demand: (a) Percentage of Failed Wires, (b) 2.5 in. Pipe Joint Rotation (rad.), Case 7	157
Figure 5-14	Sample Probabilistic Seismic Demand: (a) Percentage of Failed Wires, (b) 2.5 in. Pipe Joint Rotation (rad.), Case 8	157

Figure 5-15	Sample Probabilistic Seismic Demand: (a) Percentage of Failed Wires, (b) 2.5 in. Pipe Joint Rotation (rad.), Case 9	158
Figure 5-16	Sample Probabilistic Seismic Demand: (a) Percentage of Failed Wires, (b) 2.5 in. Pipe Joint Rotation (rad.), Case 10	158
Figure 5-17	Schematic Definition of Threaded Joint Damage States	162
Figure 5-18	Schematic Definition of Grooved Joint Damage States	163
Figure 5-19	Component Fragility Curves for Piping System of Case 1	166
Figure 5-20	Component Fragility Curves for Piping System of Case 2	167
Figure 5-21	Component Fragility Curves for Piping System of Case 3	167
Figure 5-22	Component Fragility Curves for Piping System of Case 4	168
Figure 5-23	Component Fragility Curves for Piping System of Case 5	168
Figure 5-24	Component Fragility Curves for Piping System of Case 6	169
Figure 5-25	Component Fragility Curves for Piping System of Case 7	169
Figure 5-26	Component Fragility Curves for Piping System of Case 8	170
Figure 5-27	Component Fragility Curves for Piping System of Case 9	170
Figure 5-28	Component Fragility Curves for Piping System of Case 10	171
Figure 5-29	Sample Comparison of Linear and Bilinear Regression Analysis on (a) Component Demands, (b) Component Fragility at Slight Limit State - Case 1	177
Figure 5-30	Sample Probability Differences for Case 1	178
Figure 5-31	Component Median Value Differences Considering Main Run Joint Variation	180
Figure 5-32	Component Median Value Differences Considering Motion Suite Variation	181
Figure 5-33	Component Median Value Differences Considering Water Weight Variation	182
Figure 5-34	Component Median Value Differences Considering Wire Restrainers Variation	183
Figure 5-35	Component Median Value Differences Considering Brace Type Variation	184
Figure 6-1	System Fragility Curves for Different Piping System Condition of Case 1	191
Figure 6-2	System Fragility Curves for Different Piping System Condition of Case 2	191
Figure 6-3	System Fragility Curves for Different Piping System Condition of Case 3	192
Figure 6-4	System Fragility Curves for Different Piping System Condition of Case 4	192
Figure 6-5	System Fragility Curves for Different Piping System Condition of Case 5	192
Figure 6-6	System Fragility Curves for Different Piping System Condition of Case 6	193
Figure 6-7	System Fragility Curves for Different Piping System Condition of Case 7	193
Figure 6-8	System Fragility Curves for Different Piping System Condition of Case 8	193

Figure 6-9	System Fragility Curves for Different Piping System Condition of Case 9	194
Figure 6-10	System Fragility Curves for Different Piping System Condition of Case 10	194
Figure 6-11	Comparison of Median PFA Values for All Piping Cases Considering All Components	198
Figure 6-12	System Median Value Differences Considering Main Run Joint Variation	199
Figure 6-13	System Median Value Differences Considering Motion Suite Variation	201
Figure 6-14	System Median Value Differences Considering Water Weight Variation	202
Figure 6-15	System Median Value Differences Considering Wire Restrainers Variation	203
Figure 6-16	System Median Value Differences Considering Brace Type Variation	203
Figure 7-1	Vertical Pipe Damage Due to Structural Deformation	207
Figure 7-2	Damage Caused by Sprinkler Head-Ceiling Interaction, Photo courtesy of; (b) Rodrigo Retamales, Rubn Boroschek & Associates (c) Robert Reitherman	208
Figure 7-3	Damage Observed at Pipe Penetration Points (Photo Courtesy of Mason Industries)	209
Figure 7-4	Damage Caused by Pounding of Pipe and Adjacent Objects (Photo Courtesy of Mason Industries)	209
Figure 7-5	Pipe Joint Fragility Curves Based on leakage Rotational Capacity (rad.) (Tian et al., 2012)	211
Figure 7-6	Schematic Relation of Riser Joint Rotation and Inter-Story Drift	212
Figure 7-7	Slight Fragility Curves for Different Riser Pipe Diameters	214
Figure 7-8	Moderate Fragility Curves for Different Riser Pipe Diameters	215
Figure 7-9	Extensive Fragility Curves for Different Riser Pipe Diameters	216
Figure 7-10	(a) String Potentiometers View (b) Displacement Demand of Piping System	218
Figure 7-11	(a) String Potentiometers View (b) Displacement demand of piping system	219
Figure 7-12	Displacement Demand of Piping System on (a) Grooved (b) Threaded on Main Run Pipe (Large Pipe Diameters)	219
Figure 7-13	Piping Interaction Fragility Curves for Main Run Pipes (Large Pipe Diameters)	221
Figure 7-14	Comparison of Median Values for Piping System Damage and Displacement for Large Pipe Diameters	223
Figure 7-15	Displacement Demand of Sprinkler Heads in (a) Grooved (b) Threaded Systems	224
Figure 7-16	Piping Interaction Fragility Curves for Sprinkler Heads (Small Pipe Diameters)	226
Figure 7-17	Comparison of Median Values for Piping System Damage and Displacement of Small Pipe Diameters	227

LIST OF TABLES

TABLE	TITLE	PAGE
Table 2-1	Calibrated Pinching4 Parameter for Various Pipe Diameter	43
Table 2-2	Backbone Parameters Calibrated for 6" Pipe Diameter	44
Table 2-3	Generic "Pinching4" Calculated Parameters-Tested	45
Table 2-4	Generic "Pinching4" Calculated Parameters-Proposed	47
Table 2-5	Fixed "Pinching4" Parameters of Grooved Fit Hinge Model	49
Table 2-6	Calibrated "Pinching4" Parameter for Various Pipe Diameter	51
Table 2-7	Generic "Pinching4" Calculated Parameters for Grooved Fit Hinges	54
Table 3-1	Summary of Rod Component Tests	60
Table 3-2	Calibrated Steel02 Material Parameters for Pipe Hangers	61
Table 3-3	Summary of Cable Component Tests	67
Table 3-4	Calibrated EPPG Material Parameters for Cable Braces	69
Table 3-5	Summary of Wire Restrainer Component Tests	72
Table 3-6	Calibrated EPPG Material Parameters for Wire Restrainers	74
Table 4-1	Summary of Used Components for Analytical Model	85
Table 4-2	Loading Protocol	94
Table 4-3	Summary of Used Components for Analytical Model	101
Table 4-4	Simulation Schedule for the TP Isolation Configuration	115
Table 4-5	Simulation Schedule for the Hybrid LR Isolation Configuration	116
Table 4-6	Simulation Schedule for the Fixed-Base Building	117
Table 4-7	Table/Floors Achieved Peak Acceleration	118
Table 4-8	Summary of Used Components for Analytical Model	119
Table 4-9	Natural Periods and Damping Ratios of the Piping System	122
Table 5-1	Considered Parameters in Piping System Cases	140
Table 5-2	Summary of Used Components for Analytical Model	141
Table 5-3	Desired Response Spectrum Parameters with Uniform S_{DS} Distribution	148
Table 5-4	Desired Response Spectrum Parameters with Lognormal S_{DS} Distribution	150
Table 5-5	Engineering Demand Parameter Estimations for Pipe Components-Case 1	153
Table 5-6	Engineering Demand Parameter Estimations for Pipe Components-Case 2	153
Table 5-7	Engineering Demand Parameter Estimations for Pipe Components-Case 3	154
Table 5-8	Engineering Demand Parameter Estimations for Pipe Components-Case 4	154
Table 5-9	Engineering Demand Parameter Estimations for Pipe Components-Case 5	154
Table 5-10	Engineering Demand Parameter Estimations for Pipe Components-Case 6	154
Table 5-11	Engineering Demand Parameter Estimations for Pipe Components-Case 7	154
Table 5-12	Engineering Demand Parameter Estimations for Pipe Components-Case 8	154

Table 5-13	Engineering Demand Parameter Estimations for Pipe Components- Case 9	155
Table 5-14	Engineering Demand Parameter Estimations for Pipe Components- Case 10	155
Table 5-15	Rotational Capacities of Threaded Joints	159
Table 5-16	Rotational Capacities of Grooved Joints	160
Table 5-17	Damage States of Threaded Joint Components	161
Table 5-18	Damage States for Grooved Joint Components	162
Table 5-19	Damage States for Pipe Supporting Components	163
Table 5-20	Medians and Dispersion Values for Piping Component Fragilities Curves of Case 1	171
Table 5-21	Medians and Dispersion Values for Piping Component Fragilities Curves of Case 2	172
Table 5-22	Medians and Dispersion Values for Piping Component Fragilities Curves of Case 3	172
Table 5-23	Medians and Dispersion Values for Piping Component Fragilities Curves of Case 4	173
Table 5-24	Medians and Dispersion Values for Piping Component Fragilities Curves of Case 5	173
Table 5-25	Medians and Dispersion Values for Piping Component Fragilities Curves of Case 6	174
Table 5-26	Medians and Dispersion Values for Piping Component Fragilities Curves of Case 7	174
Table 5-27	Medians and Dispersion Values for Piping Component Fragilities Curves of Case 8	175
Table 5-28	Medians and Dispersion Values for Piping Component Fragilities Curves of Case 9	175
Table 5-29	Medians and Dispersion Values for Piping Component Fragilities Curves of Case 10	176
Table 6-1	Medians and Dispersions for 4 Different Piping System of Case1	195
Table 6-2	Medians and Dispersions for 4 Different Piping System of Case 2	195
Table 6-3	Medians and Dispersions for 4 Different Piping System of Case 3	195
Table 6-4	Medians and Dispersions for 4 Different Piping System of Case 4	195
Table 6-5	Medians and Dispersions for 4 Different Piping System of Case 5	196
Table 6-6	Medians and Dispersions for 4 Different Piping System of Case 6	196
Table 6-7	Medians and Dispersions for 4 Different Piping System of Case 7	196
Table 6-8	Medians and Dispersions for 4 Different Piping System of Case 8	196
Table 6-9	Medians and Dispersions for 4 Different Piping System of Case 9	196
Table 6-10	Medians and Dispersions for 4 Different Piping System of Case 10	197
Table 7-1	Damage States of Pipe Joints	211
Table 7-2	Damage States of Pipe Joints	213
Table 7-3	Medians and Dispersion Values for Piping Displacement Fragilities for Large Pipe Diameters	220
Table 7-4	Medians and Dispersion Values for Piping Displacement Fragilities for Small Pipe Diameters	225

SECTION 1

INTRODUCTION

1.1 Motivation and Background

In general, nonstructural systems account for 75-85% of a building investment in commercial buildings while structural components account for the remaining 15-25% of the cost for new construction (Whittaker and Soong, 2003). Nonstructural systems are susceptible to seismic damage because their threshold to shaking intensities is lower than those that typically result in structural damage. Therefore, it is not surprising that in several past earthquakes, extensive damage to nonstructural systems forced the closure of critical buildings such as hospitals. As stated in FEMA 366 (2000), nonstructural damage accounts for 78.6% of total loss in the U.S. due to structural and built-in nonstructural damages.

A fire sprinkler piping system is a primary nonstructural system that provides the safety of a structure in case of fire. Damage to this system may result in a decrease or loss of functionality of the fire protection of buildings and an increase in fire hazard (Maragakis, 2007). Therefore, their loss of functionality may result in loss of property, complete closure of a building, and casualties in the case of fire-following-earthquake scenarios. Despite the importance of fire sprinkler systems, limited research has been conducted to better understand the behavior of their elements.

The seismic vulnerability of a system represented through fragility curves has widely been used for buildings and bridges. However, due to lack of past earthquake data, experimental studies, and analytical works, the development and availability of fragility curves for nonstructural systems are very limited. A recent Applied Technology Council (ATC)-sponsored document (ATC-58 50% draft, 2009) presented selected efforts to develop fragility curves for nonstructural systems, including ceiling systems and partitions. This document highlighted the need for a performance-based design based on statistical approaches in nonstructural systems. Therefore, probabilistic seismic fragility studies on fire sprinkler piping systems are vital in mitigating risk and achieving reliable designs.

In light of the importance of the operation of fire sprinkler systems after earthquakes, there is a need for additional research to develop reliable performance-based design criteria. The study

presented supports this field of research through the development of a reliable analytical model for a better understanding of seismic risk assessment of fire sprinkler piping systems.

1.2 Literature Review

This section is divided into two main parts: 1) Fire Sprinkler Piping Systems; and 2) Fragility Curves. In the first part, the general definition of a sprinkler piping system is provided, followed by a brief overview of available guidelines and standards. Next, a short summary of sprinkler piping performance during past earthquakes is given. Finally, the most recent experimental and analytical studies on sprinkler systems are presented. The second part presents a brief overview of developing fragility curves.

1.2.1 Fire Sprinkler Piping Systems

A fire sprinkler system is a network of fixed water pipes supplied by water sources with sprinkler heads fitted at recommended distances apart. Historically, these systems were only used in factories and large commercial buildings. However, in recent years, the use of fire sprinkler systems has become common in critical facilities such as power plants, hospitals, industrial units, and even homes and small buildings (Industrial Fire Sprinklers, 2013). As an example of the pervasiveness of these systems, worldwide use rate data suggests that more than 40 million sprinkler heads are fitted each year (Fire Sprinklers, 2013).

In 1812, the world's first recognizable sprinkler system was installed in a theatre in the United Kingdom. The system consisted of a reservoir of 95,000 liters fed by a 10 in water main which branched to all parts of the theatre. A series of smaller pipes fed from the distribution pipe were pierced with a series of 1/2 in holes that poured water in the event of a fire (Wormald, 1923). The first automatic sprinkler system was patented by Philip W. Pratt in 1872. Sprinkler systems have been used in the United States since 1874, and were used in factory applications where fires at the turn of the century were often catastrophic in terms of both human and property losses.

A typical fire sprinkler piping system is composed of a water pressure tank, pipe runs, sprinkler heads, hangers, braces, and restrainers. Pressure tanks provide enough pressure behind the water in a system. Sprinkler heads spray the pressurized water onto an area in case of fire or smoke. Pipe runs are composed of: 1) risers: vertical supply pipes; 2) main runs: pipes that

supply branch line water; 3) branch lines: provide drop pipe water; and 4) drops: armover or straight drops that supply sprinkler head water. Hangers carry the dead weight of a piping system. Braces resist the seismic load of a piping system. Braces can be solid or tension-only (cable) braces. Wire restrainers limit the displacement movement of branch lines. The schematic of a typical fire sprinkler piping system is presented in Figure 1-1.

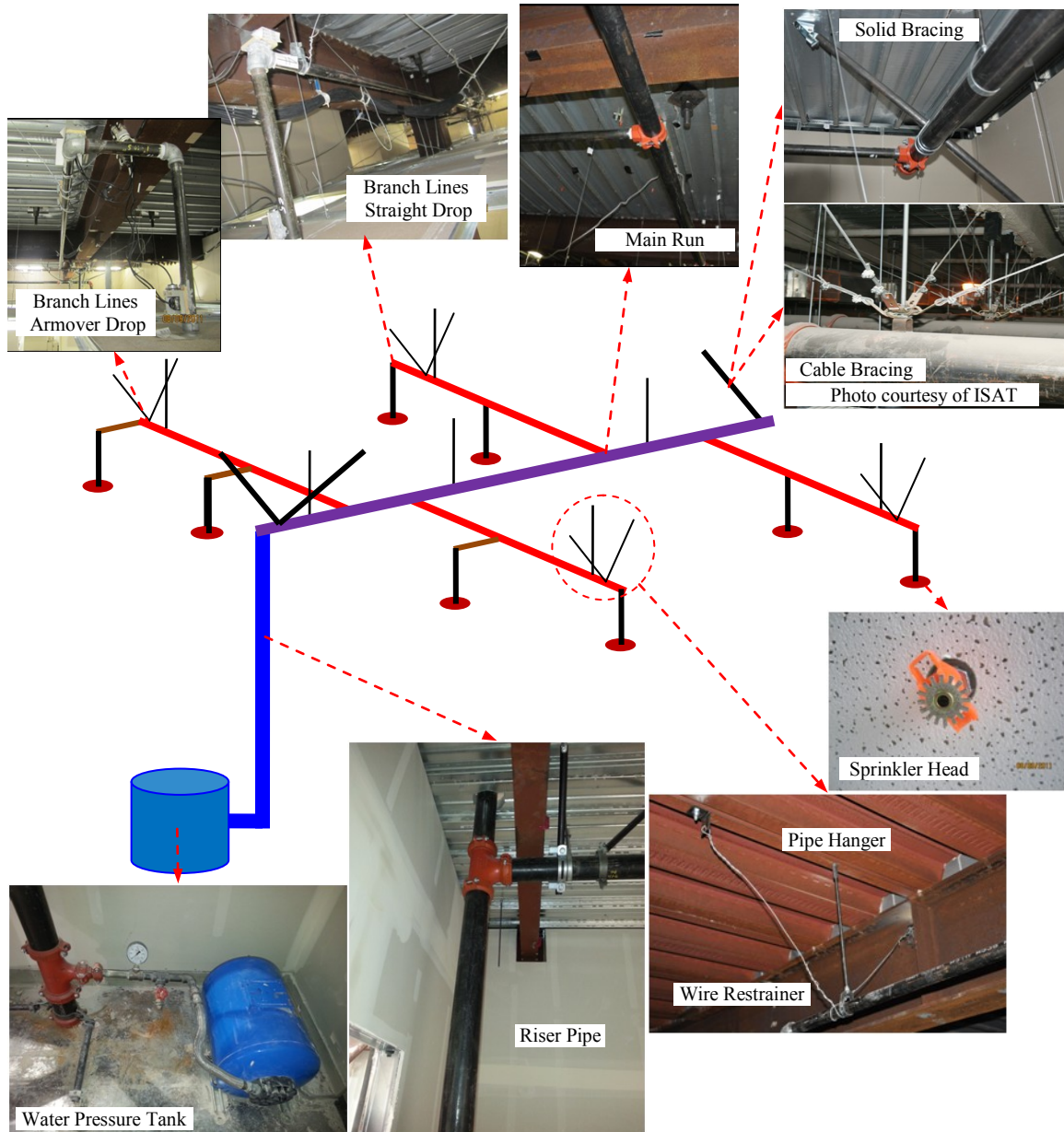


Figure 1-1 Schematic of a Typical Fire Sprinkler Piping System

1.2.1.1 Guidelines and Specifications

Several factors have been recognized as the main sources of nonstructural (fire sprinkler piping system) damage as expressed below (FEMA E-74, 2011):

- **Inertial Forces:** In general, the acceleration is greater in locations higher than the base. As a consequence, the inertial force experienced above the base of a building by an object can be several times larger than that experienced at the base. Therefore, acceleration-sensitive components (such as horizontal pipe runs) may experience damage during earthquake shaking.
- **Building Deformation:** Due to deformations of structural members, buildings are subjected to differential horizontal movement between floor levels, which is known as story drift. Therefore, drift-sensitive components (such as vertical pipe runs) may experience damage during earthquake shaking.
- **Building Separations:** Nonstructural components (such as horizontal pipe runs that passed across the structural separation joints) may experience damage due to differential movements between adjacent structures across the separation joints.
- **Nonstructural Interaction:** The main reason for this type of damage is the interaction between adjacent nonstructural systems, which move separately from one another. Some examples of damaging piping interactions include: 1) sprinkler head and ceiling interaction causing the sprinkler head to break and water to leak; 2) interaction of adjacent pipes with one another; and 3) pipe interaction with adjacent structural members or equipment.

These sources of damage can cause a partial or complete functionality loss of the fire sprinkler systems. The consequence of loss of fire sprinkler systems can pose a serious risk to life safety. Also in the case of water leakage, a portion of or the entire floor level may become flooded. Consequently, significant building equipment may get damaged, causing the building to be shut down. This is one of the most costly types of nonstructural damage.

In recent years, engineers, researchers, and code committees have devoted substantial attention to the issue of nonstructural performance in order to enhance the performance of these components. Approximately 27 codes and standards and 54 guidelines are now available with topics related to nonstructural components (References are available in FEMA E-74, 2011). For all nonstructural systems (including fire sprinklers), the design solutions must meet the minimum requirements defined by building codes such as IBC 2012 International Building Code (ICC, 2012) and ASCE/SEI 7-10 Minimum Design Loads for Buildings and Other Structures (ASCE, 2010). The nonstructural design forces from the codes are defined as:

$$0.3S_{DS}I_pW_p \leq F_p = \frac{0.4 a_p S_{DS} W_p}{\left(\frac{R_p}{I_p}\right)} \left(1 + 2 \frac{z}{h}\right) \leq 1.6S_{DS}I_pW_p \quad (1-1)$$

where:

F_p = seismic design force

S_{DS} = design response spectral acceleration at short periods

a_p = component amplification factor that varies from 1.00 to 2.50

I_p = component importance factor that varies from 1.00 to 1.50

W_p = component operating weight

R_p = component response modification factor that varies from 1.00 to 12

z = height in structure of point of attachment of component with respect to the base

h = average roof height of structure with respect to the base

The design philosophy of construction of an ordinary use is to provide a minimum level of life safety. However for essential facilities such as fire stations and hospitals, a higher level of performance (such as immediate occupancy) is required for structural and nonstructural performance. Therefore, the design of systems for a higher (different) level of damage control —

known as a performance-based design approach — has become important for engineers, researchers, and code committees. Performance-based design provides terminology to characterize seismic risk and seismic performance and provides a framework for making comparisons between varying levels of seismic hazard, structural and nonstructural performance, post-earthquake functionality, acceptable and unacceptable damage, and total earthquake losses over the expected life of the facility (FEMA E-74). The need for a performance-based design approach was highlighted in building guidelines such as ATC-58 (2009). Therefore, determining the probabilistic seismic assessments and fragility curves is a critical initial step to achieve a reliable performance-based design approach.

The current practice of piping system design, plan review, and construction inspection relies heavily on nationally accepted standards. For example, 2009 IBC accepts seismic restraint of fire protection systems designed in accordance with the National Fire Protection Association's NFPA 13 Standard for the Installation of Sprinkler Systems (2011). As a result, verification of NFPA 13 compliance is a common occurrence in the field. These construction/design standards such as ASME B31 Process Piping (ASME, 2008), NFPA 13, and SMACNA Sheet Metal and Air Conditioning Contractor's National Association (SMACNA, 2003) all prescribe brace, restrainer, and hanger locations based on such tabulated characteristics as pipe sizes and spans (FEMA E-74, 2011; GC Proposal, 2007). The following text provides a brief overview of the two current guidelines that are widely used for design and installation of piping systems. The design requirements for pipes, braces, and restrainers are provided throughout the following sections of this document, while this section only provides the historical summary of the two main guidelines for piping systems.

- **SMACNA:** Following the 1971 San Fernando earthquake, the State of California required that hospital buildings remain fully functional during and after an earthquake. The California Office of Statewide Health Planning and Development (OSHPD) approved the design guidelines for the bracing of piping and duct systems as specified by SMACNA in 1976. SMACNA provides the design guidelines and seismic restraint detailing for piping and duct systems. SMACNA has added several seismic restraints such as transverse and longitudinal bracing types over the decades (Gupta et al., 2011).

- **ASME:** In critical facilities such as fuel and natural gas lines, power plants, hospitals, and industrial piping, even when prompt restorative measures are taken, any leakage can produce serious harm to people of the building. Therefore, higher damage control and more stringent design requirements are provided in this standard. Many of the code requirements based on this standard are evolved from the experimental and analytical research on nuclear power plants. In addition to braces, restrainers, and hangers, this standard characterizes the performance of piping components such as pipe-bends (elbows) or tee-joints in terms of the controlled extent of nonlinearity, which is defined as “Plastic Collapse” rotation (FEMA E-74, 2011; Gupta et al., 2011).
- **NFPA-13:** NFPA 13 is the standard known as the industry benchmark for design and installation of automatic fire sprinkler systems. This standard addresses sprinkler system design approaches, system installation, and component options to prevent fire deaths and property loss. In this standard, the requirements include sprinkler system design, installation, and acceptance testing; hanging and bracing systems; underground piping; and ensuring seismic protection is in line with ASCE 7-10 (2010).

In 1947, for the first time in U.S. national installation rules, earthquake provisions were considered for fire sprinkler piping systems. In 1950, the NFPA document was published as NFPA 13 instead of NDFU 13 ("Standard of the National Board of Fire Underwriters for the Installation of Sprinkler Equipments as Recommended by the National Fire Protection Association"). However, there was no change in the earthquake recommendations in 1950 edition. Major changes were made to the 1951 edition based on the requirement to laterally brace the piping to carry a force of 50% of the weight of the piping. From 1951 until the current edition, several modifications and changes were made to improve the behavior of fire sprinkler piping system during the earthquakes.

It should be mentioned that the NFPA13 (2011) is considered the main document in this study for designing and performing experimental/analytical studies.

1.2.1.2 Past Earthquakes

According to FEMA E-74 (2011), a fire sprinkler piping system might become damaged during an earthquake due to several reasons such as:

- These systems are both acceleration and deformation sensitive. Vulnerable locations include joints, bends (elbow), connections, braces, hangers, restrainers and risers subjected to significant relative movement between floors.
- The possible impact of sprinkler heads and ceiling systems may cause damage to the ceiling or break sprinkler heads and cause subsequent water leakage.
- Fluids may leak from damaged joints or broken pipe; property losses and operation losses are often attributed to fluid leaks from fire suppression piping. Facilities may need to be evacuated if the fire suppression system is compromised.
- Damage to any part of the fire protection system may compromise its functionality; in addition to piping, the pumps, holding tanks, control panels, control sensors, smoke detection equipment, fire doors, etc. must all be operational. If a fire breaks out following an earthquake and the fire suppression system is not functional, significant property losses may result.

The following subsection presents a brief performance overview of fire sprinkler piping systems during selected earthquakes.

- **The Alaska Earthquake in 1964**

The Alaska earthquake caused extensive damage to nonstructural damage including plumbing, ventilation, air-conditioning, and fire protection systems (Ayres et al., 1973). In most cases, the cost to repair nonstructural systems was considerably higher than the cost of repairing the structure. During the Alaska earthquake, most of the fire sprinkler damage occurred at pipe fittings. Overall, the fittings in welded steel pipes and soldered or brazed copper lines had very little damage, while threaded fittings were the primary sources of damage. Some of the failures of threaded elbows were located where the long pipelines turned into small segments. This type of failure was believed to happen by excessive swaying of long pipe runs and inability of the short run to cope with the movement (Figure 1-2, NRC, 1973).

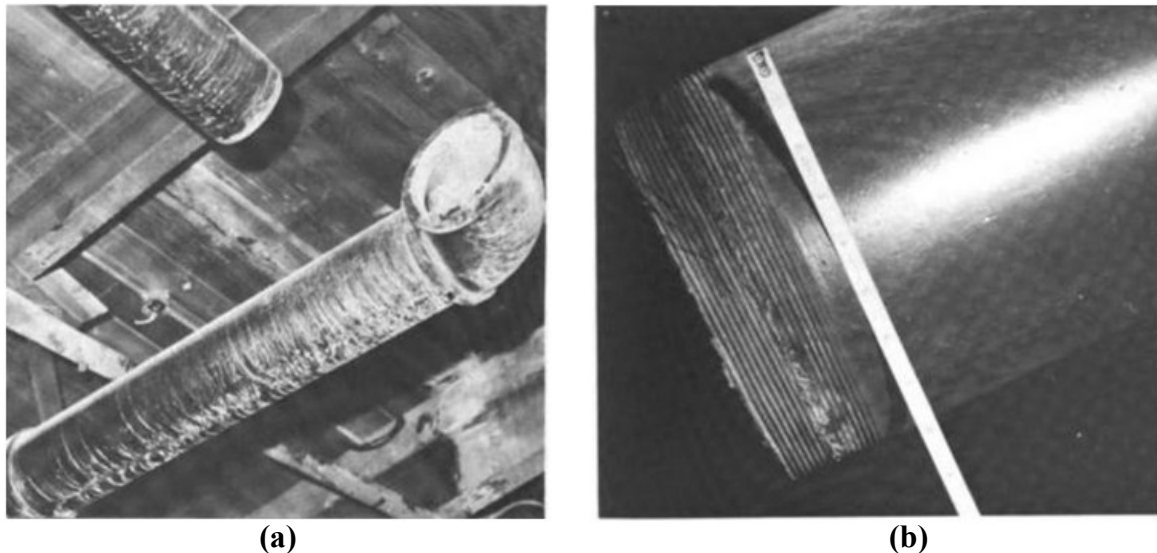


Figure 1-2 (a) Pipe Pulled out from Elbow at Elmendorf AFB Warehouse (b) Close up View of Figure (a) (NRC, 1973)

- **The San Fernando Earthquake in 1971**

A comprehensive study was performed by the U.S. Department of Commerce on 44 structures during the San Fernando earthquake. Based on this document, extensive nonstructural damage including ceilings, partitions, and piping systems were observed following the earthquake. For example, it cost \$145,000 to repair the Holiday Inn located on Van Nuys. This amount represented approximately 11% of initial costs of this hotel. Structural damage amounted to less than \$2,000; The remainder was nonstructural damage (Ayres et al., 1973). Figure 1-3 shows a sample of damage resulting from the San Fernando Earthquake.

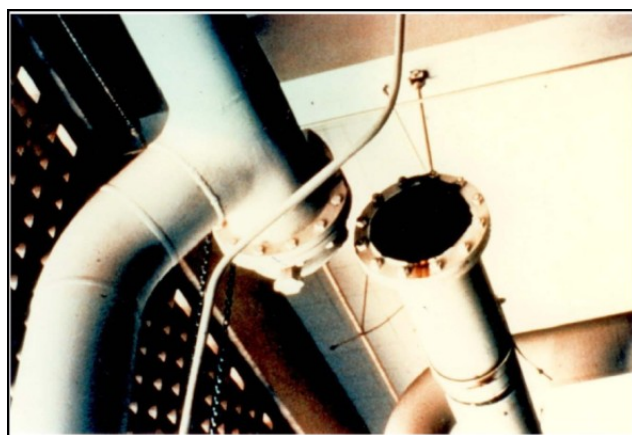


Figure 1-3 Pipe Joint Failure (Photo by John F. Meehan)

Due to the damage observed after the San Fernando earthquake, OSHPD required that hospital buildings remain fully operational after an earthquake. As a result, the seismic design of buildings and nonstructural components changed significantly (Gupta et al., 2011).

- **The Northridge Earthquake in 1994**

The performance of nonstructural components was not satisfactory during the 1994 Northridge earthquake. After this magnitude 6.8 earthquake, nonstructural components received considerable attention and several changes were applied to the fire protection system codes afterwards.

According to a report by Fleming (1998), significant damage occurred to nonstructural components during this earthquake. In one warehouse, approximately 2,200 feet of Schedule 40 steel pipes (up to 8 in. size) fell down off the ceiling. Threaded joints broke at several points, and a pipe hanger rod pulled out from the structure, which resulted in failure of the whole branch line. In some locations, threaded joints broke or pipe hangers failed due to insufficient lateral and longitudinal sway braces. In six warehouses, the grooved coupling leaked during the earthquake because of old and hard rubber gaskets and lack of lateral and longitudinal bracing. In general, the lack of bracing or inadequate bracing was reported as the main cause of significant damage to the fire sprinkler systems. In a few cases, due to the large vertical floor acceleration, many

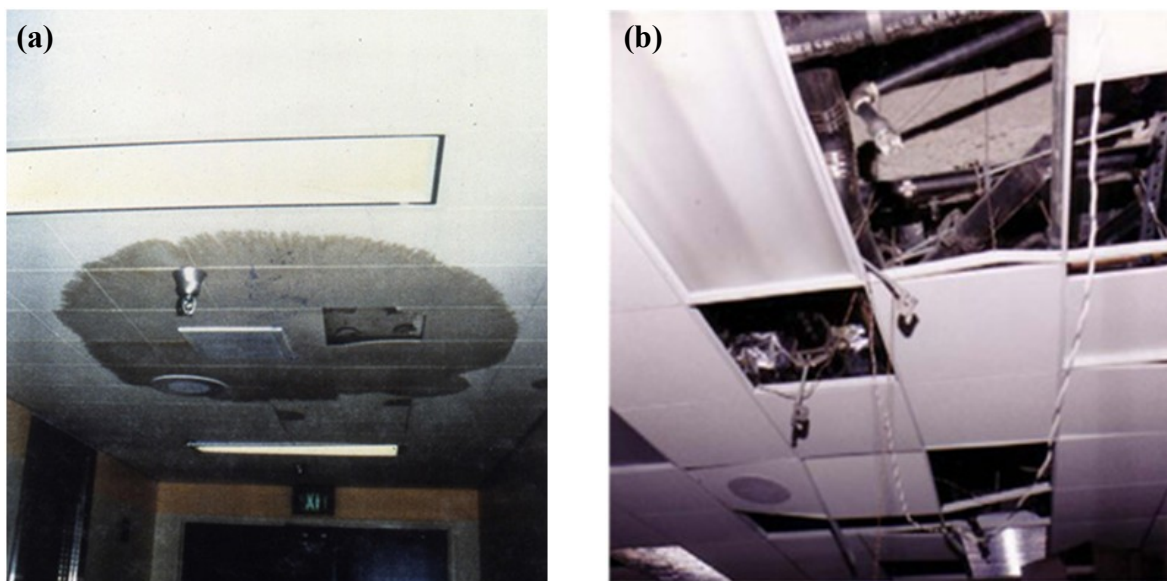


Figure 1-4 (a) Leakage Caused by Pipe Damage at Joint (Photo courtesy of Degenkolb Engineers) (b) Damage to Suspended Fire Protection Piping (Photos Courtesy of Mason Industries)

sprinklers were damaged. Pulling sprinklers through the ceiling, then pushing the sprinklers back through the substantial ceiling, caused damage to the sprinklers because of upward and downward movements of the branch lines. The ceiling-piping interaction, which resulted in damage to either piping or the ceiling system, was a common mode of failure during the Northridge earthquake (see Figure 1-4).

- **The Chile Earthquake in 2010**

In recent major earthquakes such as the 2010 Chile earthquake, most of the hospitals in the central south region of Chile were subjected to strong ground motion. Engineers inspected a total of 16 hospitals after the earthquake (Miranda et al., 2012). Four hospitals were closed due to the loss of functionality, and approximately 75% of function was lost in the remaining 12. (Ju and Gupta, 2012).

Miranda et al. (2012) reported that buildings in Chile, except newer structures, are not equipped with active fire sprinkler systems. About 50% of inspected buildings (those that had a fire sprinkler system) experienced pipe leakage. One of the most common causes of leakage was breakage of sprinkler heads interacting with ceiling systems or failure of the pipes at or near joints (Figure 1-5a). Also, several pipe hangers experienced permanent rotation (offset) due to excessive pipe movement (Figure 1-5b).



Figure 1-5 (a) Failures of Water Sprinkler Piping Near Joints (Miranda et al. 2012), and (b) Permanent Offset of Pipe Hanger (Photo: P. Correa)

Although in many cases the fire sprinklers were not adequately braced, in others cases bracing practices similar to those used in the U.S. in main and secondary sprinkler lines experienced shear failures. The latter was typical of post-installed mechanical drop-in devices. In other cases the anchorage of the braces was either sheared off or pulled out of the composite slab (Miranda et al., 2012).

- **Tohoku Pacific Earthquake in 2011**

After the great 2011 Tohoku earthquake, many structures were inspected. A study conducted by Mizutani et al. (2012), examined the relationship between equipment damage rate and type of building structure (shown in Figure 1-6a).

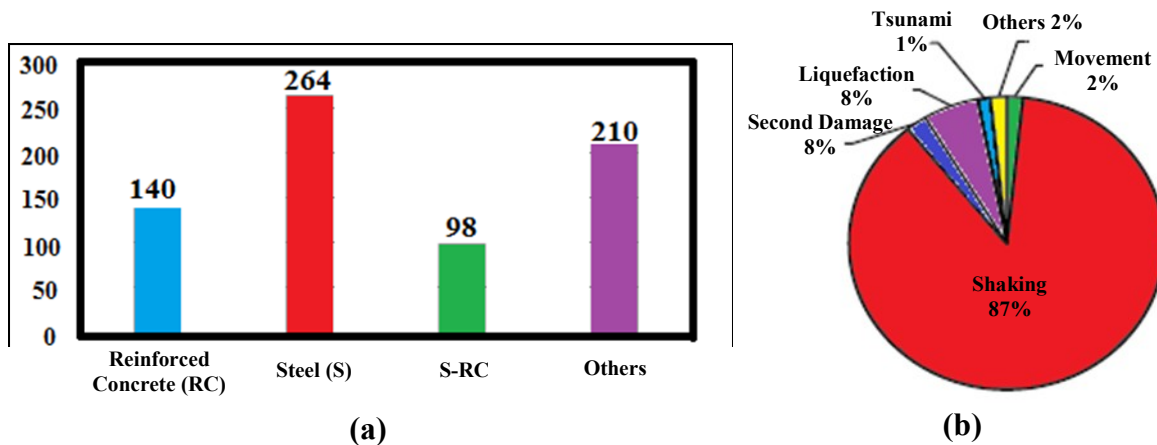


Figure 1-6 (a) Relationship Between Building Damage Rate and Type of Building Structure (b) Equipment Damage Factor (Mizutani et al., 2012)

Scientists in this study reported that the damage caused by shaking was approximately 87%, while the damage caused by liquefaction and tsunami accounted for 8% and 1% of total damage, respectively (Figure 1-6b). In this study, damage in the buildings that were directly hit by tsunami waves was not considered.

In this earthquake, damage to fire protection systems accounted for 10% of the entire cost of equipment damage, while plumbing accounted for 27% of the entire cost of equipment damage. The percentage of cost for damage to the different components of fire protection systems is shown in the pie chart in Figure 1-7a. The damage to the piping adds up to approximately 50%

of the total cost with the damage to sprinkler heads second to that. Figure 1-7b shows that 42% of the damaged piping systems also showed signs of water leakage (Mizutani et al., 2012).

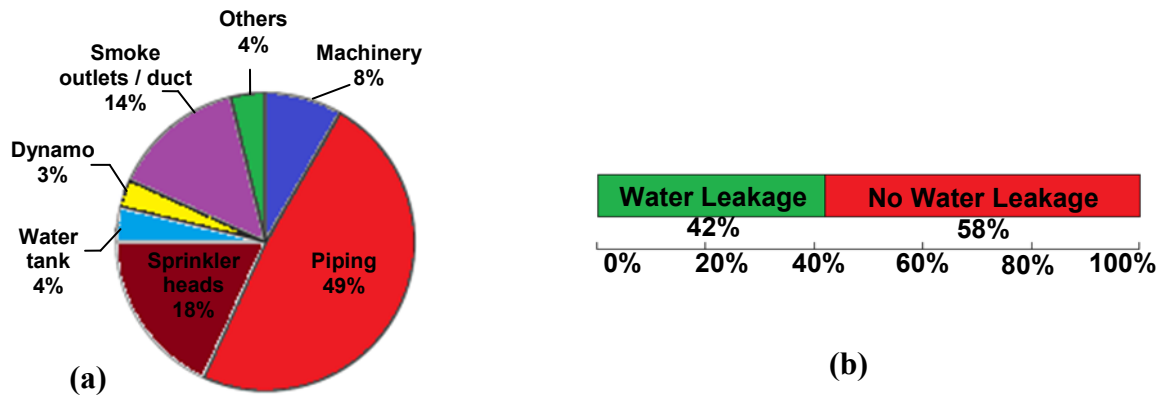


Figure 1-7 Fire Sprinkler System Damage in the Tohoku Earthquake (a) Graph of Damaged Parts (b) Percent of Damaged Pipes that Leaked Water

1.2.1.3 Experimental Studies

Experimental studies are one of the crucial steps for observing and recognizing the failure modes of piping systems. Also the data obtained from these experiments can provide valuable experimental-analytical bases. Therefore, these experimental studies can lead to the development of future reliable analytical studies. However, not many experimental studies have been conducted during past years on piping systems. A few are associated with component level experiments but do not examine the system-level performance (Larson et al., 1975; Rodabaugh et al., 1978; Gerdeen et al., 1979; Wais, 1995; Masri et al., 2002; Matzen et al., 2002). However, some studies conducted shake table testing on piping subsystems (Nims, 1991; Shimizu et al., 1998; Chiba et al., 1998; Nakamura et al., 2000). In the following subsection, a brief description of the most recent experiments on piping systems is presented, followed by a short summary of the outcome of these experiments.

- **Static Test of Pipe Joints**

A series of static tests have been made on threaded, copper, and grooved pipe joints, all commonly used in fire protection systems. The tests were intended to help researchers understand the behavior and failure mode of these joints under extreme lateral loads. Antaki and

Guzy (1998) conducted a study on the load deflection of joints at different stages like loss of stiffness, onset of leaking, and ultimate capacity of the joints. They performed a total of 24 tests (16 grooved, four copper, and four threaded). The pipes were filled with 150 psi pressurized water. Figure 1-8 shows the test setup of described bending experiment.

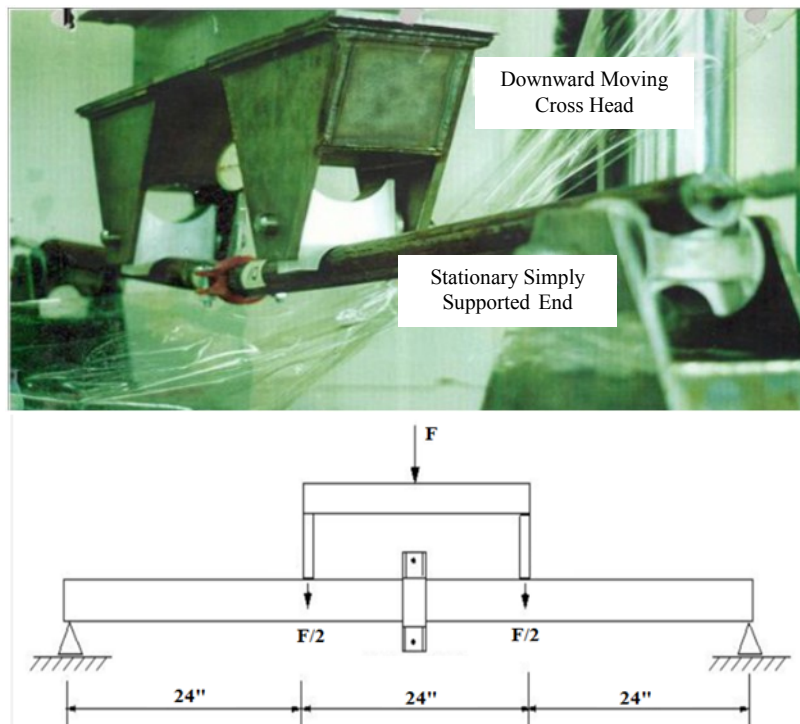


Figure 1-8 Test Setup of Static Bending Test of Joints (Antaki and Guzy, 1998)

The researchers observed consistent damage in grooved connections, which was a cracked housing followed by a loss of gasket preload and leakage; in threaded connections, a common failure started from exposed pipe thread, and one specimen failed by stripping of the engaged threads. In copper couplings, three specimens experienced rupture of the copper fitting at the coupling's centerline. One specimen buckled at the bearing point between the machine's cross head and the pipe (Antaki and Guzy, 1998).

- **Dynamic Test of Grooved Coupling and Threaded Joints**

Analysts conducted a series of dynamic tests on threaded and grooved pipe joints, commonly used in fire protection systems. The tests were designed to help engineers understand the behavior and failure mode of these joints under cyclic/seismic loads. Antaki and Guzy (1998)

performed tests on a total of 20 specimens (16 grooved and 4 threaded). Each specimen consisted of a 6-foot-long pipe filled with 150 psi pressurized water. Figure 1-9 shows the test setup of described experiment.

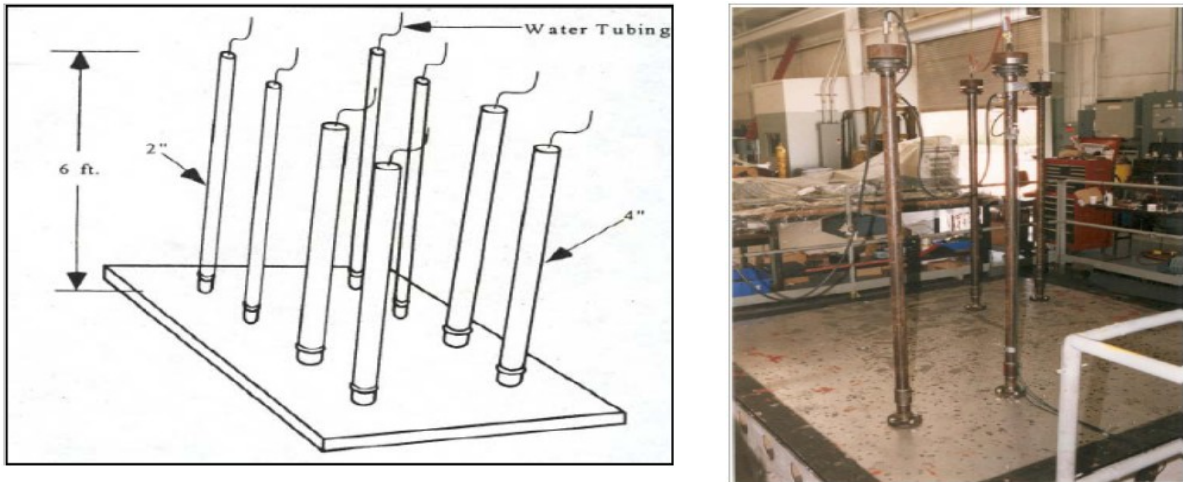


Figure 1-9 Test Setup for Dynamic Test of Grooved Coupling and Threaded Joints
(Antaki and Guzy, 1998)

Antaki and Guzy (1998) reported that rigid and flexible grooved coupling leaked at 70% of the table capacity, while the leakage of the threaded joints was observed at 50% and 25% of the table capacity. Figure 1-10 shows samples of damage during these tests.

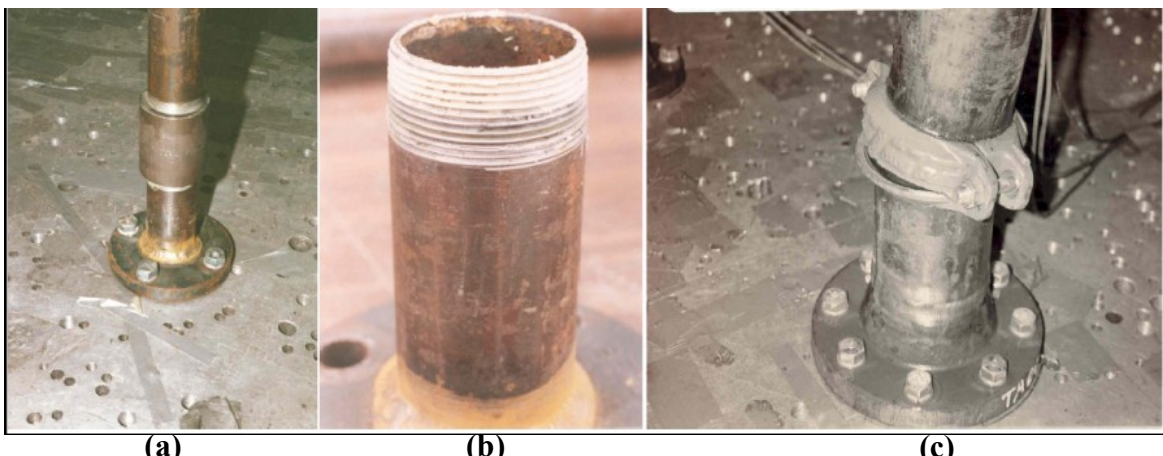


Figure 1-10 (a) Threaded Specimen Mounted on Shake Table (b) Threads Do Not Exhibit Damage After Dynamic Test to Leak (c) Failed Mechanical Coupling During Dynamic Test
(Antaki and Guzy, 1998)

- **Dynamic Test of a Sprinkler System Inside a Hospital Room**

Another study (Filiatrault et al., 2008) investigated the fire protection system for a hospital room, which was composed of vertical and horizontal Schedule-40 pipe runs $\frac{1}{2}$ -inch in diameter. Figure 1-11 presents a plan view and an elevation showing the layout of the pipe runs. The riser pipe runs were attached to the UB-NCS concrete slabs using a combination of flanges and pipe clamps. The horizontal sprinkler pipe run was attached to the partition walls using a combination of flanges and pipe clamps and to the top UB-NCS concrete slab using 3/8-inch all threaded rod hangers 7 inches in length. A Standard Spray Pendant sprinkler head was considered to interact with the suspended ceiling system. During testing, the fire extinguishing system was connected to a hydrant, providing typical working pressure.

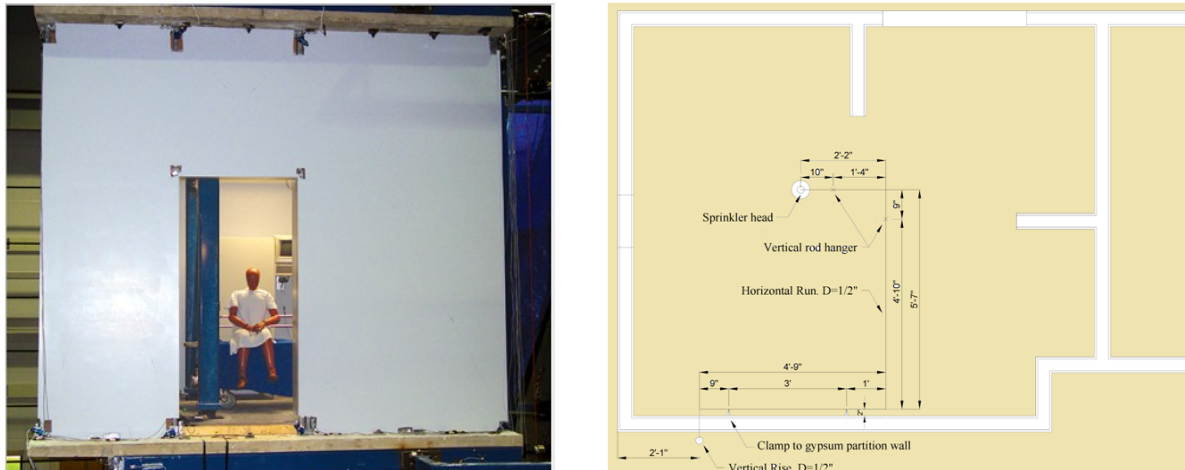


Figure 1-11 (a) Hospital Room Elevation View (b) Plan View of Sprinkler System (Filiatrault et al., 2008)

In this set of experiments, researchers observed no damage in the sprinkler system. During the test for 100% of the testing protocol, the achieved peak floor acceleration and interstory drift was 0.77g and 0.87%, respectively. The maximum scale factor that was applied to the hospital room was 150% (Filiatrault et al., 2008).

- **Other Static and Dynamic Tests of Piping Systems**

Several experiments have been conducted on piping systems during recent years such as shake table experiments on four hospital piping assemblies (Zaghi et al, 2012), shake table experiments on two hospital piping assemblies with sliding roof (will be presented in this study), monotonic

and cyclic tests on 48 pipe tee joints (Tian et. al, 2012), dynamic test of full-scale piping systems (Soroushian et al, 2012), and dynamic tests of six piping subsystem configurations (Tian, 2012). Researchers used the data from these experiments to calibrate the analytical model that will be proposed in this study. Therefore, each of these experiments will be explained briefly in the following sections.

1.2.1.4 Analytical Studies

Due to a lack of historical and experimental data, researchers have conducted very few analytical studies during the past years on evaluating the response of fire sprinkler and piping systems (such as: Baker et al., 2004; Fujita et al., 2004; Semke et al., 2006). However, recent experimental studies in this field are resulting in increasing amounts of analytical work for fire sprinkler piping systems. In the following text, a brief summary of the most recent analytical works is presented.

- **Finite Element Model (FEM) of a Coupled Piping System**

Research conducted by Martinez and Hodgson (2007) generated a finite element model of a Victaulic coupled piping system tested at Lehigh University. In their study, they investigated a welded pipe (rigid connection) and a coupled pipe that accounted for rotational stiffness in the model.

ABAQUS software was used for static and dynamic analysis of the piping system. FEM models were designed and compared with two separate test results of the piping system, using four in and eight in pipe diameters. Two finite element models were created and analyzed for each piping size. In welded pipe models, the connections between lengths of pipe were the same stiffness as the pipes themselves, while in the coupled pipe model — in which couplings joining the pipes were modeled to behave like Victaulic couplings — they were less rotationally stiff than the pipe itself (Martinez and Hodgson, 2007).

The researchers predicted approximately 70% of the acceleration obtained from the experiment by the analytical model. However, the analytical model was not able to capture the pipe and bracing strain in an acceptable range (Martinez and Hodgson, 2007).

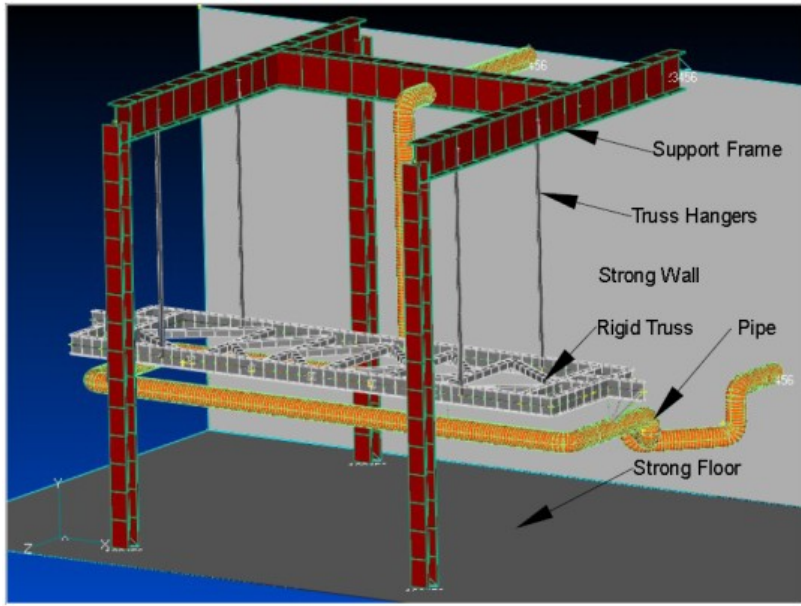


Figure 1-12 Finite Element Model of the 8 inch Victaulic Test Setup (Martinez and Hodgson, 2007)

- **Seismic Analysis of Fire Sprinkler Systems**

Sorourshian et. al (2011) analytically modeled one of the four sections of the UCSF Hospital fire sprinkler system including risers, main distribution lines, branches, sprinkler heads, hangers, and braces. This model was built in the OpenSees platform (OpenSees, 2012). This was done to investigate the influence of the type, quantity, and distribution of seismic braces on the dynamic response of fire sprinkler systems. They included in the investigation the effect of nonlinear structural response, as well through the implementation of triaxial floor response excitations obtained from an incremental dynamic analysis IDA for a set of 21 far-field ground motions of a three-story hospital building (Figure 1-13a).

Investigators in this study used OpenSees software (Mazzoni et al., 2007) to model the piping system and perform linear time-history analysis. The pipes and pipe hangers were modeled as linear elastic frame elements with their gross section properties. In this model, pipe joints were not explicitly modeled, and they were assumed rigid in all direction. They calculated the effective stiffness of the cable restrainers to be 1/10 of the gross section of the cables to account for the initial slack in the cable. The connection of the riser to the ground level was such that no

moment demand was imposed on the base of the riser pipe. The braces, hangers, and wires were assumed to be pin-ended truss members (Figure 1-13b) (Soroushian et. al, 2011).

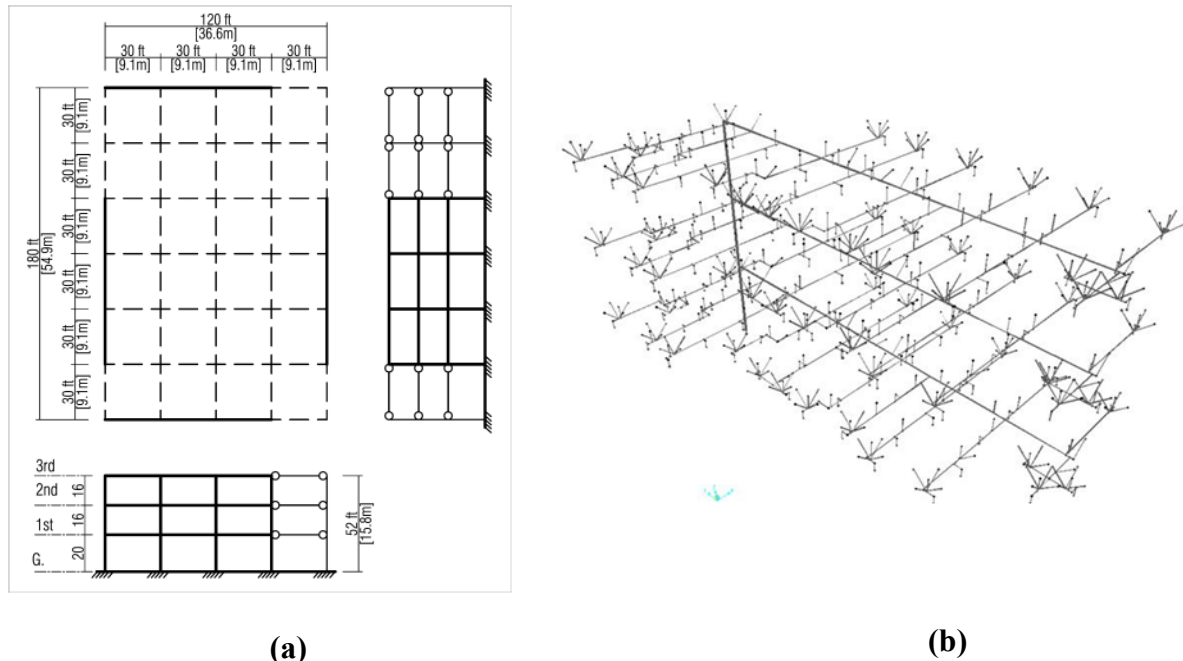


Figure 1-13 (a) Geometry of the Three-Story Hospital Building (b) Three Dimensional View of Fire Piping Model (Soroushian et. al, 2011)

Researchers, including the author of this report, concluded that increased levels of yielding in the supporting structure reduces both sprinkler head displacement demands as well as seismic brace and wire restraint forces. Also, they determined that the effect of unbraced branches significantly increased the peak sprinkler head displacements (Soroushian et. al, 2011).

- **Fragility Analysis of Threaded Tee-Joint I**

Ju and Gupta (2012) performed this study at the University at Buffalo, in which they calibrated the 2-inch black iron threaded joint by component test. They defined three limit states — minor, moderate, and severe — according to a guideline specified in the ASME (2004) for nuclear power plant piping systems based on the rotational demand of threaded joints.

Afterwards, they modeled the piping system of the UCSF Hospital with rigid connection of the joints, then applying a total of 75 earthquake ground motions directly to the piping system. At this point, they chose two different approaches in their study (Ju and Gupta, 2012):

- 1) At a maximum of three critical locations, they inserted the nonlinear threaded joint and plotted the fragility curves at these three points. Furthermore, they analyzed the effect of inserting/removing nonlinear tee joints at one location on fragility curves at a different location. The results showed that this effect is negligible (Ju and Gupta, 2012).
- 2) In this procedure, which has been named “decoupled,” they analyzed the main run piping by linear response history analysis using the mentioned motions. They also calculated the displacement history demand of a specified location on main run. They then applied the displacement history to the tee joint component model and then plotted fragility curves (Ju and Gupta, 2012).

The authors determined the results of these two approaches are quite different, and therefore the mass interaction and tuning between the main line piping and the branch piping had a considerable effect on seismic fragilities (Ju and Gupta, 2012).

- **Fragility Analysis of Threaded Tee-Joint II**

In this study, the piping model is similar to the system presented in the previous subsection. The main goal of this research: to investigate the effect of interaction between the building and the piping on piping fragility. To do so, the researchers modeled two low-rise, five-story and high-rise, 20-story buildings using OpenSees software (Mazzoni et al., 2007) (see Figure 1-14). They then analyzed the structures under 22 ground motion records and used the floor responses of 5th, 10th, 15th, and 20th floors of a 20-story building and all floors of five-story building for piping fragility analysis. In order to compare the effect of structural nonlinearity, they evaluated piping fragilities by considering the building to exhibit significant nonlinearity in the beams and columns as well as considering the buildings to remain linear (Ju and Gupta, 2012).

The researchers reported that since piping system modes are local in nature, fundamental building mode is not necessarily the critical mode in the evaluation of piping fragilities. Also by studying the effect of nonlinearity on the structure, they showed that the vulnerability of piping might be higher in linear frames whose modes have greater degree of tuning with the piping system. They also demonstrated that the vulnerability of a piping system will not necessarily increase in relationship to the height of the structure.

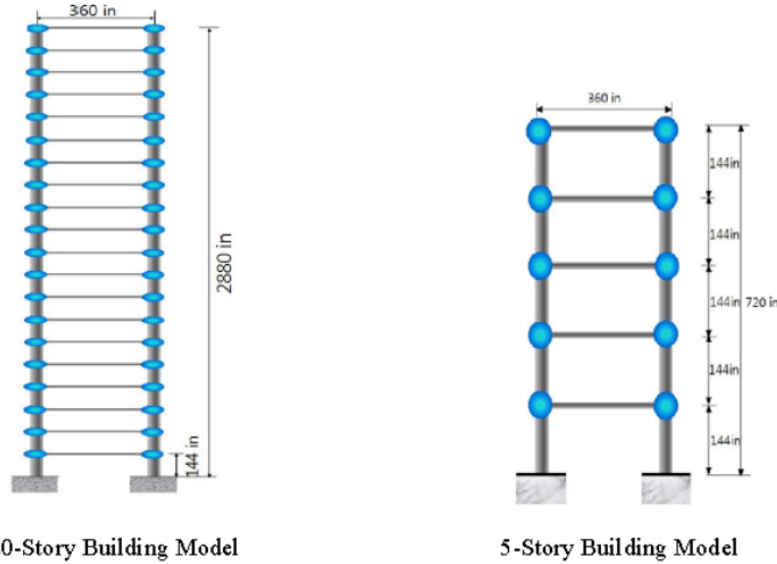


Figure 1-14 RC Moment Frame Building Configurations (Ju and Gupta, 2012)

- **Simplified Computational Model of Hospital Piping Assemblies**

Zaghi et al (2012) developed a simplified analytical model in order to capture kinematic and dynamic responses, maximum bending stresses, and optimum location cable restrainers of piping systems.

The researchers used SAP 2000 software (CSI 2009) to model the piping system and perform linear time-history analysis. The pipes and pipe hangers are modeled as linear elastic frame elements with their gross section properties. In this model, they did not explicitly model pipe joints (threaded and welded); they assumed they were rigid in all directions. They calculated the effective stiffness of the cable restrainers to be 1/10 of the gross section of the cables to account for the initial slack (Zaghi et al, 2012).

The analytical results had close correlation to fundamental periods and displacement results that they obtained from the experiment data. However, the spectral acceleration of the analytical and experimental are comparatively different in mid-range (0.2-0.7sec) periods (Zaghi et al, 2012).

1.2.2 Fragility Study

According to construction importance levels, the design of fire sprinkler systems may vary based on performance expectations and seismic risk tolerance. So, a logical and consistent

methodology that facilitates an efficient decision-making process for mitigating seismic risk is a critical step.

1.2.2.1 Seismic Risk Assessment (SRA)

Seismic risk describes the potential for damage or losses that a nonstructural (or structural) system is prone to experience from a seismic event. Seismic risk can also be defined as the spatially and temporally integrated product of the seismic ground shaking hazard, the value of assets and the fragility of assets (Jacob, 1992).

Basoz and Kiremidjian (1996) present a seismic event timeline that demonstrates the events that take place before and after a seismic event (see Figure 1-15). The first event in this timeline is seismic risk assessment, which estimates the potential losses that may occur as a result of a seismic event (Nielson, 2005). The assessment of these potential losses is conducted through the use of seismic risk assessment tools such as HAZUS (FEMA, 2003) and Performance Assessment Calculation Tool — or PACT (PACT, 2012). The fragility curves for piping systems are the critical input for the above mentioned tools to estimate damage to the piping system and, consequently, to predict the effect of piping damage on economic loss and restoration time of the entire building. Although few recent studies have generated a set of fragility curves, a comprehensive study is needed to: 1) develop new fragility curves based on recent research, and 2) improve existing fragility curves. It should be mentioned, in this study, component and system fragility curves are limited to piping components and systems installed in a building. The structural and nonstructural fragility curves and their interaction with piping system was not considered in this study.

The assessment of seismic vulnerability for an entire piping system must be made by combining the effects of the various components within the system. Fragility curves of critical piping components should be developed in order to attain a reliable fragility curve of the piping system. The component fragilities offer valuable insight as to the relative vulnerability of different piping components and the impact of retrofit on their susceptibility to damage.

However, the end goal of the fragility study is to develop a system level risk assessment of piping systems. The system fragility curves are defined by combining the component fragility

curves of all critical components of a piping system. The system failure definition is associated with the assumption that damage to any component may inhibit the functionality of the piping system. In other words, systems fragility analysis is an approach to derive a particular damage for a piping system as the union of damage probabilities of each component in that piping system.

Furthermore, a building network fragility curve can be determined by combining the system fragility curves of structural systems, nonstructural systems (e.g. piping, partition, and ceiling), and all contents of the entire building. The network fragility curves provide valuable insight as to the relative vulnerability of different systems and the impact of their damage on economic loss and restoration time of the entire building. The network fragility curves can also be expanded to metropolitan areas. However, as only piping systems are considered in this study, the network fragility is not included in the scope of this dissertation.

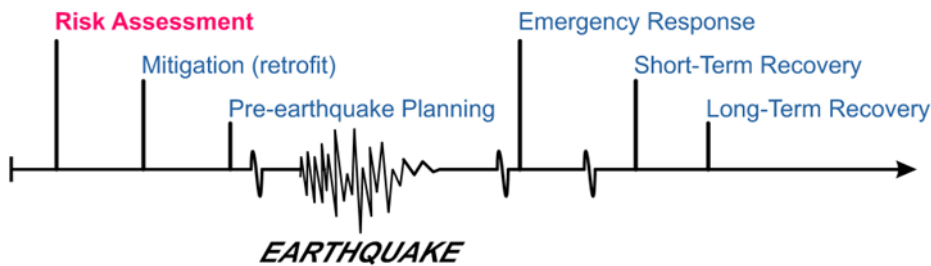


Figure 1-15 Seismic Event Timeline (Basoz and Kiremidjian, 1996)

1.2.2.2 Fragility Studies

As mentioned earlier, analysis of fragility curves of fire sprinkler piping systems is a crucial step for performing a seismic risk assessment of these systems and their parent structures. In this section, the definitions and different methodologies for generating fragility curves are presented.

Fragility curves are conditional statements that give the probability that a structure will meet or exceed a specified level of damage for a given ground motion intensity measure as:

$$f_{DS}(IM) = P(DS|IM) \quad (1-2)$$

where DS is the specified damage state for the piping component and IM represents the ground motion intensity measure. An example of a fragility curve is presented in Figure 1-16.

In general, fragility curves can be classified into four generic groups of empirical, experiential, analytical, and hybrid, according to whether the damage data used in their generation is derived mainly from observed post-earthquake surveys, expert opinion, analytical simulations, or combinations of these, respectively (Jeong and Elnashai, 2007).

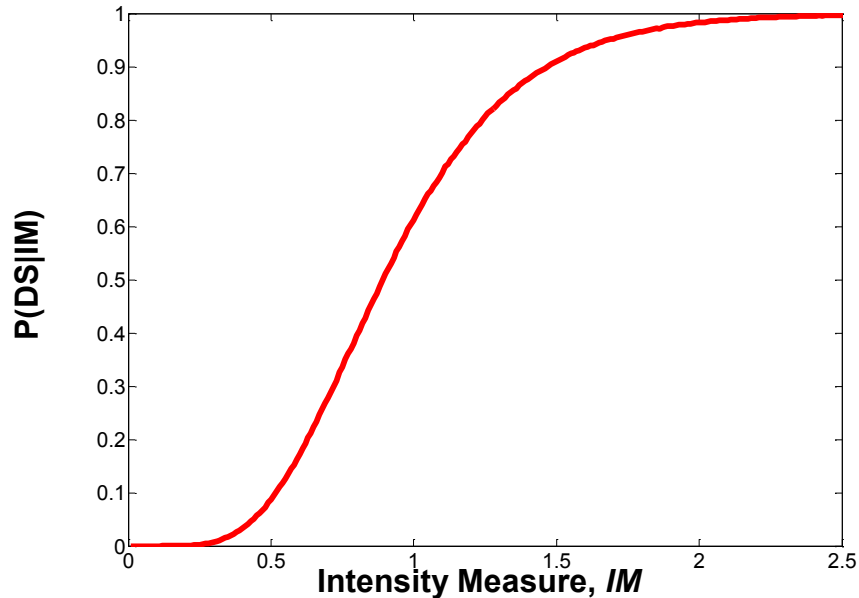


Figure 1-16 Sample Fragility Curve

Empirical: Empirical fragility curves are constructed based on statistics of observed damage from past earthquakes. The observational source is the most realistic, as all practical details of the exposed stock are taken into consideration (Rossetto and Elnashai, 2003). However, empirical data are highly specific to a particular situation. Almost all of these limitations should be considered for the experimental fragility curves, which usually have been considered in this category (Almaraz et al., 2007). However, experimental fragility curves also are subject to additional limitations such as dimensions, amplitudes of intensities, and experimental setup (which does not always result in the most widely applicable observations).

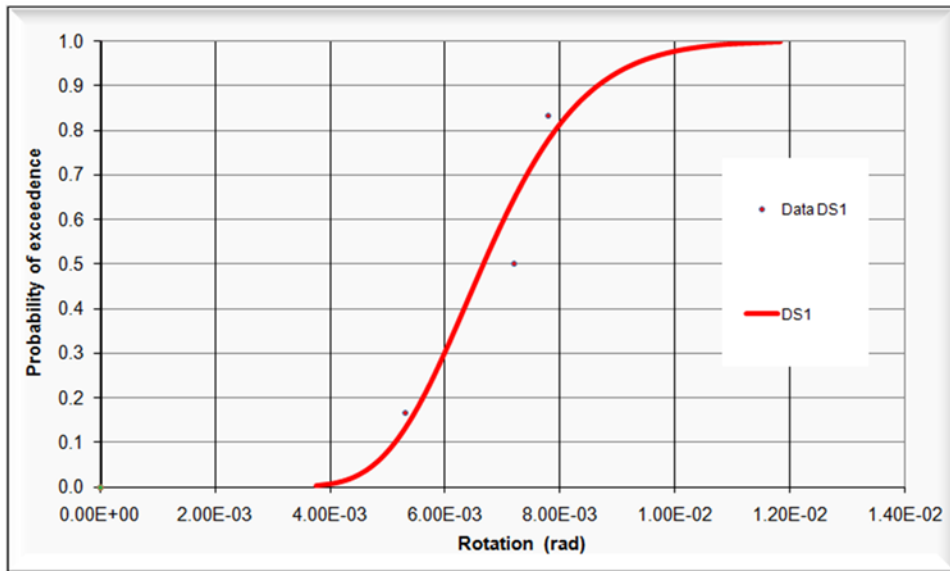


Figure 1-17 Sample Empirical Fragility Curves for Pipe Tee-Joint (Tian et al., 2012)

- **Experiential:** This type of fragility assessment (e.g. ATC-13, 1985 and FEMA, 2003) depends on judgment from experts. There is no limitation in this category in terms of quantity and quality of structural damage statistics, as the experts can be asked to provide damage estimates for any number of systems. However, these fragility curves are highly dependent on individual experience of the experts (Jeong and Elnashai, 2007).
- **Analytical:** This type of fragility curve can be more generic and diverse, as it is typically obtained from a large number of analyses. The extensive analyses usually result in a reduced bias and increased reliability of the damage distribution for systems, when compared to the other approaches (Chrysanthopoulos et al., 2000; Reinhorn et al., 2001). However, the drawback of this approach is that several aspects of elaborated modeling in a system like fire sprinklers still remain challenges that may significantly affect the analysis results. Therefore, it is desirable to either calibrate the analytical models with experiential data or compare the analytical curves with damage study survey studies in cases where appropriate observational data are available (Jeong and Elnashai, 2007).

After developing the system models, various approaches can be incorporated to generate analytical fragility curves, including elastic spectral response (Hwang et al., 2000a), nonlinear static analysis (Mander and Basoz, 1999; Shinozuka et al., 2000), and nonlinear response history

analysis (Shinozuka et al., 2000; Hwang et al., 2000b; Karim and Yamazaki, 2001). The latter analysis is the most rigorous approach to develop analytical fragility curves — the most computationally expensive but reliable methodology (Shinozuka et al., 2000; Hormozaki, 2013). Ju and Gupta (2012) used the nonlinear response history analysis for developing seismic fragility curves of fire sprinkler piping systems (see Figure 1-18).

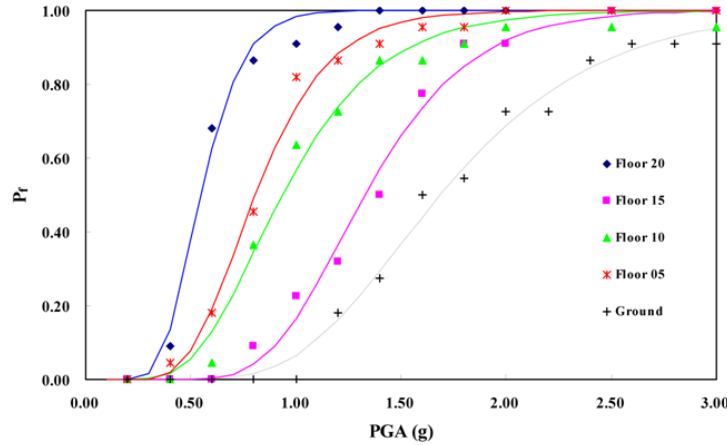


Figure 1-18 Sample Analytical Fragility Curves for Piping Systems (Ju and Gupta, 2012)

In this approach, researchers subjected fire sprinkler piping systems with several variations on design parameters to a suit of acceleration histories representing floor motions. Nonlinear response history analyses are performed, and the maximum responses are recorded to build Probabilistic Seismic Demand Models (PSDMs). As seen in Figure 1-19, the equation of PSDM representing linear regression of logarithms of peak response (Structural Demand S_D or D) and intensity measure (IM) can be written as:

$$EDP = aIM^d \quad \text{or} \quad \ln(EDP) = \ln(a) + d \ln(IM) \quad (1-3)$$

where a and b are the unknown regression coefficients and IM is the selected ground motion intensity parameter (Cornell et al., 2002).

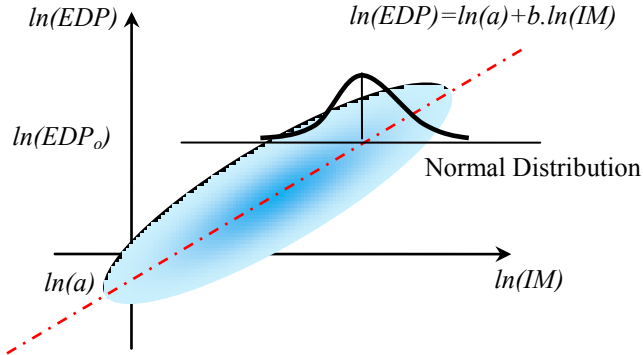


Figure 1-19 Probabilistic Seismic Demand Model (Zaghi et al., 2012)

Then, component fragility curves are developed considering their pre-defined damage states. Failure probability of a system also can be expressed as the probability that seismic demand (S_D) will exceed the structural capacity (S_C):

$$P_f = P\left(\frac{S_D}{S_C}\right) < 1.0 \quad (1-4)$$

The probabilities for fragility curve by a lognormal cumulative probability density function were defined by Choi (2002) as:

$$P(DS|IM) = \Phi\left(\frac{\ln\left(\frac{S_D}{S_C}\right)}{\sqrt{\beta_d^2 + \beta_c^2}}\right) \quad (1-5)$$

where β_d ($\beta_{EDP|IM}$) and β_c are the lognormal standard deviations (dispersions) of the demand and capacity, respectively; $\Phi(\bullet)$ is the standard normal cumulative distribution function; S_d is the median value for the limit state; and S_D (EDP) is the median for the seismic demand, which is a function of the intensity measure (IM). The composite logarithmic standard deviation of $\sqrt{\beta_d^2 + \beta_c^2}$ is known as the dispersion.

The authors of this study performed a comprehensive, three-dimensional, nonlinear model of a typical hospital sprinkler piping system, initially developing the PSDMs of various components of piping systems. Damage states of different components were also determined and described and fragility curves were developed.

For the first time, an analytical modeling methodology for fire sprinkler piping systems was developed. This methodology is used to generate seismic fragility parameters of these systems. The analytical model accounts for inelastic behavior constituents of the system including: threaded joints, grooved joints, solid braces, cable braces, hangers, and restrainers. The model incorporates a newly developed hysteresis model for threaded and grooved tee joints that is validated by the experimental results of several tee subassemblies. The modeling technique at the subsystem level is validated using the experimental results of four different piping subsystems. The methodology is used to obtain the seismic response of the fire sprinkler piping system of UCSF Hospital under two different suites of 96 artificially generated tri-axial floor acceleration histories.

The author considered a total of eight classes of piping systems with variations on types of braces, weights, joints, and location of restrainers in this study. After the component fragility parameters are obtained for the components of all piping cases, system-level fragility parameters are defined, and a joint probabilistic seismic demand model is utilized to develop system fragility parameters. The effect of variation on eight classes of piping systems are examined through component and system level fragility curves.

- Hybrid: This type of fragility curve is usually obtained from combining all of the above-mentioned fragility curves. Hybrid fragility curves are intended to compensate for scarcity, subjectivity, and modeling deficiency in experimental, judgmental, and analytical fragility curves, respectively. Two approaches are generally used to derive hybrid fragility curves: fragility relationships calibrated with other sources and fragility relationships combined with others. In the first one, empirical data generally is used to calibrate judgmental or analytical fragility curves. In the latter, two different types of fragility curves are combined to derive fragility relationships, such as analytical curves along with empirical curves from historical earthquakes (Lin Lin et al., 2011). This approach can be done by combining the empirical, experiential, and analytical fragility curves through Bayesian updating. The Bayesian updating procedure is used to improve the robustness of the fragility curve and produces confidence bounds on estimates of the probability of failure (Schultz et al., 2010).

1.3 Objectives and Scope

This study focuses on the development of analytical fragility curves for fire sprinkler piping systems. Although the use of this system is very common on essential facilities and newly standard constructions, it rarely has been investigated, and the effect of different design cases on the seismic response of these elaborated systems has never been evaluated.

The vision of this study is to provide key information and tools that will facilitate the enhancement of seismic resilience of fire sprinkler piping systems. To realize this vision, the objectives are to:

- 1) Develop a series of analytical nonlinear models for threaded and grooved fitting joints that have been calibrated with the tee-joint experimental data using the OpenSees platform;
- 2) Develop a series of nonlinear behaviors for critical fire sprinkler supporting elements such as hangers, braces, and wire restrains that have been calibrated with component-level experimental data using the OpenSees platform;
- 3) Validate and calibrate the proposed component level nonlinear behaviors of different fire sprinkler components with four different subsystem level experiments. The 3D analytical model of each of these experiments is built using the OpenSees platform and SAP2000;
- 4) Redesign a comprehensive fire sprinkler piping plan for performing analytical fragility studies on fire sprinkler piping systems. Eight different design scenarios are considered for studying the effect of design parameters on local and overall responses of fire sprinkler piping systems. This model contains 973 pipe joints, 201 pipe hangers, 168 wire restrainers, and 24 solid braces (48 cable bracing);
- 5) Generate a comprehensive analytical model using the OpenSees platform and SAP200. Perform response history analysis of all 10 fire sprinkler-motion samples and generate probabilistic seismic demand models (PSDMs) for the various components under investigation;

- 7) Identify all limit states for various components of fire sprinkler systems. Develop fragility curves for various components and, consequently, system fragility curves for all 10 fire sprinkler cases;
- 9) Conduct an extensive study on the effect of all design scenarios on component response and system fragility curves of fire sprinkler piping systems;
- 10) Generate component fragility curves based on interstory drift ratio;
- 11) Conduct an extensive study on displacement demand on piping systems and generate interaction fragility curves for piping systems;
- 12) Compare the fragility curves obtained from damage to the piping systems and those from displacement demands.

1.4 Report Organization

This report is categorized into the following sections:

Section 2 presents the development of analytical models of nonlinear hinges for threaded and grooved fittings with Schedule 40 steel material. This study uses experimental data obtained from test series at University at Buffalo for calibration of proposed analytical data. Also, several behaviors for these types of joints are proposed for the pipe diameters that were not part of the experimental test matrix. All of these models are created using the OpenSees platform.

Section 3 describes development of nonlinear analytical models for pipe segments, braces, hangers, and restrainers. This study uses experimental data obtained from past component level tests for calibration of cable braces, hangers, and wire restrainers. Computational time optimization is performed for pipe hangers. All of these models are created using the OpenSees platform.

Section 4 presents the proposed methodology for system-level modeling of fire sprinkler systems. This methodology is validated and calibrated with four different subsystem-level experiments. The 3D analytical model of each of these experiments is built using the OpenSees platform and SAP2000.

Section 5 presents a comprehensive fire sprinkler piping plan for performing analytical fragility studies on fire sprinkler piping systems. Eight different design scenarios are considered for studying the effect of design parameters on local and overall responses of fire sprinkler piping systems. This model is generated using the OpenSees platform and SAP2000 (only for verification of OpenSees model). The response history analysis of all 10 fire sprinkler-motion samples is performed, and probabilistic seismic demand models (PSDMs) for the various components under investigation are obtained. The limit states for various components of fire sprinkler systems are defined. The fragility curves for various components are generated, followed by sensitivity assessments of fragility curves to design parameter variables.

Section 6 presents the system-level fragility curves of sprinkler systems, which are obtained from the joint probabilistic seismic demand model. The sensitivity assessment of system-level fragility curves to design parameter variables are performed.

In Section 7, the component fragility curves were developed based on interstory drift rotation. The displacement fragility curves were generated based on displacement demands on small and large pipe diameters. At the end, a simple comparison is made between the fragility curves based on the displacements and those from damage to piping systems.

Finally, in Section 8, a summary and conclusions are drawn from the research, and future research needs are outlined.

SECTION 2

ANALYTICAL MODEL FOR PIPING TEE JOINTS

2.1 Introduction

As mentioned before, total losses in U.S. earthquakes due to nonstructural damage or damage resulting from the malfunction of nonstructural components are greater than damages related to the structure itself (Taghavi and Miranda, 2003). The damage to fire sprinkler piping systems can cause three consequential losses: 1) cost of repair or replacement of damaged fire sprinkler systems in a building and in the case of a fire-following-earthquake scenario; 2) loss of building contents, which in extreme cases leads to total closure of a building; and 3) threatening human life and safety.

Improving the functionality of fire sprinkler systems in cases of fire after an earthquake is the main goal and design criterion of these systems. Damage to components in these systems may not always cause loss of functionality. However, damage to the pipe joints such as spraying, dripping, or significant leaking may affect the overall functionality of fire sprinkler piping systems. Therefore, the vulnerability assessment of these joints such as threaded joints and grooved fittings is crucial.

Due to the limited available component-level experimental data and limitations on analytical tools, the capacity of these joints previously has been unknown. However, in recent years, researchers have completed several piping joint tests and developed comprehensive damage and response databases. Hence, reliable analytical tools for these joints are needed for generating sophisticated system-level analytical studies for piping systems.

Therefore, this section introduces a set of unified procedures for the development of analytical models for threaded and grooved piping joints. The validity and accuracy of the techniques, procedures, and tools are verified through a series of component-level experiments. This study uses the OpenSees platform (2012) for modeling, analysis, comparison, and calibration of test data. In this section, each pipe joint is defined and described in detail, modeling techniques are presented, the validation of the model is performed, and at the conclusion, analytical models are proposed for pipe components that were not previously included in experimental test programs.

2.2 Tee-Joint Tests at the University at Buffalo

Scientists at the University at Buffalo Network for Earthquake Engineering Simulation (NEES) site tested a total of 48 tee joints comprised of four different materials, diameters, and joint types. They then developed a diverse database categorizing the monotonic and cyclic responses and damages of tee joints; however, the main focus of this section is the results of the Schedule 40 black iron threaded joint and grooved fitted connections. These test series were designed and performed by University at Buffalo, and the outcome of these tests can be found in Tian et al. (2012). The description and experimental observation of these experiments is described in the following subsections for convenience.

2.2.1 Test Setup

In this test, University at Buffalo engineers designed a setup composed of two pipe runs with a length of L on each side of the tee-joint specimen. One end of each segment of the pipe run was attached to the tee joint, and the other end was supported using a moment free connection attached to a load cell. One end of a perpendicular pipe segment was attached to the tee joint, and the other end was connected to an actuator, which applied a mid-span point load (Figure 2-1). To capture the leakage during the test, all of the specimens were pressurized with 40 psi of water. They then calculated the moment demand of each tee joint by multiplying the force measured by

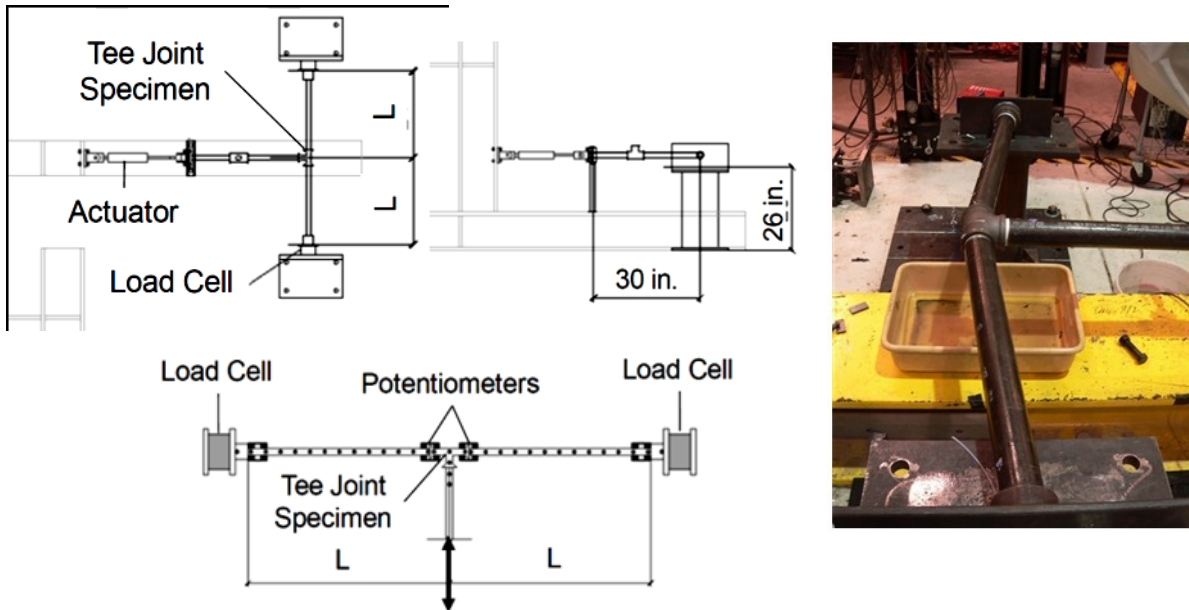


Figure 2-1 Tee Joint Experimental Set-Up (Tian et al., 2012)

the shear load cells by the distance L , measuring cord rotation using linear potentiometers attached to each side of the tee joint.

2.2.2 Loading Protocol

For each pipe section, researchers conducted one monotonic test and three cyclic tests. In the monotonic test, they applied the unidirectional ramp of actuator displacement at a low speed rate of 0.01 in/sec (Figure 2-2a). In the cyclic tests, they conducted the history of actuator displacement at a low speed rate of 0.02 in/sec (Figure 2-2b). These scientists borrowed cyclic loading parameters from a study performed by Retamales et al. (2008, 2011) on drift-sensitive nonstructural components. The 6-inch stroke of the actuator limited the maximum cyclic amplitude of ± 3 inches.

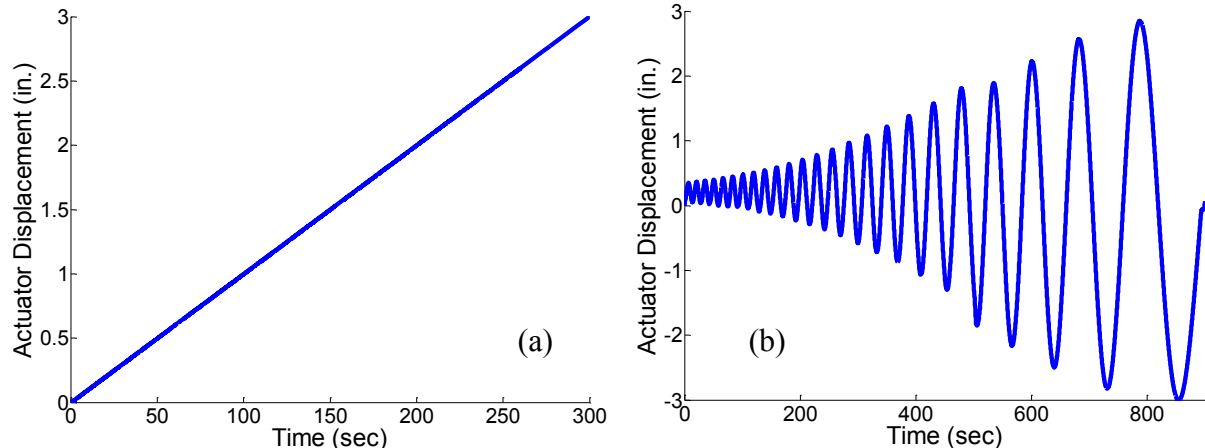


Figure 2-2 Tee Joint Experimental Loading Protocol (a) Monotonic (b) Cyclic (Tian et al., 2012)

2.2.3 Summary of the Joint Observations

A total number of 20 and eight experiments (monotonic and cyclic, respectively) for Schedule 40 black iron threaded and grooved fitted joints were performed. They tested pipe diameters of 3/4-in., 1-in., 2-in., 4-in., and 6-in. for threaded joints, while 4-in. and 6-in. pipe diameters were tested for grooved fitting connections. For each pipe diameter, they tested three subassemblies. Considering the left and right sides of each tee joint, a set of six moment-rotation relationships was obtained for each pipe size. This section of the report summarizes the experimental observations of these tests from cyclic loading.

2.2.3.1 Threaded Joints

Subassemblies were subjected to increasing cycles of loading to capture significant leakage of the tee joint. This leakage occurred due to several reasons, including slippage of pipe threads from the tee threads, erosion of pipe threads, degradation of thread sealant (Teflon tape), and bending of pipe ends (see Figure 2-3). Due to the stroke limitation of the actuator, subsequent damage such as total failure were not achieved.



Figure 2-3 Observed Damage in Threaded Tee Joints (Tian et al., 2012)

Figure 2-4 shows examples of moment-rotation hysteresis responses of tee joints for different pipe diameters. The general trend of moment-rotation relationships shows that pinching effects are more pronounced in the larger pipe diameters.

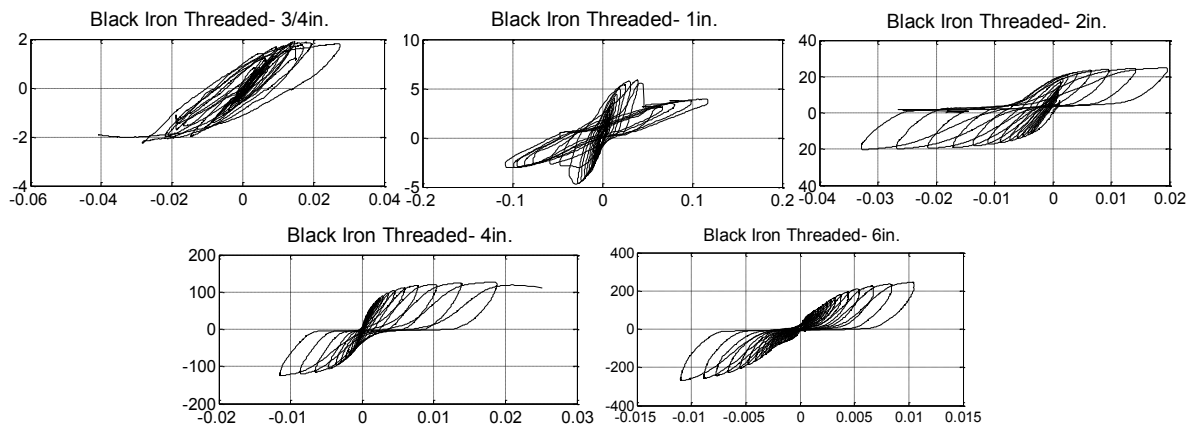


Figure 2-4 Moment-Rotation Hysteresis Response of Tee Joint Subassemblies with Different Diameters (Tian et al., 2012)

2.2.3.2 Grooved Joints

Scientists in this study also subjected the subassemblies to increasing cycles of loading to capture significant leakage of the tee joint, which accompanied the physical fracture of joints. These damages were seen due to several factors such as fracture of coupling flanges, tearing away of pipe's groove, and bending of pipe ends (see Figure 2-5).



Figure 2-5 Observed Damage in Grooved Tee Joints (Tian et al., 2012)

Figure 2-6 shows examples of moment-rotation hysteresis responses of tee joints for different pipe diameters. The general trend of moment-rotation relationships highlights the importance of pinching behavior on these types of joints. Additionally, the plots illustrate that loading and unloading stiffness increases in larger rotations.

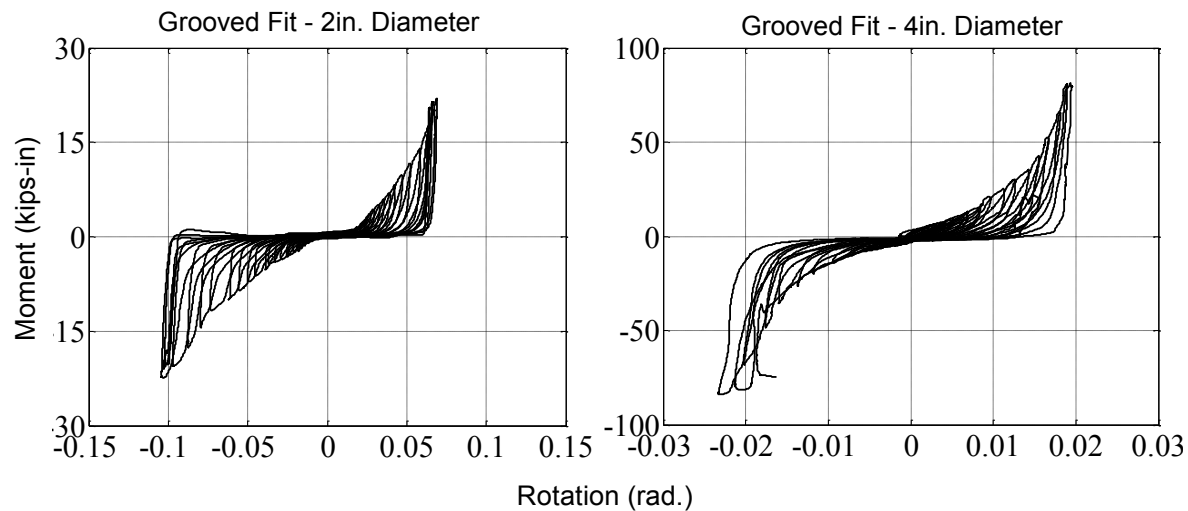


Figure 2-6 Moment-Rotation Hysteresis Response of Tee Joint Subassemblies with Different Diameters (Tian et al., 2012)

2.3 Development of an Analytical Model for Piping Tee Joints

In this report, the tee-joint experimental data was utilized by the authors to develop an adaptable nonlinear hinge model in OpenSees (2012) for tee joints of different pipe diameters.

2.3.1 Element and Material Mode

Uniaxial material models were used for modeling the behavior of pipe tee joints. Uniaxial materials in OpenSees represent stress-strain or force-displacement relationships in a single direction. A pinched load-deformation material that was implemented into OpenSees as “Pinching4” was used for modeling the tee-joint behavior in the model. The “Pinching4” material enabled the simulation of pinched load-deflection responses accounting for degradations under cyclic loading for different pipe diameters. This material requires the definition of 39 parameters (Figure 2-7), including the shape of the backbone curve, pinching parameters, damage parameters, etc. The key parameters of this material in Positive (P) and Negative (N) directions used in this study are: 1) points defining response envelope ($e(P-N)di$, $e(P-N)fi$); 2) ratio of reloading/maximum historic deformation ($rDisp(P-N)$); 3) ratio of reloading/maximum historic force ($rForce(P-N)$); 4) ratio of negative (positive) unloading/maximum (minimum) monotonic strength ($uForceP(N)$); and 5) ratios defining the unloading stiffness degradation (gK_i). A detailed description of these parameters can be found in OpenSees (2012).

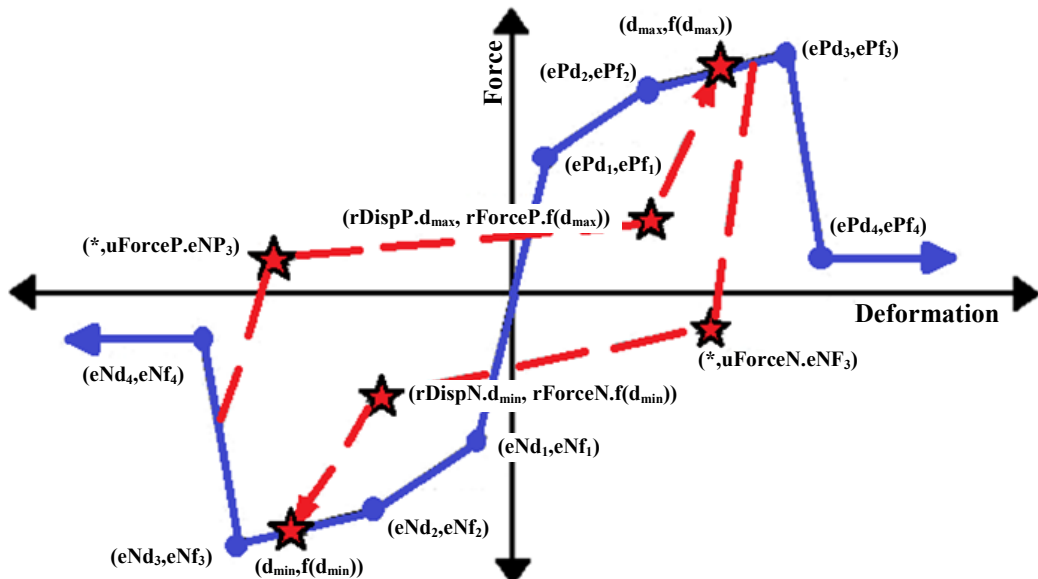


Figure 2-7 Pinching4 Material Properties (OpenSees, 2012)

The “Pinching4” uniaxial material, along with a “zeroLength” element, were used to simulate the moment-rotation response of a tee-joint pipe connecting two piping nodes. The “zeroLength” element is an element that is defined by two nodes at the same location.

2.3.2 Analytical Models of Threaded Joints

In this subsection, first the calibration process of “Pinching4” material is performed based on all available component data that was part of the University at Buffalo test matrix. Next, a generic model is defined for each pipe section included in the test matrix. Finally, a model is proposed for the missing pipe diameters.

2.3.2.1 Calibration of Analytical Model for All Tested Joints

The material model was calibrated using the tee joint moment-rotation hysteresis of all pipe diameters. For each component, the moment-rotation hysteresis curve, the value of cumulative dissipated energy, and moment histories were used in the calibration process in the visual basis. Moreover, the parameters were calibrated in the way that maximum cumulative dissipated energy of each component which, obtained from the analytical work, stays within 10% error of the results realized from the experiment. The support rotation history was imputed to the model

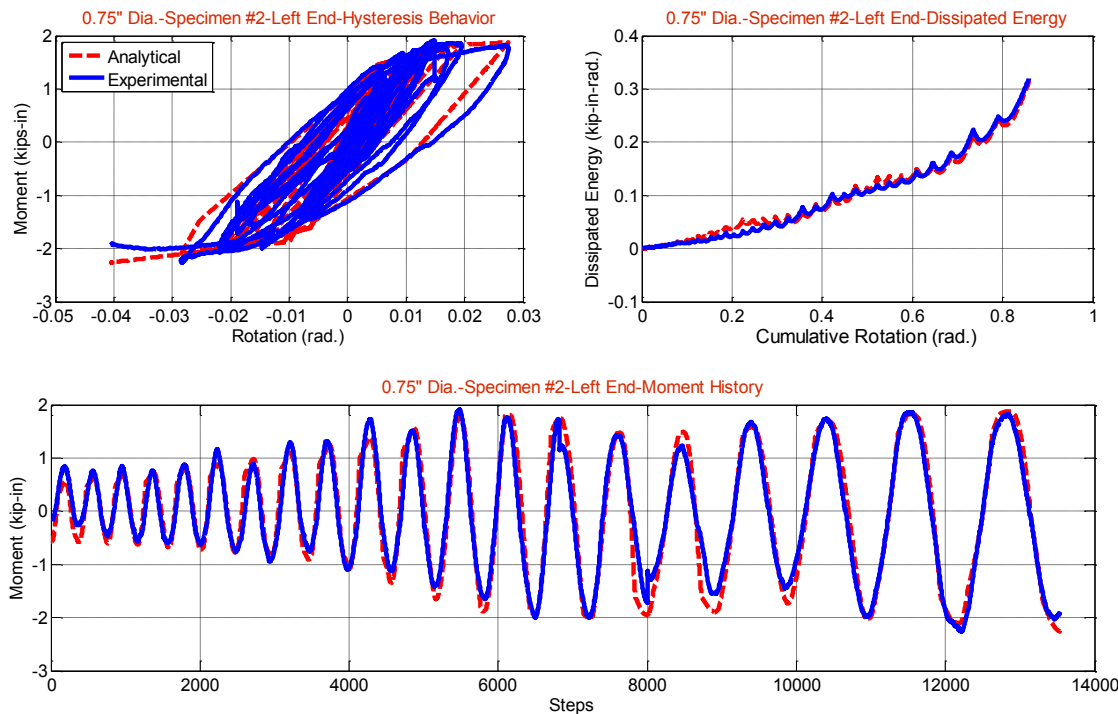


Figure 2-8 Analytical-Experimental Comparison of Second 3/4 in. Specimen on Left Side of Tee Joint

for each of the three varying diameter experiments. Due to the malfunction of some of the potentiometers, the moment-rotation data was not available on both sides of the tee joint for some of the experiments, but at least three moment-rotation data sets were available for each pipe diameter. Figure 2-8 shows the aforementioned three characteristics of the calibrated model for one of the 3/4-inch tee joints. After performing a sensitivity analysis on the material parameters (staying within 10% energy error), 10 out of 39 parameters were assigned a fixed value independent of the pipe diameter.

The OpenSees “Pinching4” material parameters $gK1$ to $gK4$, and $gKLim$ — all of which define the unloading stiffness degradation characteristic of the material — were set to the same value as gK (Mazzoni et al., 2007). The “cyclic damage” was used to determine cyclic stiffness and strength degradation, and in all the cases, the gD and gF material parameters were assumed to be zero. The rest of the parameters were used to fit the analytical data with the experimental data. Figure 2-9 to Figure 2-13 illustrate comparisons of analytical and experimental data for all five different pipe diameters. Table 2-1 presents the values of critical material parameters for different diameters. Each material parameter has a consistent relationship with the pipe diameter. This allows the determination of these parameters for other pipe diameters through interpolation.

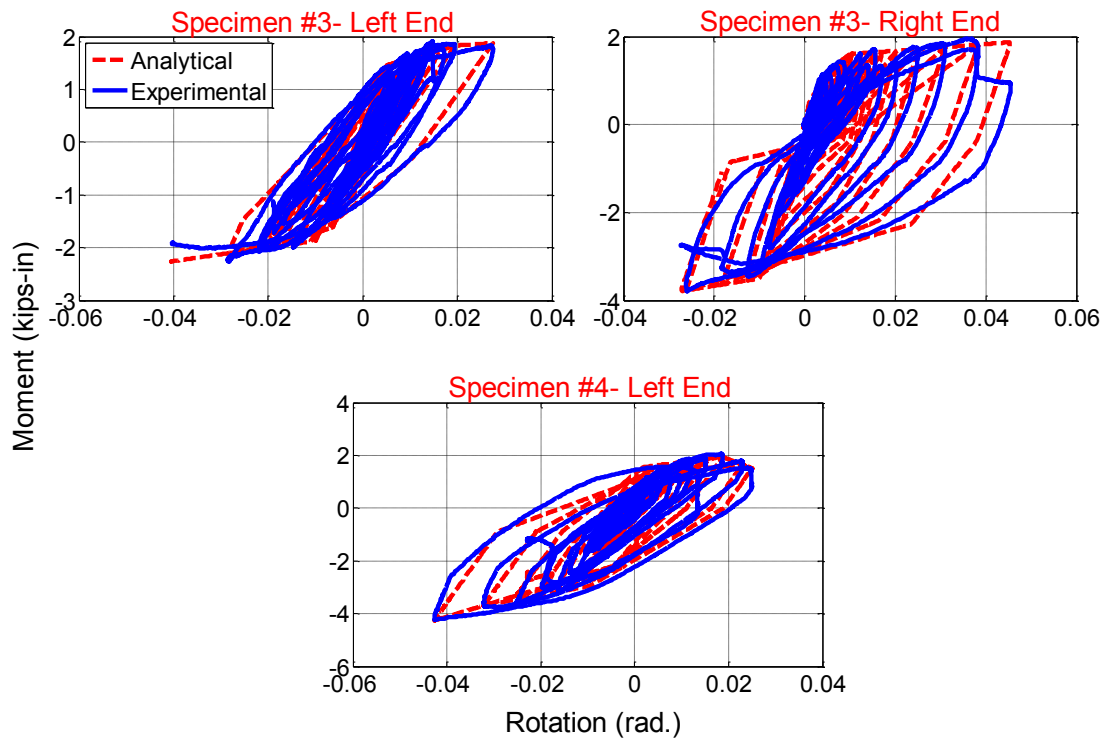


Figure 2-9 Analytical-Experimental Hysteresis Comparison of 3/4 in. Pipe Diameter

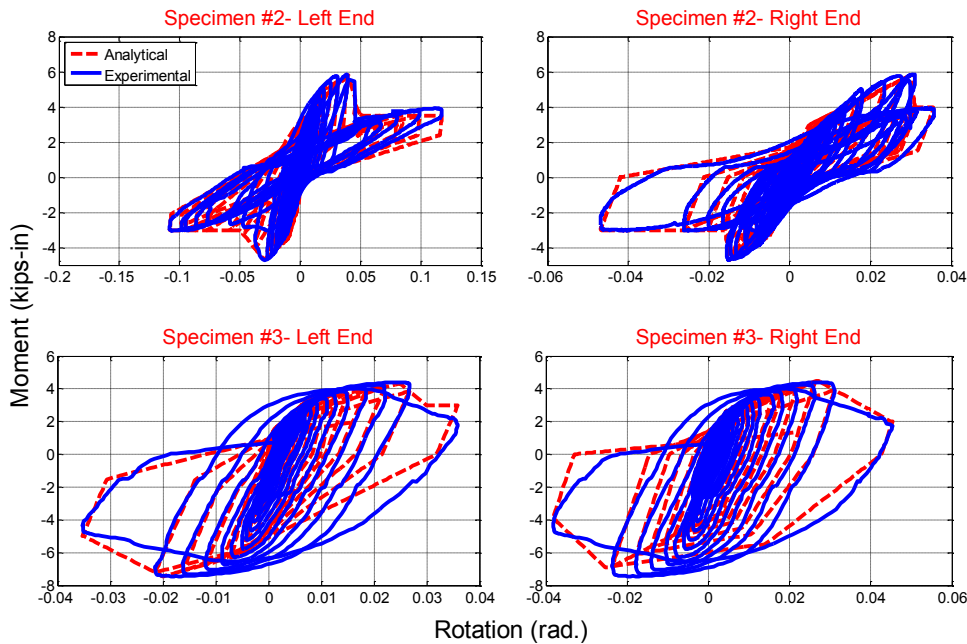


Figure 2-10 Analytical-Experimental Hysteresis Comparison of 1 in. Pipe Diameter

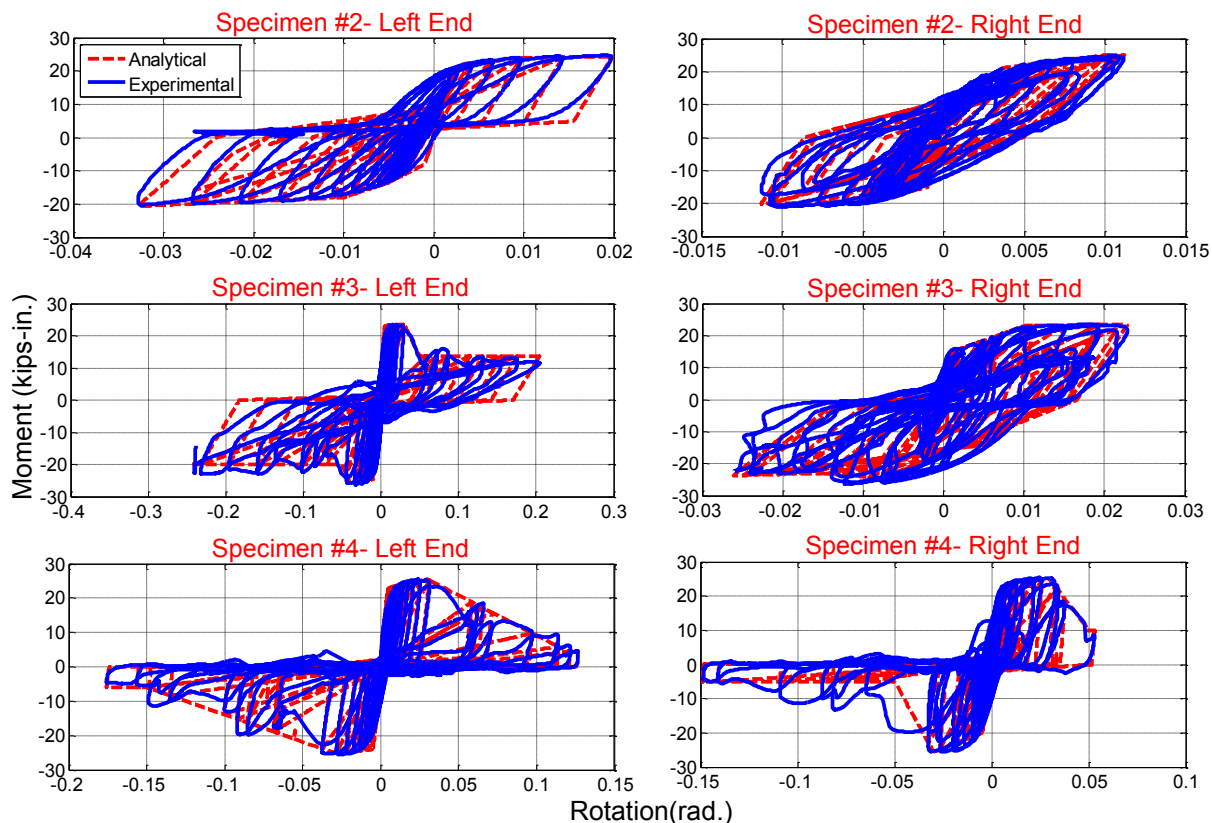


Figure 2-11 Analytical-Experimental Hysteresis Comparison of 2 in. Pipe Diameter

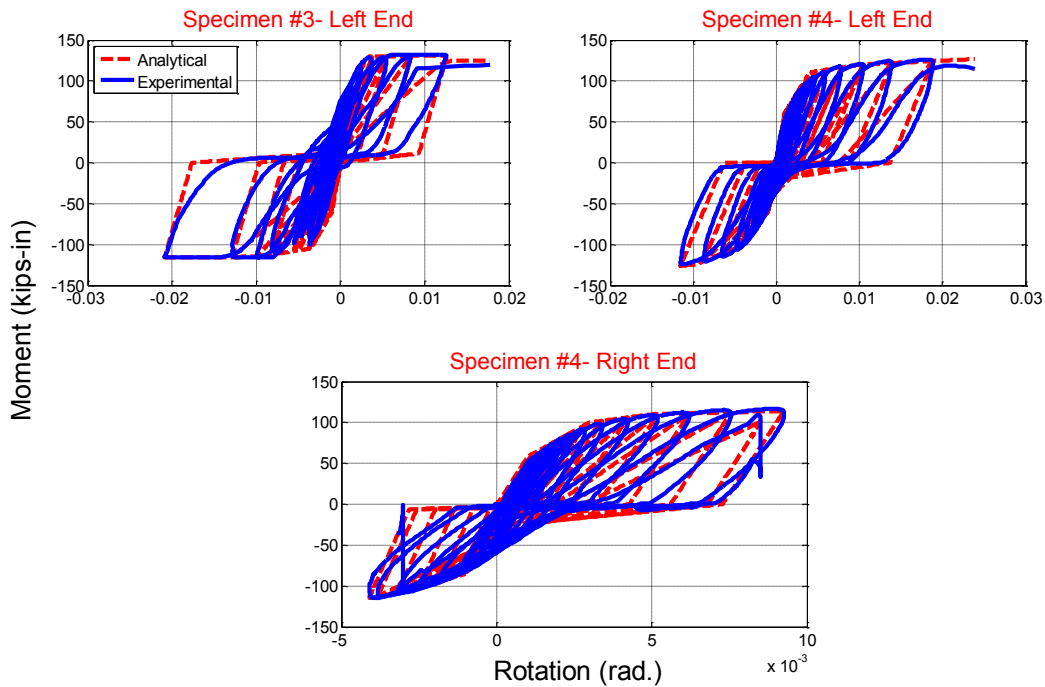


Figure 2-12 Analytical-Experimental Hysteresis Comparison of 4 in. Pipe Diameter

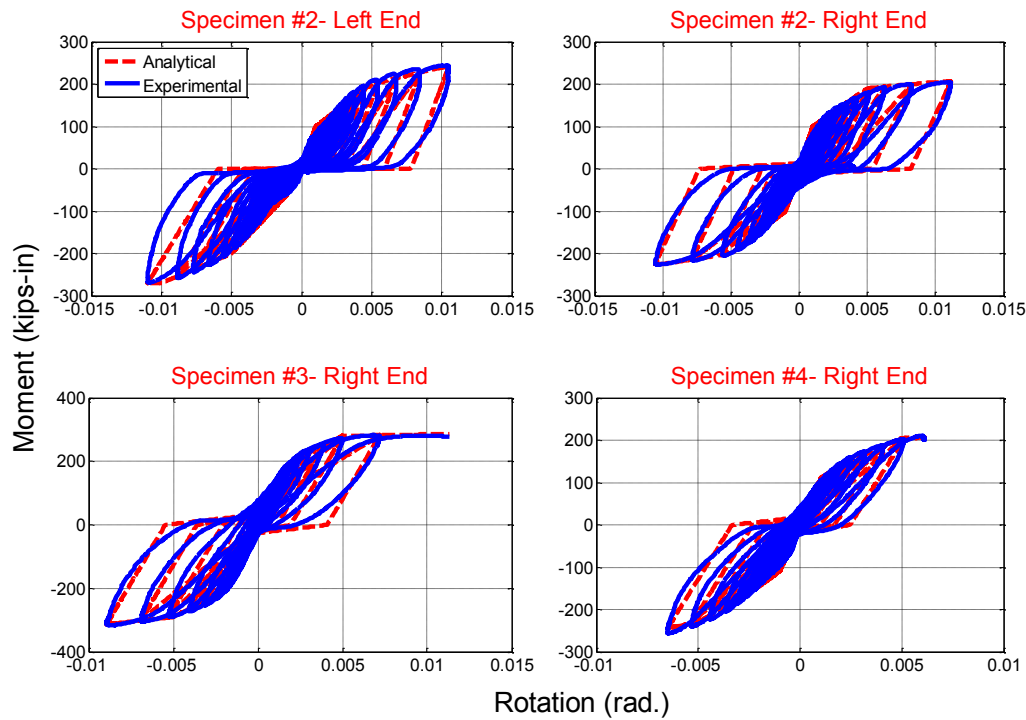


Figure 2-13 Analytical-Experimental Hysteresis Comparison of 6 in. Pipe Diameter

Table 2-1 Calibrated Pinching4 Parameter for Various Pipe Diameter

Component Name	ePf1 ePd1	ePf2 ePd2	ePf3 ePd3	ePf4 ePd4	eNf1 eNd1	eNf2 eNd2	eNf3 eNd3	eNf4 eNd4	rDispP rDispN	rForceP rForceN	uForceP uForceN	gK
3/4" Pipe Diameter												
Specimen #3 Left End	0.32 0.001	0.7 0.005	1.8 0.015	1.85 0.023	-0.5 -0.001	-0.95 -0.002	-1.87 -0.010	-2.1 -0.028	0.30 0.30	0.80 0.80	-0.80 0.15	0.60
Specimen #3 Right End	0.5 0.001	1.2 0.005	1.6 0.010	1.7 0.023	-0.5 -0.001	-1.5 -0.002	-3.5 -0.010	-3.8 -0.028	0.30 -0.90	-0.10 0.60	-0.50 0.10	0.40
Specimen #4 Left End	0.5 0.001	0.6 0.002	2 0.018	1.5 0.025	-0.5 -0.001	-1 -0.007	-2.5 -0.010	-4.22 -0.042	0.10 0.30	0.80 0.80	-0.60 0.0001	0.50
1" Pipe Diameter												
Specimen #2 Left End	1.5 0.001	5 0.020	5.8 0.040	3.5 0.050	-1.5 -0.001	-3.5 -0.010	-4.7 -0.030	-3 -0.050	-0.1 0.1	0.5 0.1	-0.6 -0.8	0.50
Specimen #2 Right End	1.5 0.001	3 0.005	5.8 0.030	4 0.030	-1.5 -0.001	-3.34 -0.005	-4.7 -0.015	-3 -0.016	0.2 0.01	0.5 0.2	0.0001 -0.5	0.60
Specimen #3 Left End	1.5 0.001	3.34 0.008	4.3 0.025	3 0.030	-1.5 -0.001	-6.1 -0.005	-7.45 -0.020	-5 -0.035	0.2 0.2	0.5 0.8	-0.5 0.0001	0.50
Specimen #3 Right End	1.5 0.001	2.8 0.005	4.5 0.027	2 0.045	-1.5 -0.001	-4.5 -0.005	-7 -0.025	-3 -0.042	0.2 -0.6	0.5 0.8	0.0001 0.0001	0.50
2" Pipe Diameter												
Specimen #2 Left End	15 0.001	22 0.003	24 0.010	24.3 0.023	-8 -0.001	-13.5 -0.005	-18 -0.010	-19.5 -0.023	0.1 0.1	0.4 -0.1	0.01 -0.25	0.70
Specimen #2 Right End	8 0.001	21 0.004	25 0.010	26.3 0.023	-15 -0.001	-20 -0.005	-20 -0.010	-21 -0.023	-0.6 -0.5	0.1 0.1	0.0001 0.0001	0.50
Specimen #3 Left End	8 0.001	23 0.005	23.5 0.030	13.5 0.050	-8 -0.001	-24.5 -0.010	-26 -0.040	20 0.050	0.1 0.1	0.1 0.1	0.0001 0.0001	0.95
Specimen #3 Right End	15 0.001	18.3 0.005	23 0.010	23.5 0.023	-8 -0.001	-25 -0.005	-23 -0.015	23.5 0.023	0.1 -0.2	0.1 0.6	-0.1 0.0001	0.75
Specimen #4 Left End	8 0.001	23 0.005	25.5 0.030	4.5 0.120	-8 -0.001	-24 -0.005	-25 -0.030	-6 0.150	0.1 0.1	0.1 0.1	0.0001 0.0001	0.50
Specimen #4 Right End	8 0.001	23 0.006	25 0.030	10 0.050	-8 -0.001	-20 -0.005	-25.5 -0.030	-5 -0.050	-0.1 0.2	0.1 0.1	0.0001 0.0001	0.10
4" Pipe Diameter												
Specimen #3 Left End	60 0.001	130 0.003	131 0.013	125 0.013	-60 -0.001	-105 -0.004	-115 -0.010	-116 -0.020	0.4 -0.2	0.001 0.15	0.0001 0.0001	0.60
Specimen #4 Left End	60 0.001	110 0.004	120 0.010	125 0.020	-60 -0.001	-105 -0.005	-125 -0.010	-130 -0.020	0.01 0.01	0.1 0.001	0.0001 -0.1	0.40
Specimen #4 Right End	58 0.001	100 0.003	110 0.005	125 0.020	-85 -0.001	-107 -0.003	-120 -0.005	-130 -0.020	0.3 -0.3	0.001 0.2	-0.5 0.0001	0.01
6" Pipe Diameter												
Specimen #2 Left End	100 0.001	200 0.005	240 0.010	250 0.023	-60 -0.001	-200 -0.005	-270 -0.010	-280 -0.023	0.4 0.1	0.001 0.001	0.0001 0.0001	0.10
Specimen #2 Right End	100 0.001	190 0.005	205 0.010	210 0.023	-100 -0.001	-200 -0.005	-225 -0.010	-230 -0.023	0.4 -0.1	0.1 0.05	0.0001 0.0001	0.30
Specimen #3 Right End	130 0.001	200 0.002	285 0.010	285 0.023	-130 -0.001	-210 -0.002	-320 -0.010	-320 -0.023	-0.1 0.1	0.1 0.1	0.0001 0.0001	0.30
Specimen #4 Right End	110 0.001	140 0.002	210 0.010	210 0.023	-110 -0.001	-145 -0.002	280 -0.010	-280 -0.023	0.1 0.1	0.1 0.1	0.0001 0.0001	0.30

2.3.2.2 Developing Generic Model for Tested Tee Joints

Throughout the calibration process, a total of 20 sets of 29 parameters for the “Pinching4” material were optimized based on all available experimental data. Although the results for each set of experiments were quite similar, there were minor discrepancies between the material

parameters for the individual experiments of each set. Therefore, for the simplicity of future analytical studies of sprinkler piping systems (not only limited to this study), one suite of material parameters was defined as the generic (representative) parameters for each pipe diameter, called “generic model” hereafter. To develop this generic model, the following assumptions were made followed by the example procedure that has been carried out for 6-inch pipe diameter. 1) A symmetric moment-rotation hysteresis behavior was used. 2) The first point of the backbone curve, ePd_1 (Figure 2-7), was defined as 0.001 rad. Table 2-2 shows positive numbers that correspond to negative and positive sides of the backbone curve, which was calibrated for each specimen. The red columns show that the first point of the backbone curves was always calculated based on 0.001 rad. This allowed the use of the average experimental moment values corresponding to 0.001 rad.. 3) The rest of the three nonlinear rotation points of the backbone curve of the generic model, ePd_2 , ePd_3 , ePd_4 (Figure 2-7), were set to 0.005, 0.01, and 0.023 rad., respectively, based on the calibrated backbone curve parameters of each set. 4) A linear interpolation was used to find the moment corresponding to the above mentioned rotations where the moment values at the calibrated backbone curves are unavailable. The blue cells in Table 2-2 depict the values calculated based on interpolation. The average of these moment values for each set were used for ePf_2 , ePf_3 , and ePf_4 (Figure 2-7) to define the backbone curve (Figure 2-14). 5) The average calibrated values were used for the rest of the parameters needed to define the generic hysteresis response. Figure 2-14 shows the average backbone curve versus all the calibrated backbone curves for a 6-in. pipe diameter.

Table 2-2 Backbone Parameters Calibrated for 6" Pipe Diameter

Component Name	6 in. Pipe Diameter									
	$e(P-N)f1$	$e(P-N)f2$	$e(P-N)f3$	$e(P-N)f4$	$e(P-N)f5$	$e(P-N)d1$	$e(P-N)d2$	$e(P-N)d3$	$e(P-N)d4$	$e(P-N)d4$
Specimen #2 Left-Positive	100	125	200	240	250	0.001	0.002	0.005	0.01	0.023
Specimen #2 Left-Negative	60	95	200	270	280	0.001	0.002	0.005	0.01	0.023
Specimen #2 Right-Positive	100	122.5	190	205	210	0.001	0.002	0.005	0.01	0.023
Specimen #2 Right-Negative	100	125	200	225	230	0.001	0.002	0.005	0.01	0.023
Specimen #3 Right-Positive	130	200	280	285	285	0.001	0.002	0.005	0.01	0.023
Specimen #3 Right-Negative	130	210	290	320	320	0.001	0.002	0.005	0.01	0.023
Specimen #4 Right-Positive	110	140	205	210	210	0.001	0.002	0.005	0.01	0.023
Specimen #4 Right-Negative	110	145	230	280	280	0.001	0.002	0.005	0.01	0.023

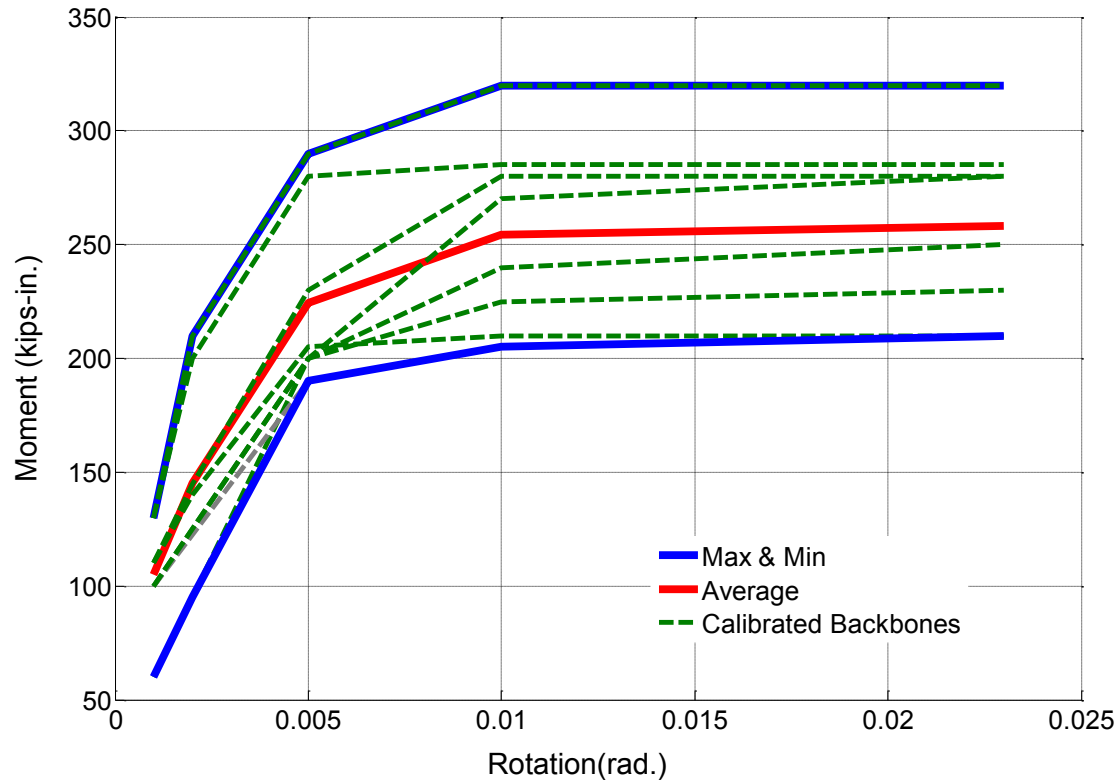


Figure 2-14 Average and Calibrated Backbone Curve for 6 in. Pipe Diameter

Note that the inconsistency between the experimental results of three sets for each pipe diameter is much larger in the smaller pipe diameter. Therefore, larger error in the hysteresis behavior between the generic model and each of the three experimental sets is the nature of this generic model. This error can be seen by comparing the generic analytical model and sample experimental result comparisons of 1-inch and 6-inch pipe diameter (see Figure 2-15). Table 2-3 shows the generic model parameters obtained using the previously mentioned assumptions. Figure 2-15 shows the comparison of the generic model with sample experimental data from each set.

Table 2-3 Generic “Pinching4” Calculated Parameters-Tested

Pipe Name	e(P-N)f1	e(P-N)f2	e(P-N)f3	e(P-N)f4	rDisp(P-N)	rForce(P-N)	uForce(P-N)	gK(P-N)
TEST SETS								
3/4"	0.47	1.19	2.00	2.36	0.07	0.62	-0.27	0.50
1"	1.50	3.37	4.07	5.08	0.03	0.49	-0.30	0.53
2"	9.75	20.18	22.81	23.43	-0.04	0.15	-0.03	0.58
4"	63.83	114.03	121.51	125.17	0.04	0.08	-0.10	0.34
6"	105.00	224.38	254.38	258.13	0.13	0.07	0.00	0.25

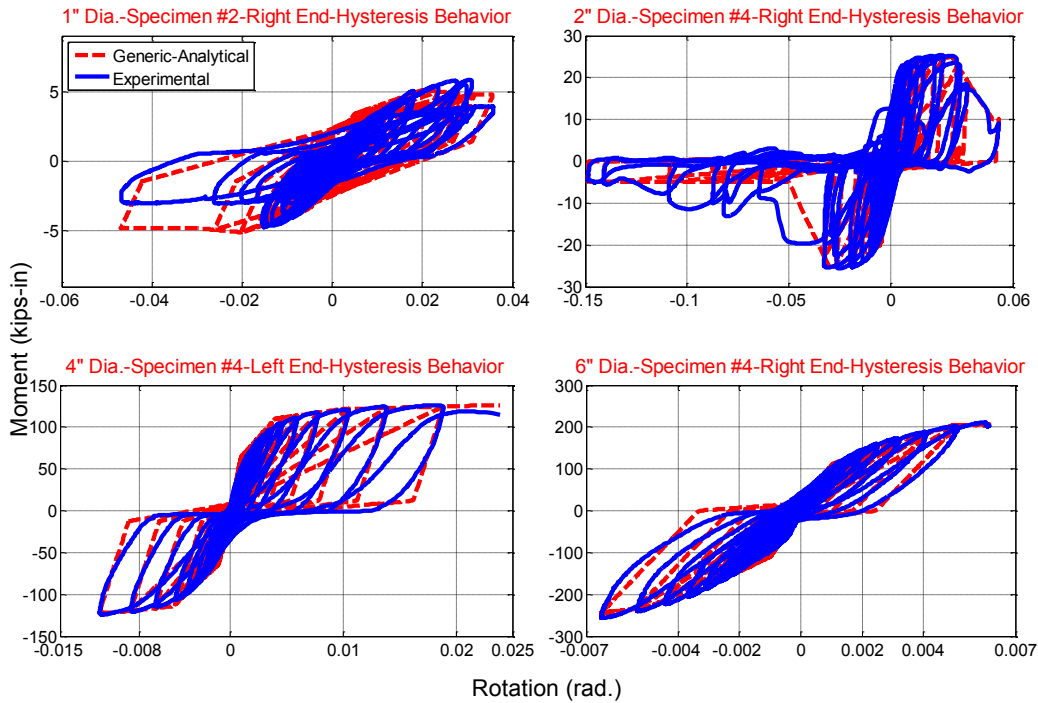


Figure 2-15 Sample Generic Analytical-Experimental Hysteresis Comparison of Different Pipe Diameters

2.3.2.3 Proposed Generic Model for Not-Tested Tee Joint Components

Based on pipe location and required water pressure, a wide range of pipe diameters is commonly used in sprinkler piping layouts. The test matrix of the University at Buffalo did not include all pipe diameters that are typically found in a system. Thus, a procedure is proposed to fill this gap in the experimental data and enable estimation of the parameters of the generic hysteresis model for the missing pipe diameters. This methodology is explained in the following steps. First, the parameters of the generic models based on the experimental data (average of minimum of three moment values obtained from the database of component tests) were plotted against the pipe diameter (red squares in Figure 2-16). The values of the moments corresponding to 0.001, 0.005, 0.01, and 0.023 rad. can be plotted against the pipe diameter, considering these rotations were kept constant for all diameters. Then, the best polynomial curve was fit to the data for each parameter. Using these algebraic functions of pipe diameter, the modeling parameters were obtained for those pipe diameters that were not tested at the University at Buffalo. Also, for each proposed pipe diameter, the linear interpolation between the two closest pipe diameters (which were obtained from the experiment) was performed for the parameters — except those that defined the backbone curves. Table 2-4 shows the values of the modeling parameters obtained

from this methodology for the missing pipe diameters. Figure 2-16 shows the trends of the modeling parameters for the “Pinching4” material (OpenSees, 2012) with respect to the pipe diameter. Figure 2-17 shows some of the proposed hysteresis plots for all pipe diameters up to 0.025 radian.

Table 2-4 Generic “Pinching4” Calculated Parameters-Proposed

Pipe Name	e(P-N)f1	e(P-N)f2	e(P-N)f3	e(P-N)f4	rDisp(P-N)	rForce(P-N)	uForce(P-N)	gK(P-N)
PROPOSED COMPONENTS								
1.25"	1.04	8.24	8.83	9.66	0.009	0.40	-0.23	0.54
1.5"	2.96	14.30	14.70	15.78	-0.008	0.32	-0.16	0.55
2.5"	20.91	44.54	46.10	48.07	-0.022	0.13	-0.05	0.52
3"	34.15	63.27	66.55	68.91	-0.003	0.11	-0.06	0.46
3.5"	48.78	84.41	90.17	92.88	0.017	0.09	-0.08	0.40
5"	90.24	162.29	180.03	183.59	0.081	0.07	-0.05	0.29

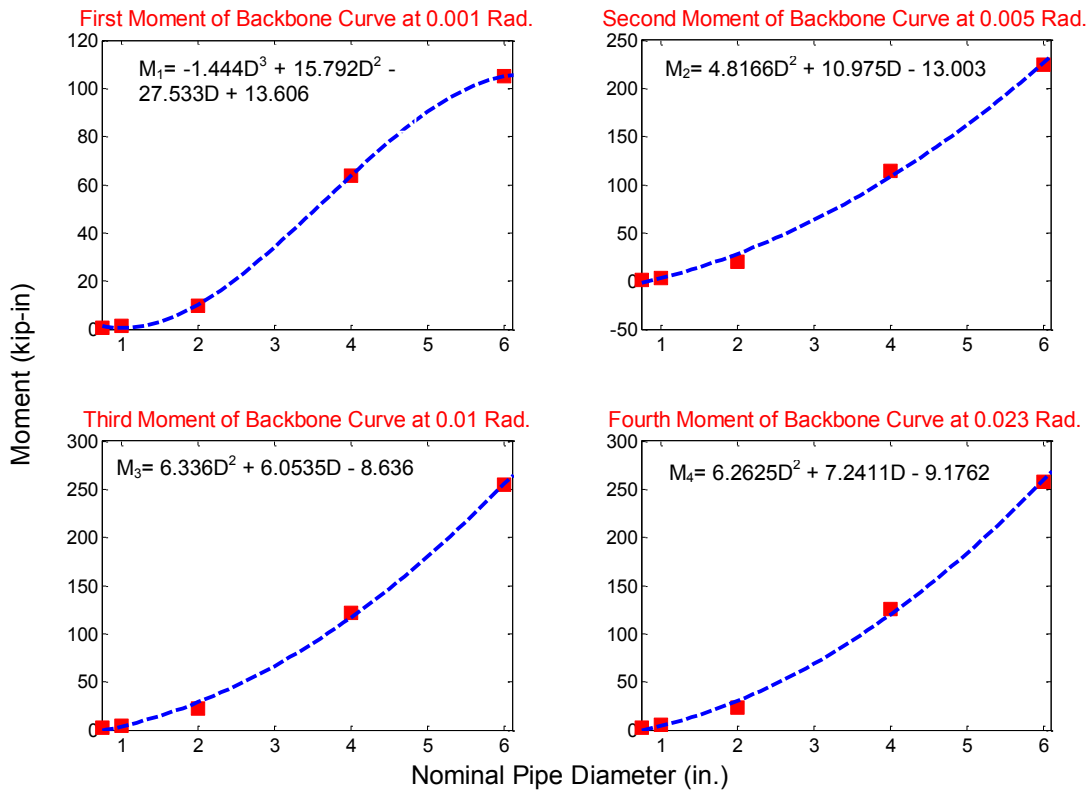


Figure 2-16 Fitted Curves on Backbone Curve Parameters of the Generic Model

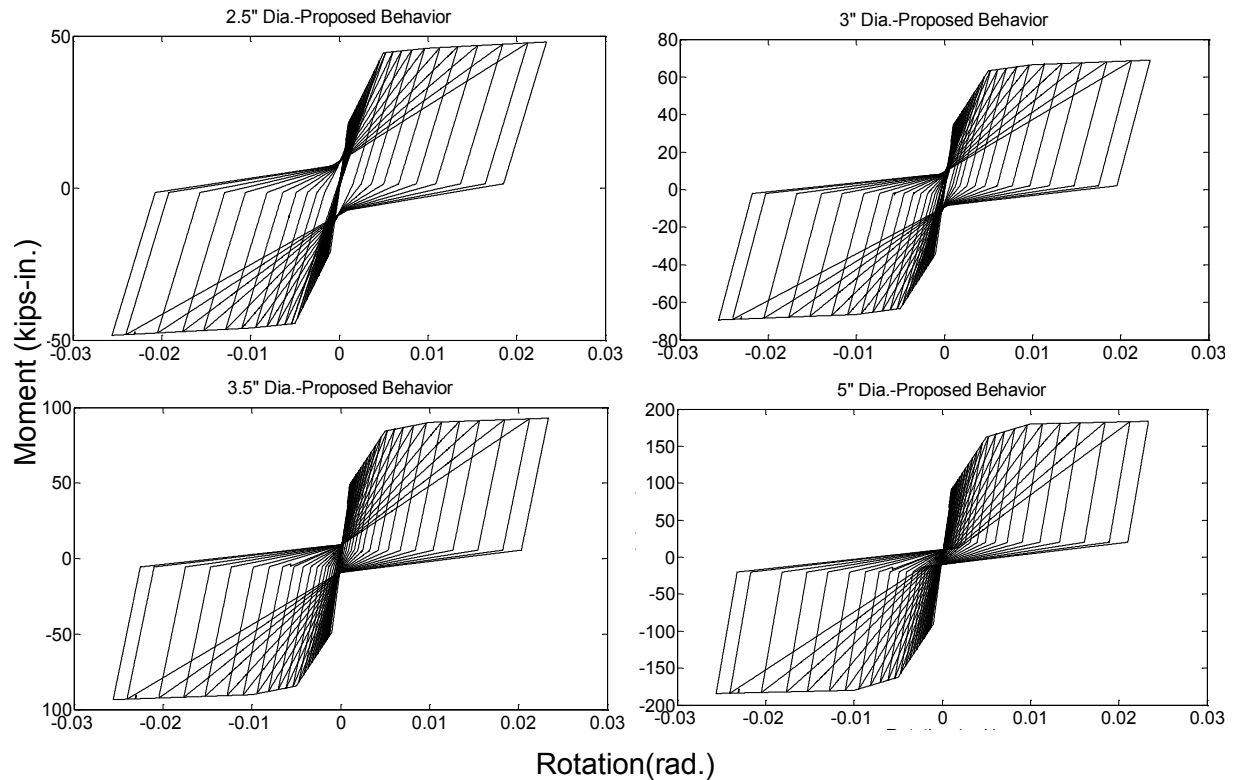


Figure 2-17 Proposed Hysteresis Behavior of Different Pipe Diameters

2.3.3 Analytical Models of Grooved Joints

Similar to the process performed for threaded joints, first the calibration process of “Pinching4” material is performed based on all available component data that was part of the University at Buffalo test matrix. Next, a generic model was defined for each pipe section that was included in the test matrix. Finally, a model is proposed for the missing pipe diameters.

2.3.3.1 Calibration of Analytical Model for All Tested Joints

The “Pinching4” material model was calibrated using the tee joint moment-rotation hysteresis of the two pipe diameters of 2-inch and 4-inch. For each component (similar to threaded joints), the moment-rotation hysteresis curve, the value of cumulative dissipated energy, and moment histories were used in the calibration process in the visual basis. Moreover, the parameters were calibrated in the way that the maximum cumulative dissipated energy of each component, which obtained from the analytical work, stays within 20% error of the results realized from the experiment. The support rotation history was applied to the model for each of the three varying diameter experiments. Due to the malfunction of some of the potentiometers, the moment-rotation data were not available on both sides of the tee joint for some of the experiments, but at

least three moment-rotation data sets were available for each pipe diameter. Figure 2-18 shows the aforementioned three characteristics used in the calibration of the model for one of the 2-inch tee joints. The shape of the curve, dissipated energy, and the moments were considered simultaneously in the calibration process to achieve the best analytical model.

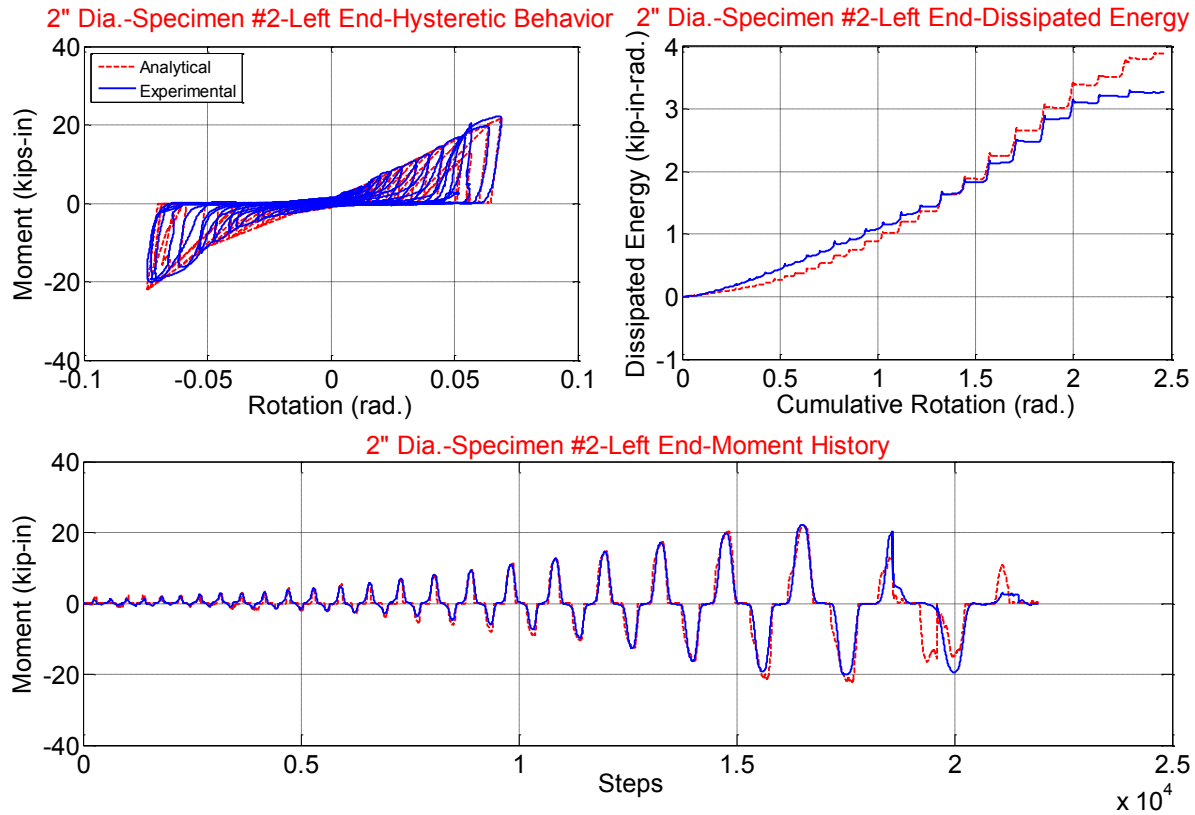


Figure 2-18 Analytical-Experimental Comparison of Second 2 in. Grooved Fit Specimen on Left Side of Tee Joint

Table 2-5 Fixed “Pinching4” Parameters of Grooved Fit Hinge Model

Parameters								
rDispP rDispN	rForceP rForceN	uForceP uForceN	gK1 gK2	gK3 gK4	gKLimit	gD gF	gE dam	
0.6	0.0001	-0.01	0.5	0.75	1	0	1	
0.6	0.0001	-0.01	0.5	0		0	cycle	

After performing a sensitivity analysis on the material parameters (staying within 20% energy error), 23 out of 39 parameters were assigned a fixed value independent of the pipe diameter. Table 2-5 shows the values that were used for the fixed parameters of the grooved fit hinge model. Table 2-6 presents the values of backbone material parameters for two different pipe

diameters of 2-inch and 4-inch. Figure 2-19 and Figure 2-20 compare analytical and experimental data for these pipe diameters.

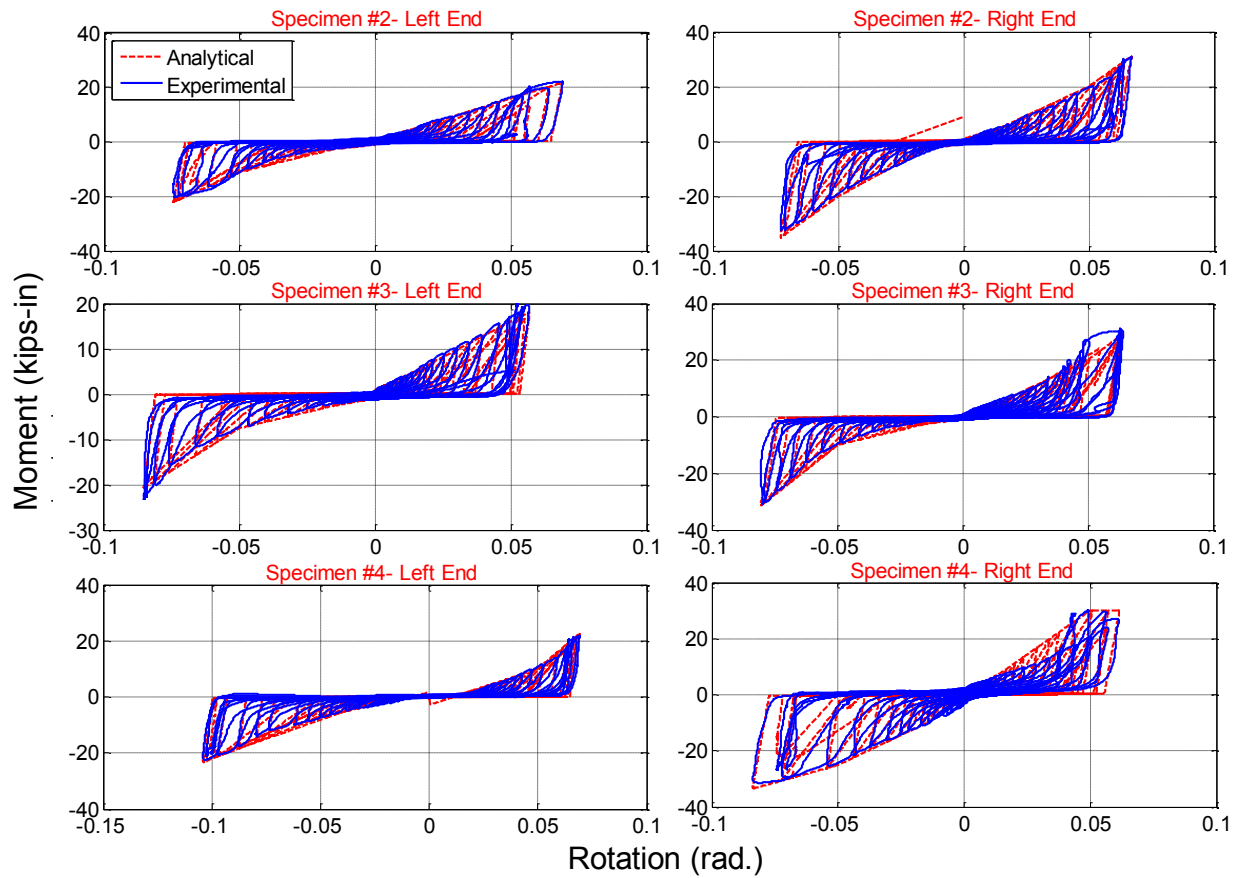


Figure 2-19 Analytical-Experimental Hysteresis Comparison of 2 in. Pipe Diameter

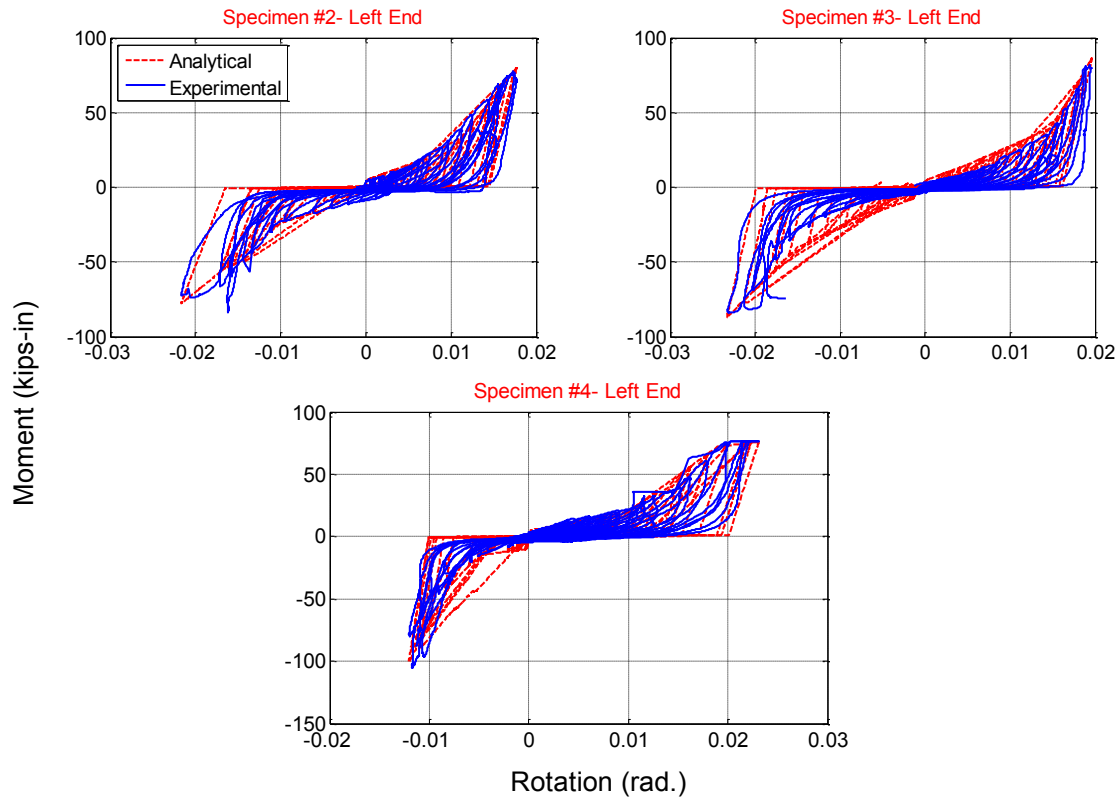


Figure 2-20 Analytical-Experimental Hysteresis Comparison of 2 in. Pipe Diameter

Table 2-6 Calibrated “Pinching4” Parameter for Various Pipe Diameter

Component Name	ePf1 ePd1	ePf2 ePd2	ePf3 ePd3	ePf4 ePd4	eNf1 eNd1	eNf2 eNd2	eNf3 eNd3	eNf4 eNd4
2" Pipe Diameter								
Specimen #2 Left End	1 0.0002	5 0.015	16 0.050	22 0.070	-1 -0.0002	-2.5 -0.015	-11 -0.050	-20 -0.070
Specimen #2 Right End	1 0.0002	5 0.015	20 0.050	33 0.070	-1 -0.0002	-2.5 -0.015	-20 -0.050	-33 -0.070
Specimen #3 Left End	1 0.0002	5 0.015	16 0.050	22 0.070	-1 -0.0002	-2.5 -0.015	-7.5 -0.050	-15 -0.070
Specimen #3 Right End	1 0.0002	5 0.015	20 0.050	33 0.070	-1 -0.0002	-2.5 -0.015	-10 -0.050	-24 -0.070
Specimen #4 Left End	1 0.0002	1 0.015	10 0.050	23 0.070	-1 -0.0002	-1 -0.015	-7 -0.050	-13 -0.070
Specimen #4 Right End	1 0.0002	8 0.015	30 0.050	30 0.070	-1 -0.0002	-10 -0.015	-25 -0.050	-30 -0.070
4" Pipe Diameter								
Specimen #2 Left End	5 0.0002	15 0.005	24 0.010	75 0.017	-3 -0.0002	-15 -0.005	-24 -0.010	-70 -0.020
Specimen #3 Left End	5 0.0002	15 0.005	40 0.015	80 0.019	-5 -0.0002	-15 -0.010	-40 -0.019	-85 -0.022
Specimen #4 Left End	5 0.0002	20 0.010	72 0.019	75 0.022	-10 -0.0002	-15 -0.005	-40 -0.008	-100 -0.012

2.3.3.2 Development of a Generic Model for Tested Tee Joints

Throughout the calibration, a total of nine sets of 16 parameters for the “Pinching4” material were optimized based on all available experimental data. Although the results for each set of experiments were quite similar, there were minor discrepancies between the material parameters for the individual experiments of each set. Therefore, for simplicity in future analytical studies of sprinkler piping systems (not only limited to this study), one suite of material parameters was defined as the generic (representative) parameters for each pipe diameter, called “generic model” hereafter. To develop this generic model, the following assumptions were made. 1) A symmetric moment-rotation hysteresis behavior was used. 2) The first point of the backbone curve, $ePd1$ (Figure 2-7), was defined as 0.0002 rad. This enabled the use of the average experimental moment values corresponding to this rotation. 3) The observed shape of the experimental grooved fit backbone curves follow a second order polynomial line, and therefore, the best second order polynomial fit was used as the backbone curve. 4) The rest of the

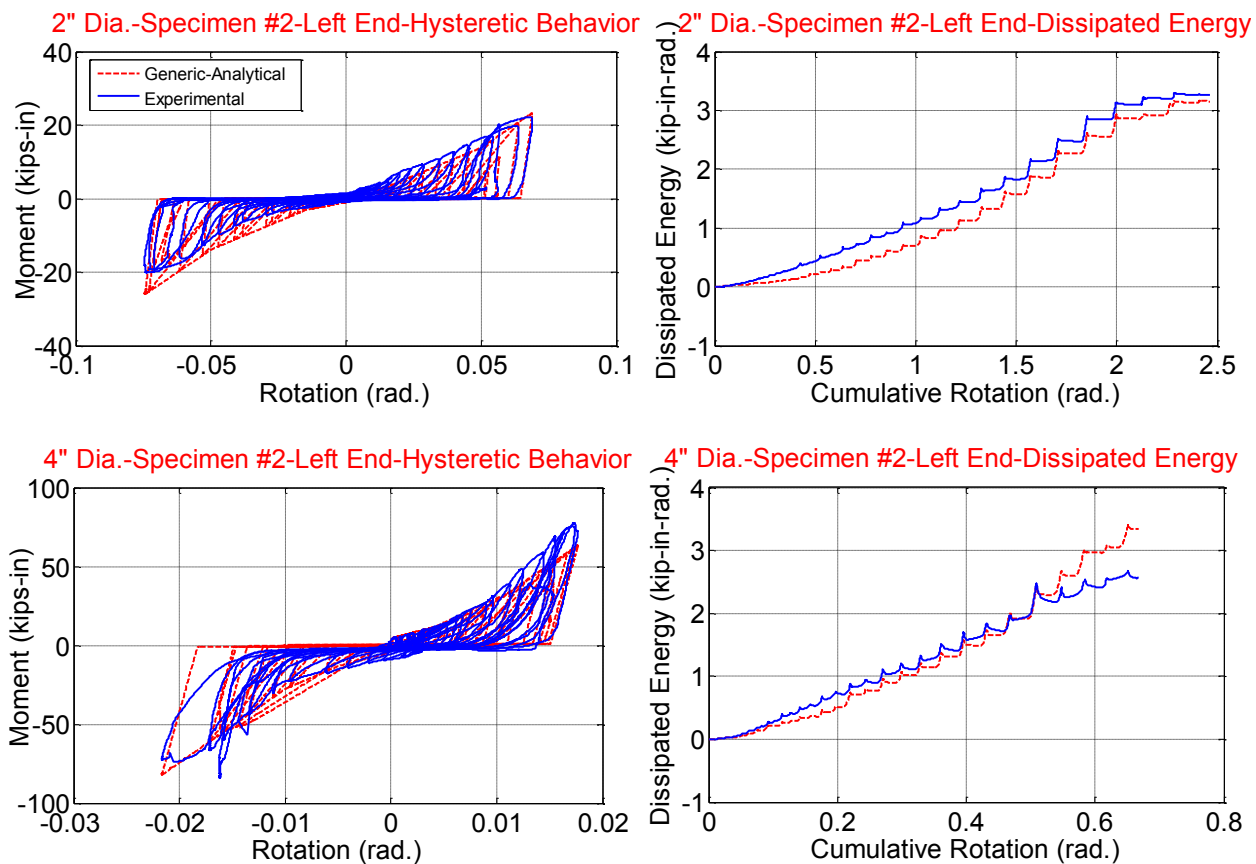


Figure 2-21 Sample Generic Analytical-Experimental Hysteresis Comparison of Different Grooved Pipe Diameters

three nonlinear rotation points of the backbone curve for the generic model, ePd2, ePd3, ePd4 (Figure 2-7), were set to the most frequent rotations that have been used throughout the calibration for each pipe diameter. 5) The second-order polynomial backbone curve was used to find the moment corresponding to rotations 0.0002 rad., ePd2, ePd3, ePd4. 6) The remainder of parameters (fixed parameters) were the same as values that are presented in Table 2-5. Figure 2-21 shows a comparison of the generic model with sample experimental data from each set. Table 2-6 also shows the generic model parameters obtained using these assumptions. The second order polynomial fitted curves are shown in Figure 2-22.

2.3.3.3 Proposed Generic Model for Not-Tested Tee Joint Components

Based on the pipe location in the system and the required water pressure, a wide range of pipe diameters is commonly used in sprinkler piping layouts. The test matrix of the University at Buffalo did not include all pipe diameters that are typically found in a system. Thus, a procedure is proposed to fill the gaps in the experimental data and enable estimation of the parameters of the generic hysteresis model for the missing pipe diameters. This methodology is explained in the following steps. First, a leakage line was defined as the line that linearly passed through the two leakage points calculated for 2-inch and 4-inch pipe diameters — obtained from Tian et al. (2012) — which is referenced in following tables. Second, a linear interpolation was made between each coefficient of experimentally (2-inch and 4-inch pipe diameter) second order fitted curves versus different pipe diameters. Third, the minimum point of the backbone curve was calculated at a rotation of 0.0002 rad., and the maximum point (leakage point) was determined from the intersection of the leakage line (see Figure 2-22) and polynomial fitted curves corresponding to each pipe diameter. Finally, the other two backbone curves were calculated from the rotations that correspond to 1/3 and 2/3 of the maximum rotation of each pipe diameter. Since the primary use of grooved fit connections is in risers and main runs, this procedure was only implemented for 2-inch and larger pipe diameters. Table 2-7 shows the values of the modeling parameters obtained from this methodology for the missing pipe diameters. Figure 2-23 shows a sample of the generic grooved fit hysteresis curves proposed for 2.5-inch and 5-inch pipe diameter.

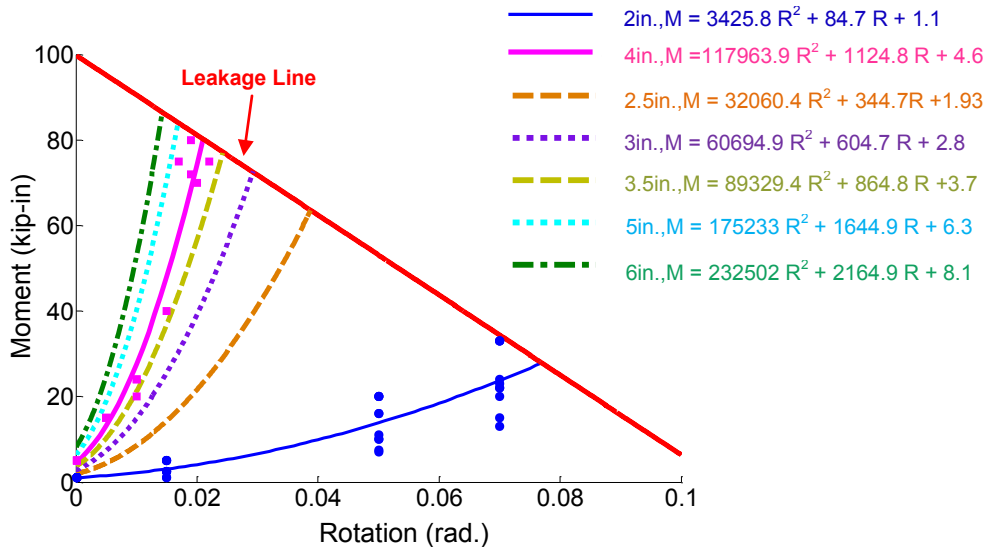


Figure 2-22 Fitted-Developed Backbone Curves of the Generic Model (Includes Moment-Rotation Equations)

Table 2-7 Generic “Pinching4” Calculated Parameters for Grooved Fit Hinges

Pipe Name	e(P-N)d1	e(P-N)d2	e(P-N)d3	e(P-N)d4	e(P-N)f1	e(P-N)f2	e(P-N)f3	e(P-N)f4
TEST SETS								
2"	1.07	3.09	13.84	23.76	0.0002	0.015	0.05	0.07
4"	4.8	13.15	27.62	74.25	0.0002	0.005	0.01	0.02
PROPOSED COMPONENTS								
2.5"	1.93	11.59	32.16	63.57	0.0002	0.013	0.026	0.038
3"	2.81	14.39	37.68	72.63	0.0002	0.010	0.019	0.029
3.5"	3.69	16.33	40.77	76.93	0.0002	0.008	0.016	0.024
5"	6.34	20.68	46.74	84.18	0.0002	0.006	0.011	0.017
6"	8.10	23.41	49.65	86.60	0.0002	0.005	0.010	0.014

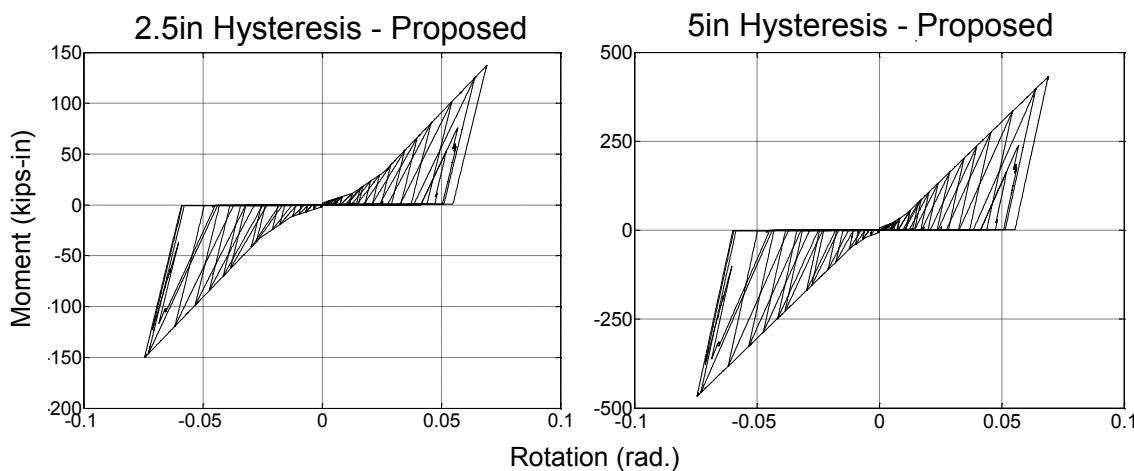


Figure 2-23 Sample of Generic Hysteresis Curves Proposed for 2.5 in. and 5 in. Pipe Diameter

2.4 Concluding Remarks

In this section, a series of nonlinear threaded and grooved joint hinges were developed for various pipe diameters based on a previous component experiment. The OpenSees program (2012) was used for modeling, analysis, comparison, and calibration of test data. The analytical model was composed of a “Pinching4” uniaxial material along with a “zeroLength” element in the rotational degree of the tee joint. Afterwards, for simplicity in future analytical studies of sprinkler piping systems (not only limited to this study), one suite of material parameters was defined as the generic (representative) parameters for each pipe diameter, called a generic model. Furthermore, as the test matrix did not include all of the pipe diameters that are typically found in a system, a procedure was proposed to fill this gap in the experimental data and enable estimation of the parameters of the generic hysteresis model for the missing pipe diameters.

SECTION 3

ANALYTICAL MODELS OF PIPING COMPONENTS

3.1 Introduction

In recent years due to improvements in technology, nonlinear response history analysis (nRHA) has become increasingly popular. This type of analysis is being used in a large number of studies to examine the performance of a wide range of systems under a variety of input motions. Undoubtedly, nRHA is the most comprehensive analytical method used to establish realistic seismic demands on systems. However, the appropriate accuracy for this type of analysis requires complex, detailed, and realistic descriptions of system parameters. Appropriate and accurate analytical definitions and representations of various sources of nonlinearities associated with materials, components, and their interactions and geometric nonlinearities are key tasks in modeling studies. This fact is mainly due to the high sensitivity of analysis results to small variations in the parameters that characterize and define such nonlinearities.

Despite the wide use of nRHA in structural and infrastructural systems, the amount of research that has been conducted on nonstructural systems is extremely limited. This is primarily because of a lack of knowledge and complexity of nonstructural systems. In order to develop a reliable analytical tool for performing nRHA, a comprehensive and methodological component-level study must also be carried out. Therefore, models used for this type of investigation should be calibrated against available experimental data from both component- and system-level experiments.

This section introduces a set of unified procedures to develop analytical models for piping components. The validity and accuracy of the techniques, procedures, and tools are verified through a series of component-level experiments. The OpenSees program (2012) was used for modeling, analysis, comparison, and calibration of test data. In this section, each piping component is defined and described in detail, modeling techniques are presented, and at the conclusion, the validation of the model is performed with available experimental data.

3.2 Pipe Hangers

Pipe hangers are one of the main components used to carry the dead load of piping systems. These elements are usually suspended from the structure and intended to carry the piping load in

tension. The main parts of pipe hangers are hanger rods, deck fasteners, hanger clips, and surge clips (see Figure 3-1).

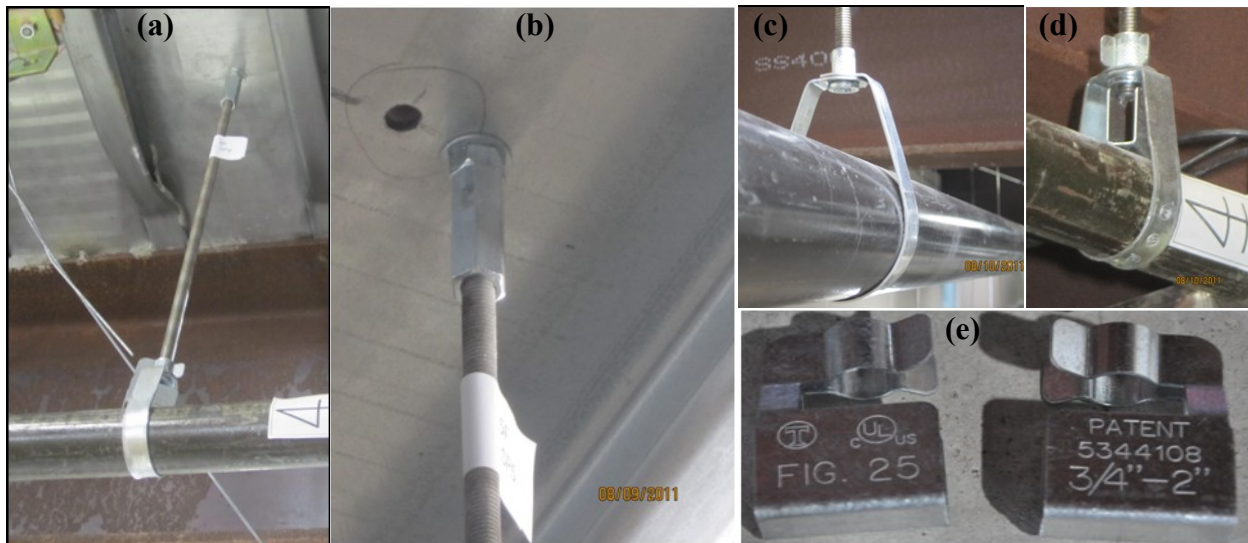


Figure 3-1 (a) Pipe hanger and (b) Deck Fastener (c) Hanger Clip (d) Hanger Clip and Surge Clip (e) Surge Clips

3.2.1 Code Requirements

The pipe hangers shall follow several requirements specified by NFPA 13 (2011). Some of these requirements can be summarized as:

- Hangers shall be ferrous.
- Hangers shall carry five times the weight of the water-filled pipe plus 250 pounds at each point of piping support.
- Threaded rod with diameter of 3/8 inch is permitted for supporting up to and including 4-inch nominal pipe diameters, while 1/2 inch shall be used for larger pipes (less than 10 inches).

3.2.2 Pipe Hanger Tests at the University of Nevada, Reno

Researchers at the University of Nevada, Reno performed three tensile tests on 5/8-inch threaded rods of pipe hangers. The outcome of these tests can be found in Goodwin et al. (2005). Hereafter, the description and experimental observation of these experiments are provided for convenience.

The tensile test was performed by applying a unidirectional ramp of displacement at a low speed rate of 0.01 in/sec (Figure 3-2a). The rods were subjected to increasing tensile loading to observe the failure point. Figure 3-2b shows the force-displacement results of these tests.

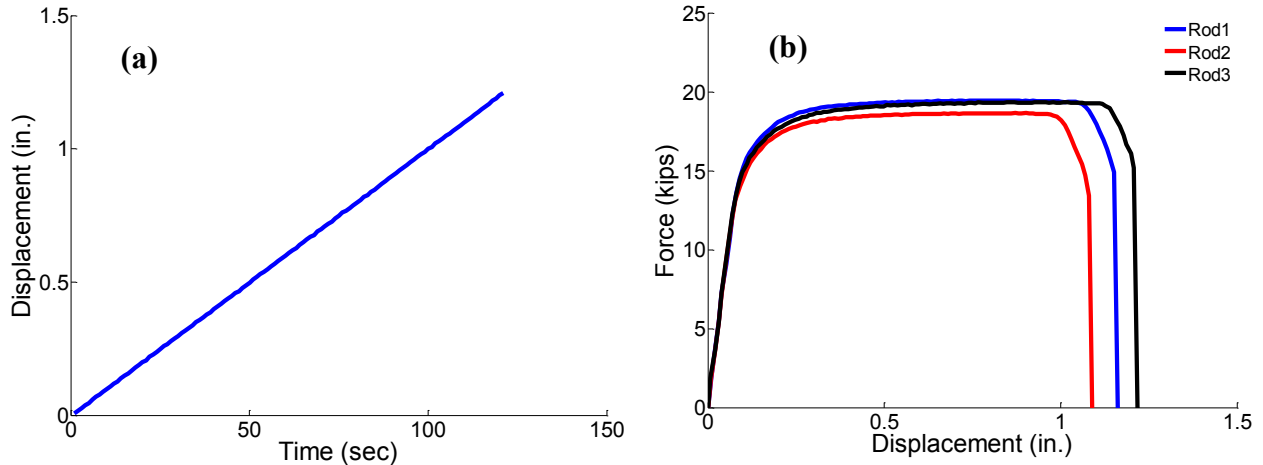


Figure 3-2 (a) Loading History of Rod Tensile Test (b) Rod Force/Displacement Curves (Goodwin et al., 2005)

The stresses and strains of the tested components were calculated based on the net tensile area of the rod. The stiffness of each rod was calculated based on the best-fitted line to the linear portion of the curve for each component. Then, the modulus of elasticity was calculated based on the gauge-distance measured for each rod and net tensile area. The gauge distance for all components was set to 30 inches. Table 3-1 shows the summary of component test results. The median value of each parameter, λ_m , and its associated logarithmic standard deviation value, β , were calculated as follows:

$$\lambda_m = e^{\frac{1}{N} \sum_{i=1}^N \ln \lambda_i} \quad (3-1)$$

$$\beta = \sqrt{\frac{1}{N-1} \sum_{i=1}^N \left[\ln \left(\frac{\lambda_i}{\lambda_m} \right) \right]^2} \quad (3-2)$$

where λ_i denotes the i^{th} measured maximum or failure response (see Table 3-1) and N is the number of tests conducted for each component ($N = 3$ in this study).

Table 3-1 Summary of Rod Component Tests

	Rod1	Rod2	Rod3	λ_m	β
Failure Displacement (in.)	1.02	0.971	1.06	1.02	0.044
Maximum Force (kips)	19.5	18.7	19.3	19.16	0.022
Max Strain	0.034	0.032	0.035	0.03	0.046
Max Stress (ksi)	86.1	82.5	85.6	84.7	0.023
E(ksi)	21866	21275	21732	21622	0.014

3.2.3 Analytical Model of Pipe Hangers

The Giuffre-Menegotto-Pinto steel material model (CEB, 1996) was adopted as the constitutive relation of the steel material. This material is implemented in OpenSees (OpenSees manual) as Steel02 material. The Steel02 material model can capture both kinematic hardening and isotropic hardening. The material behavior is controlled by: (1) yield stress σ_y ; (2) initial stiffness E; (3) post-yield stiffness ratio $b = E_p/E$; (4) parameters R_0, cR_1, cR_2 that control the transition from elastic to plastic branches; and (5) optional parameters that control isotropic behavior (not used in this model). Values of $R_0 = 10$ to 20 , $cR_1 = 0.925$ and $cR_2 = 0.15$ are recommended (OpenSees manual). The monotonic and cyclic stress-strain relations for this material with kinematic hardening are shown in Figure 3-3.

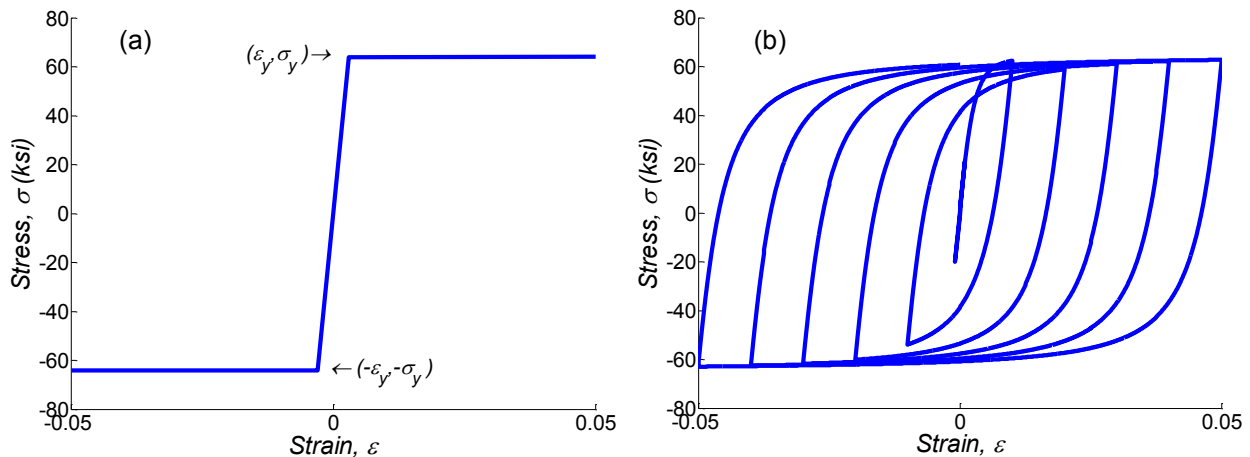


Figure 3-3 Behavior of Steel Material Model (a) Backbone Curve (b) Hysteresis Loop Due to Cyclic Load

Force-based nonlinear elements along with fiber sections were used to model the pipe hangers. These elements were tested several times for the models, and they are known for their improved accuracy compared to displacement-base elements (Neuenhofer and Filippou, 1997). This

element was formulated based on force distribution interpolation. The interpolation function in force-based elements is almost exact (except under P-D effect) because the element has a linear moment distribution. The element behavior is defined by: (1) end nodes; (2) number of integration points along the elements (in this study five points were used); and (3) previously defined section. The remaining parameters are intended for defining element mass density and more iteration control, which was not used in this study.

3.2.4 Calibration of Material Model for Pipe Hangers

The calibration process of the pipe hanger analytical model was performed based on all available component data found in the University of Nevada, Reno's test matrix. The tensile test results of threaded rods were used to calibrate the parameters of the Steel02 material model along force-based nonlinear element. The number of fibers associated to pipe hanger section was set to 48, which will be discussed later.

The optimum material was defined as the material that provides a force-displacement relationship within approximately 10% of all tensile test results of threaded rods using equation (3-3). The parameters of calibrated Steel02 material are presented in Table 3-2.

$$Error (\%) = \frac{abs(P_{i-Analytical} - P_{i-Rod_j})}{abs(P_{i-Analytical})} \times 100 \quad (3-3)$$

In this equation, $P_{i-Analytical}$ and P_{i-Rod_j} are the tensile force values corresponding to the i^{th} displacement of analytical and component tests of j^{th} rod, respectively.

Table 3-2 Calibrated Steel02 Material Parameters for Pipe Hangers

σ_y	E	b	R0	cR1	cR2	Optional (Refer to OpenSees Manual)				
						a1	a2	a3	a4	sigInit
64	21642	0.0001	2	0.5	0.15	0	1	0	1	0

Results of a calibration analysis on the force displacement of a 30-inch (gauge length of tensile machine) pipe hanger — Figure 3-4 (a) — were used to find the accurate experimentally

validated model. Figure 3-4 (b) shows the results of a force displacement analysis, and Figure 3-4 (c) shows the error in the forces between three tensile test results and analytical responses.

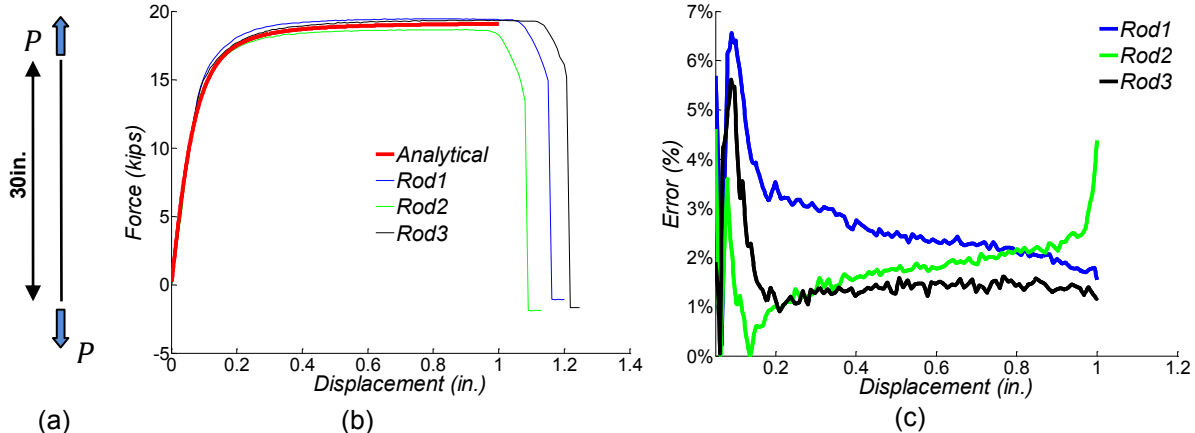


Figure 3-4 Accuracy of Analytical Hanger Modeling (a) Tensile Member, (b) Force-Displacement Relationship, and (c) Error in Force Between Members

3.2.5 Element Model for Pipe Hangers

Fiber section modeling was used to consider the nonlinearity in the pipe hangers. Using a nonlinear fiber section consisting of Steel02 material will allow the flexural yielding and permanent rotation of pipe hangers. In order to find the number of fibers for providing the accurate nonlinear behavior, a wide range of fiber numbers were used. However, no effort has been made to minimize the computational time in this calculation. A summary of this procedure is presented in Figure 3-5. This figure shows three sections using 5, 15 and 16 subdivisions in radial (nr) and circumferential (nc) direction. The 225-fiber (15x15) section provides a moment rotation relationship within 1% of the 256-fiber (16x16) section (see Equation (3-4)). Therefore, the hanger section with 225 fibers was named as the “accurate” model.

$$Error (\%) = \frac{abs(M_{i-Accurate} - M_{i-trial})}{abs(M_{i-Accurate})} \times 100 \quad (3-4)$$

In this equation, $M_{i-accurate}$ and $M_{i-trial}$ are the moment values corresponding to the i^{th} displacement of accurate (225-fiber section) and trial models, respectively.

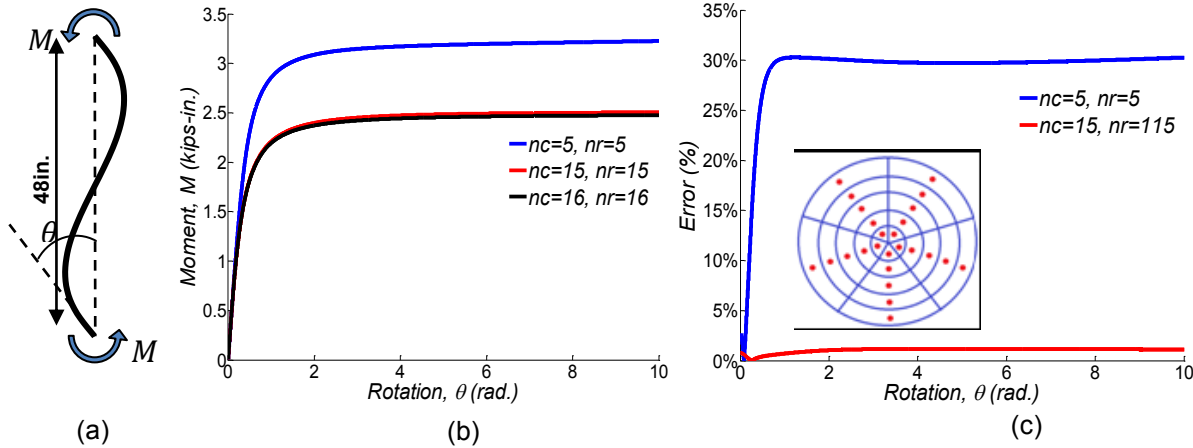


Figure 3-5 Sample Behavior of a Bending Members (a) Bending Member, (b) Moment-Rotation Relationships, and (c) Error in Moment Between Members

Through section analysis, it was observed that the behavior of hanger sections is not sensitive to radial subdivisions. Therefore, the value of nr was reduced to three and nc was set equal to 16 in order to provide appropriate accuracy. Hence, 48-fiber circular-shape sections were used to minimize the computational effort while still providing accurate nonlinear behavior. The generalized distribution of fibers for circular shape sections (5/8-inch pipe hangers) of the hangers can be seen in Figure 3-6. Results of a sensitivity analysis on the moment rotation of a typical pipe hanger — illustrated in Figure 3-6 (a) — were used to find the optimum number of fibers. Figure 3-6(b) shows the results of a moment rotation analysis, and Figure 3-6(c) shows the error in the moment between sections with various numbers of fibers. The 48-fiber section provides a moment rotation relationship within approximately 1% of the “accurate” section. The

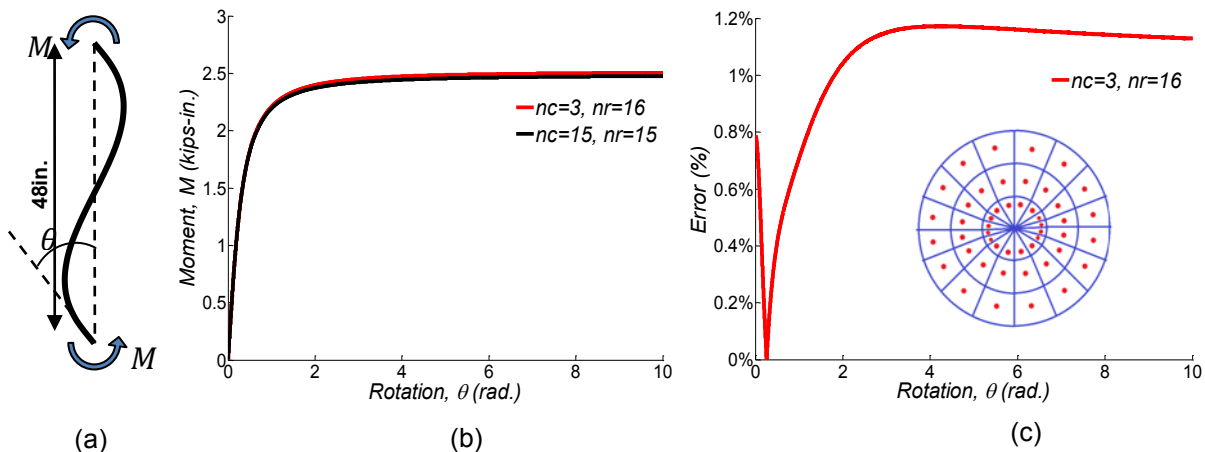


Figure 3-6 Behavior of a Bending Member with $nc=16, nr=3$ (a) Bending Member, (b) Moment-Rotation Relationship, and (c) Error in Moment Between Members

48-fiber section splits the sections into three radial and 16 circumferential fibers in order to calculate the moment of inertia about the two axes of the section and assure numerical stability.

The fiber sections defined in OpenSees using the uniaxial material do not consider the torsional degrees of freedom of the members. The torsional constant of element section, J , along with the shear modulus of steel material, G , define the torsional stiffness of hanger sections. Afterwards the section aggregator command was used to assemble the degrees of freedom of the hanger section. Shear deformations in the members were neglected.

In order to develop the analytical model for pipe hangers with other diameters, the same modeling approach was used. Samples of analytical models for tensile and bending behavior of 3/8in, 1/2in, and 5/8in pipe hangers are presented in Figure 3-7. The only changes implemented included:

- Using the fiber section with actual rod diameter of pipe hangers.
- Choosing an appropriate torsional constant of section, J , to define the torsional stiffness of hanger sections.

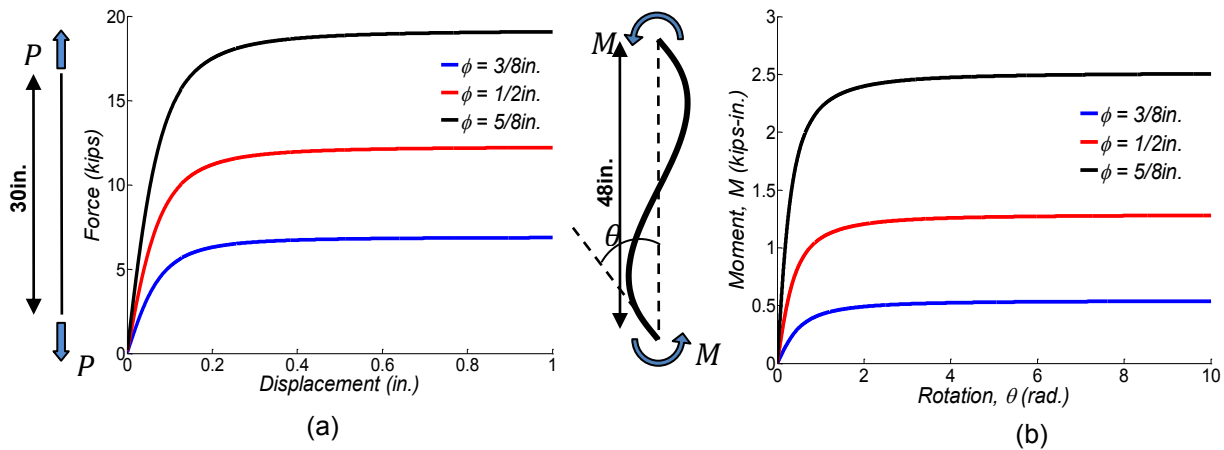


Figure 3-7 Proposed Analytical Model of Pipe Hangers (a) Tensile Behavior, (b) Bending Behavior

3.3 Seismic Sway Braces

Seismic sway braces are a critical component of piping systems used to carry the seismic loads of piping systems. These elements are usually suspended from the structure and intended to resist

horizontal and vertical seismic loads. The braces that are intended to resist movement perpendicular and parallel to the axis of the pipe are defined as lateral and longitudinal sway braces, respectively.

3.3.1 Code Requirements

The seismic sway braces shall follow several requirements specified by NFPA 13 (2011). Some of these requirements are summarized here.

- Two tension-only brace components opposing each other can be used instead of each lateral or longitudinal brace location.
- The horizontal force, F_{pw} , acting on the brace shall be calculated as:

$$F_{pw} = C_p \times W_P \quad (3-5)$$

where C_p is the seismic coefficient selected in Table 9.3.5.6.2 of NFPA13 (2011) utilizing the short period response parameter, S_s . The upper bounds of F_{pw} are presented in Table 9.3.5.3.2 (a-f) and Tables 9.3.5.8.7 (a-c) of NFPA13 (2011). These tables are presented in Appendix A.

- Sway braces shall be installed at least 45 degrees from the vertical plane

3.3.2 Solid Sway Braces

The seismic sway braces either can be a steel section capable of resisting compression as well as tension, called solid braces (1-inch pipe section is the most common) or two tension-only

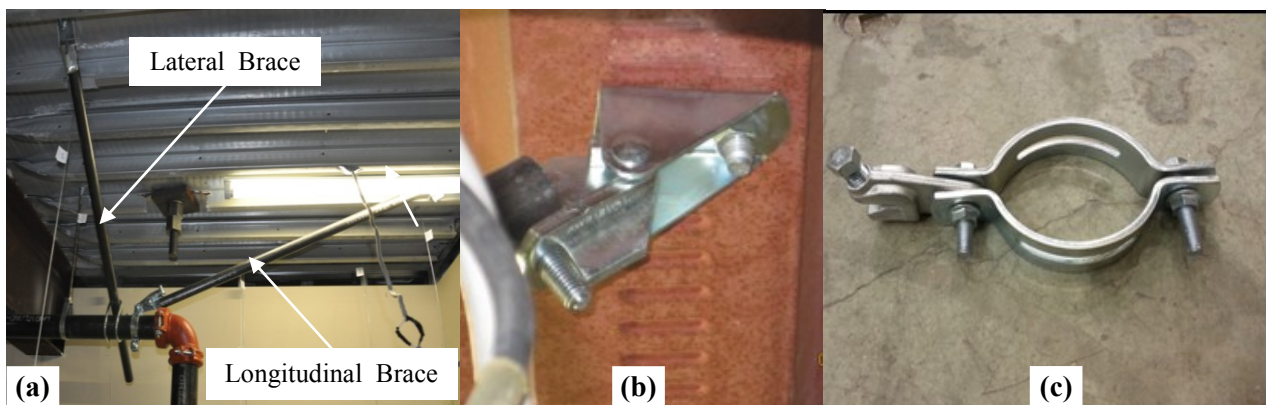


Figure 3-8 (a) Lateral and Longitudinal Solid Braces (b) Deck Fastener(c) Longitudinal Pipe-Attachment Clip

members. The main components of seismic braces are brace sections (pipes, angles, cables, etc.), deck fasteners, and pipe-attachment clips. Figure 3-8 shows an example of a solid seismic sway brace and its attachment parts.

3.3.2.1 Analytical Model of Solid Sway Braces

Since the maximum design force of solid braces are well below the yield force associated with these types of braces, nonlinearity has not been considered for these elements. Therefore, these types of braces were modeled using an elastic section. In this study, the 1-inch pipe shape section was used to represent solid sway braces. The definition of this section requires: (1) modulus of elasticity ($E=29000$ ksi); (2) area of pipe section ($A=0.4939$ in 2); (3) moment of inertia ($I = 0.0873$ in 4); (4) shear modulus ($G=11153$ ksi); and (5) torsional constant ($J=0.1747$ in 4). This section was used along with the force-based element to model the solid sway braces.

3.3.3 Tension Only Sway Braces

Seismic cable braces (SCBs) can be replaced with seismic solid sway braces because of their effectiveness and ease of installation. Figure 3-9 shows an example of tension-only (cable) seismic sway bracing.

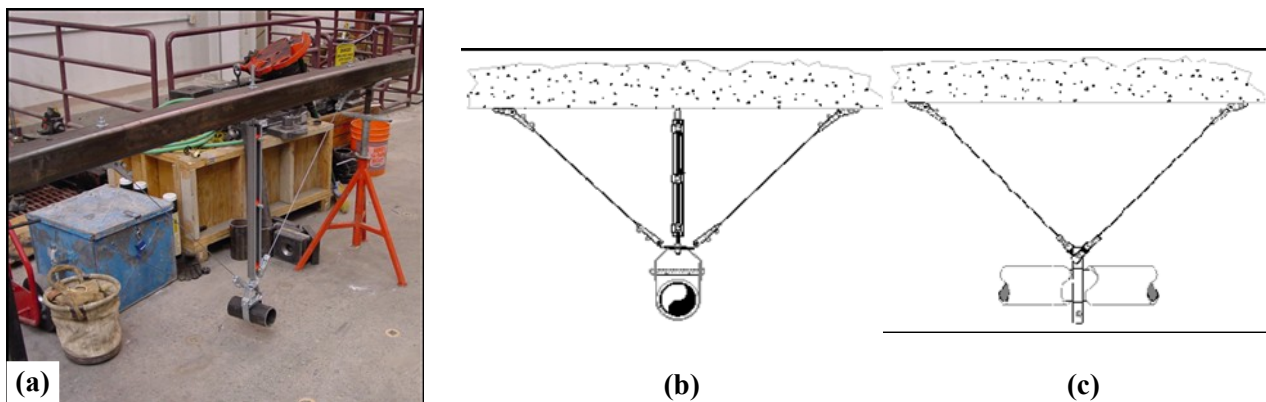


Figure 3-9 (a) Photograph of Tension-Only Braces (Cables) (b) Lateral and (c) Longitudinal Bracing (Goodwin et al., 2005)

3.3.3.1 Cable Tests at the University of Nevada, Reno

The cables used in the tensile tests were made of $\frac{1}{8}$ -inch diameter galvanized 7 x 19 (number of strands x wires per strand) aircraft-grade steel with a specified minimum break strength of 1700 pounds (Mason, 2009). Three tensile tests were performed for the cable bracing assembly. These

tests were designed and performed by University of Nevada, Reno and the outcome of these tests can be found in Goodwin et al. (2005). Hereafter, the description and experimental observation of these experiments are provided for convenience.

The tensile test was performed by applying a unidirectional ramp of displacement at a low speed rate of 0.01 in/sec (Figure 3-10a). The cables were subjected to increased tensile loading to observe the failure point. Figure 3-10b shows the force-displacement results of these tests.

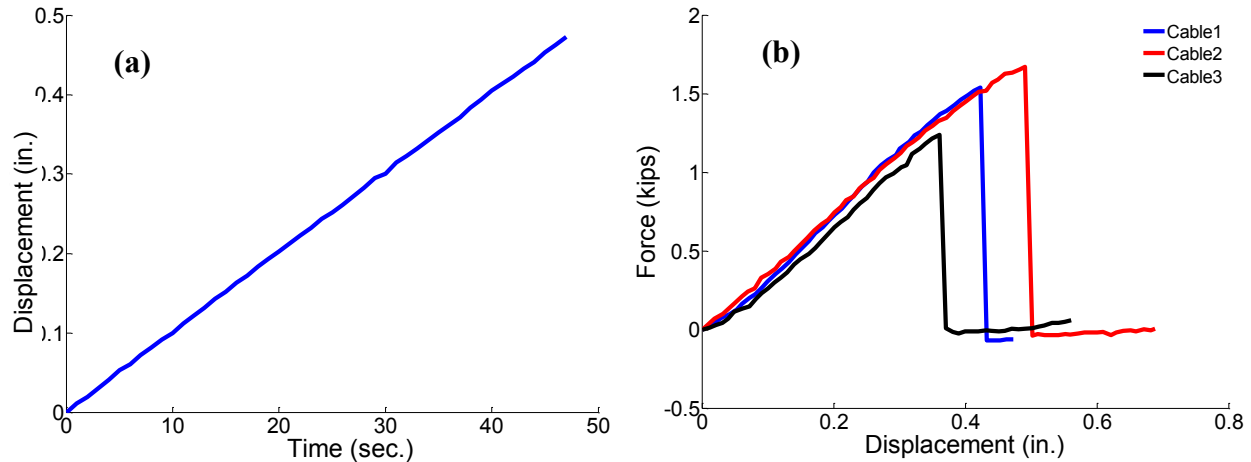


Figure 3-10 (a) Loading History of Cable Tensile Test (b) Cable Force/Displacement Curves (Goodwin et al., 2005)

The cables were tested using the same configuration found in construction. The cable support was threaded, and a screw was clamped on top. All of the cables failed at the clamped portion of the cable. This indicates that the clamping effect produces the governing damages in the failure of the cables (Goodwin et al., 2005). The stress and strain of the tested components were calculated based on the net tensile area of the cables and the gauge distance measured for each cable. The modulus of elasticity was calculated based on maximum stress and strain. The gauge distances were 28.625 inches, 29.10 inches, and 28.75 inches for cables 1, 2 and 3, respectively. Table 3-1 shows a summary of component test results. The median value of each parameter, λ_m ,

Table 3-3 Summary of Cable Component Tests

	Cable1	Cable2	Cable3	λ_m	β
Failure Displacement (in.)	0.423	0.491	0.369	0.425	0.143
Maximum Force (kips)	1.538	1.670	1.240	1.471	0.154
Max Strain	0.015	0.017	0.013	0.01	0.137
Max Stress (ksi)	125	136	101	119.89	0.154
E(ksi)	8481	8065	7873	8135.75	0.038

and its associated logarithmic standard deviation value, β , was calculated based on equations (3-1) and (3-2).

3.3.3.2 Analytical Model of Tension-Only Sway Braces

A bilinear material model that incorporated the initial gap was adopted as the constitution of the seismic cable bracing material. This material is implemented in OpenSees (OpenSees manual) as Elastic Perfectly Plastic Gap (EPPG) material. The EPPG material model can capture either compression or tension behavior at the same time. The material behavior is controlled by: (1) initial stiffness, E ; (2) yield stress, σ_y ; (3) initial gap strain, (gap); (4) post-yield stiffness ratio, $b = E_p/E$; and (5) damage type (not used in this model), which is an optional parameter to specify whether damage is accumulated or not in the material model. Figure 3-11 shows the behavior of EPPG material with and without initial gap strain with the same parameters. The initial gap strain and deformation was useful for capturing the initial slack of cable bracing, which is common in construction. Compression capacity was not considered for the analytical model of cable bracing (see Figure 3-11).

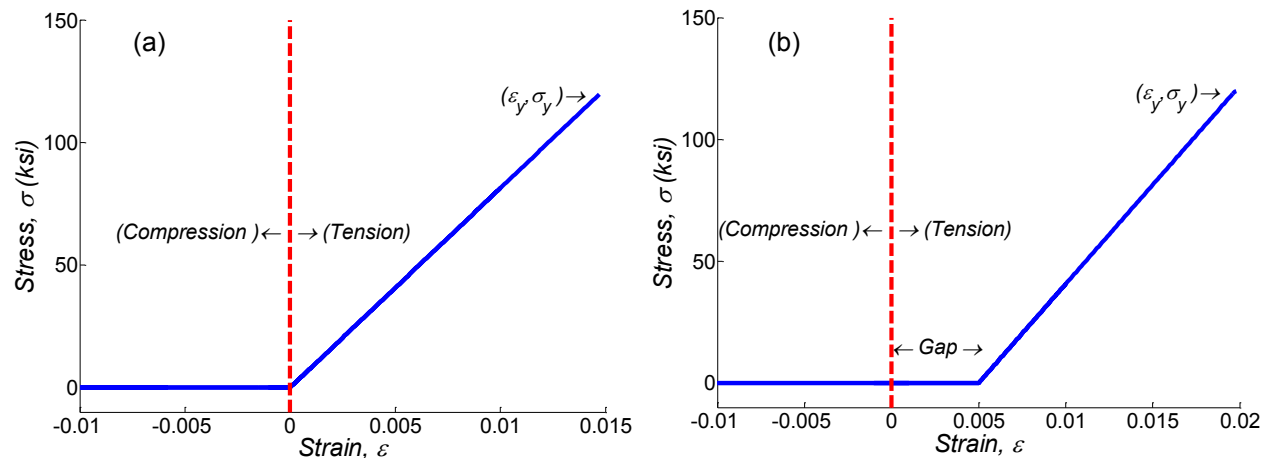


Figure 3-11 Behavior of EPPG Material for Cable Bracing (a) Model without Gap (b) Model with Gap

Truss elements were used to model the cable bracing. These elements are suitable for modeling the elements with pin-to-pin conditions at both ends. The element behavior is defined by: (1) end nodes; (2) cross-sectional area of element A; and (3) previously defined material. The remaining parameters are optional for defining element mass density and to specify whether or not to account for Rayleigh damping in the element model, which was not used in this study.

3.3.3.3 Calibration of Analytical Model for Cable Bracing

The calibration process of the mentioned seismic cable bracing analytical model was performed based on all available component data that was part of the University of Nevada, Reno test matrix. To calibrate the bracing model, the parameters of the EPPG material model, along with the truss element, were calibrated using test results from a monotonic tensile test of cable bracing.

The optimum material was considered as the material that provides a force-displacement relationship within approximately 10% of all tensile test results of cable bracing using equation (3-6). The parameters of the calibrated EPPG material are presented in Table 3-2.

$$\text{Error (\%)} = \frac{\text{abs} (P_{i-\text{Analytical}} - P_{i-\text{Cable}_j})}{\text{Max} (\text{abs}(P_{i-\text{Analytical}}))} \times 100 \quad (3-6)$$

In this equation, $P_{i-\text{Analytical}}$ and $P_{i-\text{Cable}_j}$ are the tensile force values corresponding to the i^{th} displacement of the analytical and component test of the j^{th} cable, respectively.

Table 3-4 Calibrated EPPG Material Parameters for Cable Braces

σ_y	E	Gap	Optional (Refer to OpenSees Manual)	
			b	damage
120	8136	Can Vary (Assumed 0)	0	"noDamage"

Results of the calibration analysis on the force displacement of a 28.825-inch cable brace (the average gauge length of tensile components) were used to experimentally validate the model. See Figure 3-12a. Figure 3-12b shows the results of a force displacement analysis, and Figure 3-12c shows the error in the forces between three tensile test results and the analytical response.

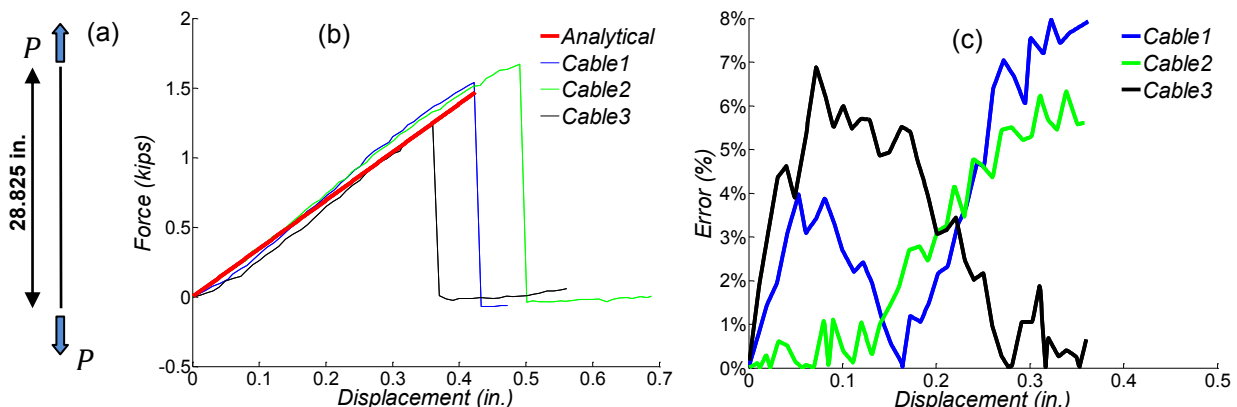


Figure 3-12 Accuracy of Analytical Cable Modeling (a) Tensile Member (b) Force-Displacement Relationship (c) Error in Force between Members

3.4 Restrainers

Restrainers are considered secondary components of piping systems. These elements are usually suspended from the structure and are intended to limit the movement of pipelines (usually branch lines). Restrainers are designed for lesser degrees of resisting force loads than bracing. Wire restrainers are the most common type of pipe restraints. The main parts of restrainers are deck fasteners, steel strap (45 degree) or steel angle, and wraparound diagonal wire restrainers (see Figure 3-13).

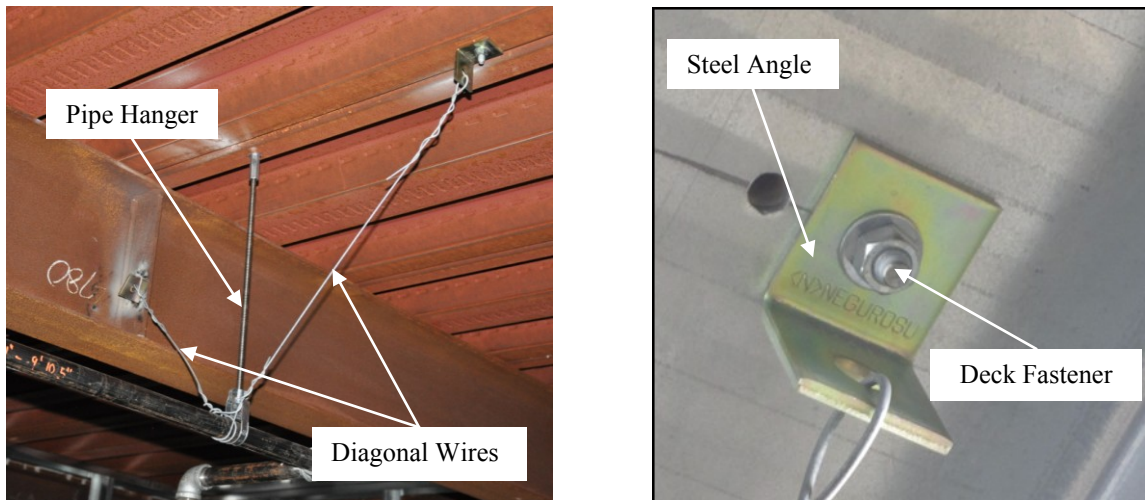


Figure 3-13 Wire Restrainers and the Deck Connection Detail

3.4.1 Code Requirements

There are a limited number of requirements specified by NFPA 13 (2011) for wire restrainers. Some of these requirements include:

- Sway brace assemblies, wraparound U-hook, and wires can be used as the pipe restrainers.
- Wire restrainers shall be gauge number 12 wires.
- Wires shall be installed at least 45 degrees from the vertical plane and on both sides of the pipe.
- The wires shall have a minimum strength capacity of 440 pounds.

3.4.2 Wire Restrainer Tests at the University of Nevada, Reno

Three tensile tests were performed for 12-gauge wires. An extensometer with a gauge distance of 8 inches was used to measure deformation in the wires. Figure 3-14 shows the testing machine along with the extensometer and one of the testing samples.

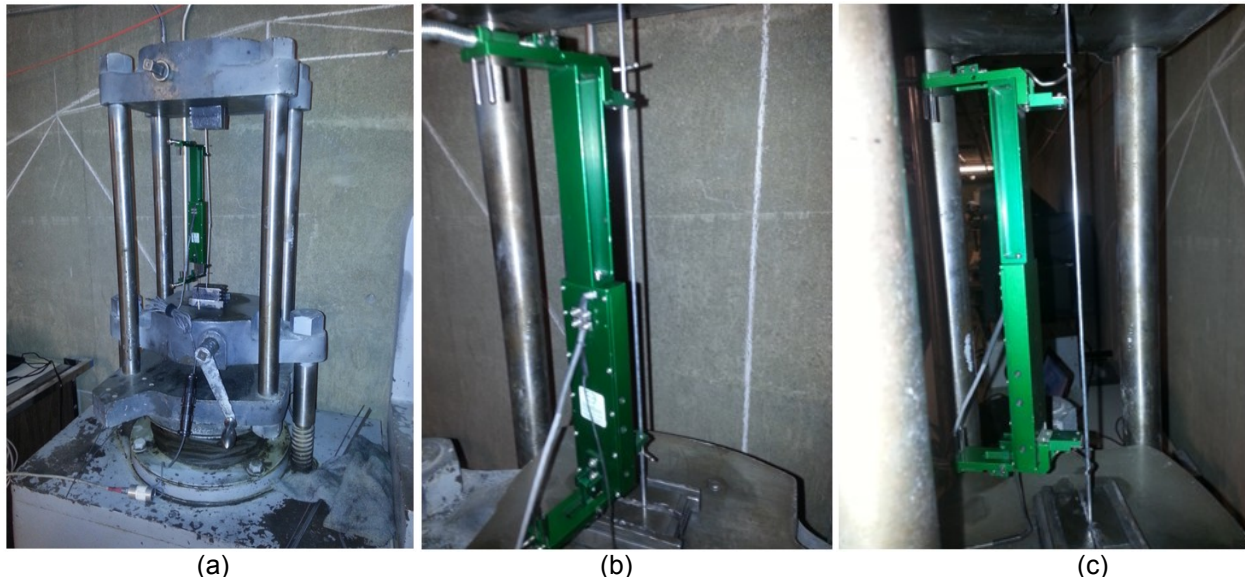


Figure 3-14 Tensile Test of Wire Restrainers (a) Testing Machine (b) Extensometer (c) Testing Sample of Wires

The tensile test was performed by applying a unidirectional ramp of displacement at a low speed rate of 0.02 in/sec (Figure 3-15a). The wires were subjected to increasing tensile loading to observe the failure point. Figure 3-15b shows the force-displacement results of these tests.

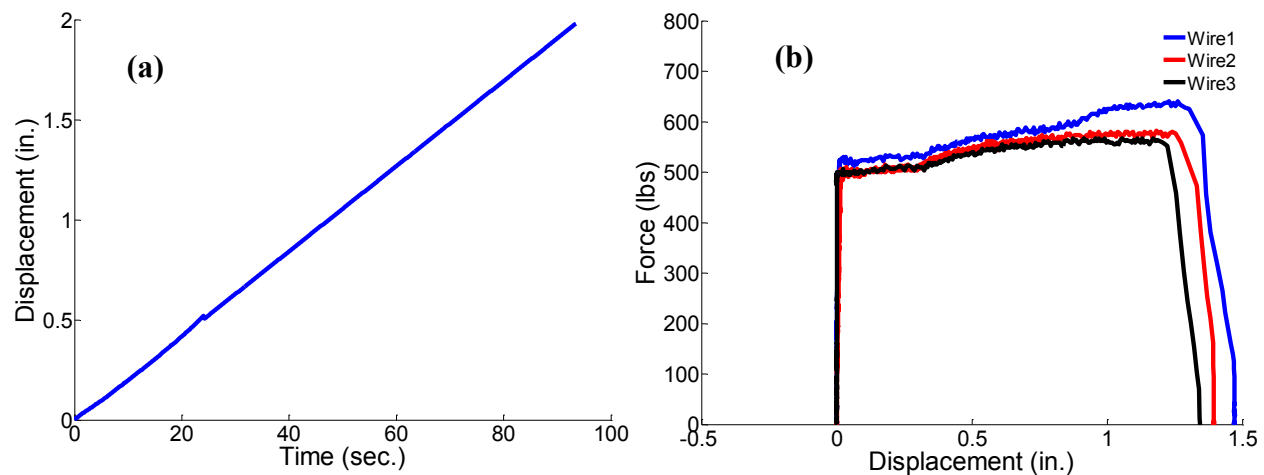


Figure 3-15 (a) Loading History of Wire Tensile Test (b) Rod Force/Displacement Curves

The stress and strain of tested components was calculated based on the net tensile area of the wires and gauge distance of components. The gauge distance for all components was set to 8 inches. Table 3-5 shows a summary of component test results. The median value of each parameter, λ_m , and its associated logarithmic standard deviation value, β , were calculated based on equations (3-1) and (3-2).

Table 3-5 Summary of Wire Restrainer Component Tests

	Wire 1	Wire 2	Wire 3	λ_m	β
Failure Displacement (in.)	1.472	1.396	1.345	1.40	0.045
Maximum Force (lbs)	640	583	567	596	0.063
Max Strain	0.184	0.175	0.168	0.175	0.045
Max Stress (ksi)	124.78	113.67	110.55	116.18	0.063

3.4.3 Analytical Model of Wire Restrainers

The Elastic Perfectly Plastic Gap (EPPG) material that was previously described is used for constitution of the wire restrainer material. As previously addressed, the material behavior is controlled by: (1) initial stiffness, E ; (2) yield stress, σ_y ; (3) initial gap strain, gap; (4) post-yield stiffness ratio, $b = E_p/E$; and (5) damage type, which is an optional parameter to specify whether to accumulate damage or not in the material model. Figure 3-16 shows the backbone curves of EPPG material with and without initial gap strain with the same parameters. The initial gap strain and deformation can be useful for capturing the initial slack of wire restrainers, which

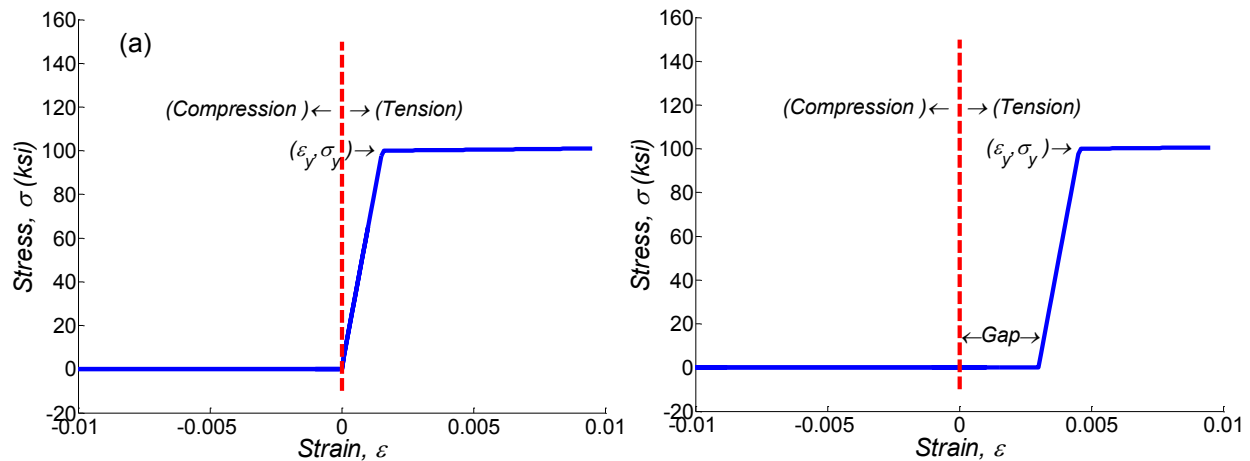


Figure 3-16 Behavior of EPPG Material for Wire Restrainers (a) Model without Gap (b) Model with Gap

is common in construction. Compression capacity was not considered for the analytical model of cable bracing (see Figure 3-16).

Despite the brittle behavior of cable bracing, wire restrainers have ductile behavior. Therefore, accounting for additional slack due to yielding is crucial. In other words, after each cycle of yielding, the length and slack of wire restrainers would increase. Hence, in the next loading cycle, the wires would engage if the differential distance between two end nodes went beyond the summation of additional slack and initial slack. In order to account for this type of behavior, the cyclic damage was considered when defining the EPPG material for wire restrainers. Figure 3-17 shows that in the model that accounted for cyclic damage, the gap is increased and started from the last maximum nonlinear displacement.

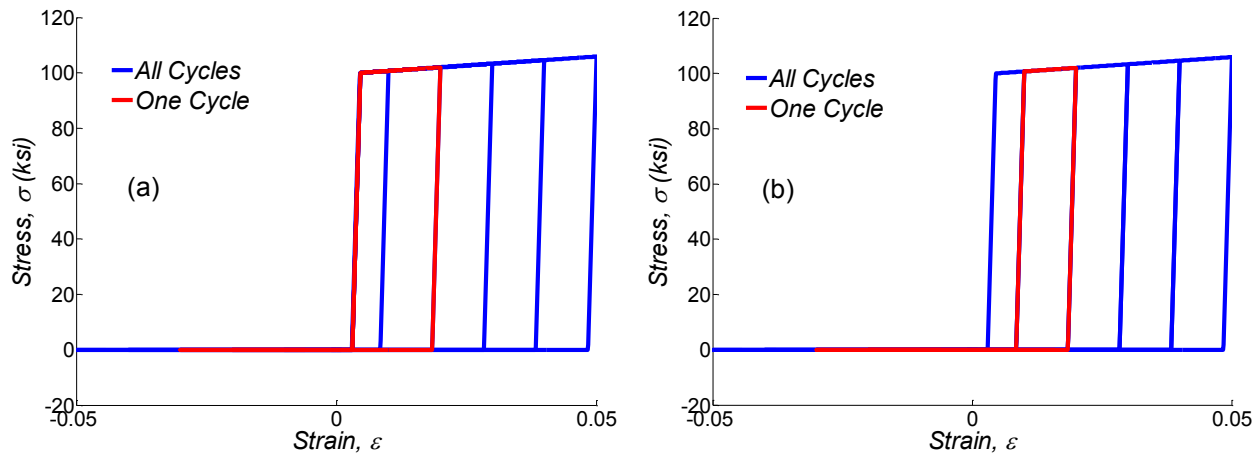


Figure 3-17 Hysteresis Behavior of EPPG Material for Wire Restrainers (a) Model without Cyclic Damage (b) Model with Cyclic Damage

Truss elements were used to model the wire restrainers. These elements are used for wire restrainers, as the wires do not have significant rotational and torsional resistance. As mentioned before, the behavior of these elements are defined by: (1) end nodes; (2) cross-sectional area of element A; and (3) previously defined material. The remaining parameters are optional for defining element mass density and to specify whether or not to account for Rayleigh damping in the element model, which was not used in this study.

3.4.4 Calibration of Analytical Model for Wire Restrainers

The calibration process of the wire restrainer analytical model was performed based on all available component data that was part of the University of Nevada, Reno test matrix. To calibrate the model, the parameters of the EPPG material model along with truss elements were calibrated using test results from a monotonic tensile test of wire restrainers.

The optimum material was considered as the material that provides a force-displacement relationship within approximately 10% of all tensile test results of cable bracing using equation (3-7). The parameters of the calibrated EPPG material are presented in Table 3-6.

$$Error (\%) = \frac{abs(P_{i-Analytical} - P_{i-Wire_j})}{Max(abs(P_{i-Analytical}))} \times 100 \quad (3-7)$$

In this equation, $P_{i-Analytical}$ and P_{i-Wire_j} are the tensile force values corresponding to the i^{th} displacement of the analytical and component test of the j^{th} wire, respectively.

Table 3-6 Calibrated EPPG Material Parameters for Wire Restrainers

σ_y	E	Gap	Optional (Refer to OpenSees Manual)	
			b	damage
100	29000	Can Vary (Assumed 0)	0.005	"Damage"

Results of the calibration analysis on the force displacement of an 8-inch wire restrainer (average gauge length of tensile components) was used to experimentally validate the model. See Figure 3-18a. Figure 3-18b shows the results of a force displacement analysis, and Figure 3-18c shows the error in the forces between three tensile test results and analytical response.

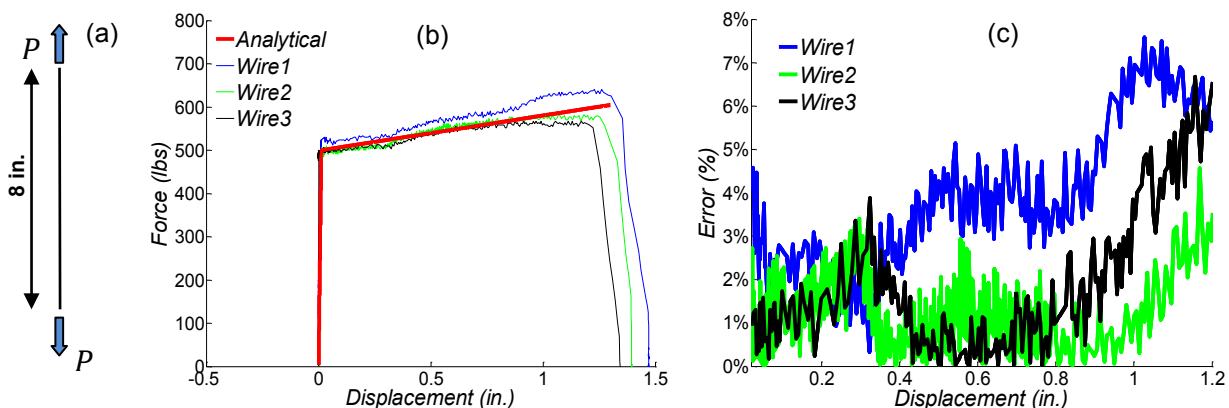


Figure 3-18 Accuracy of Analytical Wire Modeling (a) Tensile Member (b) Force-Displacement Relationship (c) Error in Force between Members

3.5 Pipe Runs

Pipe runs are perhaps the most important components of a piping system. These elements feed the sprinkler heads in a fire sprinkler system. They are usually sized through the piping system based on numbers of outlets, pressure, and performance. Pipe runs are categorized as risers, main runs, branch lines, armovers, and drops. The riser pipes are the vertical supply pipes in a sprinkler system. The main run pipes supply branch lines, which are the pipes supplying sprinklers — either directly or through drops. The horizontal pipes that extend from the branch line to a single sprinkler head are called armovers. Drop pipes are the vertical pipes that feed sprinkler heads from branch lines or armovers (see Figure 3-19). As mentioned previously, fittings are the elements that connect two or more pipe segments. The most common types of fittings are threaded, grooved, welded, and chlorinated polyvinyl chloride (CPVC) with cement joints. The main focus of this study is on threaded and grooved fittings.

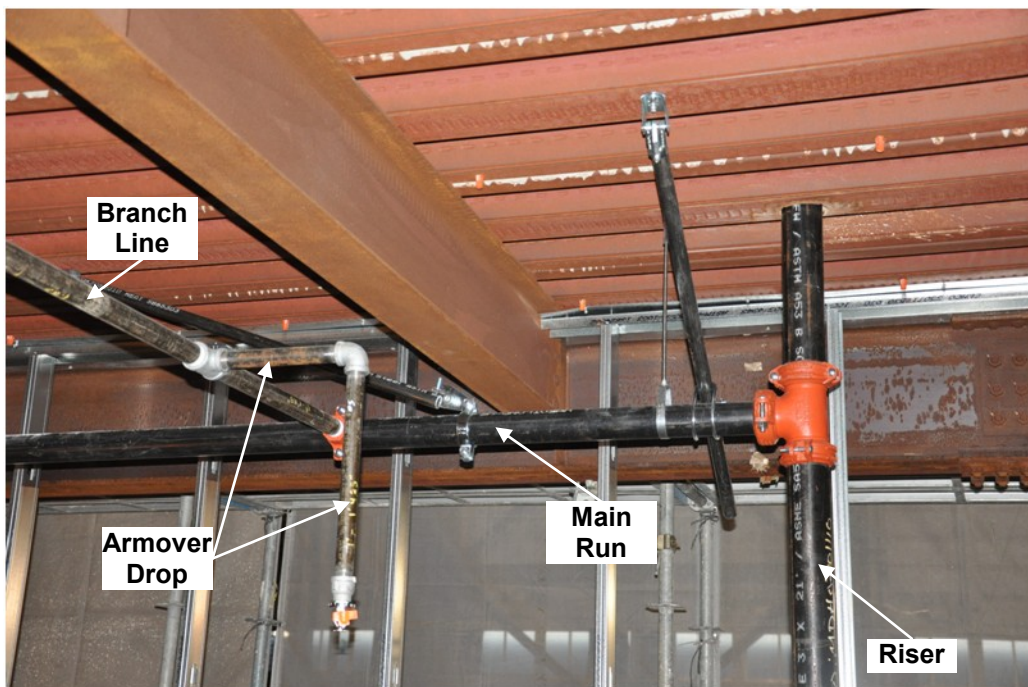


Figure 3-19 Typical Pipe Runs of a Sprinkler Piping System

3.5.1 Code Requirements

Pipe runs and sections shall meet several requirements specified by NFPA 13 (2011). However, only the wall thickness requirements for threaded and grooved joints are presented below.

- In grooved fitted pipes, the minimum nominal wall thickness for pressures up to 300 psi shall be in accordance with Schedule 10 for pipe sizes up to 5 inches, 0.134 inches for 6-inch pipe, 0.188 inches for 8-inch and 10-inch pipe, and 0.330 inches for 12-inch pipe.
- In threaded pipes, the minimum wall thickness of pipes shall be in accordance with Schedule 30 pipe (in sizes 8 inch and larger) or Schedule 40 pipe (in sizes less than 8 inches) for pressures up to 300 psi.

3.5.2 Analytical Model of Pipe Runs

Since the moment capacity of pipe sections is much larger than their grooved or threaded joints, nonlinearity has not been considered for these elements (excluding the end joints). Therefore, it has been assumed that the nonlinearity of pipe runs are only concentrated at the end joints. Hence, pipe segments were modeled using an elastic section. As mentioned before, the definition of this section requires: (1) modulus of elasticity, $E=29000$ ksi; (2) area of pipe section A ; (3) pipe section moment of inertia I ; (4) shear modulus, $G=11153$ ksi; and (5) pipe section torsional constant, J . This section was used along with the force-based element to model the pipe segments. As previously stated, the “Pinching4” uniaxial material along with a “zeroLength”

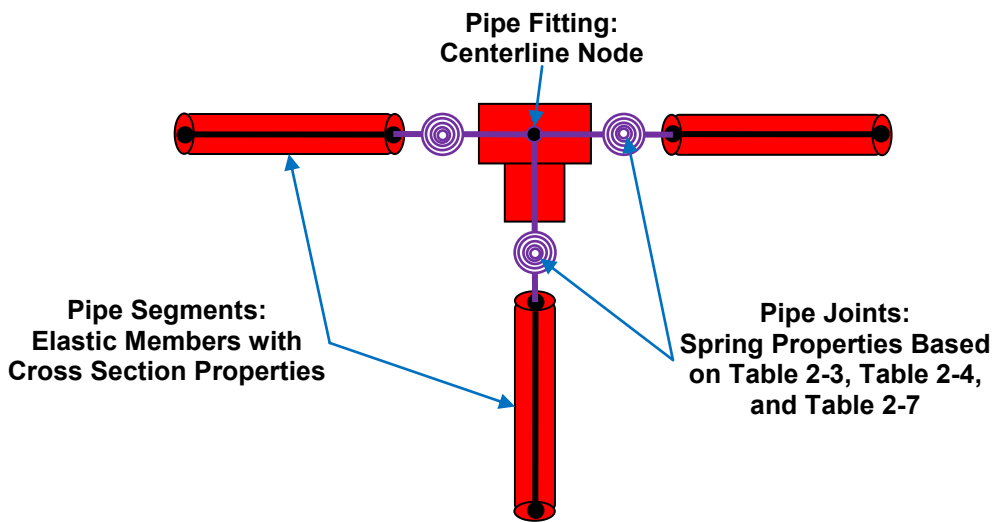


Figure 3-20 Schematic of Analytical Modeling for Pipe Runs

element were used to simulate the moment-rotation response of a pipe joint connecting two piping nodes (OpenSees, 2012). The other four degrees (axial, two shears, torsional) of the “zeroLength” element were defined using four elastic materials. The properties of these materials

were defined based on an element with the connected pipe section properties and unit length (see Figure 3-20).

3.6 Concluding Remarks

In this section, the analytical models were developed for supporting elements of fire sprinkler piping systems. An element model was built for representing pipe hangers. This model consisted of fiber section modeling along with force-based nonlinear elements. The optimum number of fibers was found to reduce the time of analysis while still providing the required accuracy. The developed pipe hanger model was compared with the tensile experimental data. Finally, the behavior of pipe hangers with different diameters was analyzed.

Analytical models were developed for two types of sway braces — solid and tension-only. An elastic section element using an elastic section along with a force-based element were proposed for 1-inch pipe section solid sway braces. A truss element using elastic perfectly plastic gap material was used for modeling the tension-only (cable) bracing components. The proposed model was calibrated with the tensile test data.

An analytical model was generated for wire restrainers. This model incorporated elastic perfectly plastic gap material and truss elements to simulate the behavior of wire restrainers. The tensile test experimental data was used to validate the analytical model of wire restrainers.

Finally, in order to analytically model the pipe runs, an assumption was made that the nonlinearity of the pipe runs is only concentrated in the connecting joint. Therefore, elastic sections along with force-based elements were used for pipe segments, while “zeroLength” elements with nonlinear “Pinching4” material were used from modeling the rotational degree of end joints. However, the other four degrees (axial, two shears, torsional) of “zeroLength” element were defined using four elastic materials.

SECTION 4 VERIFICATION OF ANALYTICAL MODEL OF PIPING SYSTEM EXPERIMENTS

4.1 Introduction

The nonlinear behavior of different piping components and their calibration using experimental level data was described in the previous sections. These nonlinear models enabled to be performed sophisticated future nonlinear response history analysis (nRHA) of piping systems. The accurate response of these elements as part of a system is crucial. Parameters such as constraints, restraints, and damping model can significantly change the behavior of a component in system-level analytical studies. Therefore, it is necessary to examine and validate the analytical models with subsystem or system-level experiments.

This section used the results of previously compared and subsystem-level experiments to verify the proposed component behavior. Furthermore, methods were developed to analytically model piping systems incorporating different types of components. The OpenSees program (2012) was used for modeling, analysis, comparison, and calibration of test data. The model accuracy was verified by comparing the analytical and experimental results. In this section, several types of responses (acceleration, displacement, hanger forces, wire restrainer forces, etc.) will be considered in different locations (main runs, branch lines, sprinkler heads, etc.) for validating the proposed analytical method.

4.2 Hospital Piping Assemblies Tested at University of Nevada, Reno, I

Four subassemblies — 1) welded unbraced, 2) welded braced, 3) threaded unbraced, and 4) threaded braced — were tested. As the behaviors of threaded pipe joints and cable braces are in the scope of this research, only the results of the fourth configuration are presented and used to calibrate the analytical model. These tests were designed and performed by the University of Nevada, Reno, and the results can be found in Goodwin et al. (2005). The description and experimental observations of these experiments are given for convenience in the following sections.

4.2.1 Test Background

The piping assembly used two water heaters, one heat exchanger, three riser branches, and horizontal runs. The assembly was fixed on a shake table and hung from, or restrained to, a stationary frame that was attached to the laboratory floor — see Figure 4-1(a) and Figure 4-1(b). The piping assemblies were tested under horizontal seismic excitations, to allow the investigation of the response to the imposed interstory drift expected to occur between adjacent floors of a multistory building (Zaghi et al, 2012).

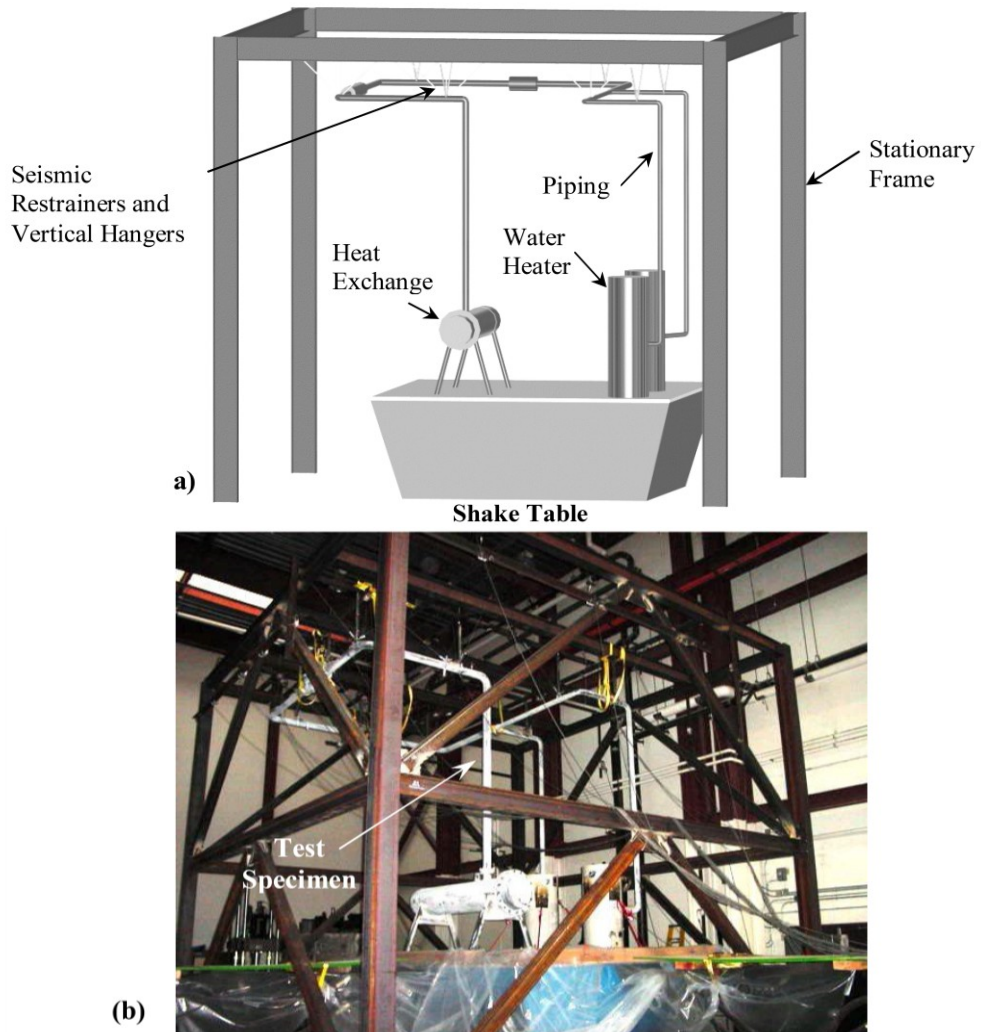


Figure 4-1 Experimental Setup a) Schematic of the Setup, b) Final Setup, (Zaghi et al., 2012).

The tested piping subsystem consisted of a 12-foot by 12-foot layout on one floor. A 12-foot-long vertical pipe riser connected the water heaters and heat exchangers that attached the shake

tables to the piping that was hung from the stationary frame — see Figure 4-2(a) and Figure 4-2(b). To detect any leaks, the system was filled with water under hydrostatic pressure.

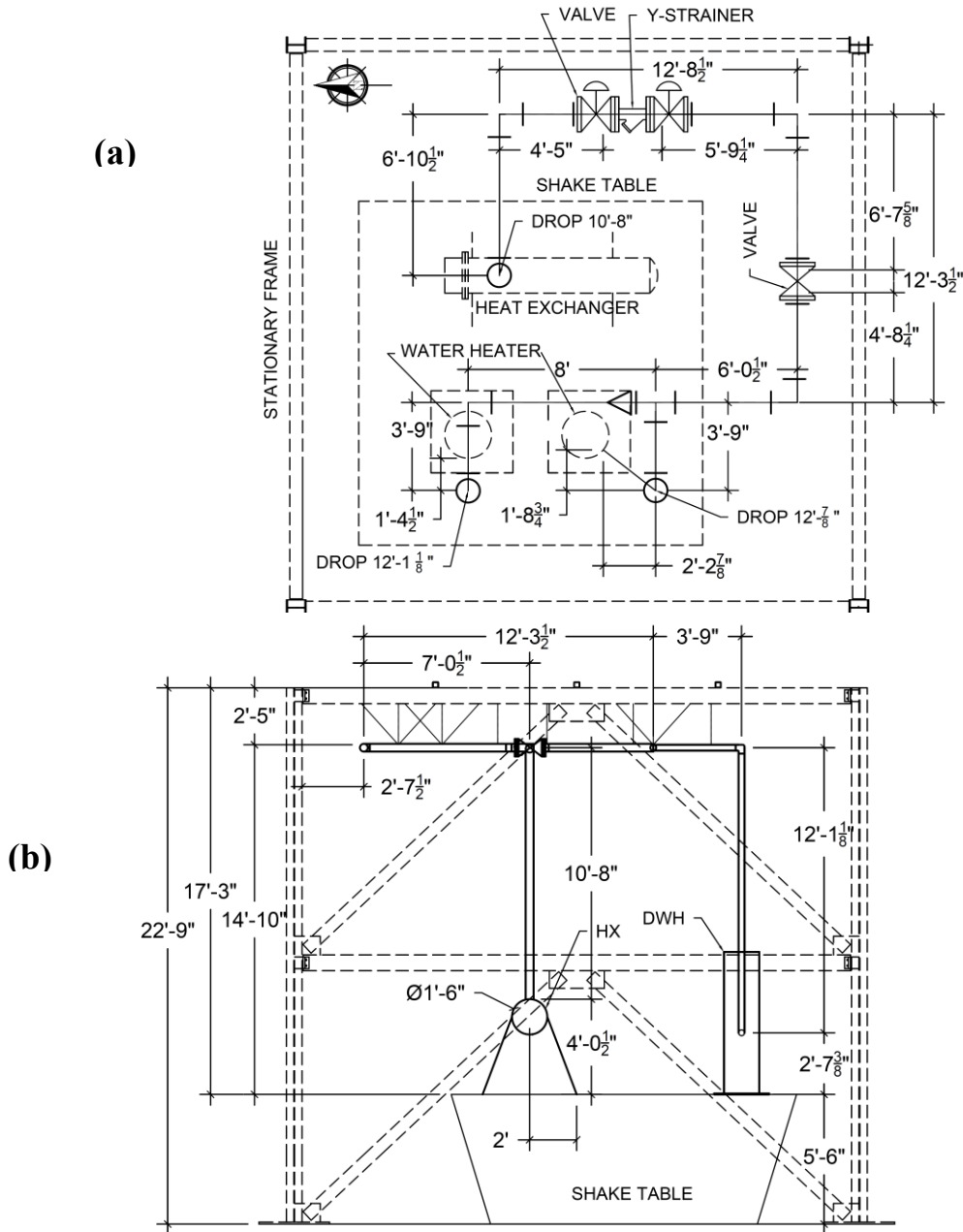


Figure 4-2 Piping Assembly a) Plan View, b)Elevation View (Zaghi et al, 2012)

The piping subsystem included 3-in. and 4-in. diameter Schedule 40 pipes. The water heaters were connected to the 3-inch pipes using four-bolt flanged connections. The heat exchanger and all valves were connected to the 4-in. pipes using eight-bolt flanged connections. A combination

of one y-strainer (61 pounds) between two gate valves (83 lbs/valve) and a separate check valve (80 pounds) were installed on the horizontal run. The entire piping system was supported by vertical hangers at 11 locations. Eight $\frac{5}{8}$ -in. diameter all-thread rods for supporting the 4-in. pipe and three $\frac{1}{2}$ -in. diameter all-thread rods supported the 3-in. pipe. The cable bracings used in the test setup instead solid sway bracing. The bracing was made of $\frac{1}{8}$ -in. diameter galvanized 7 x 19 (number of strands x wires per strand) aircraft grade steel and had a specified minimum break strength of 1700 pounds. These cable bracings were attached to the pipe hangers at seven locations (out of 11). Two out of the seven bracing points had cable bracings in the longitudinal and lateral directions (Figure 4-3). Further information about the test setup is provided in Zaghi et al. (2012).

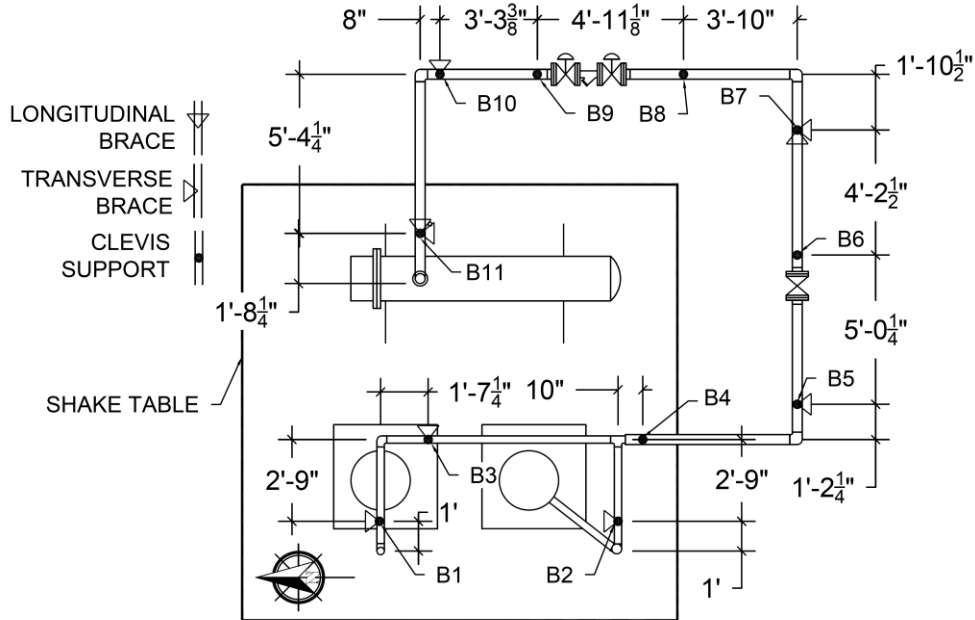


Figure 4-3 Seismic Bracing Layout (Zaghi et al, 2012)

4.2.2 Instrumentation Plan

Data collected from the experiments consisted of the displacement of the piping subsystem measured relative to the stationary frame and the accelerations at critical locations on the pipes (Figure 4-4). A total of 28 displacement transducers and 16 accelerometers were used to measure

the overall response of piping subassemblies. A detailed instrumentation plan is reported in Goodwin et al. (2005).

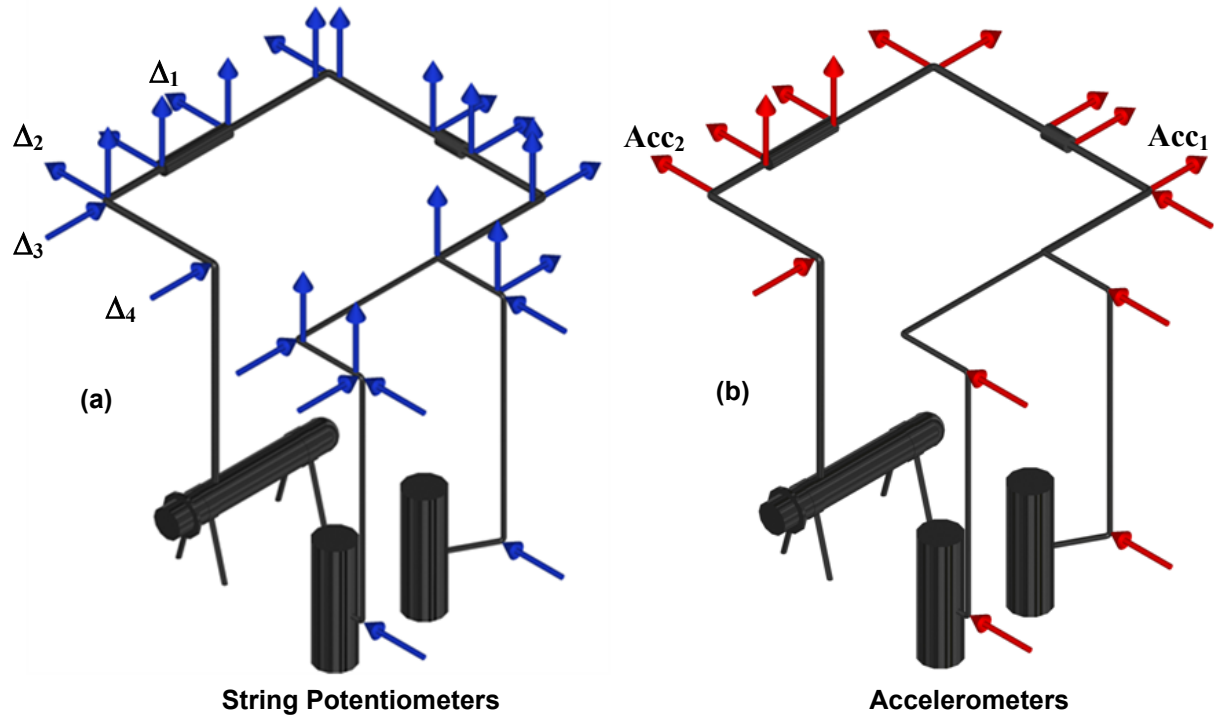


Figure 4-4 Instrumentation View

4.2.3 Loading Protocol

The loading history protocols used in this experiment were table motion compatible with the requirements of AC156, assuming conservative values that are typical of Seismic Design Category D (Zaghi et al., 2012). Each experimental setup was subjected to increasing intensities of the input motion ranging from 5% to 100% of the full-scale motion. These excitations were applied independently along each of the main axes, referred to as N-S, E-W. Biaxial excitation was also applied at 45° with respect to these axes (Goodwin et al., 2005). Figure 4-5 shows a sample of achieved loading histories corresponding to 60% of full-scale motion (60% IM, N-S). The experimental results of the piping subsystem under this excitation were used for validating the analytical OpenSees model. Further information about the loading protocol is provided in Zaghi et al. (2012).

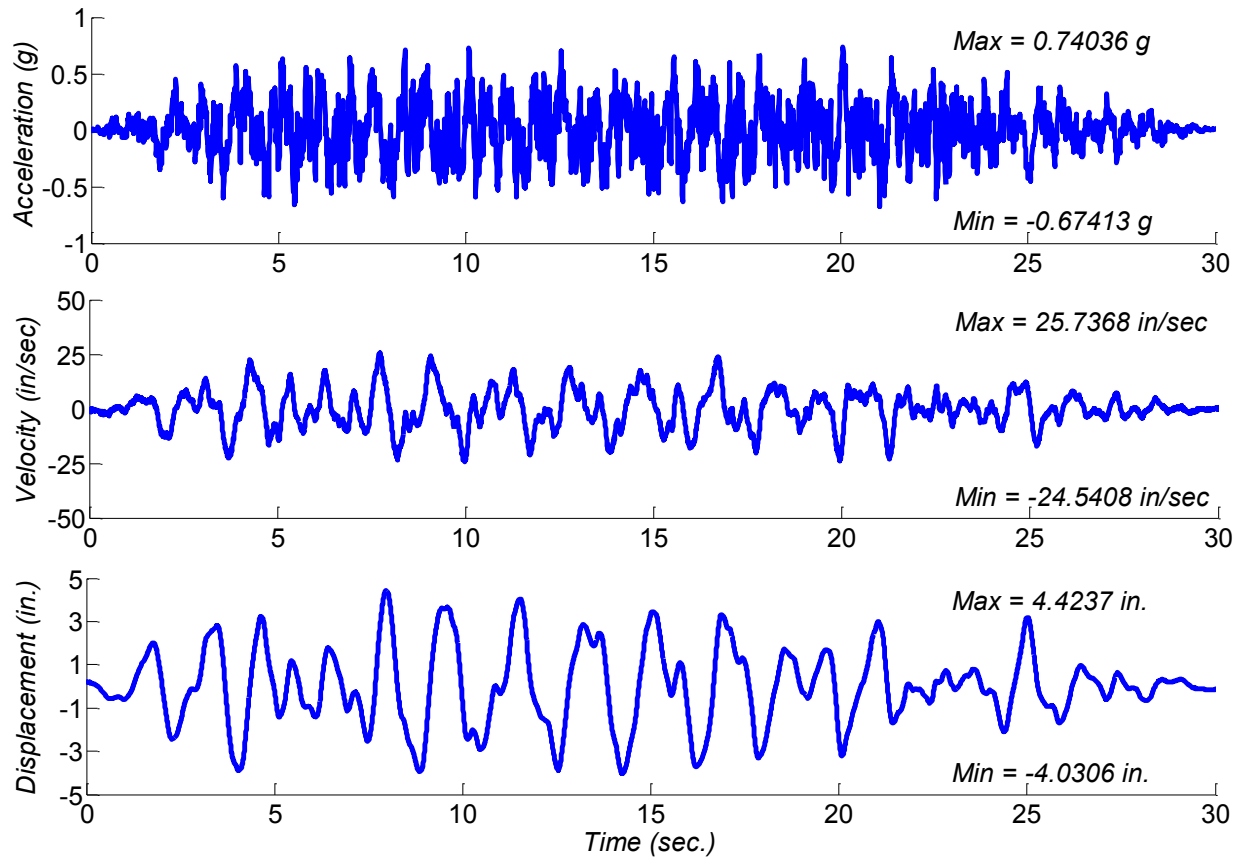


Figure 4-5 Achieved Table Motion on 60% IM in N-S Direction

4.2.4 Generation of the Analytical Model

An analytical model of the piping subassemblies was developed both in SAP2000 v15 and OpenSees v2.4.0. The OpenSees model was the primary model for analysis, comparison with

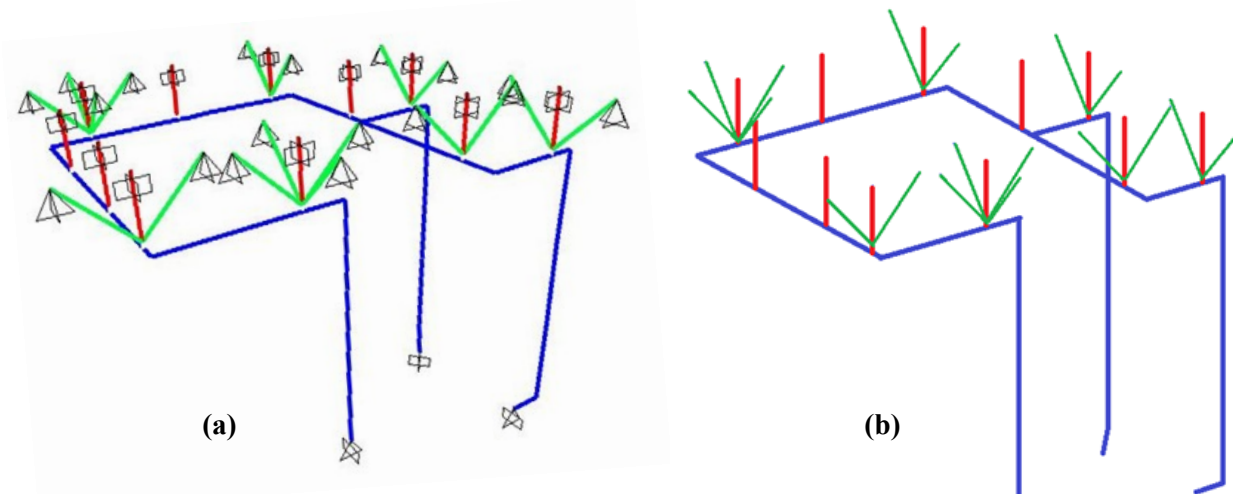


Figure 4-6 Models of the Piping Subassemblies (a) SAP Model (b) OpenSees Model

and calibration of test data, and further investigation. The SAP model — see Figure 4-6(a) — computed nodal gravity load and lumped mass distribution, which was transferred to the OpenSees model. The SAP model verified the static response and modal analysis of the OpenSees model — as illustrated in Figure 4-6 (b).

The model included elements that were presented earlier in this study. A summary of the components used is presented in Table 4-1.

Table 4-1 Summary of Used Components for Analytical Model

	Reference	Material	Section	Element
Pipe Segments	3.5.2	NA	Elastic	Force-Based
Pipe Joints	3.5.2	Pinching4	NA	ZeroLength
Hangers	3.2.4	Steel02	Fiber	Force Based
Cables	3.3.3.3	EPPG	NA	Truss

Throughout the calibration process, 0.008 initial gap strain for the cable bracing gave the best match between the analytical and experimental displacement results. However, this initial strain impacted the acceleration results in the analytical model, which was not observed in experimental results. In order to prevent this phenomenon, a second EPPG material without initial gap strain and with the elastic modulus of approximately 1/27 of cable modulus was added to the cable model in parallel. In order to combine the effect of these two EPPG, the parallel uniaxial material was used. This procedure is presented in Figure 4-7.

The connections of the pipes to the heat exchanger and heaters were assumed rigid in all directions except rotationally about the longitudinal axis. Both ends of the cable braces were modeled using truss elements with a pin connection. A fixed connection was used for the pipe hangers — stationary frame attachment. However, a pin type attachment was used for the connection of pipe hangers to the pipe runs. The main reason for choosing a pin connection was because the hanger clips have negligible rotational resistance. A uniform excitation pattern was used to excite the piping system under the achieved table accelerations. This excitation pattern applies a uniform excitation to the model acting in a certain direction.

Static analysis of the SAP model, which calculated the gravity load, was used to transfer distributed loads to the frame elements and the associated nodal masses into the OpenSees model. The mass of the piping system was determined using the wet weight of the pipes.

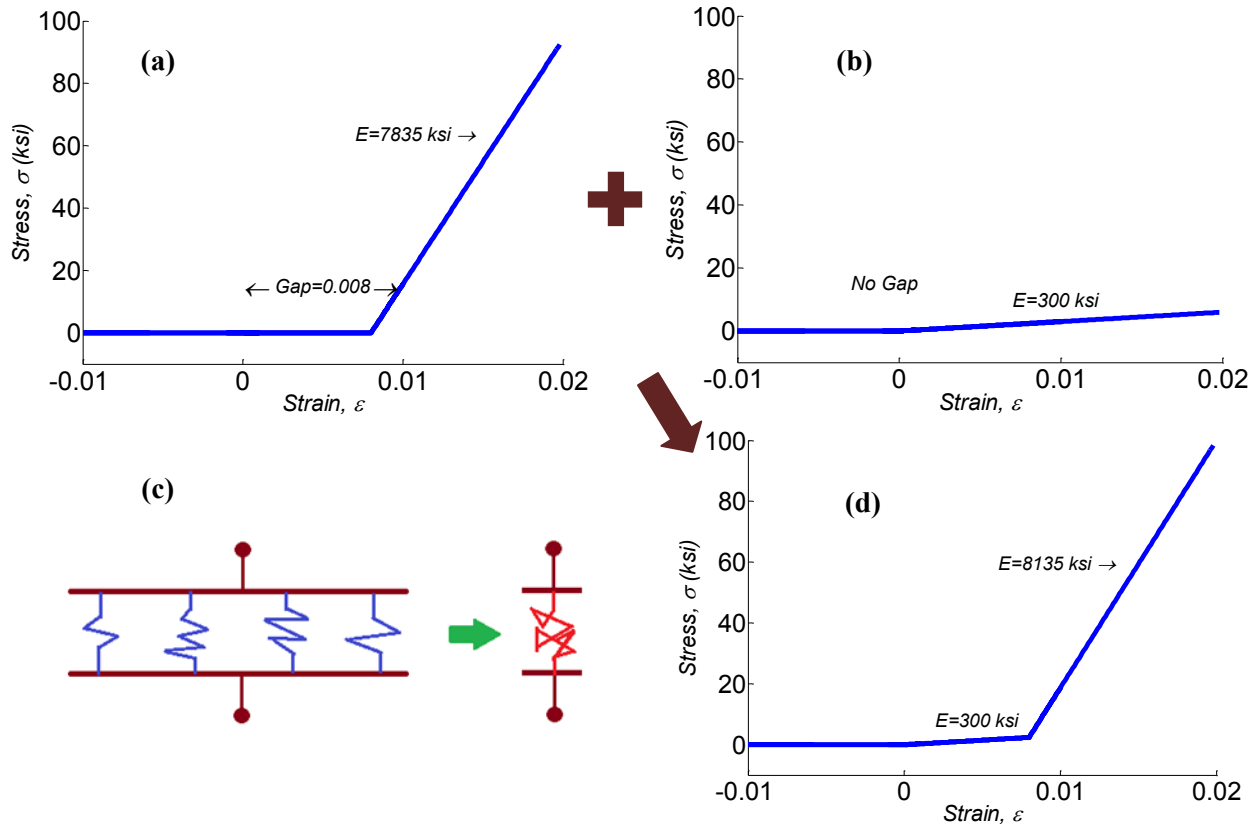


Figure 4-7 (a) First EGGP Material (b) Second EGGP Material (c) Combining Diagram (d) Combined EGGP Material for Cable Bracing

Rayleigh damping, a convenient damping model for applying classical damping, was used to represent energy dissipation in the structure. This damping model is the combination of mass and stiffness proportional components and is a form of classical damping, which means that the damping matrix in modal coordinates is diagonal. As shown by Chopra (2007), the damping matrix for Rayleigh damping can be determined as:

$$[C] = a_M [M] + a_K [K] \quad (4-1)$$

where $[C]$, $[M]$ and $[K]$ are the global damping matrix, mass matrix and stiffness matrix, and a_M and a_K are mass and stiffness proportional constants. The damping ratio ζ_n for the n^{th} mode is:

$$\zeta_n = \frac{a_M}{2} \frac{1}{\omega_n} + \frac{a_K}{2} \omega_n \quad (4-2)$$

where ω_n is angular frequency of n^{th} mode. The constants a_M and a_K can be determined by prescribing the damping ratios ζ_i, ζ_j of 2 different modes, according to:

$$\frac{1}{2} \begin{bmatrix} 1/\omega_i & \omega_i \\ 1/\omega_j & \omega_j \end{bmatrix} \begin{Bmatrix} a_M \\ a_K \end{Bmatrix} = \begin{Bmatrix} \zeta_i \\ \zeta_j \end{Bmatrix} \quad (4-3)$$

A Rayleigh damping of 5% was assigned to the first and third modes piping subassembly.

4.2.5 Experimental-Analytical Result Comparison

Sampling frequency of all channels was 160 Hz. All recorded data presented in the study was low-pass filtered using the 4-pole Butterworth filter with a cutoff frequency of 20 Hz. The low-pass filter “filtered out” or eliminated the high frequency components of the signal while preserving lower frequency components. The filter shape as a function of normalized frequency is shown in Figure 4-8. Afterwards, a polynomial baseline correction was applied, if needed.

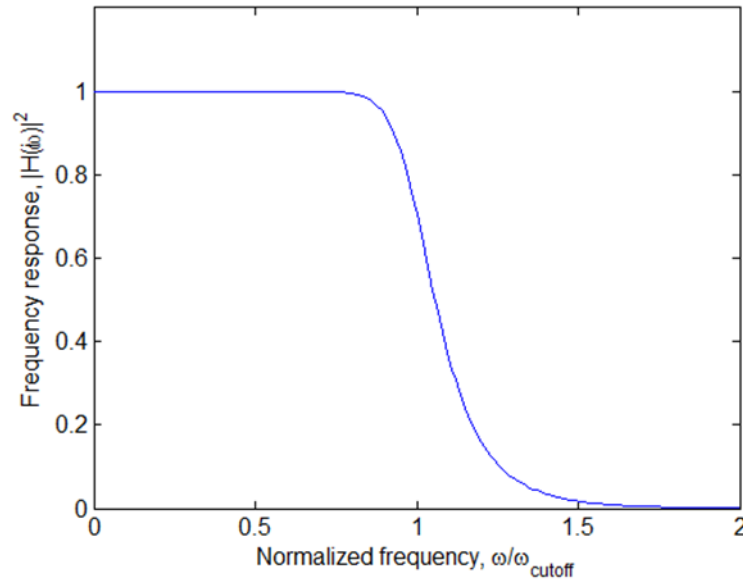


Figure 4-8 Magnitude of Low-Pass Butterworth Filter Transfer Function

The first two vibration periods of the piping subsystem based on experimental data were 0.33 and 0.23 seconds, respectively. The corresponding periods obtained from the analytical model were 0.31 and 0.23 seconds. The mode shapes of these two first modes are presented in Figure 4-9.

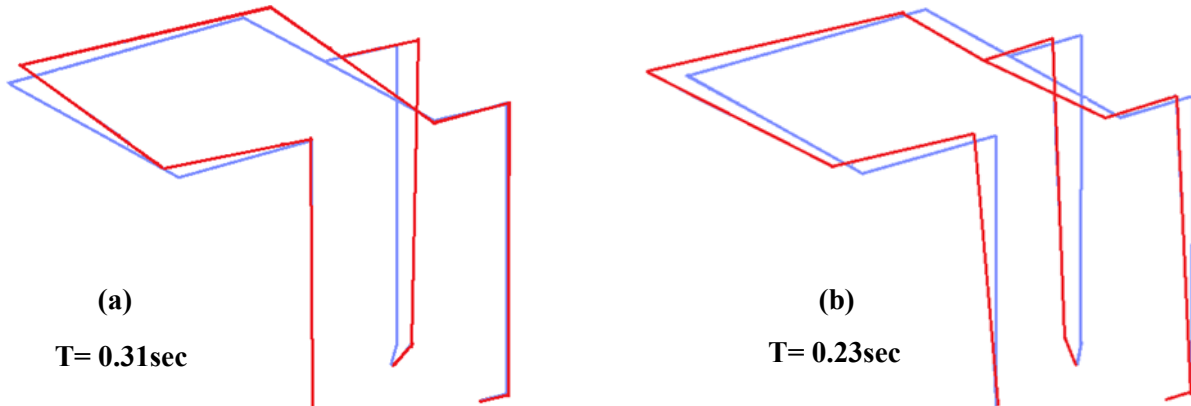


Figure 4-9 The First Two Modes of Piping Subassembly (a) First mode (b) Second mode

The responses of the locations labeled “ Δ_1 ” through “ Δ_4 ” — see (Figure 4-4(a)) — were used to compare the analytical and experimental results of piping displacements in Figure 4-10. Also the 5% damped spectral acceleration of analytical results was compared with the experimental responses at points “ Acc_1 ” and “ Acc_2 ” — see Figure 4-4(b). The comparisons show that the model was able to predict the most detail of the response, including the frequency content of piping responses. However, the general trend shows that the peak displacements estimated from analytical model were slightly smaller than displacements observed from the experiment.

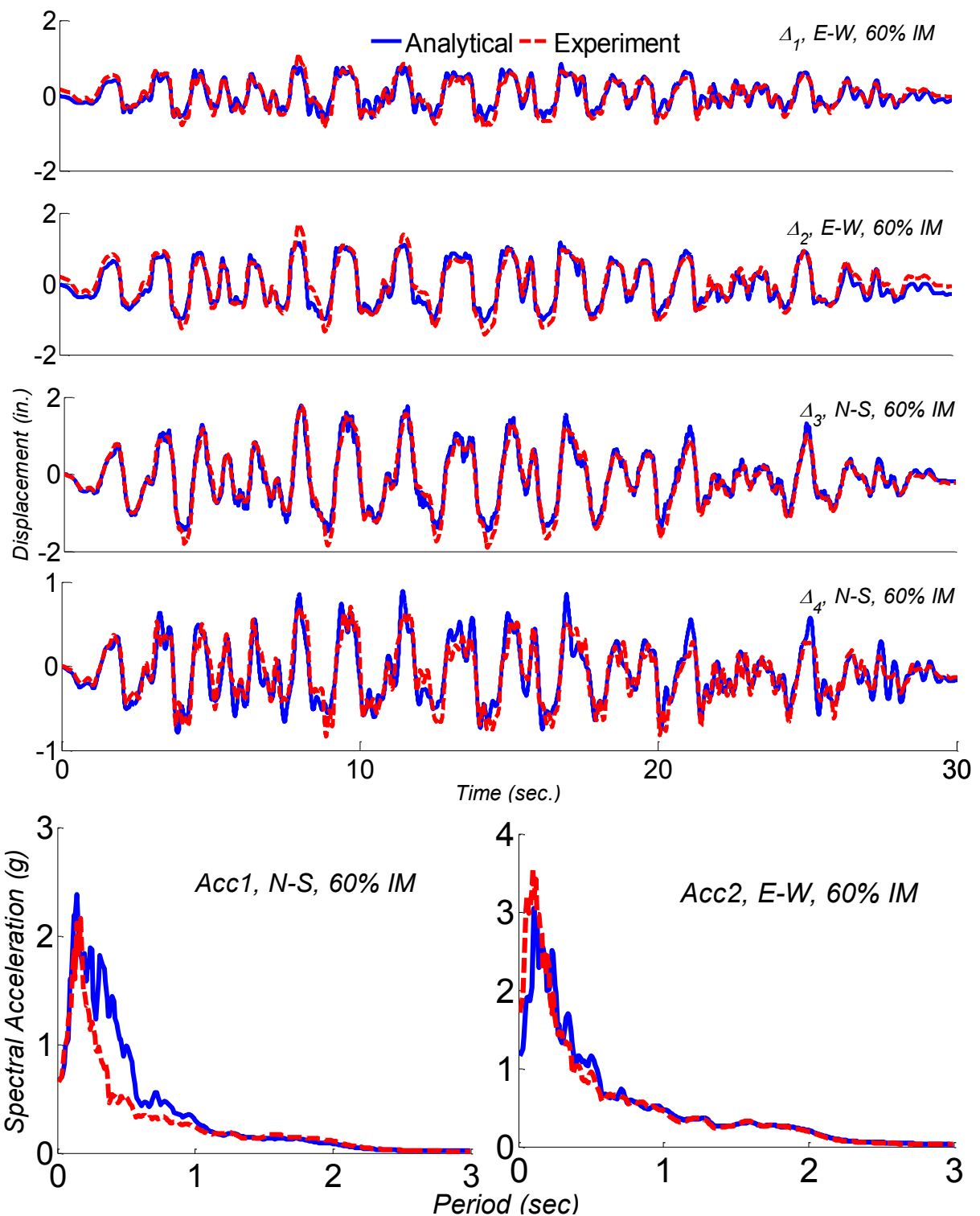


Figure 4-10 Comparison of Experimental and Analytical Results: Displacement History at Locations “ Δ_1 ” through “ Δ_4 ”, 5% Damped Spectral Acceleration at locations “ Acc_1 ” and “ Acc_2 ”

4.3 Hospital Piping Assemblies Tested at University of Nevada, Reno, II

A total of two subassemblies — 1) threaded unbraced and 2) threaded braced — were tested in this testing program. In this study, only the results of latter configuration are presented and used for calibration of the analytical model. A summary of the test setup is presented in this subsection, followed by the comparison of experimental-analytical results.

4.3.1 Test Background

The geometry of the piping assembly was made up of approximately 100 feet of 3-in. and 4-in. diameter Schedule 40 steel pipe, which was the same piping system discussed in the previous subsection. The only difference between these two tests was the experimental test setup, which will be discussed below.

The experimental setup shown in Figure 4-11 was designed to simulate the first floor motions and the third floor motions of a four-story building, which will be described in the following subsections. The first floor motion was used as input for the shake table, whereas the third floor motion was used as input for the horizontal sliding top frame. The sliding frame is supported by the stationary frame, which is anchored at the laboratory floor. Figure 4-12 shows the plan view of the sliding frame with the actuator. The 55-kips, 24-in. stroke, 180-gpm valve actuator was attached to the stationary frame at point A, which served as the reaction frame. The actuator was then attached to the sliding frame at point B in the figure. To ensure smooth sliding between the sliding and stationary frames, Teflon pads glazed with grease were attached at locations where the sliding and stationary frame came into contact. In addition, wheels at four corners shown in Figure 4-13 prevented it from moving sideways. Steel tube braces were provided to keep the sliding frame as rigid as possible (Figure 4-13). This setup, however, limits the amount of story drift that could be applied. With the braced hanger configuration, the sliding frame could only go ± 6 inches due to low clearance between the braces and the top beams of the stationary frame.



Figure 4-11 Experimental Setup

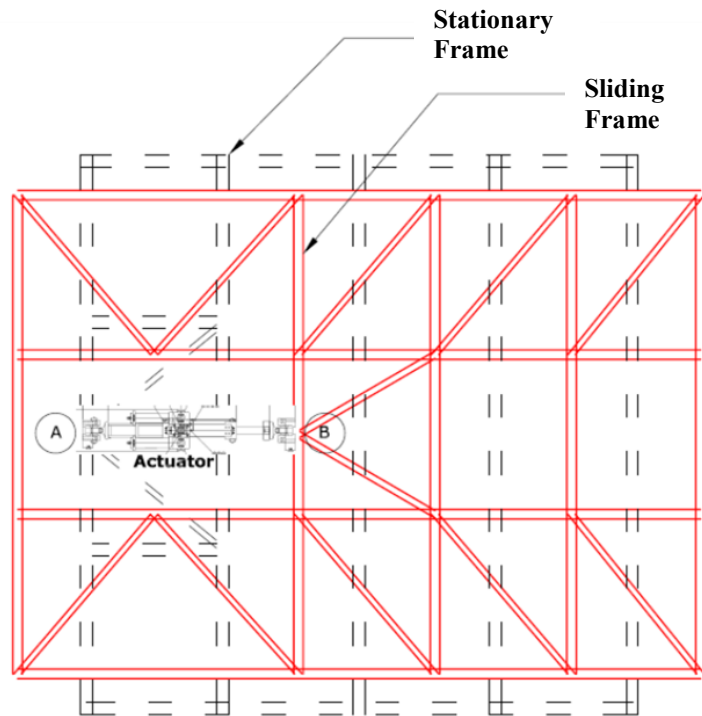


Figure 4-12 Plan View of Horizontal Sliding Top Frame

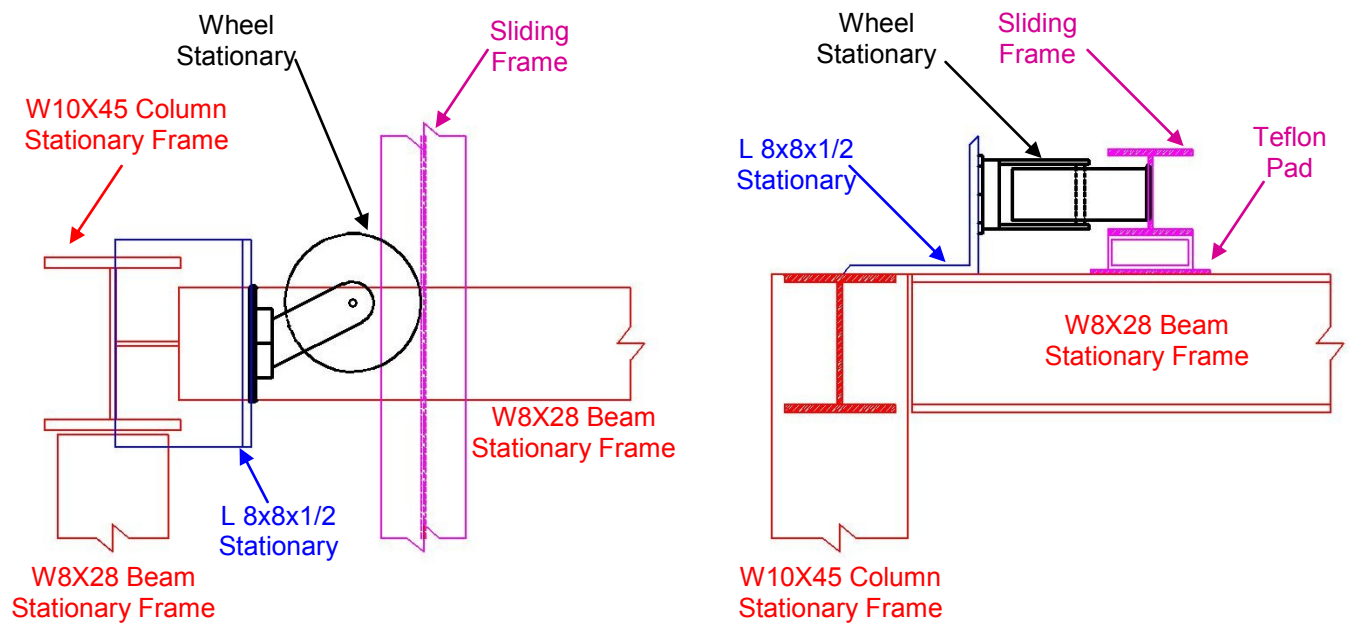


Figure 4-13 Detail at Wheel Locations

4.3.2 Instrumentation Plan

The instrumentation layout shown in Figure 4-14 was designed for the experiment to accurately record the physical response of the system. The instrumentation consisted of 29 unimeasure

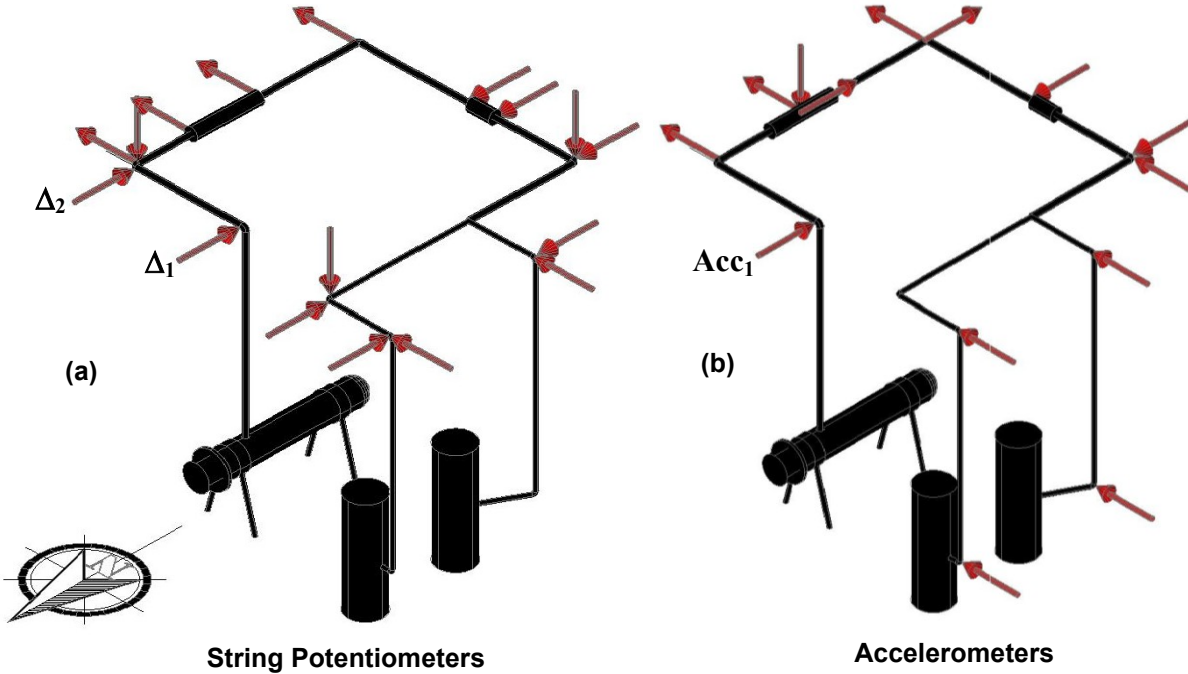


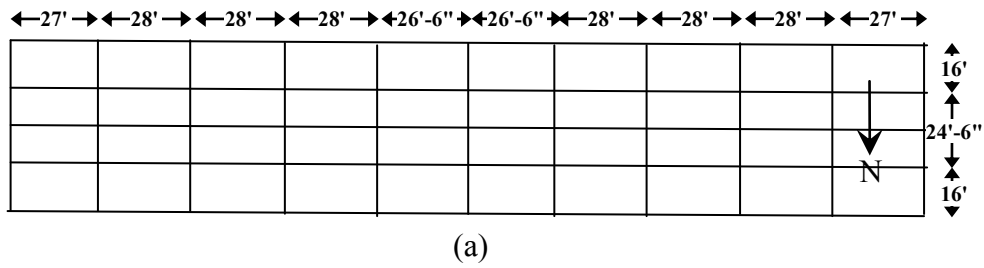
Figure 4-14 Instrumentation View

Stringpot (SP) Celesto Displacement Transducers (+20 inch [+510 mm] stroke) and 16 Crossbow (xbow) Kinematics (+4g) Accelerometers. The displacement transducers were anchored to the stationary frame, which allowed the direct measurements of piping displacements with respect to the stationary frame.

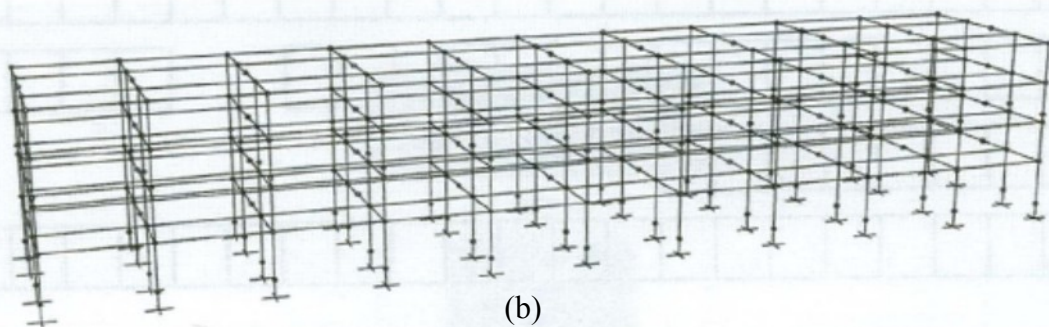
4.3.3 Loading Protocol

The input motions were derived using the simulated ground motions generated by the Specific Barrier Model (Wanitkorkul and Filiatrault, 2005). These synthetic motions were designed specifically to develop analytical and experimental fragility curves for nonstructural components contained in hypothetical hospital sites on the west and east coasts of the United States. The standardized accelerograms were generated for 2% probability of exceedance of the Northridge earthquake in 50 years. For this earthquake event, two acceleration components were simulated – fault-normal and fault-parallel horizontal components. Within these parameters, there were 25 earthquakes all with different peak ground accelerations.

Dynamic analyses were performed using the WC70 model (Astrella and Whittaker, 2005) in conjunction with the above-mentioned Northridge Near-Fault Ground Motions using OpenSees (Mazzoni et al., 2007). The WC70 model, shown in Figure 4-15a and Figure 4-15b, represents a



(a)



(b)

Figure 4-15 (a) Plan View of the WC70 Structure (b) OpenSees Structural Model

typical west coast hospital construction consisting of a four-story steel structure with typical story heights of 12.5 feet. The plan dimensions of this model are equal to 275 feet in the east-west direction and 56.5 feet in the north-south direction.

The relative floor drifts were then calculated from the displacement responses that were recorded at each floor level. The maximum drifts and their corresponding acceleration were then found for the 2% probability of exceedance. Of the two acceleration components that were simulated, fault-normal and fault-parallel, the fault-normal component reported the greatest drifts. The input motion was selected to ensure setup limitations were not exceeded. This includes the capacity of the actuator driving the sliding frame and clearance between the braces and the stationary frame.

Table 4-2 shows the experimental protocol for the piping subassembly. The motions were run in the north-south direction with the braced and unbraced configuration. The experimental protocol started out with 10% of full intensity, then increased to 50% and 100%. In the first set of runs (Runs 1 to 6), the shake table and the sliding top were running in-phase with each other. In the second set of runs (Runs 7 to 12), the shake table and sliding top were running out-of-phase with each other.

Table 4-2 Loading Protocol

Run No.	Shake Table	Sliding Top	Direction	Condition
1	10%	10%	N - S	Braced
2	50%	50%	N - S	Braced
3	100%	100%	N - S	Braced
4	10%	10%	N - S	Unbraced
5	50%	50%	N - S	Unbraced
6	100%	100%	N - S	Unbraced
7	-10%	100%	N - S	Unbraced
8	-50%	100%	N - S	Unbraced
9	-100%	100%	N - S	Unbraced
10	-10%	100%	N - S	Braced
11	-50%	100%	N - S	Braced
12	-100%	100%	N - S	Braced

The story drift that can be applied is limited by the clearances between the braces and stationary frame. To increase the story drifts, the shake table was run out-of-phase with the sliding top as indicated in Runs 7 to 12. For example, in Run 8 (unbraced configuration), the shake table was

running at 10% intensity while the sliding top is running at +100% intensity, which means the shake table is running 10% in the opposite direction as the sliding top.

Figure 4-16 shows a sample of achieved loading histories corresponding to the 50% of full scale motion (50% IM, N-S). These motions were applied only in the north-south direction. The experimental results of the piping subsystem under this excitation were used for validating the analytical OpenSees model.

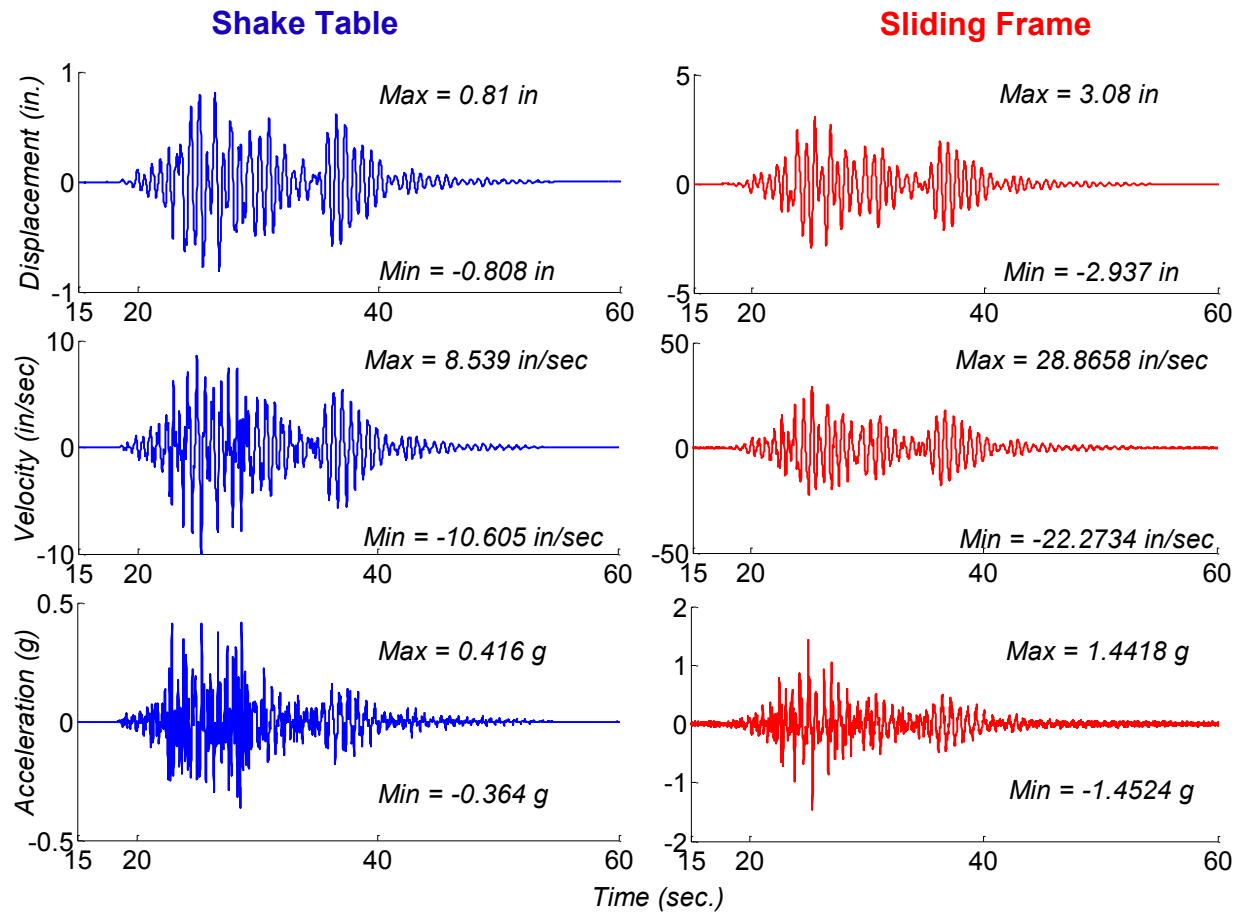


Figure 4-16 Achieved Table-Slider Motion on 50% IM in N-S Direction

4.3.4 Generation of the Analytical Model

The model of the introduced piping subsystem was developed in OpenSees (Mazzoni et al., 2007). The exact same modeling assumptions and techniques were used as those used in Section 4.2.4. However, there are two differences between these two models as follows:

- The achieved table and slider motion was defined as multiple support displacement history in the direction of shaking, while in Section 4.2.4 the table motion was defined as acceleration uniform excitation.
- Throughout the calibration process, 0.001 initial gap strain for the cable bracing gave the best match between the analytical and experimental displacement results. However, the initial gap strain equal to 0.008 was used in Section 4.2.4.

4.3.5 Experimental-Analytical Result Comparison

Sampling frequency of all channels was 128 Hz. All recorded data presented in the study was low pass filtered using the 4-pole Butterworth filter with a cutoff frequency of 20 Hz. The low-pass filter “filtered out” or eliminated the high frequency components of the signal while preserving lower frequency components.

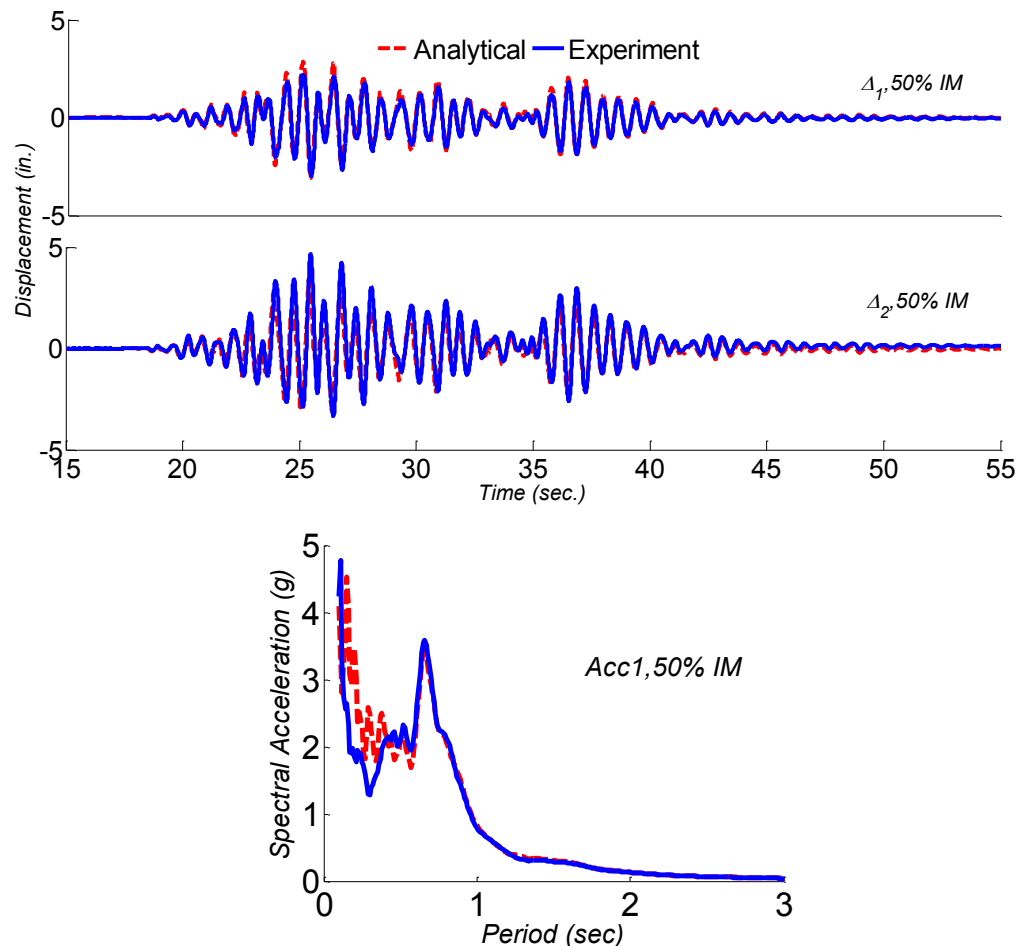


Figure 4-17 Comparison of Experimental and Analytical Results: Displacement History at Locations “ Δ_1 ” and “ Δ_2 ” and 5% Damped Spectral Acceleration at location “ Acc_1 ”

The responses of the locations labeled “ Δ_1 ” and “ Δ_2 ” in Figure 4-17a were used to compare the analytical and experimental results of piping displacements. Also in Figure 4-17b, the 5% damped spectral acceleration of analytical results was compared with the experimental responses at location “Acc₁”. Figure 4-46 through Figure 4-52 compare sample horizontal acceleration responses of the analytical model and test data. The results show that the analytical model was able to predict the frequency content and amplitudes of piping displacements obtained from the experiment. The comparison between the spectral accelerations shows that the analytical model predicted the spectral acceleration achieved from experiment very well.

4.4 Piping Subsystem Tested at University of Buffalo

A total of three different materials and joint arrangements (steel groove fit Schedule 40 and Schedule 10 used for main lines and riser, black iron threaded Schedule 40 and Schedule 10, CPVC cemented joint, and Dynaflow grooved fit used for branch lines) were tested in this experimental phase. In this study, only the results of the subsystem with Schedule 40 grooved fit connections for main lines and risers and Schedule 40 threaded joints for branch lines are presented and used for calibration of the analytical model. These tests were designed and performed at the University at Buffalo, and their outcome can be found in Tian (2012). The following descriptions and experimental observations of these experiments are provided for convenience.

4.4.1 Test Background

A two-story, full-scale sprinkler piping subsystem was tested under dynamic loading using the University at Buffalo Nonstructural Component Simulator (UB-NCS). The UB-NCS is a two-level shake table that simulates the seismic motions of two adjacent floors (Figure 4-18 a). This equipment subjects its content to large magnitudes of acceleration, velocity, and interstory drift. A more detailed description of the UB-NCS can be found in Mosqueda et al. (2008).

The tested piping subsystem consisted of two 30-foot by 11-foot layouts over two adjacent floors. These two floor layouts were connected by a 15-foot-long vertical pipe riser (Figure 4-18 b). To detect leaking, the specimen was filled with water under a typical city pressure of 40 psi. To simulate the interactions between the ceiling system and sprinkler heads, six sprinkler heads were placed in common ceiling tiles made up of acoustic material and gypsum drywall using

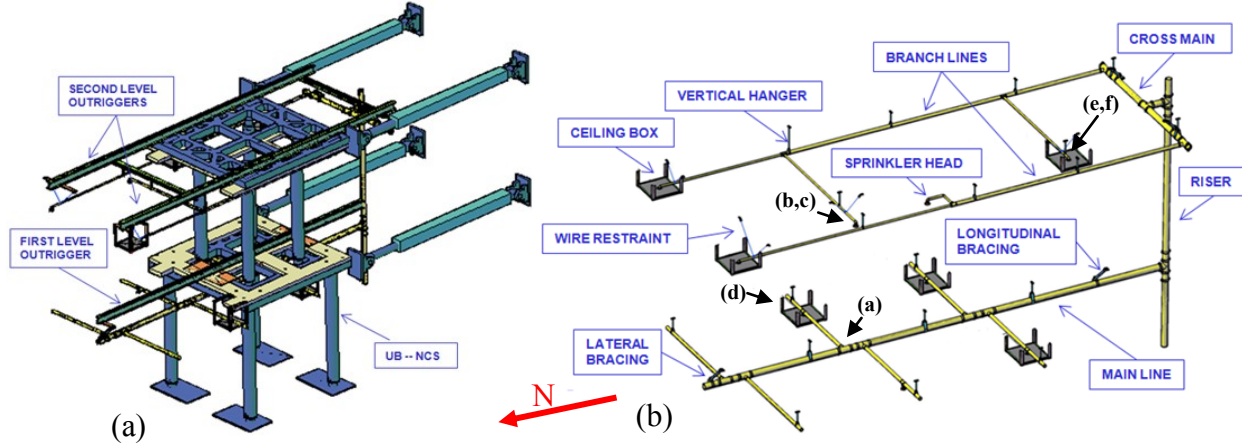


Figure 4-18 Test Set-Up for Sprinkler Piping Subsystem Testing (Tian, 2012)

through-ceiling fittings that were suspended 2 feet above from the UB-NCS deck or outrigger beam (Figure 4-18 b). At the end of the branch lines on the first floor, 0.49lb additional weight was added to replicate the mass of longer branch lines. The piping subsystem was hung from and braced to the UB-NCS per NFPA 13 (NFPA 2011).

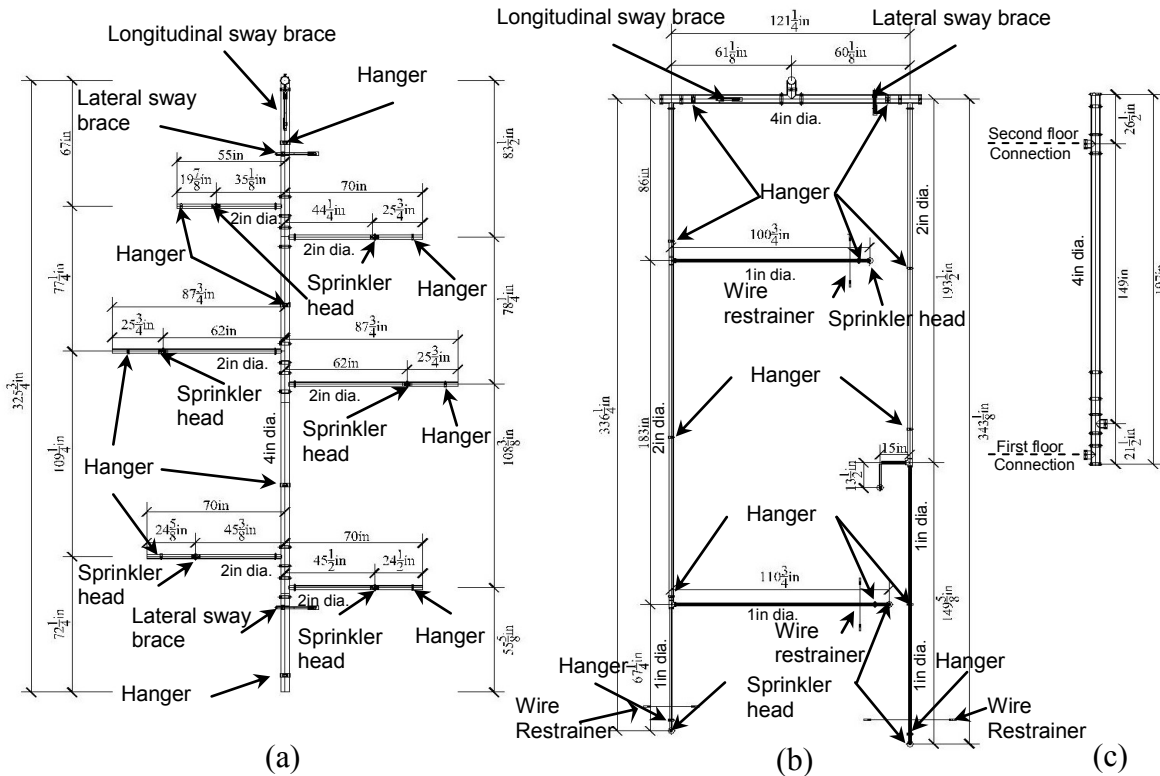


Figure 4-19 Piping System Plan View of (a) the First Floor (b) the Second Floor (c) and the Elevation View of the Riser Pipe (Tian, 2012).

The layout of the piping system, location of hangers and braces, and diameter of the pipes are shown in Figure 4-19 for both floors. The piping subsystem included 4-inch diameter pipes for the riser and the main runs, 2-inch diameter branch lines on the first floor, and 2-inch and 1-inch diameter branch lines on the second floor. The connections on the riser and the main runs were groove fit, but the rest of the fittings were threaded joints. On the first floor, the piping system was supported by vertical pipe hangers at 11 locations — five main runs and six branch lines. On the second floor, 12 hangers were used — two main runs and 10 branch lines. The hangers consisted of 3/8-inch, 22-inch and 24-inch long threaded rods on the first and second floors, respectively. Sway bracing was provided on the main run of pipe near the riser using 1-inch diameter pipes in both longitudinal and lateral directions. At the end of the main run of pipe on the first floor, a lateral brace was installed using the same 1-inch diameter brace pipe (Figure 4-19). On the second floor, the ends of the branch lines were restrained with two diagonal 12-gauge splay wires; however, no end braces were utilized on the branches of the first floor.

4.4.2 Instrumentation Plan

Data collected from the experiments consisted of displacements of the piping subsystem measured relative to the reaction wall, rotations at critical tee joints, accelerations of the sprinkler heads and critical pipe locations, and the axial forces of vertical hangers and wire restraints. A total number of 33 accelerometers, 46 displacement transducers, 31 load cells, and nine string pots were used to measure the detailed responses of piping subsystem. A detailed instrumentation set up is reported in Tian (2012).

4.4.3 Loading Protocol

The loading history protocols used in this experiment were developed specifically for the qualification of nonstructural systems (Retamales et al., 2011). The unidirectional motions were applied in the north-south direction (see Figure 4-18). Figure 4-20 shows a sample of loading histories corresponding to the Maximum Considered Earthquake (MCE). Under these experiments, the experimental results of the piping subsystem were used to validate the analytical OpenSees model. Further information about the test setup and loading protocol is provided in Tian et al. (2012b).

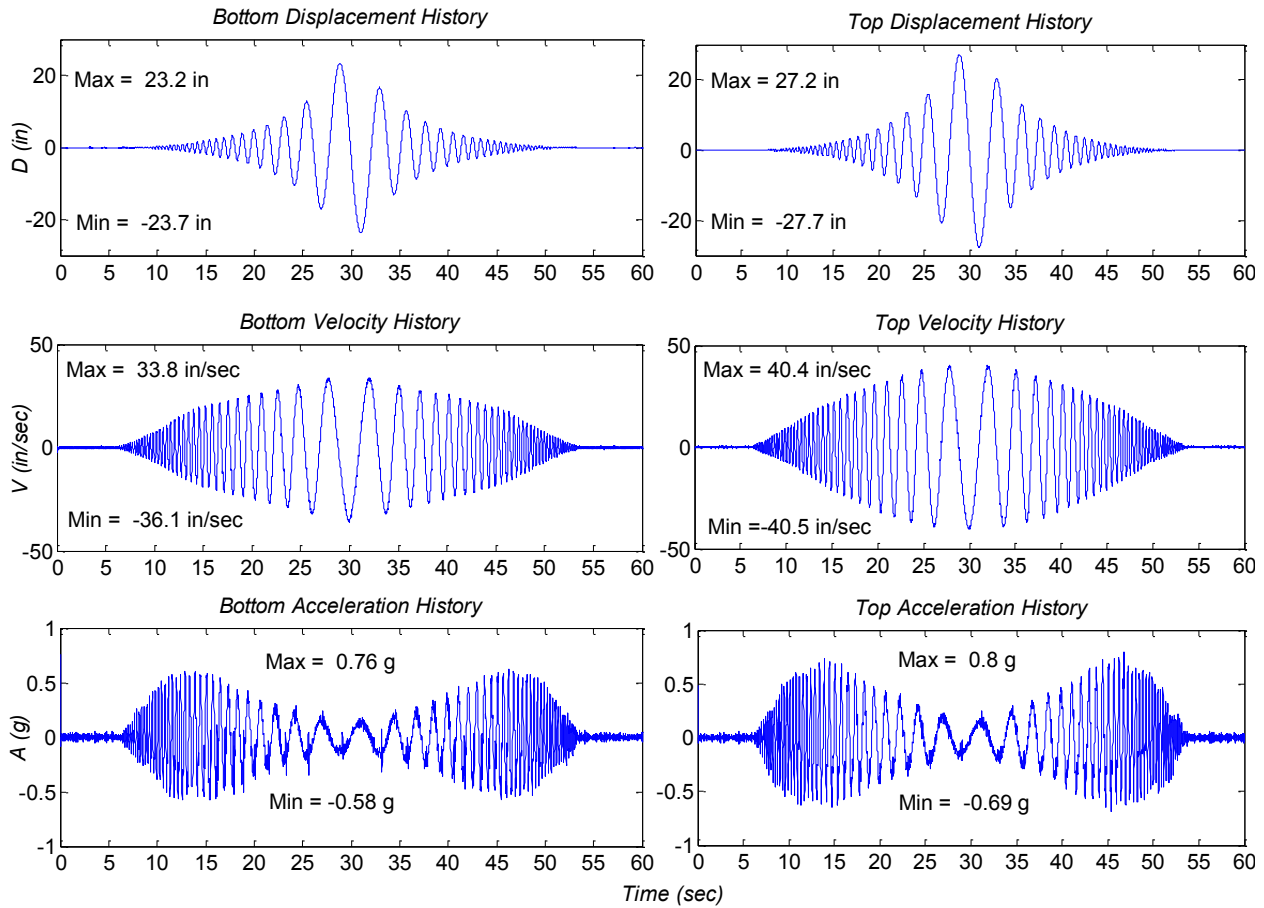


Figure 4-20 Sample of Achieved, Displacement, Velocity, and Acceleration Histories at Maximum Considered Earthquake (MCE) Level

4.4.4 Generation of the Analytical Model

An analytical model of the piping subsystem was developed both in SAP2000 v15 and OpenSees v2.4.0. The OpenSees model was the primary model for analysis, comparison, and calibration of test data, and further investigation. The SAP model (Figure 4-21a) was used to compute nodal gravity load and lumped mass distribution for the OpenSees model. The SAP model also verified the static response and modal analysis of the OpenSees model (Figure 4-21b).

The model was composed of elements that were presented earlier in this study. However, a summary of components used is presented in Table 4-3. Pin type connections were used for both ends of the wire, as they were modeled using truss elements. Fixed connections were used for the pipe hangers-UB NCS machine attachment. However, pin attachments were used for the connection of pipe hangers to the pipe runs. The main reason for choosing a pin connection was because the hanger clips have negligible rotational resistance. The connection of the seismic

braces was assumed to be rigid at both ends. The achieved actuator displacements for the first and second floor were defined as multiple support displacement history in the direction of shaking. This excitation pattern allowed the application of a multiple support excitation to the model acting in a certain direction.

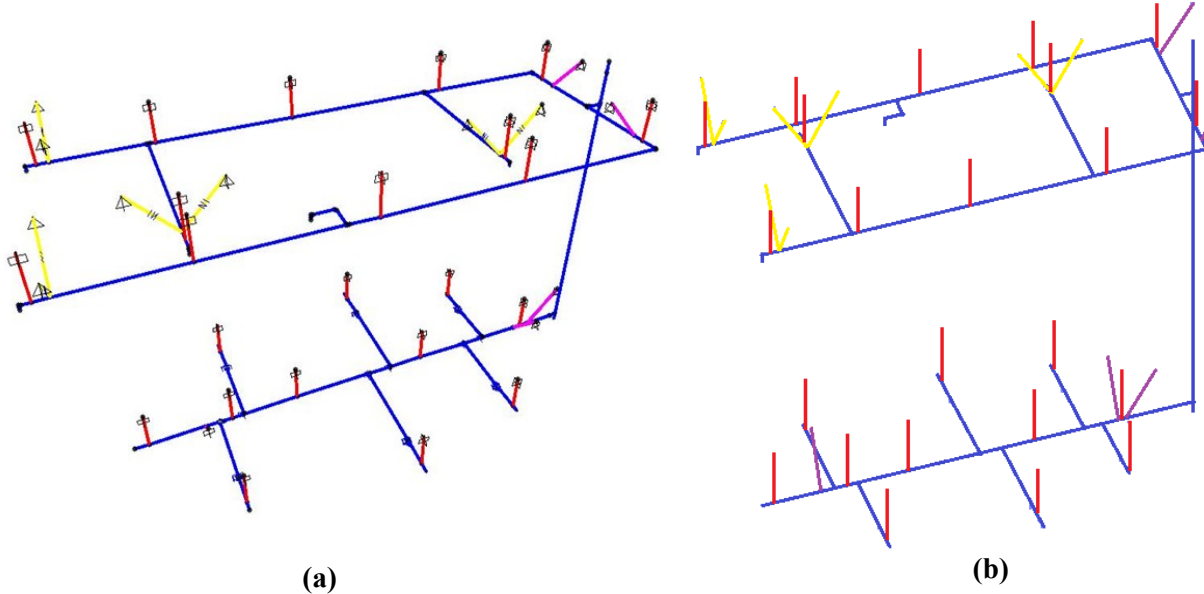


Figure 4-21 Models of the Piping Subsystem (a) SAP Model (b) OpenSees Model

Table 4-3 Summary of Used Components for Analytical Model

	Reference	Material	Section	Element
Pipe Segments	3.5.2	NA	Elastic	Force-Based
Pipe Joints	3.5.2	Pinching4	NA	ZeroLength
Hangers	3.2.4	Steel02	Fiber	Force Based
Solid Braces	3.3.2.1	NA	Elastic	Force-Based
Restrainers	3.4.4	EPPG	NA	Truss

The static analysis of the SAP model, which calculated the gravity load, was used to compute distributed loads to the frame elements and associated nodal masses for the OpenSees model. The mass of the piping system was determined using the wet weight (steel and water weight) of the pipes. An additional mass of 0.2 pounds was used for each sprinkler head. A classical Rayleigh damping was used for accounting the inherent damping of the piping system.

4.4.5 Experimental-Analytical Result Comparison

The sampling frequency of all channels was 128 Hz. All recorded data presented was low pass filtered using the 4-pole Butterworth filter with a cutoff frequency of 20 Hz. Based on experimental data, the first three vibration periods of the piping subsystem were 0.58, 0.53, and 0.46 seconds. The corresponding periods obtained from the analytical model were 0.58, 0.55, and 0.42 seconds. As mentioned in Gupta and Ju (2011), a fire sprinkler piping system has many localized modes instead of a few fundamental modes like buildings and bridges. In other words, the fundamental mode shape of the piping system does not excite the entire piping system, but instead a localized region. The first mode shape of the piping subsystem is shown in Figure 4-22.

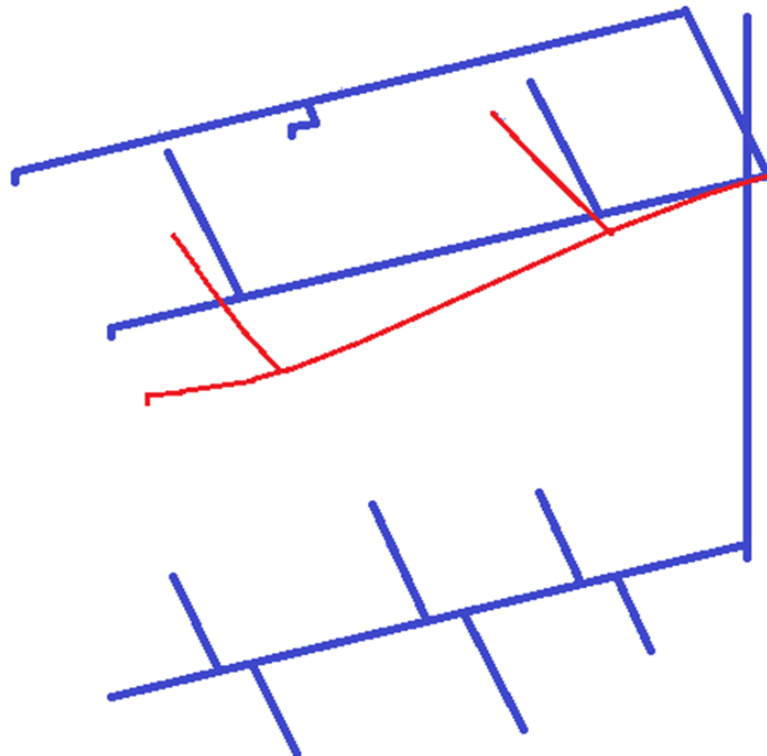


Figure 4-22 The First Local Mode of Piping Subsystem

The responses of the elements labeled “a” through “f” in Figure 4-18 were used to compare the analytical and experimental results. Figure 4-23 compares the results obtained from the experiment and the analytical model. These plots show that the analytical model predicted the joint rotation and pipe displacement very well. The results show that the model cannot predict

every detail of the acceleration and force responses, but it can predict the trend of response very well. The model captured the range of axial forces in pipe hangers, but it was not able to capture the experimental response trend.

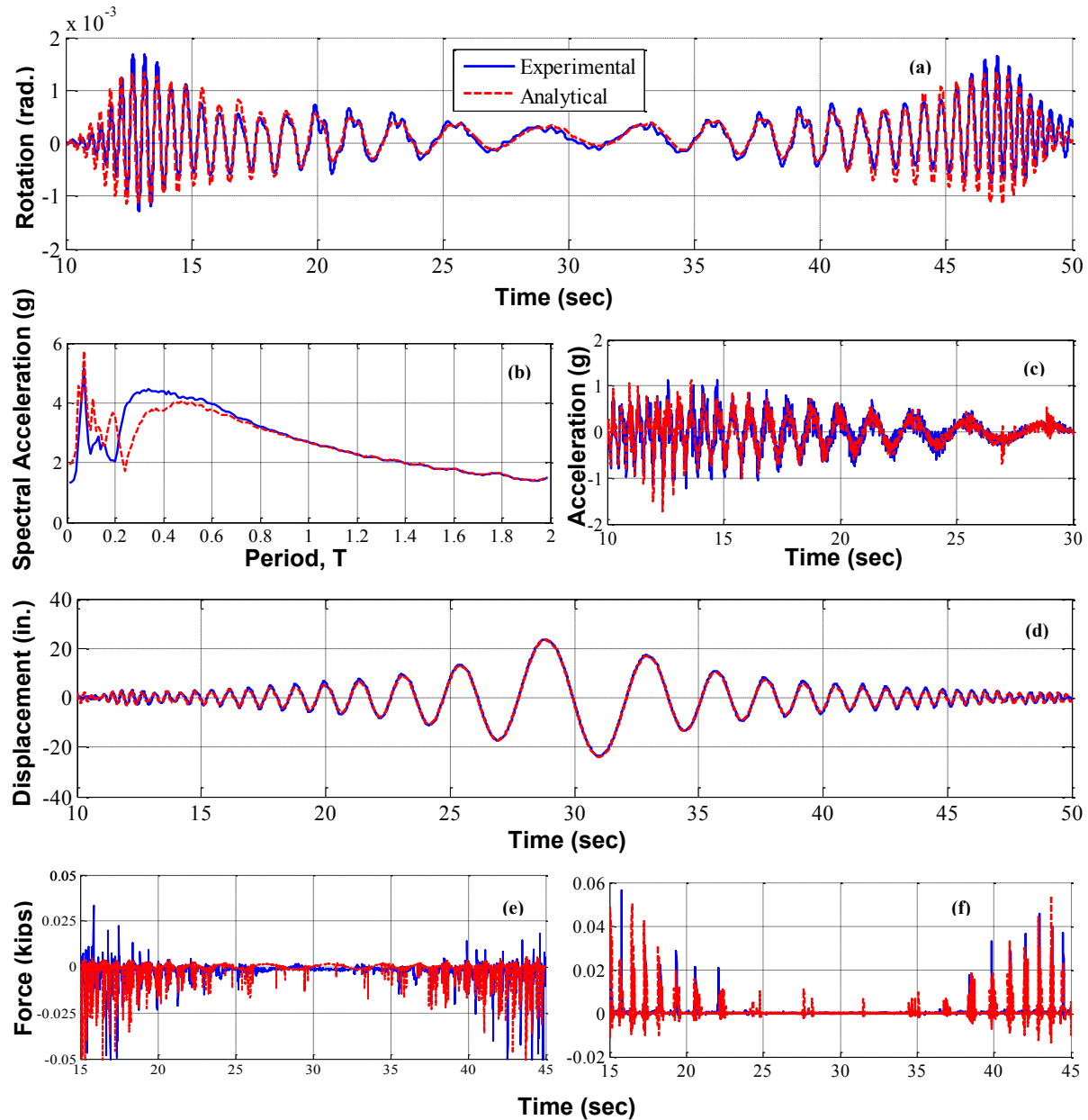


Figure 4-23 Comparison of Experimental and Analytical Results: a) Tee Joint Rotation History at Location “a”, b) 5% Damped Spectral Acceleration at the Tip of the Branch Line Labeled “b”, c) Acceleration History at the Tip of the Branch Line Labeled “c”, d) Absolute Displacement History at the Tip of the Branch Line Labeled “d”, e), f) Axial Force in the Hanger Labeled “e”, and f) Axial Force at the Wire Restrainer Labeled “f”

4.5 Piping System at Full Scale 5-Story Building at E-Defense Experiment

As part of a collaboration between the Network for Earthquake Engineering Simulation-Grand Challenge project (“NEES-GC: Simulation of the Seismic Performance of Nonstructural System”) and the National Research Institute for Earth Science and Disaster Prevention (NIED) of Japan, a series of system-level, full-scale experiments — including partitions-ceilings-sprinkler piping systems — were conducted at the Hyogo Earthquake Engineering Research Center, also known as E-Defense, of the NIED agency. In this study, only the results of the fire sprinkler piping subsystem were used to calibrate the analytical model. This piping system was installed in a full-scale building that was tested in three different configurations: 1) base isolated with triple pendulum (TP) bearings; 2) base isolated with a combination of lead-rubber bearings and cross linear (LR/CL) bearings; and 3) base fixed.

4.5.1 Test Background

Nonstructural elements were installed in a five-story steel moment frame building (Figure 4-24) that was tested for the NEES TIPS/E-Defense project. The building was approximately 53 feet tall and asymmetric in plan with dimensions measuring 33 feet by 40 feet (2 bays by 2 bays — see Figure 4-24). Further information about the building is provided in Dao (2012).

The building weighed approximately 1070 kips. A 124 kips steel mass was added on the east side and middle of the roof to represent a penthouse and to intentionally introduce eccentricity in mass. The fundamental period and damping ratio of the building, determined from system identification based on a white noise signal, were 0.65 sec and 3.3% in the North-South direction, and 0.68 sec and 2.5% in the East-West direction (Dao, 2012).

Two isolation systems were considered and designed in addition to the base fixed configuration in this experiment. The first isolation system incorporated nine identical TP bearings, one beneath each column, which were manufactured by Earthquake Protection Systems. The second isolation system incorporated 4 LR bearings manufactured by Dynamic Isolation Systems and 5 CL bearings manufactured by THK according to design specified by Aseismic Devices Company (ADC). Additional details of the isolation design are provided in Dao (2012) and Ryan et al. (2012).

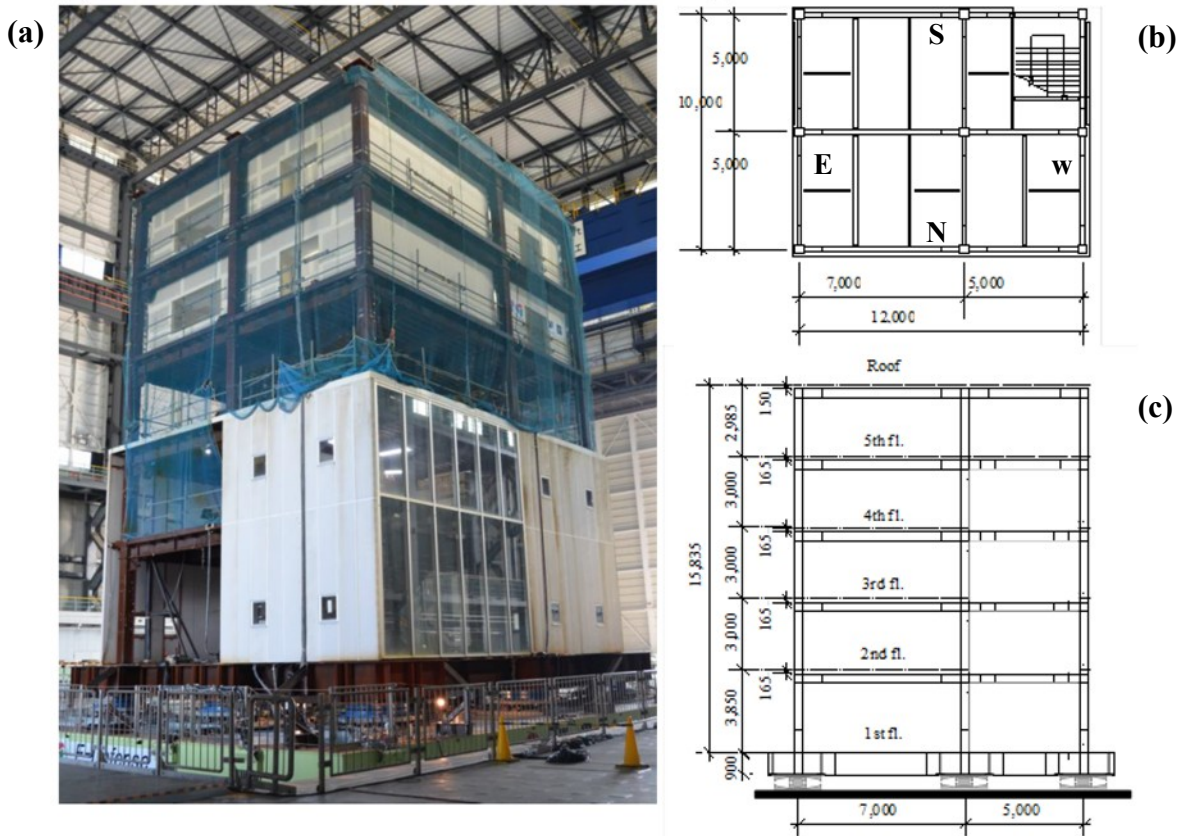


Figure 4-24 (a) 5-Story Steel Moment Frame Specimen Set on Triple Pendulum Isolators (b) Plan View (c) Elevation View

A Ceiling-Partition-Sprinkler Piping (CPP) subassembly was designed and installed in nearly identical configuration over two complete floors of the building specimen. These components were installed on the fourth and fifth floors, which were expected to draw the maximum floor accelerations (Figure 4-25).

In this experiment, the piping system installed in both floors was designed to be exactly the same in order to investigate the performance of two different ceilings interacting with the same piping geometry and detail. However, the piping system was designed to include as many variables as possible that could be studied in this experiment. In general, the piping system variables that were intended to be compared were the armover versus straight-drop branch lines, the “No Gap” versus 2-inch oversized ceiling hole around sprinkler heads, and flex hose versus conventional drop pipes.

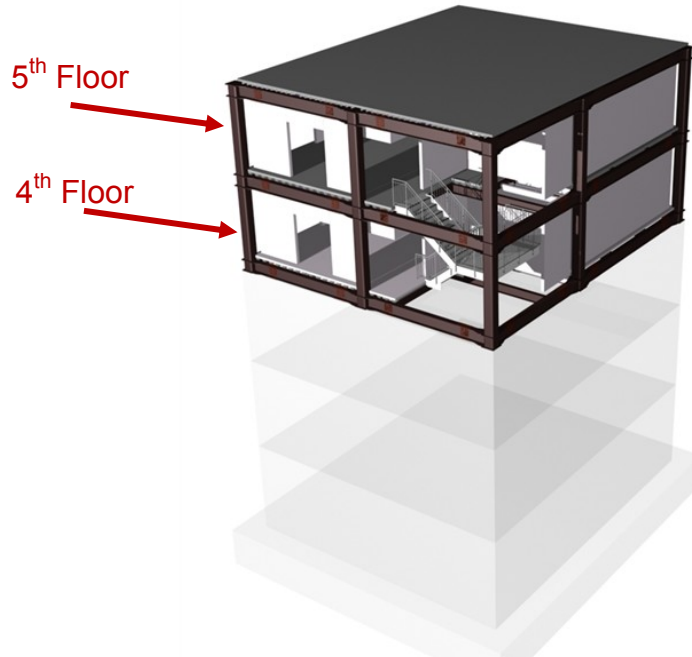


Figure 4-25 Schematic of Test Building along with the Installed Nonstructural Floors

A standard Schedule 40 piping system was attached to the specimen per NFPA 13 (NFPA13, 2011). The piping system included one 3-inch diameter riser pipe, one 2.5-inch diameter main run and three (north-south) 1.25-1 in diameter branch lines (Figure 4-26).

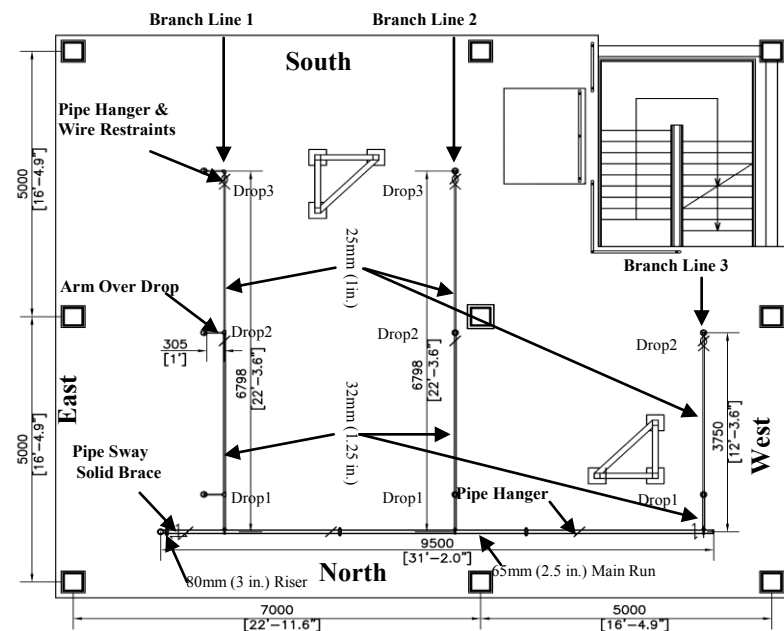


Figure 4-26 Overall Plan View of Piping System

All connections on the riser, the main run, and the branch line to the main-run intersections were grooved fit, while the rest of the connections were threaded (Figure 4-27). Branch Lines 1 and 2, each with three 12-inch drops, incorporated armover drops and straight drops, respectively.

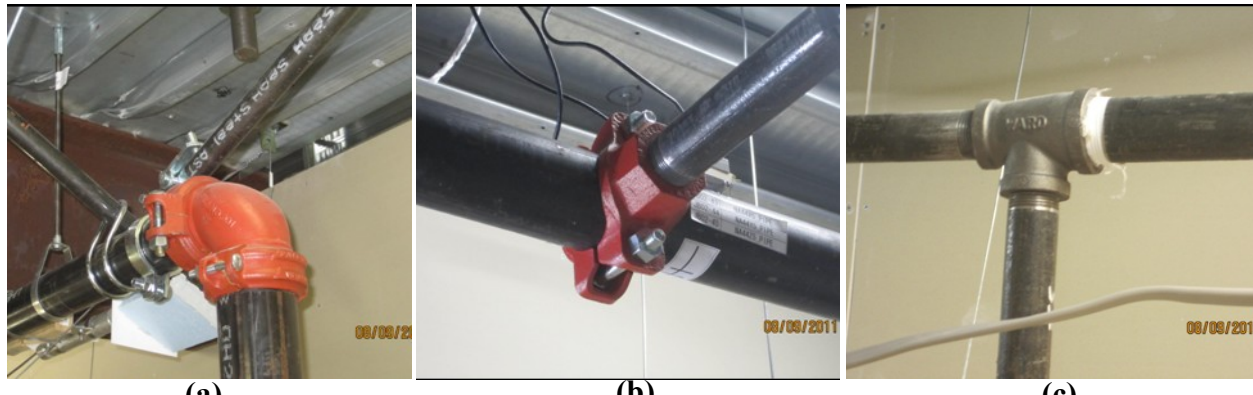


Figure 4-27 Pipe Connections (a) Riser-Main Run Grooved Fit Connection (b) Main Run- Branch Line Grooved Fit Connection (c) Branch Line Threaded Connection

The piping system was supported by vertical pipe hangers at nine locations — four for the main run and five for the branch lines on each floor. The hangers consisted of 3/8-in. diameter, 18-in. long all-threaded rods. Surge clips were used at the hangers that were near the sprinkler heads (branch lines) to prevent the vertical movement of sprinkler heads (See Figure 4-28 a-e).

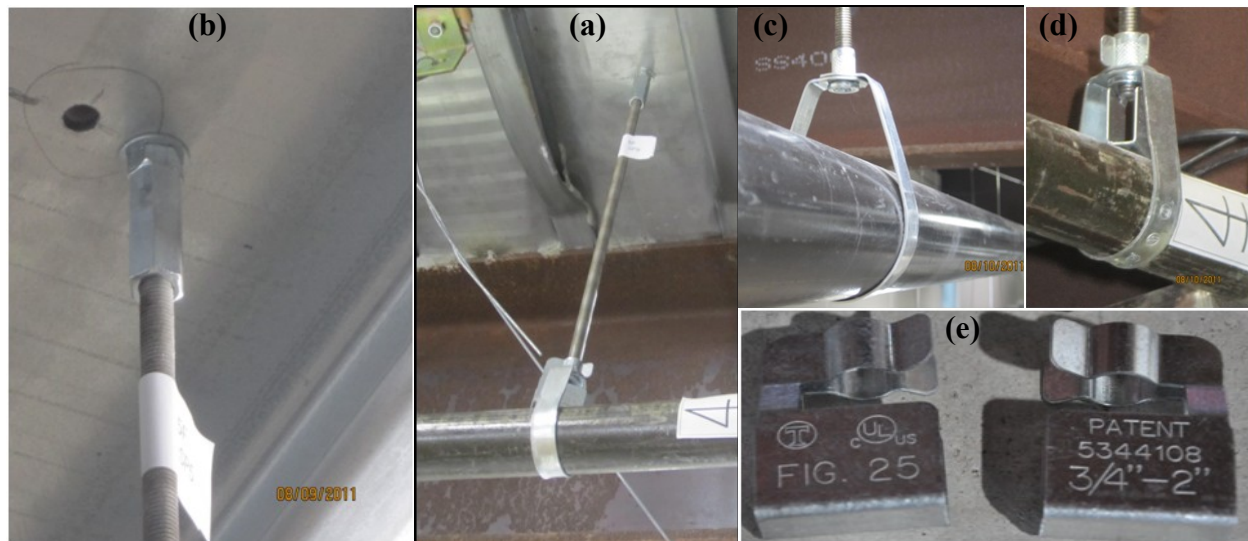


Figure 4-28 Pipe hanger and (b) Top Connection (c)Main Run Bottom Connection (d) Branch Line bottom Connection (e) Surge Clips

At the first drop of each branch line, a 2-in. oversized ring was used at the location of the sprinkler heads (oversized gap configuration, Figure 4-29a), while only minimal gap was provided for the rest of the drops (no gap configuration, Figure 4-29b). A Victaulic Aquaflex Flexible drop was used at Drop 2 of Branch Line 3 (Figure 4-29c).

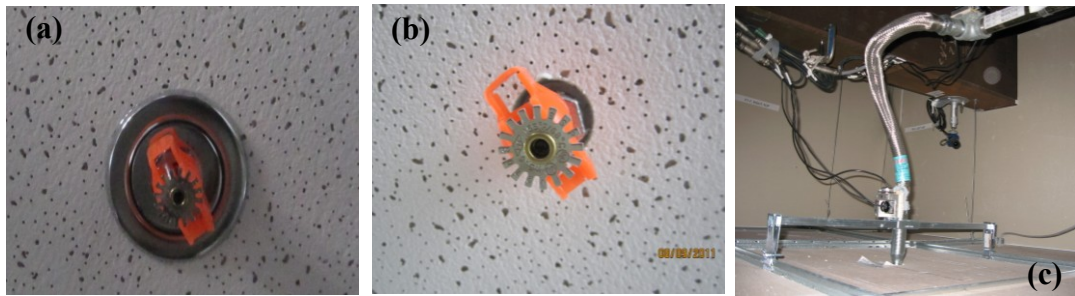


Figure 4-29 Sprinkler Heads and Drops: (a) 2 in. Oversized Gap Configuration, (b) No Gap Configuration, and (c) Flexible Drop

Lateral resistance was provided by inclined 1-inch diameter longitudinal and lateral pipe sway braces on the main run near the riser pipe (Figure 4-30a) and a lateral pipe sway brace at the end of the main run (Figure 4-30b). As the riser pipe was not continued down to the shake tables (it stopped at fourth floor), two longitudinal braces at the end of the riser pipe were used to simulate the realistic boundary condition. These braces forced the riser pipe to experience differential movement imposed by structural story drift (Figure 4-30c).

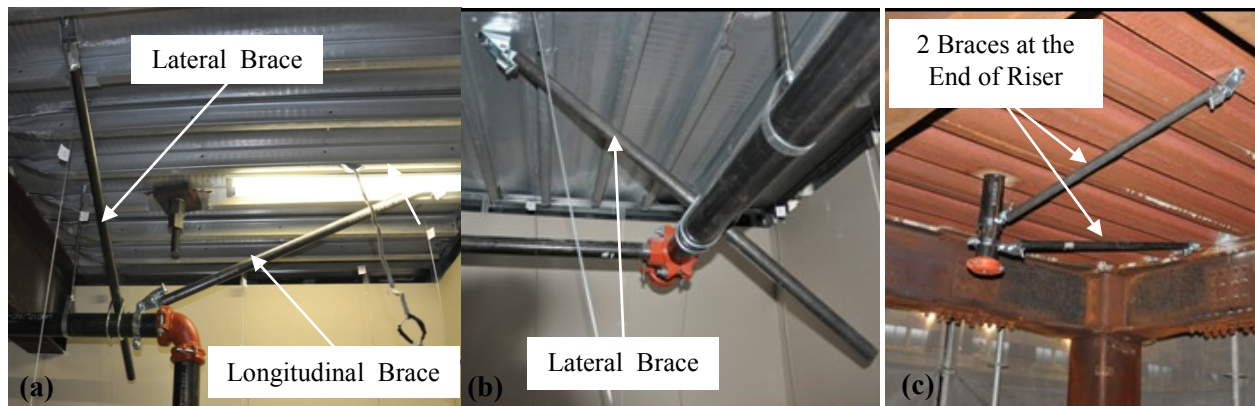


Figure 4-30 (a) Lateral and Longitudinal Brace Near Riser (b) Lateral Brace at the End of Main Run (c) Two Longitudinal Braces at the End of Riser on Fourth Floor

The ends of the branch lines were restrained with two diagonal splay wires to limit the lateral movement (Figure 4-31a). These wires were attached to the deck through steel angle and 3/8-

inch diameter Hilti KB-TZ expansion bolts. In some locations, steel angles were welded to the structural girders in order to provide a maximum 45-degree angle of wire direction relative to the horizontal piping plane.

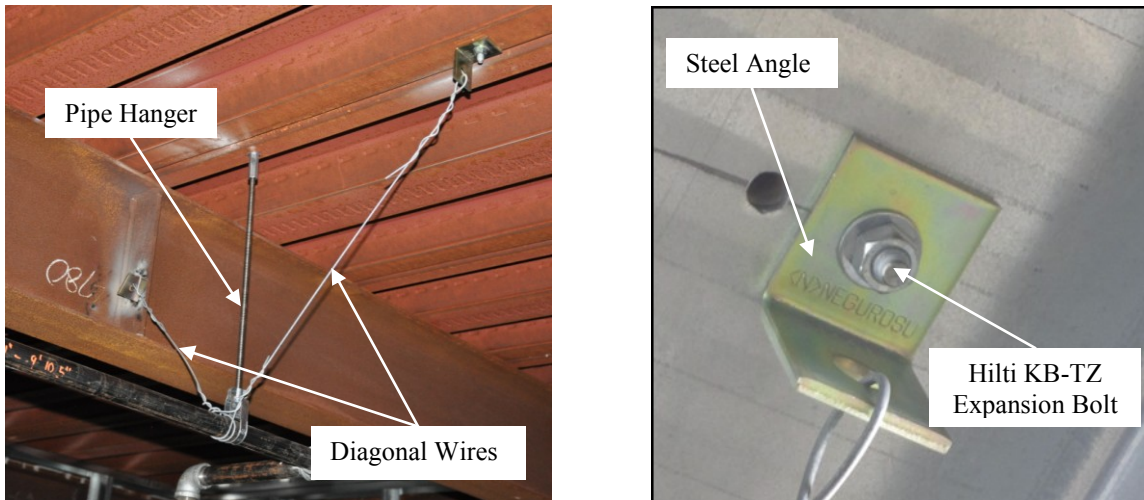


Figure 4-31 Wire Restrainers and the Top Connection Detail

4.6 Instrumentation

A maximum 615 sensor channels were used for measuring the table motion and the responses of structural and nonstructural components. Sampling frequency of all channels was 1000 Hz. Unless otherwise noted, all recorded data presented in the study was low pass filtered using the 4-pole Butterworth filter with a cutoff frequency of 25 Hz. The low-pass filter “filtered out” or eliminated the high-frequency components of the signal while preserving lower frequency components, including the dominant isolation frequency.

4.6.1 Structural Instrumentation

As mentioned, the number of used sensor channels was changed in each isolation and fixed-base system because of different structure-table connection details. In this report, the detailed instrumentation of isolators will not be provided. The detailed instrumentation for the TPB isolators can be found in Dao and Ryan (2012) and for LRB/CLB in Ryan et al. (2012). However, the summary of structure instrumentation is provided below.

4.6.1.1 Displacement Transducers

Laser displacement transducers were used for measuring story drift. Each sensor was attached to a truss built on the concrete mass block on the bottom floor, and its reflecting plate was attached to the top floor as shown in Figure 4-32. A pair of transducers measures the relative displacement between the two floors in each direction at two locations (Figure 4-33). Using a rigid floor diaphragm assumption, three unparallel displacement transducers are needed for



Figure 4-32 Instrumentation for Measuring Story Drift

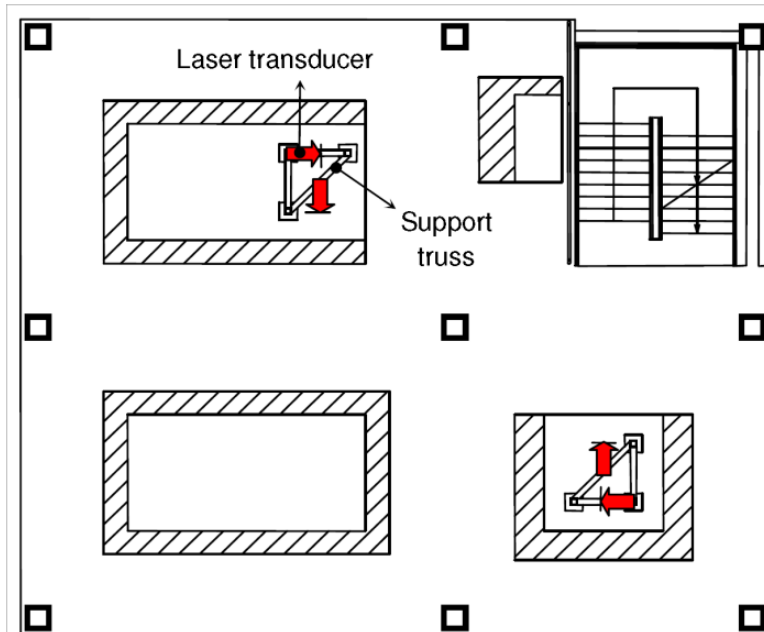


Figure 4-33 Layout of Displacement Transducers to Measure Story Drift in 2nd to 5th Stories

determining relative displacement between the adjacent floors. An additional displacement transducer was placed at each story for redundancy. The layout of the four displacement transducers was added at the second through fifth stories, consistent with Figure 4-33. At the first story, the four displacement transducers were installed at the southeast and northwest columns.

4.6.1.2 Accelerometers

Floor accelerations (2 horizontal and vertical components) were measured using 3 triaxial accelerometers installed at the SE, NE and NW corners of every floor. These triaxial accelerometers were attached to the column face just above the floor slab. Vertical accelerations at other locations on the floor slab were also recorded. Figure 4-34 shows the layout of accelerometers on the 5th floor, which was a typical layout for all floors. The vertical accelerometers were attached to the bottoms of the slabs.

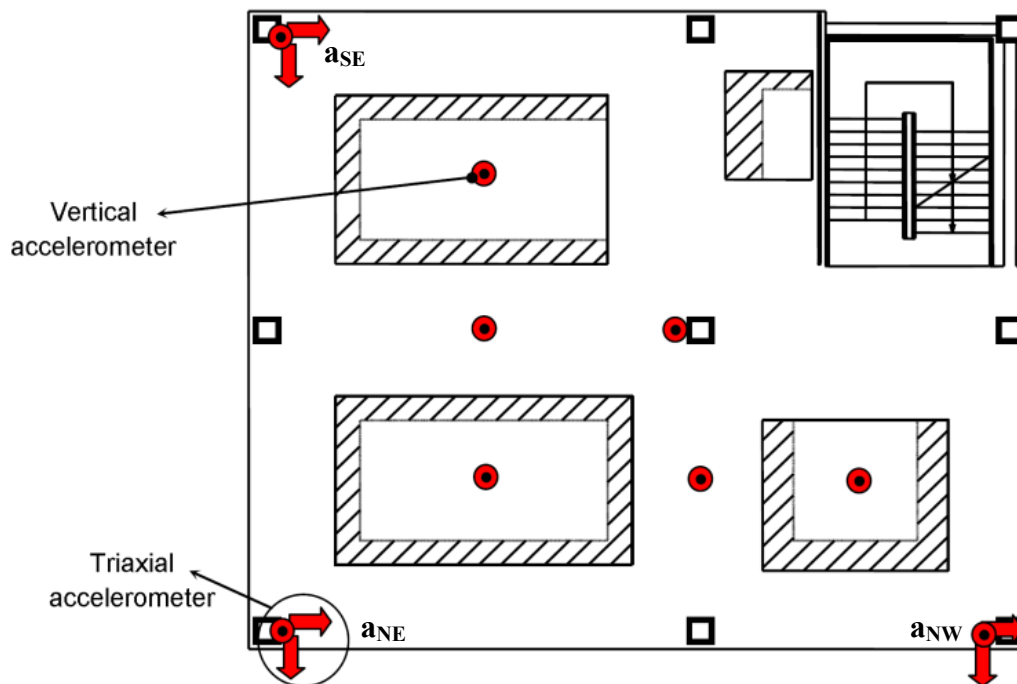


Figure 4-34 Layout of Accelerometers at the 5th Floor

4.6.2 Piping System

A maximum of 204 sensor channels were used for measuring the responses of nonstructural components. A total number of 102 sensor channels were used for measuring the responses of the piping system, which will be summarized in the following subsection.

4.6.2.1 Displacement Transducers

A total number of 12 displacement transducers (12 channels, two floors) were placed on the piping system to measure the overall response of this system. Four displacement transducers (four channels, two floors) were mounted on main run pipe close to the lateral sway braces and pipe hangers to measure the sliding of these elements relative to the main run pipes. Four displacement transducers (four channels, two floors) were mounted on branch line pipes close to the pipe hangers to measure the sliding of hangers relative to the branch line pipes. Four displacement transducers (string pots) (four channels, two floors) were mounted on main run pipes to measure the displacement of the piping system relative to the building structure in both horizontal directions. Figure 4-35 demonstrates the view of these displacement transducers and their instrumentation detail.

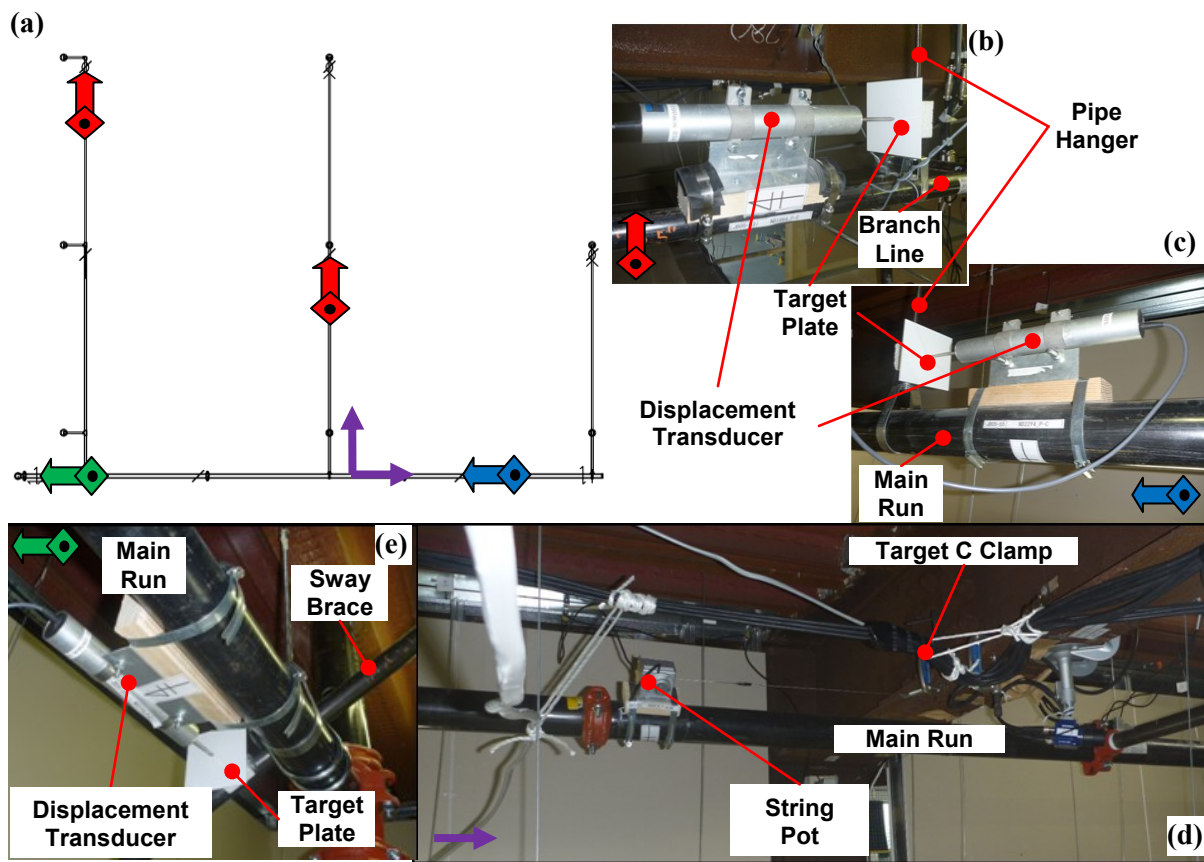


Figure 4-35 (a) Layout of Displacement Transducer at Piping System (b-e) Instrument Detail

4.6.2.2 Accelerometers

A total of six triaxial accelerometers (18 channels, two floors) were mounted on main run pipe at the branch line-main run attachment point. Furthermore, 10 triaxial accelerometers (30 channels, two floors) were placed on branch lines at the drop-branch line connection points. Figure 4-36 demonstrates the view of these accelerometers and their instrumentation detail.

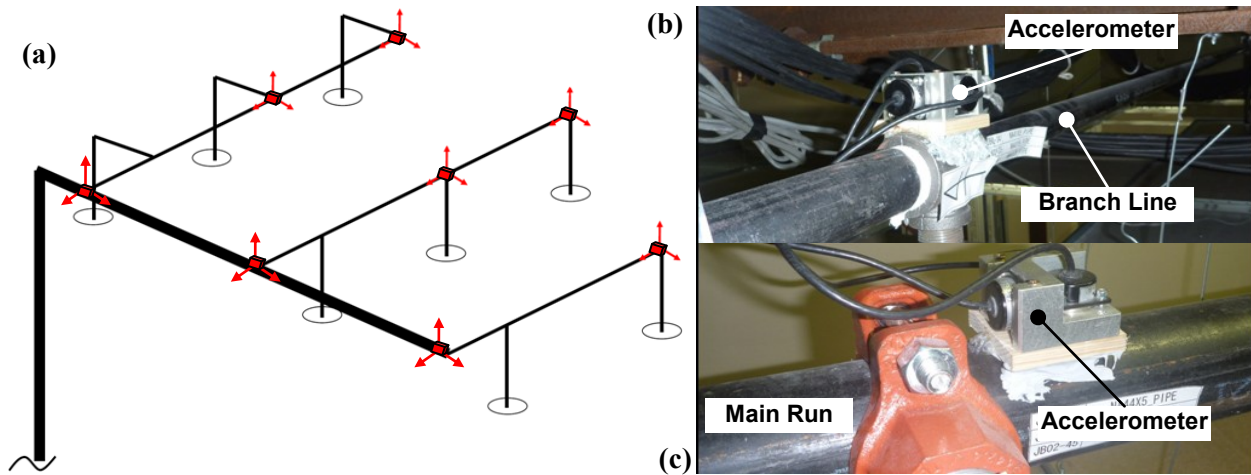


Figure 4-36 (a) View of Accelerometers on Main Run and Branch Line Pipes (b,c) Instrument Detail

A total of 14 triaxial accelerometers (42 channels, two floors) were placed on the sprinkler heads in order to capture the acceleration amplification of these locations compared to the pipe runs and the impact acceleration caused by ceiling-to-piping interaction.

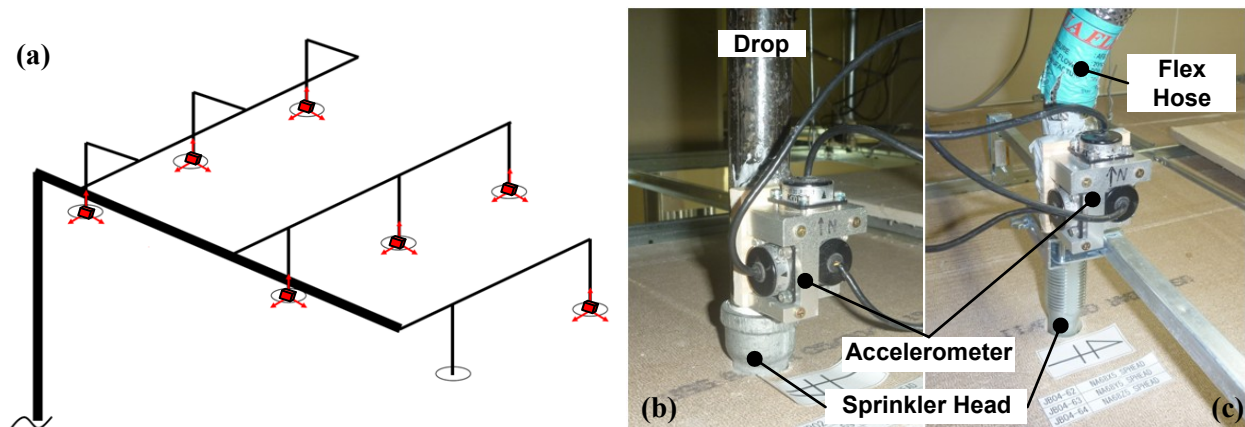


Figure 4-37 (a) View of Accelerometers on Sprinkler Heads (b,c) Instrument Detail

4.6.3 Excitation Plan

Several motions were studied for selecting the best suite of motions for each building configuration. The preference of choosing motions was given to real, strong, and un-scaled motions. However, due to safety limitations and possibility of performance comparisons between three different building configurations, motions were scaled to different factors when it was needed. The author was not involved in motion selection. The detailed description of motion selection can be found in Dao (2012) and Ryan et al. (2012).

The test schedule included three days of shaking (21 simulations) for the TP isolation (TPB) configuration, two days of shaking (15 simulations) for the hybrid LR (CLB/LRB) configuration, and one day of shaking (five simulations along with white noise and sine sweep) for the fixed-base configuration. The test schedule is presented in Table 4-4, Table 4-5, and Table 4-6. The abbreviation consists of the first three letters of the station name with the scale factor. If the input excitation is not 3D, then “(XY)” is added for bidirectional horizontal input and “(Y)” or “(X)” is added for unidirectional input in the y or x direction. If the simulation is repeated with the same input, the repetitions are labeled “-1” and “-2”.

Peak horizontal acceleration (achieved) shake table and two top floors of the buildings (piping system mounted from these two floors) is listed in Table 4-7. The peak values in horizontal direction are calculated at geometric center of table and floor (formulation will be given later) and based on the vector sum values of the X- and Y-components. The peak floor acceleration in vertical direction (Z- component) is calculated based on maximum peak recorded acceleration in that floor (most of the time at the center of deck).

Table 4-4 Simulation Schedule for the TP Isolation

Date (dd/mm/yy)	Time	Simulation abbreviation	Motion	Scale factor			Damage inspection
				X	Y	Z	
17/08/11	12:01:46	SIN65(X)	Sine-wave	0.65	0	0	
	12:49:54	SIN100(X)	Sine-wave	1.00	0	0	
	13:42:20	WSM80	Superstition Hills, Westmorland, Imperial Valley, El Centro	0.80	0.80	0.80	
	14:30:21	ELC130	Northridge, Rinaldi Rec. Sta.	1.30	1.30	1.30	
	15:20:16	RRS88	Northridge, Sylmar	0.88	0.88	0.88	Yes
	17:16:16	SYL100	Tabas, Tabas Sta.	1.00	1.00	1.00	
	17:48:56	TAB50	Tabas, Tabas Sta.	0.50	0.50	0.50	Yes
18/08/11	11:35:31	LGP70	Loma Prieta Los Gatos Pres. Ctr.	0.70	0.70	0.70	
	12:25:40	TCU50(XY)	ChiChi, TCU065	0.50	0.50	0	
	13:55:30	TCU70(XY)	ChiChi, TCU065	0.70	0.70	0	
	14:31:59	IWA100(XY)	Tohoku, Iwanuma	1.00	1.00	0	
	15:45:46	SAN100(XY)	Sannomaru	1.00	1.00	0	
	16:34:58	TAK100	Kobe, JMA Takatori	1.00	1.00	1.00	
	17:05:03	KJM100	Kobe, Kobe JMA	1.00	1.00	1.00	Yes
19/08/11	11:29:55	RRS88(XY)	Northridge, Rinaldi Rec. Sta.	0.88	0.88	0	
	12:16:55	TCU80(XY)	ChiChi, TCU065	0.80	0.80	0	
	13:08:07	TAB80	Tabas, Tabas Sta.	0.80	0.80	0.80	
	14:02:19	TAB90(XY)	Tabas, Tabas Sta.	0.90	0.90	0	
	14:50:46	TAB100(XY)	Tabas, Tabas Sta.	1.00	1.00	0	
	15:28:19	SCT100(XY)	Michoacan, SCT	1.00	1.00	0	
	16:19:03	TAK115	Kobe, JMA Takatori	1.15	1.15	1.00	Yes

Table 4-5 Simulation Schedule for the Hybrid LR Isolation

Date (dd/mm/yy)	Time	Simulation abbreviation	Motion	Scale factor			Damage inspection
				X	Y	Z	
25/08/11	11:19:52	WSM80	Superstition Hills, Westmorland	0.80	0.80	0.80	
	12:21:52	SIN100(Y)-1	Sine-wave	0	1.00	0	
	13:06:04	VOG75-1	Vogtle #13	0.75	0.75	0.75	
	13:56:09	VOG100	Vogtle #13	1.00	1.00	1.00	
	14:33:53	VOG125	Vogtle #13	1.25	1.25	1.25	
	15:15:09	VOG150	Vogtle #13	1.50	1.50	1.50	
	16:17:50	VOG175	Vogtle #13	1.75	1.75	1.75	
	16:52:49	DIA80	Diablo #15	0.80	0.80	0.80	Yes
26/08/11	12:03:09	DIA95(XY)	Diablo #15	0.95	0.95	0	
	12:48:49	ELC130	Imperial Valley, El Centro	1.30	1.30	1.30	
	13:44:36	IWA100(XY)	Tohoku, Iwanuma	1.00	1.00	0	
	14:37:30	RRS88(XY)	Northridge Rinaldi Rec. Sta.	0.88	0.88	0	
	15:20:52	RRS88	Northridge Rinaldi Rec. Sta.	0.88	0.88	0.88	
	16:15:12	VOG75-2	Vogtle #13	0.75	0.75	0.75	
	16:59:19	SIN100	Sine-wave	0	1.00	0	Yes

Table 4-6 Simulation Schedule for the Fixed-Base Building

Date (dd/mm/yy)	Time	Simulation abbreviation	Motion	Scale factor			Damage inspection
				X	Y	Z	
	10:19:52	WHT100(X)-1	White noise	1.00	0	0	
	10:30:02	WHT100(Y)-1	White noise	0	1.00	1.00	
	10:38:32	WHT100(Z)-1	White noise	1.00	1.00	1.00	
	10:50:35	WSM80	Superstition Hills, Westmorland	0.80	0.80	0.80	
	11:02:50	WHT100-1	White noise	1.00	1.00	1.00	Yes
	12:06:31	WHT100-2	White noise	1.00	1.00	1.00	
	12:18:47	RRS35(XY)	Northridge, Rinaldi Rec. Sta.	0.35	0.35	0	
	12:28:02	WHT100-3	White noise	1.00	1.00	1.00	Yes
	13:37:34	WHT100-4	White noise	1.00	1.00	1.00	
31/08/11	13:51:20	RRS35	Northridge, Rinaldi Rec. Sta.	0.35	0.35	0.35	
	14:03:01	WHT100-5	White noise	1.00	1.00	1.00	Yes
	15:12:50	WHT100-6	White noise	1.00	1.00	1.00	
	15:24:53	RRS35(XY)88(Z)	Northridge, Rinaldi Rec. Sta.	0.35	0.35	0.88	
	15:33:51	WHT100-7	White noise	1.00	1.00	1.00	Yes
	17:07:04	WHT100-8	White noise	1.00	1.00	1.00	
	17:22:33	IWA70(XY)	Tohoku, Iwanuma	0.70	0.70	0	
	17:35:28	WHT100(X)-2	White noise	1.00	0	0	
	17:43:12	WHT100(Y)-2	White noise	0	1.00	0	
	17:52:47	WHT100(Z)-2	White noise	1.00	1.00	1.00	Yes

Table 4-7 Table/Floors Achieved Peak Acceleration

Name	System	Scale Factor	Table		5th Floor		6th Floor	
			PGA _{xy} (g)	PGA _z (g)	PFA _{xy} (g)	PFA _z (g)	PFA _{xy} (g)	PFA _z (g)
1-1987 Superstition Hills - Westmorland (3D)	TPB	80%	0.19	0.14	0.15	0.81	0.15	1.18
2-1940 Imperial Valley - El Centro (3D)	TPB	130%	0.51	0.26	0.25	1.40	0.33	1.70
3-1994 Northridge – Rinaldi Rec. Sta. (3D)	TPB	88%	1.21	1.24	0.90	6.77	0.85	6.44
4-1994 Northridge – Sylmar (3D)	TPB	100%	1.14	0.54	0.41	2.69	0.60	4.56
5-1978 Tabas – Tabas Sta. (3D)	TPB	50%	0.58	0.36	0.24	1.30	0.33	2.04
6-1989 Loma Prieta – Los Gatos (3D)	TPB	70%	0.57	0.69	0.27	2.22	0.42	2.95
7-1999 Chichi – TCU065 (XY)	TPB	50%	0.47	0.02	0.16	0.12	0.18	0.22
8-1999 Chichi – TCU065 (XY)	TPB	70%	0.66	0.03	0.18	0.28	0.23	0.30
9-2011 Tohoku – Iwanuma (XY)	TPB	100%	0.59	0.03	0.22	0.25	0.34	0.42
10-Sannomaru (XY)	TPB	100%	0.23	0.02	0.16	0.18	0.22	0.28
11-1995 Kobe – Takatori (3D)	TPB	100%	1.00	0.26	0.38	1.81	0.66	1.69
12-1995 Kobe – JMA Kobe (3D)	TPB	100%	1.04	0.41	0.53	1.26	0.66	2.17
13-1994 Northridge – Rinaldi Rec. Sta. (XY)	TPB	88%	1.20	0.10	0.34	0.85	0.38	1.03
14-1999 Chichi – TCU065 (XY)	TPB	80%	0.76	0.03	0.17	0.27	0.21	0.29
15-1978 Tabas – Tabas Sta. (3D)	TPB	80%	0.92	0.59	0.39	2.77	0.77	4.05
16-1978 Tabas – Tabas Sta. (XY)	TPB	90%	1.00	0.10	0.23	0.78	0.39	0.94
17-1978 Tabas – Tabas Sta. (XY)	TPB	100%	1.12	0.12	0.24	0.77	0.46	0.98
18-1985 Mexico City – SCT (XY)	TPB	100%	0.18	0.02	0.16	0.14	0.18	0.22
19-1995 Kobe – Takatori (3D)	TPB	115% XY 100% Z	1.16	0.28	0.36	1.67	0.69	1.70
20-1987 Superstition Hills - Westmorland (3D)	LRB/CLB	80%	0.19	0.15	0.14	0.92	0.13	0.71
21-Vogtle #13 (3D)	LRB/CLB	75%	0.38	0.21	0.24	0.89	0.23	1.13
22-Vogtle #13 (3D)	LRB/CLB	100%	0.54	0.30	0.32	1.25	0.32	1.68
23-Vogtle #13 (3D)	LRB/CLB	125%	0.68	0.37	0.40	1.80	0.40	2.31
24-Vogtle #13 (3D)	LRB/CLB	150%	0.83	0.44	0.49	2.42	0.48	2.93
25-Vogtle #13 (3D)	LRB/CLB	175%	1.00	0.49	0.53	3.03	0.52	3.61
26-Diablo Canyon #28 (3D)	LRB/CLB	80%	0.89	0.45	0.40	2.82	0.50	2.76
27-Diablo Canyon #28 (XY)	LRB/CLB	95%	1.10	0.06	0.35	0.37	0.44	0.47
28-1940 Imperial Valley - El Centro (3D)	LRB/CLB	130%	0.51	0.28	0.24	1.33	0.27	1.35
29-2011 Tohoku – Iwanuma (XY)	LRB/CLB	100%	0.58	0.02	0.31	0.07	0.37	0.10
30-1994 Northridge – Rinaldi Rec. Sta. (XY)	LRB/CLB	88%	1.14	0.05	0.42	0.18	0.56	0.22
31-1994 Northridge – Rinaldi Rec. Sta. (3D)	LRB/CLB	88%	1.15	1.26	0.67	4.76	1.12	7.03
32-Vogtle #13 (3D)	LRB/CLB	75%	0.38	0.22	0.24	0.82	0.24	1.19
33-1987 Superstition Hills - Westmorland (3D)	Fixed	80%	0.22	0.14	0.46	0.96	0.54	0.68
34-1994 Northridge – Rinaldi Rec. Sta. (XY)	Fixed	35%	0.40	0.01	0.97	0.09	1.01	0.10
35-1994 Northridge – Rinaldi Rec. Sta. (3D)	Fixed	35%	0.41	0.35	0.97	1.46	1.06	2.17
36-1994 Northridge – Rinaldi Rec. Sta. (3D)	Fixed	35% XY 88% Z	0.41	1.06	1.19	4.49	1.22	6.11
37-2011 Tohoku – Iwanuma (XY)	Fixed	70%	0.37	0.01	0.93	0.09	1.13	0.11

4.6.4 Generation of the Analytical Model

An analytical model of the piping subsystem was developed in SAP2000 v15 and OpenSees v2.4.0. The OpenSees model was the primary model for analysis, comparison and calibration of test data, and further investigation. The SAP model (Figure 4-38a) computed nodal gravity load and lumped mass distribution, which was transferred to the OpenSees model. The SAP model verified the static response and modal analysis of the OpenSees model (Figure 4-38b). The solid braces in the longitudinal and lateral directions near the riser-main run isolated the dynamic response of the piping system of each floor from the adjacent floor response. Therefore, in this study, only the piping layout of one floor is analytically modeled. It should be mentioned that the

piping layout of each floor was the same. Hence, the response of the piping system installed on the fourth floor was analytically considered here.

The model was composed of elements that were presented earlier in this study. However, a summary of components used is presented in Table 4-8. Both end connections of wire restrainers were assumed pin connection, as they modeled using truss elements. Fixed connections were used for the pipe hangers-structural deck attachment. However, a pin-type attachment was used for the connection of pipe hangers to the pipe runs. The connection of the seismic braces was assumed to be rigid at both ends. The achieved floor accelerations were defined as uniform acceleration history in the direction of shaking. This excitation pattern applied a uniform-support excitation to the model acting in a certain direction.

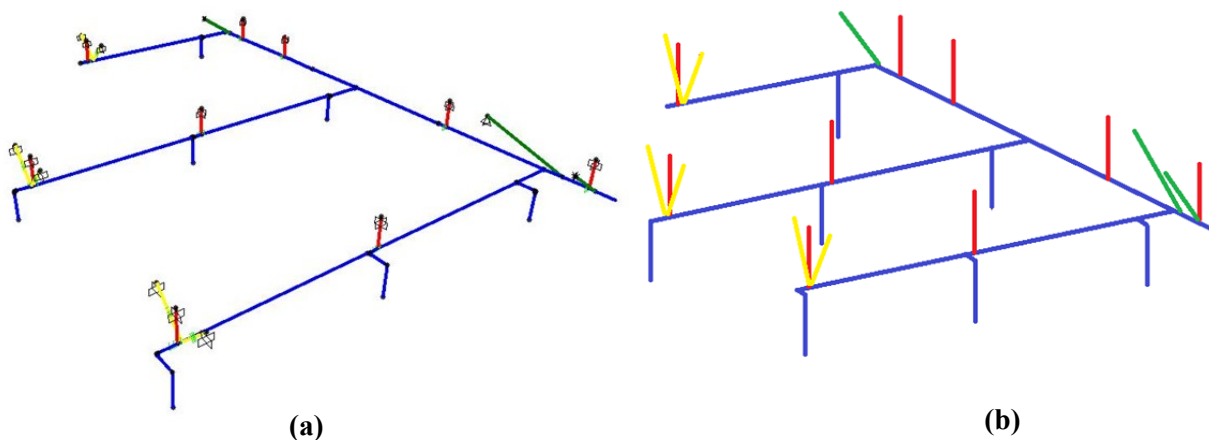


Figure 4-38 Models of the Piping Subsystem (a) SAP Model (b) OpenSees Model

Static analysis of the SAP model, which calculated the gravity load, was used to transfer distributed loads to the frame elements and the associated nodal masses to the OpenSees model. The mass of the piping system was determined using the dry weight of the pipes. An additional

Table 4-8 Summary of Used Components for Analytical Model

	Reference	Material	Section	Element
Pipe Segments	3.5.2	NA	Elastic	Force-Based
Pipe Joints	3.5.2	Pinching4	NA	ZeroLength
Hangers	3.2.4	Steel02	Fiber	Force Based
Solid Braces	3.3.2.1	NA	Elastic	Force-Based
Restrainers	3.4.4	EPPG	NA	Truss

mass of 0.5 pounds was used for each sprinkler head. A classical Rayleigh damping was used to account for the inherent damping of the piping system.

Throughout the calibration process, 0.003 initial gap strain for the wire restrainers gave the closest match between the analytical and experimental acceleration and displacement results. In the calibration process, the initial gap of all wire restrainers and their horizontal angles were assumed to be the same, which may not replicate the actual construction.

4.6.5 Experimental-Analytical Result Comparison

The natural periods and damping of the piping system were determined directly from the transfer functions. The transfer functions were obtained from the white-noise excitation conducted for the fixed-base case prior to the primary excitations. As mentioned before, piping systems have many localized modes instead of few fundamental modes. Therefore, an effort is made to find as many as possible localized modes of piping system tested at this experiment. The damping ratio of each mode is then plotted versus the natural frequency of that mode to estimate the experimental damping ratio versus the natural frequencies. Then, the assumed analytical damping model is compared with experimental damping values. The theoretical transfer function (TF) is defined as the ratio of absolute acceleration of the target point to a reference point of the piping system in the frequency domain:

$$\frac{\ddot{a}_{target}(\omega)}{\ddot{a}_{reference}(\omega)} = TF = \left(\frac{i\omega c + k}{-m\omega^2 + i\omega c + k} \right) \quad (4-4)$$

where i , ω , c , k , m are $\sqrt{-1}$, circular frequency, viscous damping coefficient, and mass, respectively. The nodal (target point) mode shapes of piping segments (branch lines or main run) were calculated with respect to the fix pints (zero mode shape value) named as reference point. For calculating the bending natural frequency of main run, two ends of main run were assumed as the reference point. Assuming that the main run pipe is axially rigid, three intersection point of branch lines-main run were considered as the reference point for calculating first and second bending modes and frequencies of branch lines. The period and damping ratio corresponding to the fundamental modes were evaluated by using the acceleration response of each segment (branch lines and main run) separately. Figure 4-39 shows the location of accelerometers that were used as the target and reference accelerometers.

$$\zeta = \frac{\omega_b - \omega_a}{2\omega_n} \quad \text{or} \quad \zeta = \frac{f_b - f_a}{2f_n} \quad (4-5)$$

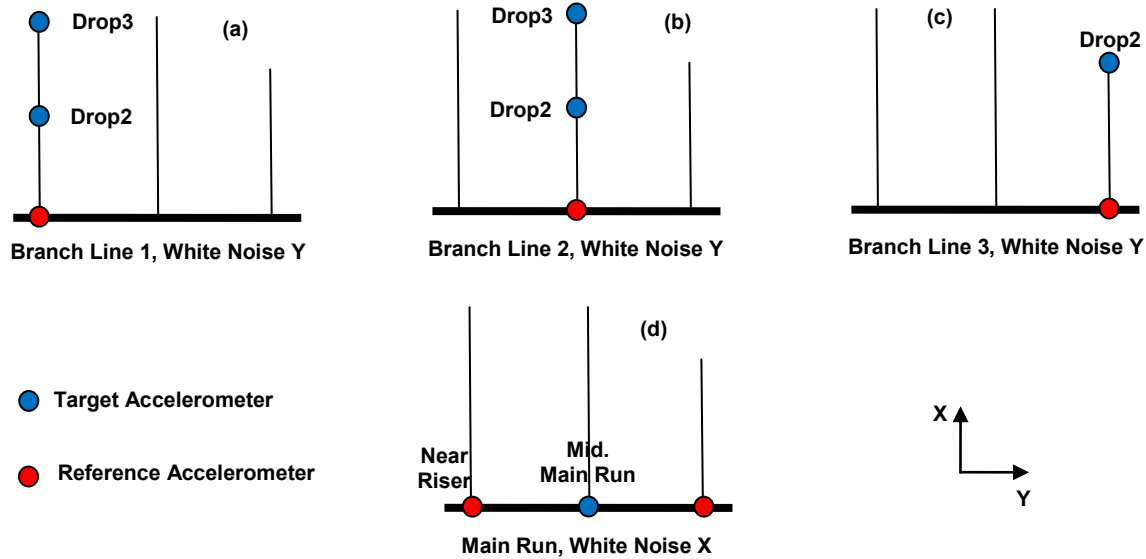


Figure 4-39 Schematic of Used Accelerometers to Obtain Transfer Functions

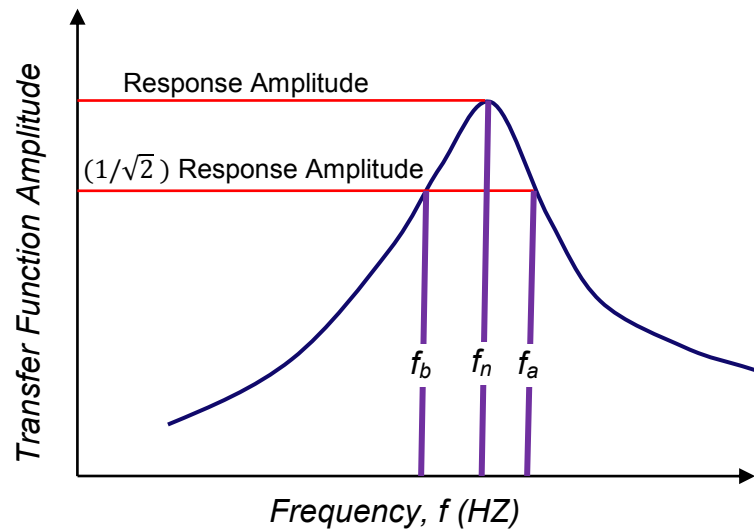


Figure 4-40 Definition of Half-Power Bandwidth

where ω_b and ω_a (f_b and f_a) are the frequencies on either side of the resonant frequency and ω_n (f_n) is the circular frequency at which the transfer function amplitude is $1/\sqrt{2}$ times the resonant amplitude (see Figure 4-40).

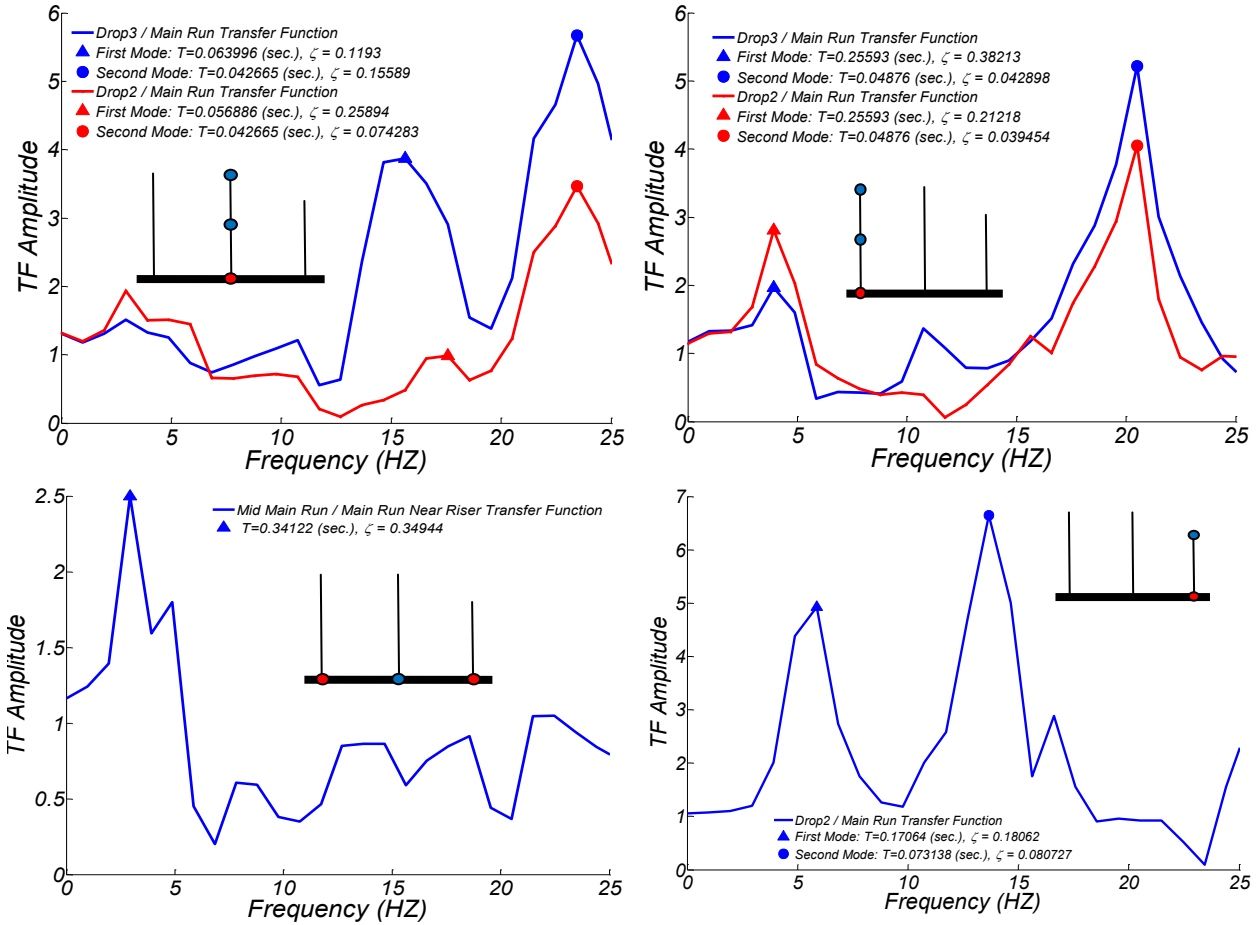


Figure 4-41 Transfer Functions for Piping System

Figure 4-41 shows the transfer functions obtained from experimental results for each piping segment. Table 4-9 summarizes the periods and damping ratios calculated based on experimental fragility curves. By comparing the analytical results and test results, the Rayleigh damping curve passing through damping ratios of 7% at periods of 0.14 s (7.16 Hz) and 0.06 s (16 Hz) was found to give a good match. This damping model was used throughout the analysis of the piping system.

Table 4-9 Natural Periods and Damping Ratios of the Piping System

Mode	Branch Line 1			Branch Line 2			Branch Line 3			Main Run	
				Target							
	Drop 3	Drop 2	Drop 3	Drop 2	Drop 2	Middle					
Period (sec)	1 st	0.25593	0.25593	0.063996	0.056886	0.17064					
Damping (%)	2 nd	0.04876	0.04876	0.042665	0.042665	0.073138					NA
	1 st	0.38213	0.21218	0.1193	0.25894	0.18062					0.34944
	2 nd	0.042898	0.039454	0.15589	0.074283	0.080727					NA

Figure 4-42 shows the selected Rayleigh damping model for the fixed-base analytical model compared to the damping values computed from test data.

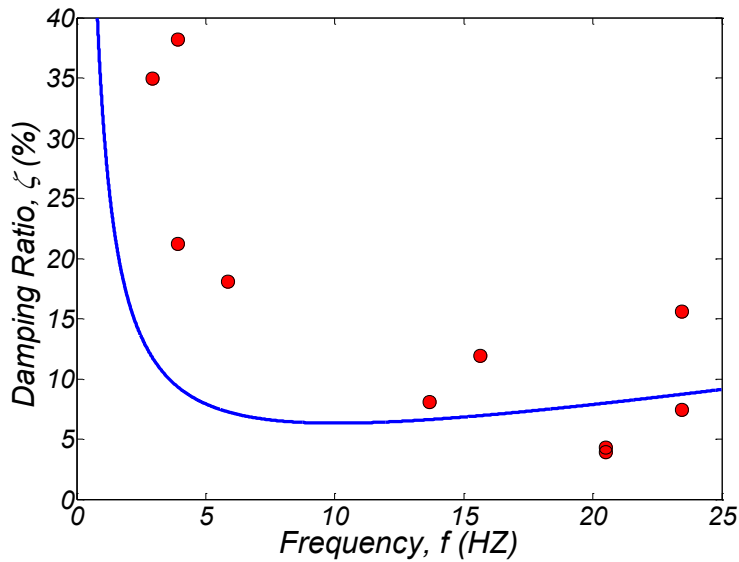


Figure 4-42 Rayleigh Damping Model

Several white-noise excitations were applied to the structure. However, the piping system was never directly subjected to white-noise excitation. Therefore, the white noise excitations were changed at the dominant frequencies of structure. Due to this effect, the damping ratios and dominant frequencies of the piping system may not be accurate. From the experimental data, the first two vibration periods of the piping system were 0.35 seconds and 0.26 seconds for the main run and first branch line, respectively. The corresponding periods obtained from the analytical model were 0.34 and 0.27 seconds. The natural period from mode three in the analytical mode was 0.26 seconds, which corresponded to the second branch line. This mode was missing from the experimental results (see Figure 4-43). The analytical dominant natural period was calculated based on the closed gap in the wire restrainers and rigid connection of pipe hangers to the pipes. The rationale behind this was: 1) as the white-noise excitation was amplified at the dominant frequencies of structure, the initial gap of wire restrainers might have closed during this excitation; 2) the white noise excitations (even those that passed through the structure) are low amplitude and they might not have generated enough rotational moment to overcome the small hanger-pipe rotational resistance.

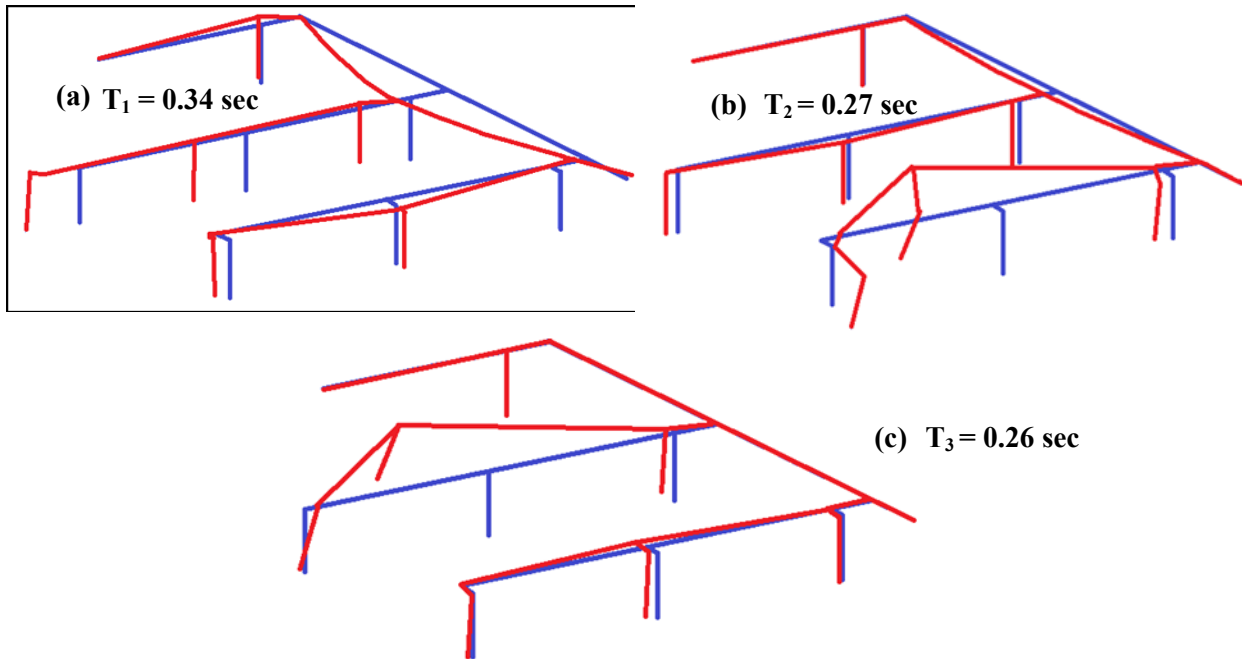


Figure 4-43 The First Three Local Modes of Piping System

Time history accelerations and displacement of the piping system subjected to 35RRS (XY) motion were selected to calibrate the analytical model. The input motions of the analytical model were based on fourth floor accelerations and calculated at the geometric center floor as:

$$a_{xc} = \frac{1}{2} \left(\frac{a_{xSE} + a_{xNE}}{2} + a_{xNW} \right) \quad (4-6)$$

$$a_{yc} = \frac{1}{2} \left(\frac{a_{yNW} + a_{yNE}}{2} + a_{ySE} \right) \quad (4-7)$$

where a_{xSE} and a_{ySE} are X and Y components of the horizontal acceleration at the southeast corner, and so on (Figure 4-34). The acceleration at geometric center of the structure has a different amplitude and frequency compared to the three corner accelerations. Due to these differences, some of the frequencies of the piping system were not recorded with the correct amplitude, and the differential movement of the piping system was not imposed to different segments of the piping system. The horizontal components of 35RRS (XY) are presented in Figure 4-44 and Figure 4-45.

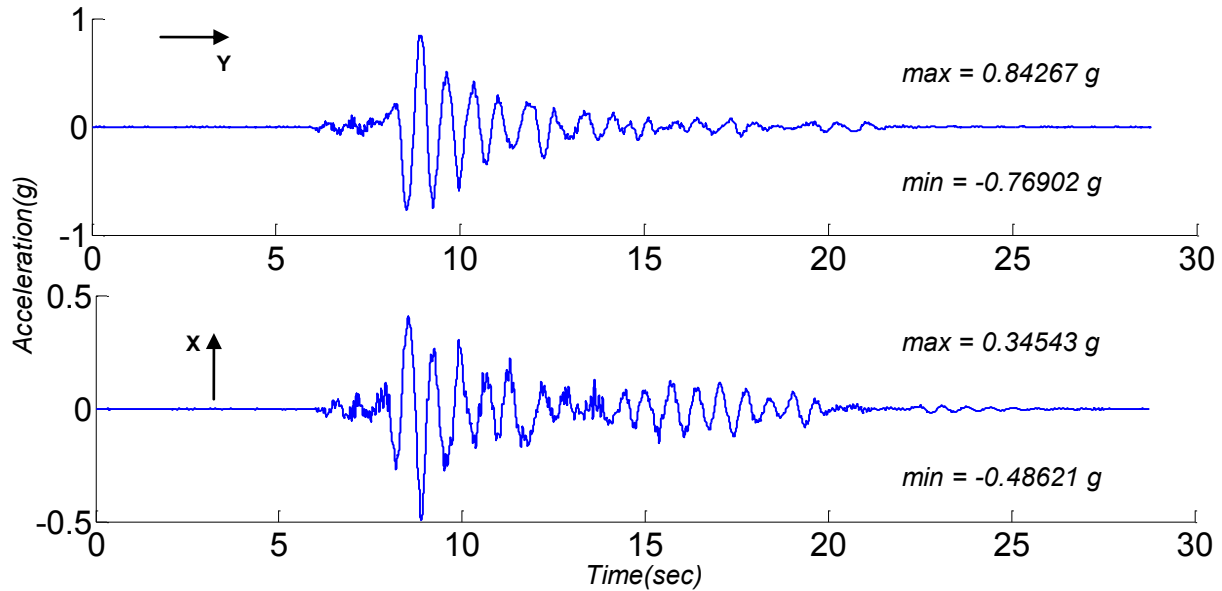


Figure 4-44 Calculated Horizontal Components of Acceleration Histories at Geometric Center of 4th Floor under 35RRS (XY-Fixed Base)

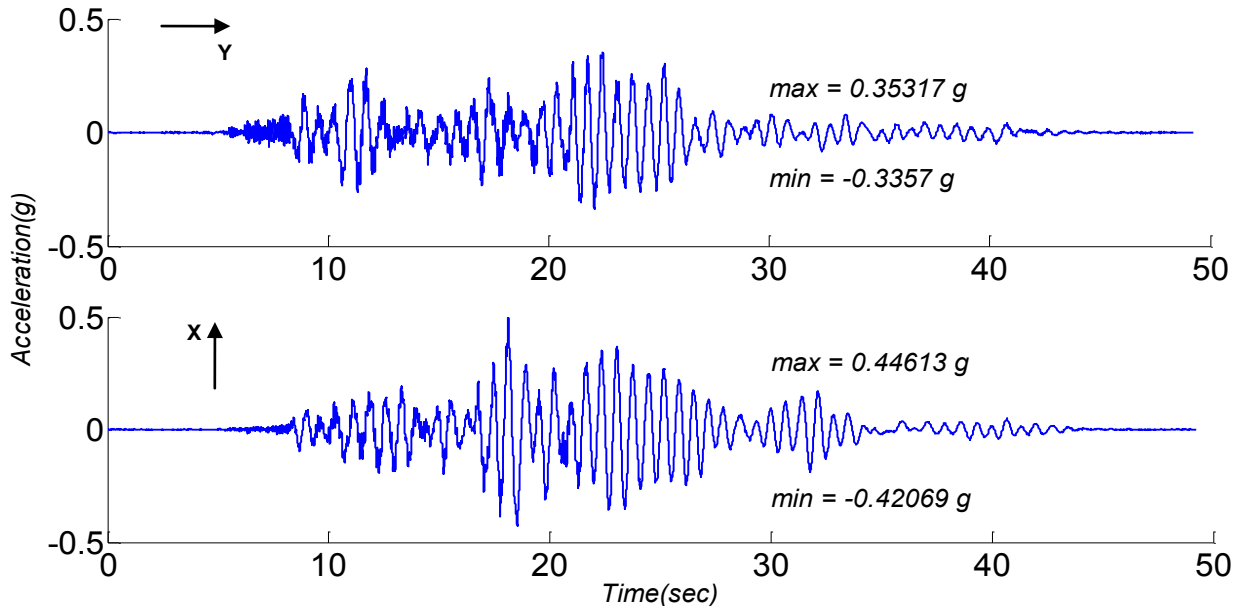


Figure 4-45 Calculated Horizontal Components of Acceleration Histories at Geometric Center of 4th Floor under WSM80 (3D-Fixed Base)

Figure 4-46 through Figure 4-52 compare sample horizontal acceleration responses of the analytical model and test data. The results show that the model cannot predict every detail of the response, but it can predict the trend of response very well. Figure 4-51 and Figure 4-52 show that the model was not able to predict the higher frequencies in some locations. In Figure 4-53, the displacement response perpendicular to the main run was compared under 35RRS (XY-Fixed Base) and WSM80 (3D-Fixed Base) excitations.

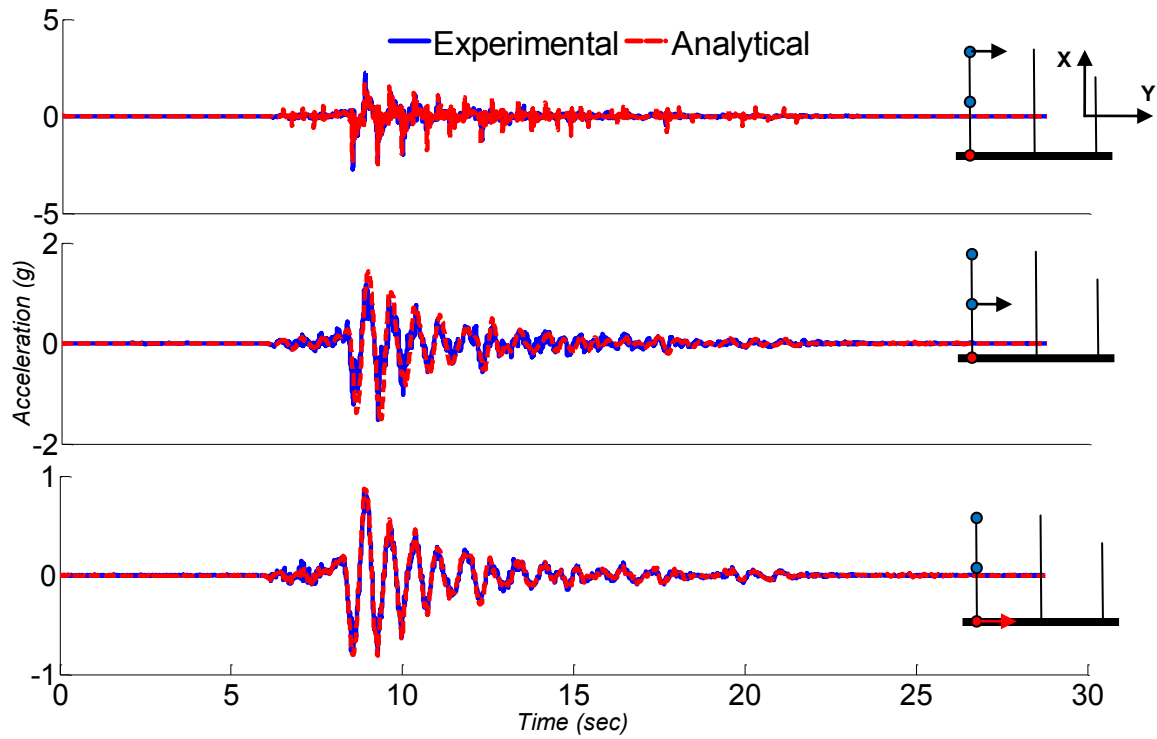


Figure 4-46 Comparison of Experimental and Analytical Acceleration History of First Branch Line in Y Direction under 35RRS (XY-Fixed Base)

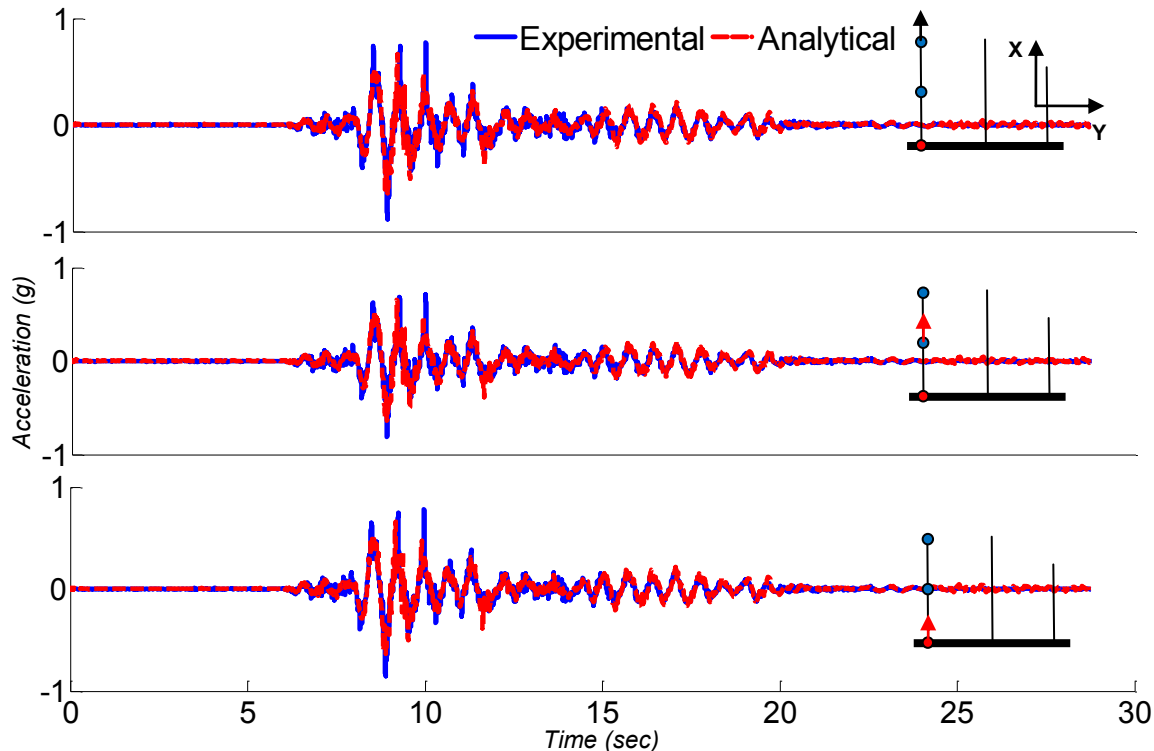


Figure 4-47 Comparison of Experimental and Analytical Acceleration History of First Branch Line in X Direction under 35RRS (XY-Fixed Base)

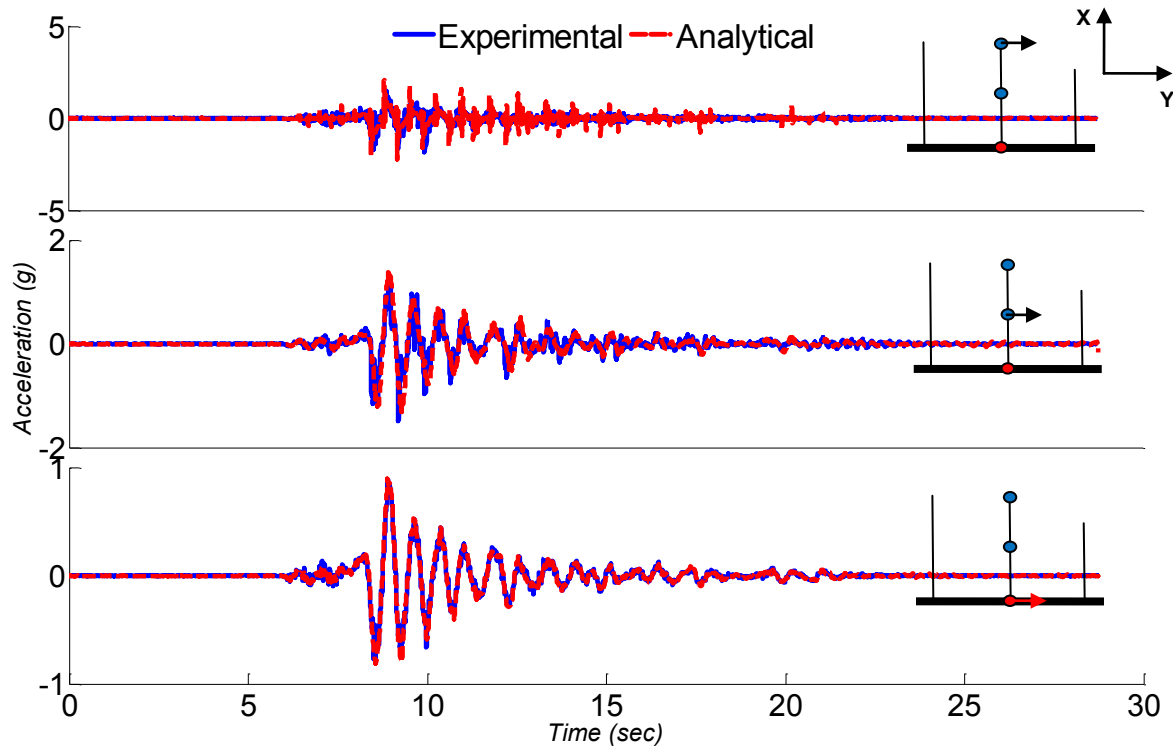


Figure 4-48 Comparison of Experimental and Analytical Acceleration History of Second Branch Line in Y Direction under 35RRS (XY-Fixed Base)

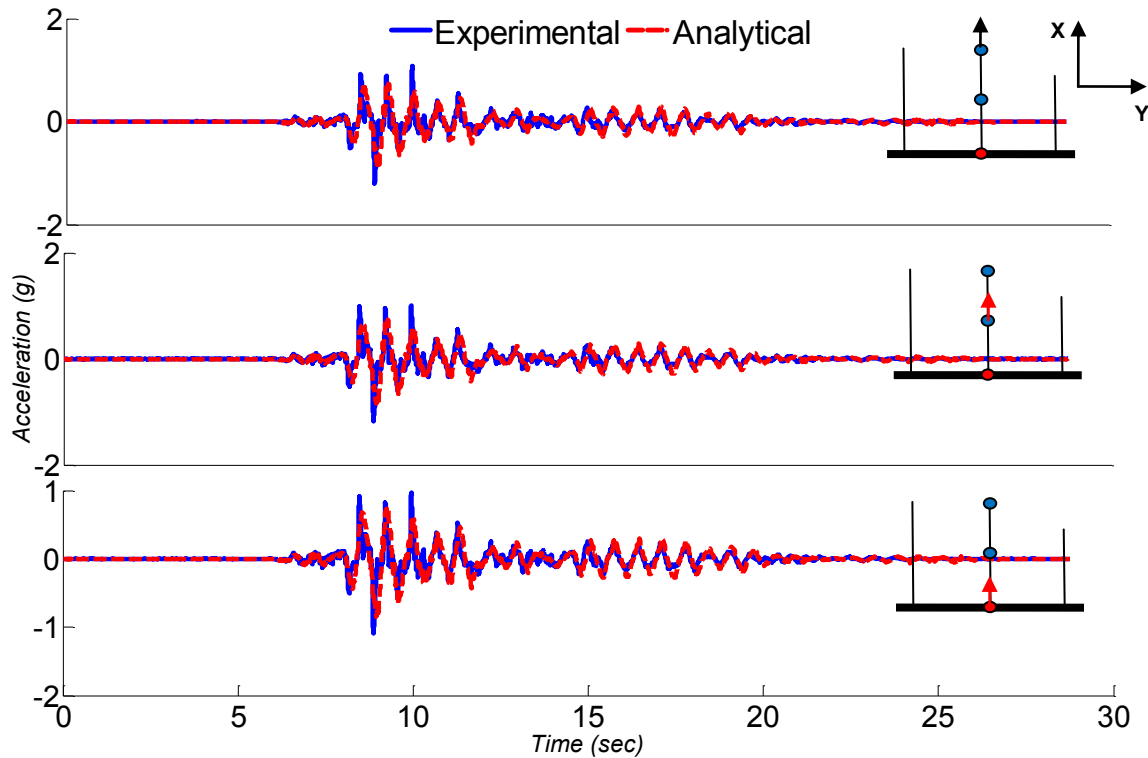


Figure 4-49 Comparison of Experimental and Analytical Acceleration History of Second Branch Line in X Direction under 35RRS (XY-Fixed Base)

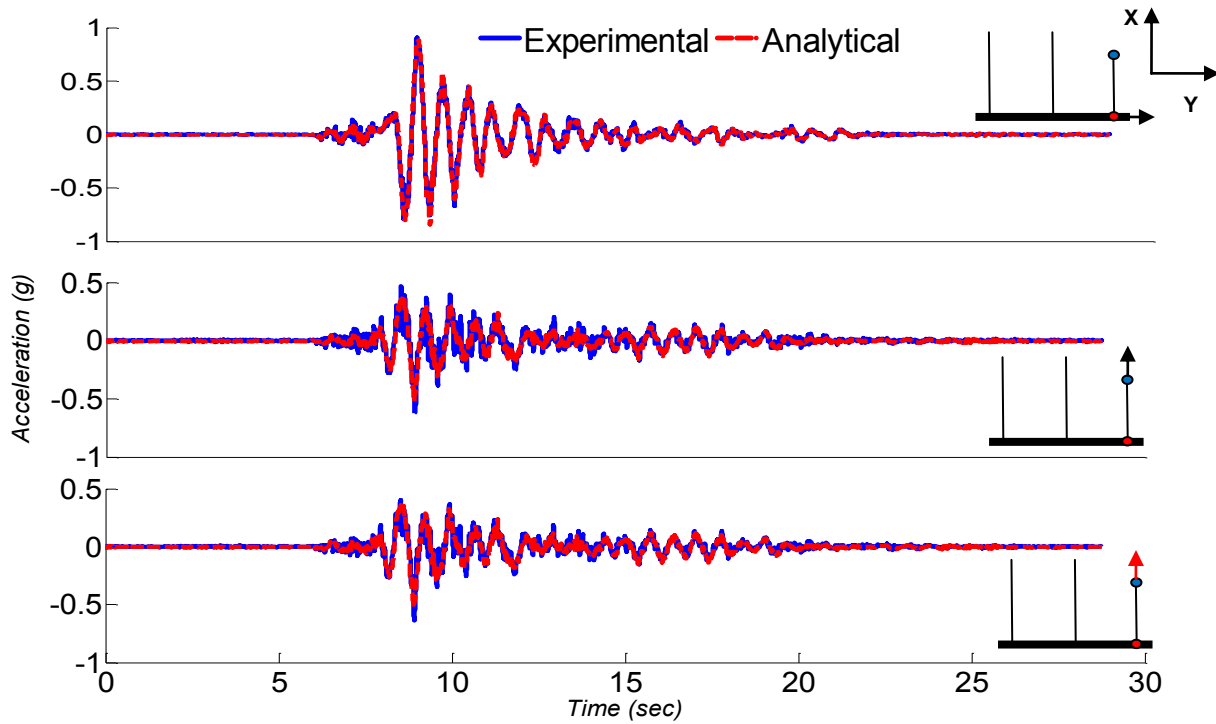


Figure 4-50 Comparison of Experimental and Analytical Acceleration History of Third Branch Line in X-Y Directions under 35RRS (XY-Fixed Base)

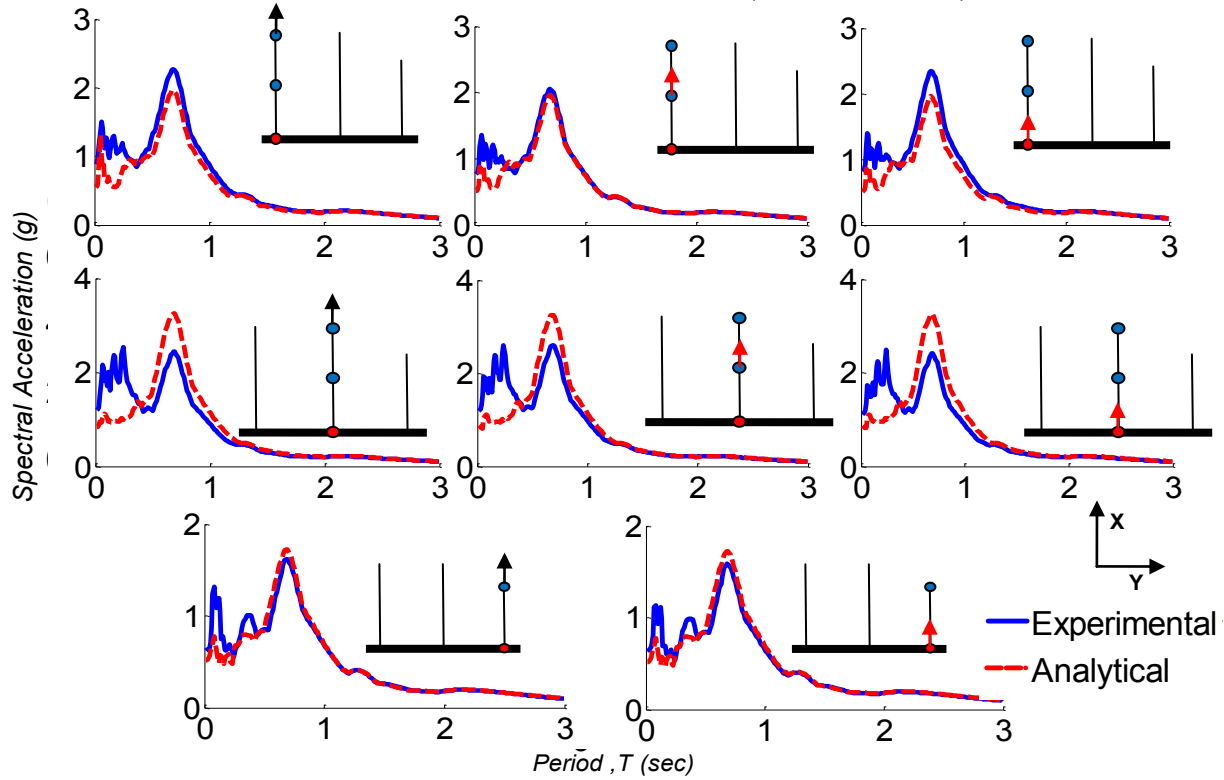


Figure 4-51 Comparison of Experimental and Analytical Spectral Acceleration of All Branch Lines in X Direction under 35RRS (XY-Fixed Base)

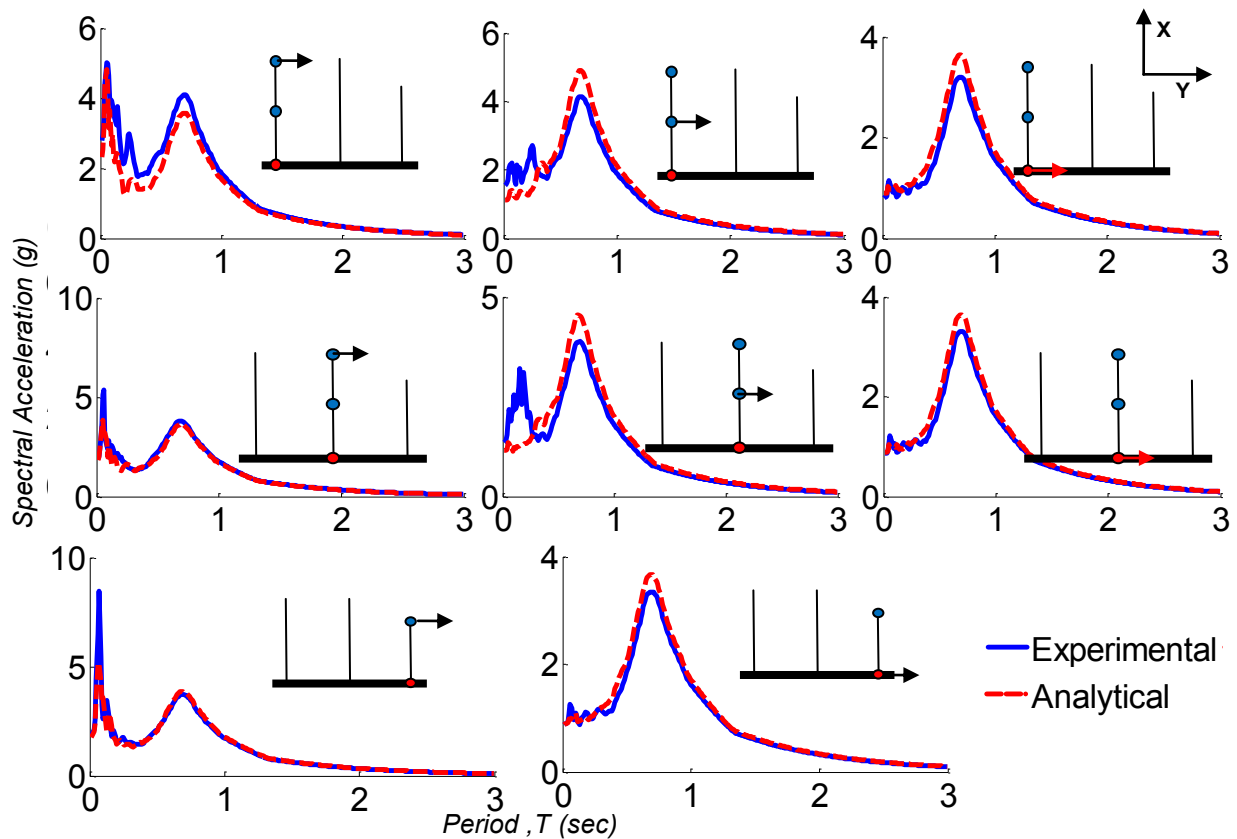


Figure 4-52 Comparison of Experimental and Analytical Spectral Acceleration of All Branch Lines in Y Direction under 35RRS (XY-Fixed Base)

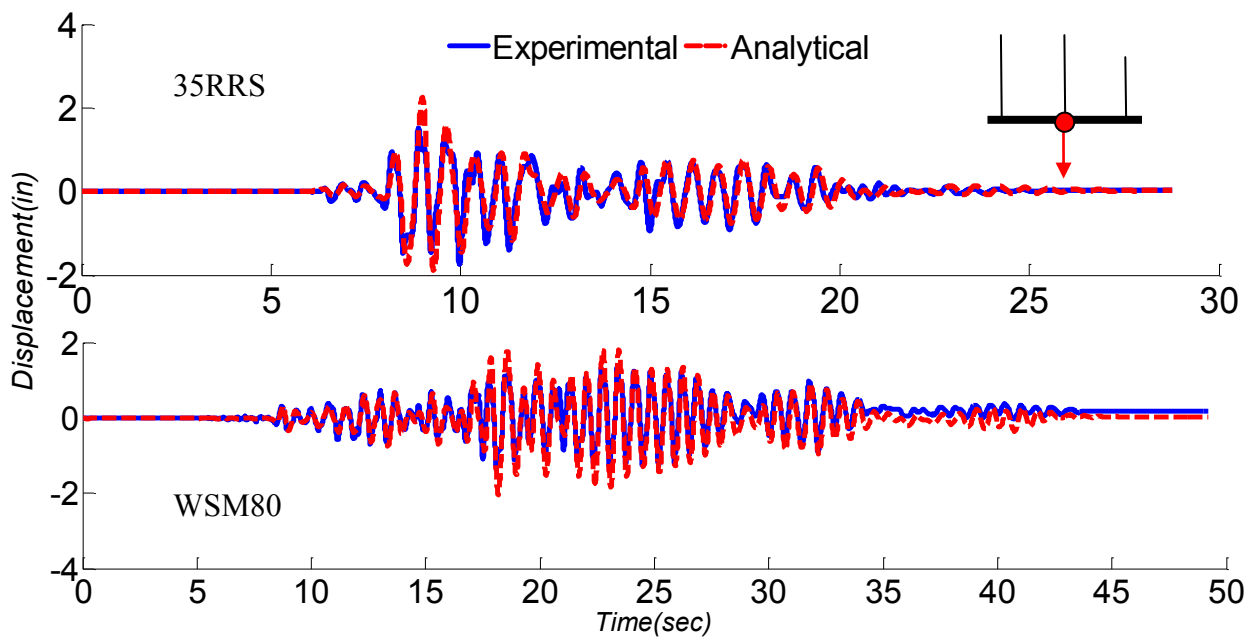


Figure 4-53 Comparison of Experimental and Analytical Displacement History of Third Main Run in X Direction under Fixed Base 35RRS (XY) and WSM80 (3D)

4.7 Concluding Remarks

In this section, the previously developed piping components were verified and calibrated with several subsystem-level experiments. The four experiments were: UNR hospital subassemblies with and without sliding frame; a two-story piping subsystem test at the University at Buffalo; and a two-story piping subsystem test at the E-Defense shake table facility. For each of these experiments, two models were built in SAP and OpenSees programs. The modeling technique of each of these experiments was presented using previously defined component-level analytical models. The results of the analytical models were compared with the experimental acceleration, displacement, restrainer axial force, pipe hanger axial force, joint rotation, and spectral acceleration responses data.

SECTION 5 COMPONENT FRAGILITY STUDIES

5.1 Introduction

Quantitative and qualitative seismic risk assessment is a crucial step in evaluating the impact of an earthquake on the performance of piping systems. This impact is typically estimated in terms of components' vulnerability and losses. Seismic risk assessment tools are used to measure the performance of systems, and seismic fragility curves are the key information to these tools. Fragility curves are conditional statements that give the probability that a structure will meet or exceed a specified level of damage for a given ground motion intensity measure as:

$$f_{DS}(IM) = P(DS|IM) \quad (5-1)$$

where DS is the specified damage state for the piping component and IM represents the ground motion intensity measure. The failure probability of a system can also be expressed as the probability that seismic demand (S_D) will exceed the structural capacity (S_C):

$$P_f = P\left(\frac{S_D}{S_C} < 1.0\right) \quad (5-2)$$

The probabilistic seismic demand analysis (PSDA), which is also known as the cloud approach, is one of the most widely used and accepted nonlinear demand approaches. PSDA is an approach to estimate the probability of exceeding a specified seismic demand on a structural system under an earthquake with a specified intensity measure (IM) such as peak floor acceleration (PFA). Probabilistic seismic demand analysis assists in the seismic risk assessment for structures with uncertainties in the response and capacity. It consists of the selection of a suite of floor motions, piping models with distribution of components and parameters, and subsequently nonlinear response history analysis of corresponding computational models. The probabilistic seismic demand models (PSDM) are the outcomes of PSDA that represent the relationship between Engineering Demand Parameters (EDPs) and Intensity Measures (IM). In this context, EDP is defined as the response of various components in the structure system during a response history analysis. Therefore, nonlinear response history analyses of all statistical samples are carried out, and maximum responses are recorded to build PSDMs.

In the previous sections, the modeling methodology and the nonlinear properties of the elements were validated using the component and subsystem experimental results. In this section, the same modeling techniques are used to complete fragility studies of typical sprinkler piping components and systems. A comprehensive three-dimensional nonlinear model of a typical hospital sprinkler piping system is developed. The PSDMs of various components of piping systems were initially developed. Damage states of different components are determined and described, and their fragility curves are developed.

5.2 Fragility Analysis Methodology

The seismic vulnerability of a structural or nonstructural component can be graphically represented through the generation of analytical fragility curves. Fragility curves are probabilistic representations of exceeding a predefined capacity or limit state (damage state) in terms of intensity measures (IMs) — peak floor acceleration in this case — and engineering demand parameters (EDPs) as a measure of piping response. Therefore, the essential steps for generating the sprinkler piping fragility curves are: 1) develop an analytical model; 2) generate a ground motion suite; 3) create probabilistic seismic demand models; 4) determine the capacity estimates; and 5) fragility formulation (component and system level). Each of these steps is presented in the following sections.

As mentioned before, one of the most common methods to develop fragility curves is the Probabilistic Seismic Demand Model. The PSDM can be developed using a “scaling” or “cloud” approach to relate the engineering demand parameter (EDP) to the ground motion intensity measure. With the scaling approach, all motions are scaled to selective intensity levels corresponding to prescribed seismic hazard levels, and incremental dynamic analysis (IDA) is performed at different hazard levels. On the other hand, the cloud approach (Probabilistic Seismic Demand Analysis, PSDA) uses unscaled (or scaled by a constant factor) earthquake ground motions (Zhang, 2008).

5.2.1 Cloud Approach (Probabilistic Seismic Demand Analysis, PSDA)

The PSDA method utilizes power law or regression logarithmic analysis between EDPs and IMs, which was proposed by Cornell et al. (2002) as:

$$EDP = aIM^b \quad \text{or} \quad \ln(EDP) = \ln(a) + b \ln(IM) \quad (5-3)$$

to obtain the mean and standard deviation for each limit state by assuming a logarithmic correlation between median engineering demand EDP and an appropriately selected intensity measure IM. In the above equation, parameters a and b are regression coefficients obtained from the response data of nonlinear response history analyses. However, the actual data from response history analyses follows:

$$\ln(EDP) = \ln(a) + b \ln(IM) + e \quad (5-4)$$

The remaining variable (e) in $\ln(EDP)$ at a given IM is assumed to have a constant variance for all IM range, and according to Baker and Cornell (2006), the standard variation is estimated as:

$$\beta_{EDP|IM} = \text{Var}(e) = \sqrt{\frac{\sum_{i=1}^n [\ln(EDP_i) - (\ln(a) + b \ln(IM_i))]^2}{n - 2}} \quad (5-5)$$

where EDP_i and IM_i are the EDP and IM value of record i , and n is the number of records. By assuming the Gaussian distribution of $\ln(EDP)$, the estimated conditional probability of exceeding an EDP level y , at a given $IM=im$ can be expressed as:

$$P(EDP = y|im) = 1 - \Phi\left(\frac{\ln(y) - \ln(a) - b \ln(im)}{\beta_{EDP|IM}}\right) \quad (5-6)$$

where $P(EDP = y|im)$ is the complementary cumulative distribution function (CCDF) of EDP at given IM, and $\Phi(\cdot)$ is the cumulative distribution function of the standard Gaussian distribution. This equation can be extended as:

$$P(DI \geq LS_i | im) = 1 - \int_0^{DS_i} \frac{1}{\sqrt{2\pi} \beta_{EDP|IM} EDP} \exp\left(\frac{[\ln(EDP_i) - (\ln(a) + b \ln(IM_i))]^2}{2 (\beta_{EDP|IM})^2}\right) d(EDP) \quad (5-7)$$

where LS_i is the limit state corresponding to different damage states (DS) and DI is the damage index.

The exceedance probabilities for a fragility curve by a lognormal cumulative probability density function were defined by Choi (2002) as:

$$P = \Phi \left(\frac{\ln \left(\frac{S_d}{S_c} \right)}{\sqrt{\beta_d^2 + \beta_c^2}} \right) \quad (5-8)$$

where β_d ($\beta_{EDP|IM}$) and β_c are the lognormal standard deviations (dispersions) of the demand and capacity, respectively, $\Phi(\bullet)$ is the standard normal cumulative distribution function, S_d is the median value for the limit state and S_d (EDP) is the median for the seismic demand, which is a function of the intensity measure IM. The composite logarithmic standard deviation of $\sqrt{\beta_d^2 + \beta_c^2}$ is known as the dispersion.

5.2.2 Scaled Approach (Incremental Dynamic Analysis, IDA)

The IDA method requires more computational effort because of the need to scale earthquake motions to different intensity levels, i.e., through increments. However, no prior assumptions need to be made in terms of probabilistic distribution of seismic demand in order to derive the fragility curves (Zhang, 2008). The damage probability is calculated as the ratio of the number of damage cases n_i at and beyond the damage state i (DS_i) over the number of total simulation cases N at a given IM level (im) (Karim and Yamazaki, 2001):

$$P (DI \geq LS_i | im) = \frac{n_i}{N} \quad (5-9)$$

The IDA fragility curves can be fitted with either a normal cumulative distribution function:

$$P (DI \geq LS_i | im) = \int_{-\infty}^{im} \frac{1}{\sqrt{2\pi}\sigma_{IM}} \exp \left(-\frac{(IM - \mu_{IM})^2}{2\sigma_{IM}^2} \right) d(IM) \quad (5-10)$$

or a log-normal cumulative distribution function:

$$P (DI \geq LS_i | im) = \int_{-\infty}^{im} \frac{1}{IM\sqrt{2\pi}\xi_{IM}} \exp \left(-\frac{(\ln(IM) - \lambda_{IM})^2}{2\xi_{IM}^2} \right) d(IM) \quad (5-11)$$

In this equation, σ_{IM} and μ_{IM} are the standard deviation and mean value of IM to reach the specified damage state based on normal distribution, while ξ_{IM} and λ_{IM} are the standard deviation and mean value of $\ln(IM)$ to reach the specified damage states based on lognormal distribution.

The responses from the IDA approach are often very sensitive to the characteristics of the individual input motion used as seismic input. Therefore, several analyses are required using different input motion records to achieve a reliable estimation of the probabilistic distribution of system response. Therefore, in this study, the cloud (probabilistic seismic demand analysis) approach is implemented to obtain the PSDMs for various components.

5.3 Specifications of Hospital Fire Sprinkler Piping System

The dimensions and layout of fire protection piping systems are individualized for each building and vary based on the architecture and occupancy of the building. Therefore, selecting a generic fire piping system is, to some extent, arbitrary. The piping system modeled in this study was adopted from the fire sprinkler of the University of California (UCSF) Medical Center Building. Slight modifications were implemented to the original design by redesigning the hangers and braces to meet the minimum spacing requirement of NFPA 13: Standard for the Installation of Sprinkler Systems (NFPA, 2011). Some of these requirements are:

- The maximum distance between the pipe hangers is 12 feet for pipe diameters smaller than 1.5 inches and 15 feet for larger (including 1.5 inch) pipe diameters.
- The maximum spacing between the lateral braces is 40 feet.
- The distance between the last longitudinal brace and the end of the pipe (2.5 inches and larger) should be less than 40 feet.
- The maximum intervals of longitudinal bracing is 80 feet.
- The distance between the last lateral brace and the end of the pipe (2.5 inches and larger) should be less than 6 feet.

- Four-way braces (attached to the horizontal piping) shall be provided within 24 inches of the centerline of the riser.

The final system incorporated a variety of commonly used components such as main runs and branch lines of various diameters, hangers, seismic braces, wire restraints, tee joints, elbow joints, and drops with sprinkler heads. It also contained a sufficiently large quantity of each component, which enabled a better statistical evaluation of the seismic performance of each component within the system. It should be noted that due to the uncertainty of material properties and other parameters such as damping ratio, variability in many of the modeling parameters such as steel yield strengths, wire restrainers and pipe hanger failure force, pipe hanger clip breakage force, and different anchorage ultimate strength can be incorporated in piping systems. However, in this model, the same modeling techniques and variables that were obtained from the calibration process (experiments in University at Buffalo) were used.

The piping system shown in Figure 5-1 covers an area of approximately 17,000 square feet. It is 250 feet long and 176 feet wide and has more than 900 threaded joints (649 x 1 in, 185 x 1.25 in, 28 x 1.5 in, 7 x 2 in, 41 x 2.5 in, 34 x 3 in, and 29 x 4 in diameter joints). A plenum height (the

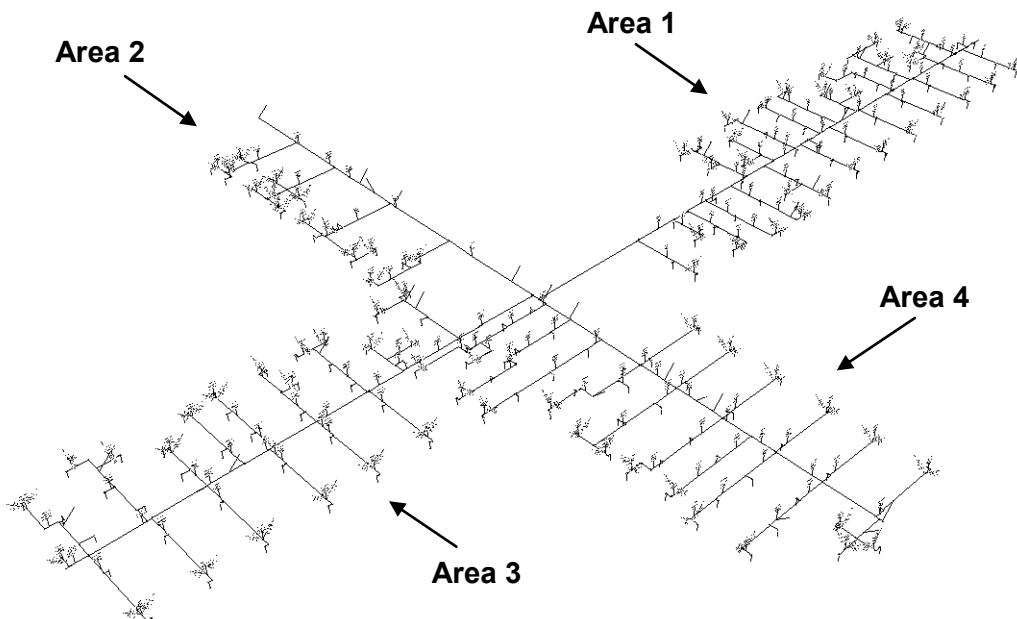


Figure 5-1 3-D View of UCSF Medical Center Sprinkler Piping System

distance between the supporting structural floor and the ceiling system) of 4 feet is used. The piping system is suspended 2.5 feet below the supporting floor, thus the sprinkler drops are 1.5 feet long. The sprinkler piping system is connected and braced to the supporting floor with 1 inch diameter longitudinal and lateral pipe sway braces or pair of 1/8-inch diameter galvanized 7 x 19 cable bracing, 3/8-inch all-threaded hangers, and 12-gauge wire restraints. The sway braces and wire restraints are oriented at 45-degree angles with respect to the plane of the supporting floor.

The piping layout was composed of four major areas. Area 1 is composed of main run pipes with total length of 154 ft with diameters varying from 2.5 to 4 in. These pipes feed 23 x 1.25 in. and 1 in diameter branch lines and 61 sprinkler heads. In Area 2, main run pipes are 97 ft long with 4 in diameter. This pipe supplies the water for 4 1.25 in and 1in branch lines and 15 sprinkler heads. Area 3 integrates 97 ft of 3 in. and 2.5 in. diameter main runs with 15 branch lines ranging in diameter from 1.5 to 1 in., and a total of 44 sprinkler heads. Area 4 consists of 82 ft of main distribution line varying in diameter from 4 to 2 in. The main distribution line feeds 16 x 1.5 to 1 in. branch lines. In this area, the main line and branch line supply 47 sprinkler heads. The original drawing of this piping system is presented in Appendix B.

According to the NFPA 13 (NFPA, 2011), flexible couplings shall be used on riser pipes passing through the structural floors allowing piping systems to accommodate interstory drifts. Therefore, riser pipes were not modeled, and their damage was not included in this study. In addition, the braces in the longitudinal and lateral directions near the riser-main run intersections are required by the NFPA 13 (NFPA, 2011). This will isolate the dynamic response of the piping system of each floor from that of the adjacent floors. Therefore, in this study, only the piping layout for one floor was analytically modeled. However, it should be noted in piping systems without braces near the riser, the overall response and performance of the system may significantly be different, and the results of this study may not hold true.

5.4 Considered Variables in Fire Sprinkler Analytical Models

In this study, several typical design variables were considered to produce 10 different piping scenarios (cases). In addition to the design variables, two types of distribution for input peak floor acceleration were considered, which will be discussed later. The considered design variables in piping systems are presented below.

- **Main Run Joints**

Threaded joints are the most common type of connection that are used in steel pipe construction. However, in new construction, the connections of larger pipe diameters (larger than 2 in) like riser and main run pipes are constructed using grooved fittings, while the connections of smaller pipe diameters such as branch lines and drop pipes (smaller than 2 in) are threaded fittings. Therefore, two types of joints (threaded and grooved) were considered as the variables for main run joints.

- **Water Supply System**

Fire sprinkler piping systems can be categorized into two distinct groups with respect to their operation technique. The first group belongs to piping systems, which have pressurized water in the pipes at all times, ready to spray, while the other is more of a “water on demand” system. Each system has its advantages and disadvantages, which are presented here.

Wet pipe sprinkler systems are the most common system among all other types of fire sprinkler systems. They are also the most reliable system, as they are simple with the only operating components being the automatic sprinklers and (commonly, but not always) the automatic alarm check valve. An automatic water supply provides water under pressure to the piping system. Leaks are more likely to develop in wet fire sprinkler piping systems since the water is constantly pressurized. Since water is stagnant for long periods of time, the system has to be maintained on a routine schedule that includes a periodic draining and refilling of the pipes.

Dry pipe systems are installed in spaces in which the ambient temperature may be cold enough to freeze the water in a wet pipe system, rendering the system inoperable. Dry pipe systems are most often used in unheated buildings, in parking garages, in outside canopies attached to heated buildings (in which a wet pipe system would be provided), or in refrigerated coolers. Dry pipe systems are the second most common type of sprinkler system. According to NFPA 13 (2011), dry pipe systems cannot be installed unless the range of ambient temperatures reaches below 40 F. In dry pipe systems, water is not present in the piping until the system operates. The piping is filled with air below the water supply pressure. When one or more of the automatic sprinklers is exposed for a sufficient time to a temperature at or above the temperature rating, it opens,

allowing the air in the piping to vent from that sprinkler. As the air pressure in the piping drops, the pressure differential across the dry pipe valve changes, allowing water to enter the piping system. Some of the disadvantages of using dry fire sprinkler systems are operation complexity, higher installation and maintenance cost, larger number of sprinkler zones due to the lower design flexibility, longer fire response time, and higher risk of corrosion.

In this study, the performance of these two systems was compared with respect to their vulnerability during earthquakes. Therefore, the only difference between these two systems was effect of water weight and mass on performance of piping systems.

- **Restrainers**

According to NFPA 13 (2011), the end sprinkler on a line shall be restrained against excessive vertical and lateral movement. This requirement is implemented in the model by restraining the end of each branch line (near to end sprinkler head). As mentioned before, the armover pipes are defined as a horizontal pipe that extends from the branch line to a single sprinkler. The NFPA13 (2011) standard requires that the cumulative horizontal length of an unsupported armover to a sprinkler should be less than 24 in. To comply with the standard, for each armover pipe longer than 24 in., at least one pipe hanger was inserted to the model. However, in order to better evaluate the armover vulnerability, two cases were defined for supporting armovers longer than 24 in. as: 1) one additional hanger was inserted into the model, and 2) wire restrainers were inserted into the model near the sprinkler head in addition to pipe hangers.

- **Bracings**

As mentioned before, two types of solid and tension-only sway braces are the most common types of braces for piping systems. Therefore, these two types were interchanged with each other in the analytical model in order to compare their performance.

5.5 Generation of Analytical Models for Fire Sprinkler Systems

Considering the number of variables mentioned previously, a total number of eight different piping systems were considered in this study. Also by combining the variation of motion distribution, a total number of 10 different piping cases were defined in this study. These cases are presented in Table 5-1. Two benchmark cases were selected based on the variation of main

run joints. These two cases have uniform S_{DS} (design spectral response acceleration at short periods) distribution, wet pipes, restrainer on armovers, and solid bracing (highlighted rows in Table 5-1).

An analytical model of the UCSF piping system was developed both in SAP2000 v15 and OpenSees v2.4.0. The OpenSees model was the primary model for analysis, comparison with and calibration of test data, and further investigation. The SAP model (Figure 5-1) was used for computing nodal gravity load and lumped mass distribution to the OpenSees model, as well as verification of the static response and modal analysis of the OpenSees model.

Table 5-1 Considered Parameters in Piping System Cases

Case #	Main Run		S_{DS} Distribution		Piping System		Restrainer on Armovers		Bracing	
	Threaded	Grooved	Uniform	Lognormal	Wet	Dry	Yes	No	Solid	Cable
1	✓	✗	✓	✗	✓	✗	✓	✗	✓	✗
2	✓	✗	✗	✓	✓	✗	✓	✗	✓	✗
3	✓	✗	✓	✗	✗	✓	✓	✗	✓	✗
4	✓	✗	✓	✗	✓	✗	✗	✓	✓	✗
5	✓	✗	✓	✗	✓	✗	✓	✗	✗	✓
6	✗	✓	✓	✗	✓	✗	✓	✗	✓	✗
7	✗	✓	✗	✓	✓	✗	✓	✗	✓	✗
8	✗	✓	✓	✗	✗	✓	✓	✗	✓	✗
9	✗	✓	✓	✗	✓	✗	✗	✓	✓	✗
10	✗	✓	✓	✗	✓	✗	✓	✗	✗	✓

The model was composed of elements that were presented earlier in this study. However, a summary of components used is presented in Table 5-2. Both end connections of wire restrainers were assumed as pin connection, as they are modeled using truss elements. Fixed connections were used for the attachment of pipe hangers to the assumed above deck. However, pin type attachments were used for connection of pipe hangers to the pipe runs. The main reason for choosing pin connections was because the hanger clips have negligible rotational resistance. The connection of the seismic braces was assumed to be rigid at both ends. A uniform excitation

pattern was used to excite the piping system under the generated accelerations. This excitation pattern allows for application of uniform excitation to a model acting in a certain direction.

As mentioned earlier, static analysis of the SAP model, which calculated the gravity load, was used to compute distributed loads to the frame elements and associated nodal masses in the OpenSees model. The mass of the piping system was determined using the wet weight of the pipes. An additional mass of 0.5 pounds was used for each sprinkler head. A classical Rayleigh damping was used for accounting the inherent damping of the piping system.

Table 5-2 Summary of Used Components for Analytical Model

	Reference	Material	Section	Element
Pipe Segments	3.5.2	NA	Elastic	Force-Based
Pipe Joints	3.5.2	Pinching4	NA	ZeroLength
Hangers	3.2.4	Steel02	Fiber	Force Based
Solid Braces	3.3.2.1	NA	Elastic	Force-Based
Restrainers	3.4.4	EPPG	NA	Truss
Cables	3.3.3.3	EPPG	NA	Truss

5.5.1 Real Time Element Removal Algorithm

A real time element removal algorithm was incorporated in the analyses to capture the progression of damage to the piping system during seismic excitations. An element removal algorithm enables the model to redistribute forces after failure occurs in an element using the “remove element” command in OpenSees software (OpenSees, 2012).

- **Restrainers**

This algorithm removed wire restrainers after they reached their rupture capacity, 0.4 kips from USG (2006). The assumed criteria made for the failure of wire restrainers was based on wire restrainer assembly (minimum of tensile failure of wire, pipe connection or raps, and deck anchorage strength). However, the failure criteria can be made based on ultimate tensile force or displacement of wire restrainers, which is not considered in this study.

- **Hangers**

Due to the large spectrum of hanger clip details, the failure force of the pipe hangers was calculated based on the minimum NFPA 13 (2011) requirements. NFPA 13 mandates that the hangers shall be designed to support five times the weight of the water-filled pipe plus 250 pounds at each point of support. This failure scenario was considered as the conservative failure criteria for pipe hangers.

In the wet piping system, the axial forces on the hanger were calculated after the dead load analysis was conducted. During the response history analyses, the program triggered the “remove element” command when the axial force of a hanger reached five times the recorded axial force plus 250 lbs.

In the dry piping system, first the dead load analysis of the wet piping system was performed. The axial forces of pipe hangers were recorded under this dead load analysis. Second, the dead load was removed from the piping system and a new dead load analysis, assuming a dry piping system, was performed. Finally, a nonlinear response history analysis was implemented.

- **Solid Braces**

Removal algorithm was set to remove the solid braces after they reached their design capacity, 6.3 kips. This number was set based on numbers provided in Table 9.3.5.8.7(a) of the NFPA 13 (2011) standard. This value corresponded to the 1in diameter pipe section solid braces with the l/r ratio less than 100 and horizontal angle equal to 45 degrees (see Appendix A).

- **Cable Braces**

The removal algorithm for cable bracing was set to remove cable bracing after they reached their rupture capacity, 1.471 kips. This number was obtained from the component test results that have been previously presented. Throughout a nonlinear response history analysis, a large number of cable braces failed (this will be presented later). As a result, the computer program experienced numerical convergence errors and instability problems after removing a few cable braces. In order to prevent the numerical

problems, cable braces were not removed during the response history analysis. However, the number of failed braces and their locations were recorded for fragility studies.

5.5.2 Modal Analysis and Damping Model

Fire sprinkler piping systems have many localized modes instead of a few fundamental modes like buildings and bridges. In other words, the fundamental mode shape of the piping system does not excite the complete piping system but a localized region (Gupta and Ju, 2011). The first 40 natural periods of all piping cases are plotted in Figure 5-2 and Figure 5-3, which correspond to piping models with and without considering initial gap strain for wire restrainers. The presented first 40 natural periods correspond to the branch lines in all cases. Wire restrainers are only located on the branch lines. Therefore, the initial gap or slack of wire restrainers (eliminating these elements from modal analysis) increased the first 40 natural periods of the UCSF piping system.

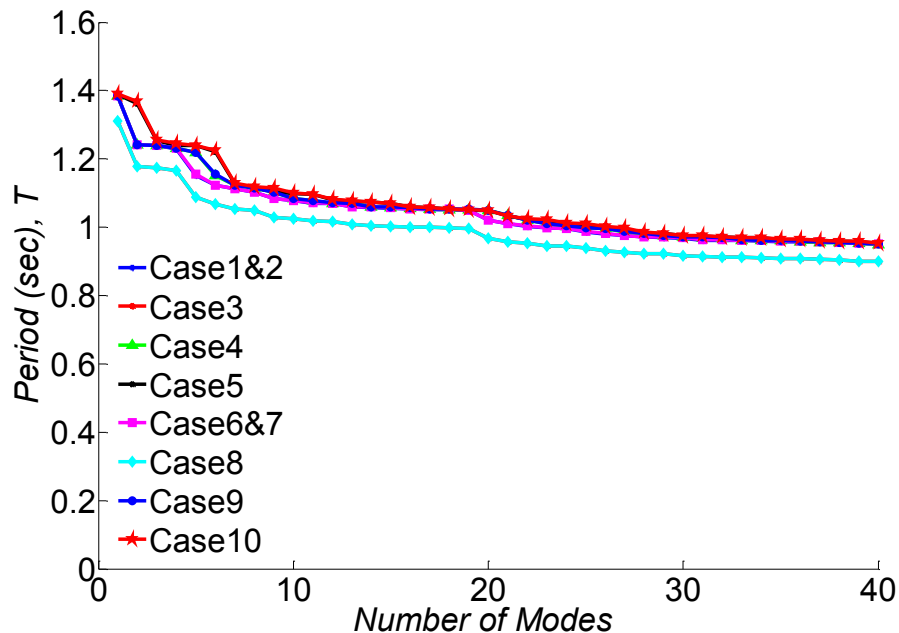


Figure 5-2 First Forty Natural Periods of All Piping Cases (0.005 Initial Gap Strain on Wire Restrainers)

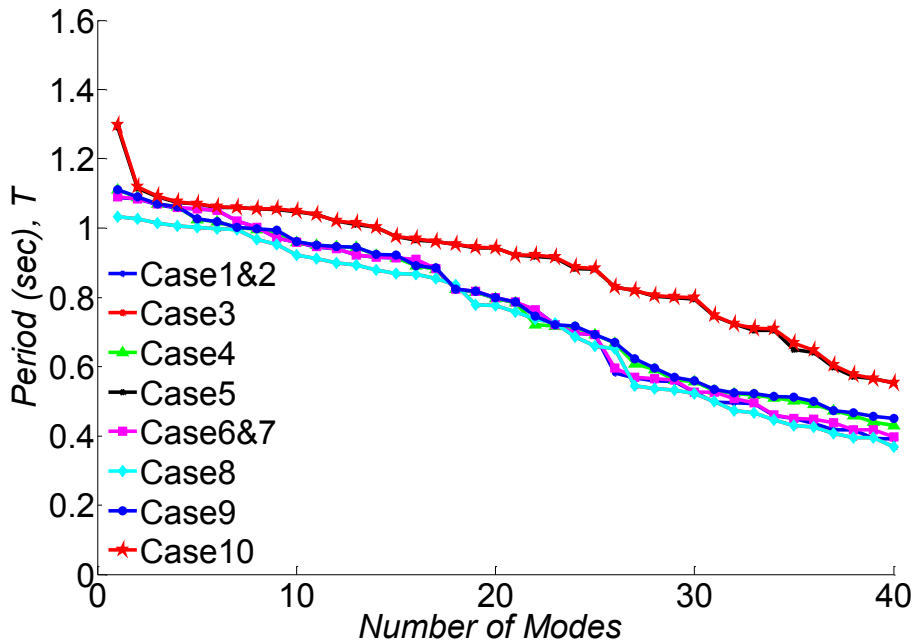


Figure 5-3 First Forty Natural Periods of All Piping Cases (Closed Gap Strain on Wire Restrainers)

Rayleigh damping was used for UCSF analytical model. The Rayleigh damping curve passed through damping ratios of 3% at the first and third fundamental periods of each case scenario of the UCSF piping system. The assumed damping model should be considered as the conservative damping model.

5.6 Generation of the Input Motions

It is crucial to assemble a suite of floor motions that accurately characterizes seismic hazard to develop PSDMs and eventually piping fragility curves. In the systems such as buildings and bridges, the input motions are mostly defined as ground motion. Per Bommer and Acevedo (2004), these ground motions can be categorized into three different groups: 1) artificial spectrum-matched accelerations; 2) synthetic accelerations generated from seismological source models by accounting for path and site effect; and 3) real accelerations recorded from past earthquakes. However, nonstructural systems are usually subjected to the floor motions. These floor motions can be classified into three groups as: 1) real floor motions recorded during past earthquakes; 2) synthetic floor accelerations obtained from floor response of range of structures subjected to synthetic or real ground motions; and 3) artificial spectrum-matched floor accelerations.

A limited number of real floor motions are available from past earthquakes mainly because of few instrumented structures. Since there is a lack of floor motion records, using synthetic floor acceleration histories may be the only solution to perform fragility studies for nonstructural components. The floor accelerations developed from the second group depend on the structural system. In other words, most of the motions that are realized by the nonstructural components are passed through the parent building, which means that some of the ground motion frequencies (near the fundamental frequencies of structure) will change (most of the time amplify). Therefore, the response of nonstructural systems will be very dependent on how close their fundamental frequencies are to the parent structure's frequencies. Considering the number of structural systems, structural nonlinearities, building dynamic properties, and height ratio of installed nonstructural components (elevation of installed component versus the total height of structure), an infinite number of floor motions may result from a ground motion. Hence, generating floor motions based on a few structural systems may not adequately represent the range of the response of nonstructural systems. Generating spectrum-matched response histories is not new, and it has been attempted several times in the past. The spectrum-matched motions usually include high energy contents. Also these motions do not account for arrivals of different types of seismic waves at different time-instants (Mukherjee and Gupta, 2002). However, as stated by Gupta and Ju (2011), piping systems have many localized modes. Therefore, a spectrum-matched approach was used to generate motions that cover a wide range of frequencies and excite most of the localized modes of the piping systems as a result. It should be noted that using a spectrum matched approach may lead to conservative results due to the high energy content of the generated motions.

Due to the inherent randomness of the seismological mechanisms and variations of structural systems, there is uncertainty in the nature of floor motions. The uncertainty of the ground motions is elaborated on by using two sets of 96 triaxial acceleration histories artificially generated using the spectrum-matching procedure. These two sets were generated based on different intensity variations of floor accelerations to study the effects of using different motion suites on piping responses. SIMQKE software (VanMarcke et al., 1976) was used to generate the artificial acceleration histories. The target response spectrum was input in the form of a spectral velocity spectrum, and the output was obtained in the form of acceleration histories with a specified peak acceleration value. All of the acceleration histories developed in this study were

incoherent and independent motions. Acceleration spectra were produced for the horizontal directions following ICC-AC156 (ICC, 2010) parameters (Figure 5-4a).

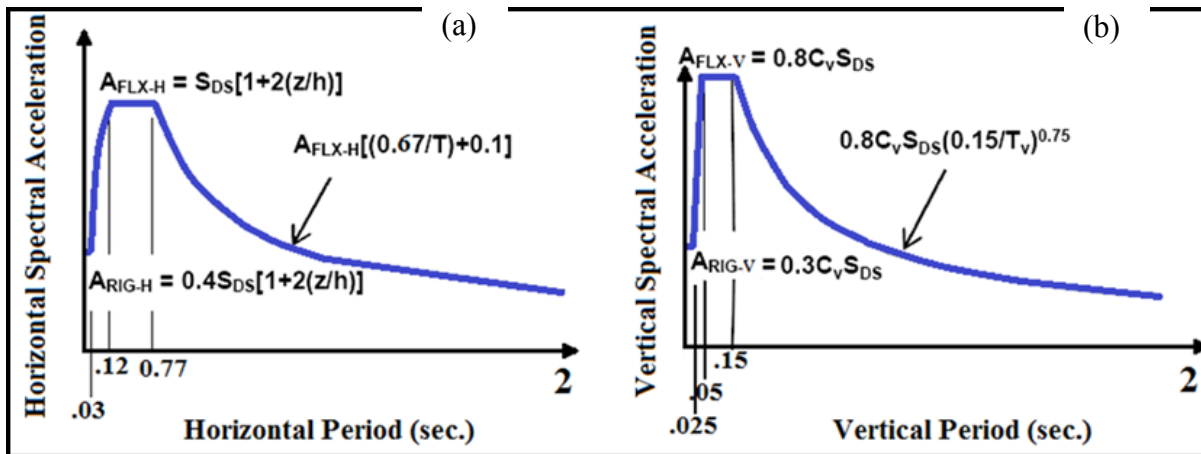


Figure 5-4 Design Response Spectrum, (a) Horizontal Response Spectra, (b) Vertical Response Spectra

The z/h parameter is the story height ratio, and S_{DS} is the design spectral response acceleration at short periods. The minimum and maximum periods for the horizontal accelerations were defined as 0.03 and 3.0 sec, respectively.

To generate the vertical component of the acceleration history sets, the vertical acceleration response spectrum introduced in ASCE/SEI 7-10 Chapter 23 (ASCE, 2010) was adopted. The S_{DS} value used to determine the vertical response spectrum for each set was the same as that of the horizontal spectra.

ASCE Chapter 11 (ASCE, 2010) was used to relate the parameters of the vertical acceleration spectra to the horizontal motion by determining S_{MS} , F_A , and S_S . The vertical coefficient, C_V , was then determined from Table 23.1-1 of ASCE/SEI 7-10 (ASCE, 2010). Site Classes D, E, and F were used to define the values of C_V . Figure 5-4b displays the vertical response spectrum from the new Chapter 23 of ASCE/SEI 7-10 (ASCE, 2010).

The minimum and the maximum periods for the vertical accelerations were defined as 0.02 and 2.0 sec, respectively. For the acceleration histories, a trapezoidal intensity envelope with a rise time, level time, and total duration of 5, 20, and 30 seconds, respectively, was specified for both

the horizontal and vertical motions. A fourth order low-pass Butterworth filter with a cut off frequency of 50 Hz was applied to the acceleration histories using Matlab (MathWorks, 2010). Afterward, the motions were baseline corrected using a linear curve fit method.

5.6.1 Motion Set 1: Motions with Uniform S_{DS} Distribution

The target horizontal floor spectra were developed by combining a uniform distribution of S_{DS} values varying from 0.1 g to 3 g and four height ratios of 0, 0.33, 0.67, and 1.0. The above procedure was executed once for the x-direction and once for the y-direction, with the same S_{DS} and z/h values generating a total of 192 frequency-independent horizontal acceleration histories. Table 5-3 presents the target response spectrum parameters used to generate the synthetic horizontal and vertical acceleration histories. The statistical distribution of the peak floor accelerations and the median 16th, 84th, and 97th percentile of the 5% damped elastic spectrum for the horizontal and vertical components are presented in Figure 5-5. The nonlinear analytical model of the UCSF piping system was subjected to the described 96 sets of triaxial motions.

Table 5-3 Desired Response Spectrum Parameters with Uniform S_{DS} Distribution

Case No.	S_{DS} (g)	Horizontal Parameters								Vertical Parameters	
		A_{FLX-H} (g)				A_{RIG-H} (g)				A_{FLX-v} (g)	A_{RIG-v} (g)
		$\frac{z}{h} = 0$	$\frac{z}{h} = \frac{1}{3}$	$\frac{z}{h} = \frac{2}{3}$	$\frac{z}{h} = 1$	$\frac{z}{h} = 0$	$\frac{z}{h} = \frac{1}{3}$	$\frac{z}{h} = \frac{2}{3}$	$\frac{z}{h} = 1$		
1	0.12	0.12	0.19	0.19	0.19	0.05	0.08	0.11	0.11	0.07	0.03
2	0.24	0.24	0.38	0.38	0.38	0.10	0.16	0.22	0.22	0.14	0.05
3	0.36	0.36	0.58	0.58	0.58	0.14	0.24	0.34	0.34	0.27	0.10
4	0.48	0.48	0.77	0.77	0.77	0.19	0.32	0.45	0.45	0.32	0.13
5	0.60	0.60	0.96	0.96	0.96	0.24	0.40	0.56	0.56	0.40	0.16
6	0.72	0.72	1.15	1.15	1.15	0.29	0.48	0.67	0.67	0.48	0.19
7	0.84	0.84	1.34	1.34	1.34	0.34	0.56	0.78	0.78	0.56	0.23
8	0.96	0.96	1.54	1.54	1.54	0.38	0.64	0.90	0.90	0.64	0.26
9	1.08	1.08	1.73	1.73	1.73	0.43	0.72	1.01	1.01	0.72	0.29
10	1.20	1.20	1.92	1.92	1.92	0.48	0.80	1.12	1.12	0.80	0.32
11	1.32	1.32	2.11	2.11	2.11	0.53	0.88	1.23	1.23	0.88	0.36
12	1.44	1.44	2.30	2.30	2.30	0.58	0.96	1.34	1.34	0.96	0.39
13	1.56	1.56	2.50	2.50	2.50	0.62	1.04	1.46	1.46	1.05	0.42
14	1.68	1.68	2.69	2.69	2.69	0.67	1.12	1.57	1.57	1.13	0.45
15	1.80	1.80	2.88	2.88	2.88	0.72	1.20	1.68	1.68	1.21	0.49
16	1.92	1.92	3.07	3.07	3.07	0.77	1.28	1.79	1.79	1.29	0.52
17	2.04	2.04	3.26	3.26	3.26	0.82	1.36	1.90	1.90	1.37	0.55
18	2.16	2.16	3.46	3.46	3.46	0.86	1.44	2.02	2.02	1.45	0.58
19	2.28	2.28	3.65	3.65	3.65	0.91	1.52	2.13	2.13	1.53	0.62
20	2.40	2.40	3.84	3.84	3.84	0.96	1.60	2.24	2.24	1.61	0.65
21	2.52	2.52	4.03	4.03	4.03	1.01	1.68	2.35	2.35	1.69	0.68
22	2.64	2.64	4.22	4.22	4.22	1.06	1.76	2.46	2.46	1.77	0.71
23	2.76	2.76	4.42	4.42	4.42	1.10	1.84	2.58	2.58	1.85	0.75
24	2.88	2.88	4.61	4.61	4.61	1.15	1.92	2.69	2.69	3.46	1.30

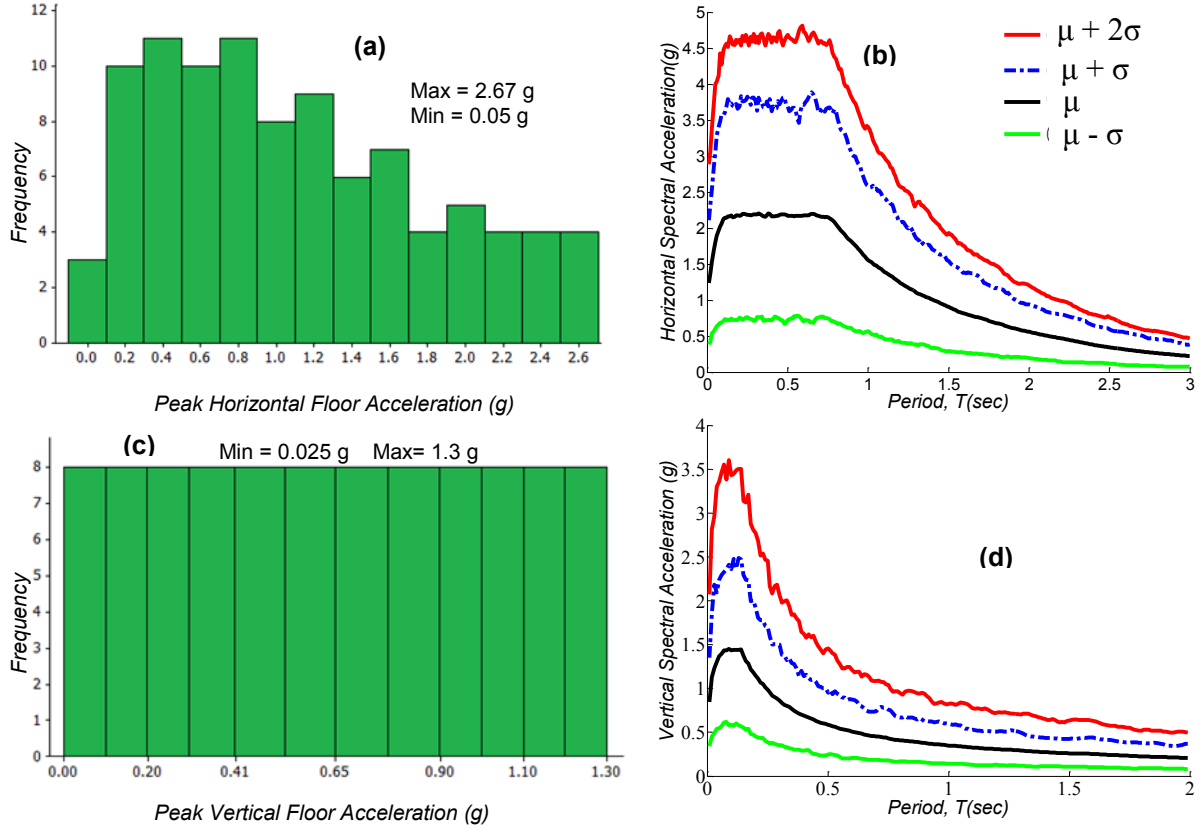


Figure 5-5 (a) Distribution of Peak Horizontal Floor Acceleration , (b) Horizontal Spectral Floor Acceleration, (c) Distribution of Peak Vertical Floor Acceleration, (d) Vertical Spectral Floor Acceleration with Uniform S_{DS} Distribution

5.6.2 Motion Set 2: Motions with Lognormal S_{DS} Distribution

The target horizontal floor spectra were developed by combining a lognormal distribution of S_{DS} values varying from 0.1 g to 3 g and four height ratios of 0, 0.33, 0.67, and 1.0. The distribution of S_{DS} and lognormal curve fitted curve with its parameters is presented in Figure 5-6a. The above procedure was executed once for the x-direction and once for the y-direction, with the same S_{DS} and z/h values generating a total of 192 frequency independent horizontal acceleration histories. Table 5-4 presents the target response spectrum parameters used to generate the synthetic horizontal and vertical acceleration histories. The statistical distribution of the peak floor accelerations and the median 16th, 84th, and 97th percentile of the 5% damped elastic spectrum for the horizontal and vertical components are presented in Figure 5-6. The nonlinear analytical model of the UCSF piping system was also subjected to the described 96 sets of triaxial motions.

Table 5-4 Desired Response Spectrum Parameters with Lognormal S_{DS} Distribution

Case No.	S_{DS} (g)	Horizontal Parameters								Vertical Parameters	
		A_{FLX-H} (g)				A_{RIG-H} (g)				A_{FLX-v} (g)	A_{RIG-v} (g)
		$\frac{z}{h} = 0$	$\frac{z}{h} = \frac{1}{3}$	$\frac{z}{h} = \frac{2}{3}$	$\frac{z}{h} = 1$	$\frac{z}{h} = 0$	$\frac{z}{h} = \frac{1}{3}$	$\frac{z}{h} = \frac{2}{3}$	$\frac{z}{h} = 1$		
1	0.12	0.12	0.19	0.19	0.19	0.05	0.08	0.11	0.11	0.07	0.03
2	0.40	0.40	0.64	0.64	0.64	0.16	0.27	0.37	0.37	0.27	0.11
3	0.80	0.80	1.28	1.28	1.28	0.32	0.53	0.75	0.75	0.54	0.22
4	0.60	0.60	0.96	0.96	0.96	0.24	0.40	0.56	0.56	0.40	0.16
5	0.80	0.80	1.28	1.28	1.28	0.32	0.53	0.75	0.75	0.54	0.22
6	0.90	0.90	1.44	1.44	1.44	0.36	0.60	0.84	0.84	0.60	0.24
7	1.00	1.00	1.60	1.60	1.60	0.40	0.67	0.93	0.93	0.67	0.27
8	1.10	1.10	1.76	1.76	1.76	0.44	0.73	1.03	1.03	0.74	0.30
9	1.20	1.20	1.92	1.92	1.92	0.48	0.80	1.12	1.12	0.80	0.32
10	1.30	1.30	2.08	2.08	2.08	0.52	0.87	1.21	1.21	0.87	0.35
11	1.40	1.40	2.24	2.24	2.24	0.56	0.93	1.31	1.31	0.94	0.38
12	0.70	0.70	1.12	1.12	1.12	0.28	0.47	0.65	0.65	0.47	0.19
13	1.35	1.35	2.16	2.16	2.16	0.54	0.90	1.26	1.26	0.90	0.36
14	0.85	0.85	1.36	1.36	1.36	0.34	0.57	0.79	0.79	0.57	0.23
15	0.95	0.95	1.52	1.52	1.52	0.38	0.63	0.89	0.89	0.64	0.26
16	1.50	1.50	2.40	2.40	2.40	0.60	1.00	1.40	1.40	1.01	0.41
17	1.70	1.70	2.72	2.72	2.72	0.68	1.13	1.59	1.59	1.14	0.46
18	1.90	1.90	3.04	3.04	3.04	0.76	1.27	1.77	1.77	1.27	0.51
19	2.10	2.10	3.36	3.36	3.36	0.84	1.40	1.96	1.96	1.41	0.57
20	2.20	2.20	3.52	3.52	3.52	0.88	1.47	2.05	2.05	1.47	0.59
21	2.40	2.40	3.84	3.84	3.84	0.96	1.60	2.24	2.24	1.61	0.65
22	0.30	0.30	0.48	0.48	0.48	0.12	0.20	0.28	0.28	0.20	0.08
23	1.55	1.55	2.48	2.48	2.48	0.62	1.03	1.45	1.45	1.04	0.42
24	2.90	2.90	4.64	4.64	4.64	1.16	1.93	2.71	2.71	1.94	0.78

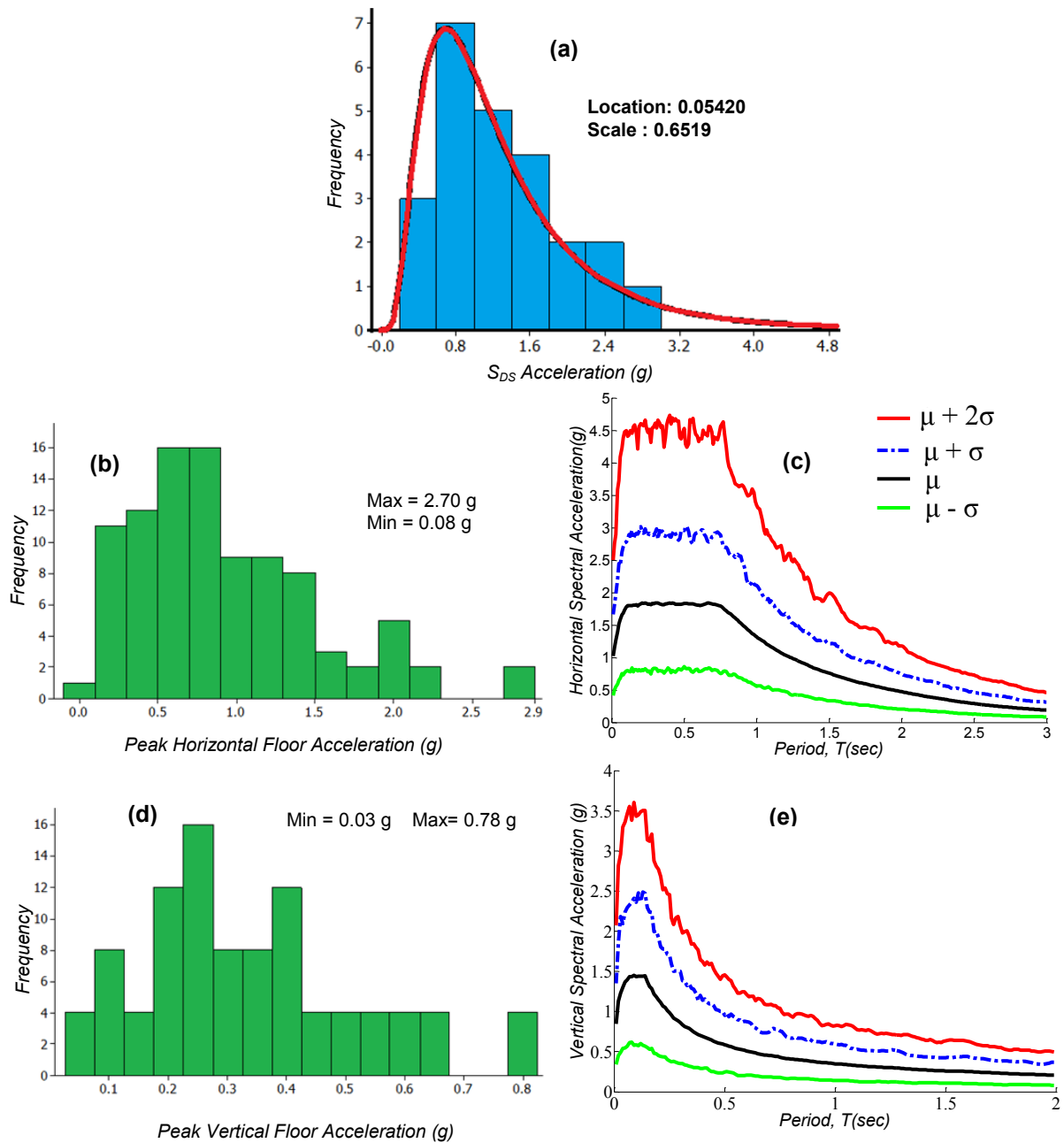


Figure 5-6 Distribution of (a) S_{DS} Acceleration (b) Peak Horizontal Floor Acceleration, (c) Horizontal Spectral Floor Acceleration, (d) Distribution of Peak Vertical Floor Acceleration, (e) Vertical Spectral Floor Acceleration of Motions with Lognormal S_{DS} Distribution

5.6.3 Intensity Measure (IM) Selection

The formulation of a PSDM shown in equations (5-3) through (5-8) is based on IM. Therefore, it is evident that the selection of an optimal IM can play a predominant role in the accuracy of the model in estimating seismic demand. Their optimal selection is instrumental in obtaining reasonable estimates of the vulnerability of various components as the uncertainty associated with the demand is dependent on the variable chosen as an IM to some extent, although this is not the only source of the uncertainty (Ramanathan, 2012).

Several researchers have used different parameters as IM selection for acceleration-sensitive nonstructural systems. The Applied Technology Council report, ATC-58 (2009), uses the peak floor acceleration (PFA) as the IM. In the experimental fragility study done by Almaraz et al. (2007), floor (shake table) spectral accelerations at 0.2, 0.5, 1.0, 1.5, and 2 seconds and also PFA was considered as intensity measure. In the work done by Sato et al. (2011), the peak floor acceleration was used as IM for generating the Japanese ceiling fragility curves. In the more recent work on piping fragility done by Soroushian et al. (2011) and Gupta and Ju (2011), the peak ground acceleration (PGA) was used as the intensity measure. The spectral acceleration at the fundamental period of parent structure or nonstructural systems can be used as the IM for fragility study of nonstructural systems. Therefore, choosing a reliable intensity measure (IM) is one of the complex key procedures for assessing fragility curves.

Piping systems have many localized modes instead of a few fundamental modes like buildings and bridges. Therefore, there is no actual fundamental period for piping systems. Also, mode shapes close to the fundamental period of the parent structure may not excite the entire piping system. So, using the spectral acceleration at a specific period may not be an appropriate choice. Since the piping systems are usually subject to floor accelerations and not ground accelerations, PGA may not be the best choice. The main reason ground motions were not used is that they usually amplify through the height of structure, and nonstructural systems installed in the upper floors are more vulnerable compared to the lower floors. Hence, the peak floor acceleration was used as the IM in this study.

5.7 Component Demands

Probabilistic seismic demand models (PSDMs) of various piping components were developed by performing a probabilistic seismic demand analysis (PSDA). Fragility curves of different key piping components were developed based on their corresponding PSDMs. These component fragility curves were further combined to obtain the system fragility curves.

Based on geometry, the response of a piping system can significantly vary. As an example, for the same pipe section, the rotational demands on long armovers (more than 2-feet) are generally larger than on straight drops (Soroushian et al., 2012). Therefore, it is necessary to categorize the *EDPs* to better represent the physical damage. To do so, *EDPs* of branch line pipes were categorized based on the pipe diameter and the type of branch line (with or without armovers). The demand parameters of the piping system were defined as the median: 1) percentage of failed wire restrainers; 2) percentage of broken hangers; 3) percentage of failed braces; 4) the rotation at the tee armovers and elbow armovers; 5) the rotation at critical joints of the branch lines; and 6) rotation of fittings on the main runs. Due to only a few numbers of failed solid braces, these components were not considered for component and system level fragility curves in some of the piping cases. Table 5-5 through Table 5-14 present the regression parameters a and b along with β_{dIM} for piping tee-joints, braces, hangers, and wires for all 10 different piping cases. Figure 5-7 through Figure 5-16 shows the demand plots for the failed wire restrainers and the rotational demands for the 2.5in pipe diameter joints.

Table 5-5 Engineering Demand Parameter Estimations for Pipe Components-Case 1

Pipe Name	a	b	β_{dIM}
ARMOVERS			
Armover-Tee Joint	0.016	1.69	0.59
Armover-Elbow Joint	0.009	1.46	0.49
BRANCH LINES			
1" Pipe	0.010	1.56	0.63
1.25" Pipe	0.009	1.32	0.60
1.5" Pipe	0.010	1.48	0.73
MAIN RUNS			
2" Pipe	0.005	1.76	0.72
2.5" Pipe	0.001	0.93	0.42
3" Pipe	0.001	1.09	0.59
4" Pipe	0.001	1.24	0.51
SUPPORTS			
Wire Restrainers	0.131	1.64	0.50
Hangers	0.057	1.90	0.60
Braces	0.040	1.23	0.50

Table 5-6 Engineering Demand Parameter Estimations for Pipe Components-Case 2

Pipe Name	a	b	β_{dIM}
ARMOVERS			
Armover-Tee Joint	0.015	1.84	0.49
Armover-Elbow Joint	0.008	1.55	0.40
BRANCH LINES			
1" Pipe	0.008	1.65	0.47
1.25" Pipe	0.008	1.29	0.50
1.5" Pipe	0.008	1.39	0.57
MAIN RUNS			
2" Pipe	0.005	1.91	0.59
2.5" Pipe	0.001	0.90	0.34
3" Pipe	0.001	1.05	0.47
4" Pipe	0.001	1.32	0.45
SUPPORTS			
Wire Restrainers	0.127	1.85	0.47
Hangers	0.059	2.09	0.54

Table 5-7 Engineering Demand Parameter Estimations for Pipe Components-Case 3

Pipe Name	a	b	β_{dIM}
ARMOVERS			
Armover-Tee Joint	0.013	1.66	0.55
Armover-Elbow Joint	0.008	1.43	0.48
BRANCH LINES			
1" Pipe	0.008	1.51	0.58
1.25" Pipe	0.007	1.25	0.53
1.5" Pipe	0.007	1.33	0.59
MAIN RUNS			
2" Pipe	0.003	1.67	0.62
2.5" Pipe	0.001	0.87	0.36
3" Pipe	0.001	0.98	0.53
4" Pipe	0.001	1.19	0.49
SUPPORTS			
Wire Restrainers	0.097	1.86	0.53
Hangers	0.037	2.16	0.59

Table 5-9 Engineering Demand Parameter Estimations for Pipe Components-Case 5

Pipe Name	a	b	β_{dIM}
ARMOVERS			
Armover-Tee Joint	0.021	1.61	0.45
Armover-Elbow Joint	0.013	1.34	0.36
BRANCH LINES			
1" Pipe	0.010	1.33	0.35
1.25" Pipe	0.008	1.08	0.40
1.5" Pipe	0.009	1.30	0.41
MAIN RUNS			
2" Pipe	0.002	1.31	0.43
2.5" Pipe	0.001	0.89	0.27
3" Pipe	0.001	0.89	0.31
4" Pipe	0.001	1.04	0.30
SUPPORTS			
Wire Restrainers	0.170	1.26	0.45
Hangers	0.005	0.08	0.19
Braces	0.542	0.96	0.48

Table 5-11 Engineering Demand Parameter Estimations for Pipe Components-Case 7

Pipe Name	a	b	β_{dIM}
ARMOVERS			
Armover-Tee Joint	0.017	1.79	0.46
Armover-Elbow Joint	0.010	1.57	0.40
BRANCH LINES			
1" Pipe	0.009	1.65	0.49
1.25" Pipe	0.007	1.28	0.52
1.5" Pipe	0.009	1.50	0.60
MAIN RUNS			
2" Pipe	0.024	2.46	1.05
2.5" Pipe	0.012	1.46	0.35
3" Pipe	0.010	1.38	0.33
4" Pipe	0.010	1.60	0.40
SUPPORTS			
Wire Restrainers	0.128	1.73	0.42
Hangers	0.046	2.00	0.53

Table 5-8 Engineering Demand Parameter Estimations for Pipe Components-Case 4

Pipe Name	a	b	β_{dIM}
ARMOVERS			
Armover-Tee Joint	0.009	1.54	0.59
Armover-Elbow Joint	0.010	1.46	0.46
BRANCH LINES			
1" Pipe	0.010	1.56	0.54
1.25" Pipe	0.010	1.39	0.56
1.5" Pipe	0.009	1.41	0.67
MAIN RUNS			
2" Pipe	0.005	1.78	0.71
2.5" Pipe	0.001	0.95	0.36
3" Pipe	0.001	1.11	0.52
4" Pipe	0.001	1.26	0.44
SUPPORTS			
Wire Restrainers	0.118	1.57	0.37
Hangers	0.061	1.87	0.54
Braces	0.044	0.65	0.31

Table 5-10 Engineering Demand Parameter Estimations for Pipe Components-Case 6

Pipe Name	a	b	β_{dIM}
ARMOVERS			
Armover-Tee Joint	0.019	1.68	0.52
Armover-Elbow Joint	0.011	1.48	0.45
BRANCH LINES			
1" Pipe	0.010	1.58	0.57
1.25" Pipe	0.009	1.34	0.57
1.5" Pipe	0.011	1.57	0.69
MAIN RUNS			
2" Pipe	0.018	2.25	1.03
2.5" Pipe	0.011	1.48	0.37
3" Pipe	0.010	1.39	0.32
4" Pipe	0.010	1.53	0.41
SUPPORTS			
Wire Restrainers	0.126	1.72	0.46
Hangers	0.048	1.92	0.55
Braces	0.041	0.43	0.27

Table 5-12 Engineering Demand Parameter Estimations for Pipe Components-Case 8

Pipe Name	a	b	β_{dIM}
ARMOVERS			
Armover-Tee Joint	0.013	1.66	0.56
Armover-Elbow Joint	0.008	1.43	0.47
BRANCH LINES			
1" Pipe	0.008	1.54	0.60
1.25" Pipe	0.008	1.26	0.54
1.5" Pipe	0.007	1.34	0.61
MAIN RUNS			
2" Pipe	0.004	1.71	0.64
2.5" Pipe	0.001	0.87	0.37
3" Pipe	0.001	0.99	0.53
4" Pipe	0.001	1.20	0.52
SUPPORTS			
Wire Restrainers	0.093	1.87	0.45
Hangers	0.040	2.09	0.57

Table 5-13 Engineering Demand Parameter Estimations for Pipe Components-Case 9

Pipe Name	<i>a</i>	<i>b</i>	$\beta_{d IM}$
ARMOVERS			
Armover-Tee Joint	0.019	1.68	0.52
Armover-Elbow Joint	0.011	1.48	0.45
BRANCH LINES			
1" Pipe	0.010	1.58	0.57
1.25" Pipe	0.009	1.34	0.57
1.5" Pipe	0.011	1.57	0.69
MAIN RUNS			
2" Pipe	0.022	2.05	0.93
2.5" Pipe	0.015	1.13	0.39
3" Pipe	0.011	1.15	0.36
4" Pipe	0.011	1.35	0.44
SUPPORTS			
Wire Restrainers	0.158	1.32	0.41
Hangers	0.006	0.52	0.31
Braces	0.477	1.14	0.50

Table 5-14 Engineering Demand Parameter Estimations for Pipe Components-Case 10

Pipe Name	<i>a</i>	<i>b</i>	$\beta_{d IM}$
ARMOVERS			
Armover-Tee Joint	0.021	1.56	0.41
Armover-Elbow Joint	0.013	1.29	0.33
BRANCH LINES			
1" Pipe	0.011	1.34	0.35
1.25" Pipe	0.008	1.04	0.41
1.5" Pipe	0.009	1.29	0.51
MAIN RUNS			
2" Pipe	0.022	2.05	0.93
2.5" Pipe	0.015	1.13	0.39
3" Pipe	0.011	1.15	0.36
4" Pipe	0.011	1.35	0.44
SUPPORTS			
Wire Restrainers	0.158	1.32	0.41
Hangers	0.006	0.52	0.31
Braces	0.477	1.14	0.50

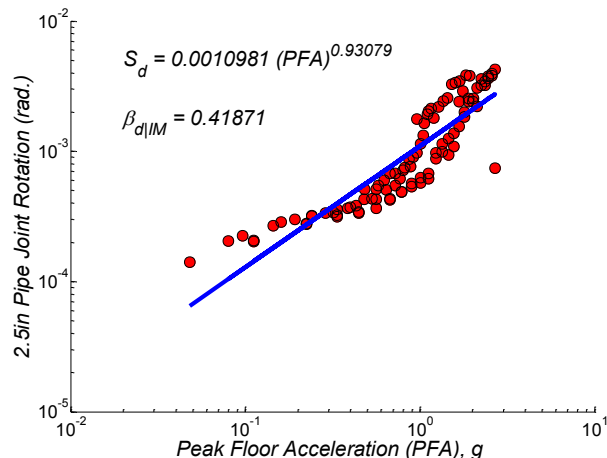
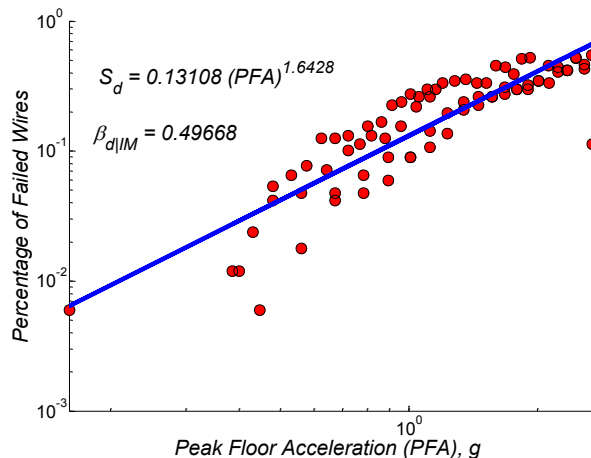


Figure 5-7 Sample Probabilistic Seismic Demand: (a) Percentage of Failed Wires, (b) 2.5 in. Pipe Joint Rotation (rad.), Case 1

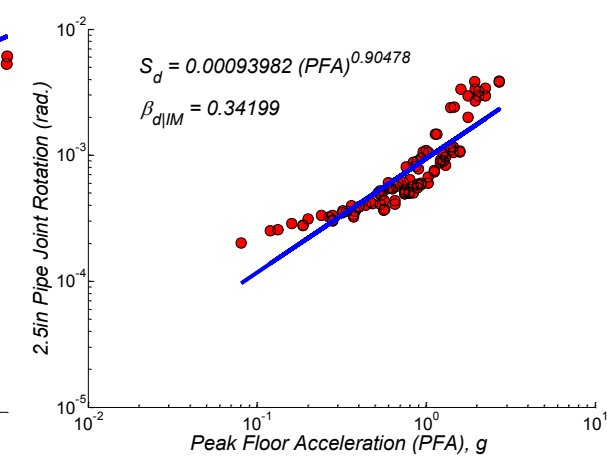
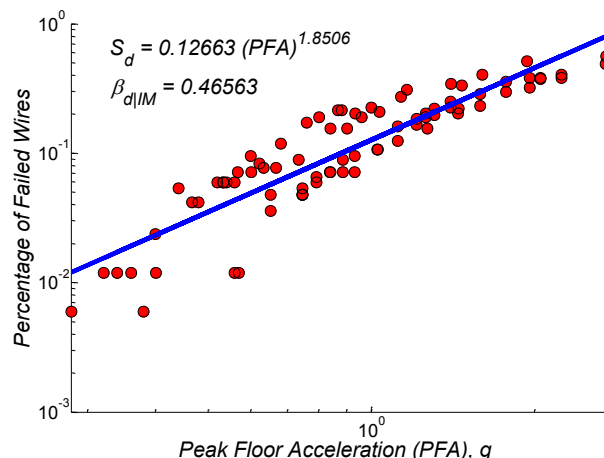


Figure 5-8 Sample Probabilistic Seismic Demand: (a) Percentage of Failed Wires, (b) 2.5 in. Pipe Joint Rotation (rad.), Case 2

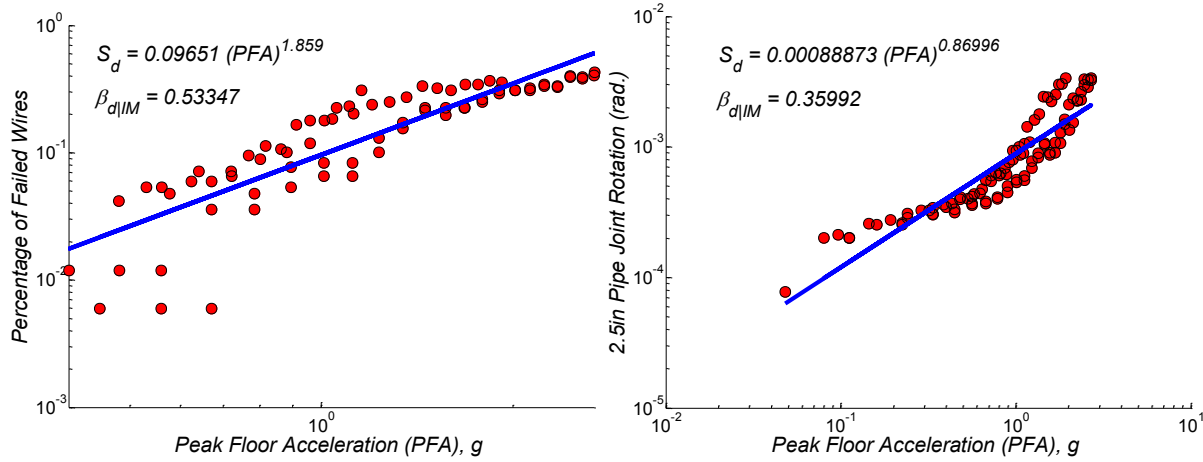


Figure 5-9 Sample Probabilistic Seismic Demand: (a) Percentage of Failed Wires, (b) 2.5 in. Pipe Joint Rotation (rad.), Case 3

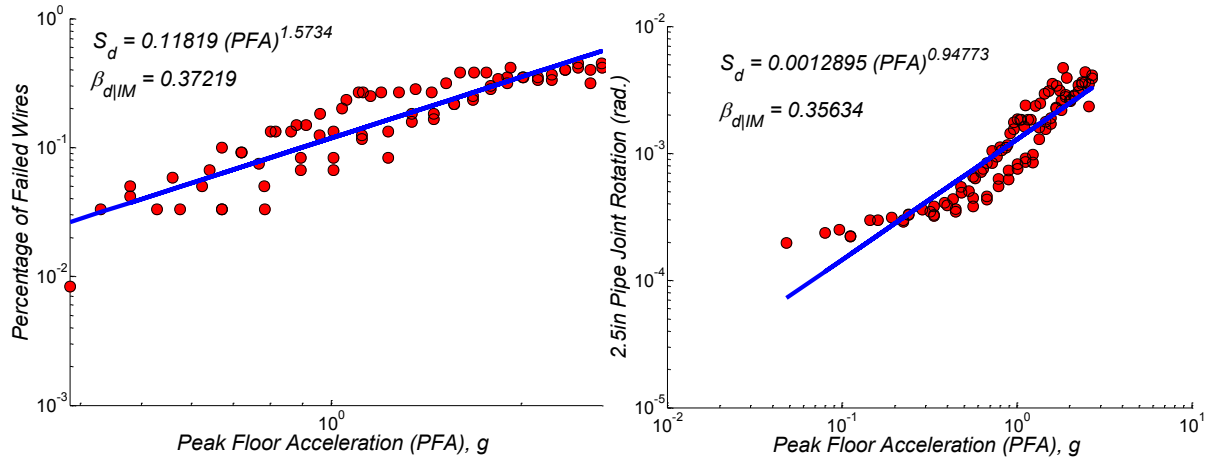


Figure 5-10 Sample Probabilistic Seismic Demand: (a) Percentage of Failed Wires, (b) 2.5 in. Pipe Joint Rotation (rad.), Case 4

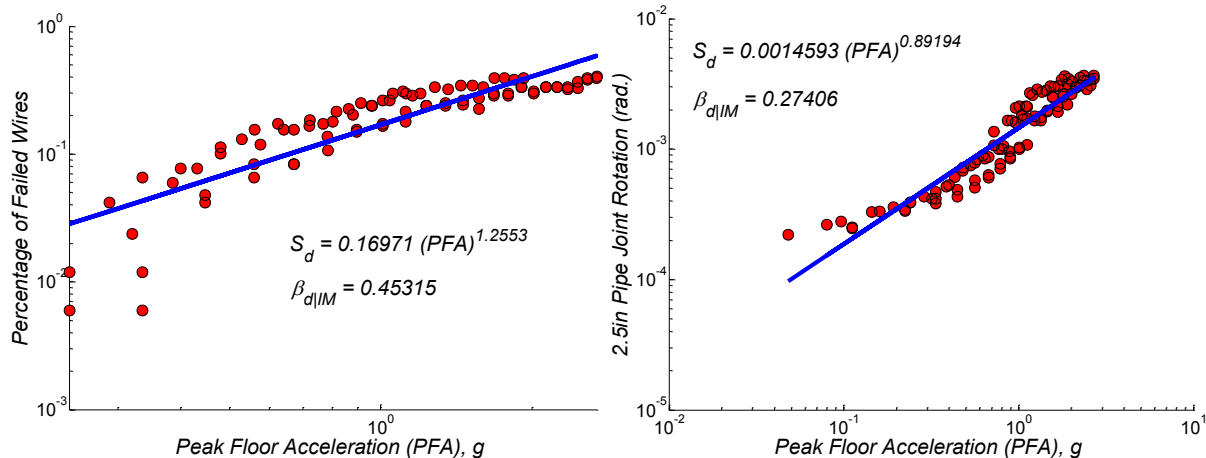


Figure 5-11 Sample Probabilistic Seismic Demand: (a) Percentage of Failed Wires, (b) 2.5 in. Pipe Joint Rotation (rad.), Case 5

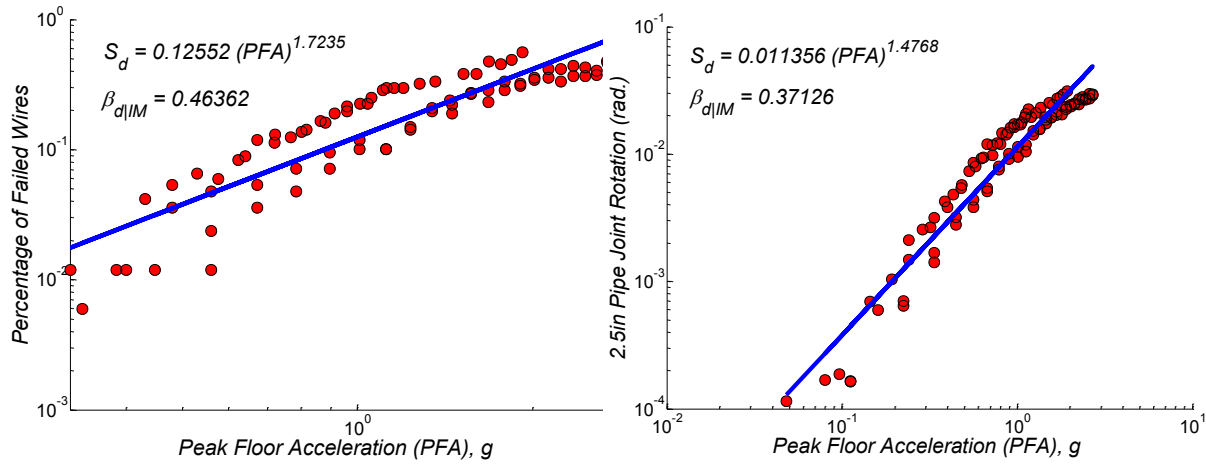


Figure 5-12 Sample Probabilistic Seismic Demand: (a) Percentage of Failed Wires, (b) 2.5 in. Pipe Joint Rotation (rad.), Case 6

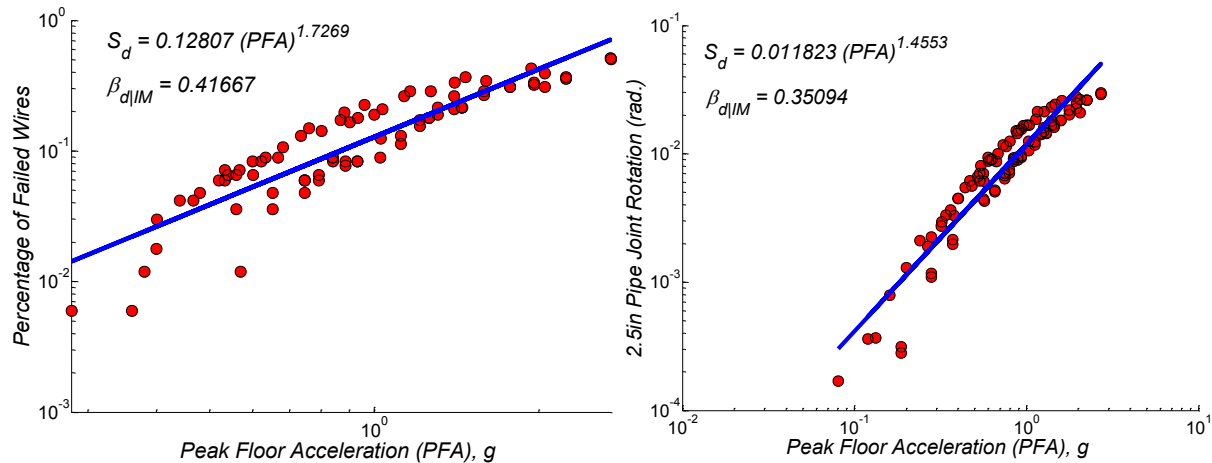


Figure 5-13 Sample Probabilistic Seismic Demand: (a) Percentage of Failed Wires, (b) 2.5 in. Pipe Joint Rotation (rad.), Case 7

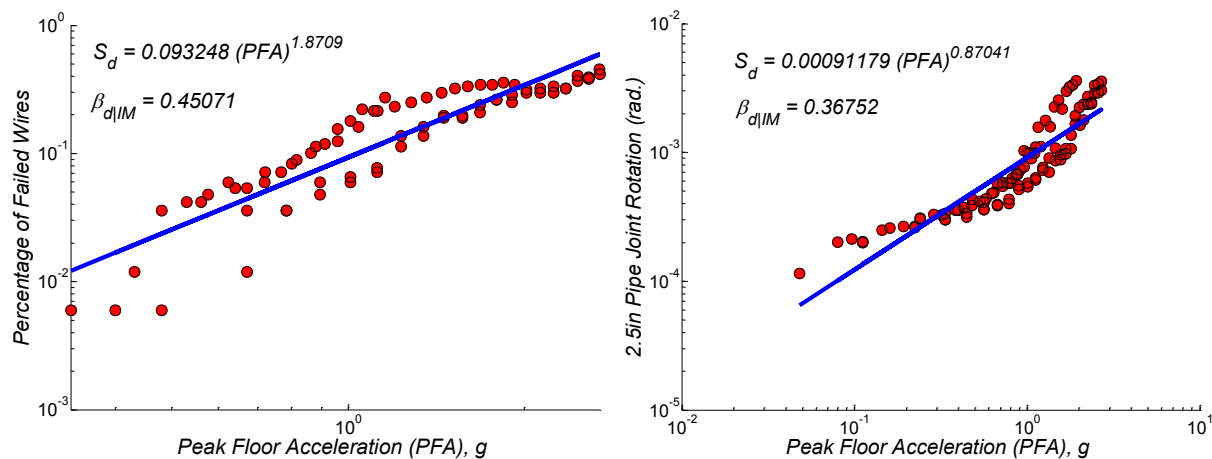


Figure 5-14 Sample Probabilistic Seismic Demand: (a) Percentage of Failed Wires, (b) 2.5 in. Pipe Joint Rotation (rad.), Case 8

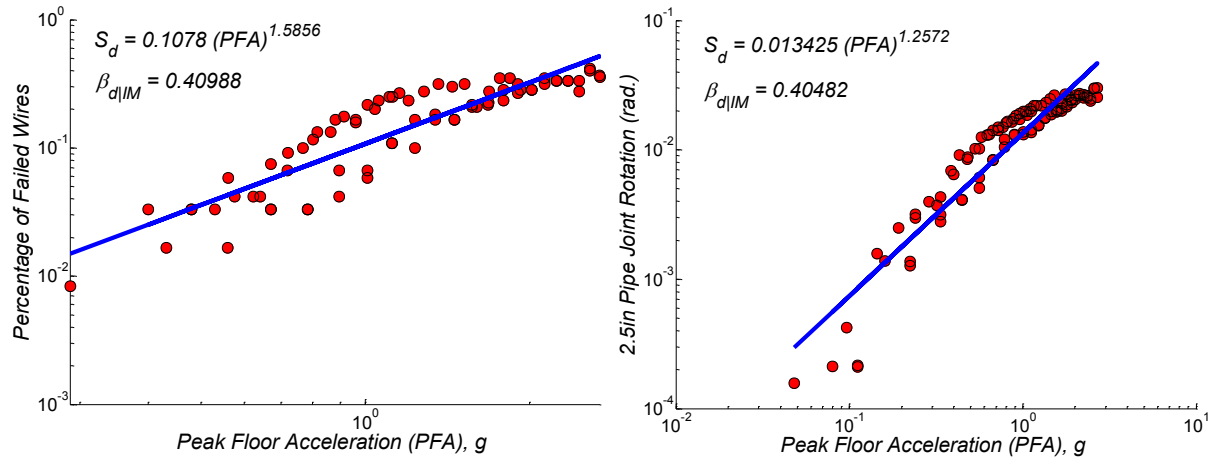


Figure 5-15 Sample Probabilistic Seismic Demand: (a) Percentage of Failed Wires, (b) 2.5 in. Pipe Joint Rotation (rad.), Case 9

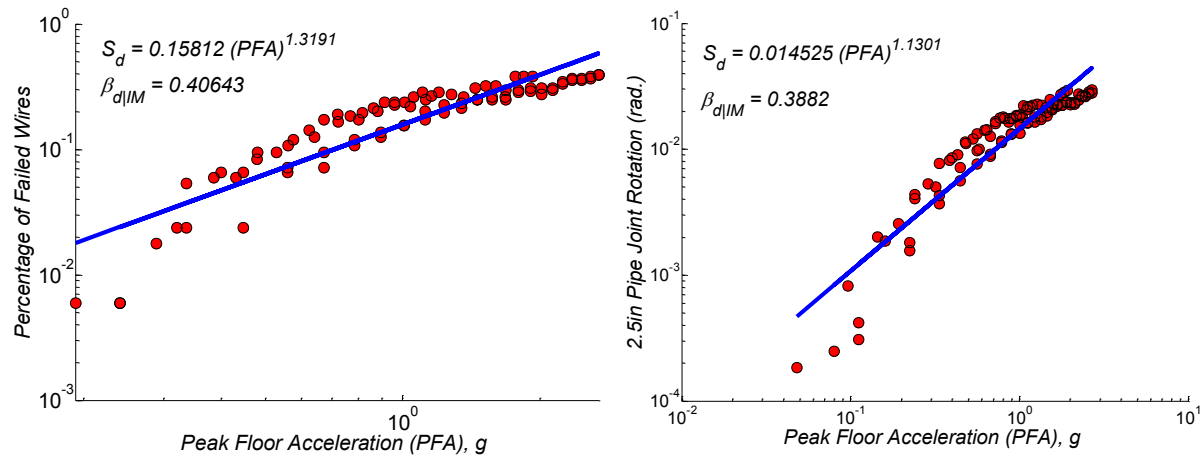


Figure 5-16 Sample Probabilistic Seismic Demand: (a) Percentage of Failed Wires, (b) 2.5 in. Pipe Joint Rotation (rad.), Case 10

5.8 Pipe Joint Capacity Parameters

In order to develop fragility curves for critical components of fire sprinkler piping systems, their corresponding damage states need to be identified and quantified statistically. In this study, the damage states corresponding to pipe joints are defined based on different plastic rotation levels until reaching their leakage capacity. Therefore, statistically quantifying the leakage capacity is a crucial step for defining the pipe joint damage states. The procedure for determining leakage capacity for threaded and grooved joints is presented below.

5.8.1 Threaded Joints

The capacity of each pipe diameter was determined from the median rotational threshold corresponding to the first significant leakage of the joint, θ_{leak} . For the pipe diameters that were tested at the University at Buffalo, θ_{leak} and β_c were borrowed from the work done by Tian et al. (2012) and are presented in Table 4. For the rest of the pipes, θ_{leak} (rad.) was calculated as (Tian et al., 2012):

$$\theta_{leak} = \frac{2 \bar{s}}{D_0} \quad (5-12)$$

In this equation, \bar{s} (average axial slip, analogous to strain in bending assuming plane section of pipes remain plane) is a constant value of 0.019 in for threaded pipe joints, and D_0 (in.) is the outside pipe diameter. Table 4 shows that the values of θ_{leak} calculated using Equation (5-12) correspond well with the experimentally determined values. This equation provides a good approximation for the median rotational capacity at first significant leakage for those pipe diameters that were not previously tested. Also for each pipe diameter in this group, values of β_c were calculated using linear interpolation between two adjacent previously tested diameters.

Table 5-15 Rotational Capacities of Threaded Joints

Pipe Name	Experiment		Eq. (2)	β_c
	θ_{leak}	β_c		
TEST SETS				
3/4" Pipe	0.040	0.206	0.037	NA
1" Pipe	0.031	0.146	0.029	NA
2" Pipe	0.014	0.094	0.016	NA
4" Pipe	0.010	0.216	0.009	NA
6" Pipe	0.006	0.204	0.006	NA
PROPOSED COMPONENTS				
1.25" Pipe	NA	NA	0.023	0.133
1.5" Pipe	NA	NA	0.020	0.120
2.5" Pipe	NA	NA	0.013	0.125
3" Pipe	NA	NA	0.011	0.155
3.5" Pipe	NA	NA	0.010	0.186
5" Pipe	NA	NA	0.007	0.210

5.8.2 Grooved Joints

The rotational capacity of each pipe diameter was determined from the median rotational threshold corresponding to the first leakage of the joint, θ_{leak} . For the pipe diameters that were tested at the University at Buffalo, θ_{leak} and β_c were adopted from the work done by Tian et al. (2012). For the proposed diameters, the median rotational capacities were calculated from the equations presented in Figure 2-22 at the intersection of fitted curves and leakage line. Also for each pipe diameter in this group, values of β_c were calculated using linear interpolation between two previously tested diameters. The same β_c as 4 in pipe diameter was used for 5 in and 6 in pipe diameters.

Table 5-16 Rotational Capacities of Grooved Joints

Pipe Size	Experiment		Calculation	
	θ_{leak}	β_c	θ_{leak}	β_c
TEST SETS				
2" Pipe	0.077	0.170	NA	NA
4" Pipe	0.021	0.049	NA	NA
PROPOSED COMPONENTS				
2.5" Pipe	NA	NA	0.038	0.140
3" Pipe	NA	NA	0.029	0.110
3.5" Pipe	NA	NA	0.024	0.079
5" Pipe	NA	NA	0.017	0.049
6" Pipe	NA	NA	0.014	0.049

5.9 Damage States

A damage state is a metric that describes the post-earthquake functionality or the level of damage sustained by a component or system subjected to a certain intensity measure. The individual damage states are defined by representative capacity values median (S_c) and dispersion (β_c), which are assumed to be lognormal akin to the demands. A continuous range of damage was assumed to exist, though the damage state definitions were discrete. This assumption enables the closed-form computation of the component fragility curves.

While only a single capacity may exist for certain components within a piping system, multiple damage states can be defined for the components and entire system. The three damage states are defined for pipe components and are named “Slight,” “Moderate,” and “Extensive.”

The damage states of pipe joints were defined based on the range of plastic rotations. A similar concept has been defined in ASME (2004) design guidelines for nuclear power plant piping systems. Unlike the piping system in hospitals and office buildings that have threaded and grooved joints, the studies related to nuclear power plant piping systems are conducted on piping systems that have welded joints (Ju and Gupta, 2012).

5.9.1 Threaded Joints

The damage states of pipe joints are defined based on the extent of plastic rotations. The second point on the generic backbone curve, θ_N , was assumed as the starting point of nonlinear behavior. The likelihood of any leakage occurring in this level is low; however, there is a possibility for permanent rotation of joints. The “Moderate” damage state was selected as the average value between “Slight” and “Extensive” rotations. The “Extensive” damage state corresponds to the observation of the first significant leakage rotation (θ_{leak}). The moderate rotational damage state, θ_M , was defined as the dripping and spraying condition of the threaded joints (Figure 5-17). The dispersion values were set to β_c for all damage states. The parameters for the damage states for threaded pipe joints are presented in Table 5-17.

Table 5-17 Damage States of Threaded Joint Components

Pipe Diameter	Slight	Moderate	Extensive	Dispersion
	Median (rad.)			β_c
TEST SETS				
3/4" Pipe	0.005	0.023	0.040	0.206
1" Pipe	0.005	0.018	0.031	0.146
2" Pipe	0.005	0.094	0.014	0.094
4" Pipe	0.005	0.075	0.010	0.216
6" Pipe	0.005	0.006	0.006	0.204
PROPOSED COMPONENTS				
1.25" Pipe	0.005	0.014	0.023	0.133
1.5" Pipe	0.005	0.013	0.020	0.120
2.5" Pipe	0.005	0.009	0.013	0.125
3" Pipe	0.005	0.008	0.011	0.155
3.5" Pipe	0.005	0.008	0.010	0.186
5" Pipe	0.005	0.006	0.007	0.210

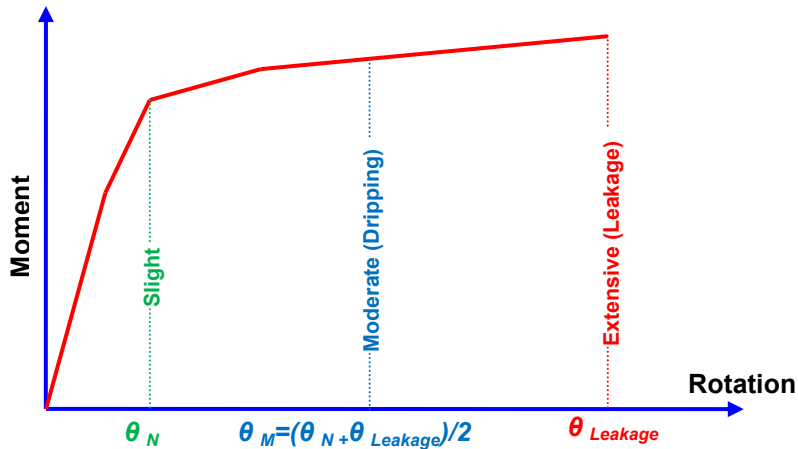


Figure 5-17 Schematic Definition of Threaded Joint Damage States

5.9.2 Grooved Joints

The damage states of pipe joints are defined based on the range of plastic rotations. The second point on the generic backbone curve, θ_N , was assumed as the starting point of nonlinear behavior. The likelihood of any leakage in this level is low; however, there is a possibility of the permanent rotation of joints. The "Moderate" damage state was selected as the third point on the generic backbone curve. The later damage state ("Extensive") corresponds to the observation of the first significant leakage rotation (θ_{leak}). The moderate rotational damage state, θ_M , was defined as the dripping and spraying condition of the grooved joints (Figure 5-18). The dispersion values were set to β_c for all damage states. The parameters for the damage states of pipe joint are presented in Table 5-18.

Table 5-18 Damage States for Grooved Joint Components

Pipe Diameter	Slight	Moderate	Extensive	Dispersion
	Median (rad.)	TEST SETS		β_c
TEST SETS				
2" Pipe	0.015	0.050	0.077	0.170
4" Pipe	0.005	0.010	0.021	0.049
PROPOSED COMPONENTS				
2.5" Pipe	0.013	0.026	0.038	0.140
3" Pipe	0.010	0.019	0.029	0.110
3.5" Pipe	0.008	0.016	0.024	0.079
5" Pipe	0.006	0.011	0.017	0.049
6" Pipe	0.005	0.010	0.014	0.049

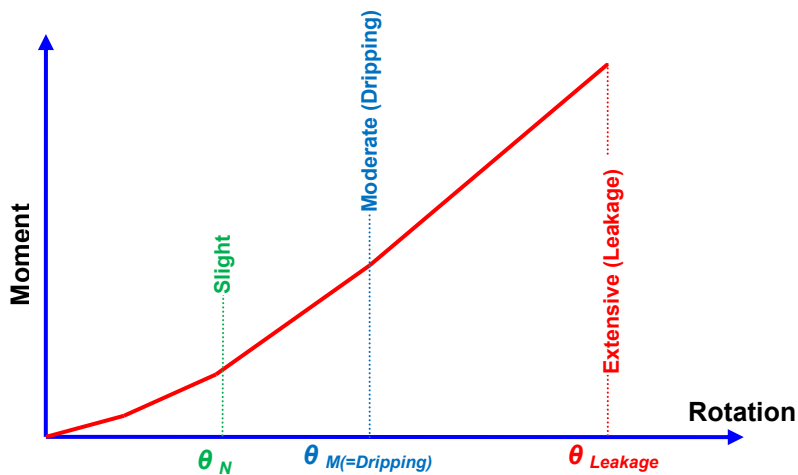


Figure 5-18 Schematic Definition of Grooved Joint Damage States

5.9.3 Supports

The damage states of the pipe hangers, braces, and wire restrainers are determined from the median percentage of failed components, θ_{break} , and the logarithmic standard deviation of the rotational capacity, β_c . A constant value of 0.4, the most frequently used value in nonstructural components (ATC 58, 2009), was assigned to β_c for pipe hangers, braces, and wire restrainers. Three damage states (DS) are defined for the percentage of failed supporting elements named “Slight,” “Moderate,” and “Extensive.”

The tolerance for support elements failing are based on the assumption that the repair time and importance level of a pipe hanger or a solid brace is almost twice that of a cable brace or a wire restrainer. The parameters for the damage states of pipe supporting elements are presented in Table 5-19.

Table 5-19 Damage States for Pipe Supporting Components

Pipe Diameter	Slight	Moderate	Extensive	Dispersion
	Median (%)			β_c
	TEST SETS			
Solid Braces	5	10	15	0.4
Cable Braces	10	20	30	0.4
Pipe Hangers	5	10	15	0.4
Wire Restrainers	10	20	30	0.4

5.10 Component Fragility Curves

Next, the fragility curves of different piping components were developed. The probability of failure of a system can be expressed as the probability that the seismic demand (S_D) will exceed the structural capacity (S_C):

$$P_f = P\left(\frac{S_D}{S_C}\right) < 1.0 \quad (5-13)$$

The component fragility can be derived using a closed form solution described in equation (5-14), where D and C denote demand and capacity, S_D and S_C denote the median values of demand and capacity, and $\beta_{D|IM}$ and β_c denote the dispersions (logarithmic standard deviation) of the demand and capacity, respectively (Ramanathan, 2012).

$$P[D > C|IM] = \Phi\left(\frac{\ln\left(\frac{S_D}{S_C}\right)}{\sqrt{\beta_{D|IM}^2 + \beta_c^2}}\right) \quad (5-14)$$

where $\Phi(\cdot)$ is the standard normal probability integral. Substituting the formula for the median demand, S_D described in the PSDM formula, and subsequent simplification, as illustrated in equation (5-15), leads to the formula in (5-16) which is representative of the lognormal distribution describing the component fragilities with median, λ_c and dispersion, ζ_c . Component fragility curves provide valuable information about the vulnerable component in the piping system thereby prioritizing the improvement and retrofit.

$$P[LS|IM] = \Phi\left(\frac{\ln(a IM^b) - \ln(S_C)}{\sqrt{\beta_{D|IM}^2 + \beta_c^2}}\right) = \Phi\left(\frac{\ln(IM) - \left(\frac{\ln(S_C) - \ln(a)}{b}\right)}{\frac{\sqrt{\beta_{D|IM}^2 + \beta_c^2}}{b}}\right) \quad (5-15)$$

$$P[LS|IM] = \Phi\left(\frac{\ln(IM) - (\lambda_c)}{\zeta_c}\right) \quad (5-16)$$

The component fragility curves for all ten designed piping cases are shown in Figure 5-19 through Figure 5-28. Among the pipe joint damage, the general trend in all cases showed that the response of tee-armovers is the most dominant component in the vulnerability of piping systems in nearly all damage states. In two cases (case 4 and case 9) where the wire restrainers are removed from the armovers, tee-armovers are not the most vulnerable component among the rest of the pipe joints. The dominancy of larger diameter branch line pipes (1.5 in and 1.25 in) on overall vulnerability of piping system increases in higher damage states. In higher damage states, the pipe hangers start to yield, and more wire restrainers fail. As a result, the branch lines behave like cantilevers, and the demand on these pipe diameters, which usually only have connections to the main runs, increases. In this study, the general trend is that the demand on the largest and smallest main runs (4 in and 2 in) is higher. Because these pipes are mainly located at the beginning and end of branch lines, in addition to the existence of solid sway braces, the bending demand at these locations is generally higher than the other locations.

The fragility plots showed that the median values of all components except the main run components are quite similar and slightly smaller (more vulnerable) in piping systems with grooved main runs. Due to the smaller initial stiffness in groove fitting connections, the main runs are more flexible compared to the threaded connections. As a result, the displacement amplitudes that are imposed on the branch lines are slightly higher. Therefore, the wire restrainer forces and rotational demand on the branch lines are slightly higher.

The plots showed that in all main run components, the rotational demand is less in the piping systems with threaded joints (in some cases except 2 in. pipe diameter). This trend can be justified with the following reasons:

1. Considering progressive damage during an earthquake, yielding occurs during the low-intensity portion of the floor motion on joints close to solid braces (2 in. and 4 in. pipes in the studied system) with a “Threaded” configuration. The presence of the generated hinges created during these lower intensities decreases the demand experienced by the rest of the main run joints at higher intensities. Technically, there is no yielding behavior in grooved fitting connections, and the stiffness of joints increases by increasing the rotational demand.

Therefore, the rotational demand will not decrease on the rest of the main run joints during the larger intensity portion of the motion.

2. Due to the hysteresis behavior of threaded joints compared to grooved joints, the dissipated energy is larger in threaded joints. As a result, the presence of the plastic hinges during lower intensities dissipates a larger portion of the energy of input motions compared to grooved fitting connections. Therefore, the rotational demand on the rest of the threaded joints will be less than that of grooved joint main runs.
3. Cable braces were found to be more vulnerable compared to solid braces. However, this vulnerability may be more pronounced in this study because cable braces were not removed through the response history analysis. Pipe hangers were determined to be less vulnerable in the system with cable bracing because of the existence of cable braces. Table 5-20 through Table 5-29 shows the median and dispersion values for the seismic fragility curves of the piping components for different piping cases.

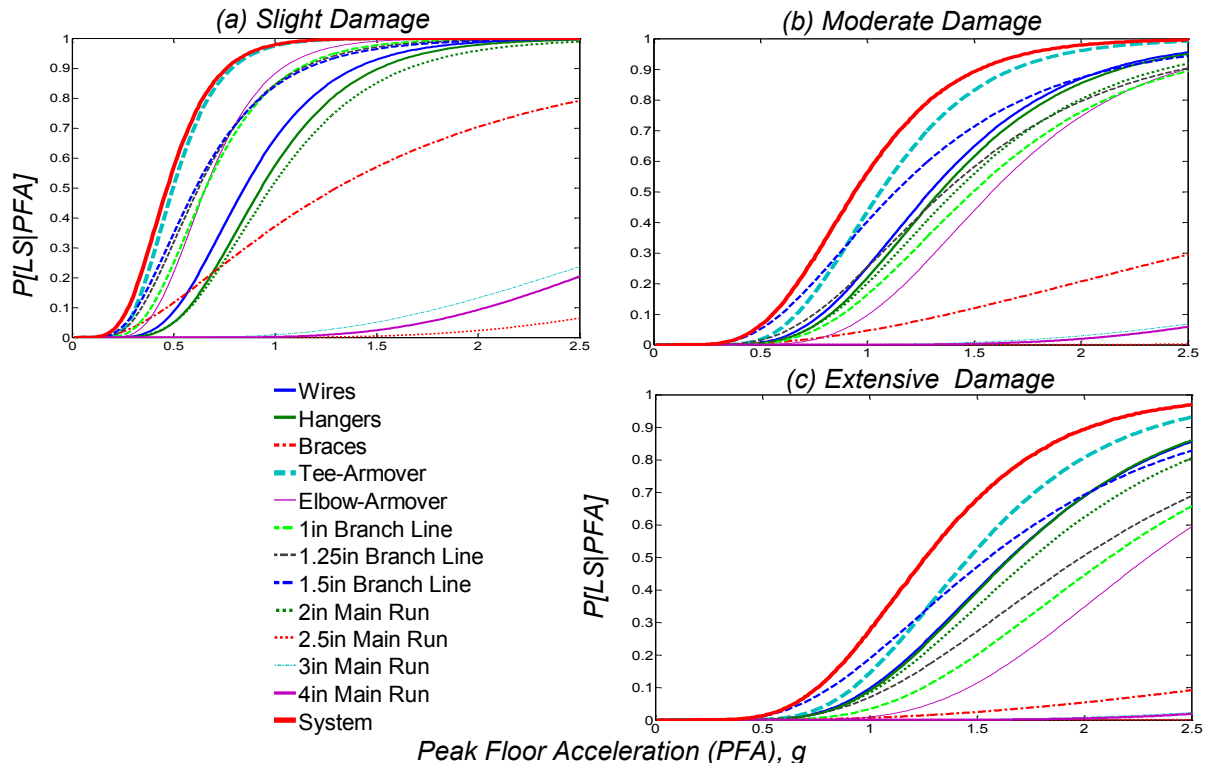


Figure 5-19 Component Fragility Curves for Piping System of Case 1

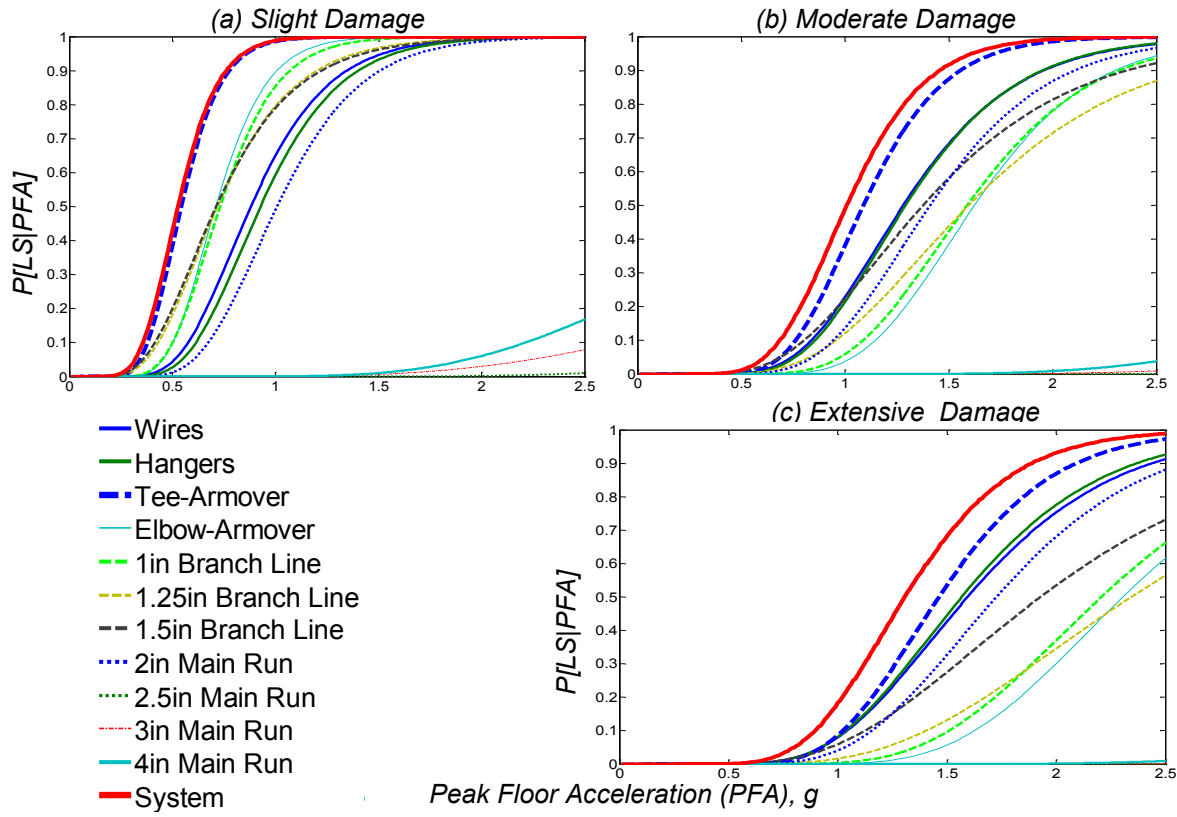


Figure 5-20 Component Fragility Curves for Piping System of Case 2

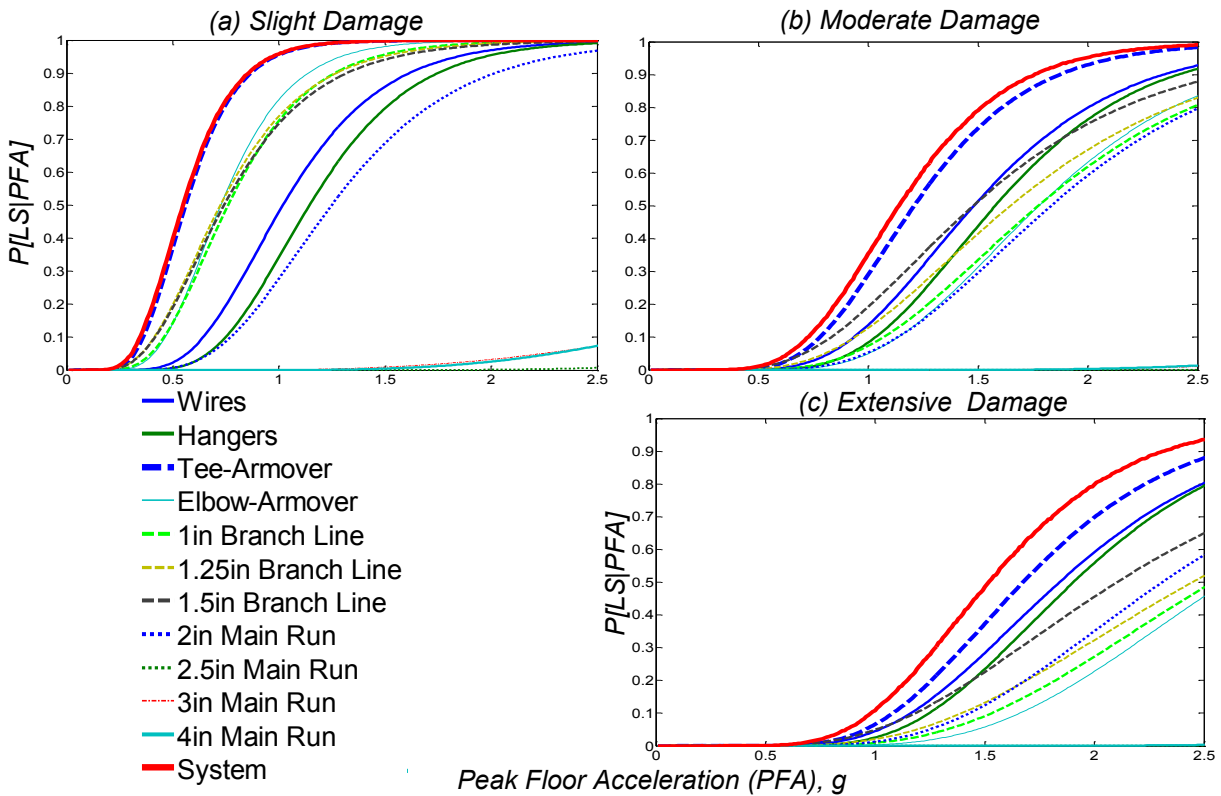


Figure 5-21 Component Fragility Curves for Piping System of Case 3

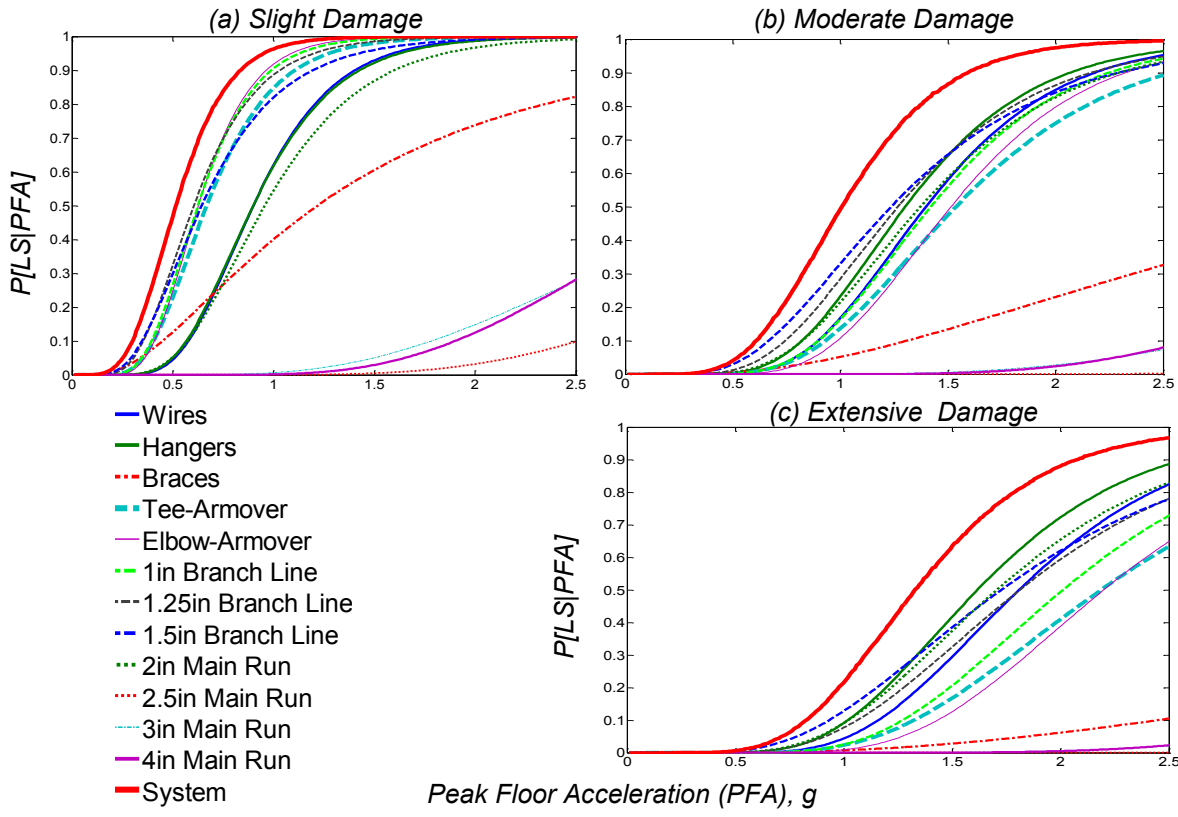


Figure 5-22 Component Fragility Curves for Piping System of Case 4

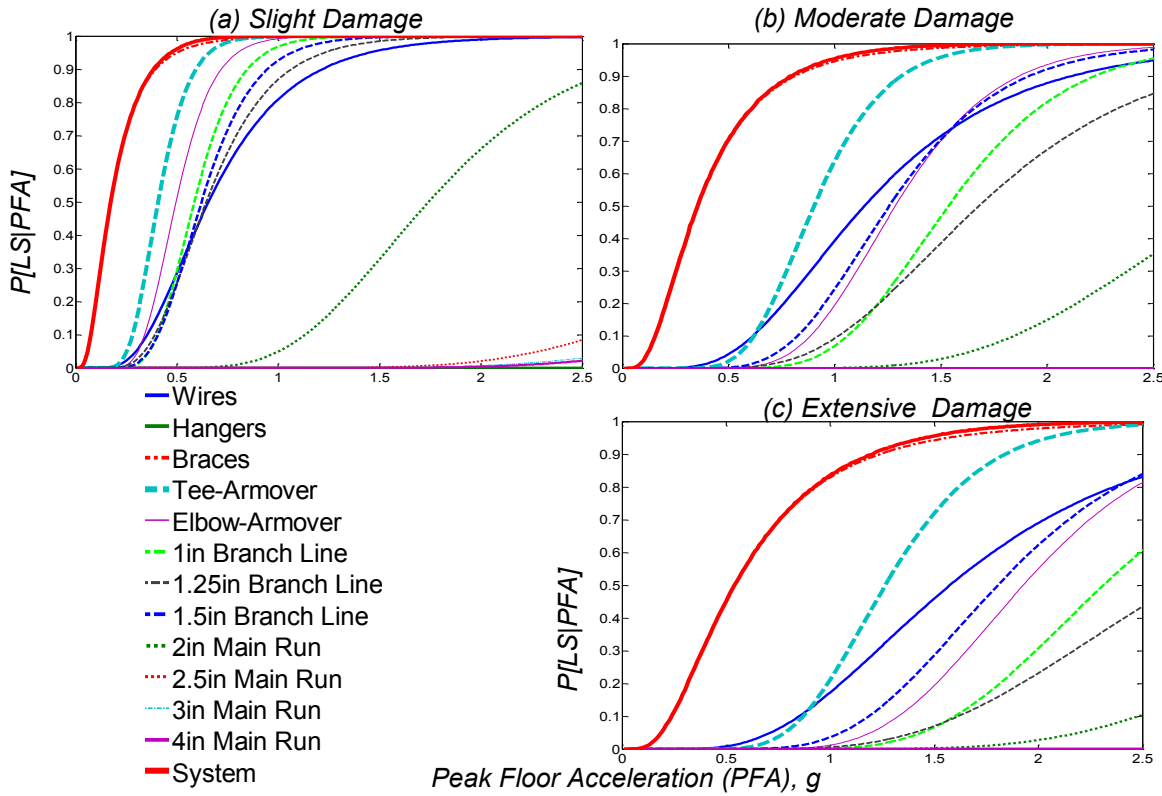


Figure 5-23 Component Fragility Curves for Piping System of Case 5

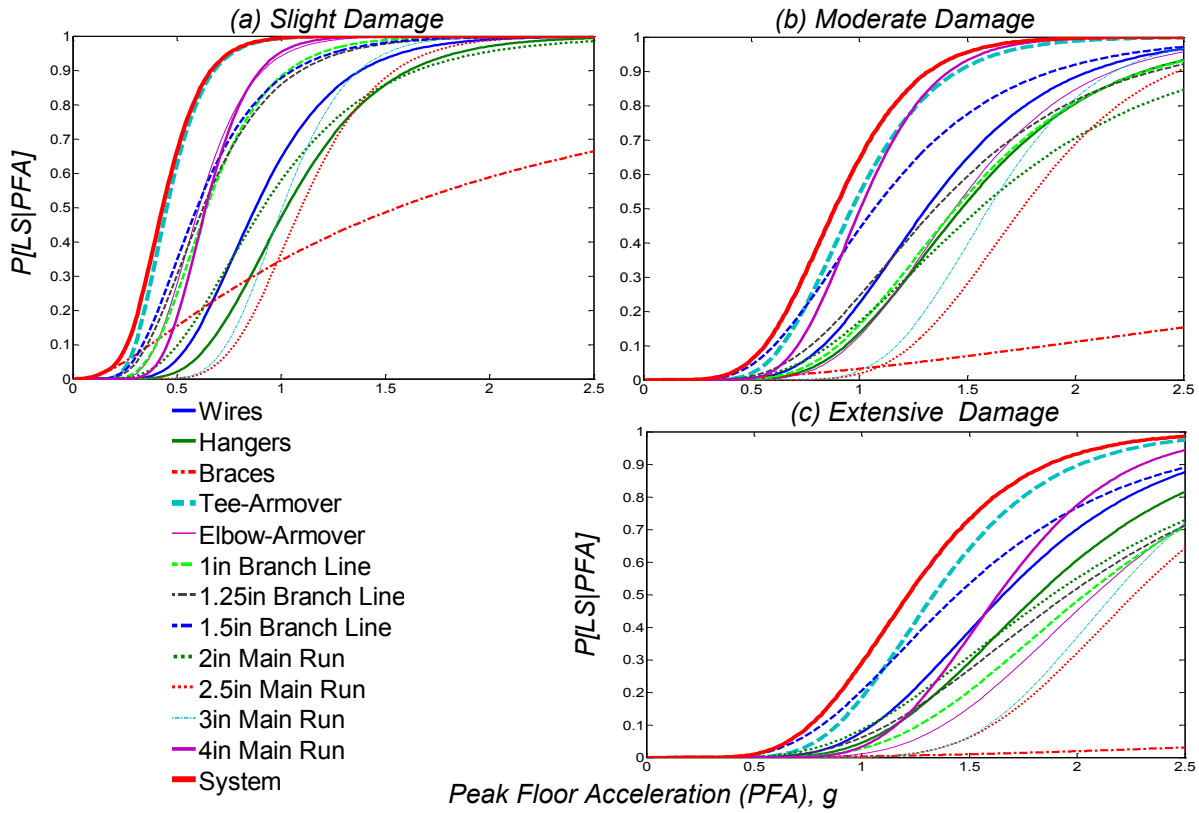


Figure 5-24 Component Fragility Curves for Piping System of Case 6

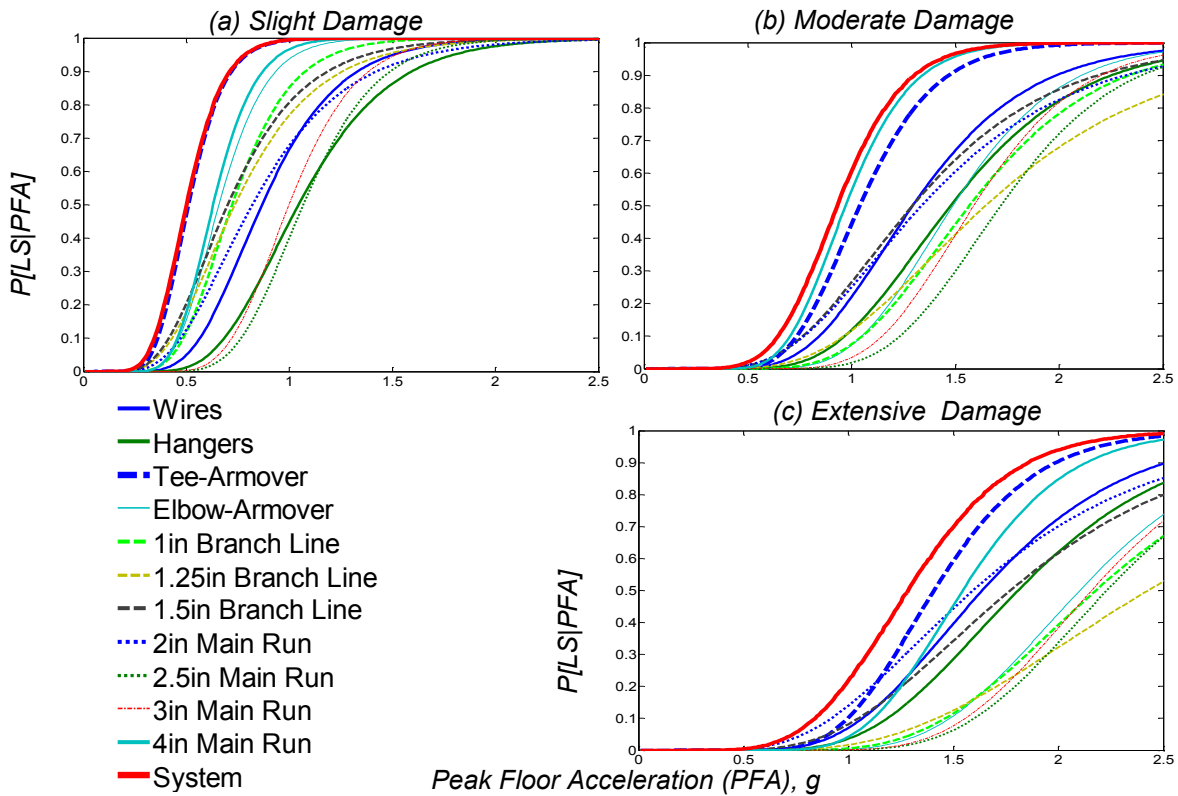


Figure 5-25 Component Fragility Curves for Piping System of Case 7

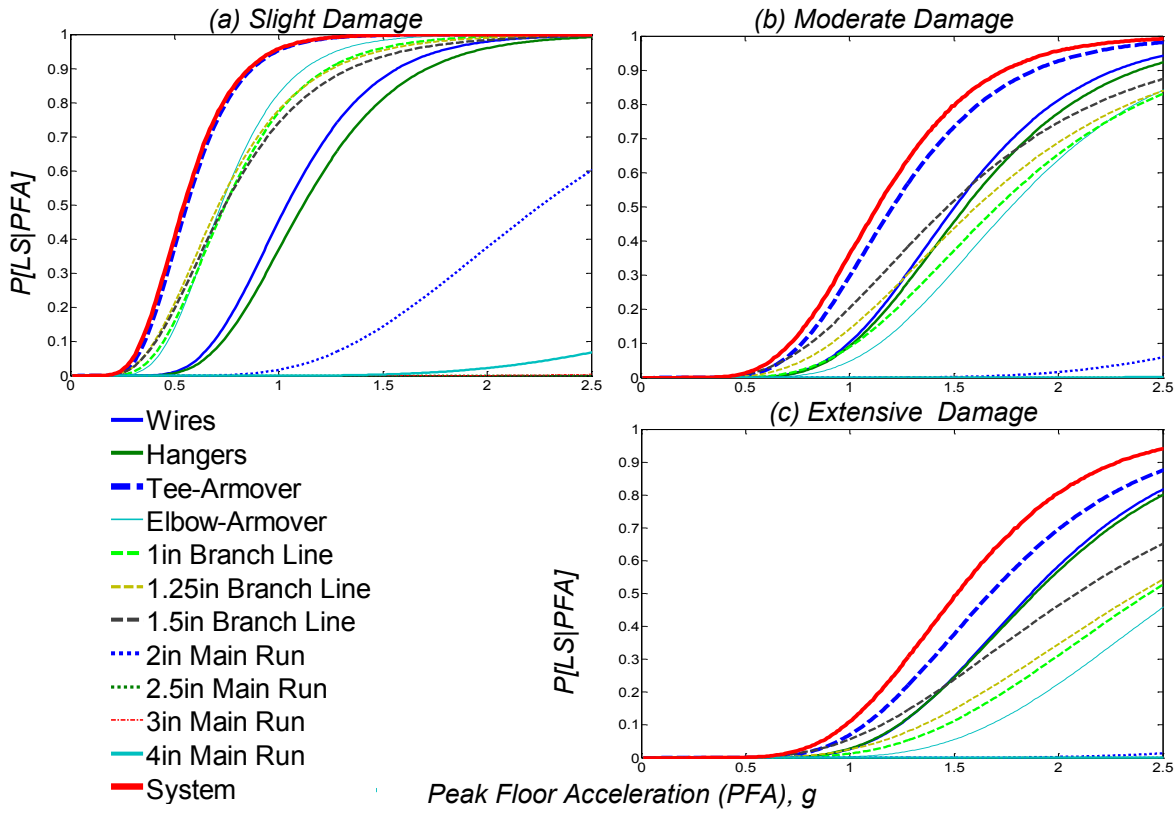


Figure 5-26 Component Fragility Curves for Piping System of Case 8

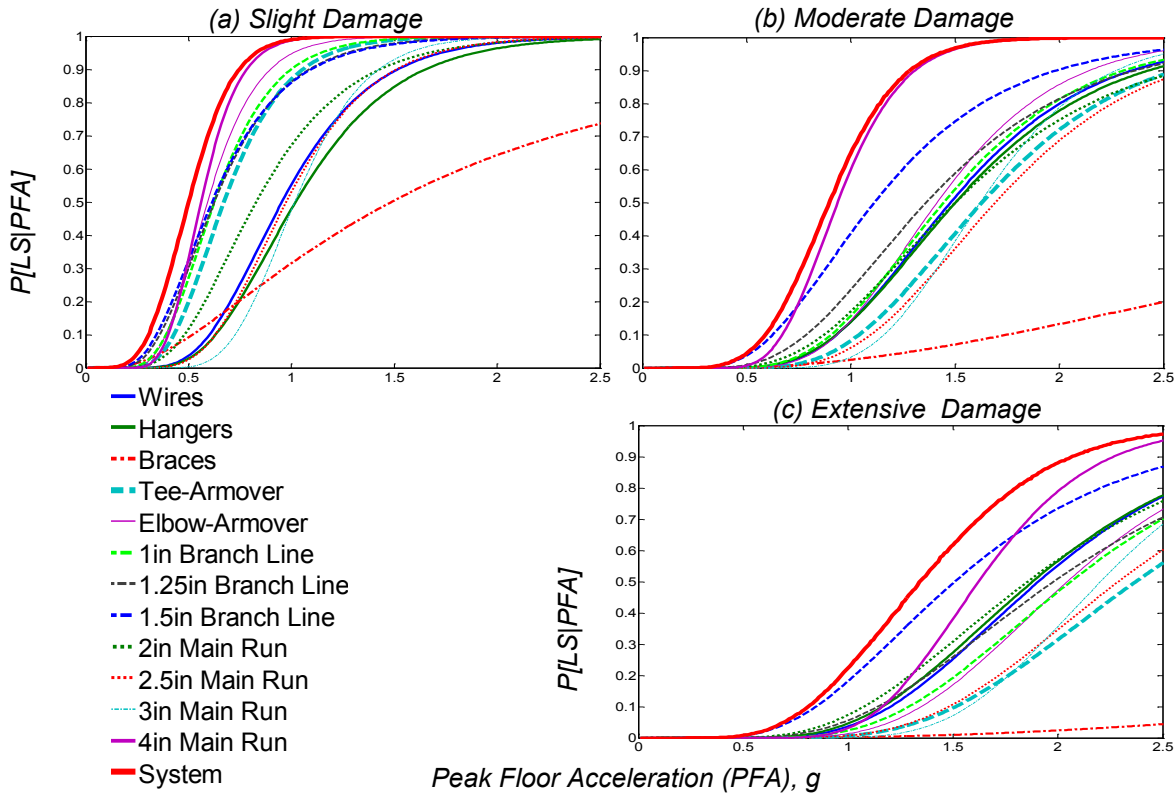


Figure 5-27 Component Fragility Curves for Piping System of Case 9

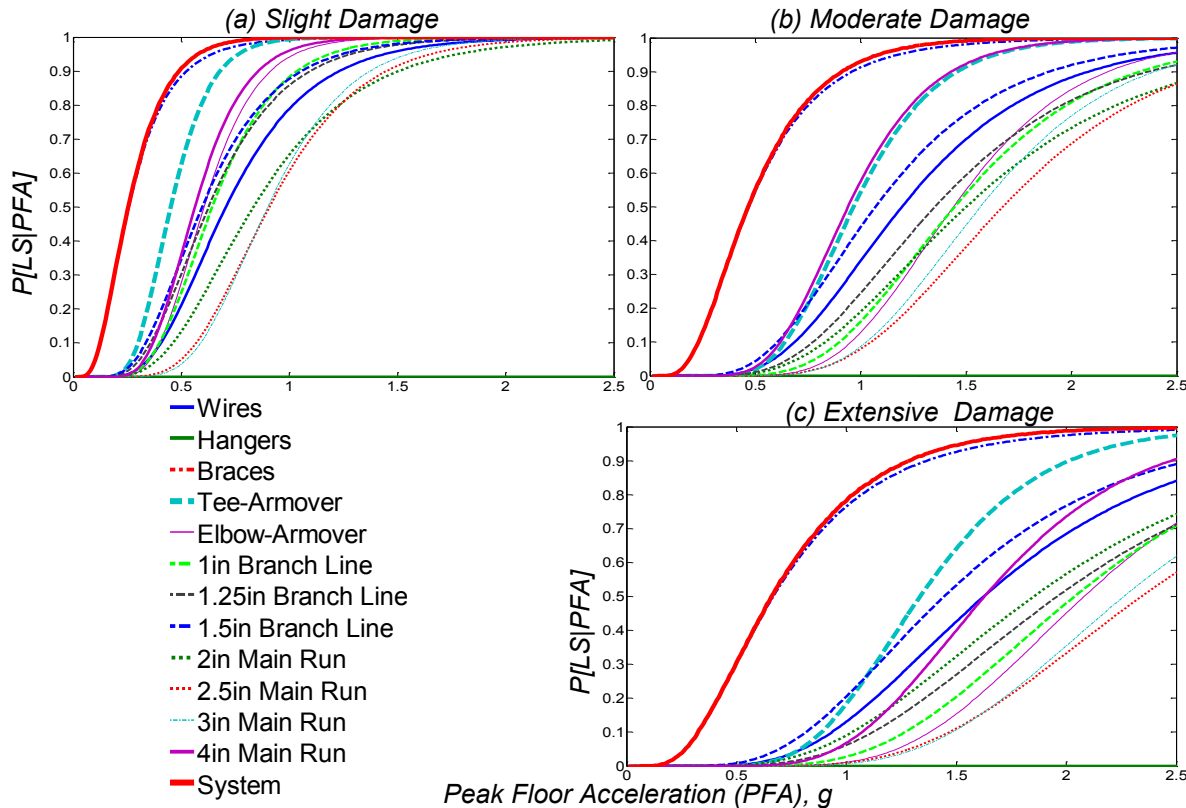


Figure 5-28 Component Fragility Curves for Piping System of Case 10

Table 5-20 Medians and Dispersion Values for Piping Component Fragilities Curves of Case 1

Component Name	Slight		Moderate		Extensive	
	Median PFA(g)	Dispersion	Median PFA(g)	Dispersion	Median PFA(g)	Dispersion
ARMOVERS						
Armover-Tee Joint	0.50	0.61	1.06	0.61	1.47	0.61
Armover-Elbow Joint	0.66	0.52	1.58	0.52	2.30	0.52
BRANCH LINES						
1" Pipe	0.66	0.64	1.50	0.64	2.12	0.64
1.25" Pipe	0.62	0.61	1.36	0.61	1.99	0.61
1.5" Pipe	0.61	0.74	1.13	0.74	1.56	0.74
MAIN RUNS						
2" Pipe	0.98	0.72	1.41	0.72	1.76	0.72
2.5" Pipe	NA*	0.44	NA*	0.44	NA*	0.44
3" Pipe	3.73	0.61	NA*	0.61	NA*	0.61
4" Pipe	3.61	0.55	NA*	0.55	NA*	0.55
SUPPORTS						
Wire restrainers	0.85	0.64	1.29	0.64	1.66	0.64
Hangers	0.93	0.72	1.34	0.72	1.66	0.72
Braces	1.30	0.51	3.85	0.51	NA*	0.51

* Estimated median values are much larger than can be appropriately extrapolated from regression analyses.

Table 5-21 Medians and Dispersion Values for Piping Component Fragilities Curves of Case 2

Component Name	Slight		Moderate		Extensive	
	Median PFA(g)	Dispersion	Median PFA(g)	Dispersion	Median PFA(g)	Dispersion
ARMOVERS						
Armover-Tee Joint	0.54	0.51	1.09	0.51	1.46	0.51
Armover-Elbow Joint	0.71	0.42	1.62	0.42	2.31	0.42
BRANCH LINES						
1" Pipe	0.73	0.49	1.59	0.49	2.21	0.49
1.25" Pipe	0.72	0.52	1.60	0.52	2.34	0.52
1.5" Pipe	0.71	0.59	1.38	0.59	1.93	0.59
MAIN RUNS						
2" Pipe	1.01	0.60	1.41	0.60	1.73	0.60
2.5" Pipe	NA*	0.36	NA*	0.36	NA*	0.36
3" Pipe	NA*	0.50	NA*	0.50	NA*	0.50
4" Pipe	3.59	0.50	NA*	0.50	NA*	0.50
SUPPORTS						
Wire restrainers	0.88	0.61	1.28	0.61	1.59	0.61
Hangers	0.93	0.67	1.29	0.67	1.57	0.67

* Estimated median values are much larger than can be appropriately extrapolated from regression analyses.

Table 5-22 Medians and Dispersion Values for Piping Component Fragilities Curves of Case 3

Component Name	Slight		Moderate		Extensive	
	Median PFA(g)	Dispersion	Median PFA(g)	Dispersion	Median PFA(g)	Dispersion
ARMOVERS						
Armover-Tee Joint	0.56	0.57	1.21	0.57	1.67	0.57
Armover-Elbow Joint	0.73	0.50	1.78	0.50	2.60	0.50
BRANCH LINES						
1" Pipe	0.76	0.60	1.77	0.60	2.54	0.60
1.25" Pipe	0.72	0.55	1.65	0.55	2.45	0.55
1.5" Pipe	0.74	0.60	1.48	0.60	2.10	0.60
MAIN RUNS						
2" Pipe	1.25	0.63	1.83	0.63	2.31	0.63
2.5" Pipe	NA*	0.38	NA*	0.38	NA*	0.38
3" Pipe	NA*	0.55	NA*	0.55	NA*	0.55
4" Pipe	NA*	0.53	NA*	0.53	NA*	0.53
SUPPORTS						
Wire restrainers	1.02	0.67	1.48	0.67	1.84	0.67
Hangers	1.14	0.71	1.58	0.71	1.90	0.71

* Estimated median values are much larger than can be appropriately extrapolated from regression analyses.

Table 5-23 Medians and Dispersion Values for Piping Component Fragilities Curves of Case 4

Component Name	Slight		Moderate		Extensive	
	Median PFA(g)	Dispersion	Median PFA(g)	Dispersion	Median PFA(g)	Dispersion
ARMOVERS						
Armover-Tee Joint	0.67	0.60	1.54	0.60	2.19	0.60
Armover-Elbow Joint	0.63	0.49	1.51	0.49	2.20	0.49
BRANCH LINES						
1" Pipe	0.62	0.56	1.42	0.56	2.01	0.56
1.25" Pipe	0.60	0.58	1.27	0.58	1.81	0.58
1.5" Pipe	0.64	0.68	1.24	0.68	1.73	0.68
MAIN RUNS						
2" Pipe	0.96	0.71	1.37	0.71	1.70	0.71
2.5" Pipe	NA*	0.38	NA*	0.38	NA*	0.38
3" Pipe	3.32	0.54	NA*	0.54	NA*	0.54
4" Pipe	3.13	0.49	NA*	0.49	NA*	0.49
SUPPORTS						
Wire restrainers	0.90	0.55	1.40	0.55	1.81	0.55
Hangers	0.90	0.67	1.30	0.67	1.62	0.67
Braces	1.22	0.50	3.55	0.50	NA*	0.50

* Estimated median values are much larger than can be appropriately extrapolated from regression analyses.

Table 5-24 Medians and Dispersion Values for Piping Component Fragilities Curves of Case 5

Component Name	Slight		Moderate		Extensive	
	Median PFA(g)	Dispersion	Median PFA(g)	Dispersion	Median PFA(g)	Dispersion
ARMOVERS						
Armover-Tee Joint	0.41	0.47	0.90	0.47	1.26	0.47
Armover-Elbow Joint	0.50	0.39	1.29	0.39	1.93	0.39
BRANCH LINES						
1" Pipe	0.59	0.38	1.54	0.38	2.31	0.38
1.25" Pipe	0.65	0.42	1.68	0.42	2.66	0.42
1.5" Pipe	0.62	0.43	1.26	0.43	1.80	0.43
MAIN RUNS						
2" Pipe	1.74	0.44	2.84	0.44	3.81	0.44
2.5" Pipe	NA*	0.30	NA*	0.30	NA*	0.30
3" Pipe	NA*	0.35	NA*	0.35	NA*	0.35
4" Pipe	NA*	0.37	NA*	0.37	NA*	0.37
SUPPORTS						
Wire restrainers	0.66	0.60	1.14	0.60	1.57	0.60
Hangers	NA*	0.44	NA*	0.44	NA*	0.44
Braces	0.17	0.62	0.36	0.62	0.54	0.62

* Estimated median values are much larger than can be appropriately extrapolated from regression analyses.

Table 5-25 Medians and Dispersion Values for Piping Component Fragilities Curves of Case 6

Component Name	Slight		Moderate		Extensive	
	Median PFA(g)	Dispersion	Median PFA(g)	Dispersion	Median PFA(g)	Dispersion
ARMOVERS						
Armover-Tee Joint	0.45	0.54	0.97	0.54	1.34	0.54
Armover-Elbow Joint	0.60	0.47	1.44	0.47	2.08	0.47
BRANCH LINES						
1" Pipe	0.64	0.59	1.45	0.59	2.04	0.59
1.25" Pipe	0.63	0.58	1.35	0.58	1.96	0.58
1.5" Pipe	0.60	0.70	1.07	0.70	1.44	0.70
MAIN RUNS						
2" Pipe	0.91	1.04	1.56	1.04	1.89	1.04
2.5" Pipe	1.10	0.40	1.75	0.40	2.27	0.40
3" Pipe	1.01	0.34	1.60	0.34	2.17	0.34
4" Pipe	0.64	0.41	1.01	0.41	1.63	0.41
SUPPORTS						
Wire restrainers	0.88	0.61	1.31	0.61	1.66	0.61
Hangers	1.03	0.68	1.47	0.68	1.82	0.68
Braces	1.56	0.48	NA*	0.48	NA*	0.48

* Estimated median values are much larger than can be appropriately extrapolated from regression analyses.

Table 5-26 Medians and Dispersion Values for Piping Component Fragilities Curves of Case 7

Component Name	Slight		Moderate		Extensive	
	Median PFA(g)	Dispersion	Median PFA(g)	Dispersion	Median PFA(g)	Dispersion
ARMOVERS						
Armover-Tee Joint	0.51	0.48	1.04	0.48	1.41	0.48
Armover-Elbow Joint	0.66	0.43	1.49	0.43	2.10	0.43
BRANCH LINES						
1" Pipe	0.72	0.52	1.57	0.52	2.18	0.52
1.25" Pipe	0.74	0.54	1.65	0.54	2.43	0.54
1.5" Pipe	0.70	0.61	1.29	0.61	1.77	0.61
MAIN RUNS						
2" Pipe	0.82	1.06	1.34	1.06	1.59	1.06
2.5" Pipe	1.07	0.38	1.72	0.38	2.23	0.38
3" Pipe	1.00	0.35	1.59	0.35	2.16	0.35
4" Pipe	0.63	0.40	0.97	0.40	1.54	0.40
SUPPORTS						
Wire restrainers	0.87	0.58	1.29	0.58	1.64	0.58
Hangers	1.04	0.66	1.48	0.66	1.81	0.66

* Estimated median values are much larger than can be appropriately extrapolated from regression analyses.

Table 5-27 Medians and Dispersion Values for Piping Component Fragilities Curves of Case 8

Component Name	Slight		Moderate		Extensive	
	Median PFA(g)	Dispersion	Median PFA(g)	Dispersion	Median PFA(g)	Dispersion
ARMOVERS						
Armover-Tee Joint	0.56	0.58	1.21	0.58	1.67	0.58
Armover-Elbow Joint	0.72	0.49	1.77	0.49	2.59	0.49
BRANCH LINES						
1" Pipe	0.74	0.61	1.71	0.61	2.43	0.61
1.25" Pipe	0.71	0.56	1.61	0.56	2.38	0.56
1.5" Pipe	0.74	0.62	1.47	0.62	2.09	0.62
MAIN RUNS						
2" Pipe	2.26	0.66	NA*	0.66	NA*	0.66
2.5" Pipe	NA*	0.39	NA*	0.39	NA*	0.39
3" Pipe	NA*	0.54	NA*	0.54	NA*	0.54
4" Pipe	NA*	0.52	NA*	0.52	NA*	0.52
SUPPORTS						
Wire restrainers	1.04	0.60	1.50	0.60	1.87	0.60
Hangers	1.12	0.70	1.56	0.70	1.89	0.70

* Estimated median values are much larger than can be appropriately extrapolated from regression analyses.

Table 5-28 Medians and Dispersion Values for Piping Component Fragilities Curves of Case 9

Component Name	Slight		Moderate		Extensive	
	Median PFA(g)	Dispersion	Median PFA(g)	Dispersion	Median PFA(g)	Dispersion
ARMOVERS						
Armover-Tee Joint	0.67	0.51	1.63	0.51	2.37	0.51
Armover-Elbow Joint	0.59	0.48	1.41	0.48	2.04	0.48
BRANCH LINES						
1" Pipe	0.62	0.56	1.44	0.56	2.06	0.56
1.25" Pipe	0.63	0.57	1.36	0.57	1.98	0.57
1.5" Pipe	0.61	0.70	1.11	0.70	1.51	0.70
MAIN RUNS						
2" Pipe	0.83	0.86	1.50	0.86	1.85	0.86
2.5" Pipe	0.97	0.43	1.69	0.43	2.29	0.43
3" Pipe	1.02	0.36	1.62	0.36	2.20	0.36
4" Pipe	0.56	0.35	0.94	0.35	1.62	0.35
SUPPORTS						
Wire restrainers	0.95	0.57	1.48	0.57	1.91	0.57
Hangers	1.02	0.68	1.50	0.68	1.88	0.68
Braces	1.48	0.47	NA*	0.47	NA*	0.47

* Estimated median values are much larger than can be appropriately extrapolated from regression analyses.

Table 5-29 Medians and Dispersion Values for Piping Component Fragilities Curves of Case 10

Component Name	Slight		Moderate		Extensive	
	Median PFA(g)	Dispersion	Median PFA(g)	Dispersion	Median PFA(g)	Dispersion
ARMOVERS						
Armover-Tee Joint	0.39	0.43	0.90	0.43	1.27	0.43
Armover-Elbow Joint	0.47	0.36	1.26	0.36	1.92	0.36
BRANCH LINES						
1" Pipe	0.58	0.38	1.49	0.38	2.24	0.38
1.25" Pipe	0.67	0.43	1.81	0.43	2.92	0.43
1.5" Pipe	0.65	0.52	1.33	0.52	1.92	0.52
MAIN RUNS						
2" Pipe	0.83	0.94	1.50	0.94	1.85	0.94
2.5" Pipe	0.91	0.41	1.67	0.41	2.34	0.41
3" Pipe	0.90	0.38	1.57	0.38	2.26	0.38
4" Pipe	0.56	0.44	0.94	0.44	1.63	0.44
SUPPORTS						
Wire restrainers	0.71	0.57	1.19	0.57	1.62	0.57
Hangers	NA*	0.51	NA*	0.51	NA*	0.51
Braces	0.26	0.64	0.47	0.64	0.67	0.64

* Estimated median values are much larger than can be appropriately extrapolated from regression analyses.

5.11 Effect of Variations of Design, Motion, and Fragility Parameters on Component Fragility Curves

In this section, different variables of fragility curves for different piping components were compared with respect to considered variables. The variables that were considered as the comparision bases are: 1) component demands; 2) joint types (threaded/grooved); 3) motion suites; 4) weight of water; 5) configuration of wire restrainers; and 6) and type of bracing (cable/solid).

5.11.1 Component Demands

The PSDA method, which utilizes power law or regression logarithmic analysis between EDPs and IMs, is one of the most popular procedures for estimating component demands. Previous plots showed a linear fit is customarily used over the domain of the data. However, these figures demonstrated that the linear logarithmic regression analysis may not be the best approach for estimating the component demands. Therefore, bilinear (piecewise linear) fits were used to reduce dispersion and increase the efficiency of the model (Mackie and Stojadinović, 2005). To do so, bilinear regression along with least-squares approach were used to find the best bilinear regression model for each component demand (minimum dispersion value) as follows:

$$\begin{aligned}
EDP &= a_1 IM^{b_1} & \text{when } IM_i < IM_{intersect} \\
EDP &= a_2 IM^{b_2} & \text{when } IM_i \geq IM_{intersect}
\end{aligned} \tag{5-17}$$

The remaining variability (e) in $\ln(EDP)$ at a given IM is assumed to have a constant variance for all IM range, and the standard variation is estimated as:

$$\beta_{EDP|IM} = \text{Var}(e) = \sqrt{\frac{\sum_{i=1}^n [\ln(EDP_i) - (\ln(a_j) + b_j \ln(IM_i))]^2}{n-2}} \tag{5-18}$$

$j=1 \text{ when } IM_i < IM_{intersect}$ and $j=2 \text{ when } IM_i \geq IM_{intersect}$

where EDP_i and IM_i are the EDP and IM value of record i , n is the number of records, a_j and b_j are the regression coefficient of each segment of bilinear curve, and $IM_{intersect}$ is the intensity at intersection of two linear segments of bilinear curve. Figure 5-29 shows the sample comparison of linear and bilinear regression analysis of component demands and fragility curves at slight limit state under Case 1 using the aforementioned procedure. The rest of the component demands and component fragility curves can be found in Appendix C and D, respectively.

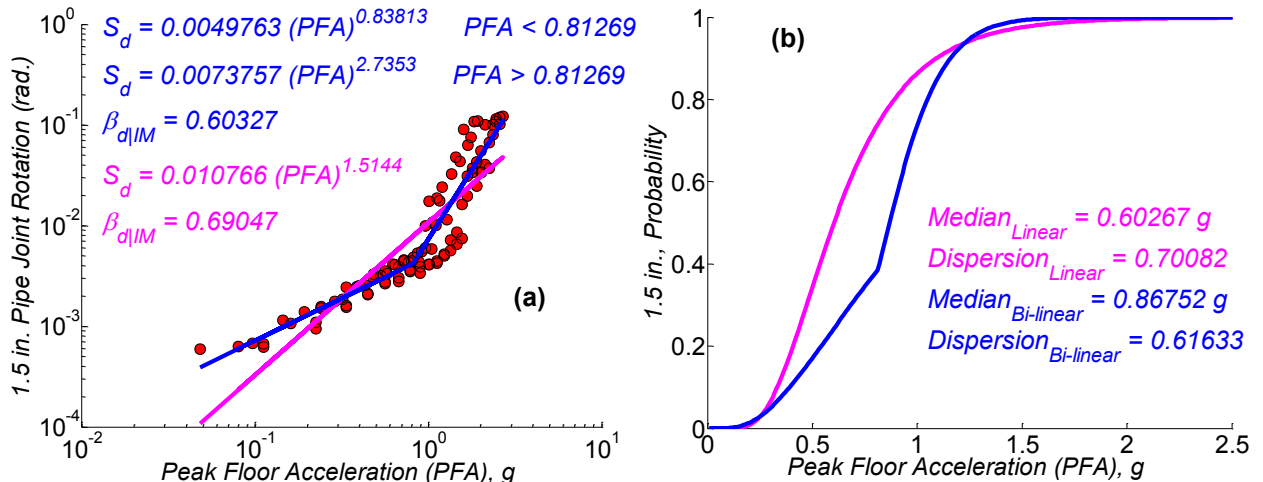


Figure 5-29 Sample Comparison of Linear and Bilinear Regression Analysis on (a) Component Demands, (b) Component Fragility at Slight Limit State - Case 1

Using bilinear regression analysis was found to be both efficient and effective. It was efficient because for all components and cases, the dispersion value was reduced. In order to highlight the

effect of using bilinear regression analysis, the differences between the failure probability of each component was calculated over the range of IMs using the following equation:

$$\text{Probability Difference} = P(\text{DS|IM})_{\text{Bilinear}} - P(\text{DS|IM})_{\text{Linear}} \quad (5-19)$$

where $P(\text{DS|IM})_{\text{Bilinear}}$ and $P(\text{DS|IM})_{\text{Linear}}$ is the probability of component failure (using equation (5-8)) calculated based on bilinear and linear regression analysis, respectively. The negative values of a probability difference show that the probabilities calculated based on linear regression analysis are more conservative. Figure 5-30 shows an example of probability difference based on three different damage states for case 1.

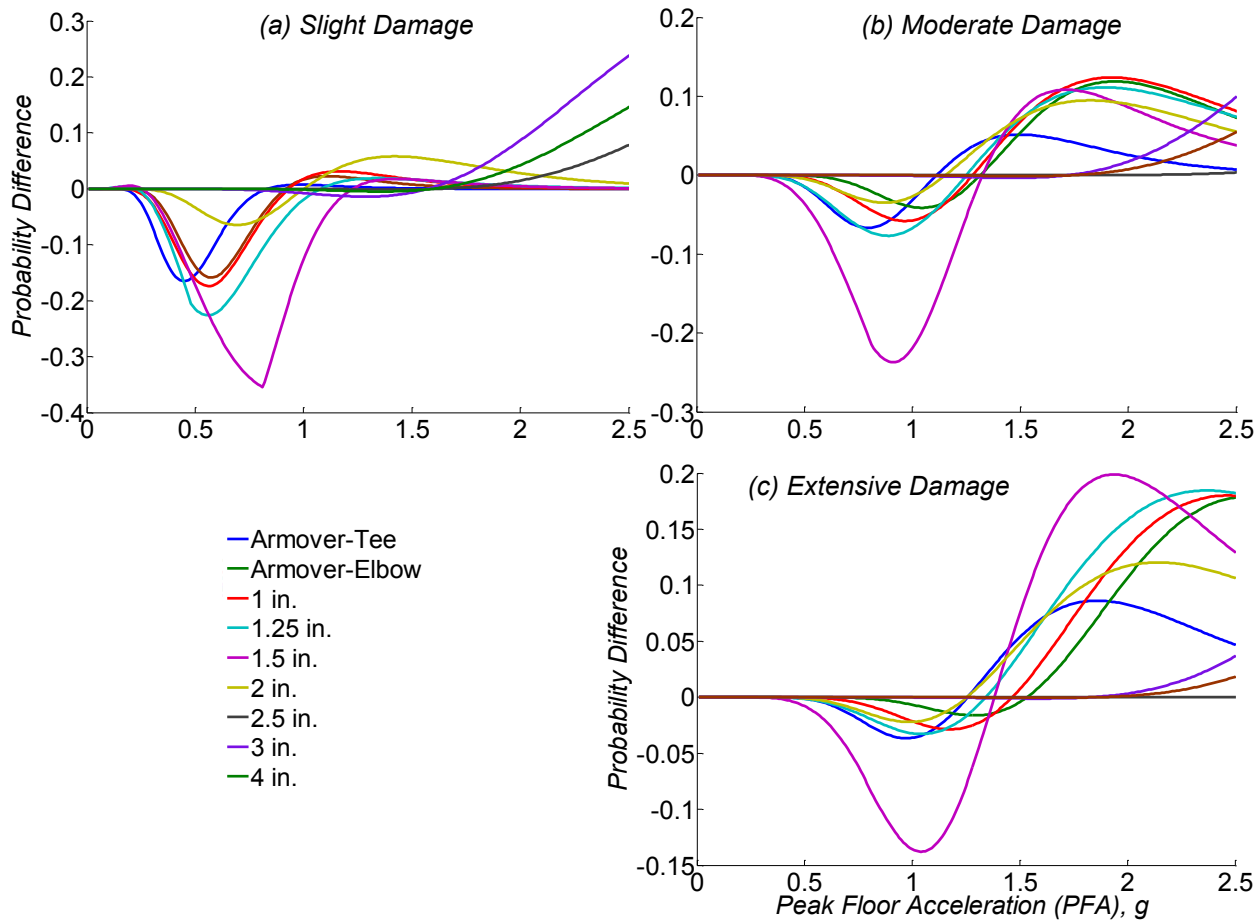


Figure 5-30 Sample Probability Differences for Case 1

The plots of Figure 5-30 imply that the probability differences are reduced in higher damage states. Also, for the PFAs less than 1.5 g, curves calculated based on bilinear regression analysis are more conservative while they are less conservative for larger PFAs.

5.11.2 Joint Types

The effect of variable joint types is considered in the following text. This study was made by comparing the median values of each damage state for pipe joint fragility curves between the piping systems with threaded and grooved main run joints. The pairs of comparison cases were chosen considering the joint type variation only (e.g. comparing case 2 with case 7). The differences between the median values are calculated using the following equation:

$$\text{Median Value Differences (MVD) (\%)} = \frac{\lambda_{\text{Threaded}} - \lambda_{\text{Grooved}}}{\lambda_{\text{Threaded}}} \times 100 \quad (5-20)$$

where $\lambda_{\text{Threaded}}$ and λ_{Grooved} are the median value component fragility curves for threaded and grooved main runs, respectively, for a specific damage state. The positive values of MVD imply more fragile components in a grooved system.

Figure 5-31 shows that in all main run components, the rotational demand is less in the piping systems with threaded joints (in some cases except 2 in. pipe diameter). This trend can be justified as follows: 1) The presence of the generated hinges in the threaded configuration created during lower intensities decreases the demand experienced by the rest of the main run joints at higher intensities. Technically, there is no yielding behavior in grooved fit connections, and the stiffness of joints increases by increasing the rotational demand. Therefore, the rotational demand will not decrease on the rest of the main run joints during the larger intensity portion of the motion. 2) Due to the ductile behavior of threaded joints compared to grooved joints, the dissipated energy is larger in threaded joints. As a result, the presence of the plastic hinges during lower intensities dissipates a larger portion of the energy of input motions compared to grooved fitting connections. Therefore, the rotational demand on the rest of the threaded joints will be less than on the grooved joint main runs. 3) The rotational capacity of 2 in. grooved fittings is larger than the capacity of a 2 in. threaded joint.

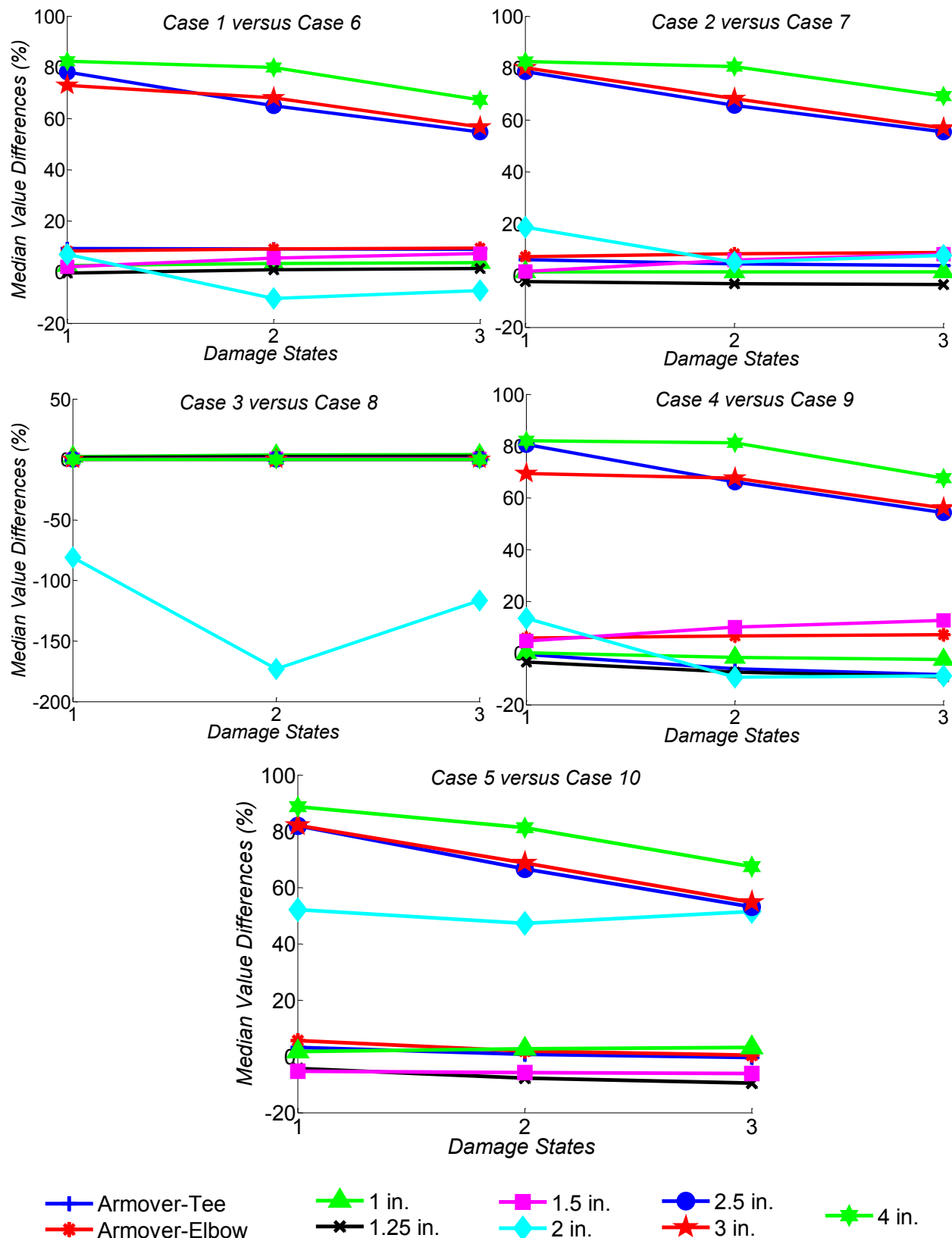


Figure 5-31 Component Median Value Differences Considering Main Run Joint Variation

5.11.3 Motion Suites

The effect of using different motion suites with different S_{DS} distributions are considered in the following text. This comparison has been made by comparing the median values of each of the damage states for pipe joint fragility curves between the piping systems under motions with uniform and lognormal S_{DS} distribution. The pairs of comparison cases are chosen considering the motion distribution variation only (e.g. comparing case 6 with case 7). The differences between the median values are calculated using the following equation:

$$\text{Median Value Differences (MVD)} (\%) = \frac{\lambda_{\text{Uniform}} - \lambda_{\text{Lognormal}}}{\lambda_{\text{Uniform}}} \times 100 \quad (5-21)$$

where λ_{Uniform} and $\lambda_{\text{Lognormal}}$ are the median value component fragility curves for the pipe joints under motion suites with uniform and lognormal S_{DS} distribution, respectively, for a specific damage state. The positive values of MVD imply more fragile component under lognormal distribution.

Figure 5-32 shows that variation on motion distributions resulted in 35% maximum differences on median values of fragility curves. In general, the motion suite with uniform S_{DS} distribution resulted in slightly more conservative results. In other words, a larger number of motions with lower intensities in a suite of motions may result in less fragile components.

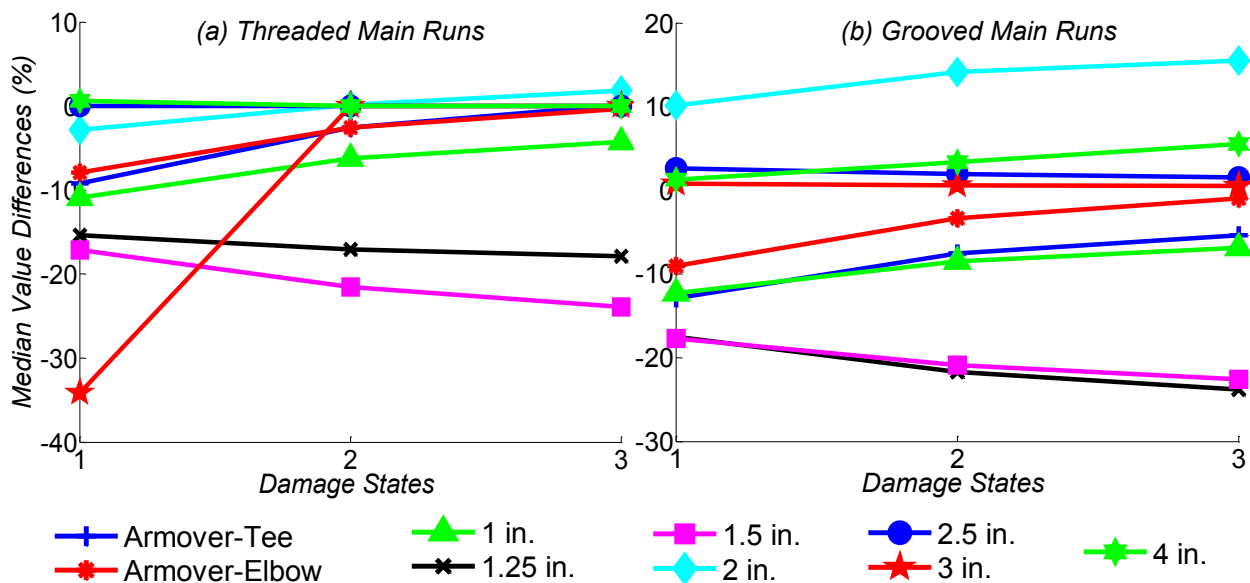


Figure 5-32 Component Median Value Differences Considering Motion Suite Variation

5.11.4 Water Weight

Fire sprinkler systems can be categorized into wet and dry piping systems. Some of the disadvantages of using a dry fire sprinkler system include its complexity, higher installation and maintenance cost, larger number of sprinkler zones, longer fire response time, and the fact that corrosion reduced their extent of use in common practice. The seismic performance of a dry system is compared with a wet piping system in the following text. This comparison has been made by comparing the median values of each damage state for pipe joint fragility curves between the wet and dry piping systems. The pairs of comparison cases are chosen considering the water weight variation only (e.g. comparing case 1 with case 3). The differences between the median values are calculated using the following equation:

$$\text{Median Value Differences (MVD)} (\%) = \frac{\lambda_{\text{Wet}} - \lambda_{\text{Dry}}}{\lambda_{\text{Wet}}} \times 100 \quad (5-22)$$

where λ_{Wet} and λ_{Dry} are the median values for component fragility curves for the pipe joints in wet and dry piping systems, respectively, for a specific damage state. The positive values of MVD imply more fragile components in a dry piping system.

Figure 5-33 shows that in all components, the rotational demand is less in the dry piping systems compared to the wet piping systems. The reduction in vulnerability is larger in piping systems

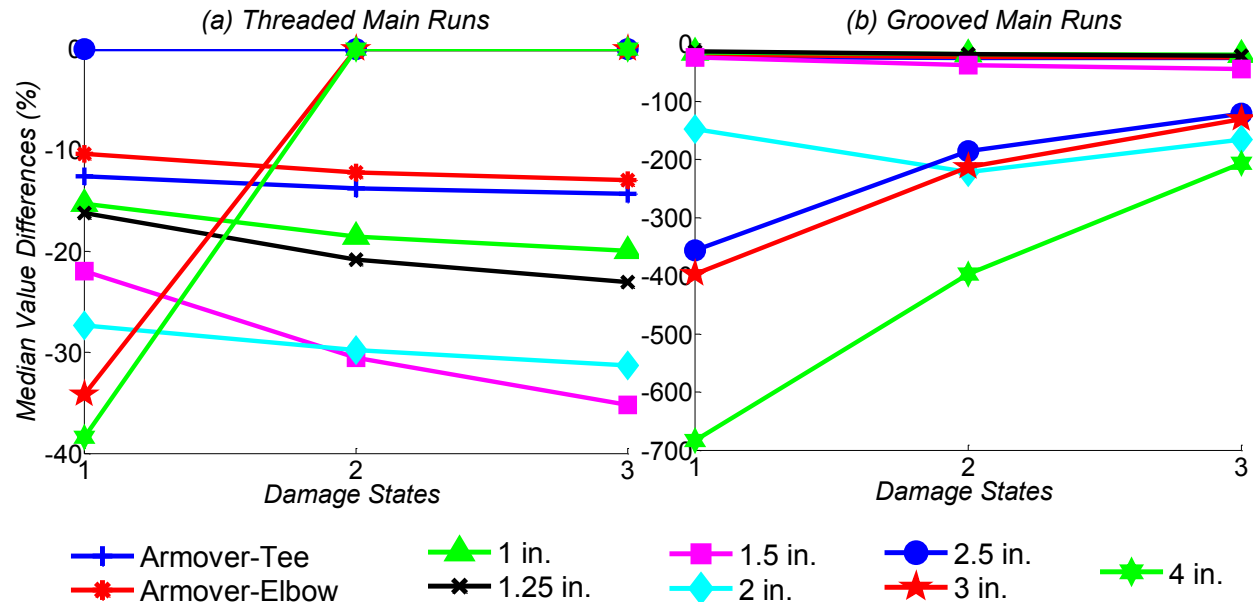


Figure 5-33 Component Median Value Differences Considering Water Weight Variation

with grooved main runs. In the piping system with threaded joints, the probability of leakage in threaded joints is very low; therefore, eliminating the water weight may not improve the piping system within the range of possible peak floor acceleration (0-4g). However, in a piping system with a grooved connection, removing the water weight may significantly improve the piping system.

5.11.5 Wire Restrainers

Two restraining configurations were studied for supporting armover pipes. This study compared the median values of each damage state for pipe joint fragility curves between piping systems with and without wire restrainers on armover pipes. In both cases, the armover pipes were supported by pipe hangers. The pairs of comparison cases were chosen considering the restraint variation only (e.g. comparing case 6 with case 9). The differences between the median values are calculated using the following equation:

$$\text{Median Value Differences (MVD)} (\%) = \frac{\lambda_{\text{Wire}} - \lambda_{\text{No-Wire}}}{\lambda_{\text{Wire}}} \times 100 \quad (5-23)$$

where λ_{Wire} and $\lambda_{\text{No-Wire}}$ are the median values for component fragility curves for the pipe joints in piping systems with and without wire restrainers on armover pipes, respectively, for a specific damage state. The positive values of MVD imply more fragile components in the piping system without wire restrainers on armovers.

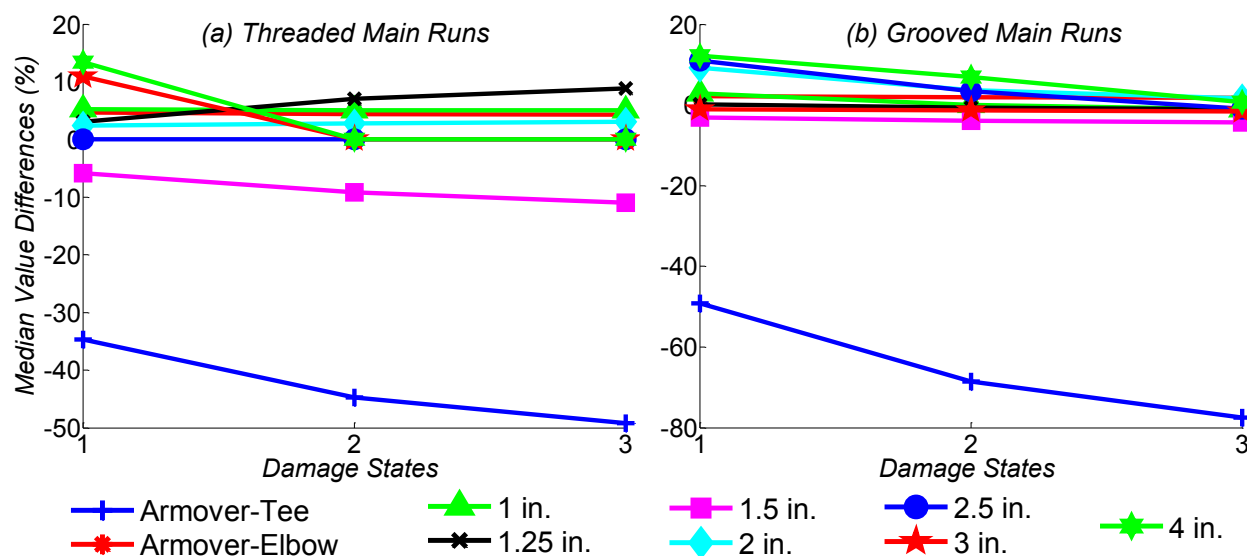


Figure 5-34 Component Median Value Differences Considering Wire Restrainers

Figure 5-34 shows that in all components, the rotational demand is less in the piping system with additional wire restrainers on armover pipes. However, as also stated in previous sections, armover joints are the most fragile component between the other pipe joints. Removing the wire restrainers clearly improved the behavior of these armover pipes.

5.11.6 Bracing

Two types of bracing were studied for seismic resistance of piping systems. This comparison has been made by comparing the median values of each damage state for pipe joint fragility curves between piping systems with solid and cable bracing. The pairs of comparison cases are chosen considering the bracing variation only (e.g. comparing case 1 with case 5). The differences between the median values are calculated using the following equation:

$$\text{Median Value Differences (MVD)} (\%) = \frac{\lambda_{\text{Solid}} - \lambda_{\text{Cable}}}{\lambda_{\text{Solid}}} \times 100 \quad (5-24)$$

where λ_{Solid} and λ_{Cable} are the median values for component fragility curves for the pipe joints in piping systems with solid and cable bracing, respectively, for a specific damage state. The positive values of MVD implies more fragile components in piping systems with cable bracing.

The general trend in Figure 5-35 shows that the rotational demand is less in the piping systems with solid bracing. However, in the threaded piping system, the vulnerability of main runs with cable bracing is less due to the less moment fixity at the end of main runs. In the grooved piping

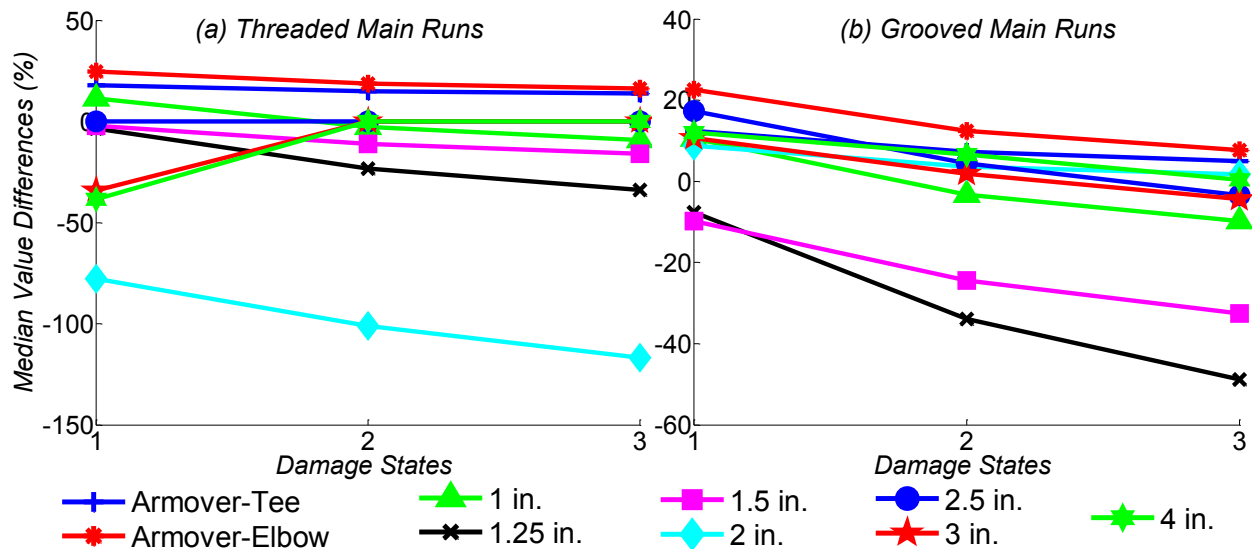


Figure 5-35 Component Median Value Differences Considering Brace Type Variation

system, the vulnerability at the end branch line joints are smaller in piping systems with cable bracing due to smaller displacement demands. As the cable braces never were removed during the response history analysis, the demands at the end of branch lines were smaller. It should be mentioned that cable braces were found to be more vulnerable compared to solid braces.

5.12 Concluding Remarks

The analytical component fragility curves of fire sprinkler piping systems were developed using a probabilistic seismic design model (PSDM). In general, PSDMs are tools for generating fragility curves that relate the engineering demand parameters (EDP) to ground motion intensity measures (peak floor acceleration used in this study). These PSDMs can be generated in two different ways: 1) incremental dynamic analysis (IDA); and 2) the cloud approach (probabilistic seismic demand analysis). In this study, the latter method is implemented, and PSDMs for various critical components in eight different classes of piping systems were obtained. In this study, a full fire sprinkler system layout incorporating a variety of common sprinkler piping systems was adopted from the University of California, San Francisco (UCSF) medical center building and was analytically simulated in OpenSees. Eight different design variables were considered for developing the UCSF piping plan. Two suites of floor motions with different design spectral accelerations at short period S_{DS} were artificially generated. Nonlinear response history analyses of the computational models of the pipings subjected to the floor motions with varying intensities were carried out next to record realistic component and piping system response. Fragility curves for various components for all different piping cases were developed.

The general trend in all cases revealed that the response of tee-armovers is the most dominant component in the vulnerability of piping systems in nearly all damage states. The dominancy of larger diameter branch line pipes (1.5-inch and 1.25-inch) on the overall vulnerability of the piping system increases in higher damage states. In higher damage states, the pipe hangers start to yield, and more wire restrainers fail. As a result, the branch lines behave like cantilevers, and the demand on these pipe diameters, which usually only have connections to the main runs, increases. In this study, the general trend is that the demand on the largest and smallest main runs (4-inch and 2-inch) is higher. Because these pipes are mainly located at the beginning and end of branch lines in addition to the existence of solid sway braces, the bending demand at these locations is generally higher than at other locations.

Several comparisons were made between component fragilities of different piping systems considering only a variable at a time. These comparisons showed that:

- 1) Using bilinear and linear power law formulation for component demand estimation may result in maximum 0.4 differences in probability values.
- 2) The median values of all components except the main run components are quite similar and slightly smaller (more vulnerable) in piping systems with grooved main runs. Due to the smaller initial stiffness in groove fitting connections, the main runs are more flexible compared to the threaded connections. As a result, the displacement amplitudes that are imposed on the branch lines are slightly higher. Therefore, the wire restrainer forces and rotational demand on the branch lines are slightly higher.
- 3) Considering progressive damage during an earthquake, yielding occurs during a low intensity portion of the floor motion on joints close to solid braces (2-in. and 4-in. pipes in the studied system) with a “Threaded” configuration. The presence of the generated hinges created during these lower intensities decreases the demand experienced by the rest of the main run joints at higher intensities. Technically, there is no yielding behavior in grooved fitting connections, and the stiffness of joints increases by increasing the rotational demand. Therefore, the rotational demand will not decrease on the rest of the main run joints during the larger intensity portion of the motion.
- 4) Cable braces were found to be more vulnerable compared to solid braces.
- 5) In this study, variation on motion distributions resulted in 35% maximum differences on median fragility curve values.
- 6) The rotational demand is less in the dry piping systems compared to the wet piping systems. The reduction in vulnerability is larger in the piping system with grooved main runs. In the piping system with threaded joints, the probability of leakage in threaded joints is very low; therefore, eliminating water weight may not improve the piping system within the range of possible peak floor acceleration (0-4g). However, in

a piping system with grooved connections, removing the water weight may significantly improve the piping system.

- 7) The rotational demand on armover pipes is larger in a piping system with additional wire restrainers. Therefore, removing the wire restrainers clearly improved the behavior of these armover pipes.
- 8) The rotational demand is less in the piping systems with solid bracing. However, in the threaded piping system, the vulnerability of main runs in cable bracing is less due to the lesser moment fixity at the end of main runs. In the grooved piping system, the vulnerability of end branch line joints is smaller in piping systems with cable bracing due to not removing the smaller displacement. Since the cable braces never were removed during the response history analysis, the demands at the end of branch lines were smaller.

SECTION 6 SYSTEM LEVEL FRAGILITY STUDIES

6.1 Introduction

The assessment of seismic vulnerability for an entire piping system must be made by combining the effects of the various components within the system. Fragility curves of critical piping components should be developed in order to reach a reliable curve of the piping system. In other words, component fragility curves are the microscopic risk assessment of piping systems. In the previous section, the fragility curves of piping components were generated. However, the end goal of the fragility study is to develop a system-level risk assessment of fire sprinkler piping systems.

In this section, a methodology for developing system level fragility curves was borrowed from the work done by Nielson (2005). A brief description of this procedure is given followed by fragility curves of different piping cases. Finally, the impact of each variable is studied on system level risk assessment of fire sprinkler piping systems.

6.2 Methodology

The assessment of seismic vulnerability for the entire piping system must be made by combining the effects of the various piping system components. Three system damage states "Slight", "Moderate", and "Extensive" were defined by combining the previously defined component damage states. A joint probabilistic seismic demand model (JPSDM) was used in this study to estimate the fragility level of the piping system. The JPSDM is developed by assessing the demands placed on individual components (marginal distribution) through regression analysis. A covariance matrix is calculated by estimating the correlation coefficients between the demands placed on the various components. The correlation coefficients between the component demands are obtained by using the results of a nonlinear response history analysis, and the resulting covariance matrix is then assembled. Using the damage state parameters and the JPSDM, Equation (6-1) can be evaluated using a Monte Carlo simulation. A correlation of 100% is considered between various damage states in developing the samples for the capacity, and as mentioned, the correlation between various components for developing the demand samples is obtained based on response history analyses. Samples (10^5 in this case) are drawn from both the demand and capacity models, and the probability of the demand exceeding the capacity is evaluated for a particular IM value.

A Monte Carlo simulation is used to compare some level of correlation realizations between component demands using the JPSDM defined by a conditional joint normal distribution in the transformed space and statistically independent component capacities to calculate the probability of system failure. This procedure is applied for each damage state for various levels of IMs. Then regression analysis is used to estimate the lognormal parameters, median, and dispersion, which characterize the piping system fragility.

The probability that the piping reaches or goes beyond a particular damage state ($\text{Fail}_{\text{system}}$) is the union of the probabilities that each of the components will reach that same damage state ($\text{Fail}_{\text{component-}i}$), as shown in Equation (6-1) (Nielson and DesRoches, 2007) :

$$P[\text{Fail}_{\text{System}}] = \bigcup_{i=1}^n P[\text{Fail}_{\text{Component}i}] \quad (6-1)$$

For a given system level damage state, the series system assumption is used to generate fragility curves. In other words, once any component in the system reaches a certain damage state, the system is said to reach corresponding damage state. This assumption means when the first component reaches certain component damage state, then the whole piping system reaches the corresponding system damage state. In the fire sprinkler piping studies, the primary components, except the supports (braces, hangers, and wire restrainers), are only pipe joints. Assuming that the repair cost and repair time of smaller pipe diameters are equal to larger pipe diameters, the series system assumption will be valid. However, a question that might arise is: “Does the significant leakage of 1in pipe have the same effect on piping functionality as the significant leakage of 4in pipe?” The answer to this question is highly related to the piping layout. As an example, damage to a 1in pipe diameter in a small piping system may significantly affect the overall functionality of the system in terms of water pressure loss. While in a large piping system, if the damage occurs in the last branch line on 1in pipe diameter, the functionality of the system might not be significantly affected. Several factors such as overall dimension of the piping system, diameter of damaged pipes, and the distance of the leaked location from the water pressure source of the floor may affect the overall functionality of the piping system. Therefore, defining a robust scenario of component contribution on the overall functionality of a piping system might be very challenging. However, the authors defined the scenarios such as “w/o Armovers” (in which the probability of armover leakage was not considered in JPSDM) to define

the fragility curves for the systems where their damage might not be affected by armover pipe leakage. Therefore, the number of components comprising the series system varies based on the system level scenarios under consideration.

6.3 System Fragility Curves

Armovers contribute to the vulnerability of the piping system more than the other components. Also, the use of over-braced main runs may reduce the vulnerability of main runs. To see the difference between all of the optional configurations, four different system-level fragility curves were developed, namely “All” (considering all the components), “w/o Armovers” (removing armover demands from JPSDMs), “w/o Main Runs” (removing main run demands from JPSDMs), and “w/o Main Runs & Armovers” (removing both main run and armover demand from JPSDMs). Figure 6-1 through Figure 6-10 show the piping system fragility curves of the four different systems for 10 piping systems.

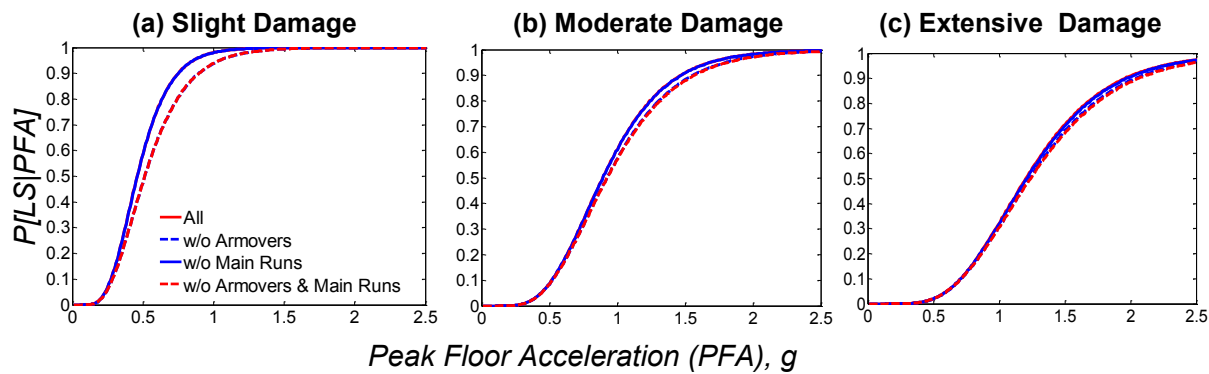


Figure 6-1 System Fragility Curves for Different Piping System Condition of Case 1

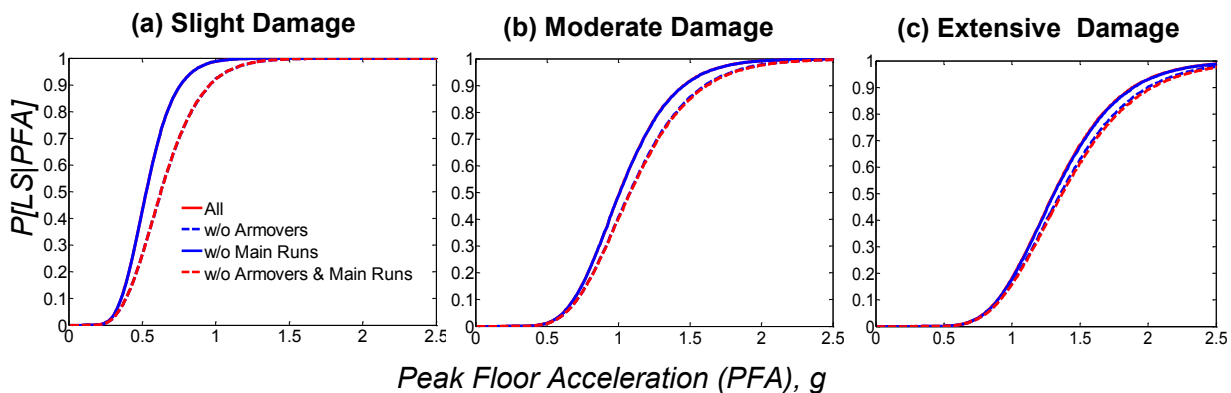


Figure 6-2 System Fragility Curves for Different Piping System Condition of Case 2

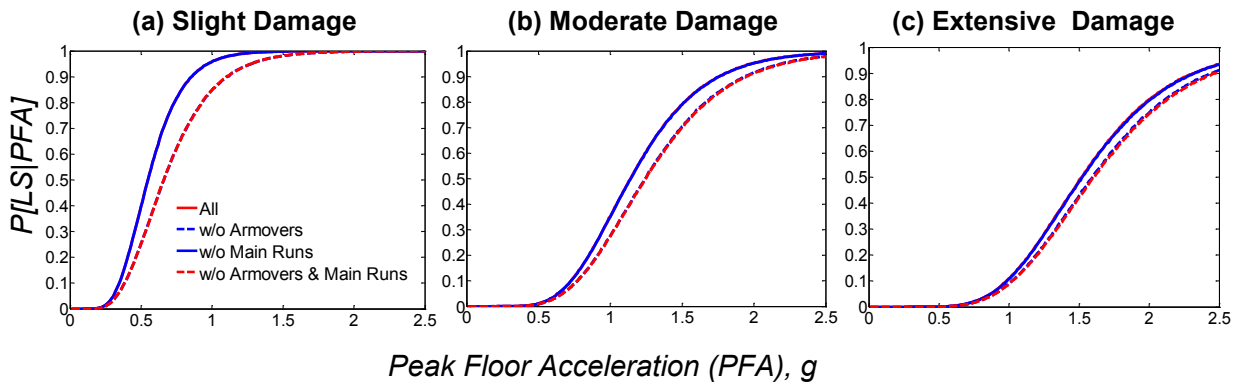


Figure 6-3 System Fragility Curves for Different Piping System Condition of Case 3

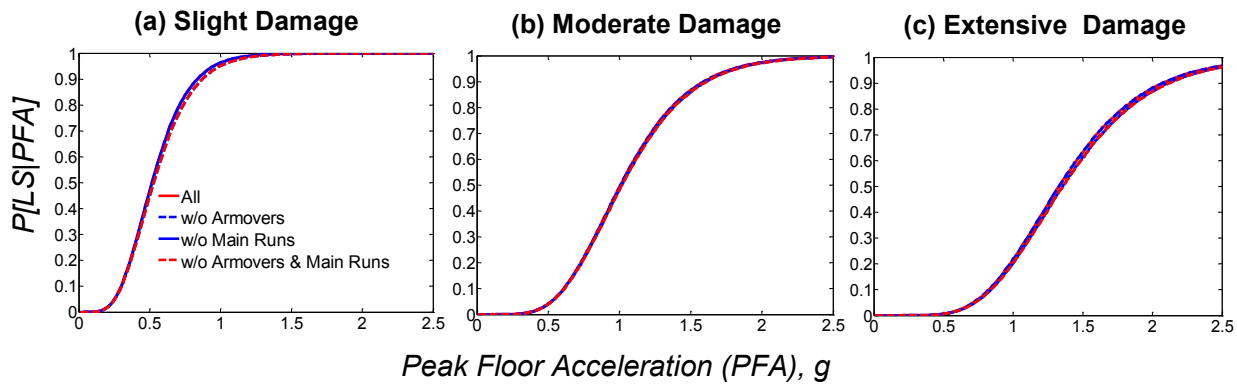


Figure 6-4 System Fragility Curves for Different Piping System Condition of Case 4

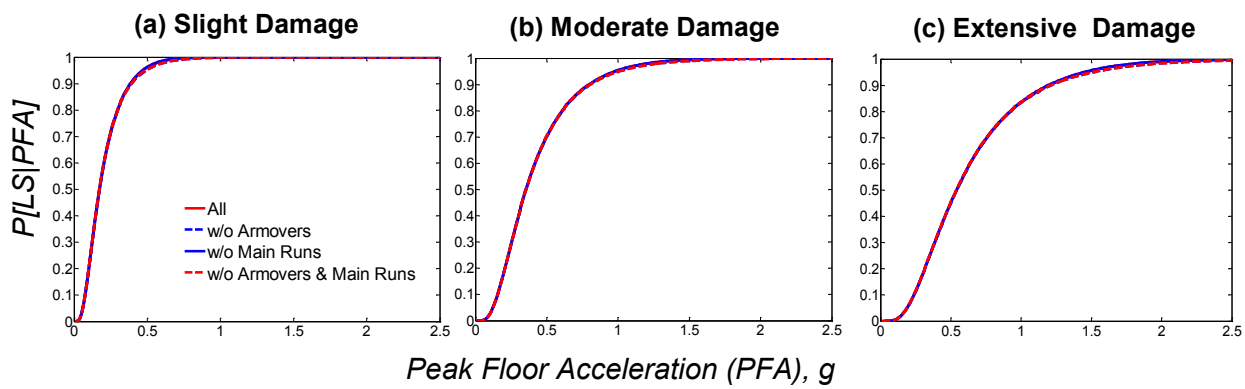


Figure 6-5 System Fragility Curves for Different Piping System Condition of Case 5

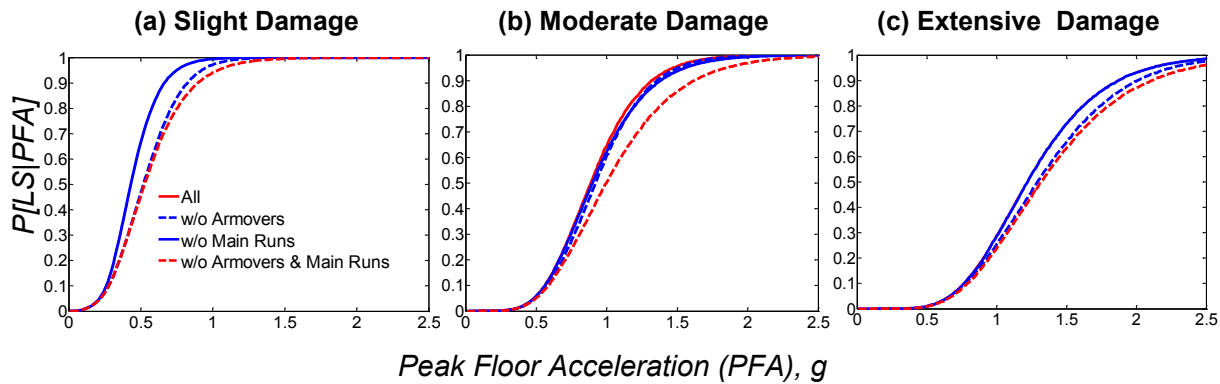


Figure 6-6 System Fragility Curves for Different Piping System Condition of Case 6

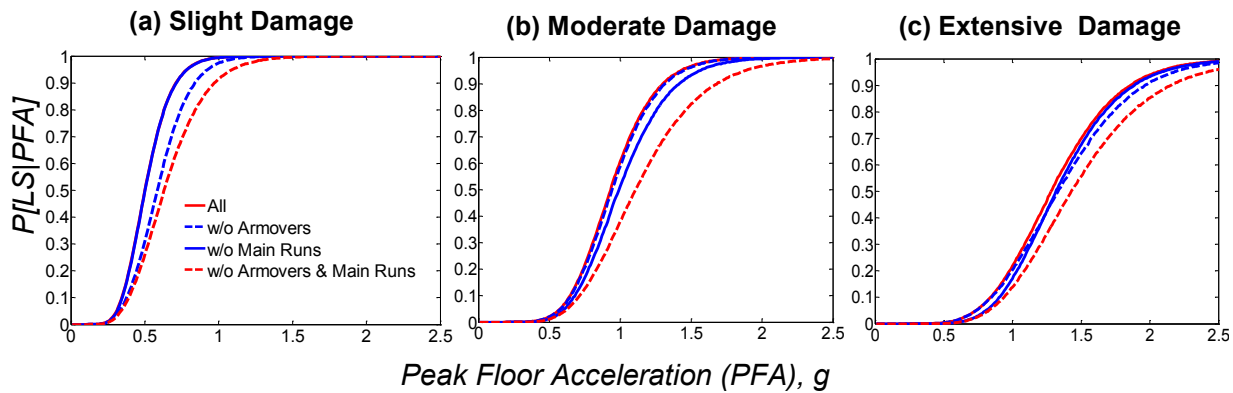


Figure 6-7 System Fragility Curves for Different Piping System Condition of Case 7

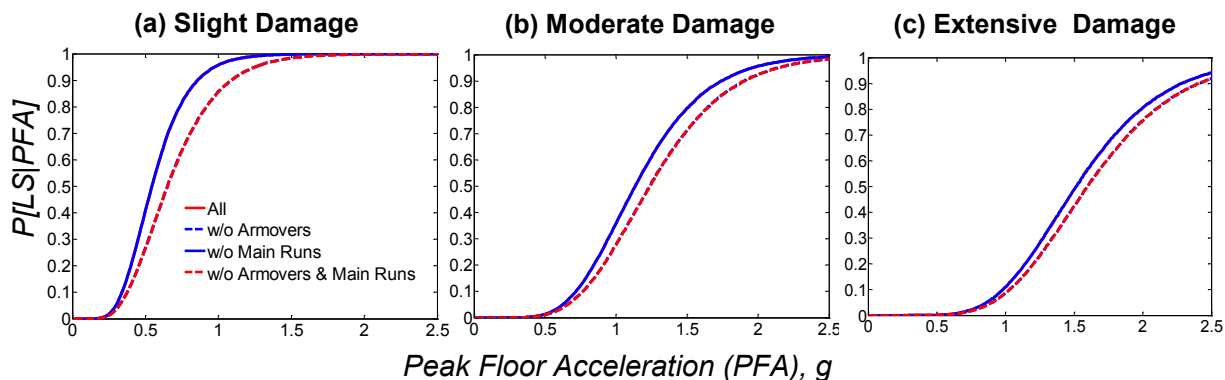


Figure 6-8 System Fragility Curves for Different Piping System Condition of Case 8

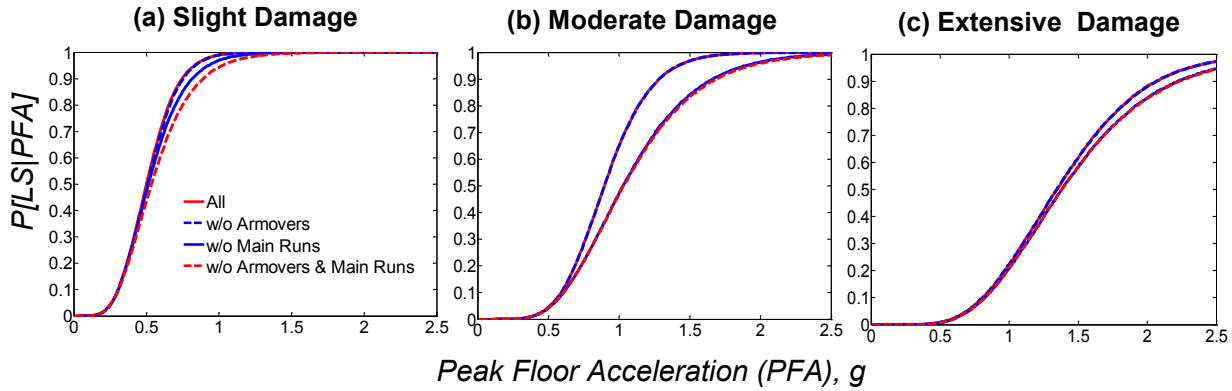


Figure 6-9 System Fragility Curves for Different Piping System Condition of Case 9

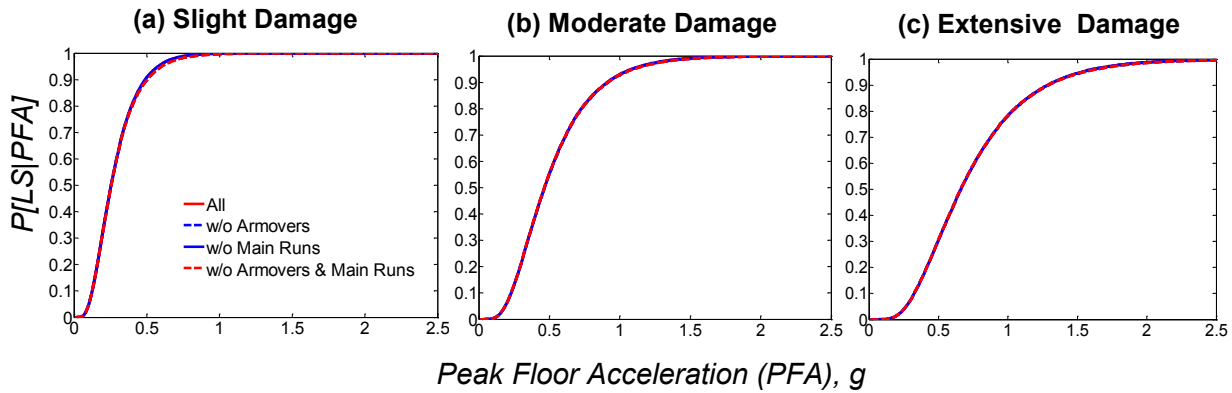


Figure 6-10 System Fragility Curves for Different Piping System Condition of Case 10

The above plots show that changes between system scenarios did not impose significant changes to any of the different piping cases. The differences were minimal in case 5 and case 10 among the other cases since system fragility curves are mostly governed by the percentage of failed cable braces in these two cases. In all cases with wire restrainers or armover drops (except cases with cable bracing), the system fragility curves were governed by armover damage. However, in the cases without wire restrainers on armover pipes (case 4 and case 9), damage to armovers was not the dominant failure mode in a piping system.

A simple approach was used to estimate the relative change in the median values of the fragility curves. The median values of the system fragility curves were calculated without considering the armover component demands in the JPSDMs. Then the armover component demands were added to the JPSMs, and the percent change in the median value of the system fragility curves

with and without considering the armovers was calculated. A positive change indicates a less vulnerable piping system. Table 6-1 through Table 6-10 show the lognormal parameters (median, λ , and logarithmic standard deviation or dispersion, ζ) that characterize the piping system fragility from regression analysis based on all four different systems for 10 piping cases.

Table 6-1 Medians and Dispersions for 4 Different Piping System of Case1

System Name	Slight			Moderate			Extensive		
	Median λ	Difference (%)	Dispersion ζ	Median λ	Difference (%)	Dispersion ζ	Median λ	Difference (%)	Dispersion ζ
ALL	0.47	NA	0.39	0.94	NA	0.39	1.26	NA	0.39
w/o Armovers	0.54	14.90	0.45	0.99	5.33	0.41	1.30	3.46	0.40
w/o Main Run	0.47	0.12	0.40	0.94	0.16	0.39	1.27	0.96	0.39
w/o Main Run & Armovers	0.54	15.08	0.45	1.00	5.99	0.42	1.32	4.94	0.40

Table 6-2 Medians and Dispersions for 4 Different Piping System of Case 2

System Name	Slight			Moderate			Extensive		
	Median λ	Difference (%)	Dispersion ζ	Median λ	Difference (%)	Dispersion ζ	Median λ	Difference (%)	Dispersion ζ
ALL	0.53	NA	0.30	1.01	NA	0.29	1.31	NA	0.29
w/o Armovers	0.63	18.81	0.35	1.08	7.03	0.32	1.36	3.84	0.31
w/o Main Run	0.53	-0.03	0.29	1.01	0.13	0.29	1.31	0.37	0.29
w/o Main Run & Armovers	0.63	18.78	0.35	1.08	7.50	0.32	1.37	4.77	0.31

Table 6-3 Medians and Dispersions for 4 Different Piping System of Case 3

System Name	Slight			Moderate			Extensive		
	Median λ	Difference (%)	Dispersion ζ	Median λ	Difference (%)	Dispersion ζ	Median λ	Difference (%)	Dispersion ζ
ALL	0.55	NA	0.35	1.14	NA	0.34	1.52	NA	0.34
w/o Armovers	0.66	20.46	0.40	1.24	8.99	0.36	1.59	5.05	0.34
w/o Main Run	0.55	-0.17	0.35	1.14	0.06	0.34	1.52	0.39	0.34
w/o Main Run & Armovers	0.66	20.40	0.40	1.25	9.33	0.36	1.60	5.50	0.35

Table 6-4 Medians and Dispersions for 4 Different Piping System of Case 4

System Name	Slight			Moderate			Extensive		
	Median λ	Difference (%)	Dispersion ζ	Median λ	Difference (%)	Dispersion ζ	Median λ	Difference (%)	Dispersion ζ
ALL	0.52	NA	0.40	1.01	NA	0.37	1.33	NA	0.36
w/o Armovers	0.53	2.54	0.41	1.01	0.03	0.37	1.33	0.08	0.36
w/o Main Run	0.52	0.16	0.40	1.02	0.82	0.37	1.36	2.14	0.36
w/o Main Run & Armovers	0.53	2.29	0.41	1.02	0.85	0.37	1.36	2.20	0.36

Table 6-5 Medians and Dispersions for 4 Different Piping System of Case 5

System Name	Slight			Moderate			Extensive		
	Median λ	Difference (%)	Dispersion ζ	Median λ	Difference (%)	Dispersion ζ	Median λ	Difference (%)	Dispersion ζ
ALL	0.18	NA	0.59	0.36	NA	0.59	0.55	NA	0.58
w/o Armovers	0.17	-0.96	0.61	0.36	-1.02	0.61	0.54	-1.46	0.61
w/o Main Run	0.18	0.08	0.58	0.36	0.32	0.59	0.55	0.04	0.58
w/o Main Run & Armovers	0.17	-1.27	0.61	0.36	-1.13	0.61	0.54	-1.86	0.61

Table 6-6 Medians and Dispersions for 4 Different Piping System of Case 6

System Name	Slight			Moderate			Extensive		
	Median λ	Difference (%)	Dispersion ζ	Median λ	Difference (%)	Dispersion ζ	Median λ	Difference (%)	Dispersion ζ
ALL	0.44	NA	0.39	0.88	NA	0.33	1.22	NA	0.35
w/o Armovers	0.52	19.03	0.43	0.92	3.71	0.33	1.29	6.15	0.36
w/o Main Run	0.44	0.24	0.39	0.90	1.90	0.35	1.22	0.32	0.35
w/o Main Run & Armovers	0.53	21.03	0.46	1.00	12.51	0.39	1.32	8.36	0.38

Table 6-7 Medians and Dispersions for 4 Different Piping System of Case 7

System Name	Slight			Moderate			Extensive		
	Median λ	Difference (%)	Dispersion ζ	Median λ	Difference (%)	Dispersion ζ	Median λ	Difference (%)	Dispersion ζ
ALL	0.50	NA	0.28	0.93	NA	0.28	1.28	NA	0.31
w/o Armovers	0.58	15.92	0.31	0.94	1.09	0.28	1.33	3.67	0.32
w/o Main Run	0.50	-0.02	0.28	0.99	6.19	0.29	1.32	2.80	0.29
w/o Main Run & Armovers	0.63	25.53	0.35	1.11	18.67	0.33	1.43	11.61	0.33

Table 6-8 Medians and Dispersions for 4 Different Piping System of Case 8

System Name	Slight			Moderate			Extensive		
	Median λ	Difference (%)	Dispersion ζ	Median λ	Difference (%)	Dispersion ζ	Median λ	Difference (%)	Dispersion ζ
ALL	0.54	NA	0.36	1.13	NA	0.34	1.51	NA	0.33
w/o Armovers	0.65	19.79	0.40	1.24	9.02	0.35	1.60	5.61	0.34
w/o Main Run	0.54	0.07	0.36	1.13	-0.14	0.34	1.51	0.04	0.33
w/o Main Run & Armovers	0.65	19.98	0.40	1.24	9.08	0.35	1.60	5.68	0.34

Table 6-9 Medians and Dispersions for 4 Different Piping System of Case 9

System Name	Slight			Moderate			Extensive		
	Median λ	Difference (%)	Dispersion ζ	Median λ	Difference (%)	Dispersion ζ	Median λ	Difference (%)	Dispersion ζ
ALL	0.50	NA	0.35	0.89	NA	0.31	1.34	NA	0.36
w/o Armovers	0.51	1.44	0.35	0.90	0.18	0.31	1.34	0.03	0.36
w/o Main Run	0.51	3.24	0.38	1.03	14.67	0.39	1.38	3.03	0.39
w/o Main Run & Armovers	0.54	7.41	0.41	1.03	15.21	0.39	1.38	3.00	0.39

Table 6-10 Medians and Dispersions for 4 Different Piping System of Case 10

System Name	Slight			Moderate			Extensive		
	Median λ	Difference (%)	Dispersion ζ	Median λ	Difference (%)	Dispersion ζ	Median λ	Difference (%)	Dispersion ζ
ALL	0.26	NA	0.47	0.47	NA	0.50	0.67	NA	0.50
w/o Armovers	0.26	0.37	0.52	0.47	-0.36	0.52	0.67	-1.38	0.53
w/o Main Run	0.26	0.22	0.47	0.47	0.36	0.50	0.67	-0.12	0.50
w/o Main Run & Armovers	0.26	0.56	0.52	0.47	-0.73	0.53	0.67	-1.25	0.54

According to the tables, the median PFA values of a slight damage state for piping systems with solid braces varies from 0.44 g to 0.66 g. The corresponding values vary from 0.88 g to 1.25 g in moderate and from 1.22 g to 1.20 g in extensive damage states. By varying the type of components considered in the system fragility curves (e.g. “all,” “w/o Main Run”), the maximum difference percentage was 26, 19, and 12 for slight, moderate, and extensive damage states, respectively. However, the differences were negligible for piping systems with cable bracing. As mentioned before, the failure of these piping systems are governed by brace failure and not by pipe joints.

A sample comparison was made between the median PFA of all the piping cases considering all components, which is shown in Figure 6-11. This figure shows that, in all damage states, dry piping systems are the least vulnerable piping systems, which is due to elimination of mass of water from the piping system (green colored bars). The piping systems with cable braces were found to be the most vulnerable piping systems (red colored bars). The failure of cable braces was always found to be the dominant damage in system level fragilities. However, the results of this may be considered subjective, as the cable braces were never removed during response history analysis. Moreover, the damage states of cable braces can be changed based on accurate cost and repair time estimation of cable braces.

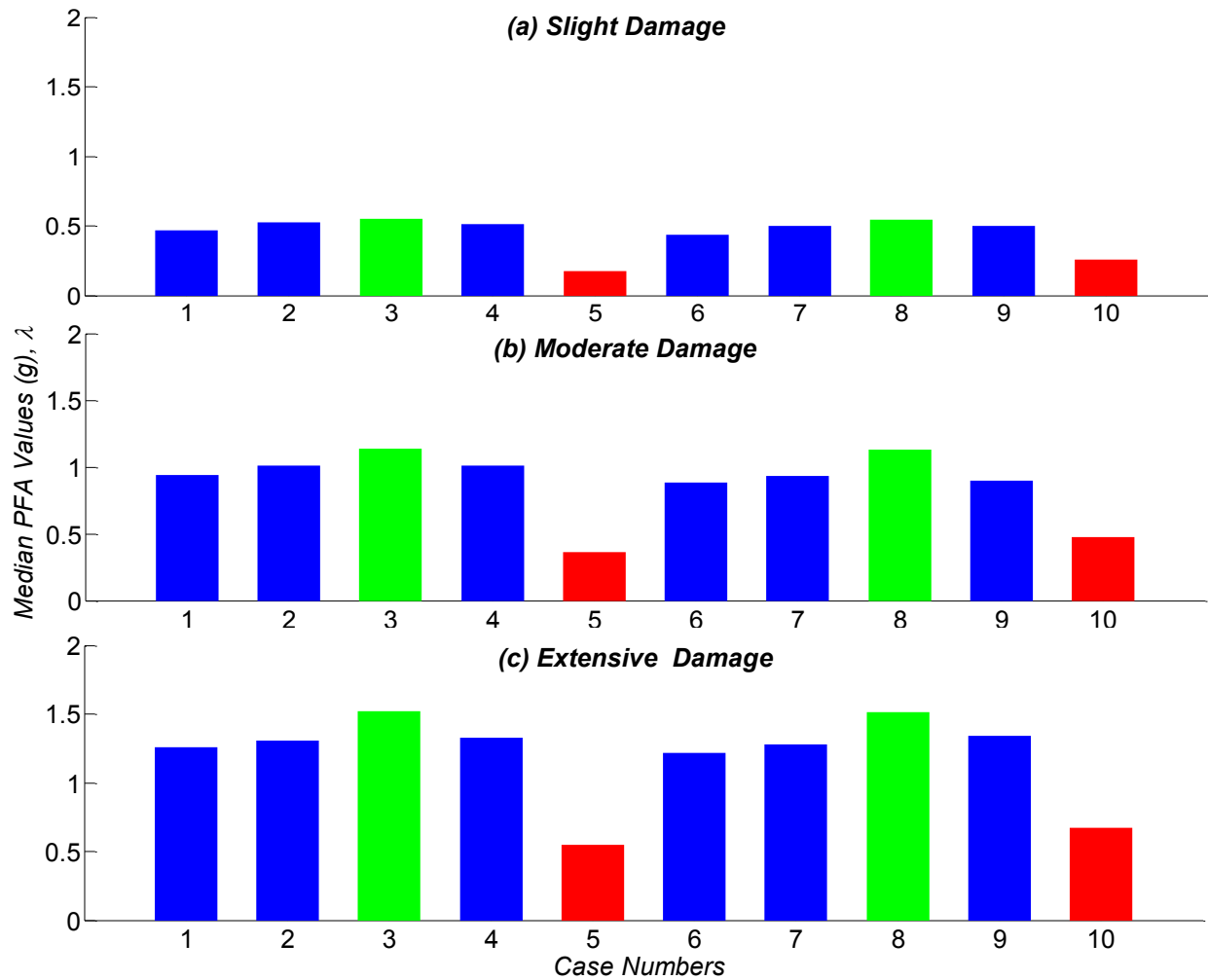


Figure 6-11 Comparison of Median PFA Values for All Piping Cases Considering All Components

6.4 Effect of Variations of Design and Motion on System Fragility Curves

In this section, the fragility curves of different piping components are compared with respect to considered variables. The variables that have been considered as the comparison bases include: 1) joint types (threaded/grooved); 2) motion suites; 3) weight of water; 4) configuration of wire restrainers; and 5) and type of bracing (cable/solid).

6.4.1 Joint Types

The effect of joint type variations on component fragility curves was studied earlier. In the following discussion, the same effect is studied in system level fragility curves. A similar procedure as that used in Section 5.11.2 is utilized in this section between the piping systems with threaded and grooved main run joints. The comparison has been made between all piping

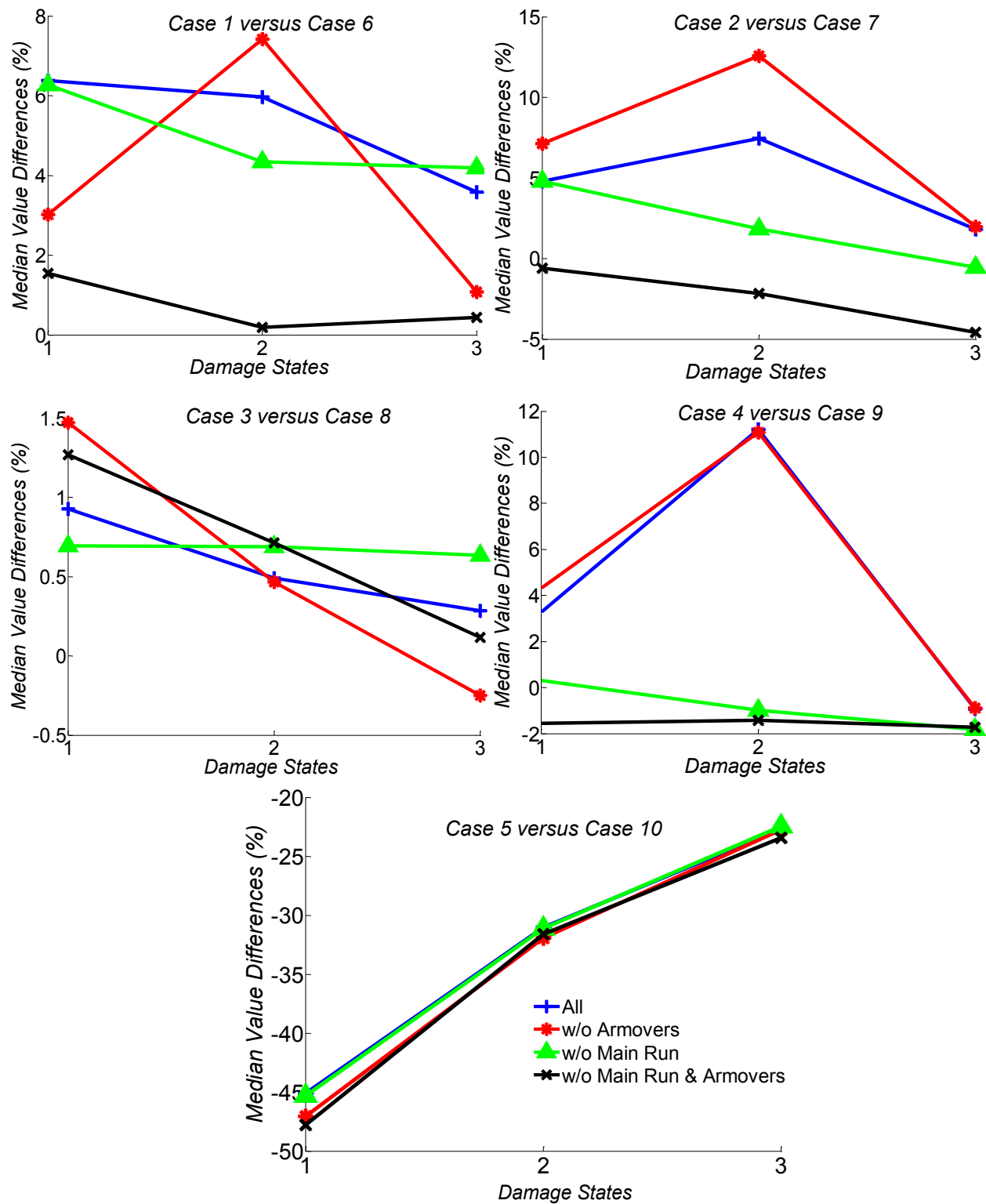


Figure 6-12 System Median Value Differences Considering Main Run Joint Variation

systems (e.g. “All,” “w/o Main Runs”). The differences between the median values, using Equation (5-20), are considered as the comparison basis. In this equation, $\lambda_{Threaded}$ and

$\lambda_{Grooved}$ are the median values of each piping system for threaded and grooved main runs, respectively, for a specific damage state. The positive values of MVD imply the more fragile system is the grooved system.

Figure 6-12 shows that in all piping systems and all cases (except with cable bracing), piping systems with grooved main run connections were slightly more fragile, which is consistent with what was concluded from component level studies. The component level plots showed that the largest differences between piping systems with different joint types were related to the main run pipe. Figure 6-12 shows the same trend, while the differences in piping systems without main run consideration were the smallest. In the piping system with cable bracing, the piping system with threaded joints was found to be more fragile, which is not governed by joint rotation and only follows the percentage of bracing failure.

6.4.2 Motion Suites

In previous sections, the effects of using different motion suites with different S_{DS} distribution on component fragility curves were studied. In the following discussion, the same effect is studied in system level fragility curves. Using a method similar to the procedure used in Section 5.11.3, a comparison was made between all piping systems (e.g. “All,” “w/o Main Runs”). The differences between the median values, using Equation (5-21), are considered for comparison. In this equation, $\lambda_{Uniform}$ and $\lambda_{Lognormal}$ are the median values of each piping system, uniform and lognormal S_{DS} distribution, respectively, for a specific damage state. The positive values of MVD imply a more fragile system under lognormal distribution.

Figure 6-13 shows that a variation on motion distributions resulted in a maximum difference of 20% between the median values of system fragility curves, which is less than the maximum differences in component level (35%). In general, the motion suite with log-normal S_{DS} distribution resulted in slightly less fragile systems compare to the motion suite with uniform S_{DS} distribution. In other words, a larger number of motions with lower intensities in a suite of motions may result in a less fragile system. A similar trend was observed in component level fragilities.

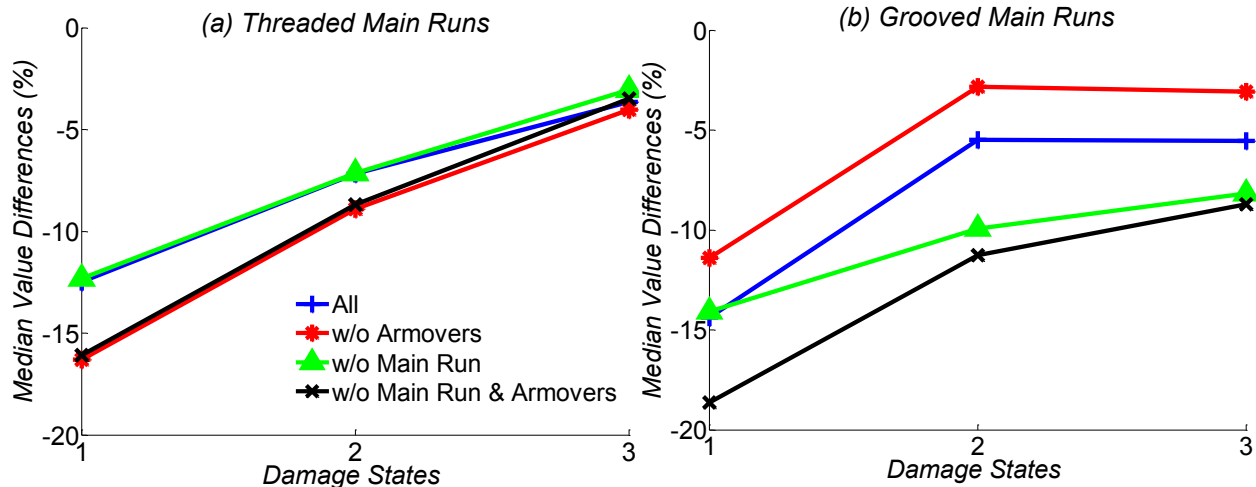


Figure 6-13 System Median Value Differences Considering Motion Suite Variation

6.4.3 Water Weight

The effect of water weight (mass) on component fragility curves was studied earlier. In the following discussion, the same effect is studied in system level fragility curves. A similar procedure used in Section 5.11.4 is utilized in this section between the dry and wet piping systems. The comparison was made between all piping systems (e.g. “All,” “w/o Main Runs”). The differences between the median values, using Equation (5-22), are considered for comparison. In this equation, λ_{Wet} and λ_{Dry} are the median values of wet and dry piping systems respectively, for a specific damage state. The positive values of MVD imply a more fragile system in dry piping system.

Figure 6-14 shows that in all piping systems, the system failure probability is less in the dry piping systems compared to the wet piping systems. The same trend was also observed in component level studies. Therefore, the piping seismic performance may be improved in dry piping systems by 15% to 35%.

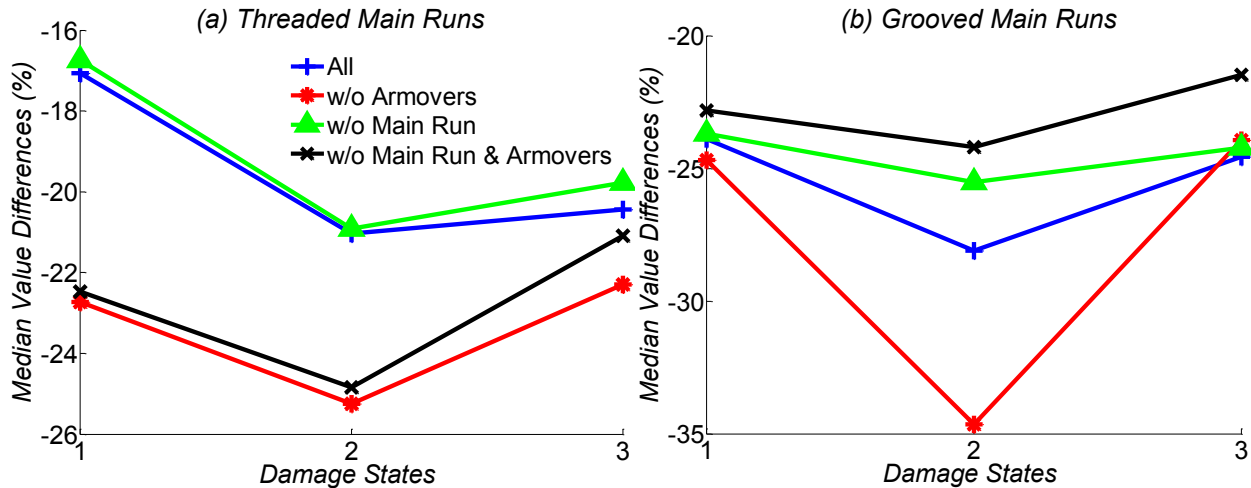


Figure 6-14 System Median Value Differences Considering Water Weight Variation

6.4.4 Wire Restrainers

The effects of removing wire restrainers from armover pipes on component fragility curves were studied in previous sections. In the following discussion, the same effect is studied in system level fragility curves. A similar procedure to that used in Section 5.11.5 is implemented in this section between the piping systems with and without wires on armover pipes. The comparison was made between all piping systems (e.g. “All,” “w/o Main Runs”). The differences between the median values, using Equation (5-23), are considered for comparison. In this equation, λ_{Wire} and $\lambda_{\text{No-Wire}}$ are the median values of piping systems with and without wire restrainer on armover pipes, respectively, for a specific damage state. The positive values of MVD imply a more fragile system in piping system without wire strainers on armovers.

Figure 6-15 shows the differences in the piping systems without armovers are negligible. However, in the piping systems with armovers, removing the wire restrainers improved the overall performance of the system. At the component level, it was shown that the vulnerability of armover tee joints was reduced after removing the wire restrainers.

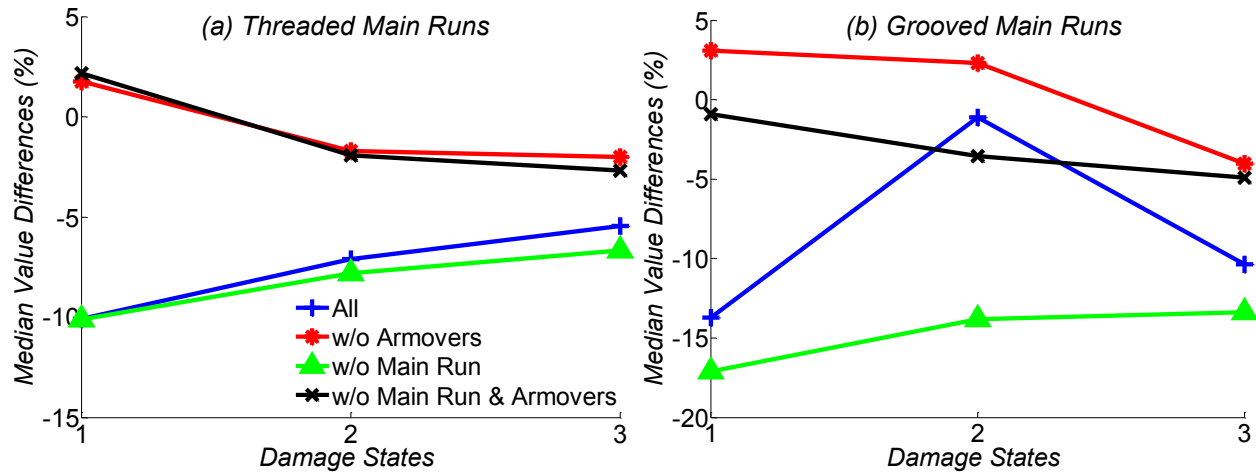


Figure 6-15 System Median Value Differences Considering Wire Restrainers Variation

6.4.5 Bracing

Previously, two types of bracing were studied for seismic resisting of piping systems. In the following discussion, the same effect is studied in system level fragility curves. A similar procedure to that used in Section 5.11.6 is implemented in this section between the piping systems with cable and solid bracing. The comparison was made between all piping systems (e.g. "All," "w/o Main Runs"). The differences between the median values, using Equation (5-24), are considered for comparison. In this equation, λ_{Solid} and λ_{Cable} are the median values of the piping system with solid and cable bracing, respectively, for a specific damage state. The positive values of MVD imply a more fragile system in a piping system with cable bracing.

According to Figure 6-16, piping systems with cable bracing are considerably weaker than

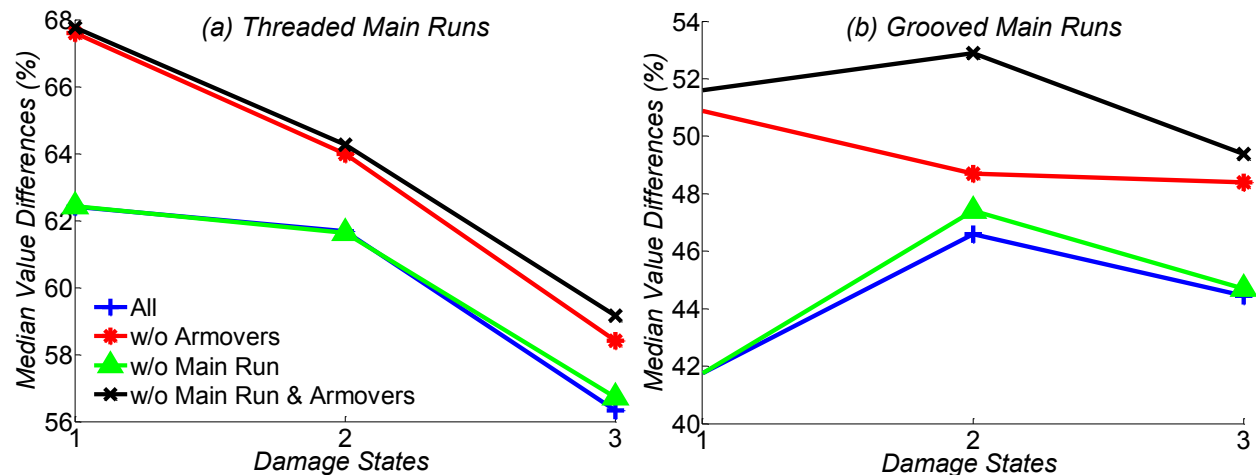


Figure 6-16 System Median Value Differences Considering Brace Type Variation

piping systems that incorporate solid braces. However, this conclusion might be subjective because the cable braces never were removed during the response history analysis and also based on the way that their damage states were defined.

6.5 Concluding Remarks

In the previous section, the analytical component fragility curves of fire sprinkler piping systems were developed using a probabilistic seismic design model (PSDM). The main purpose of this section was to establish system fragility curves by combining component fragility curves. To do so, a joint probabilistic seismic demand model (JPSDM) was used to estimate piping system level fragility. A JPSDM was developed by assessing the demands placed on individual components (marginal distribution) through regression analysis. Four different system level fragility curves were developed, namely, “All” (considering all the components), “w/o Armovers” (removing armover demands from JPSDMs), “w/o main runs” (removing main run demands from JPSDMs), and “w/o main runs & armovers” (removing both main run and armover demand from JPSDMs) to examine the difference between all of the optional piping configurations. A simple approach was used to estimate the relative change in the median values of the fragility curves for all 10 piping cases.

Several comparisons were made between system fragilities of different piping systems considering only one variable at a time. These comparisons showed that:

- 1) In all piping systems and all cases (except with cable bracing), piping systems with grooved main run connections are slightly more fragile than threaded joints. In the piping system with cable bracing, the piping system with threaded joints was found to be more fragile, which is not governed by joint rotation and only follows the percentage of bracing failure.
- 2) Variation on motion distributions resulted in maximum differences of 20% in the median values of system fragility curves, which is smaller than the maximum differences in component level (35%). In general, the motion suite with lognormal S_{DS} distribution resulted in slightly more conservative results.

- 3) In all piping systems, the system failure probability is less in the dry piping systems compared to the wet piping systems. Piping seismic performance may be improved by 15%-35% in dry piping systems.
- 4) In piping systems with armovers, removing wire restrainers improved the overall performance of piping systems. However, differences in piping systems without armovers were negligible.
- 5) Piping systems with cable bracing were considerably weaker than piping systems that incorporated solid braces. However, this conclusion might be subjective, as the cable braces never were removed during the response history analysis and also based on the way their damage states were defined.

SECTION 7 DISPLACEMENT FRAGILITY ANALYSIS

7.1 Introduction

As mentioned before, the assessment of seismic vulnerability for the entire piping system must be performed by combining the effects of the various piping components. Therefore, the procedures for developing component fragility curves and a methodology for obtaining the system level curves were described in previous sections. These types of fragility curves were developed for acceleration sensitive parts of piping systems. However, fire sprinkler piping systems are susceptible to other types of damage, which are usually associated with structural or piping displacements such as the following (FEMA E-74, 2011):

- **Building Deformation:** Due to deformations of structural members, buildings are subjected to differential horizontal movement through building floors, which is also known as story drift. Therefore, drift sensitive components such as vertical pipe runs may experience damage under large story drifts (see Figure 7-1). In general, vertical pipe runs are one of the critical members of a piping system. They supply the water to horizontal

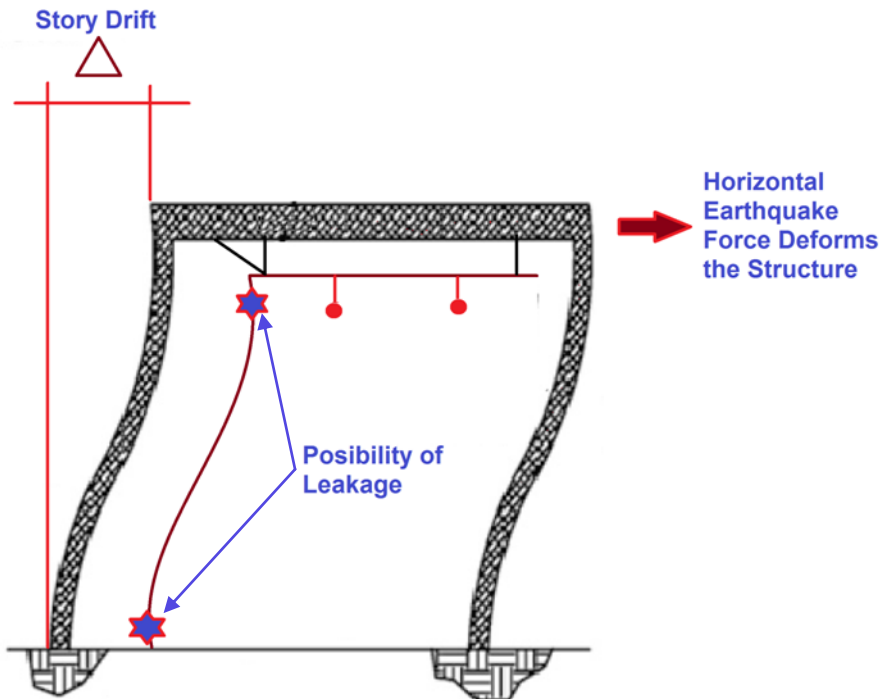


Figure 7-1 Vertical Pipe Damage Due to Structural Deformation

pipes. Consequently, the assessment of seismic vulnerability of riser pipes is a crucial step for overall performance of a piping system.

- **Nonstructural Interaction:** Due to the differential movement of adjacent nonstructural systems, nonstructural systems may become damaged during earthquakes caused by collision to their surrounding members. Some examples of damaging pipe interactions include:
 - 1) Sprinkler head and ceiling interaction, causing the sprinkler head to break and water to leak or damage to the ceiling system (see Figure 7-2).



Figure 7-2 Damage Caused by Sprinkler Head-Ceiling Interaction, Photo courtesy of; (b) Rodrigo Retamales, Rubn Boroschek & Associates (c) Robert Reitherman

- 2) Pipe movements at penetrated areas (e.g. partitions) can result in damage to architectural finishes, fireproofing, and insulation. Also, pipe poundings at penetrated joints may increase the chance of leakage and consequently cause further damage to interacting objects and potential failure of the piping system. Examples of this type of damage during previous earthquakes are shown in Figure 7-3.

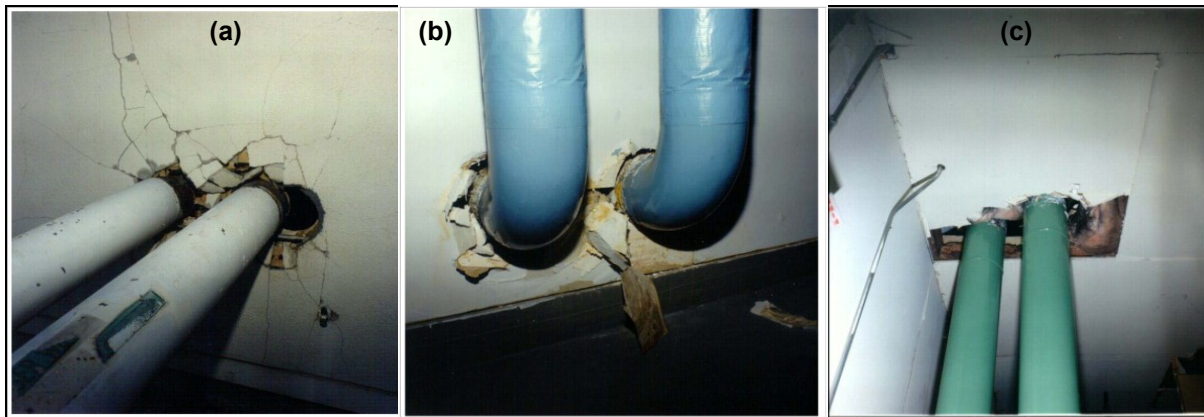


Figure 7-3 Damage Observed at Pipe Penetration Points (Photo Courtesy of Mason Industries)

- 1) The interaction of pipes with adjacent equipment or objects. This type of damage may result in pipe damage or may affect the functionality of interacting equipment (Figure 7-4). In critical facilities such as a surgery room of a hospital, this type of damage can cause serious problems, and in some cases it can be life threatening.

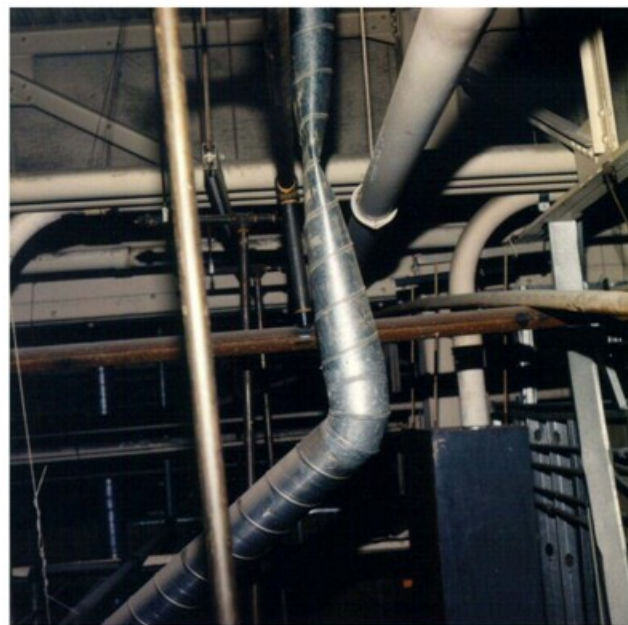


Figure 7-4 Damage Caused by Pounding of Pipe and Adjacent Objects (Photo Courtesy of Mason Industries)

In this section, the pipe joint fragility curves are developed based on story drift ratios. Next, the displacement fragility curves for large pipe diameters were developed based on the data obtained from two experiments and analytical models presented in Section 4. Finally, displacement fragility curves for smaller pipe diameters (using the sprinkler head representative nodes) were developed using the analytical models presented in Section 4.

7.2 Drift Sensitive Pipe Runs

Vertical pipe runs are one of the critical members in a piping system that supplies water to horizontal pipes. Riser pipes are recognized as the most important and common type of vertical pipe runs in fire sprinkler piping systems. However, other types of vertical pipe runs such as wall mounted pipes (Filiatrault et al., 2008) can be used in a piping system. As mentioned before, vertical pipes are the most drift sensitive part of a fire sprinkler piping system. Consequently, the assessment of seismic vulnerability of riser pipes is a crucial step for evaluating overall performance of piping system.

7.2.1 Fragility Analysis Methodology

As mentioned earlier, fragility curves are probabilistic representations of exceeding a predefined capacity or limit state (damage state) in terms of intensity measures (*IMs*), story drift ratio, and engineering demand parameters (*EDPs*) as a measure of piping response. The steps implemented in this study to generate vertical pipes fragility curves are: 1) determine the pipe joint damage states; 2) relate the pipe joint rotational damage states to story drift ratio damage states; and 3) calculate the fragility parameters based on median and logarithmic standard deviation of damage states. Each of these steps is presented in the following sections.

7.2.2 Pipe Joint Damage States

Pipe joint damage states for threaded and grooved pipe joints are provided in Section 5.9. Damage state values were borrowed from Section 5.9 and are presented here for convenience.

Table 7-1 Damage States of Pipe Joints

Pipe Diameter	Slight	Moderate	Extensive	Dispersion
	Median (rad.)			β_c
THREADED				
3/4" Pipe	0.005	0.023	0.040	0.206
1" Pipe	0.005	0.018	0.031	0.146
1.25" Pipe	0.005	0.014	0.023	0.133
1.5" Pipe	0.005	0.013	0.020	0.120
2" Pipe	0.005	0.0094	0.014	0.094
2.5" Pipe	0.005	0.009	0.013	0.125
3" Pipe	0.005	0.008	0.011	0.155
3.5" Pipe	0.005	0.008	0.010	0.186
4" Pipe	0.005	0.010	0.010	0.216
5" Pipe	0.005	0.006	0.007	0.210
6" Pipe	0.005	0.006	0.006	0.204
GROOVED				
2" Pipe	0.015	0.050	0.077	0.170
2.5" Pipe	0.013	0.026	0.038	0.140
3" Pipe	0.010	0.019	0.029	0.110
3.5" Pipe	0.008	0.016	0.024	0.079
4" Pipe	0.005	0.010	0.021	0.049
5" Pipe	0.006	0.011	0.017	0.049
6" Pipe	0.005	0.010	0.014	0.049

7.2.3 Joint Rotation/ Story Drift Ratio

The proper selection of IM can pay an important role on applicability of fragility studies. According to the work done by Tian et al. (2012), the proposed fragility curves are based on pipe joint rotation as IM (see Figure 7-5) .

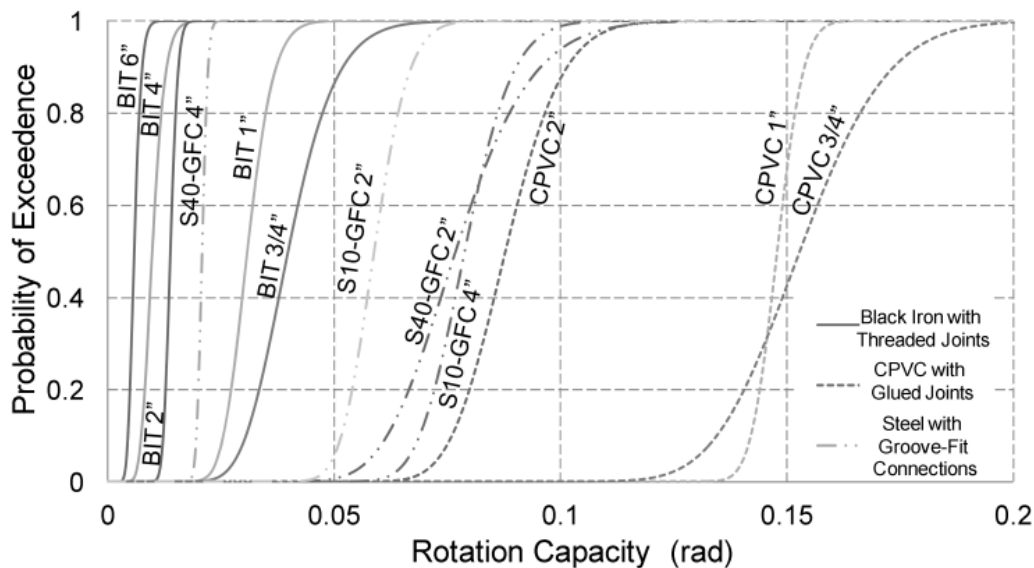


Figure 7-5 Pipe Joint Fragility Curves Based on leakage Rotational Capacity (rad.) (Tian et al., 2012)

Similar fragility curves can be produced for proposed pipe diameters and for different damage states based on rotational capacities. However, an appropriate transition from rotational capacities to story drift ratio as an intensity measure can convert these plots to be more applicable with respect to levels of structural deformation.

Assuming that the rotation on vertical pipes imposed by building deformation (drift) is only concentrated at end joint rotations, simply, the joint rotation can be related to story drift ratio. The following assumptions have been made: 1) flexural and shear deformation of pipe segments is negligible; and 2) the top and bottom of risers at each floor is fixed by solid sway braces. Therefore, as shown in Figure 7-6, the vertical joint rotation can be converted to story drift ratio as:

$$\theta_{RJ} \times 100 \cong \frac{\Delta}{H} (\%) \quad (7-1)$$

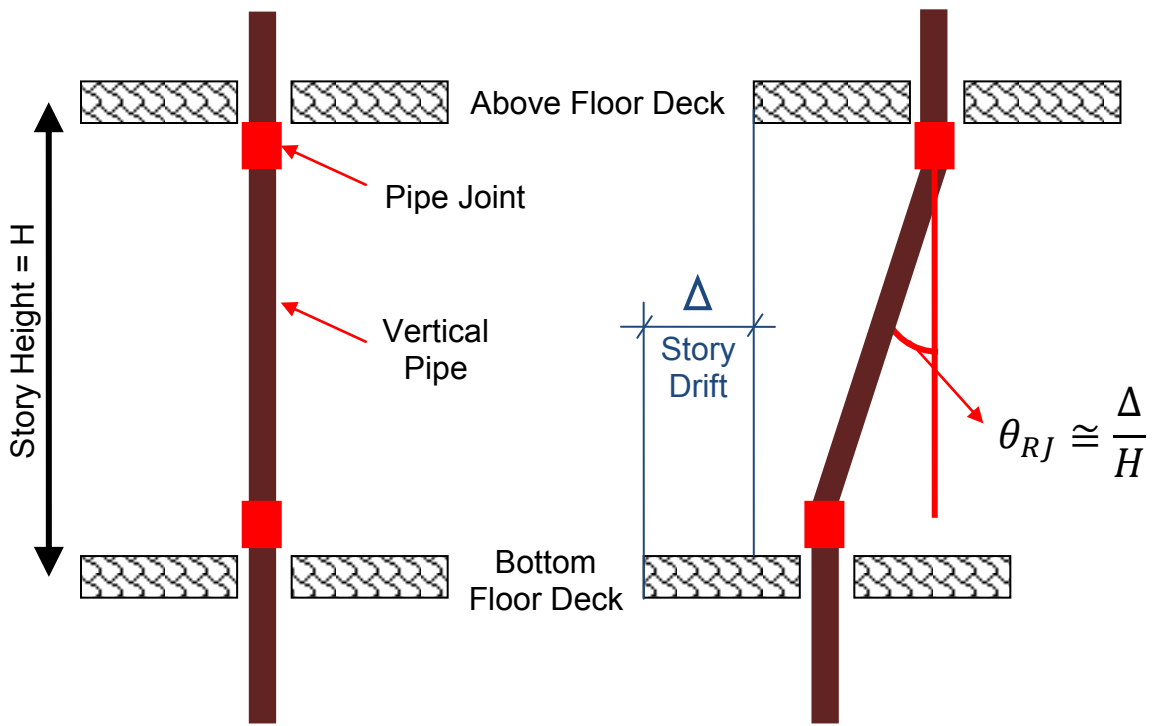


Figure 7-6 Schematic Relation of Riser Joint Rotation and Inter-Story Drift

where θ_{RJ} , Δ , and H are riser joint rotation, building deformation, and story height, respectively. Using the mentioned relation and assumptions, pipe joint damage states based in rotation (see Table 7-1) can be converted to damage states presented in Table 7-2 based on inter-story drift ratio.

Table 7-2 Damage States of Pipe Joints

Pipe Diameter	Slight	Moderate	Extensive	Dispersion
	Median (Drift (%))			
THREADED				
3/4" Pipe	0.5	2.3	4.0	0.206
1" Pipe	0.5	1.8	3.1	0.146
1.25" Pipe	0.5	1.4	2.3	0.133
1.5" Pipe	0.5	1.3	2.0	0.120
2" Pipe	0.5	0.94	1.4	0.094
2.5" Pipe	0.5	0.9	1.3	0.125
3" Pipe	0.5	0.8	1.1	0.155
3.5" Pipe	0.5	0.8	1.0	0.186
4" Pipe	0.5	1.0	1.0	0.216
5" Pipe	0.5	0.6	0.7	0.210
6" Pipe	0.5	0.6	0.6	0.204
GROOVED				
2" Pipe	1.5	5.0	7.7	0.170
2.5" Pipe	1.3	2.6	3.8	0.140
3" Pipe	1.0	1.9	2.9	0.110
3.5" Pipe	0.8	1.6	2.4	0.079
4" Pipe	0.5	1.0	2.1	0.049
5" Pipe	0.6	1.1	1.7	0.049
6" Pipe	0.5	1.0	1.4	0.049

7.2.4 Fragility Curves

As mentioned before, fragility parameters can be derived using the closed form solution described in equation (7-2), where, D and C denote demand and capacity, S_D and S_C denote the median values of demand and capacity, and $\beta_{D|IM}$ and β_C denote the dispersions (logarithmic standard deviation) of the demand and capacity, respectively (Ramanathan, 2012).

$$P[D > C|IM] = \Phi\left(\frac{\ln\left(\frac{S_D}{S_C}\right)}{\sqrt{\beta_{D|IM}^2 + \beta_C^2}}\right) \quad (7-2)$$

where $\Phi(.)$ is the standard normal probability integral. By assuming the uniform distribution of IM (0 to 10% drift) and assuming $\beta_{D|IM} = 0$ (other values can be used), values presented in

Table 7-2 can be used as median and dispersion values for the seismic fragility curves of the piping components under structural interstory drift ratios. Since pipe diameters larger than 2 inches are more common to use as riser pipes, the fragility curves of these pipe diameters are compared for different pipe joint types and damage states in Figure 7-7 through Figure 7-9. According to the NFPA 13 (2011), flexible couplings shall be used on riser pipes passing through the structural floors, allowing piping systems to accommodate interstory drifts. Flexible couplings are a type of fitting that allows axial displacement, rotation, and at least 1 degree of angular movement of the pipe without inducing harm on the pipe. The following plots show the probability of reaching each damage state in cases of flexible coupling. Figure 7-7 shows slight fragility curves for different riser pipe diameters. In all pipe diameters, these curves indicate that threaded joints are more vulnerable compared to grooved joints. The curve differences are reduced when the pipe diameters are increased.

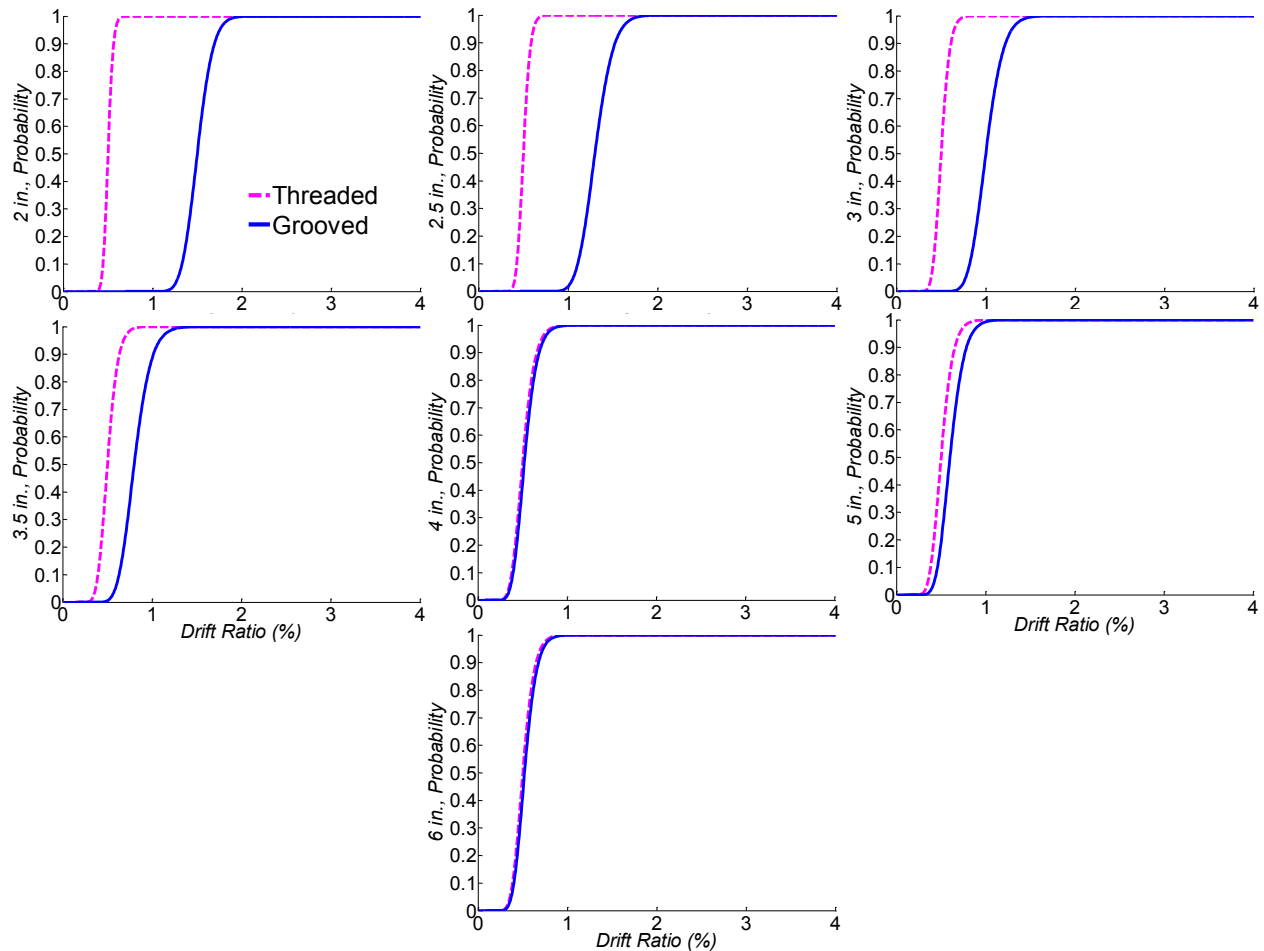


Figure 7-7 Slight Fragility Curves for Different Riser Pipe Diameters

Figure 7-8 shows moderate fragility curves for different riser pipe diameters. These curves reveal, in all pipe diameters, threaded joints are more vulnerable compared to grooved joints. The curve differences are reduced as the pipe diameters increased. The curves demonstrate that the overall probability of dripping in threaded joints are occurred in drift ratios less than 1%.

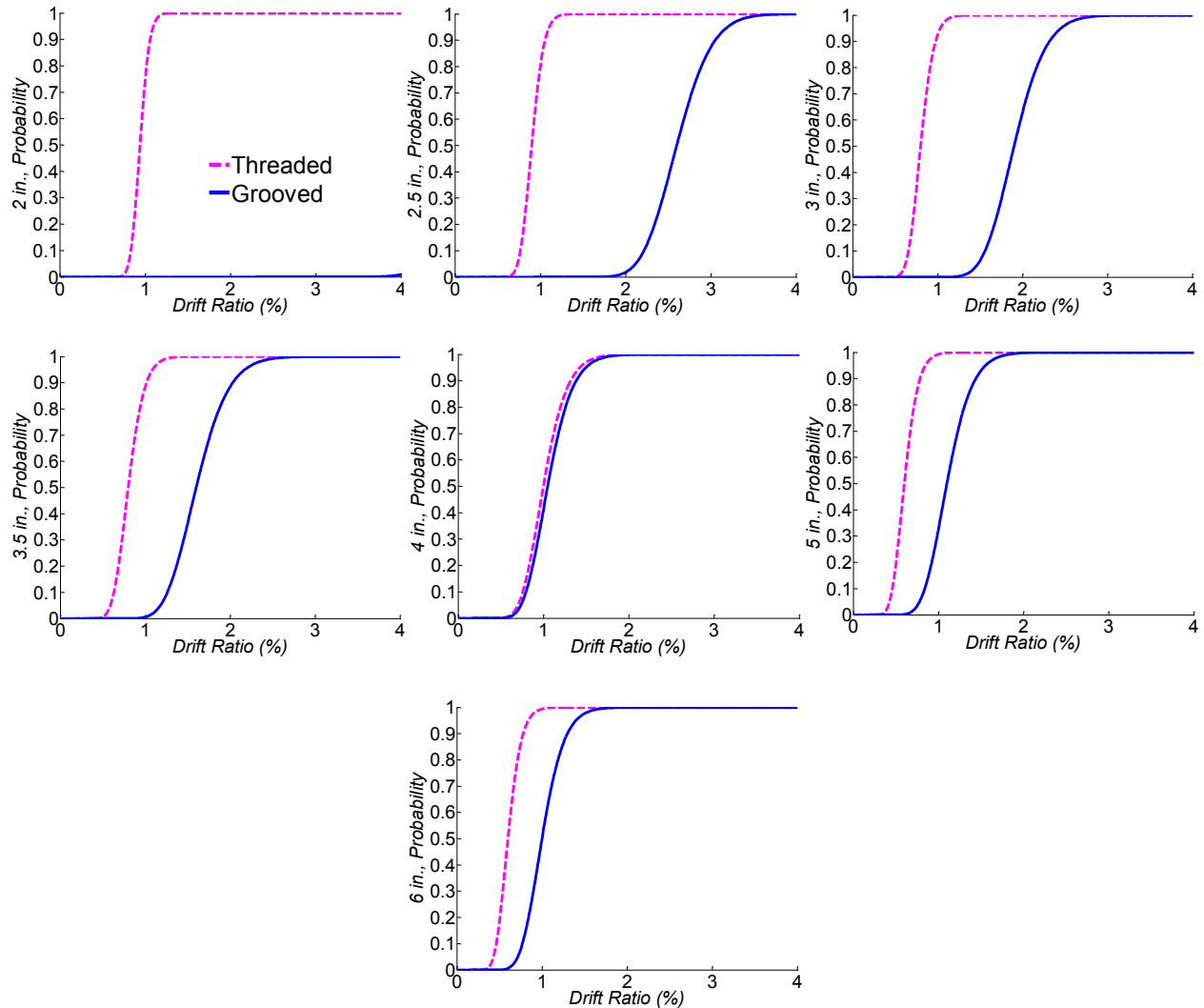


Figure 7-8 Moderate Fragility Curves for Different Riser Pipe Diameters

Figure 7-9 shows extensive fragility curves for different riser pipe diameters. These curves reveal, in all pipe diameters, threaded joints are more vulnerable compared to grooved joints.

The curve differences are reduced as the pipe diameters are increased. The curves demonstrate that the overall probability of leakage in threaded joints was observed if drift ratios were less than 1%. The probability of leakage in grooved connections for small pipe diameters (less than 3 inches) is very low. However, in larger pipe diameters, the probability of leakage in grooved joints was less than 1.5 % drift. Therefore, using flexible coupling can improve the riser pipes either with grooved or threaded joints.

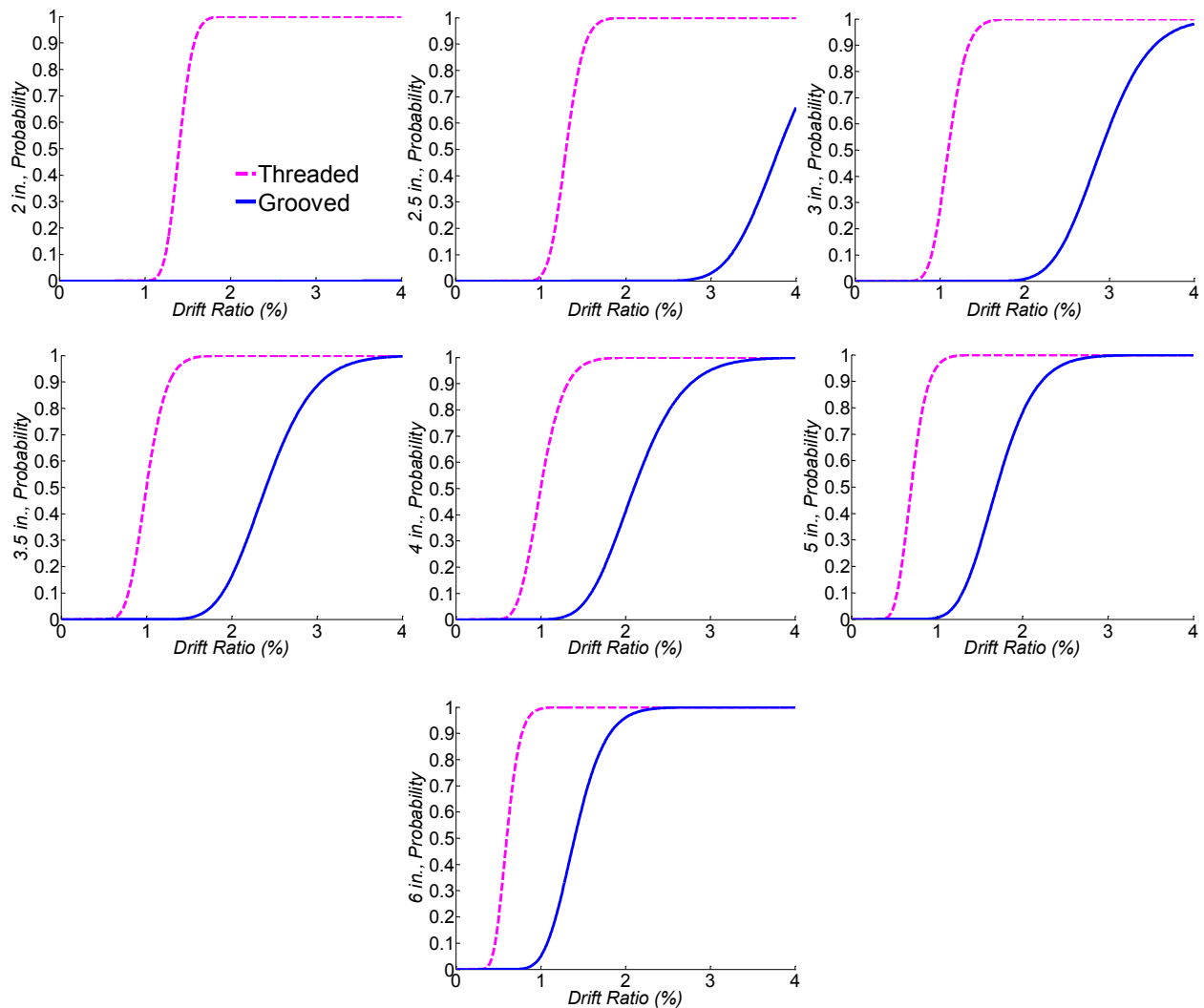


Figure 7-9 Extensive Fragility Curves for Different Riser Pipe Diameters

7.3 Displacement Demand on Large Pipe diameters

As mentioned before, excessive movement of large horizontal pipes and interaction with adjacent objects may result in damage to a partition's architectural finishes, fire proofing, and insulation. Also, the pounding of pipe runs to their surroundings may increase the probability of leakage on pipe runs or damage to critical equipment. The damage can result in property loss, building functionality loss, and in extreme cases, can be life threatening. Therefore, a realistic displacement assessment of large pipes is one of the necessary steps for evaluating the seismic vulnerability of fire sprinkler piping systems.

7.3.1 Code Requirements

According to Section 9.3.4 of NFPA 13 (NFPA, 2011), clearance shall be provided around all piping extending through walls, floors, platforms, and foundations. The summary of these requirements is stated below:

- Where a pipe passes through holes, the holes shall be sized such that the diameter of the holes is nominally 2 inches larger than the pipe for pipe 1 inch nominal to 3.5 inch nominal and 4 inches larger than the pipe for pipe 4 inch nominal and larger.
- No clearance shall be required for piping passing through gypsum board or equally frangible construction that is not required to have a fire resistance rating.
- No clearance shall be required where horizontal piping passes perpendicularly through successive studs or joists that form a wall or floor/ceiling assembly.
- Where required, the clearance shall be filled with a flexible material that is compatible with the piping material.

7.3.2 Displacement Demands

The displacement responses of two experimental piping systems and two benchmark analytical models, which were presented in Sections 5 and 6 (case 1 and case 6), were used to establish the *EDPs* following by the development of Probabilistic Seismic Demand Models (PSDMs) of piping displacements. A quick summary of each piping system is presented below.

7.3.2.1 Piping Subassembly at University of Nevada, Reno

The detailed description of this experiment, instrumentation, and loading protocol is presented in Section 4.3. However, a summary of instruments used is presented here for convenience. Data

collected from the experiments was comprised of the displacement of the piping subsystem measured relative to the stationary frame and the accelerations at critical locations on the pipes. The responses of the locations labeled “ $\Delta 1$ ” through “ $\Delta 8$ ” (in the direction of motion) in Figure 7-10 (a) were used to estimate the displacement demand of the piping subassembly. Figure 7-10 (b) shows the demand plots for the piping displacement at all recorded locations versus peak floor acceleration along with regression curves and parameters using equations (5-3) and (5-5). This plot shows that the unbraced piping system's overall displacement demand is slightly higher than the braced configuration, while the maximum recorded displacement is higher in the braced configuration.

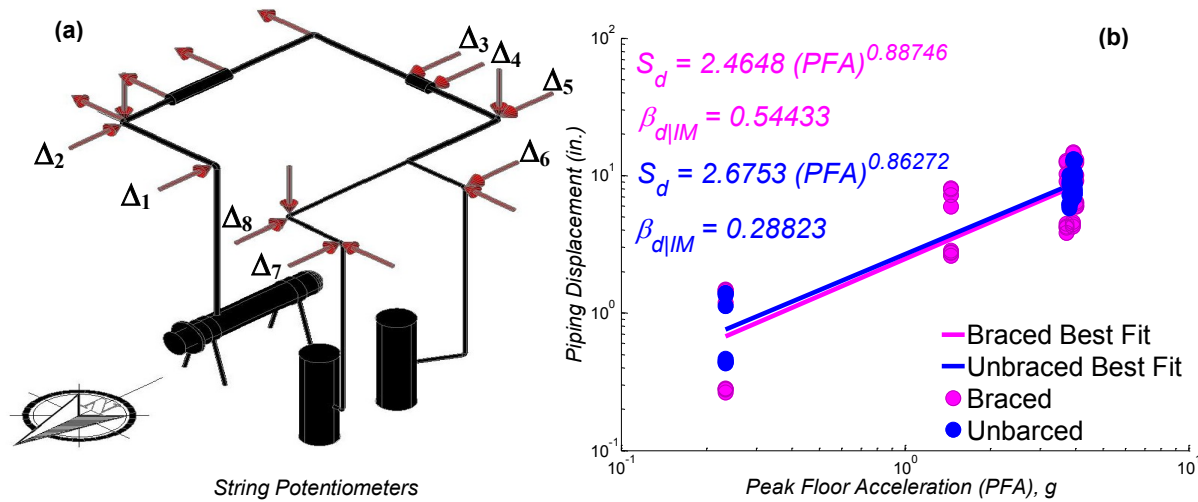


Figure 7-10 (a) String Potentiometers View (b) Displacement Demand of Piping System

7.3.2.2 Piping System at E-Defense Experiment

A detailed description of this experiment, instrumentation, and loading protocol is presented in Section 4.5. However, a summary of instruments used is presented here for convenience. Figure 7-11(a) shows the string pots that were placed on the main run pipe (near second branch line) to measure the movement of the piping system relative to the structure. Since two ends of the main run pipe were restrained by solid sway braces and assuming that the pipe is axially rigid, only the displacements in the perpendicular direction of the main run pipe were considered. Figure 7-11(b) also shows the displacement results from this study and the regression parameters.

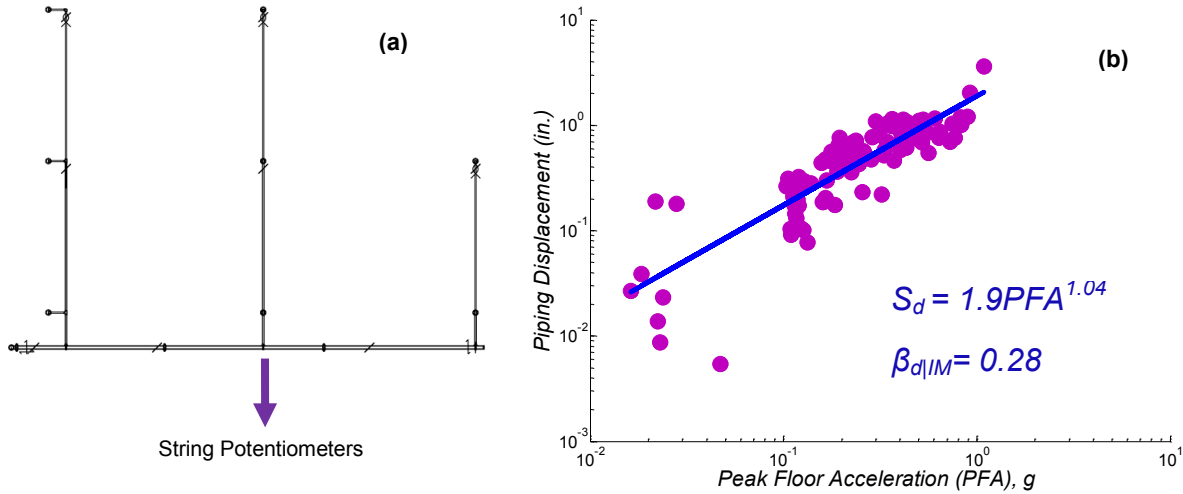


Figure 7-11 (a) String Potentiometers View (b) Displacement demand of piping system

7.3.2.3 UCSF Analytical Fire Sprinkler Piping System

A detailed description of this analytical model is presented in Section 5. A node displacement recorder was assigned to all of the joints (228 points) located at the main run pipes. These recorders were set only to measure the piping displacement in the perpendicular direction to the main run pipe run (horizontal only). The median displacement demands on grooved and threaded main runs are shown in Figure 7-12 versus peak floor acceleration along with regression curves and parameters.

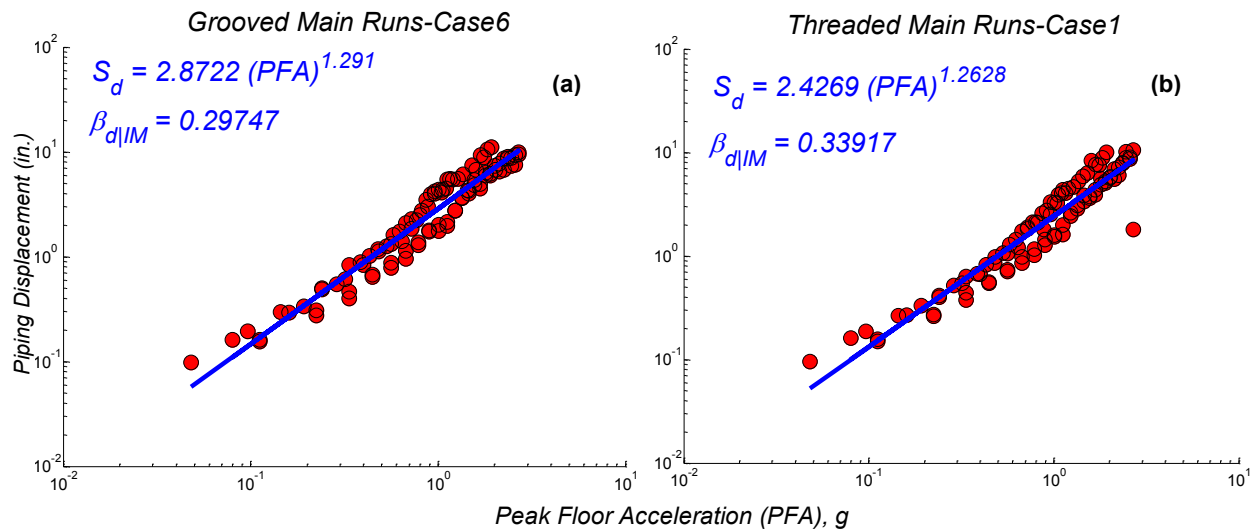


Figure 7-12 Displacement Demand of Piping System on (a) Grooved (b) Threaded on Main Run Pipe (Large Pipe Diameters)

7.3.3 Limit States

As mentioned before, according to Section 9.3.4 of NFPA 13 (NFPA, 2011), clearance shall be provided around all piping extending through walls, floor, platforms, and foundations. The most frequently used oversized diameters of holes around the pipes are 2 in. for 1 in to 3.5 in. diameter pipes and 4 in for larger pipes. Therefore, four limit states were defined herein to discuss the seismic response of piping interaction. These limit states (*LS*) were defined as 0.5 in., 1 in., 2 in., and 3 in. clearance, which correspond to "no gap", 2 in., 4 in., and 6 in. oversized hole configurations. The 0.5 in. clearance was chosen to study the possibility of piping interaction with the objects that have a minimum gap. The 3 in. clearance was used as the extreme gap scenario for main runs. These limit states were defined by θ_{int} (median clearance of piping interaction) and β_C (logarithmic standard deviation). The constant value 0.4 was assigned to β_C , which is the most frequently used parameter in nonstructural components.

7.3.4 Fragility Curves

In this section, fragility curves of piping displacements for large pipe diameters (larger/equal to 2 in.) were developed using equation (5-13). Table 7-3 shows the lognormal parameters (median and logarithmic standard deviation or dispersion) that characterized the piping displacement fragility from the regression analysis based on all five different piping systems. Figure 7-13 shows the fragility curves corresponded to the piping displacement for all different systems along with the median line and values of piping system fragilities with threaded and grooved fit main runs (case 1 and case 6 presented in Sections 5 and 6). These lines and values were borrowed from Table 6-1 and Table 6-8.

Table 7-3 Medians and Dispersion Values for Piping Displacement Fragilities for Large Pipe Diameters

Component Name	LS1	LS2	LS3	LS4	Dispersion
	Median PFA(g)	Median PFA(g)	Median PFA(g)	Median PFA(g)	
UNR-Braced	0.17	0.36	0.79	1.25	0.67
UNR-Unbraced	0.14	0.32	0.71	1.14	0.49
E-Defense	0.28	0.54	1.05	1.55	0.49
Analytical-Grooved	0.26	0.44	0.76	1.03	0.50
Analytical-Threaded	0.29	0.50	0.86	1.18	0.52

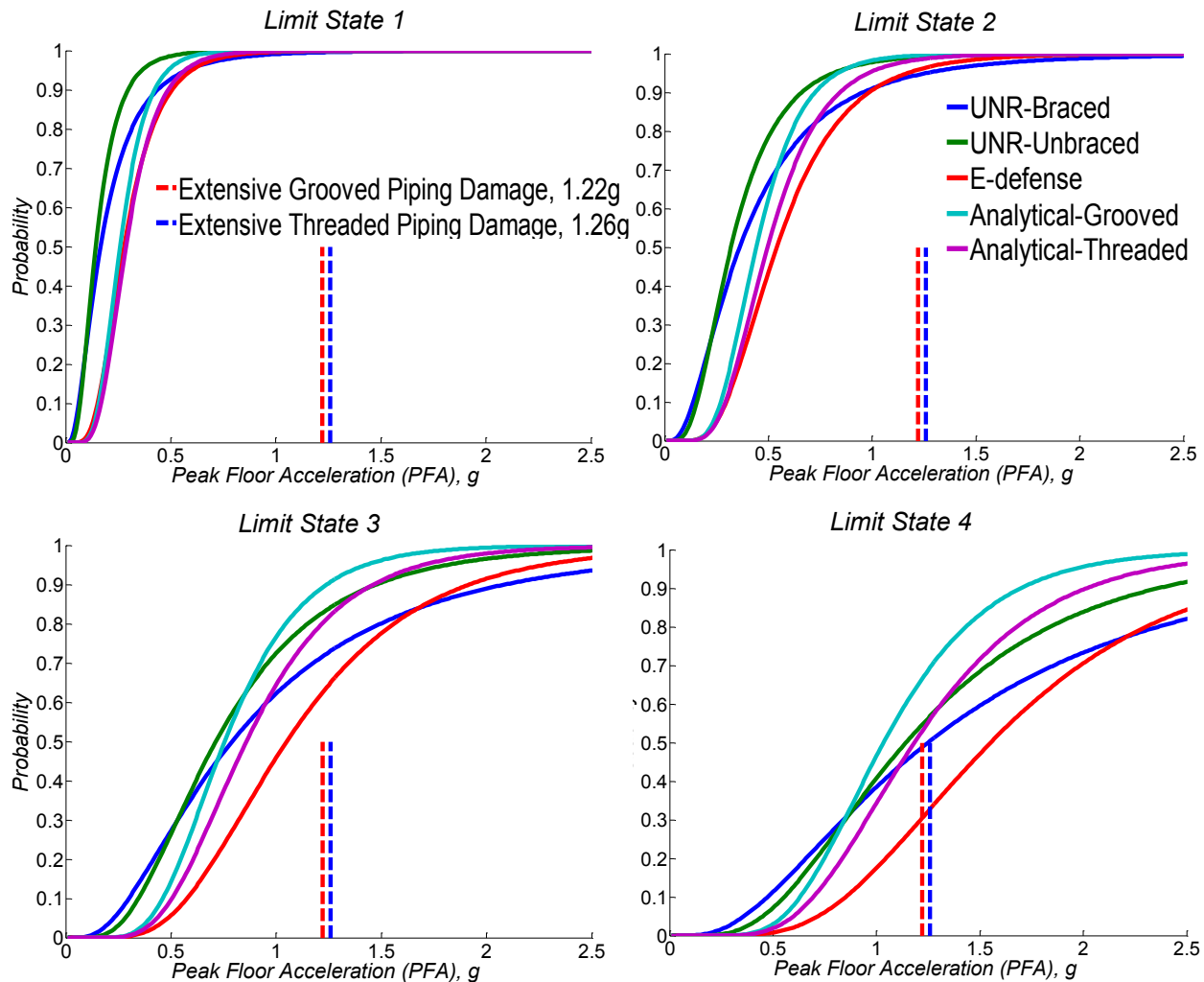


Figure 7-13 Piping Interaction Fragility Curves for Main Run Pipes (Large Pipe Diameters)

These four fragility curves imply:

- The values related to LS1 show that the objects closer than 0.5 inches collided with the piping system in excitations with very low intensities (median values less than 0.3g).
- By studying the median values of the UNR experiment, it can be concluded that removing braces from the piping system (UNR setup) increased the probability of reaching each limit state (median) by at least 10%.
- The piping system test at E-Defense was the least vulnerable piping among studied cases in terms of piping displacement. Since this system was a dry piping system (pipes were not filled with water), the displacement demand on this system is less than the others.

- The second least vulnerable piping system (in terms of piping displacements) in higher limit states was the UNR braced piping system. The displacement demand of this system is lower due to the smaller pipe dimensions and a closer brace spacing. Also, the applied motions in this experiment were uniaxial excitation.
- In almost all limit states (except LS1), the largest displacement corresponds to the analytical model with grooved fit connections. This system experienced more displacement compared to the threaded joint main runs because of lower initial stiffens in grooved fit joints.
- The components that were used in the E-Defense experiment were exactly the same as materials that were modeled in the analytical grooved piping system. However the E-Defense piping system was not filled with water, and also it was studied on a smaller scale. Due to these differences, the E-Defense piping system displacement demand was smaller than the analytical models.
- Based on the median values of extensive piping damage, a 3-inch clearance (6-inch oversized hole) from the pipe runs may prevent the collision of piping components until extensive damage to the piping system.

Another type of study is performed herein to compare the median values of different limit states for large pipe displacements and piping damages (see Figure 7-14). To do so, the median values of piping damage states corresponding to case 1 and case 6 presented in Section 6 (for “All” scenario) are divided by median values of piping displacement as:

$$Ratio = \frac{\lambda_{Pipe}}{\lambda_{Disp.}} \quad (7-3)$$

where λ_{Pipe} is the median value of the piping system for a specific damage state and $\lambda_{Disp.}$ is the median value of the piping displacement for a specific limit state. In Figure 7-14, the different piping damage state is differentiated by colors, while the piping displacement limit state is presented in each subplot. The displacement medians for each of the cases can be distinguished by the horizontal axes of the plots, while the dashed and solid lines differentiated the damage medians of systems with grooved and threaded main runs, respectively. Figure 7-14 shows that providing 1-inch clearance may coincide with the occurrence of slight damage in piping systems. However, providing 3-inch clearance (6-inch oversized hole) for the large diameter pipe runs

may mitigate the piping interaction until extensive damage (possibility of leakage) to the piping system occurs.

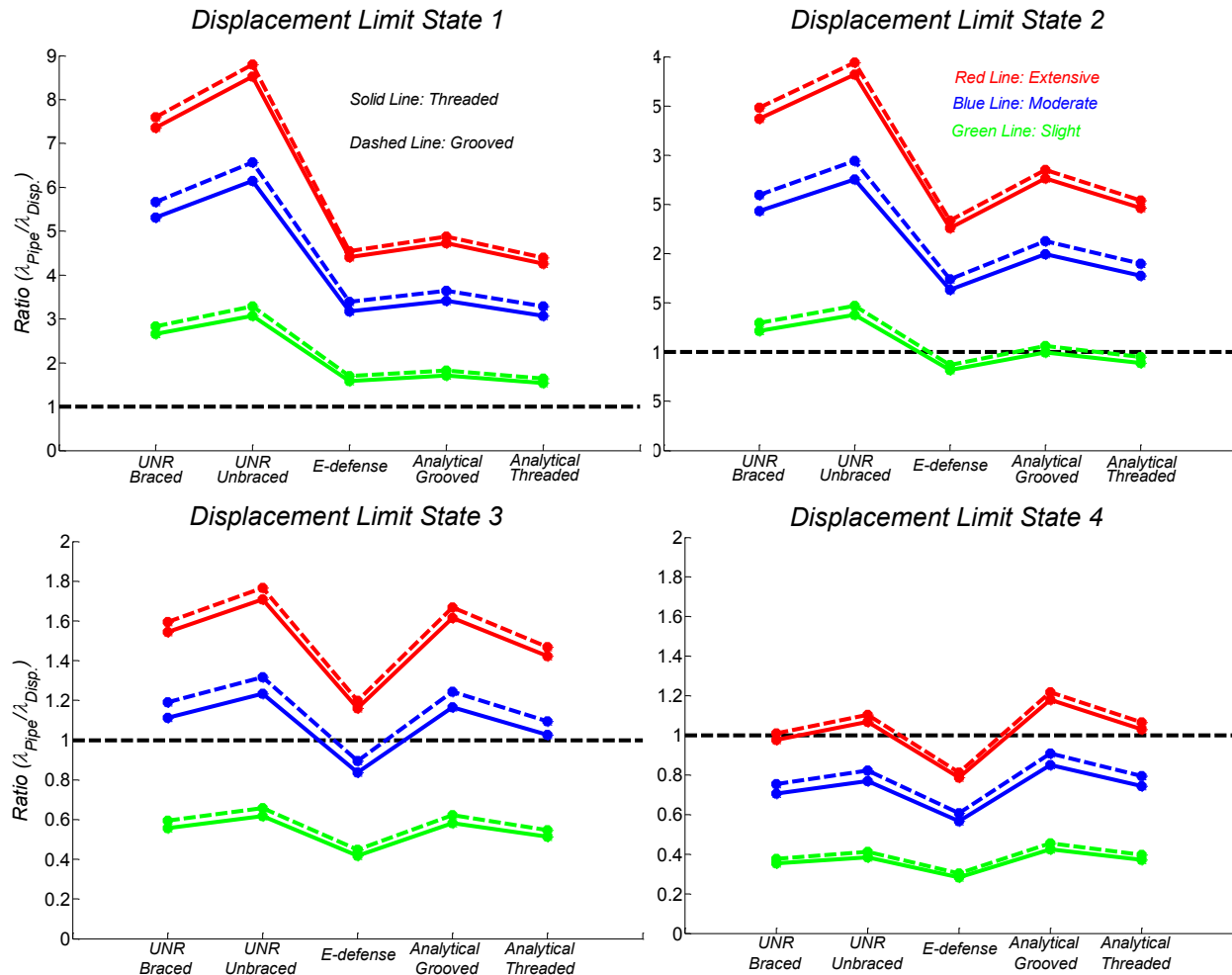


Figure 7-14 Comparison of Median Values for Piping System Damage and Displacement for Large Pipe Diameters

7.4 Displacement Demand on Small Pipe Diameters

One of the most common types of damage to fire sprinkler systems is breakage of sprinkler heads. Sprinkler heads can collide with ceiling systems, and this collision may result in damage to the ceiling system or water leakage in the piping system. Similar to what was mentioned before for large pipe diameters, excessive movement of horizontal pipes and interaction with their adjacent objects may result in damage to equipment or increase the probability of leakage on pipe runs (branch lines, armovers, and drops). Therefore, a realistic displacement assessment

of small pipe diameters can be one of the necessary steps for evaluating the seismic vulnerability of a fire sprinkler piping systems.

7.4.1 Code Requirements

According to Section 9.3.4 of NFPA 13 (NFPA, 2011), clearance shall be provided around all piping extending through walls, floors, platforms, and foundations. A summary of these requirements was presented in Section 7.3.1.

7.4.2 Displacement Demands

The displacement responses of two benchmark analytical models, which were presented in Sections 5 and 6 (case 1 and case 6), were used to establish the *EDPs* followed by the development of Probabilistic Seismic Demand Models (PSDMs) of piping displacements. A node displacement recorder was assigned for all of the sprinkler head representative joints (163 points) located at the branch line pipes. These recorders were set to measure the horizontal displacement of sprinkler heads in both horizontal directions. The median vector sum horizontal displacement demands on grooved and threaded main run systems is shown in Figure 7-15 versus peak floor acceleration along with regression curves and parameters.

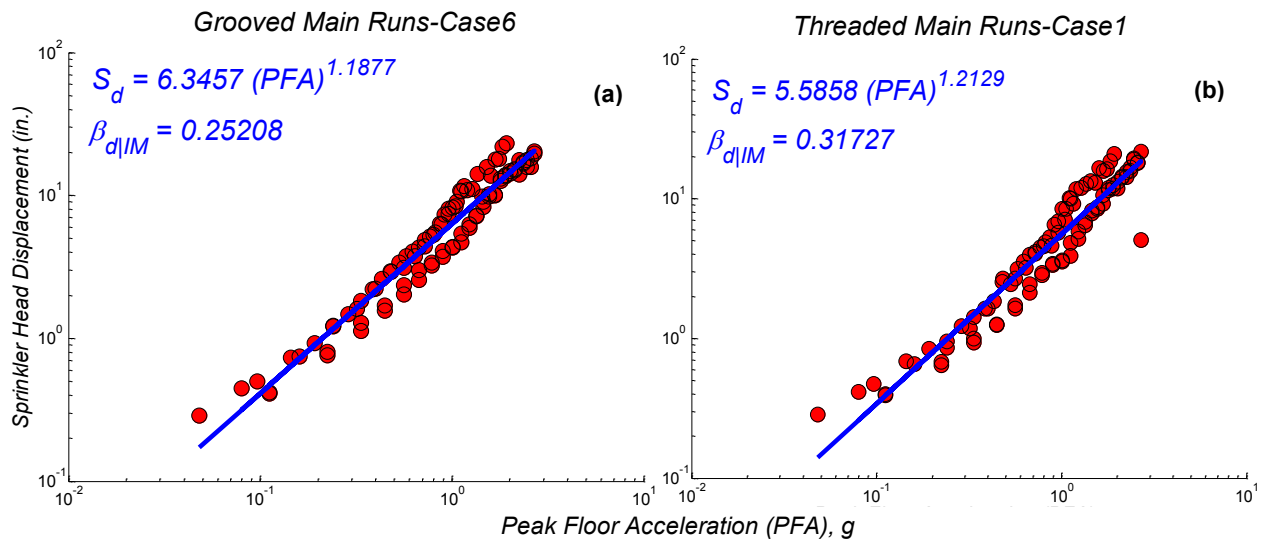


Figure 7-15 Displacement Demand of Sprinkler Heads in (a) Grooved (b) Threaded Systems

7.4.3 Limit States

According to Section 9.3.4 of NFPA 13 (NFPA, 2011), clearances should be provided around the pipes that pass through the holes. However, due to several architectural limitations (e.g. where sprinkler heads penetrate the ceiling panels), minimum gap (“no gap”) is commonly used in typical constructions. Except in these special cases, the most frequently used oversized diameter of holes around the pipes are 2 in. for 1 in. to 3.5 in. diameter pipes. Therefore, four limit states were defined herein to discuss the seismic response of piping interaction. These limit states (*LS*) were defined as 1 in., 2 in., 5 in., and 8 in. clearance, which correspond to 2 in, 4 in., 10 in, and 16 in. oversized hole configurations. The 1 in clearance was chosen to study the possibility of piping interaction with the objects (ceiling tiles) that have minimum gap. The 2 in clearance was used as a gap used for large pipe diameters. 5 in and 8 in clearances were used as two extreme cases for displacement interaction of small pipe diameters. These limit states were defined by θ_{int} (median clearance of piping interaction) and β_C (logarithmic standard deviation). The constant value 0.4 was assigned to β_C , which is the most frequent use of this parameter in nonstructural components.

7.4.4 Fragility Curves

In this section, the fragility curves of piping displacements for small pipe diameters (smaller than 2 in.) are developed using equation (5-13). Table 7-4 shows the lognormal parameters (median and logarithmic standard deviation or dispersion) that characterize the piping displacement fragility from regression analysis based on two different piping systems. Figure 7-16 shows the fragility curves corresponding to the piping displacement for all different systems along with the median line and values of piping system fragilities with threaded and grooved fit main runs (case 1 and case 6 presented in Sections 5 and 6). These lines and values were borrowed from the Table 6-1 and Table 6-8.

Table 7-4 Medians and Dispersion Values for Piping Displacement Fragilities for Small Pipe Diameters

Component Name	LS1	LS2	LS3	LS4	Dispersion
	Median PFA(g)	Median PFA(g)	Median PFA(g)	Median PFA(g)	
Analytical-Grooved	0.21	0.38	0.82	1.22	0.47
Analytical-Threaded	0.24	0.43	0.91	1.34	0.51

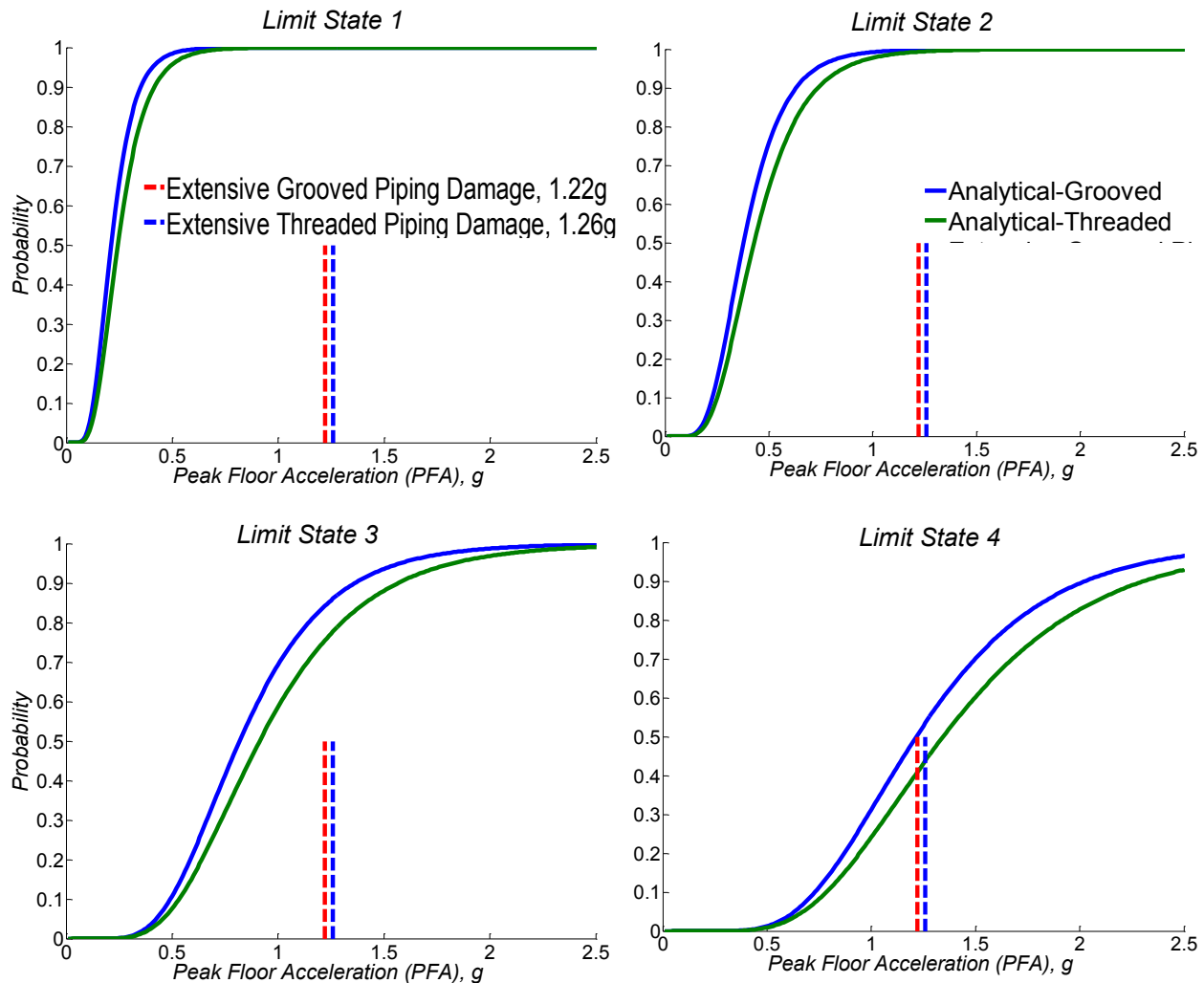


Figure 7-16 Piping Interaction Fragility Curves for Sprinkler Heads (Small Pipe Diameters)

These four fragility curves imply:

- In all of the limit states, the displacement (vulnerability) corresponding to the analytical model with grooved fitting main runs is higher than the model with threaded fitting main runs. This system observed more displacement compared to the threaded joint main runs because of lower initial stiffening of these joints.
- Based on median values of extensive piping damage, the 8-in. clearance (16 in. oversized hole) from the pipe runs may postpone the possibility of piping (small diameters) interaction until extensive damage of piping system. This large size of clearance (8 in.) may confirm that

using the flexible hose drops at the penetration location of sprinkler heads to ceiling systems can improve or eliminate the piping/ceiling system interactions.

Similar to the procedure presented in Section 7.3.4, the median values of different limit states for large pipe displacements and piping damages (see Figure 7-14) were compared with one another. To do so, the median values of piping damage states corresponded to case 1 and case 6 presented in Section 6 (for “All” scenario) are divided by the median values of piping displacement based on equation (7-3). In Figure 7-17, the different piping damage states are differentiated by colors, while piping displacement limit state is presented in each subplot. The displacement medians for

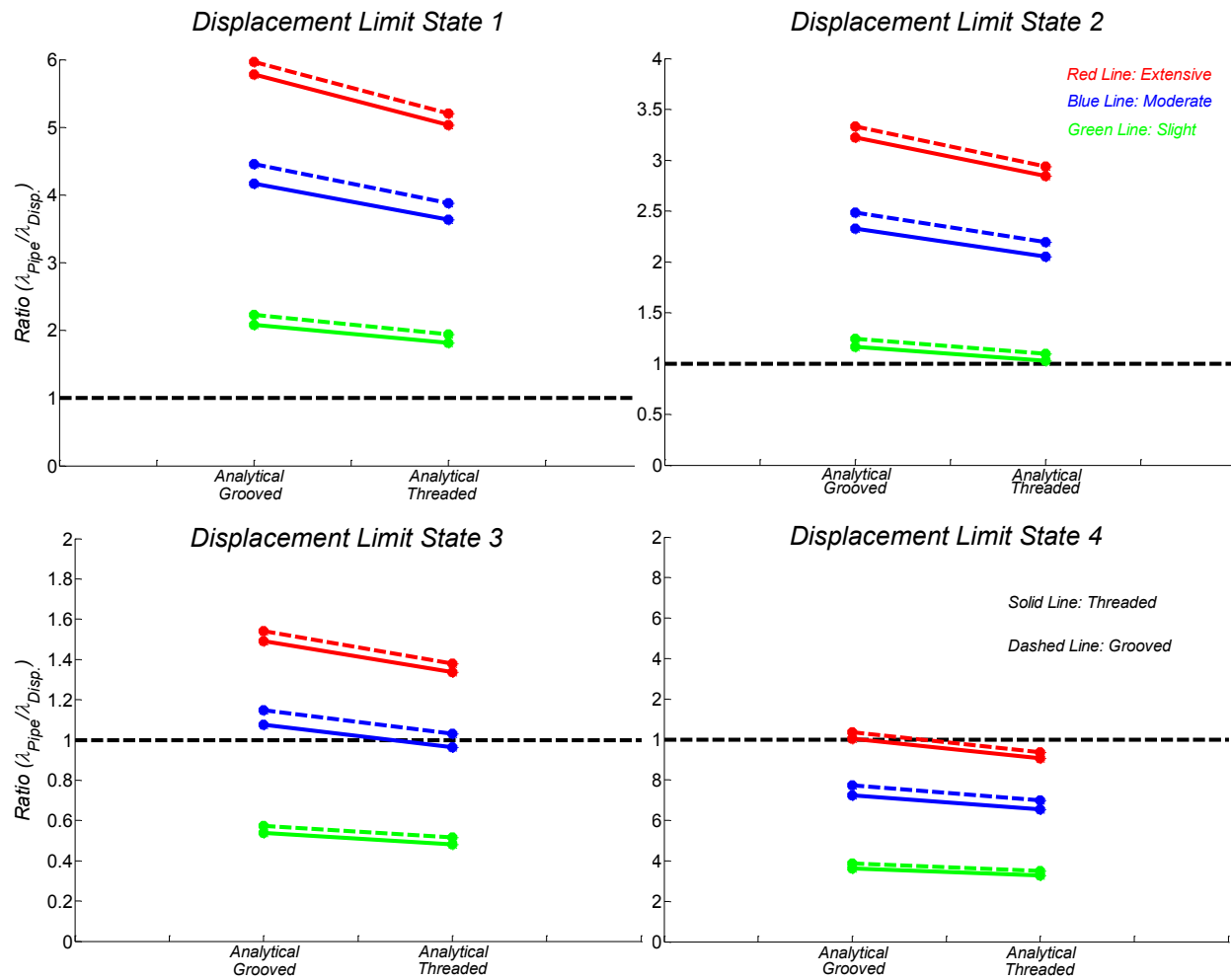


Figure 7-17 Comparison of Median Values for Piping System Damage and Displacement of Small Pipe Diameters

each case can be distinguished by the horizontal axes of the plots, while the dashed and solid lines differentiate the damage medians of systems with grooved and threaded main runs, respectively.

Figure 7-17 shows that, providing 2 in clearance may coincide with the occurrence of slight damage in piping systems. However, providing 8 in. clearance (16 in. oversized hole) from the small diameter pipes may postpone the piping interaction until the extensive damage (possibility of leakage) to the piping system.

7.5 Concluding Remarks

In this section, a simple approach was implemented to obtain pipe joint fragility curves based on interstory drift ratio from rotational capacities. These curves showed that in all pipe diameters, threaded joints are more vulnerable compared to grooved joints. Also, the curves demonstrated that using flexible couplings can improve the seismic performance of riser pipes either with grooved or threaded joints. Afterwards, the large pipe diameter (larger/equal to 2 inches) displacement fragility curves were developed for three experimental piping systems and two benchmark analytical models, which were presented in Sections 5 and 6 (case 1 and case 6). The results of these displacement fragility curves were compared with the piping damage states provided in previous sections. Comparisons between curves showed that providing 1 in. clearance may coincide with the occurrence of slight damage in piping systems. However, providing 3 in. clearance (6 in. oversized hole) from the large diameter pipe runs may postpone the piping interaction until the extensive damage (possibility of leakage) to the piping system occurs. Finally, small pipe diameter (smaller than 2 in.) displacement fragility curves were developed for two benchmark analytical models (case 1 and case 6). Similar to the procedure used for large pipe diameters, the results of these displacement fragility curves were compared with the piping damage states provided in previous sections. These comparisons showed that providing 2 in. clearance may coincide with the occurrence of slight damage in piping systems. However, providing 8 in. clearance (16 in. oversized hole) from the small diameter pipes may mitigate the piping interaction until the extensive damage (possibility of leakage) to the piping system occurs.

SECTION 8

SUMMARY AND CONCLUSIONS

8.1 Summary

Because they provide safety inside the building in case of fire, fire sprinkler piping systems are one of the most widely used nonstructural systems in the United States. Even though they are found in all critical facilities, limited studies have been conducted to evaluate the seismic vulnerability of fire sprinkler piping systems. The purpose of this study was to develop analytical fragility curves for fire sprinkler piping systems to be implemented in earthquake loss estimation tools.

The first task in this study was to develop analytical nonlinear threaded and grooved joint hinges for various pipe diameters based on previous component experiments. The OpenSees (2012) platform was used for modeling, analysis, comparison, and calibration of test data. Afterwards, for the simplicity of future analytical studies of sprinkler piping systems (not only limited to this study), one suite of material parameters was defined as the generic (representative) parameters for each pipe diameter, called the generic model. Furthermore, as the test matrix did not include all of the pipe diameters that are typically found in a system, a procedure is proposed to fill this gap in the experimental data and enable estimation of the parameters of the generic hysteresis model for the missing pipe diameters.

Element models were built for representing the pipe hangers, sway braces, wire restrainers, and pipe segments in Section 3. The developed analytical model for pipe hangers, cable braces, and wire restrainers was calibrated by experimental monotonic tensile data. In one case, the optimum analytical model was determined to reduce the time of analysis while still providing the required accuracy.

The previously developed piping components were verified and calibrated with several subsystem level experiments described in Section 4. The four experiments considered were: UNR hospital subassemblies with and without sliding frame; a two-story piping subsystem test at the University of Buffalo; and a two-story piping subsystem test at E-Defense shake table facilities. For each of these experiments, two models were built in SAP2000 (V15.0.1, 2011) and

OpenSees (2012) platform. The modeling technique of each of these experiments was presented using previously defined component level analytical models. The results of the analytical models were compared with the experimental acceleration, displacement, restrainer axial force, pipe hanger axial force, joint rotation, and spectral acceleration response data.

In Section 5, analytical component fragility curves of fire sprinkler piping systems were developed using a probabilistic seismic design model (PSDM). In general, the PSDMs are tools for generating fragility curves, which relates engineering demand parameters (EDP) to ground motion intensity measure (peak floor acceleration used in this study). A full fire sprinkler system layout incorporating a variety of common sprinkler piping systems was adopted from the University of California, San Francisco (UCSF) medical center building and was analytically simulated in OpenSees (2012) platform. Eight different design variables were considered for developing the UCSF piping plan. Two suites of floor motions with different design spectral accelerations at short period S_{DS} were artificially generated. A nonlinear response history analysis of the computational models of the pipings subjected to the floor motions with varying intensities was carried out next to record realistic component and piping system response. Fragility curves for various components for all different piping cases were developed. Afterwards, several comparisons were made between component fragilities of different piping systems considering only one variable (such as joint types, motion distribution, etc.) at a time.

The component fragility curves were combined to develop system fragility curves within Section 6. The statistical samples of demand and capacity for individual components with consideration of their correlation were produced using Monte Carlo simulation and were then utilized to develop system fragility curves. In this section, four different system level fragility curves were developed considering some of the components and their contribution toward system level fragility curves. Then, a simple approach was used to estimate the relative change in the median values of the fragility curves for all 10 piping cases.

A simple approach was implemented in Section 7 to obtain pipe joint fragility curves based on interstory drift ratio from rotational capacities. Afterwards, the large pipe diameter (larger/equal to 2 inches) displacement fragility curves of three experimental piping systems and two benchmark analytical models, which were presented in Sections 5 and 6 (case 1 and case 6),

were developed. The results of these displacement fragility curves were compared with the piping damage states provided earlier. Finally, small pipe diameter (smaller than 2in) displacement fragility curves of two benchmark analytical models (case 1 and case 6) were developed. Similar to the procedure used for large pipe diameters, the results of these displacement fragility curves were compared with the piping damage states.

8.2 Findings and Conclusions

An analytical model methodology was proposed in this study for fire sprinkler piping systems. This methodology was used for capturing the progression of damage in pipe joints as well as supporting elements such as braces, hangers, and restrainers. This modeling methodology can be applied to other types of piping systems such as plumbing and distribution pipe lines.

In Section 2, various pipe joint components (threaded and grooved) were modeled using the most up-to-date hysteretic models available in the OpenSees platform. Properties and the values assigned to the materials and elements were described in detail and calibrated with the experimental data. These descriptions were implemented into similar models to study the response of piping systems.

Different supporting elements (braces, hangers, restrainers) were modeled using different types of elements and materials through Section 3. Each of these materials and elements were described in detail and calibrated with the available experimental data.

The accuracy of component level analytical models, proposed in Section 2 and 3, was examined and validated in Section 4, within the subsystem or system level experiments.

In Section 5, fragility curves for various components for all different piping cases were developed. Some main conclusions were made and are listed below:

- The general trend in all cases shows that the response of tee-armovers is the most dominant component in the vulnerability of piping systems in nearly all damage states (except piping systems with cable bracing).
- The dominancy of larger diameter branch line pipes (1.5 in and 1.25 in) on overall vulnerability of piping system increases in higher damage states. In higher damage states,

the pipe hangers start to yield, and more wire restrainers fail. As a result, the branch lines behave like cantilevers, and the demand on these pipe diameters, which usually only have connections to the main runs, increases.

- The demand on the largest and smallest main runs (4 in and 2 in) is higher (except piping systems with cable bracing). The bending demand at these locations is generally higher than at other locations because these pipes are mainly located at the beginning and end of branch lines in addition to the existence of solid sway braces.
- Using bilinear and linear power law formulation for component demand estimation may result in maximum 0.4 differences in probability values.
- The median values of all components except the main run components were quite similar and slightly smaller (more vulnerable) in piping systems with grooved main runs. Due to the smaller initial stiffness in groove fitting connections, the main runs were more flexible compared to the threaded connections. As a result, the displacement amplitudes that are imposed on the branch lines were slightly higher. Therefore, the wire restrainer forces and rotational demand on the branch lines were slightly higher.
- Considering progressive damage during an earthquake, yielding occurs during the low intensity portion of the floor motion on joints close to solid braces (2 in and 4 in pipes in the studies system) with “Threaded” configuration. The presence of the generated hinges created during these lower intensities decreases the demand experienced by the rest of the main run joints at higher intensities. Technically, there is no yielding behavior in grooved fitting connections, and the stiffness of joints increased by increasing the rotational demand. Therefore, the rotational demand would not decrease on the rest of the main run joints during the larger intensity portion of the motion.
- The cable braces were found to be more vulnerable compared to the solid braces.
- In this study, variation on motion distributions resulted in maximum differences of 35% in median values of fragility curves.
- The rotational demand is less in the dry piping systems compared to the wet piping systems. The reduction in vulnerability is larger in piping systems with grooved main runs. In piping systems with threaded joints, the probability of leakage in threaded connections is very low; therefore, eliminating water weight may not improve the piping system within the range of possible peak floor acceleration (0-4g). However, in piping systems with grooved

connections, removing the water weight may significantly improve the seismic performance of the piping system.

- The rotational demand is less in the piping system with additional wire restrainers on armover pipes. However, as also stated in previous sections, armover joints are the most fragile component between the other pipe joints. Removing the wire restrainers clearly improved the behavior of these armover pipes.

The system fragility curves for all different piping cases were developed in Section 6. Some main conclusions were made and are listed below:

- In all piping systems and all cases (except with cable bracing), the piping systems with grooved main run connections are slightly more fragile. In the piping system with cable bracing, the piping system with threaded joints was found to be more fragile, which is not governed by joint rotation and only follows the percentage of bracing failure.
- Variation on motion distributions resulted in maximum differences of 20% in median values of system fragility curves, which was smaller than the maximum differences in component level (35%). In general, the motion suite with lognormal SDS distribution resulted in slightly more conservative results.
- In all piping systems, the system failure probability is less in the dry piping systems compared to the wet piping systems, and the piping seismic performance may be improved by 15%-35% in dry piping systems.
- In the piping systems with armovers, removing the wire restrainers improved the overall performance of the piping system. However, the differences in the piping systems without armovers was negligible.
- Piping systems with cable bracing were considerably weaker than piping systems that incorporated solid braces. However, this conclusion might be subjective as the cable braces never were removed during the response history analysis and also based on the way that their damage states were defined.

In Section 7, the displacement fragility curves for all different piping cases were developed. Some main conclusions were made and are listed below:

- In all pipe diameters, threaded joints were more vulnerable to interstory drift compared to grooved joint.
- Using flexible couplings can improve the performance of riser pipes either with grooved or threaded joints as many of the pipe joints may leak in low interstory drifts (1% drift).
- For large pipe diameters (larger/equal to 2 in.), providing a 1 in. clearance may coincide with the occurrence of slight damage in piping systems.
- Providing 3 in. clearance (6 in. oversized hole) from the large diameter pipe runs may postpone the piping interaction until the extensive damage (possibility of leakage) to the piping system. Finally, small pipe diameter (smaller than 2 in.) displacement fragility curves of two benchmark analytical models (case 1 and case 6), were developed. Similar to the procedure that was used for large pipe diameters, the results of these displacement fragility curves were compared with the piping damage states provided in previous sections.
- For small pipe diameters (smaller than 2 in.), providing 2 in. clearance may coincide with the occurrence of slight damage in piping systems.
- Providing 8 in. clearance (16 in. oversized hole) from the small diameter pipes may postpone the piping interaction until the extensive damage (possibility of leakage) to the piping system.

8.3 Future Work and Recommendations

In this section, a list of recommended future works is listed as follows:

- *Systematically developing input motions appropriate for developing nonstructural system fragility curves.* One of the critical steps in developing fragility curves is selecting suitable input motions. Although several studies have been done on generating and selecting ground motions, only a few works have been conducted on floor motions. Floor motion sets should cover a wide range of seismicity, structural systems, and structural height. Unless a comprehensive floor motion database is prepared, the results of nonstructural systems may deviate from their realistic responses. Due to unavailability of such a data base as of the date this report, a spectrum match procedure was used in this study.

- *Influence of material uncertainty on component and system fragility curves of fire sprinkler piping systems.* The material properties were obtained from the component tests that were presented in this report. However, these properties can change due to the inherent uncertainties in the production process. The type of material varies between different products. Therefore, using appropriate typology for considering these types of uncertainties may result in more accurate results.
- *Implementation of modeling methodology on other piping systems.* The modeling methodology presented in this report can be expanded to piping systems other than fire sprinklers such as plumbing and distribution pipe lines. The fragility curves developed in this study were based on a UCSF piping plan which has adequate numbers of each component. However, using different piping plans for generating piping fragility curves may result in more robust fragility curves.
- *Effect of interaction with structure or other nonstructural components.* Studies of the physical interaction of piping systems with the structures or other nonstructural systems can significantly change the damage observation and propagation in the piping system. Therefore, implementing interaction techniques into the piping system can be one of the critical future steps.
- *Effectiveness of vertical motion variation through the plane of piping system.* In this study, a uniform excitation was assigned to the all attachment points of piping system. Due to the flexibility of structural decks, the motions at the center of decks are usually amplified relative to column locations. Therefore, the vertical excitation of a piping system with multiple attach points can vary from one location to the other. So, defining systematic variation procedure for vertical input excitation can result in more realistic results for piping systems.

SECTION 9

REFERENCES

Almaraz , H. B., Whittaker A. S., and Reinhorn A. M. *Seismic Fragility of Suspended Ceiling Systems*, Earthquake Spectra 23, 21–40, 2007.

Antaki, G. *Seismic Capacity of Threaded, Brazed and Grooved Clamped Joints*, ASME 2004, PVP-Vol. 486-1, Seismic Engineering, 135-145, 2004.

Antaki, G. and Guzy, D. *Seismic Testing of Grooved and Threaded Fire Protection Joints and Correlation with NFPA Seismic Design Provisions*, ASME 1998, PVP-Vol. 364, Seismic Engineering-1998, 69-75, 1998.

Applied Technology Council (ATC-58 50% Draft). *Guidelines for Seismic Performance Assessment of Buildings*, Redwood City, California, 2009.

Applied Technology Council (ATC). *Earthquake Damage Evaluation Data for California*, Applied Technology Council Report ATC-13, 1985.

ASCE. *Minimum Design Loads for Buildings and Other Structures*, ASCE/SEI 7-10, American Society of Civil Engineers, Reston, Virginia, 2010.

ASME. *Rule for Construction of Nuclear Facility Components*, ASME Boiler and Pressure Vessel Code, Section III, American Society of Mechanical Engineers, 2004.

ASME. *Process Piping, B31.3*, American Society of Mechanical Engineers, New York, New York, 2008.

Astrella, M.J., and Whittaker, A.S. *The Performance-Based Design Paradigm*, Technical Report MCEER-05-0011, Multidisc. Ctr. for Earthq. Eng. Res., Buffalo, NY, 2005.

Ayres, J. Marx, Sun, T. Y., and Brown, F. R. “Nonstructural damage to buildings.” *The great Alaska earthquake of 1964: Engineering*, National Academy of Sciences, Washington, D.C., 1973.

Ayres, J. Marx, and Sun, T. Y. "Nonstructural damage." *The San Fernando, California Earthquake of February 9, 1971*, National Oceanic and Atmospheric Administration, Washington, D.C., 1973.

Baker, J. W., Cornell, A. C. *Vector-Valued Ground Motion Intensity Measures for Probabilistic Seismic Demand Analysis, Report No. PEER 2006/08*, Pacific Earthquake Engineering Research Center, University of California, Berkeley, CA, 2006.

Baker, S., Jangid, R., and Reddy, G. *Seismic Response of Piping Systems with Isolation Devices*, 13WCEE: 13th World Conference on Earthquake Engineering Conference Proceedings, 2004.

Basoz, N. and Kiremidjian, Anne, S. *Risk Assessment for Highway Transportation Systems*, Report No. NCEER-118, John A. Blume Earthquake Engineering Center, 1996.

Bommer, J.J, and Acevedo, A.B. *The Use of Real Earthquake Accelerograms as Input to Dynamic Analysis*, Journal of Earthquake Engineering, Vol. 8: Special Issue I, pp. 43-91, 2004.

Chiba, T., and R. Koyanagi. *Dynamic Response Studies of Piping Supports Systems*, American Society of Mechanical Engineering, Seismic Engineering, Vol. 364, 1998.

Choi, E. *Seismic Analysis and Retrofit of Mid-America Bridges*, PhD Dissertation, Georgia Institute of Technology, 2002.

Chopra, AK. Dynamics of structures, 3rd edition. Pearson Prentice Hall, New Jersey, 2007.

Chryssanthopoulos, M.K., Dymiotis , C., and Kappos, A.J. *Probabilistic Evaluation of Behaviour Factors in EC8-designed R/C Frame*, Engineering Structures, Vol. 22, pp. 1028-1041, 2000.

Comite Euro-international du Beton. *RC Elements Under Cyclic Loading*, State of the Art Report. Thomas Telford Publications, London, England, 1996.

Committee on the Alaska Earthquake of the Division of Earth Sciences National Research Council. *The Great Alaska Earthquake of 1964*. National Academy of Sciences, Washington, D.C, 1973.

Cornell, A.C., Jalayer, F., and Hamburger, R. O. *Probabilistic Basis for 2000 SAC Federal Emergency Management Agency Steel Moment Frame Guidelines*, Journal of Structural Engineering, Vol. 128, pp. 526–532, 2002.

Computers and Structures, Inc. *CSi Analysis Reference Manual*, Computers and Structures, Inc., (2009).

Dao, ND. *Seismic Response of a Full-scale Steel Frame Building Isolated with Triple Pendulum Bearings under 3D Excitation*, PhD Dissertation, University of Nevada, Reno, 2012.

FEMA 74 (Federal Emergency Management Agency). *Reducing the Risks of Nonstructural Earthquake Damage: A Practical Guide*, Redwood City, California, 2011.

FEMA (Federal Emergency Management Agency). *HAZUS-MH MR1: Technical Manual, Vol. Earthquake Model*, Federal Emergency Management Agency, Washington DC, 2003.

FEMA (Federal Emergency Management Agency), 2000. HAZUS 99 Estimated Annualized Earthquake Losses for the United States (FEMA 366). FEMA 366 only publishes the underlying study's aggregate loss figures. An analyst who conducted runs for FEMA for the study, Jawhar Bouabid of PBS & J, disaggregated the results into the structural and nonstructural figures cited here. (Bouabid, personal communication, January 2004). See also a study of estimated New York City annualized earthquake losses that found that 79% of the property damage was due to nonstructural and contents damage, 21% to structural damage. (Tantala et al., 2003).

Filiatrault, A., Mosqueda, G., Reinhorn, A., Pitman, M., Weinreber, S., and Retamales, R. *Nonstructural Component Simulator University at Buffalo Preliminary Report Seismic Performance Assessment of a Full-Scale Hospital Emergency Room*, UB-NCS Preliminary Results ER Tests, 2008.

Fire Sprinklers. *Fire Sprinklers Scotland*, Retrieved 6 February, 2013.

Fleming, R. P. *Analysis of Fire Sprinkler Systems Performance in the Northridge Earthquake*, National Institute of Standards and Technology, NIST-GCR-98-736, 1998.

Fujita, K., Kimura, T., and Ohe, Y. *Seismic Response Analysis of Piping Systems with Nonlinear Supports Using Differential Algebraic Equations*, Journal of Pressure Vessel Technology, American Society of Mechanical Engineers, New York, NY, Volume 126, Issue 1, pp. 91-97, 2004.

Gerdeen, J. C., Rodabaugh, E. C., and O'Donnell, W. JJ.. *A Critical Evaluation of Plastic Behavior Data and A Unified Definition of Plastic Loads for Pressure Components*, Welding Research Council Bulletin, Bulletin No. 254, 1979.

Goodwin, E., Maragakis, M., Itani, A., and Luo, S. *Experimental Evaluation of the Seismic Performance of Hospital Piping Subassemblies*, Report No. CCEER-05-5, Center for Civil Engineering Earthquake Research, Department of Civil Engineering, University of Nevada, Reno, NV, 2005.

Gupta, A., and Ju, B.S. *Review of Existing Literature on Real-life Failures, Seismic Design Guidelines, and Experimental Tests for Piping Systems in Buildings*. Report, Department of Civil, Construction & Environmental Engineering, North Carolina State University, Raleigh, NC, 30 p, 2011.

Hormozaki, E. A. *Analytical Fragility Curves for Horizontally Curved Steel Girder Highway Bridges*, Doctoral Dissertation, Department of Civil & Environmental Engineering, University of Nevada, Reno, 2013.

Huang NY., Whittaker AS., Kennedy RP., and Mayes RL. *Assessment of Base-Isolated Nuclear Structures for Design and Beyond-Design Basis Earthquake Shaking*, Tech. Report MCEER-09-0008, University at Buffalo, 2009.

Hwang, H., Jernigan, J. B., and Lin, Y. W. *Evaluation of Seismic Damage to Memphis Bridges and Highway Systems*. Journal of Bridge Engineering, Vol. 5, No. 4, pp. 322–330, 2000a.

Hwang, H., Liu, J. B., and Chiu, Y. H. *Seismic Fragility Analysis of Highway Bridges*, Technical Report No. MAEC RR-4, Mid-America Earthquake Center, Urbana, IL.

IBC. *International Building Code*, International Code Council, Inc., Falls Church, Virginia, 2012.

ICC Evaluation Service. *AC 156 Acceptance Criteria for Seismic Certification by Shake Table Testing of Nonstructural Components*, ICC Evaluation Service, 2010.

Industrial Fire Sprinklers. *Fire Safety Advice Centre*, Retrieved 6 February, 2013.

Jacob, K. H. *Seismic Hazards in the Eastern U.S. and the Impact on Transportation Lifelines*. Lifeline Earthquake Engineering in the Central and Eastern U.S., Monograph No. 5, ASCE, New York NY USA, 1992.

Jeong, S., and Elnashai, A.S. *Probabilistic fragility analysis parameterized by fundamental response quantities*, Engineering Structures, Vol. 29, pp. 1238–1251, 2007.

Ju, B.S. and Gupta, A. *Seismic Fragility of Piping System*, Doctoral Dissertation, Department of Civil & Environmental Engineering, North Carolina State University, Raleigh, NC, 2012.

Karim, K.R., and Yamazaki, F. *Effect of Earthquake Ground Motions on Fragility Curves of Highway Bridge Piers Based on Numerical Simulation*, Earthquake. Eng Struct. Dyn 30, 1839 – 1856, 2001.

Larson, L. D., Stokey, W. F., and Frangen, W. E. *An Approximate Model for an Elastic-Plastic Pipe Element Under Combined Loading*, ASME Journal OF Pressure Vessel Technology, pp. 22-28, February 1975.

Lin Lin, S., Elnashai, A. S., Spencer, B. F., Hashash Y. M. A., Fahnestock, L. A. *An Integrated Earthquake Impact Assessment System*, Mid-America Earthquake Center, Report No. 11-02, 2011.

Mackie, K., and Stojadinovic., B. *Fragility Basis for California Highway Overpass Bridge Seismic Decision Making*, PEER Center Research Report No. PEER 2005/12, June 2005, pp. 239, 2005.

Mander, J. B., and Basoz, N. *Seismic Fragility Curve Theory for Highway Bridges*, 5th US Conference on Lifeline Earthquake Engineering, Seattle, WA, USA. ASCE, 1999.

Maragakis, E. *NEESR-GC: Simulation of the Seismic Performance of Nonstructural Systems*. Proposal for NEESR-GC project funded by the US National Science Foundation, 2007.

Martinez, G. E. S., and Hodgson, I. C. *A Comparative Study of a Piping System Subjected to Earthquake Loads Using Finite Element Modeling and Analysis*. Proceeding of the 2007 Earthquake Engineering Symposium for Young Researchers, Seattle, WA, 2007.

Mason Industries. *Seismic Restraint Guidelines for Suspended Piping, Ductwork and Electrical System*, Smithtown, New York, 2009.

Masri, S. F., Caffrey, J. P., Myrtle, R., Nigbor, R., Agbabian, M., Johnson, E., Petak, W. Shinozuka, M., Tranquada, R., and Wellford, L. 2002. *Nonstructural Mitigation in Hospitals: the FEMA-USC Hospital Project*, Proceedings of the Seventh US National Conference on Earthquake Engineering, Boston, July, CD, 2002.

MathWorks. (2010). Matlab User Guide, The MathWorks, Inc.

Matzen, V. C., and Y. Tan. *Using Finite Element Analysis to Determine Piping Elbow Bending Moment (B2) Stress Indices*, Welding Research Council Bulletin, Bulletin No. 472, 2002.

Mazzoni, S., McKenna, F., Scott, M. H., and Fenves, G. L. *OpenSees Command Language Manual*, Berkeley, CA, 2007.

McGuire RK., Silva WJ., and Costantino CJ. *Technical Basis for Revision of Regulatory Guidance on Design Ground Motions: Hazard- and Risk-Consistent Ground Motion Spectra Guidelines*, NUREG/CR-6728, U.S. Nuclear Regulatory Commission, Washington, D.C, 2001.

Miranda, E. *Building Specific Loss Estimation for Performance Based Design*, Pacific Conference on Earthquake Engineering. University of Canterbury, Christchurch, New Zealand, 2003.

Miranda, E., and Taghavi, S. *Estimation of Seismic Demands on Acceleration- Sensitive Nonstructural Components in Critical Facilities*, Proceedings of Seminar on Seismic Design, Performance, and Retrofit of Nonstructural Components in Critical Facilities, ATC-29-2, Newport Beach, California, 2003.

Miranda, E., Mosqueda, G., Retamales, R., and Pekcan, G. *Performance of Nonstructural Components during the February 27, 2010 Chile Earthquake*, Earthquake Spectra 28, 453-471, 2012.

Mizutani, K., Kim, H., Kikuchihara, M., Nakai, T., Nishino, M., and Sunouchi, S. *The Damage of the Building Equipment under the 2011 Tohoku Pacific Earthquake*, 9th International Conference on Urban Earthquake Engineering & 4th Asia Conference on Earthquake Engineering, Tokyo Institute of Technology, Tokyo, Japan, 2012.

Mosqueda, G., Retamales, R., Filiault, A., and Reinhorn, A. M. *Testing Facility for Experimental Evaluation of Nonstructural Components under Full-scale Foor Motions*, Journal of Structural Design of Tall and Special Buildings, 18(4), 387–404, 2008.

Mukherjee, S., and Gupta, V. K. *Wavelet-Based Generation of Spectrum-Compatible Time-Histories*, Journal of Soil Dynamics and Earthquake Engineering, Elsevier, 22, 799–804, 2002.

Nakamura, I., Ogawa, N., Otani, A., and Shiratori, M.. *An Experimental Study of Dynamic Behavior of Piping Systems with Local Degradation*, American Society of Mechanical Engineering, Seismic Engineering, Vol. 402, No. 1, 2000.

Neuenhofer, A., and Filippou, FC. *Evaluation of Nonlinear Frame Finite-element Models*, Journal of Structural Engineering (ASCE); 123(7): 958-966, 1997.

NFPA13. *Standard for the Installation of Sprinkler Systems*. National Fire Protection Association, 2010 Edition, Quincy, MA, 2011.

Nielson, B. G. *Analytical Fragility Curves for Highway Bridges in Moderate Seismic Zones*, Ph.D. Dissertation. School of Civil and Environmental Engineering, Georgia Institute of Technology, Atlanta, 2005.

Nims, D. K. *Large Scale Experimental Studies of Two Alternate Support System for the Seismic Restraint of Piping*, PhD Dissertation, University of California, Berkeley, CA, 1991.

NRC. *The Great Alaska Earthquake of 1964*. National Research Council, National Academy of Sciences, Washington, D.C., 1973.

Open System for Earthquake Engineering Simulation (OpenSees) website, 2012.: <http://www.opensees.berkeley.edu> . PEER, Berkeley: University of California

PACT (Performance Assessment Calculation Tool). *ATC-58 Guidelines for Seismic Performance Assessment of Buildings*, Redwood City, California, 2012.

Pan, P., Zamfirescu, D., Nakashima, M., Nakayasu, N., and Kashiwa, H. *Base-isolation Design Practice in Japan: Introduction to the Post-Kobe Approach*. Journal of Earthquake Engineering; 9(1): 147-171, 2005.

Porter, K., Kennedy, R., and Bachman, R. *Creating Fragility Functions for Performance-based Earthquake Engineering*, Earthquake Spectra, 23(2): 471-489, 2007.

Ramanathan, K. N. *Next Generation Seismic Fragility Curves for California Bridges Incorporating the Evolution in Seismic Design Philosophy*, Doctoral Dissertation, School of Civil & Environmental Engineering, Georgia Institute of Technology, Atlanta, 2012.

Reinhorn, A.M., Barron-Corvera, R., and Ayala, A.G. *Spectral Evaluation of Seismic Fragility of Structures*, Proceedings ICOSSAR 2001, Newport Beach CA, 2001.

Retamales, R., Mosqueda, G., Filiatrault, A., and Reinhorn, A.M. *New Experimental Capabilities and Loading Protocols for Seismic Qualification and Fragility Assessment of Nonstructural Components*, Technical Report MCEER-08-0026, MCEER, State University of New York at Buffalo, New York, 2008.

Retamales, R., Mosqueda, G., Filiatrault, A., and Reinhorn, A.M. *Testing Protocol for Experimental Seismic Qualification of Distributed Nonstructural Systems*, Earthquake Spectra, 27(3):835-856, 2011.

Rodabaugh, E. C., and S. E. Moore. *Evaluation of the Plastic Characteristics of Piping Products in Relation to ASME Code Criteria*, USNRC NUREG Report No. NUREG/CR-0261, July, 1978.

Rossetto, T., and Elnashai, A. *Derivation of Vulnerability Functions for European-type RC Structures Based on Observational Data*, Engineering Structures, 25(10):1241-1263, 2003.

Ryan, K. L., Coria, C. B., and Dao, N. D. *Full Scale Earthquake Simulation of a Hybrid Lead Rubber Isolation System Designed for a Nuclear Facility*. United States Nuclear Regulatory Commission (U.S. NRC) Report, “Under Review,” Washington, DC, 2012.

SAP2000. (V15.0.1, 2011), CSI Computer & Structures Inc. *Linear and Nonlinear Static and Dynamic Analysis of Three-dimensional Structures*. Berkeley (CA): Computer & Structures, Inc.

Sato, Y., Motoyui, S., MacRae, G.A., and Dhakal, R.P. *Ceiling Fragility of Japanese Ceiling Systems*, Proceedings of the Ninth Pacific Conference on Earthquake Engineering Building an Earthquake-Resilient Society, Auckland, New Zealand1, 4-16 April, 2011.

Schultz, M., Gouldby, B., Simm, J., and Wibowo, J. *Beyond the Factor of Safety: Developing Fragility Curves to Characterize System Reliability*, ERDC SR-10-1. G. a. S. Laboratory, USACE, 2010.

Semke, W. H., Bibel, G. D., Jerath, S., Gurav, B. S., and Webster, A. L. *Efficient Dynamic Structural Response Modeling OF Bolted Flange Piping Systems*, International Journal of Pressure Vessels and Piping, Volume 83, Issue 10, 767-776, October 2006.

Shimizu, N., and Hanawa, Y. *Seismic Experiment of Piping Systems Simultaneously Subjected to Shake Table Excitation and Actuator Input*, American Society of Mechanical Engineering, Seismic Engineering, Vol. 364, 1998.

Shinozuka, M., Feng, M.Q., Lee, J., and Naganuma, T. *Statistical Analysis of Fragility Curves*, Journal of Engineering Mechanics, Vol. 126, pp. 1224–1231, 2000.

SMACNA. *Seismic Restraint Manual Guidelines for Mechanical Systems*, Sheet Metal and Air Conditioning Contractors’ National Association, Inc., 2003.

Soroushian, S., Maragakis, M., Ryan, K., Sato, E., Sasaki, T., Okazaki, T., Tedesco, L., Zaghi, E., Mosqueda, G., Alvarez, D. *Seismic response of ceiling/sprinkler piping nonstructural systems in NEES TIPS/NEES nonstructural/NIED collaborative tests on a full scale 5-story building*, Proceeding of 43rd Structures Congress, ASCE, Chicago, IL, 2012.

Sorourshian, S., Zaghi, A. E., Wieser, J., Maragakis, E. M., Pekcan, G., and Itani, M. *Seismic Analysis of Fire Sprinkler Systems*, Eighth International Conference on Structural Dynamics EURODYN 2011, Leuven, Belgium, 2011.

Tian, Y. *Experimental Seismic Study of Pressurized Fire Suppression Sprinkler Piping System*, Doctoral Dissertation, Department of Civil & Environmental Engineering, State University of New York at Buffalo, Buffalo, NY, 2012.

Tian, Y., Filiatrault, A., and Mosqueda, G. *Experimental Seismic Fragility of Pressurized Fire Suppression Sprinkler Piping Joints*, Earthquake Spectra, In press, 2012.

USG Corporation. (2006). Seismic Ceiling Resources Center. <http://www.usg.com/rc/technical-articles/seismic-technical-guide-hanger-wire-attachment-en-SC2522.pdf>.

VanMarcke, Dario, Gasparini, A., and Eric, H. *SIMQKE User's Manual and Documentation*, National Science Foundation. 1976.

Wais, E. A. *Recent Changes to ASME Section III Welded Attachments (Lugs) Code Cases*, PVP-Vol.313-2, International Pressure Vessels and Piping Codes and Standard: Vol. 2-Current Perspectives, ASME, pp. 29-31, 1995.

Wanitkorkul, A., Filiatrault, A. *Simulation of strong ground motions for seismic fragility evaluation of nonstructural components in hospitals*, Technical Report MCEER-05-0005, MCEER, State University of New York at Buffalo, NY, 2005.

Whittaker, A.S., and Soong, T.T. *An Overview of Nonstructural Component Research at Three U.S. Earthquake Engineering Research Centers*, in Proceedings of Seminar on Seismic Design, Performance, and Retrofit of Nonstructural Components in Critical Facilities, Applied Technology Council, ATC-29-2, pp. 271-280, Redwood City, California, 2003.

Wormald, John (December, 1923). *History Automatic Fire Sprinklers*. Olyfire.com. Retrieved 8 February, 2013.

Zaghi, A. E., Maragakis, E. M., Itani, A., and Goodwin, E. *Experimental and Analytical Studies of Hospital Piping Subassemblies Subjected to Seismic Loading*, Earthquake Spectra 26,367–384, 2012.

Zhang, J., and Huo, Y. *Optimum Isolation Design for Highway Bridges Using Fragility Function Method*, Proceedings of 14th World Conference on Earthquake Engineering, Beijing, China, 2008.

Appendix A

HANGING, BRACING, AND RESTRAINT OF SYSTEM PIPING

NFPA 13 was used as the design standard for the fire sprinkler systems in this study. A section of this standard is presented in this appendix, which is related to the requirements for the supporting elements of fire sprinkler piping systems.

8.17.4.6.2 Retroactive Installation. When backflow prevention devices are to be retroactively installed on existing systems, a thorough hydraulic analysis, including revised hydraulic calculations, new fire flow data, and all necessary system modifications to accommodate the additional friction loss, shall be completed as a part of the installation.

8.17.5 Hose Connections.

8.17.5.1 Small [1½ in. (38 mm)] Hose Connections. See Section C.5.

8.17.5.1.1* Where required, small [1½ in. (38 mm)] hose connections shall be installed. Valves shall be available to reach all portions of the area with 100 ft (30.5 m) of hose plus 30 ft (9.1 m) of hose stream distance.

8.17.5.1.1.1 Where the building is protected throughout by an approved automatic sprinkler system, the presence of 1½ in. (38 mm) hose lines for use by the building occupants shall not be required, subject to the approval of the authority having jurisdiction.

8.17.5.1.2 The hose connections shall not be required to meet the requirements of Class II hose systems defined by NFPA 14, *Standard for the Installation of Standpipe and Hose Systems*.

8.17.5.1.3 Hose connections shall be supplied from one of the following:

- (1) Outside hydrants
- (2) A separate piping system for small hose connections
- (3) Valved hose connections on sprinkler risers where such connections are made upstream of all sprinkler control valves
- (4) Adjacent sprinkler systems
- (5) In rack storage areas, the ceiling sprinkler system in the same area (as long as in-rack sprinklers are provided in the same area and are separately controlled)

8.17.5.1.4* Hose connections used for fire purposes only shall be permitted to be connected to wet pipe sprinkler systems only, subject to the following restrictions:

- (1) Hose connection's supply pipes shall not be connected to any pipe smaller than 2½ in. (65 mm) in diameter.
- (2) The requirements of 8.17.5.1.4(1) shall not apply to hydraulically designed loops and grids, where the minimum size pipe between the hose connection's supply pipe and the source shall be permitted to be 2 in. (51 mm).
- (3) For piping serving a single hose connection, pipe shall be a minimum of 1 in. (25.4 mm) for horizontal runs up to 20 ft (6.1 m), a minimum of 1½ in. (38 mm) for the entire run for runs between 20 ft and 80 ft (6.1 m and 24.4 m), and a minimum of 1½ in. (38 mm) for the entire run for runs greater than 80 ft (24.4 m). For piping serving multiple hose connections, runs shall be a minimum of 1½ in. (38 mm) throughout.
- (4) Piping shall be at least 1 in. (25 mm) for vertical runs.
- (5) Where the residual pressure at a 1½ in. (38 mm) outlet on a hose connection exceeds 100 psi (6.9 bar), an approved pressure-regulating device shall be provided to limit the residual pressure at the outlet to 100 psi (6.9 bar).
- (6) Where the static pressure at a 1½ in. (38 mm) hose connection exceeds 175 psi (12.1 bar), an approved pressure-regulating device shall be provided to limit static and residual pressures at the outlet to 100 psi (6.9 bar).

8.17.5.2 Hose Connections for Fire Department Use.

8.17.5.2.1 In buildings of light or ordinary hazard occupancy, 2½ in. (64 mm) hose valves for fire department use shall be permitted to be attached to wet pipe sprinkler system risers.

8.17.5.2.2* The following restrictions shall apply:

- (1) Each connection from a standpipe that is part of a combined system to a sprinkler system shall have an individual control valve and check valve of the same size as the connection.
- (2) The minimum size of the riser shall be 4 in. (102 mm) unless hydraulic calculations indicate that a smaller size riser will satisfy sprinkler and hose stream allowances.
- (3) Each combined sprinkler and standpipe riser shall be equipped with a riser control valve to permit isolating a riser without interrupting the supply to other risers from the same source of supply. (For fire department connections serving standpipe and sprinkler systems, refer to Section 6.8.)

Chapter 9 Hanging, Bracing, and Restraint of System Piping

9.1 Hangers.

9.1.1* General.

9.1.1.1 Unless the requirements of 9.1.1.2 are met, types of hangers shall be in accordance with the requirements of Section 9.1.

9.1.1.2 Hangers certified by a registered professional engineer to include all of the following shall be an acceptable alternative to the requirements of Section 9.1:

- (1) Hangers shall be designed to support five times the weight of the water-filled pipe plus 250 lb (114 kg) at each point of piping support.
- (2) These points of support shall be adequate to support the system.
- (3) The spacing between hangers shall not exceed the value given for the type of pipe as indicated in Table 9.2.2.1(a) or Table 9.2.2.1(b).
- (4) Hanger components shall be ferrous.
- (5) Detailed calculations shall be submitted, when required by the reviewing authority, showing stresses developed in hangers, piping, and fittings and safety factors allowed.

9.1.1.3 Where water-based fire protection systems are required to be protected against damage from earthquakes, hangers shall also meet the requirements of 9.3.7.

9.1.1.4 Listing.

9.1.1.4.1 Unless permitted by 9.1.1.4.2 or 9.1.1.4.3, the components of hanger assemblies that directly attach to the pipe or to the building structure shall be listed.

9.1.1.4.2* Mild steel hangers formed from rods shall be permitted to be not listed.

9.1.1.4.3* Fasteners as specified in 9.1.3, 9.1.4, and 9.1.5 shall be permitted to be not listed.

9.1.1.4.4 Other fasteners shall be permitted as part of a hanger assembly that has been tested, listed, and installed in accordance with the listing requirements.

9.1.1.5 Component Material.

9.1.1.5.1 Unless permitted by 9.1.1.5.2 or 9.1.1.5.3, hangers and their components shall be ferrous.

9.1.1.5.2 Nonferrous components that have been proven by fire tests to be adequate for the hazard application, that are listed for this purpose, and that are in compliance with the other requirements of this section shall be acceptable.

9.1.1.5.3 Holes through solid structural members shall be permitted to serve as hangers for the support of system piping provided such holes are permitted by applicable building codes and the spacing and support provisions for hangers of this standard are satisfied.

9.1.1.6* Trapeze Hangers.

9.1.1.6.1 For trapeze hangers, the minimum size of steel angle or pipe span between purlins or joists shall be such that the section modulus required in Table 9.1.1.6.1(a) does not

exceed the available section modulus of the trapeze member from Table 9.1.1.6.1(b).

9.1.1.6.2 Any other sizes or shapes giving equal or greater section modulus shall be acceptable.

9.1.1.6.3 All angles shall be installed with the longer leg vertical.

9.1.1.6.4 The trapeze member shall be secured to prevent slippage.

9.1.1.6.5* All components of each hanger assembly that attach to a trapeze member shall conform to 9.1.1.4 and be sized to support the suspended sprinkler pipe.

9.1.1.6.6 The ring, strap, or clevis installed on a pipe trapeze shall be manufactured to fit the pipe size of the trapeze member.

9.1.1.6.7 Holes for bolts shall not exceed $\frac{1}{16}$ in. (1.6 mm) greater than the diameter of the bolt.

9.1.1.6.8 Bolts shall be provided with a flat washer and nut.

Table 9.1.1.6.1(a) Section Modulus Required for Trapeze Members (in.³)

Span of Trapeze	Nominal Diameter of Pipe Being Supported											
	1 in. 25 mm	1 1/4 in. 32 mm	1 1/2 in. 40 mm	2 in. 50 mm	2 1/2 in. 65 mm	3 in. 80 mm	3 1/2 in. 90 mm	4 in. 100 mm	5 in. 125 mm	6 in. 150 mm	8 in. 200 mm	10 in. 250 mm
1 ft 6 in. (0.46 m)	0.08 0.08	0.09 0.09	0.09 0.09	0.09 0.10	0.10 0.11	0.11 0.12	0.12 0.13	0.13 0.15	0.15 0.18	0.18 0.22	0.24 0.30	0.32 0.41
2 ft 0 in. (0.61 m)	0.11 0.11	0.12 0.12	0.12 0.12	0.13 0.13	0.13 0.15	0.15 0.16	0.16 0.18	0.17 0.20	0.20 0.24	0.24 0.29	0.32 0.40	0.43 0.55
2 ft 6 in. (0.76 m)	0.14 0.14	0.14 0.15	0.15 0.15	0.16 0.16	0.17 0.18	0.18 0.21	0.20 0.22	0.21 0.25	0.25 0.30	0.30 0.36	0.40 0.50	0.54 0.68
3 ft 0 in. (0.91 m)	0.17 0.17	0.17 0.18	0.18 0.18	0.19 0.20	0.20 0.22	0.22 0.25	0.24 0.27	0.26 0.30	0.31 0.36	0.36 0.43	0.48 0.60	0.65 0.82
4 ft 0 in. (1.2 m)	0.22 0.22	0.23 0.24	0.24 0.24	0.25 0.26	0.27 0.29	0.29 0.33	0.32 0.36	0.34 0.40	0.41 0.48	0.48 0.58	0.64 0.80	0.87 1.09
5 ft 0 in. (1.5 m)	0.28 0.28	0.29 0.29	0.30 0.30	0.31 0.33	0.34 0.37	0.37 0.41	0.40 0.45	0.43 0.49	0.51 0.60	0.59 0.72	0.80 1.00	1.08 1.37
6 ft 0 in. (1.8 m)	0.33 0.34	0.35 0.35	0.36 0.36	0.38 0.39	0.41 0.44	0.44 0.49	0.48 0.54	0.51 0.59	0.61 0.72	0.71 0.87	0.97 1.20	1.30 1.64
7 ft 0 in. (2.1 m)	0.39 0.39	0.40 0.41	0.41 0.43	0.44 0.46	0.47 0.51	0.52 0.58	0.55 0.63	0.60 0.69	0.71 0.84	0.83 1.01	1.13 1.41	1.52 1.92
8 ft 0 in. (2.4 m)	0.44 0.45	0.46 0.47	0.47 0.49	0.50 0.52	0.54 0.59	0.59 0.66	0.63 0.72	0.68 0.79	0.81 0.96	0.95 1.16	1.29 1.61	1.73 2.19
9 ft 0 in. (2.7 m)	0.50 0.50	0.52 0.53	0.53 0.55	0.56 0.59	0.61 0.66	0.66 0.74	0.71 0.81	0.77 0.89	0.92 1.08	1.07 1.30	1.45 1.81	1.95 2.46
10 ft 0 in. (3.0 m)	0.56 0.56	0.58 0.59	0.59 0.61	0.63 0.65	0.68 0.74	0.74 0.82	0.79 0.90	0.85 0.99	1.02 1.20	1.19 1.44	1.61 2.01	2.17 2.74

For SI units, 1 in. = 25.4 mm; 1 ft = 0.3048 m.

Notes:

(1) Top values are for Schedule 10 pipe; bottom values are for Schedule 40 pipe.

(2) The table is based on a maximum allowable bending stress of 15 ksi and a midspan concentrated load from 15 ft (4.6 m) of water-filled pipe, plus 250 lb (114 kg).

Table 9.1.1.6.1(b) Available Section Modulus of Common Trapeze Hangers (in.³)

Pipe	Modulus	Angles (in.)	Modulus (in. ³)
in.	(in. ³)	in.	
Schedule 10			
1	25	0.12	1½ × 1½ × 3/16
1½	32	0.19	2 × 2 × 1/8
1½	40	0.26	2 × 1½ × 3/16
2	50	0.42	2 × 2 × 3/16
2½	65	0.69	2 × 2 × 1/4
3	80	1.04	2½ × 1½ × 3/16
3½	90	1.38	2½ × 2 × 3/16
4	100	1.76	2 × 2 × 5/16
5	125	3.03	2½ × 2½ × 3/16
6	150	4.35	2 × 2 × 3/8
			2½ × 2½ × 1/4
			3 × 2 × 3/16
Schedule 40			
1	25	0.13	3 × 2½ × 3/16
1½	32	0.23	3 × 3 × 3/16
1½	40	0.33	2½ × 2½ × 3/16
2	50	0.56	3 × 2 × 1/4
2½	65	1.06	2½ × 2 × 3/8
3	80	1.72	2½ × 2½ × 3/8
3½	90	2.39	3 × 3 × 1/4
4	100	3.21	3 × 3 × 3/16
5	125	5.45	2½ × 2½ × 1/2
6	150	8.50	3½ × 2½ × 1/4
			3 × 2½ × 3/8
			3 × 3 × 3/8
			3½ × 2½ × 3/16
			3 × 3 × 5/16
			4 × 4 × 1/4
			3 × 3 × 1/2
			4 × 3 × 3/16
			4 × 4 × 5/16
			4 × 3 × 3/8
			4 × 4 × 3/8
			5 × 3½ × 3/16
			4 × 4 × 1/2
			4 × 4 × 3/8
			4 × 4 × 1/4
			6 × 4 × 3/8
			6 × 4 × 1/2
			6 × 4 × 3/4
			6 × 6 × 1

For SI units, 1 in. = 25.4 mm; 1 ft = 0.3048 m.

9.1.1.7* **Support of Non-System Components.** Sprinkler piping or hangers shall not be used to support non-system components.

9.1.2 Hanger Rods.

9.1.2.1 Unless the requirements of 9.1.2.2 are met, hanger rod size shall be the same as that approved for use with the hanger assembly, and the size of rods shall not be less than that given in Table 9.1.2.1.

9.1.2.2 Rods of smaller diameters than indicated in Table 9.1.2.1 shall be permitted where the hanger assembly

Table 9.1.2.1 Hanger Rod Sizes

Pipe Size			
in.	mm	in.	mm
Up to and including 4	100	5/8	9.5
5	125	1/2	12.7
6	150		
8	200		
10	250	5/8	15.9
12	300		

has been tested and listed by a testing laboratory and installed within the limits of pipe sizes expressed in individual listings.

9.1.2.3 Where the pitch of the branch line is 6 in 12 or greater, a reduction in the lateral loading on branch line hanger rods shall be done by one of the following:

- (1) A second hanger installed in addition to the required main hangers
- (2) Lateral sway brace assemblies on the mains
- (3) Branch line hangers utilizing an articulating structural attachment
- (4) Equivalent means providing support to the branch line hanger rods

9.1.2.4 U-Hooks. The size of the rod material of U-hooks shall not be less than that given in Table 9.1.2.4.

Table 9.1.2.4 U-Hook Rod Sizes

Pipe Size			
in.	mm	in.	mm
Up to and including 2	50	5/16	7.9
2½ to 6	65 to 150	5/8	9.5
8	200	1/2	12.7

9.1.2.5 Eye Rods.

9.1.2.5.1 The size of the rod material for eye rods shall not be less than specified in Table 9.1.2.5.1.

9.1.2.5.2 Eye rods shall be secured with lock washers to prevent lateral motion.

9.1.2.5.3 Where eye rods are fastened to wood structural members, the eye rod shall be backed with a large flat washer bearing directly against the structural member, in addition to the lock washer.

9.1.2.6 Threaded Sections of Rods. Threaded sections of rods shall not be formed or bent.

Table 9.1.2.5.1 Eye Rod Sizes

Pipe Size		Diameter of Rod			
		With Bent Eye		With Welded Eye	
in.	mm	in.	mm	in.	mm
Up to and including 4	100	3/8	9.5	3/8	9.5
5	125	1/2	12.7	1/2	12.7
6	150	1/2	12.7	1/2	12.7
8	200	5/8	19.1	5/8	19.1

9.1.3 Fasteners in Concrete.

9.1.3.1 Unless prohibited by 9.1.3.2 or 9.1.3.3, the use of listed inserts set in concrete and listed post-installed anchors to support hangers shall be permitted for mains and branch lines.

9.1.3.2 Post-installed anchors shall not be used in cinder concrete, except for branch lines where the post-installed anchors are alternated with through-bolts or hangers attached to beams.

9.1.3.3 Post-installed anchors shall not be used in ceilings of gypsum or other similar soft material.

9.1.3.4 Unless the requirements of 9.1.3.5 are met, post-installed anchors shall be installed in a horizontal position in the sides of concrete beams.

9.1.3.5 Post-installed anchors shall be permitted to be installed in the vertical position under any of the following conditions:

- (1) When used in concrete having gravel or crushed stone aggregate to support pipes 4 in. (100 mm) or less in diameter
- (2) When post-installed anchors are alternated with hangers connected directly to the structural members, such as trusses and girders, or to the sides of concrete beams [to support pipe 5 in. (125 mm) or larger]
- (3) When post-installed anchors are spaced not over 10 ft (3 m) apart [to support pipe 4 in. (100 mm) or larger]

9.1.3.6 Holes for post-installed anchors in the side of beams shall be above the centerline of the beam or above the bottom reinforcement steel rods.

9.1.3.7 Holes for post-installed anchors used in the vertical position shall be drilled to provide uniform contact with the shield over its entire circumference.

9.1.3.8 The depth of the post-installed anchor hole shall not be less than specified for the type of shield used.

9.1.3.9 Powder-Driven Studs.

9.1.3.9.1 Powder-driven studs, welding studs, and the tools used for installing these devices shall be listed.

9.1.3.9.2 Pipe size, installation position, and construction material into which they are installed shall be in accordance with individual listings.

9.1.3.9.3* Representative samples of concrete into which studs are to be driven shall be tested to determine that the studs will hold a minimum load of 750 lb (341 kg) for 2 in. (50 mm) or smaller pipe; 1000 lb (454 kg) for 2 1/2 in., 3 in., or 3 1/2 in. (65 mm, 80 mm, or 90 mm) pipe; and 1200 lb (545 kg) for 4 in. or 5 in. (100 mm or 125 mm) pipe.

9.1.3.9.4 Increaser couplings shall be attached directly to the powder-driven studs.

9.1.3.10 Minimum Bolt Size for Concrete.

9.1.3.10.1 The size of a bolt used with a hanger and installed through concrete shall not be less than specified in Table 9.1.3.10.1.

Table 9.1.3.10.1 Minimum Bolt Size for Concrete

Pipe Size	Size of Bolt
in.	mm
Up to and including 4	100
5	125
6	150
8	200
10	250
12	300

9.1.3.10.2 Holes for bolts shall not exceed 1/16 in. (1.6 mm) greater than the diameter of the bolt.

9.1.3.10.3 Bolts shall be provided with a flat washer and nut.

9.1.4 Fasteners in Steel.

9.1.4.1* Powder-driven studs, welding studs, and the tools used for installing these devices shall be listed.

9.1.4.2 Pipe size, installation position, and construction material into which they are installed shall be in accordance with individual listings.

9.1.4.3 Increaser couplings shall be attached directly to the powder-driven studs or welding studs.

9.1.4.4 Welding studs or other hanger parts shall not be attached by welding to steel less than U.S. Standard, 12 gauge (2.78 mm).

9.1.4.5 Minimum Bolt Size for Steel.

9.1.4.5.1 The size of a bolt used with a hanger and installed through steel shall not be less than specified in Table 9.1.4.5.1.

9.1.4.5.2 Holes for bolts shall not exceed 1/16 in. (1.6 mm) greater than the diameter of the bolt.

9.1.4.5.3 Bolts shall be provided with a flat washer and nut.

9.1.5 Fasteners in Wood.

9.1.5.1 Drive Screws.

9.1.5.1.1 Drive screws shall be used only in a horizontal position as in the side of a beam and only for 2 in. (50 mm) or smaller pipe.

9.1.5.1.2 Drive screws shall only be used in conjunction with hangers that require two points of attachments.

Table 9.1.4.5.1 Minimum Bolt Size for Steel

Pipe Size		Size of Bolt	
in.	mm	in.	mm
Up to and including 4	100	3/8	10
5	125	1/2	12
6	150		
8	200		
10	250	5/8	15
12	300	3/4	20

9.1.5.2 Ceiling Flanges and U-Hooks with Screws.

9.1.5.2.1 Unless the requirements of 9.1.5.2.2 or 9.1.5.2.3 are met, for ceiling flanges and U-hooks, screw dimensions shall not be less than those given in Table 9.1.5.2.1.

9.1.5.2.2 When the thickness of planking and thickness of flange do not permit the use of screws 2 in. (50 mm) long, screws 1 3/4 in. (45 mm) long shall be permitted with hangers spaced not over 10 ft (3 m) apart.

9.1.5.2.3 When the thickness of beams or joists does not permit the use of screws 2 1/2 in. (60 mm) long, screws 2 in. (50 mm) long shall be permitted with hangers spaced not over 10 ft (3 m) apart.

9.1.5.3 Bolt or Lag Screw.

9.1.5.3.1 Unless the requirements of 9.1.5.3.2 are met, the size of bolt or lag screw used with a hanger and installed on the side of the beam shall not be less than specified in Table 9.1.5.3.1.

9.1.5.3.2 Where the thickness of beams or joists does not permit the use of screws 2 1/2 in. (64 mm) long, screws 2 in. (50 mm) long shall be permitted with hangers spaced not over 10 ft (3 m) apart.

9.1.5.3.3 All holes for lag screws shall be pre-drilled 1/8 in. (3.2 mm) less in diameter than the maximum root diameter of the lag screw thread.

9.1.5.3.4 Holes for bolts shall not exceed 1/16 in. (1.6 mm) greater than the diameter of the bolt.

9.1.5.3.5 Bolts shall be provided with a flat washer and nut.

9.1.5.4 Wood Screws. Wood screws shall be installed with a screwdriver.

9.1.5.5 Nails. Nails shall not be acceptable for fastening hangers.

9.1.5.6 Screws in Side of Timber or Joists.

9.1.5.6.1 Screws in the side of a timber or joist shall be not less than 2 1/2 in. (64 mm) from the lower edge where supporting branch lines and not less than 3 in. (76 mm) where supporting main lines.

9.1.5.6.2 The requirements of 9.1.5.6.1 shall not apply to 2 in. (51 mm) or thicker nailing strips resting on top of steel beams.

Table 9.1.5.2.1 Screw Dimensions for Ceiling Flanges and U-Hooks

Pipe Size		Two Screw Ceiling Flanges	
in.	mm		
Up to and including 2	50	Wood screw No. 18 x 1 1/2 in. or Lag screw 3/16 in. x 1 1/2 in.	
			Three Screw Ceiling Flanges
Up to and including 2	50	Wood screw No. 18 x 1 1/2 in.	
2 1/2	65	Lag screw 5/8 in. x 2 in.	
3	80		
3 1/2	90		
4	100	Lag screw 1/2 in. x 2 in.	
5	125		
6	150		
8	200	Lag screw 3/8 in. x 2 in.	
			Four Screw Ceiling Flanges
Up to and including 2	50	Wood screw No. 18 x 1 1/2 in.	
2 1/2	65	Lag screw 5/8 in. x 1 1/2 in.	
3	80		
3 1/2	90		
4	100	Lag screw 1/2 in. x 2 in.	
5	125		
6	150		
8	200	Lag screw 3/8 in. x 2 in.	
			U-Hooks
Up to and including 2	50	Drive screw No. 16 x 2 in.	
2 1/2	65	Lag screw 5/8 in. x 2 1/2 in.	
3	80		
3 1/2	90		
4	100	Lag screw 1/2 in. x 3 in.	
5	125		
6	150		
8	200	Lag screw 3/8 in. x 3 in.	

9.1.5.7 Coach Screw Rods.

9.1.5.7.1 Minimum Coach Screw Rod Size. The size of coach screw rods shall not be less than the requirements of Table 9.1.5.7.1.

9.1.5.7.2 The minimum plank thickness and the minimum width of the lower face of beams or joists in which coach screw rods are used shall be not less than that specified in Table 9.1.5.7.2.

Table 9.1.5.3.1 Minimum Bolt or Lag Screw Sizes for Side of Beam Installation

Pipe Size		Size of Bolt or Lag Screw		Length of Lag Screw Used with Wood Beams	
in.	mm	in.	mm	in.	mm
Up to and including 2	50	3/8	10	2 1/2	64
2 1/2 to 6 (inclusive)	65 to 150	1/2	12	3	76
8	200	5/8	15	3	76

Table 9.1.5.7.1 Minimum Coach Screw Rod Size

Pipe Size		Diameter of Rod		Minimum Penetration	
in.	mm	in.	mm	in.	mm
Up to and including 4	100	3/8	10	3	76
Larger than 4	100	NP	NP	NP	NP

NP: Not permitted.

Table 9.1.5.7.2 Minimum Plank Thicknesses and Beam or Joist Widths

Pipe Size		Nominal Plank Thickness		Nominal Width of Beam or Joist Face	
in.	mm	in.	mm	in.	mm
Up to and including 2	50	3	76	2	51
2 1/2	65	4	102	2	51
3	80				
3 1/2	90				
4	100	4	102	3	76

9.1.5.7.3 Coach screw rods shall not be used for support of pipes larger than 4 in. (100 mm) in diameter.

9.1.5.7.4 All holes for coach screw rods shall be predrilled $\frac{1}{8}$ in. (3.2 mm) less in diameter than the maximum root diameter of the wood screw thread.

9.2* Installation of Pipe Hangers.

9.2.1 General.

9.2.1.1 Ceiling Sheathing.

9.2.1.1.1* Unless the requirements of 9.2.1.1.2 are met, sprinkler piping shall be supported independently of the ceiling sheathing.

9.2.1.1.2 Toggle hangers shall be permitted only for the support of pipe 1 1/2 in. (40 mm) or smaller in size under ceilings of hollow tile or metal lath and plaster.

9.2.1.2 Storage Racks. Where sprinkler piping is installed in storage racks, piping shall be supported from the storage rack structure or building in accordance with all applicable provisions of Sections 9.2 and 9.3.

9.2.1.3* Building Structure.

9.2.1.3.1 Unless the requirements of 9.2.1.3.3 apply, sprinkler piping shall be substantially supported from the building structure, which must support the added load of the water-filled pipe plus a minimum of 250 lb (114 kg) applied at the point of hanging, except where permitted by 9.2.1.1.2, 9.2.1.3.3, and 9.2.1.4.1.

9.2.1.3.2 Trapeze hangers shall be used where necessary to transfer loads to appropriate structural members.

9.2.1.3.3* Flexible Sprinkler Hose Fittings.

9.2.1.3.3.1 Listed flexible sprinkler hose fittings and their anchoring components intended for use in installations connecting the sprinkler system piping to sprinklers shall be installed in accordance with the requirements of the listing, including any installation instructions.

9.2.1.3.3.2 When installed and supported by suspended ceilings, the ceiling shall meet ASTM C 635, *Standard Specification for the Manufacture, Performance, and Testing of Metal Suspension Systems for Acoustical Tile and Lay-In Panel Ceilings*, and shall be installed in accordance with ASTM C 636, *Standard Practice for Installation of Metal Ceiling Suspension Systems for Acoustical Tile and Lay-In Panels*.

9.2.1.3.3.3* Where flexible sprinkler hose fittings exceed 6 ft (1.83 m) in length and are supported by a suspended ceiling in accordance with 9.2.1.3.3.2, a hanger(s) attached to the structure shall be required to ensure that the maximum unsupported length does not exceed 6 ft (1.83 m).

9.2.1.3.3.4* Where flexible sprinkler hose fittings are used to connect sprinklers to branch lines in suspended ceilings, a label limiting relocation of the sprinkler shall be provided on the anchoring component.

9.2.1.4 Metal Deck.

9.2.1.4.1* Branch line hangers attached to metal deck shall be permitted only for the support of pipe 1 in. (25 mm) or smaller in size, by drilling or punching the vertical portion of the metal deck and using through bolts.

9.2.1.4.2 The distance from the bottom of the bolt hole to the bottom of the vertical member shall be not less than $\frac{3}{8}$ in. (9.5 mm).

9.2.1.5 Where sprinkler piping is installed below ductwork, piping shall be supported from the building structure or from the ductwork supports, provided such supports are capable of handling both the load of the ductwork and the load specified in 9.2.1.3.1.

9.2.2* Maximum Distance Between Hangers.

9.2.2.1 The maximum distance between hangers shall not exceed that specified in Table 9.2.2.1(a) or Table 9.2.2.1(b), except where the provisions of 9.2.4 apply.

9.2.2.2 The maximum distance between hangers for listed nonmetallic pipe shall be modified as specified in the individual product listings.

9.2.3 Location of Hangers on Branch Lines.

9.2.3.1 Subsection 9.2.3 shall apply to the support of steel pipe or copper tube as specified in 6.3.1 and subject to the provisions of 9.2.2.

9.2.3.2* Minimum Number of Hangers.

9.2.3.2.1 Unless the requirements of 9.2.3.2.2 or 9.2.3.2.3 are met, there shall be not less than one hanger for each section of pipe.

9.2.3.2.2* Where sprinklers are spaced less than 6 ft (1.8 m) apart, hangers spaced up to a maximum of 12 ft (3.7 m) shall be permitted.

9.2.3.2.3* Starter lengths less than 6 ft (1.8 m) shall not require a hanger, unless on the end line of a sidefeed system or where an intermediate cross main hanger has been omitted.

9.2.3.3 Clearance to Hangers. The distance between a hanger and the centerline of an upright sprinkler shall not be less than 3 in. (76 mm).

9.2.3.4* Unsupported Lengths.

9.2.3.4.1 The unsupported horizontal length between the end sprinkler and the last hanger on the line shall not be

greater than 36 in. (0.9 m) for 1 in. (25 mm) pipe, 48 in. (1.2 m) for 1½ in. (32 mm) pipe, and 60 in. (1.5 m) for 1½ in. (40 mm) or larger pipe.

9.2.3.4.2 For copper tube, the unsupported horizontal length between the end sprinkler and the last hanger on the line shall not be greater than 18 in. (457 mm) for 1 in. (25 mm) pipe, 24 in. (610 mm) for 1½ in. (32 mm) pipe, and 30 in. (762 mm) for 1½ in. (40 mm) or larger pipe.

9.2.3.4.3 Where the limits of 9.2.3.4.1 and 9.2.3.4.2 are exceeded, the pipe shall be extended beyond the end sprinkler and shall be supported by an additional hanger.

9.2.3.4.4* Unsupported Length with Maximum Pressure Exceeding 100 psi (6.9 bar) and a Branch Line Above a Ceiling Supplying Sprinklers in a Pendent Position Below the Ceiling.

9.2.3.4.4.1 Where the maximum static or flowing pressure, whichever is greater at the sprinkler, applied other than through the fire department connection, exceeds 100 psi (6.9 bar) and a branch line above a ceiling supplies sprinklers in a pendent position below the ceiling, the hanger assembly supporting the pipe supplying an end sprinkler in a pendent position shall be of a type that prevents upward movement of the pipe.

9.2.3.4.4.2 The unsupported length between the end sprinkler in a pendent position or drop nipple and the last hanger on the branch line shall not be greater than 12 in. (305 mm) for steel pipe or 6 in. (152 mm) for copper pipe.

9.2.3.4.4.3 When the limit of 9.2.3.4.4.2 is exceeded, the pipe shall be extended beyond the end sprinkler and supported by an additional hanger.

9.2.3.4.4.4 The hanger closest to the sprinkler shall be of a type that prevents upward movement of the pipe.

Table 9.2.2.1(a) Maximum Distance Between Hangers (ft-in.)

	Nominal Pipe Size (in.)											
	¾	1	1¼	1½	2	2½	3	3½	4	5	6	8
Steel pipe except threaded lightwall	N/A	12-0	12-0	15-0	15-0	15-0	15-0	15-0	15-0	15-0	15-0	15-0
Threaded lightwall steel pipe	N/A	12-0	12-0	12-0	12-0	12-0	12-0	N/A	N/A	N/A	N/A	N/A
Copper tube	8-0	8-0	10-0	10-0	12-0	12-0	12-0	15-0	15-0	15-0	15-0	15-0
CPVC	5-6	6-0	6-6	7-0	8-0	9-0	10-0	N/A	N/A	N/A	N/A	N/A
Ductile iron pipe	N/A	N/A	N/A	N/A	N/A	N/A	15-0	N/A	15-0	N/A	15-0	15-0

Table 9.2.2.1(b) Maximum Distance Between Hangers (m-mm)

	Nominal Pipe Size (m)											
	20	25	32	40	50	65	80	90	100	125	150	200
Steel pipe except threaded lightwall	N/A	3.66	3.66	4.57	4.57	4.57	4.57	4.57	4.57	4.57	4.57	4.57
Threaded lightwall steel pipe	N/A	3.66	3.66	3.66	3.66	3.66	3.66	N/A	N/A	N/A	N/A	N/A
Copper tube	2.44	2.44	3.05	3.05	3.66	3.66	3.66	4.57	4.57	4.57	4.57	4.57
CPVC	1.68	1.83	1.98	2.13	2.44	2.74	3.05	N/A	N/A	N/A	N/A	N/A
Ductile iron pipe	N/A	N/A	N/A	N/A	N/A	N/A	4.57	N/A	4.57	N/A	4.57	4.57

9.2.3.5* Unsupported Armover Length.

9.2.3.5.1 The cumulative horizontal length of an unsupported armover to a sprinkler, sprinkler drop, or sprig shall not exceed 24 in. (610 mm) for steel pipe or 12 in. (305 mm) for copper tube.

9.2.3.5.2* Unsupported Armover Length with Maximum Pressure Exceeding 100 psi (6.9 bar) and a Branch Line Above a Ceiling Supplying Sprinklers in a Pendent Position Below the Ceiling.

9.2.3.5.2.1 Where the maximum static or flowing pressure, whichever is greater at the sprinkler, applied other than through the fire department connection, exceeds 100 psi (6.9 bar) and a branch line above a ceiling supplies sprinklers in a pendent position below the ceiling, the cumulative horizontal length of an unsupported armover to a sprinkler or sprinkler drop shall not exceed 12 in. (305 mm) for steel pipe and 6 in. (152 mm) for copper tube.

9.2.3.5.2.2 The hanger closest to the sprinkler shall be of a type that prevents upward movement of the pipe.

9.2.3.6* Wall-mounted sidewall sprinklers shall be restrained to prevent movement.

9.2.3.7 Sprigs. Sprigs 4 ft (1.2 m) or longer shall be restrained against lateral movement.

9.2.4 Location of Hangers on Mains.

9.2.4.1 Unless the requirements of 9.2.4.2, 9.2.4.3, 9.2.4.4, or 9.2.4.5 are met, hangers for mains shall be in accordance with 9.2.2, between each branch line, or on each section of pipe, whichever is the lesser dimension.

9.2.4.2 For cross mains in steel pipe systems in bays having two branch lines, the intermediate hanger shall be permitted to be omitted, provided that a hanger attached to a purlin is installed on each branch line located as near to the cross main as the location of the purlin permits.

9.2.4.2.1 The remaining branch line hangers shall be installed in accordance with 9.2.3.

9.2.4.3 For cross mains in steel pipe systems only in bays having three branch lines, either side or center feed, one (only) intermediate hanger shall be permitted to be omitted, provided that a hanger attached to a purlin is installed on each branch line located as near to the cross main as the location of the purlin permits.

9.2.4.3.1 The remaining branch line hangers shall be installed in accordance with 9.2.3.

9.2.4.4 For cross mains in steel pipe systems only in bays having four or more branch lines, either side or center feed, two intermediate hangers shall be permitted to be omitted, provided the maximum distance between hangers does not exceed the distances specified in 9.2.2 and a hanger attached to a purlin on each branch line is located as near to the cross main as the purlin permits.

9.2.4.5 At the end of the main, intermediate trapeze hangers shall be installed unless the main is extended to the next framing member with a hanger installed at this point, in which event an intermediate hanger shall be permitted to be omitted in accordance with 9.2.4.2, 9.2.4.3, and 9.2.4.4.

9.2.5 Support of Risers.

9.2.5.1 Risers shall be supported by riser clamps or by hangers located on the horizontal connections within 24 in. (610 mm) of the centerline of the riser.

9.2.5.2 Riser clamps supporting risers by means of set screws shall not be used.

9.2.5.3* Riser clamps anchored to walls using hanger rods in the horizontal position shall not be permitted to vertically support risers.

9.2.5.4 Multistory Buildings.

9.2.5.4.1 In multistory buildings, riser supports shall be provided at the lowest level, at each alternate level above, above and below offsets, and at the top of the riser.

9.2.5.4.2* Supports above the lowest level shall also restrain the pipe to prevent movement by an upward thrust where flexible fittings are used.

9.2.5.4.3 Where risers are supported from the ground, the ground support shall constitute the first level of riser support.

9.2.5.4.4 Where risers are offset or do not rise from the ground, the first ceiling level above the offset shall constitute the first level of riser support.

9.2.5.5 Distance between supports for risers shall not exceed 25 ft (7.6 m).

9.2.6* Pipe Stands.

9.2.6.1 Pipe stands shall be sized to support a minimum of 5 times the weight of the water-filled pipe, plus 250 lb (114 kg).

9.2.6.2 Where pipe stands are utilized, they shall be approved.

9.3 Protection of Piping Against Damage Where Subject to Earthquakes.

9.3.1* General.

9.3.1.1 Where water-based fire protection systems are required to be protected against damage from earthquakes, the requirements of Section 9.3 shall apply, unless the requirements of 9.3.1.2 are met.

9.3.1.2 Alternative methods of providing earthquake protection of sprinkler systems based on a seismic analysis certified by a registered professional engineer such that system performance will be at least equal to that of the building structure under expected seismic forces shall be permitted.

9.3.1.3 Obstructions to Sprinklers. Braces and restraints shall not obstruct sprinklers and shall comply with the obstruction rules of Chapter 8.

9.3.2* Couplings.

9.3.2.1 Listed flexible pipe couplings joining grooved end pipe shall be provided as flexure joints to allow individual sections of piping 2½ in. (65 mm) or larger to move differentially with the individual sections of the building to which it is attached.

9.3.2.2 Couplings shall be arranged to coincide with structural separations within a building.

9.3.2.3 Systems having more flexible couplings than required by this section shall be provided with additional sway bracing as required in 9.3.5.3.8. The flexible couplings shall be installed as follows:

(1)*Within 24 in. (610 mm) of the top and bottom of all risers, unless the following provisions are met:

(a) In risers less than 3 ft (0.9 m) in length, flexible couplings are permitted to be omitted.

- (b) In risers 3 ft to 7 ft (0.9 m to 2.1 m) in length, one flexible coupling is adequate.
- (2) Within 12 in. (305 mm) above and within 24 in. (610 mm) below the floor in multistory buildings. When the flexible coupling below the floor is above the tie-in main to the main supplying that floor, a flexible coupling shall be provided in accordance with one of the following:
 - (a)*On the horizontal portion within 24 in. (610 mm) of the tie-in where the tie-in is horizontal
 - (b)*On the vertical portion of the tie-in where the tie-in incorporates a riser
- (3) On both sides of concrete or masonry walls within 1 ft (305 mm) of the wall surface, unless clearance is provided in accordance with 9.3.4
- (4)*Within 24 in. (610 mm) of building expansion joints
- (5) Within 24 in. (610 mm) of the top of drops exceeding 15 ft (4.6 m) in length to portions of systems supplying more than one sprinkler, regardless of pipe size
- (6) Within 24 in. (610 mm) above and 24 in. (610 mm) below any intermediate points of support for a riser or other vertical pipe

9.3.2.4* Flexible Couplings for Drops. Flexible couplings for drops to hose lines, rack sprinklers, and mezzanines shall be installed regardless of pipe sizes as follows:

- (1) Within 24 in. (610 mm) of the top of the drop
- (2) Within 24 in. (610 mm) above the uppermost drop support attachment, where drop supports are provided to the structure, rack, or mezzanine
- (3) Within 24 in. (610 mm) above the bottom of the drop where no additional drop support is provided

9.3.3* Seismic Separation Assembly.

9.3.3.1 An approved seismic separation assembly shall be installed where sprinkler piping, regardless of size, crosses building seismic separation joints at ground level and above.

9.3.3.2 Seismic separation assemblies shall consist of flexible fittings or flexible piping so as to allow movement sufficient to accommodate closing of the separation, opening of the separation to twice its normal size, and movement relative to the separation in the other two dimensions in an amount equal to the separation distance.

9.3.3.3* The seismic separation assembly shall include a four-way brace upstream and downstream within 6 ft (1.83 m) of the seismic separation assembly.

9.3.3.4 Bracing shall not be attached to the seismic separation assembly.

9.3.4* Clearance.

9.3.4.1 Clearance shall be provided around all piping extending through walls, floors, platforms, and foundations, including drains, fire department connections, and other auxiliary piping.

9.3.4.2 Unless the requirements of 9.3.4.3 through 9.3.4.7 are met, where pipe passes through holes in platforms, foundations, walls, or floors, the holes shall be sized such that the diameter of the holes is nominally 2 in. (50 mm) larger than the pipe for pipe 1 in. (25 mm) nominal to 3½ in. (90 mm) nominal and 4 in. (100 mm) larger than the pipe for pipe 4 in. (100 mm) nominal and larger.

9.3.4.3 Where clearance is provided by a pipe sleeve, a nominal diameter 2 in. (50 mm) larger than the nominal diameter

of the pipe shall be acceptable for pipe sizes 1 in. (25 mm) through 3½ in. (90 mm), and the clearance provided by a pipe sleeve of nominal diameter 4 in. (100 mm) larger than the nominal diameter of the pipe shall be acceptable for pipe sizes 4 in. (100 mm) and larger.

9.3.4.4 No clearance shall be required for piping passing through gypsum board or equally frangible construction that is not required to have a fire resistance rating.

9.3.4.5 No clearance shall be required if flexible couplings are located within 1 ft (305 mm) of each side of a wall, floor, platform, or foundation.

9.3.4.6 No clearance shall be required where horizontal piping passes perpendicularly through successive studs or joists that form a wall or floor/ceiling assembly.

9.3.4.7 No clearance shall be required where nonmetallic pipe has been demonstrated to have inherent flexibility equal to or greater than the minimum provided by flexible couplings located within 1 ft (305 mm) of each side of a wall, floor, platform, or foundation.

9.3.4.8 Where required, the clearance shall be filled with a flexible material that is compatible with the piping material.

9.3.4.9 Clearance from structural members not penetrated or used, collectively or independently, to support the piping shall be at least 2 in. (50 mm).

9.3.5* Sway Bracing Design.

9.3.5.1 General.

9.3.5.1.1 The system piping shall be braced to resist both lateral and longitudinal horizontal seismic loads and to prevent vertical motion resulting from seismic loads.

9.3.5.1.2 The structural components to which bracing is attached shall be determined to be capable of resisting the added applied seismic loads.

9.3.5.1.3* Horizontal loads on system piping shall be determined in accordance with 9.3.5.6.

9.3.5.2 Sway Bracing Design.

9.3.5.2.1 Sway braces shall be designed to withstand forces in tension and compression, unless the requirements of 9.3.5.2.2 are met.

9.3.5.2.2* Tension-only bracing systems shall be permitted for use where listed for this service and where installed in accordance with their listing limitations, including installation instructions.

9.3.5.2.3 For all braces, whether or not listed, the maximum allowable load shall be based on the weakest component of the brace with safety factors.

9.3.5.3 Lateral Sway Bracing.

9.3.5.3.1* Lateral sway bracing shall be provided on all feed and cross mains regardless of size and all branch lines and other piping with a diameter of 2½ in. (65 mm) and larger.

9.3.5.3.2* Lateral sway bracing shall be in accordance with either Table 9.3.5.3.2(a), (b), (c), (d) or (e) or 9.3.5.3.3, based on the piping material of the sprinkler system.

9.3.5.3.2.1 Specially listed nonstandard pipe shall be permitted using the values in Table 9.3.5.3.2(c) or with values provided by the manufacturer.

Table 9.3.5.3.2(a) Maximum Load (F_{pw}) in Zone of Influence (lb), ($F_y = 30$ ksi) Schedule 10 Steel Pipe

Pipe (in.)	Lateral Sway Brace Spacing (ft) ^a				
	20 ^b	25 ^b	30 ^c	35 ^c	40 ^d
1	111	89	73	63	52
1 1/4	176	141	116	99	83
1 1/2	241	193	158	136	114
2	390	312	256	219	183
2 1/2	641	513	420	360	301
3	966	773	633	543	454
3 1/2	1281	1025	840	720	603
4	1634	1307	1071	918	769
5	2814	2251	1844	1581	1324
6 and larger	4039	3231	2647	2269	1900

^a The tables for the maximum load F_{pw} in zone of influence are based on specific configurations of mains and branch lines.

^b Assumes branch lines at center of pipe span and near each support.

^c Assumes branch lines at third-points of pipe span and near each support.

^d Assumes branch lines at quarter-points of pipe span and near each support.

^e Larger diameter pipe may be used when justified by engineering analysis.

^f ASTM A 106 Grade B or A 53 Grade B has an $F_y = 35$ ksi. An $F_y = 30$ ksi was used also as a conservative value to account for differences in material properties as well as other operational stresses.

Table 9.3.5.3.2(c) Maximum Load (F_{pw}) in Zone of Influence (lb), ($F_y = 30$ ksi) Schedule 5 Steel Pipe

Pipe (in.)	Lateral Sway Brace Spacing (ft) ^a				
	20 ^b	25 ^b	30 ^c	35 ^c	40 ^d
1	71	56	46	40	33
1 1/4	116	93	76	65	55
1 1/2	154	124	101	87	73
2	246	197	161	138	116
2 1/2	459	367	301	258	216
3	691	552	453	388	325
3 1/2	910	728	597	511	428
4 ^e	1160	928	760	652	546

^a The tables for the maximum load F_{pw} in zone of influence are based on specific configurations of mains and branch lines.

^b Assumes branch lines at center of pipe span and near each support.

^c Assumes branch lines at third-points of pipe span and near each support.

^d Assumes branch lines at quarter-points of pipe span and near each support.

^e Larger diameter pipe may be used when justified by engineering analysis.

^f ASTM A 106 Grade B or A 53 Grade B has an $F_y = 35$ ksi. An $F_y = 30$ ksi was used also as a conservative value to account for differences in material properties as well as other operational stresses.

Table 9.3.5.3.2(b) Maximum Load (F_{pw}) in Zone of Influence (lb), ($F_y = 30$ ksi) Schedule 40 Steel Pipe

Pipe (in.)	Lateral Sway Brace Spacing (ft) ^a				
	20 ^b	25 ^b	30 ^c	35 ^c	40 ^d
1	121	97	79	68	57
1 1/4	214	171	140	120	100
1 1/2	306	245	201	172	144
2	520	416	341	292	245
2 1/2	984	787	645	553	463
3	1597	1278	1047	897	751
3 1/2	2219	1775	1455	1247	1044
4	2981	2385	1954	1675	1402
5	5061	4049	3317	2843	2381
6 and larger	7893	6314	5173	4434	3713

^a The tables for the maximum load F_{pw} in zone of influence are based on specific configurations of mains and branch lines.

^b Assumes branch lines at center of pipe span and near each support.

^c Assumes branch lines at third-points of pipe span and near each support.

^d Assumes branch lines at quarter-points of pipe span and near each support.

^e Larger diameter pipe may be used when justified by engineering analysis.

^f ASTM A 106 Grade B or A 53 Grade B has an $F_y = 35$ ksi. An $F_y = 30$ ksi was used also as a conservative value to account for differences in material properties as well as other operational stresses.

Table 9.3.5.3.2(d) Maximum Load (F_{pw}) in Zone of Influence (lb), ($F_y = 8$ ksi) CPVC Pipe

Pipe (in.)	Lateral Sway Brace Spacing (ft) ^a				
	20 ^b	25 ^b	30 ^c	35 ^c	40 ^d
3/4	15	12	10	8	7
1	28	22	18	15	13
1 1/4	56	45	37	30	26
1 1/2	83	67	55	45	39
2	161	129	105	87	76
2 1/2	286	229	188	154	135
3 ^e	516	413	338	278	243

^a The tables for the maximum load F_{pw} in zone of influence are based on specific configurations of mains and branch lines.

^b Assumes branch lines at center of pipe span and near each support.

^c Assumes branch lines at third-points of pipe span and near each support.

^d Assumes branch lines at quarter-points of pipe span and near each support.

^e Larger diameter pipe may be used when justified by engineering analysis.

^f ASTM A 106 Grade B or A 53 Grade B has an $F_y = 35$ ksi. An $F_y = 30$ ksi was used also as a conservative value to account for differences in material properties as well as other operational stresses.

Table 9.3.5.3.2(e) Maximum Load (F_{pw}) in Zone of Influence (lb), ($F_y = 32$ ksi) Type M Copper Tube

Pipe (in.)	Lateral Sway Brace Spacing (ft) ^a				
	20 ^b	25 ^b	30 ^c	35 ^c	40 ^d
3/4	17	14	11	9	8
1	31	25	21	17	15
1 1/4	56	45	37	30	27
1 1/2	92	74	60	49	43
2 ^e	192	154	126	103	90

^a The tables for the maximum load F_{pw} in zone of influence are based on specific configurations of mains and branch lines.

^b Assumes branch lines at center of pipe span and near each support.

^c Assumes branch lines at third-points of pipe span and near each support.

^d Assumes branch lines at quarter-points of pipe span and near each support.

^e Larger diameter pipe may be used when justified by engineering analysis.

^f ASTM A 106 Grade B or A 53 Grade B has an $F_y = 35$ ksi. An $F_y = 30$ ksi was used also as a conservative value to account for differences in material properties as well as other operational stresses.

9.3.5.3.2.2 Spacing shall not exceed a maximum interval of 40 ft (12.2 m) on center.

9.3.5.3.2.3 The maximum permissible load in the zone of influence of a sway brace shall not exceed the values given in Table 9.3.5.3.2(a) through Table 9.3.5.3.2(e) or the values calculated in accordance with 9.3.5.3.3.

9.3.5.3.3 The maximum load (F_{pw}) in the zone of influence for specially listed pipe shall be calculated. (See Annex E.)

9.3.5.3.4 The requirements of 9.3.5.3.1 shall not apply to 2 1/2 in. (65 mm) starter pieces that do not exceed 12 ft (3.66 m) in length.

9.3.5.3.5 The distance between the last brace and the end of the pipe shall not exceed 6 ft (1.8 m).

9.3.5.3.6 The last length of pipe at the end of a feed or cross main shall be provided with a lateral brace.

9.3.5.3.7 Lateral braces shall be allowed to act as longitudinal braces if they are within 24 in. (610 mm) of the centerline of the piping braced longitudinally and the lateral brace is on a pipe of equal or greater size than the pipe being braced longitudinally.

9.3.5.3.8 Where flexible couplings are installed on mains other than as required in 9.3.2, a lateral brace shall be provided within 24 in. (610 mm) of every other coupling, including flexible couplings at grooved fittings, but not more than 40 ft (12.2 m) on center.

9.3.5.3.9 The requirements of 9.3.5.3 shall not apply to pipes individually supported by rods less than 6 in. (152 mm) long measured between the top of the pipe and the point of attachment to the building structure.

9.3.5.3.10 The requirements of 9.3.5.3 shall not apply where U-type hooks of the wraparound type or those U-type hooks arranged to keep the pipe tight to the underside of the structural element shall be permitted to be used to satisfy the requirements for lateral sway bracing, provided the legs are bent

out at least 30 degrees from the vertical and the maximum length of each leg and the rod size satisfies the conditions of Table 9.3.5.8.7(a), Table 9.3.5.8.7(b), and Table 9.3.5.8.7(c).

9.3.5.4 Longitudinal Sway Bracing.

9.3.5.4.1 Longitudinal sway bracing spaced at a maximum of 80 ft (24.4 m) on center shall be provided for feed and cross mains.

9.3.5.4.2 Longitudinal braces shall be allowed to act as lateral braces if they are within 24 in. (610 mm) of the centerline of the piping braced laterally.

9.3.5.4.3 The distance between the last brace and the end of the pipe shall not exceed 40 ft (12.2 m).

9.3.5.5 Risers.

9.3.5.5.1* Tops of risers exceeding 3 ft (1 m) in length shall be provided with a four-way brace.

9.3.5.5.2 Riser nipples shall be permitted to omit the four-way brace required by 9.3.5.5.1.

9.3.5.5.3 When a four-way brace at the top of a riser is attached on the horizontal piping, it shall be within 24 in. (610 mm) of the centerline of the riser and the loads for that brace shall include both the vertical and horizontal pipe.

9.3.5.5.4 Distance between four-way braces for risers shall not exceed 25 ft (7.6 m).

9.3.5.5.5 Four-way bracing shall not be required where risers penetrate intermediate floors in multistory buildings where the clearance does not exceed the limits of 9.3.4.

9.3.5.6* Horizontal Seismic Loads.

9.3.5.6.1* The horizontal seismic load for the braces shall be as determined in 9.3.5.6.4 or 9.3.5.6.5, or as required by the authority having jurisdiction. The weight of the system being braced (W_p) shall be taken as 1.15 times the weight of the water-filled piping. (See A.9.3.5.6.1.)

9.3.5.6.2* The horizontal force, F_{pw} , acting on the brace shall be taken as $F_{pw} = C_p W_p$, where C_p is the seismic coefficient selected in Table 9.3.5.6.2 utilizing the short period response parameter, S_s . The value of S_s used in Table 9.3.5.6.2 shall be obtained from the authority having jurisdiction or from seismic hazard maps. Linear interpolation shall be permitted to be used for intermediate values of S_s .

9.3.5.6.2.1* The horizontal force, F_{pw} , acting on the brace shall be permitted to be determined in accordance with Section 13.3.1 of SEI/ASCE 7, *Minimum Design Loads for Buildings and Other Structures*, multiplied by 0.7 to convert to allowable stress design (ASD).

9.3.5.6.3* Where the authority having jurisdiction does not specify the horizontal seismic load, the horizontal seismic force acting on the braces shall be determined as specified in 9.3.5.6.2 with $C_p = 0.5$.

9.3.5.6.4* The zone of influence for lateral braces shall include all branch lines and mains tributary to the brace, except branch lines that are provided with longitudinal bracing.

9.3.5.6.5 The zone of influence for longitudinal braces shall include all mains tributary to the brace.

9.3.5.7 Net Vertical Reaction Forces. Where the horizontal seismic loads used exceed 0.5 W_p and the brace angle is less than 45 degrees from vertical or where the horizontal seismic

Table 9.3.5.6.2 Seismic Coefficient Table

S_s	C_p
0.33 or less	0.35
0.40	0.38
0.50	0.40
0.60	0.42
0.70	0.42
0.75	0.42
0.80	0.44
0.90	0.48
0.95	0.50
1.00	0.51
1.10	0.54
1.20	0.57
1.25	0.58
1.30	0.61
1.40	0.65
1.50	0.70
1.60	0.75
1.70	0.79
1.75	0.82
1.80	0.84
1.90	0.89
2.00	0.93
2.10	0.98
2.20	1.03
2.30	1.07
2.40	1.12
2.50	1.17
2.60	1.21
2.70	1.26
2.80	1.31
2.90	1.35
3.00	1.40

load exceeds $1.0 W_r$ and the brace angle is less than 60 degrees from vertical, the braces shall be arranged to resist the net vertical reaction produced by the horizontal load.

9.3.5.8* Sway Brace Installation.

9.3.5.8.1 Sway bracing shall be tight.

9.3.5.8.2 For individual braces, the slenderness ratio (l/r) shall not exceed 300, where l is the length of the brace and r is the least radius of gyration.

9.3.5.8.3 Where threaded pipe is used as part of a sway brace assembly, it shall not be less than Schedule 30.

9.3.5.8.4 All parts and fittings of a brace shall lie in a straight line to avoid eccentric loadings on fittings and fasteners.

9.3.5.8.5 For longitudinal braces only, the brace shall be permitted to be connected to a tab welded to the pipe in conformance to 6.5.2.

9.3.5.8.6 For tension-only braces, two tension-only brace components opposing each other must be installed at each lateral or longitudinal brace location.

9.3.5.8.7* The loads determined in 9.3.5.6 shall not exceed the lesser of the maximum allowable loads provided in Table 9.3.5.8.7(a), Table 9.3.5.8.7(b), and Table 9.3.5.8.7(c) or the manufacturer's certified maximum allowable horizon-

tal loads for brace angles of 30 to 44 degrees, 45 to 59 degrees, 60 to 89 degrees, or 90 degrees.

9.3.5.8.8* Other pipe schedules and materials not specifically included in Table 9.3.5.8.7(a), Table 9.3.5.8.7(b), and Table 9.3.5.8.7(c) shall be permitted to be used if certified by a registered professional engineer to support the loads determined in accordance with the criteria in the tables. Calculations shall be submitted where required by the authority having jurisdiction.

9.3.5.8.9 C-type clamps including beam and large flange clamps, with or without restraining straps, shall not be used to attach braces to the building structure.

9.3.5.8.10 Powder-driven fasteners shall not be used to attach braces to the building structure, unless they are specifically listed for service in resisting lateral loads in areas subject to earthquakes.

9.3.5.9* Fasteners.

9.3.5.9.1* For individual fasteners, the loads determined in 9.3.5.6 shall not exceed the allowable loads provided in Figure 9.3.5.9.1.

9.3.5.9.2 The type of fasteners used to secure the bracing assembly to the structure shall be limited to those shown in Figure 9.3.5.9.1 or to listed devices.

9.3.5.9.3* For connections to wood, through-bolts with washers on each end shall be used, unless the requirements of 9.3.5.9.4 are met.

9.3.5.9.4 Where it is not practical to install through-bolts due to the thickness of the wood member in excess of 12 in. (305 mm) or inaccessibility, lag screws shall be permitted. Holes shall be pre-drilled $\frac{1}{8}$ in. (3.2 mm) smaller than the maximum root diameter of the lag screw.

9.3.5.9.5 Holes for through-bolts and similar listed attachments shall be $\frac{1}{16}$ in. (1.6 mm) greater than the diameter of the bolt.

9.3.5.9.6 The requirements of 9.3.5.9 shall not apply to other fastening methods, which shall be acceptable for use if certified by a registered professional engineer to support the loads determined in accordance with the criteria in 9.3.5.6. Calculations shall be submitted where required by the authority having jurisdiction.

9.3.5.9.7 Concrete Anchors.

9.3.5.9.7.1* Concrete anchors shall be prequalified for seismic applications in accordance with ACI 355.2, *Qualification of Post-Installed Mechanical Anchors in Concrete and Commentary*, and installed in accordance with the manufacturer's instructions.

9.3.5.9.7.2 Concrete anchors other than those shown in Figure 9.3.5.9.1 shall be acceptable for use where designed in accordance with the requirements of the building code and certified by a registered professional engineer.

9.3.5.10 Assemblies.

9.3.5.10.1 Sway bracing assemblies shall be listed for a maximum load rating, unless the requirements of 9.3.5.10.2 are met.

9.3.5.10.2 Where sway bracing utilizing pipe, angles, flats, or rods as shown in Table 9.3.5.8.7(a), Table 9.3.5.8.7(b), and Table 9.3.5.8.7(c) is used, the components shall not require listing.

Table 9.3.5.8.7(a) Maximum Horizontal Loads for Sway Braces with $l/r = 100$ for Steel Braces with $F_y = 36$ ksi

Brace Shape and Size (in.)	Area (in. ²)	Least Radius of Gyration (r) (in.)	Maximum Length for $l/r = 100$	Max. Horizontal Load (lb)				
				ft	in.	30° to 44° Angle from Vertical	45° to 59° Angle from Vertical	60° to 90° Angle from Vertical
Pipe Schedule 40	1	0.494	0.421	3	6	3,150	4,455	5,456
	1 1/4	0.669	0.540	4	6	4,266	6,033	7,389
	1 1/2	0.799	0.623	5	2	5,095	7,206	8,825
	2	1.07	0.787	6	6	6,823	9,650	11,818
Angles	1 1/2 x 1 1/2 x 1/4	0.688	0.292	2	5	4,387	6,205	7,599
	2 x 2 x 1/4	0.938	0.391	3	3	5,982	8,459	10,360
	2 1/2 x 2 x 1/4	1.06	0.424	3	6	6,760	9,560	11,708
	2 1/2 x 2 1/2 x 1/4	1.19	0.491	4	1	7,589	10,732	13,144
	3 x 2 1/2 x 1/4	1.31	0.528	4	4	8,354	11,814	14,469
	3 x 3 x 1/4	1.44	0.592	4	11	9,183	12,987	15,905
Rods (all thread)	3/8	0.07	0.075	0	7	446	631	773
	1/2	0.129	0.101	0	10	823	1,163	1,425
	5/8	0.207	0.128	1	0	1,320	1,867	2,286
	3/4	0.309	0.157	1	3	1,970	2,787	3,413
	7/8	0.429	0.185	1	6	2,736	3,869	4,738
Rods (threaded at ends only)	5/8	0.11	0.094	0	9	701	992	1,215
	1/2	0.196	0.125	1	0	1,250	1,768	2,165
	3/8	0.307	0.156	1	3	1,958	2,769	3,391
	3/4	0.442	0.188	1	6	2,819	3,986	4,882
	7/8	0.601	0.219	1	9	3,833	5,420	6,638
Flats	1 1/2 x 1/4	0.375	0.0722	0	7	2,391	3,382	4,142
	2 x 1/4	0.5	0.0722	0	7	3,189	4,509	5,523
	2 x 3/8	0.75	0.1082	0	10	4,783	6,764	8,284

9.3.5.10.2.1 Bracing fittings and connections used with those specific materials shall be listed.

9.3.5.10.3 The loads shall be reduced as shown in Table 9.3.5.10.3 for loads that are less than 90 degrees from vertical.

9.3.5.11 Attachments.

9.3.5.11.1 Bracing shall be attached directly to feed and cross mains.

9.3.5.11.2 Each run of pipe between changes in direction shall be provided with both lateral and longitudinal bracing, unless the requirements of 9.3.5.11.3 are met.

9.3.5.11.3 Pipe runs less than 12 ft (3.7 m) in length shall be permitted to be supported by the braces on adjacent runs of pipe.

9.3.5.12 Braces to Buildings with Differential Movement. A length of pipe shall not be braced to sections of the building that will move differentially.

9.3.6 Restraint of Branch Lines.

9.3.6.1* Restraint is considered a lesser degree of resisting loads than bracing and shall be provided by use of one of the following:

(1) A listed sway brace assembly

(2) A wraparound U-hook satisfying the requirements of 9.3.5.3.10

(3) No. 12, 440 lb (200 kg) wire installed at least 45 degrees from the vertical plane and anchored on both sides of the pipe

(4) Other approved means

(5)*A hanger not less than 45 degrees from vertical installed within 6 in. (152 mm) of the vertical hanger arranged for restraint against upward movement, provided it is utilized such that l/r does not exceed 400, where the rod shall extend to the pipe or have a surge clip installed

9.3.6.2 Wire used for restraint shall be located within 2 ft (610 mm) of a hanger. The hanger closest to a wire restraint shall be of a type that resists upward movement of a branch line.

9.3.6.3 The end sprinkler on a line shall be restrained against excessive vertical and lateral movement.

9.3.6.4* Branch lines shall be laterally restrained at intervals not exceeding those specified in Table 9.3.6.4(a) or (b) based on branch line diameter and the value of C_p .

Table 9.3.5.8.7(b) Maximum Horizontal Loads for Sway Braces with $l/r = 200$ for Steel Braces with $F_y = 36$ ksi

Brace Shape and Size (in.)	Area (in. ²)	Least Radius of Gyration (r) (in.)	Maximum Length for $l/r = 200$		Max. Horizontal Load (lb)			
					ft	in.	Brace Angle	
			30° to 44° Angle from Vertical	45° to 59° Angle from Vertical	60° to 90° Angle from Vertical			
Pipe Schedule 40	1	0.494	0.421	7	0	926	1310	1604
	1½	0.669	0.540	9	0	1254	1774	2173
	1½	0.799	0.623	10	4	1498	2119	2595
	2	1.07	0.787	13	1	2006	2837	3475
Angles	1½ × 1½ × ¼	0.688	0.292	4	10	1290	1824	2234
	2 × 2 × ¼	0.938	0.391	6	6	1759	2487	3046
	2½ × 2 × ¼	1.06	0.424	7	0	1988	2811	3442
	2½ × 2½ × ¼	1.19	0.491	8	2	2231	3155	3865
	3 × 2½ × ¼	1.31	0.528	8	9	2456	3474	4254
	3 × 3 × ¼	1.44	0.592	9	10	2700	3818	4677
Rods (all thread)	¾	0.07	0.075	1	2	131	186	227
	½	0.129	0.101	1	8	242	342	419
	½	0.207	0.128	2	1	388	549	672
	¾	0.309	0.157	2	7	579	819	1004
	¾	0.429	0.185	3	0	804	1138	1393
Rods (threaded at ends only)	¾	0.11	0.094	1	6	206	292	357
	½	0.196	0.125	2	0	368	520	637
	½	0.307	0.156	2	7	576	814	997
	¾	0.442	0.188	3	1	829	1172	1435
	¾	0.601	0.219	3	7	1127	1594	1952
Flats	1½ × ¼	0.375	0.0722	1	2	703	994	1218
	2 × ¼	0.5	0.0722	1	2	938	1326	1624
	2 × ¾	0.75	0.1082	1	9	1406	1989	2436

9.3.6.5 Where the branch lines are supported by rods less than 6 in. (152 mm) long measured between the top of the pipe and the point of attachment to the building structure, the requirements of 9.3.6.1 through 9.3.6.4 shall not apply and additional restraint shall not be required for the branch lines.

9.3.6.6* Sprigs 4 ft (1.2 m) or longer shall be restrained against lateral movement.

9.3.6.7 Drops and armovers shall not require restraint.

9.3.7 Hangers and Fasteners Subject to Earthquakes.

9.3.7.1 Where seismic protection is provided, C-type clamps (including beam and large flange clamps) used to attach hangers to the building structure shall be equipped with a restraining strap unless the provisions of 9.3.7.1.1 are satisfied.

9.3.7.1.1 As an alternative to the installation of a required restraining strap, a device investigated and specifically listed to restrain the clamp to the structure is permitted where the intent of the device is to resist the worst-case expected horizontal load.

9.3.7.2 The restraining strap shall be listed for use with a C-type clamp or shall be a steel strap of not less than 16 gauge (1.57 mm) thickness and not less than 1 in. (25.4 mm) wide for pipe diameters 8 in. (200 mm) or less and 14 gauge (1.98 mm) thickness and not less than 1½ in. (31.7 mm) wide for pipe diameters greater than 8 in. (200 mm).

9.3.7.3 The restraining strap shall wrap around the beam flange not less than 1 in. (25.4 mm).

9.3.7.4 A lock nut on a C-type clamp shall not be used as a method of restraint.

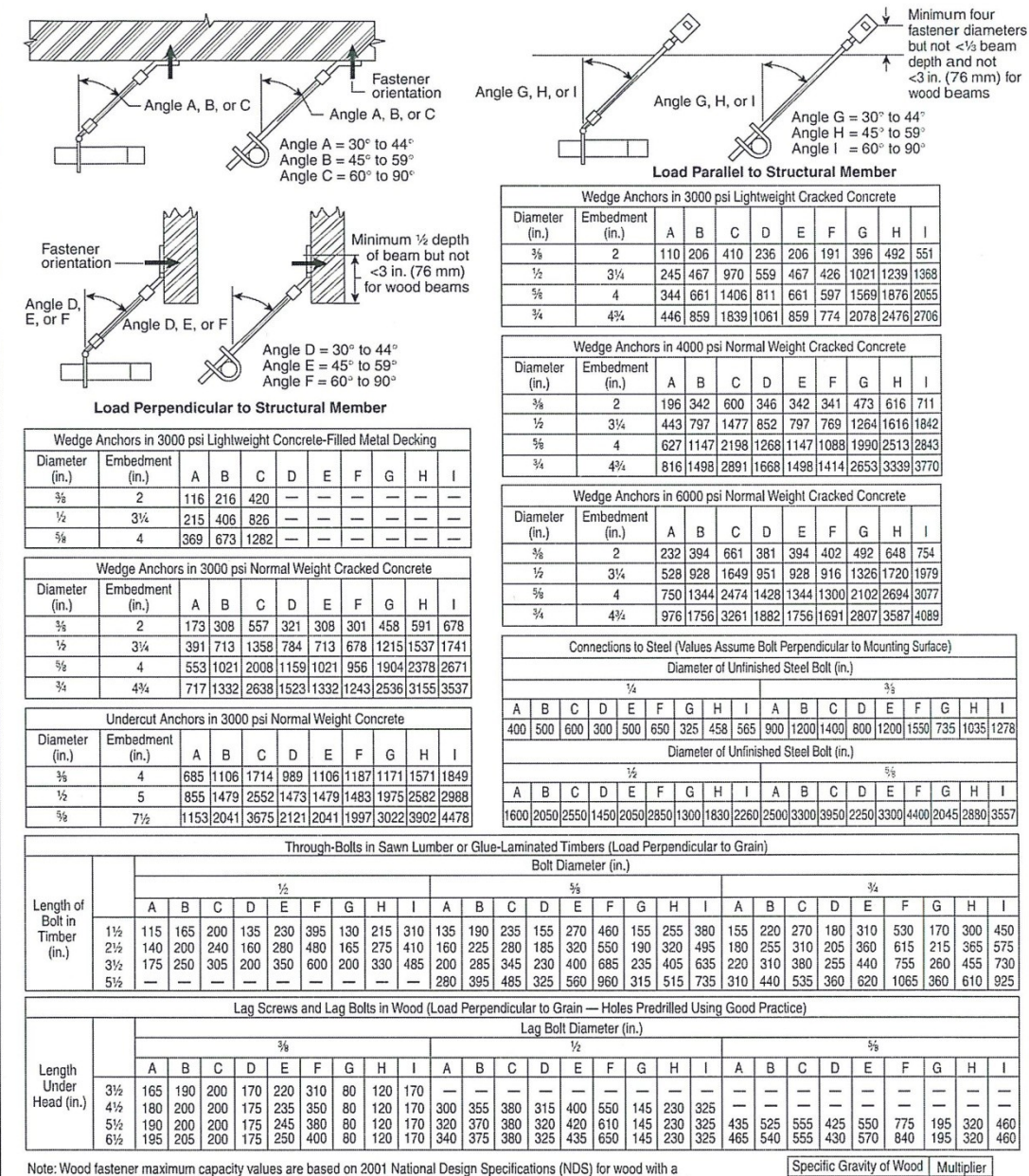
9.3.7.5 A lip on a "C" or "Z" purlin shall not be used as a method of restraint.

9.3.7.6 Where purlins or beams do not provide a secure lip to a restraining strap, the strap shall be through-bolted or secured by a self-tapping screw.

9.3.7.7 In areas where the horizontal force factor exceeds 0.50 W_p , powder-driven studs shall be permitted to attach hangers to the building structure where they are specifically listed for use in areas subject to earthquakes.

Table 9.3.5.8.7(c) Maximum Horizontal Loads for Sway Braces with $l/r = 300$ for Steel Braces with $F_y = 36$ ksi

Brace Shape and Size (in.)	Area (in. ²)	Least Radius of Gyration (r) (in.)	Maximum Length for $l/r = 300$		Max. Horizontal Load (lb)			
					ft	in.	Brace Angle	
			30° to 44° Angle from Vertical	45° to 59° Angle from Vertical	60° to 90° Angle from Vertical			
Pipe Schedule 40	1	0.494	0.421	10	6	412	582	713
	1 1/4	0.669	0.540	13	6	558	788	966
	1 1/2	0.799	0.623	15	6	666	942	1153
	2	1.07	0.787	19	8	892	1261	1544
Angles	1 1/2 x 1 1/2 x 1/4	0.688	0.292	7	3	573	811	993
	2 x 2 x 1/4	0.938	0.391	9	9	782	1105	1354
	2 1/2 x 2 x 1/4	1.06	0.424	10	7	883	1249	1530
	2 1/2 x 2 1/2 x 1/4	1.19	0.491	12	3	992	1402	1718
	3 x 2 1/2 x 1/4	1.31	0.528	13	2	1092	1544	1891
	3 x 3 x 1/4	1.44	0.592	14	9	1200	1697	2078
Rods (all thread)	3/8	0.07	0.075	1	10	58	82	101
	1/2	0.129	0.101	2	6	108	152	186
	5/8	0.207	0.128	3	2	173	244	299
	3/4	0.309	0.157	3	11	258	364	446
	7/8	0.429	0.185	4	7	358	506	619
Rods (threaded at ends only)	3/8	0.11	0.094	2	4	92	130	159
	1/2	0.196	0.125	3	1	163	231	283
	5/8	0.307	0.156	3	10	256	362	443
	3/4	0.442	0.188	4	8	368	521	638
	7/8	0.601	0.219	5	5	501	708	867
Flats	1 1/2 x 1/4	0.375	0.0722	1	9	313	442	541
	2 x 1/4	0.5	0.0722	1	9	417	589	722
	2 x 3/8	0.75	0.1082	2	8	625	884	1083



Note: Wood fastener maximum capacity values are based on 2001 National Design Specifications (NDS) for wood with a specific gravity of 0.35. Values for other types of wood can be obtained by multiplying the above values by the following factors:

For SI values, 1 in. = 25.4 mm.

Specific Gravity of Wood	Multiplier
0.36 thru 0.49	1.17
0.50 thru 0.65	1.25
0.66 thru 0.73	1.50

FIGURE 9.3.5.9.1 Maximum Loads for Various Types of Structures and Maximum Loads for Various Types of Fasteners to Structures.

Table 9.3.5.10.3 Allowable Horizontal Load on Brace Assemblies Based on the Weakest Component of the Brace Assembly

Brace Angle	Allowable Horizontal Load
30 to 44 degrees from vertical	Listed load rating divided by 2,000
45 to 59 degrees from vertical	Listed load rating divided by 1,414
60 to 89 degrees from vertical	Listed load rating divided by 1,155
90 degrees from vertical	Listed load rating

Table 9.3.6.4(a) Maximum Spacing (ft) of Steel Branch Line Restraints (ft)

Pipe (in.)	Seismic Coefficient (C_p)		
	$C_p \leq 0.50$	$0.5 < C_p \leq 0.71$	$C_p > 0.71$
1	43	36	26
1 1/4	46	39	27
1 1/2	49	41	29
2	53	45	31

Table 9.3.6.4(b) Maximum Spacing (ft) of CPVC and Copper Branch Line Restraints

Pipe (in.)	Seismic Coefficient (C_p)		
	$C_p \leq 0.50$	$0.5 < C_p \leq 0.71$	$C_p > 0.71$
3/4	31	26	18
1	34	28	20
1 1/4	37	31	22
1 1/2	40	34	24
2	45	38	27

Chapter 10 Underground Piping

10.1* Piping Materials. [24:10.1]

10.1.1* Listing. Piping shall be listed for fire protection service or shall comply with the standards in Table 10.1.1. [24:10.1.1]

10.1.2 Steel Pipe. Steel piping shall not be used for general underground service unless specifically listed for such service. [24:10.1.2]

10.1.3 Steel Pipe Used with Fire Department Connections. Where externally coated and wrapped and internally galvanized, steel pipe shall be permitted to be used between the check valve and the outside hose coupling for the fire department connection. [24:10.1.3]

10.1.4* Pipe Type and Class. The type and class of pipe for a particular underground installation shall be determined through consideration of the following factors:

- (1) Fire resistance of the pipe
- (2) Maximum system working pressure
- (3) Depth at which the pipe is to be installed
- (4) Soil conditions
- (5) Corrosion
- (6) Susceptibility of pipe to other external loads, including earth loads, installation beneath buildings, and traffic or vehicle loads

[24:10.1.4]

10.1.5* Working Pressure. Piping, fittings, and other system components shall be rated for the maximum system working pressure to which they are exposed but shall not be rated at less than 150 psi (10.4 bar). [24:10.1.5]

10.1.6* Lining of Buried Pipe. [24:10.1.6]

10.1.6.1 Unless the requirements of 10.1.6.2 are met, all ferrous metal pipe shall be lined in accordance with the applicable standards in Table 10.1.1. [24:10.1.6.1]

10.1.6.2 Steel pipe utilized in fire department connections and protected in accordance with the requirements of 10.1.3 shall not be additionally required to be lined. [24:10.1.6.2]

10.2 Fittings. [24:10.2]

10.2.1 Standard Fittings. Fittings shall meet the standards in Table 10.2.1(a) or shall be in accordance with 10.2.2. In addition to the standards in Table 10.2.1(b), CPVC fittings shall also be in accordance with 10.2.2 and with the portions of the ASTM standards specified in Table 10.2.1(b) that apply to fire protection service. [24:10.2.1]

10.2.2 Special Listed Fittings. Other types of fittings investigated for suitability in automatic sprinkler installations and listed for this service, including, but not limited to, polybutylene, CPVC, and steel differing from that provided in Table 10.2.1(a), shall be permitted when installed in accordance with their listing limitations, including installation instructions. [24:10.2.2]

10.2.3 Pressure Limits. Listed fittings shall be permitted for system pressures as specified in their listings, but not less than 150 psi (10 bar). [24:10.2.3]

10.2.4* Buried Joints. Joints shall be approved. [24:10.2.4]

10.2.5* Buried Fittings. Fittings shall be of an approved type with joints and pressure class ratings compatible with the pipe used. [24:10.2.5]

10.3 Joining of Pipe and Fittings. [24:10.3]

10.3.1 Threaded Pipe and Fittings. All threaded steel pipe and fittings shall have threads cut in accordance with ASME B1.20.1, *Pipe Threads, General Purpose (Inch)*. [24:10.3.1]

10.3.2 Groove Joining Methods. Pipes joined with grooved fittings shall be joined by a listed combination of fittings, gaskets, and grooves. [24:10.3.2]

10.3.3 Brazed and Pressure Fitting Methods. Joints for the connection of copper tube shall be brazed or joined using pressure fittings as specified in Table 10.2.1(a). [24:10.3.3]

Appendix B

UCSF FIRE SPRINKLER PIPING PLAN

A brief description of the UCSF fire sprinkler piping plan was presented in Section 5. The detailed original drawing of the UCSF fire sprinkler piping plan is presented in this appendix.

System Layout

Section 1

95.5600

Section 4

Section 4

1.6934

1.6934

Section 2

97.1866

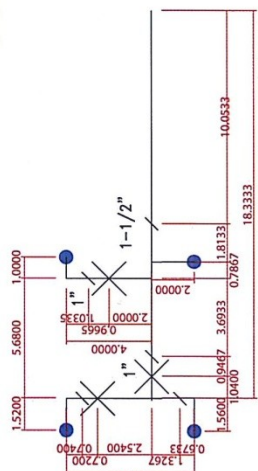
153.6533

Section 3

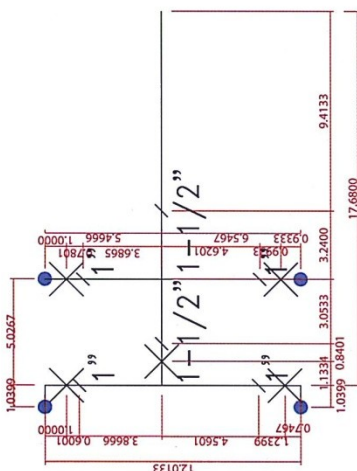
N

0 $\sqrt{2}$ 1
0 1 $\sqrt{2}$
SCALE 1/8 = 1'-0"

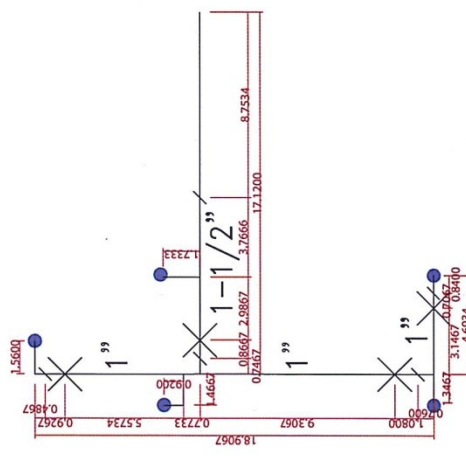
Section 1



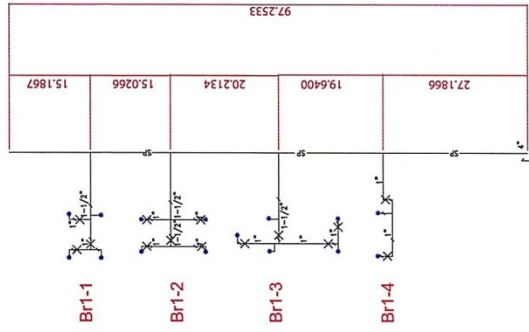
Br1-1



Br1-2



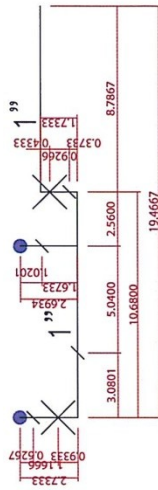
Br1-3



Br1-1

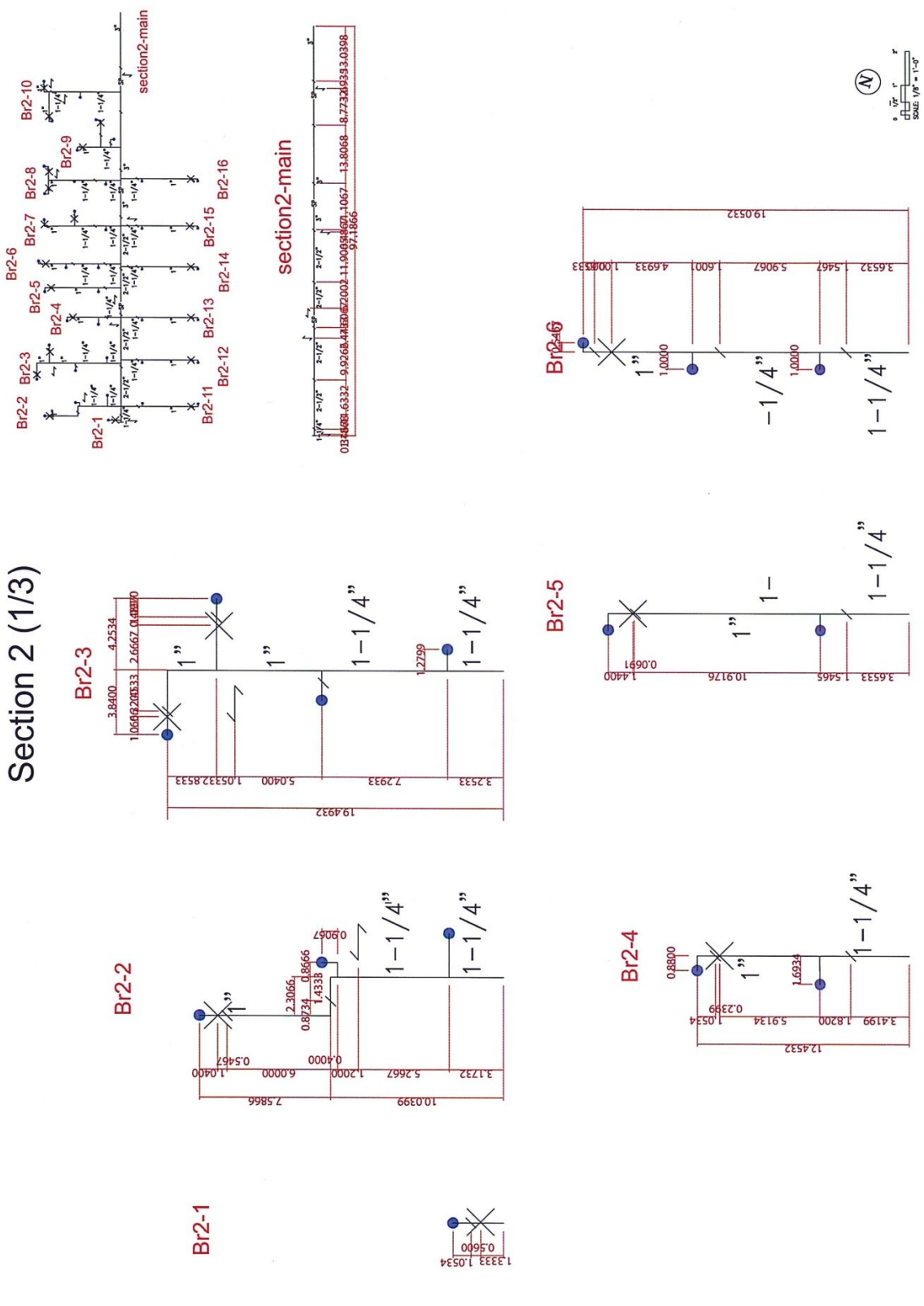
Br1-2

Br1-3

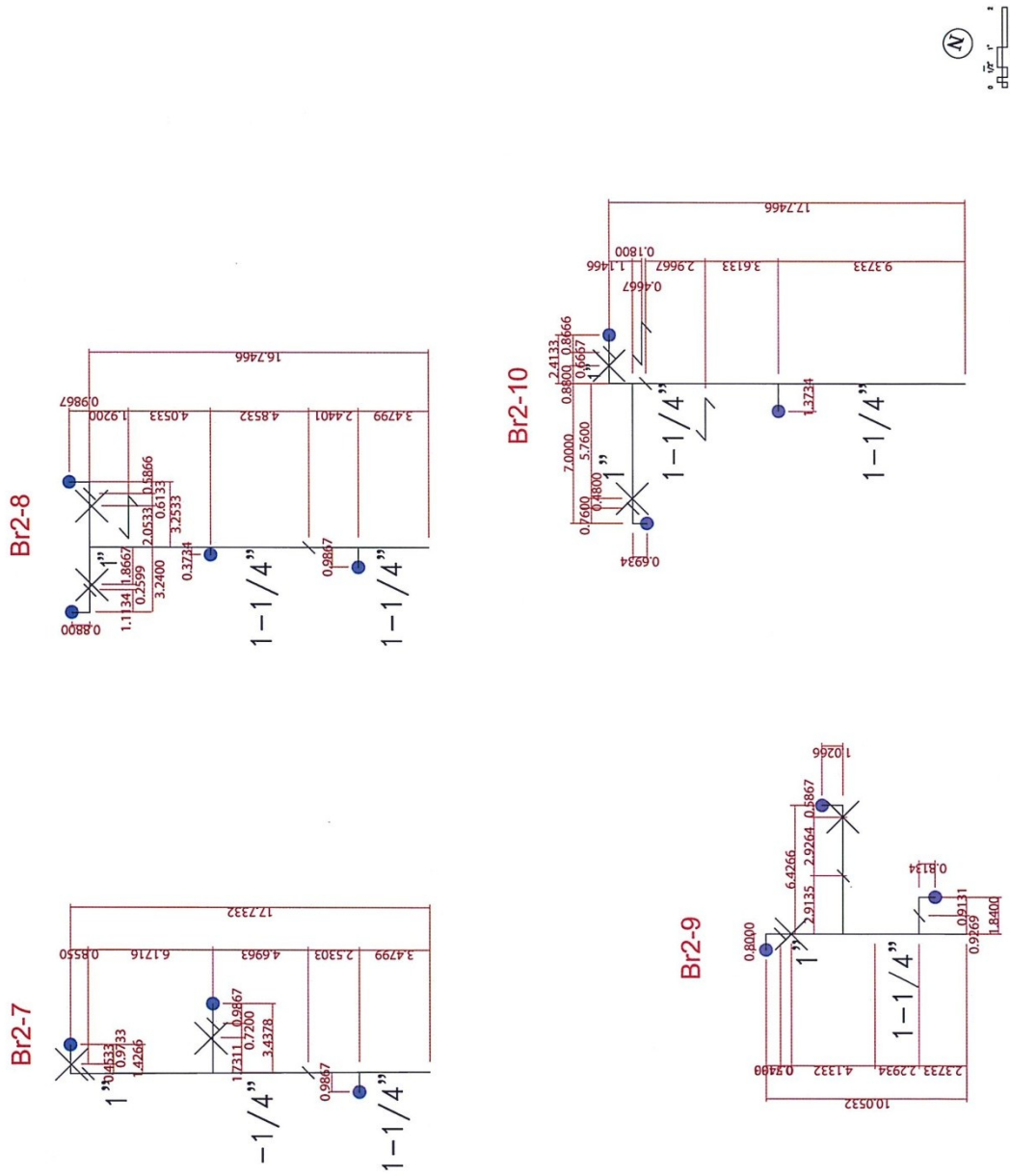


Br1-4

Section 2 (1/3)

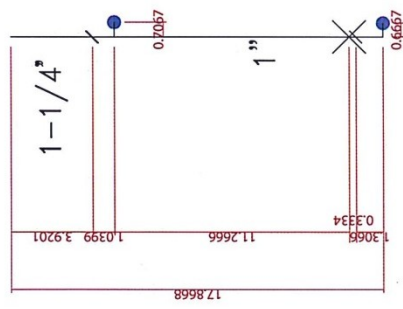


Section 2 (2/3)

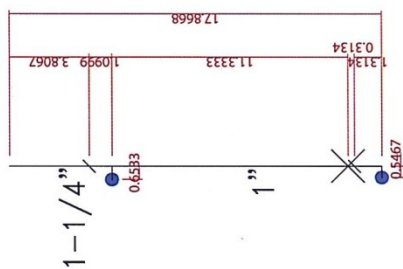


Section 2 (3/3)

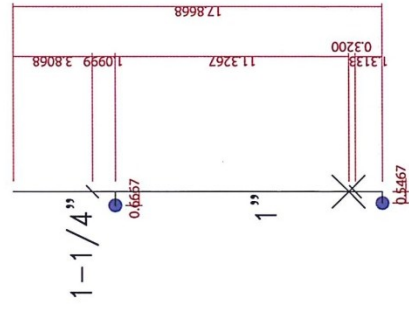
Br2-11



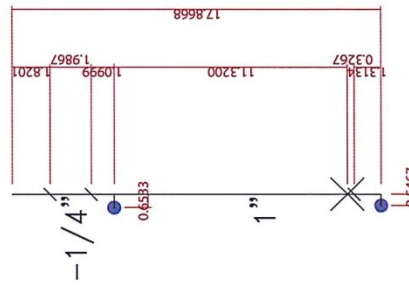
Br2-12



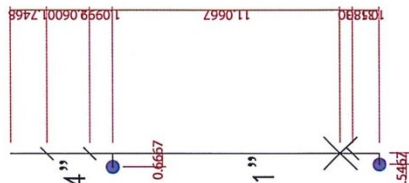
Br2-13



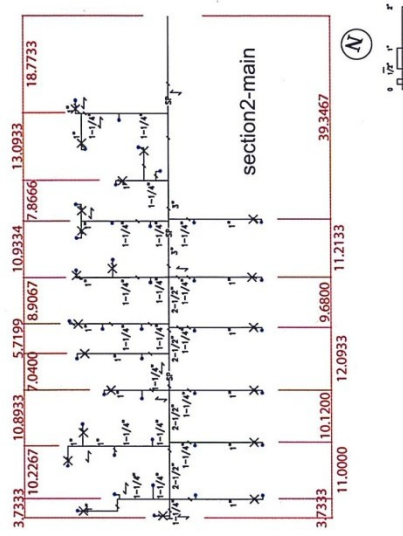
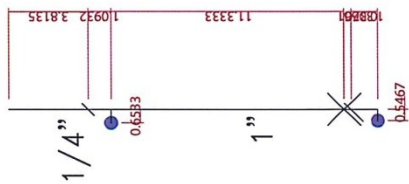
Br2-14



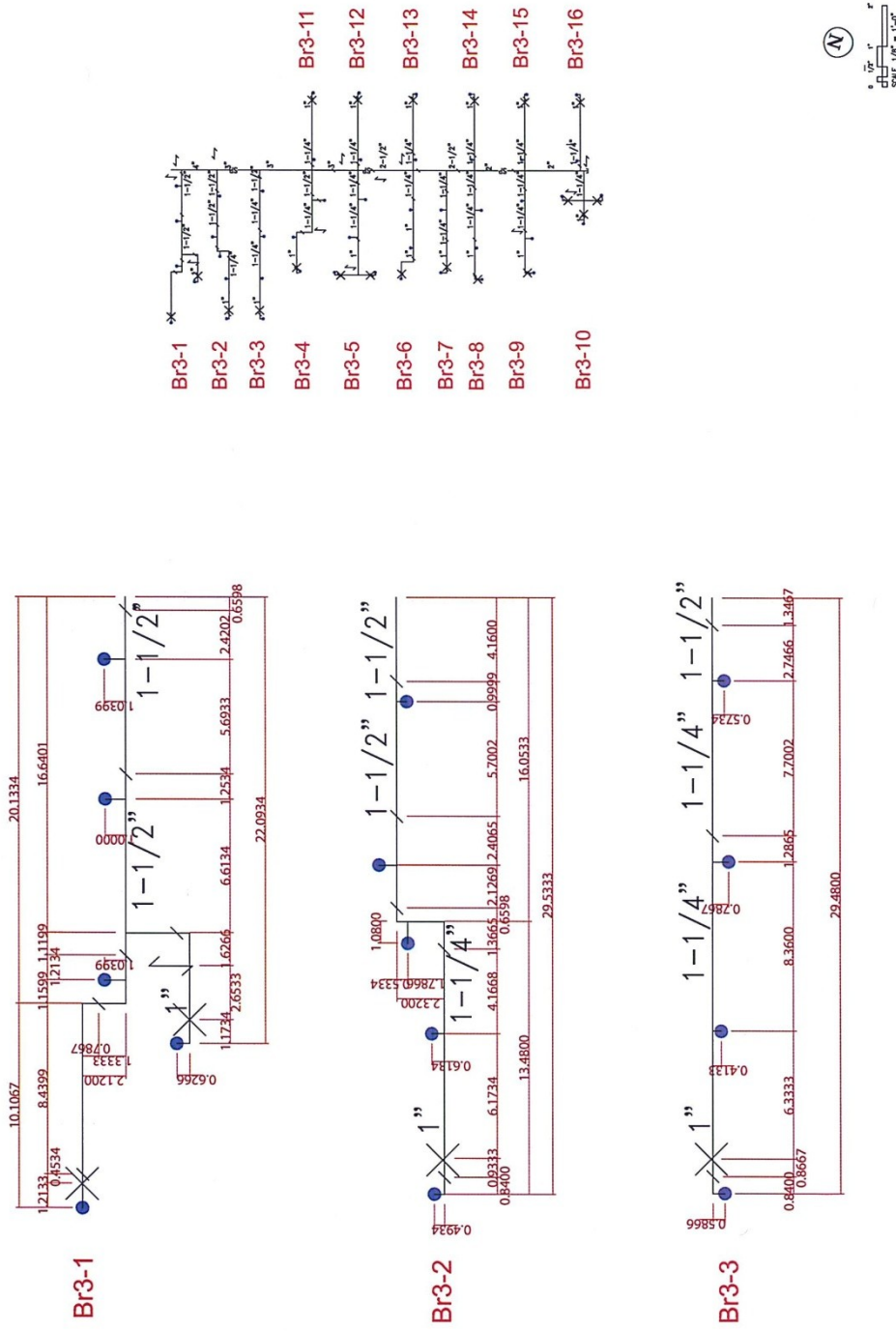
Br2-15



Br2-16

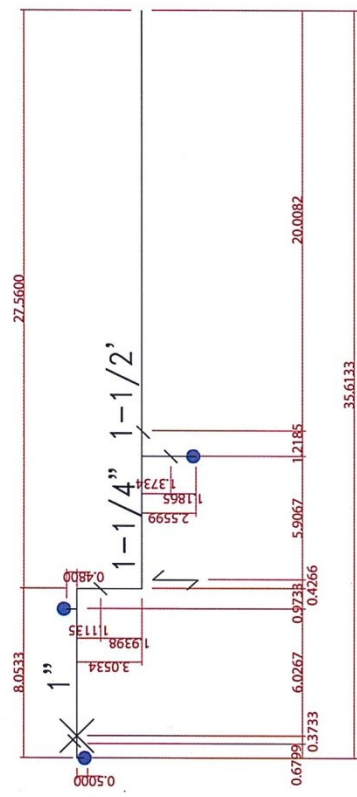


Section 3 (1/4)

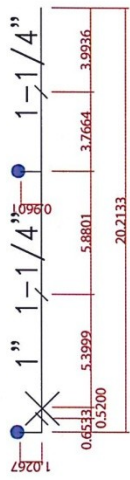


Section 3 (2/4)

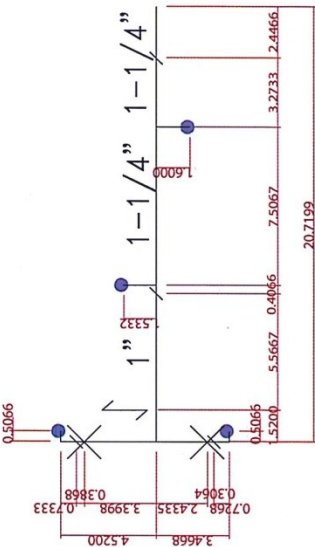
Br3-4



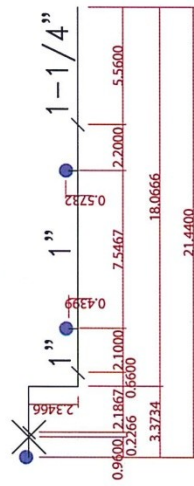
Br3-7



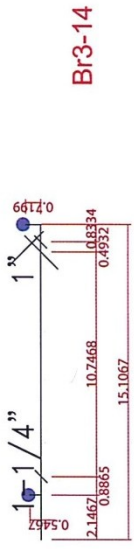
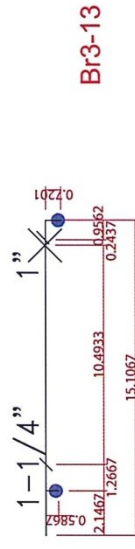
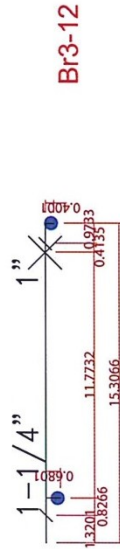
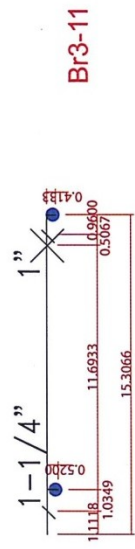
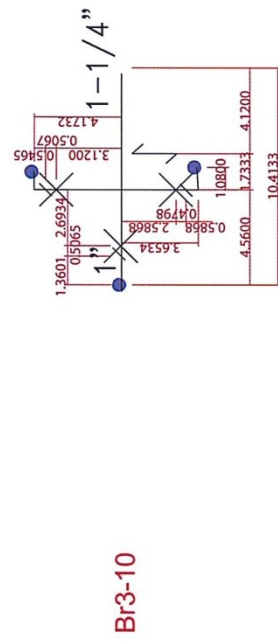
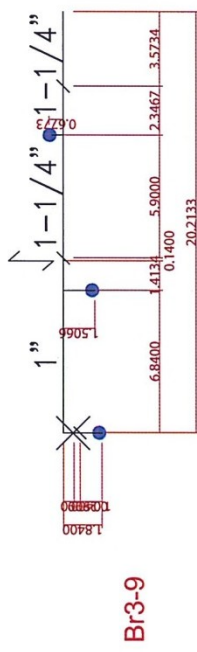
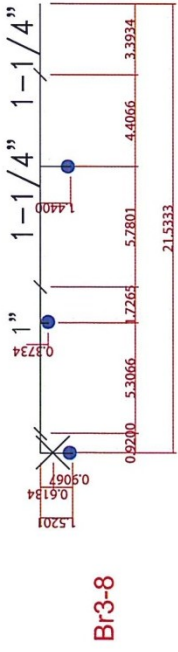
Br3-5



Br3-6

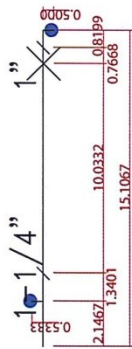


Section 3 (3/4)

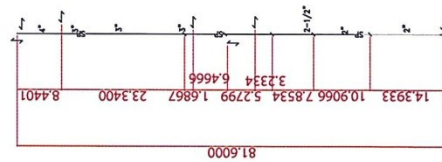


Section 3 (4/4)

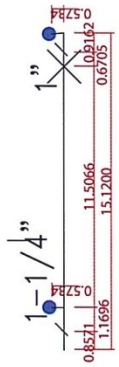
Br3-15



section3-main

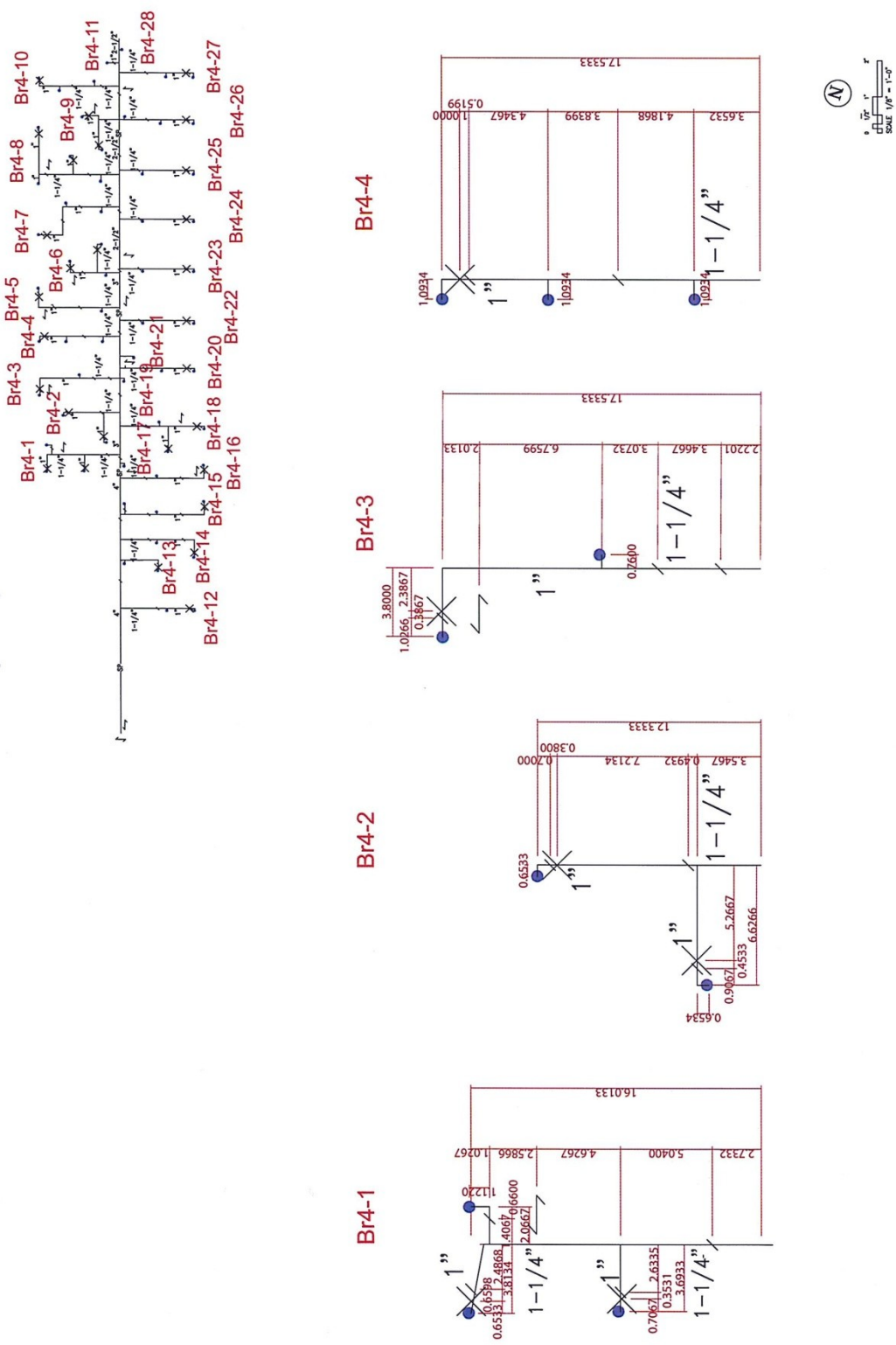


Br3-16



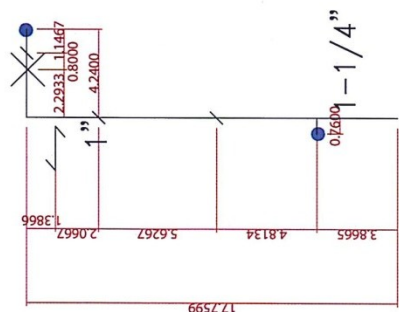
78.9466	11.5999	9.8800	8.3600	9.0132	10.2400	10.9067	5.5065	9.5334	10.2400	10.9067	9.0132	27.5334	27.5334	10.9067	9.8800	11.5999
---------	---------	--------	--------	--------	---------	---------	--------	--------	---------	---------	--------	---------	---------	---------	--------	---------

Section 4 (1/5)

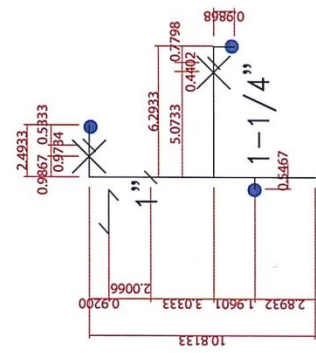


Section 4 (2/5)

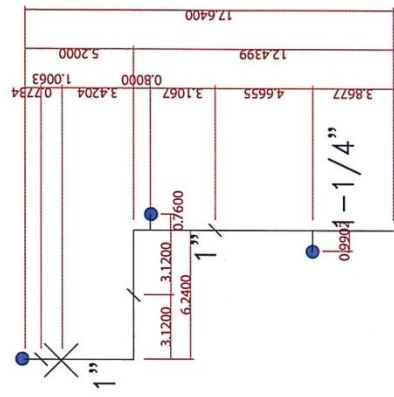
Br4-5



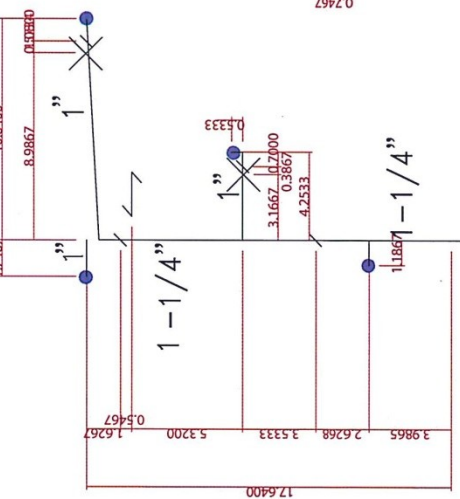
Br4-6



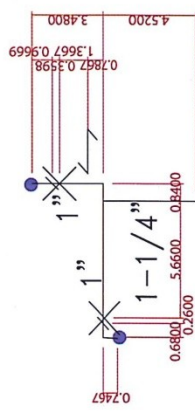
Br4-7



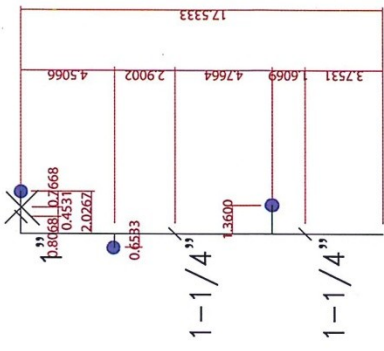
Br4-8



Br4-9

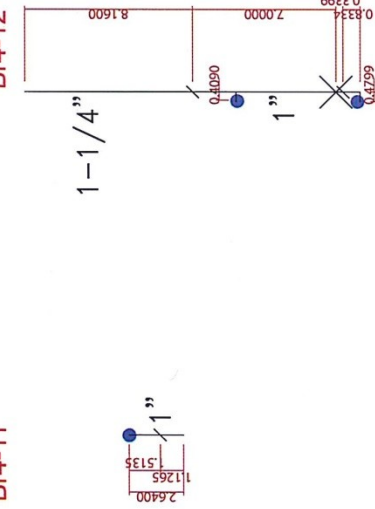


Br4-10

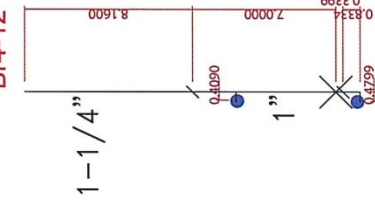


Section 4 (3/5)

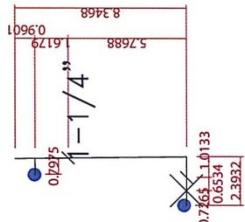
Br4-11



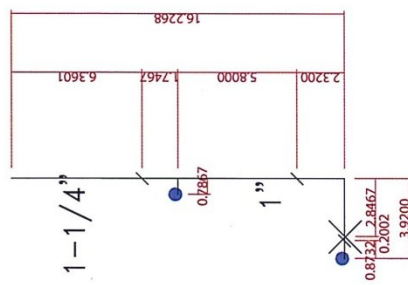
Br4-12



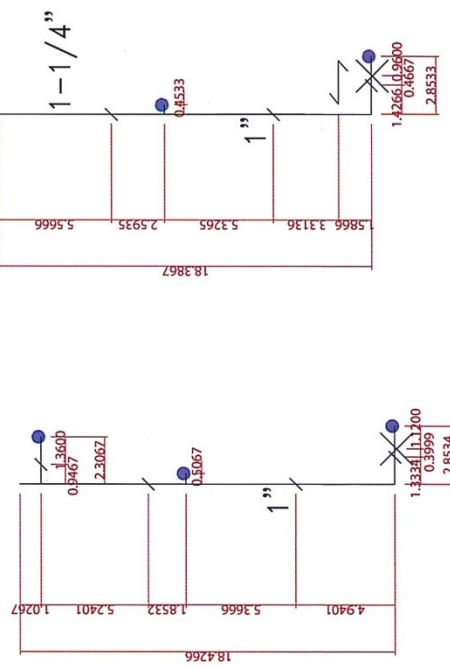
Br4-13



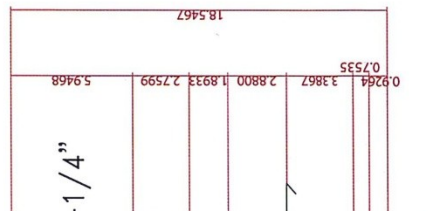
Br4-14



Br4-15



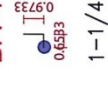
Br4-16



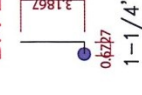
Br4-17



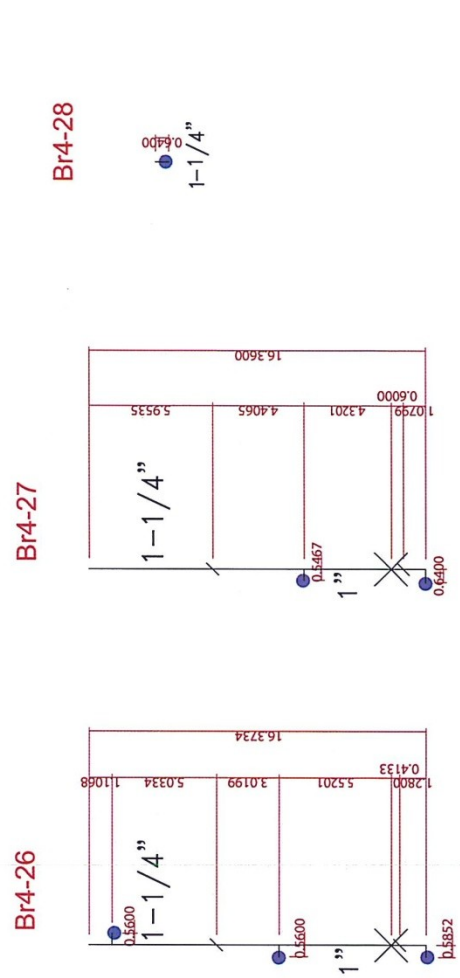
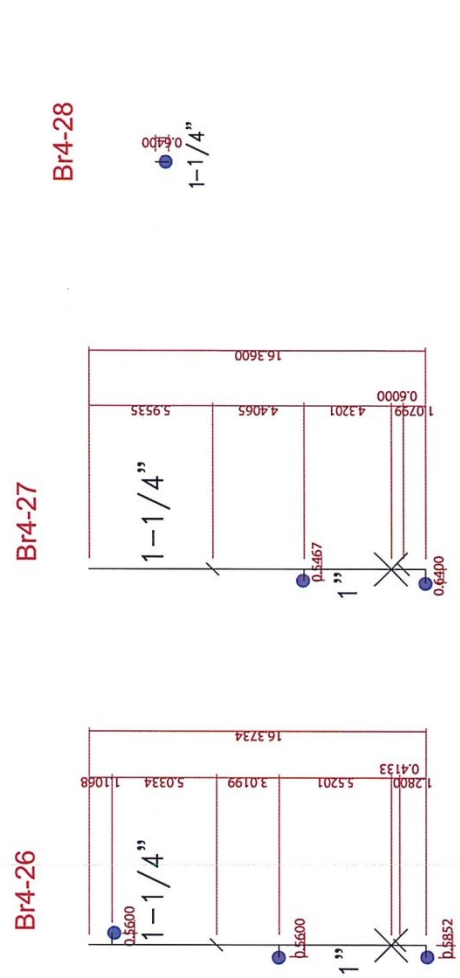
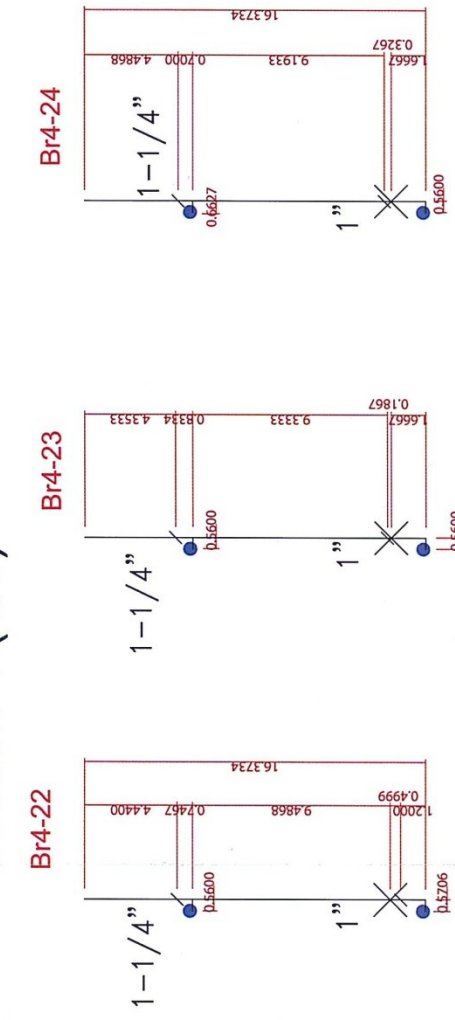
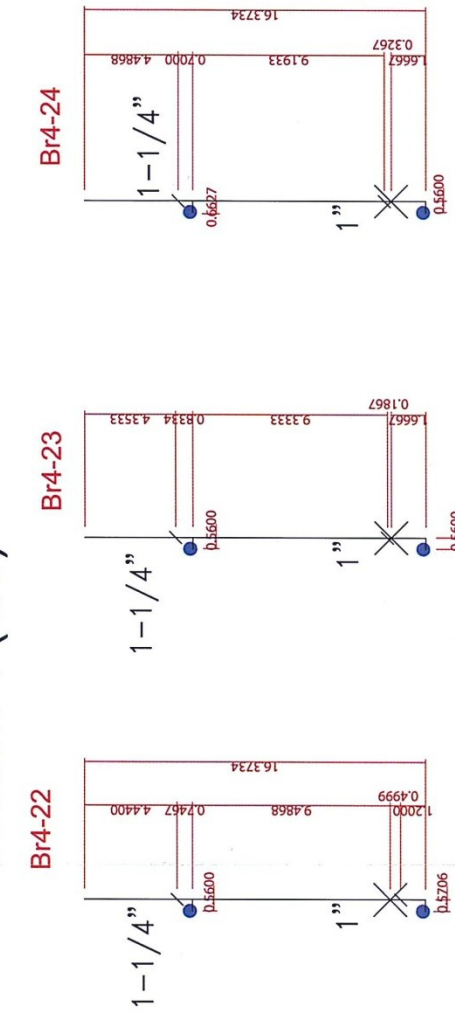
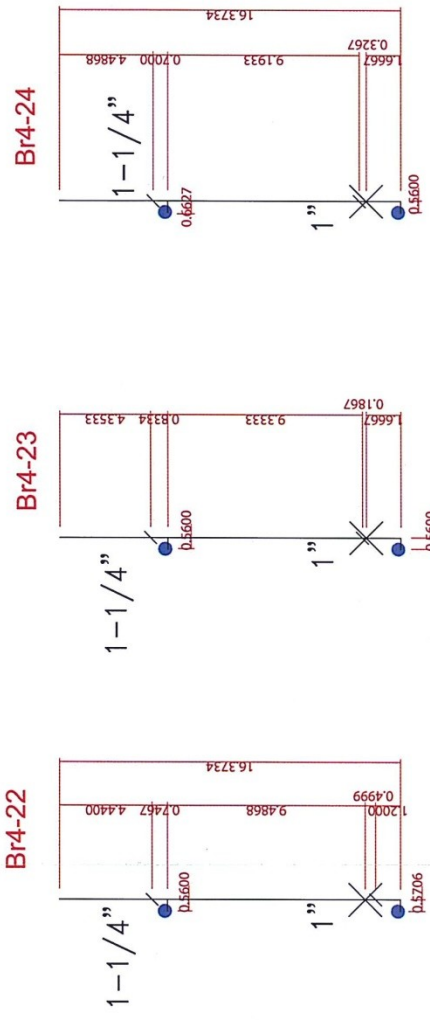
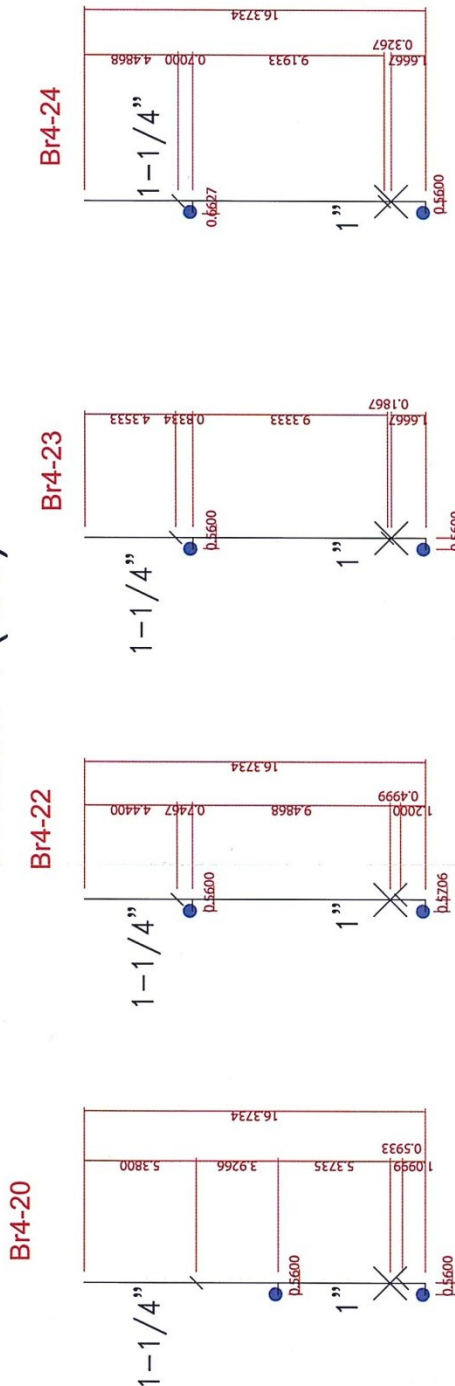
Br4-19



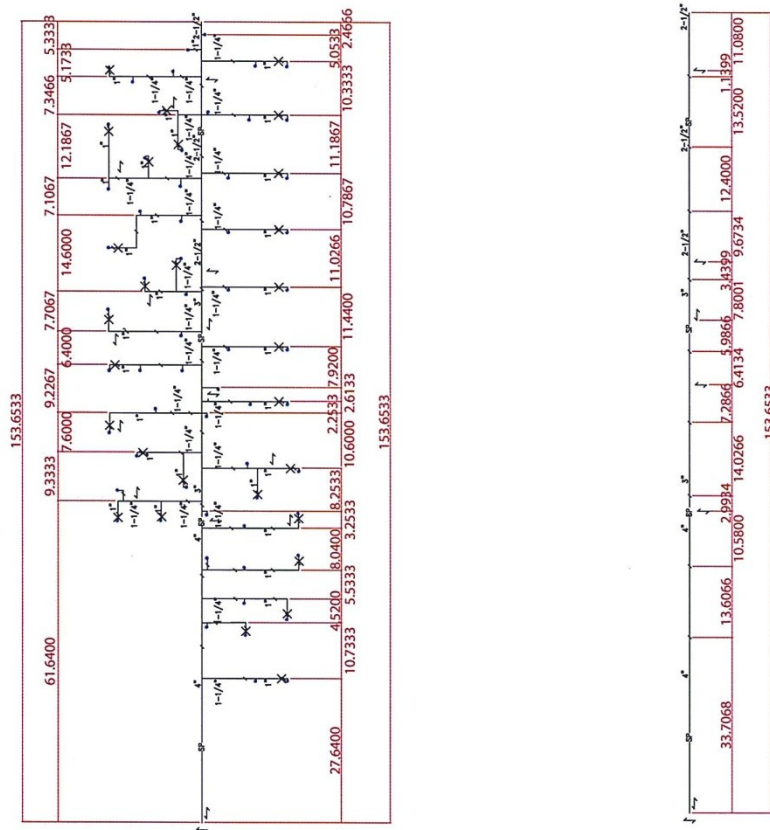
Br4-21



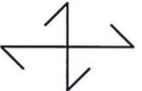
Section 4 (4/5)



Section 4 (5/5)



Layout Legend

Legend	Note
	Sprinkler pipe
	Existing Fire Sprinkler
	Existing Hanger
	Existing 2-ay Seismic Brace
	Existing 4-way seismic brace
	New wire restraint. Transverse sway braces may be used in lieu of wire restraints.
	New support and bracing in accordance with the structural drawings.

-Pipe: ASTM A53 GRADE B. SCHEDULE 40. (1" to 4")

-UNITS: FEET (LENGTH)

Appendix C

PSDMs OF FIRE SPRINKLER PIPING SYSTEMS

PSDMs of 2.5in pipe joints and wire restrainers were addressed in Section 5. The rest of the PSDMs are illustrated in this appendix.

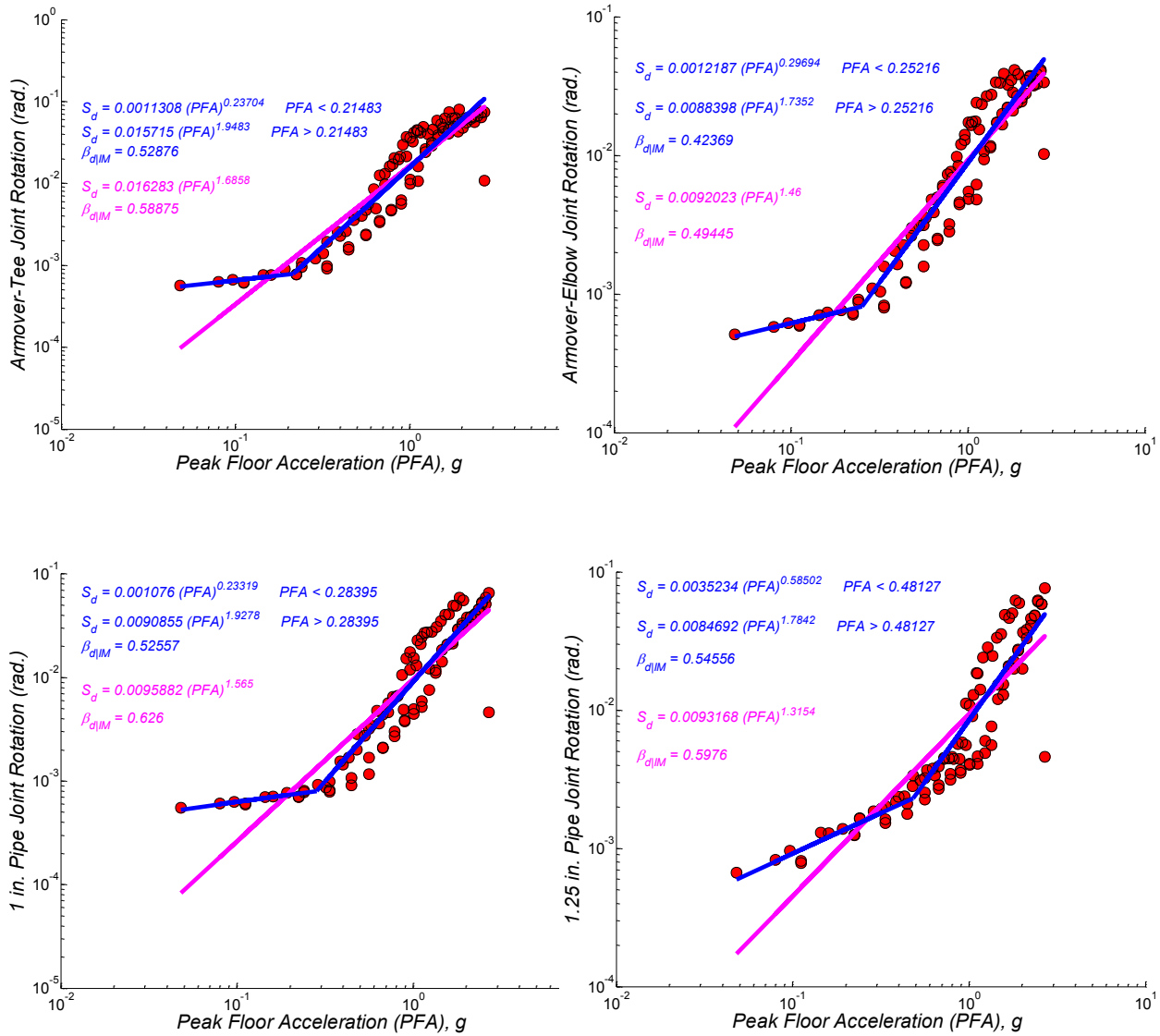


Figure C- 1 PSDMs for Pipe Components - Case1

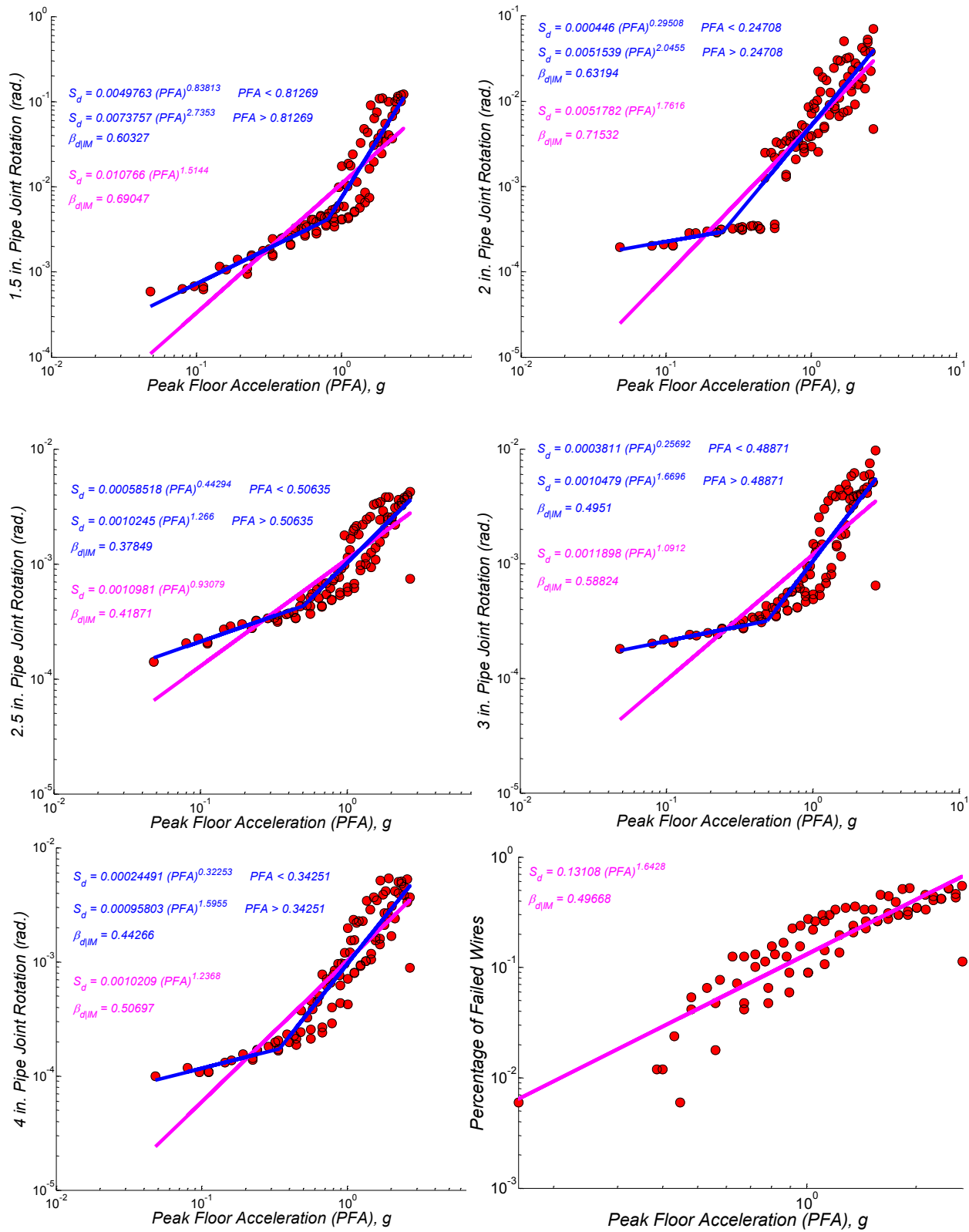


Figure C- 2 PSDMs for Pipe Components - Case 1

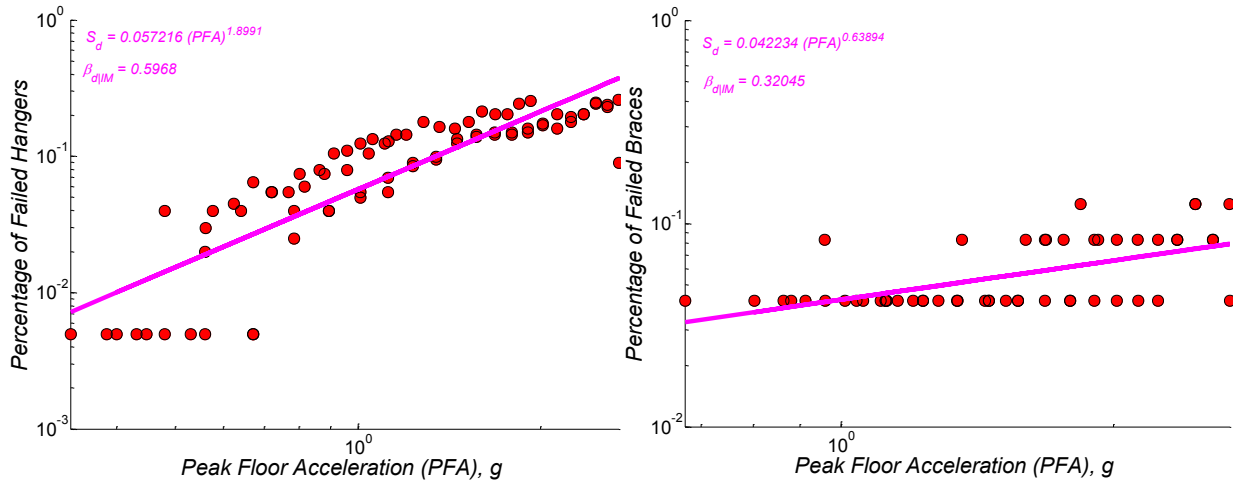


Figure C- 3 PSDMs for Pipe Components - Case 1

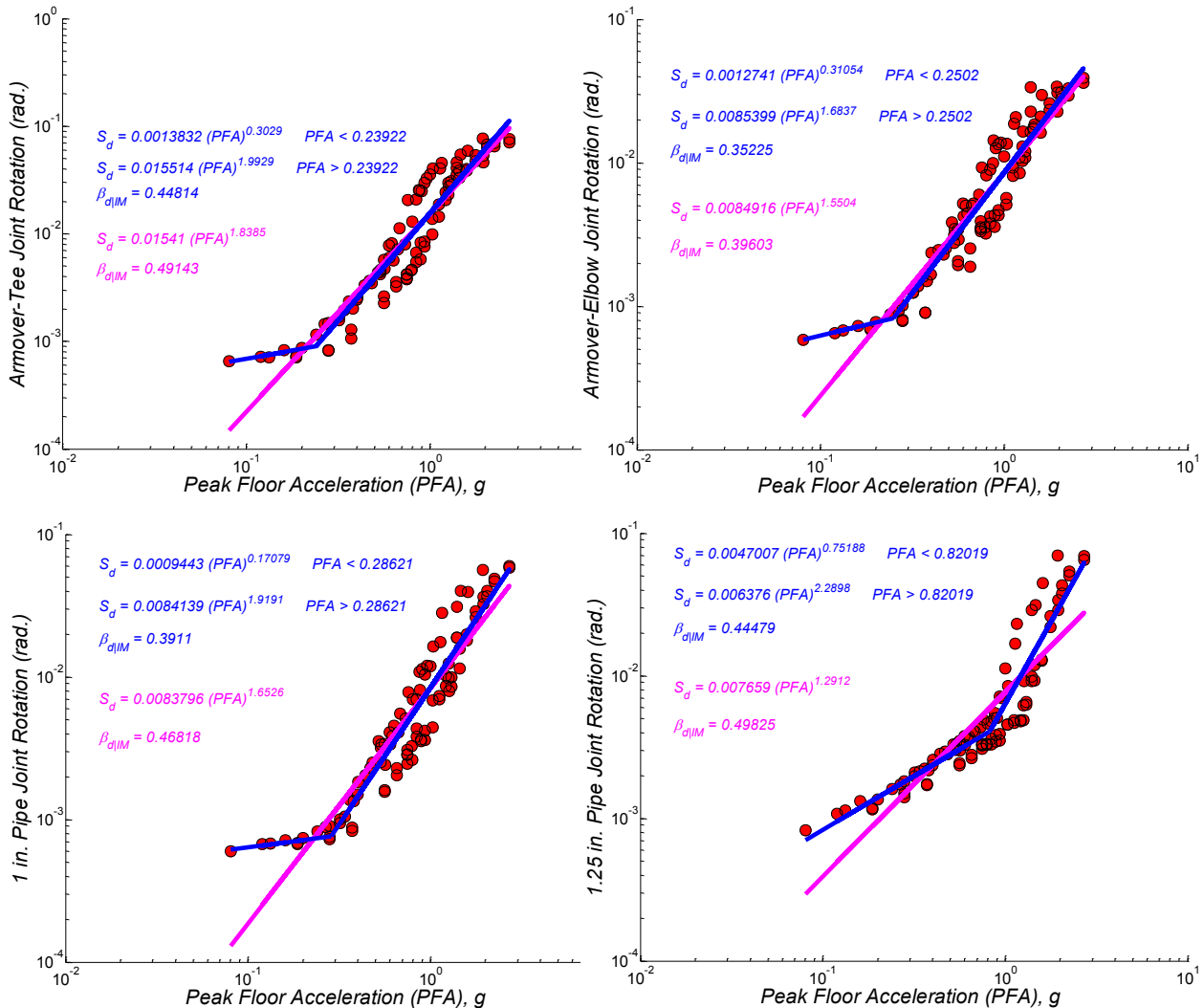


Figure C- 4 PSDMs for Pipe Components - Case 2

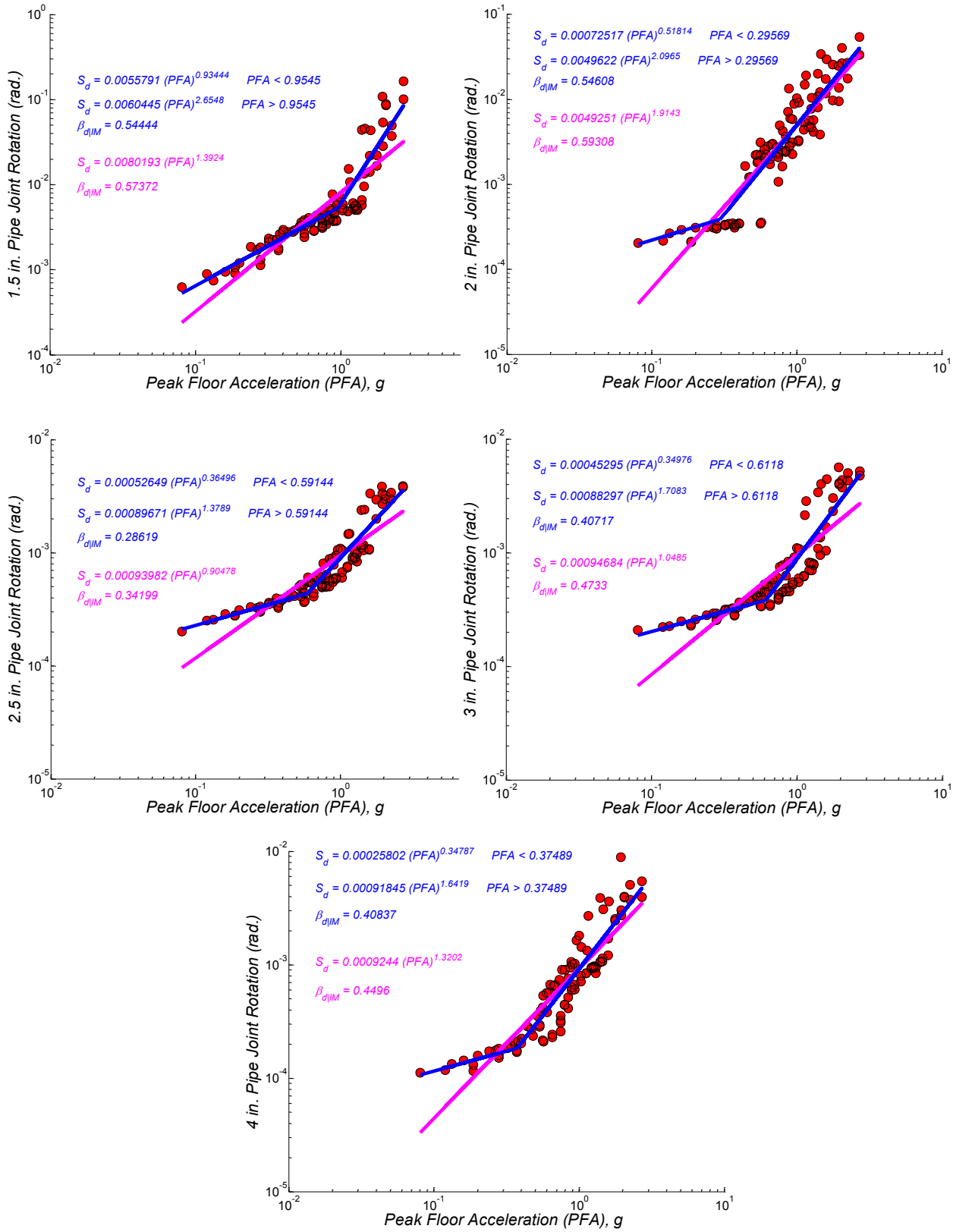


Figure C- 5 PSDMs for Pipe Components - Case 2

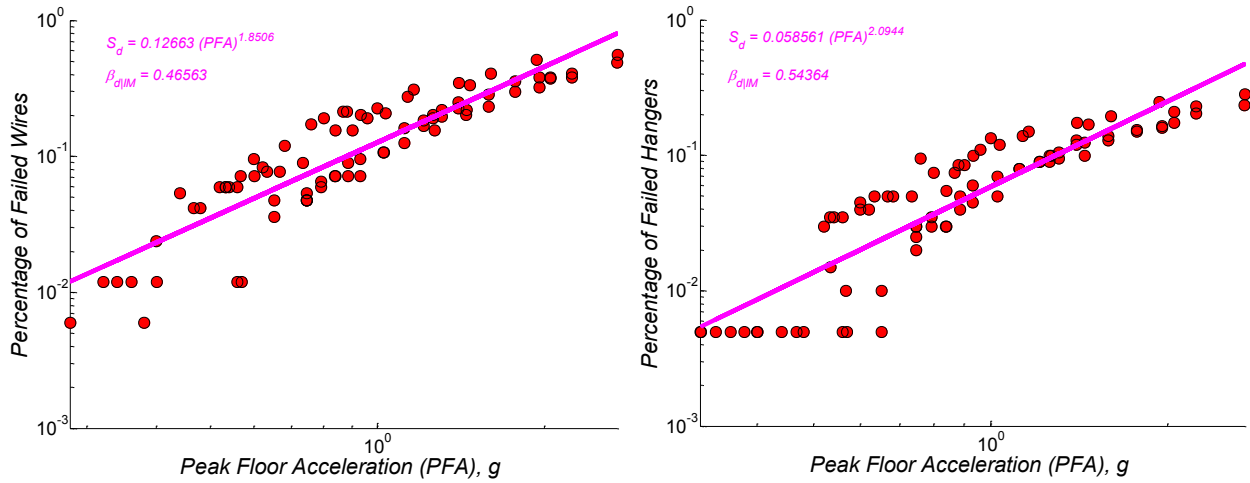


Figure C- 6 PSDMs for Pipe Components - Case 2

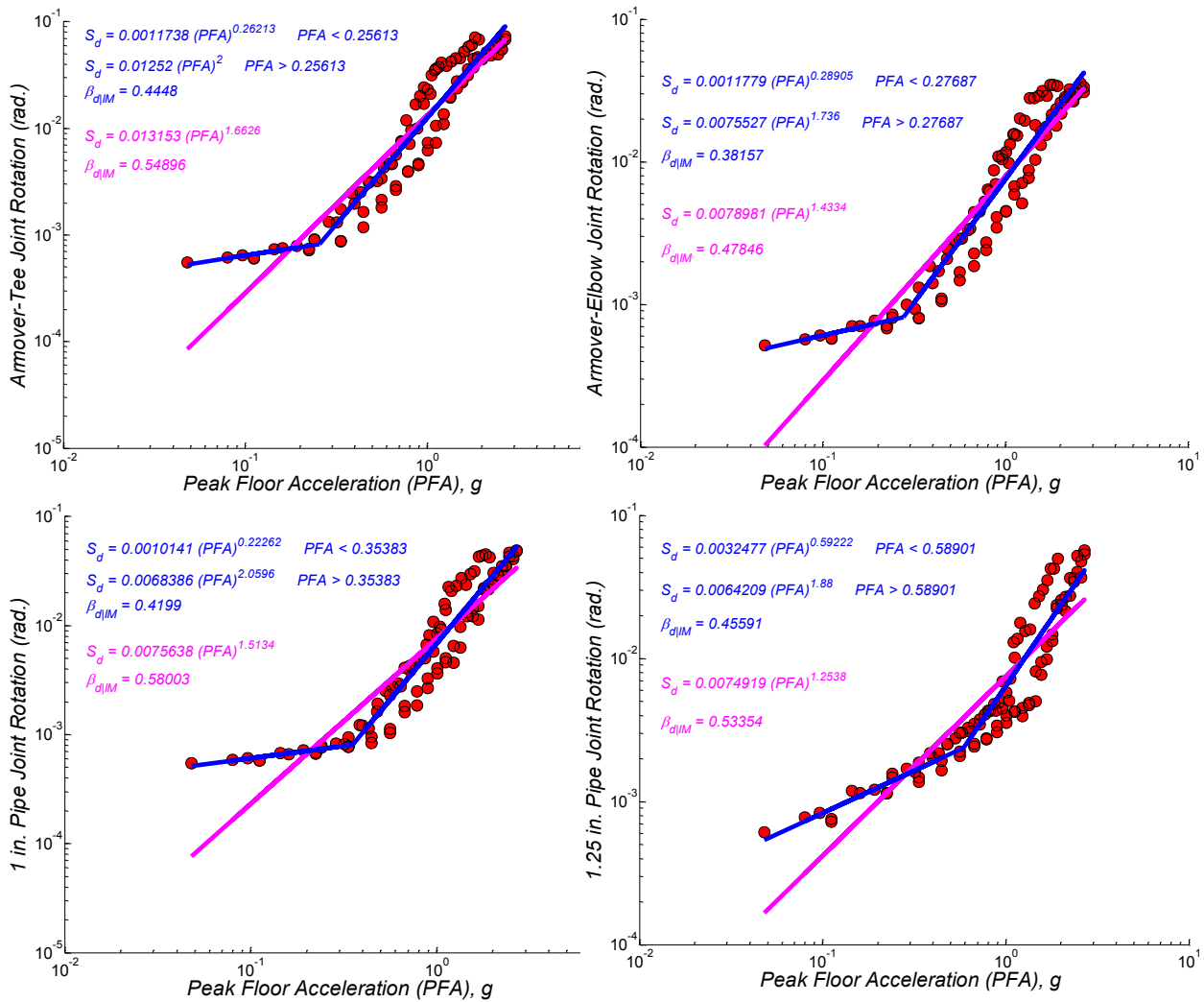


Figure C- 7 PSDMs for Pipe Components - Case 3

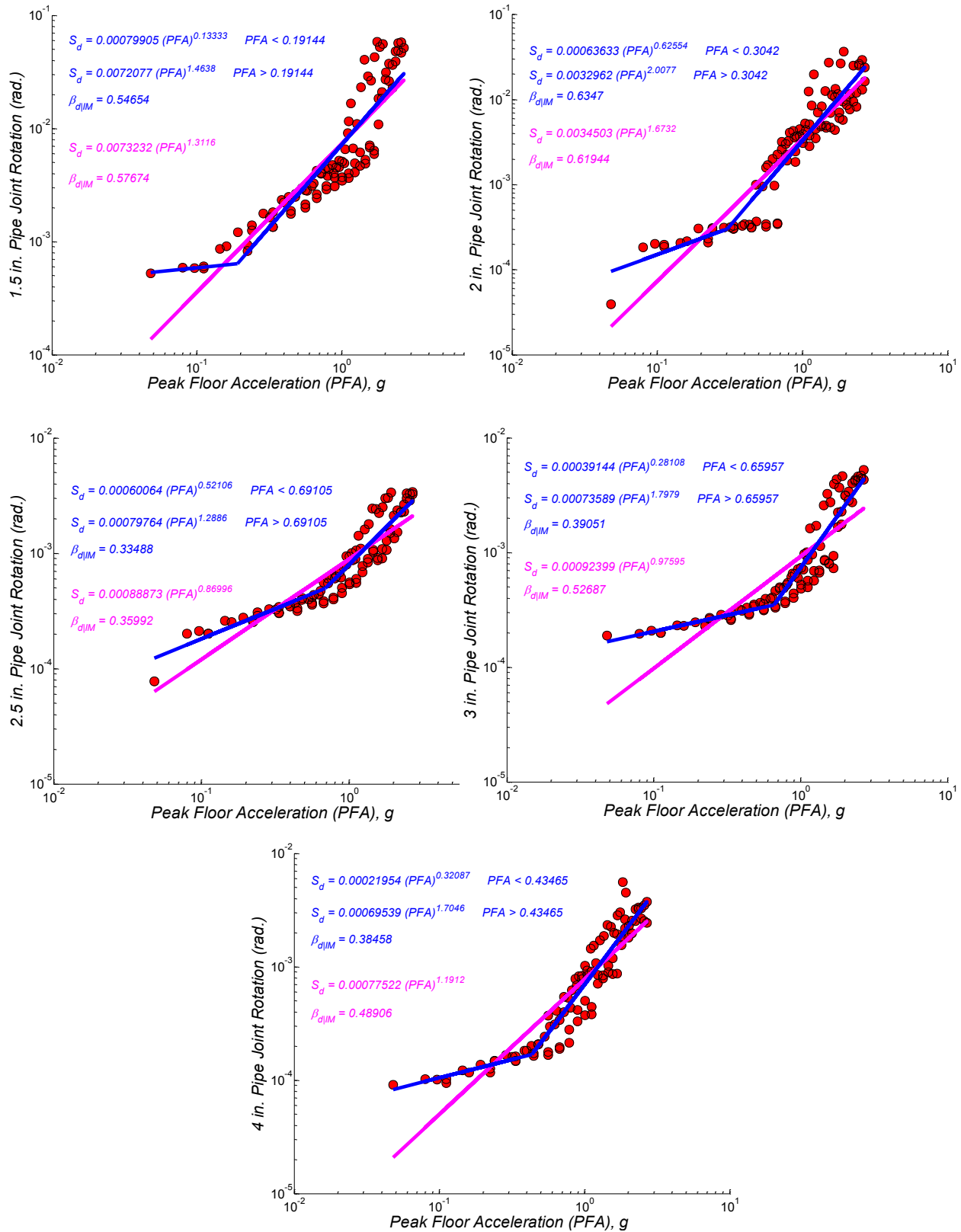


Figure C-8 PSDMs for Pipe Components - Case 3

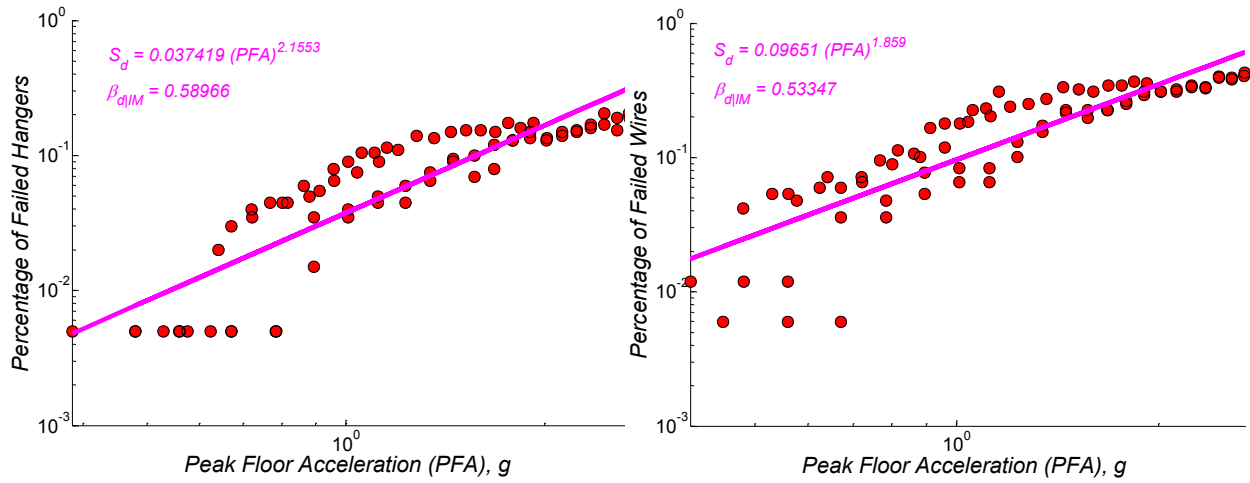


Figure C- 9 PSDMs for Pipe Components - Case 3

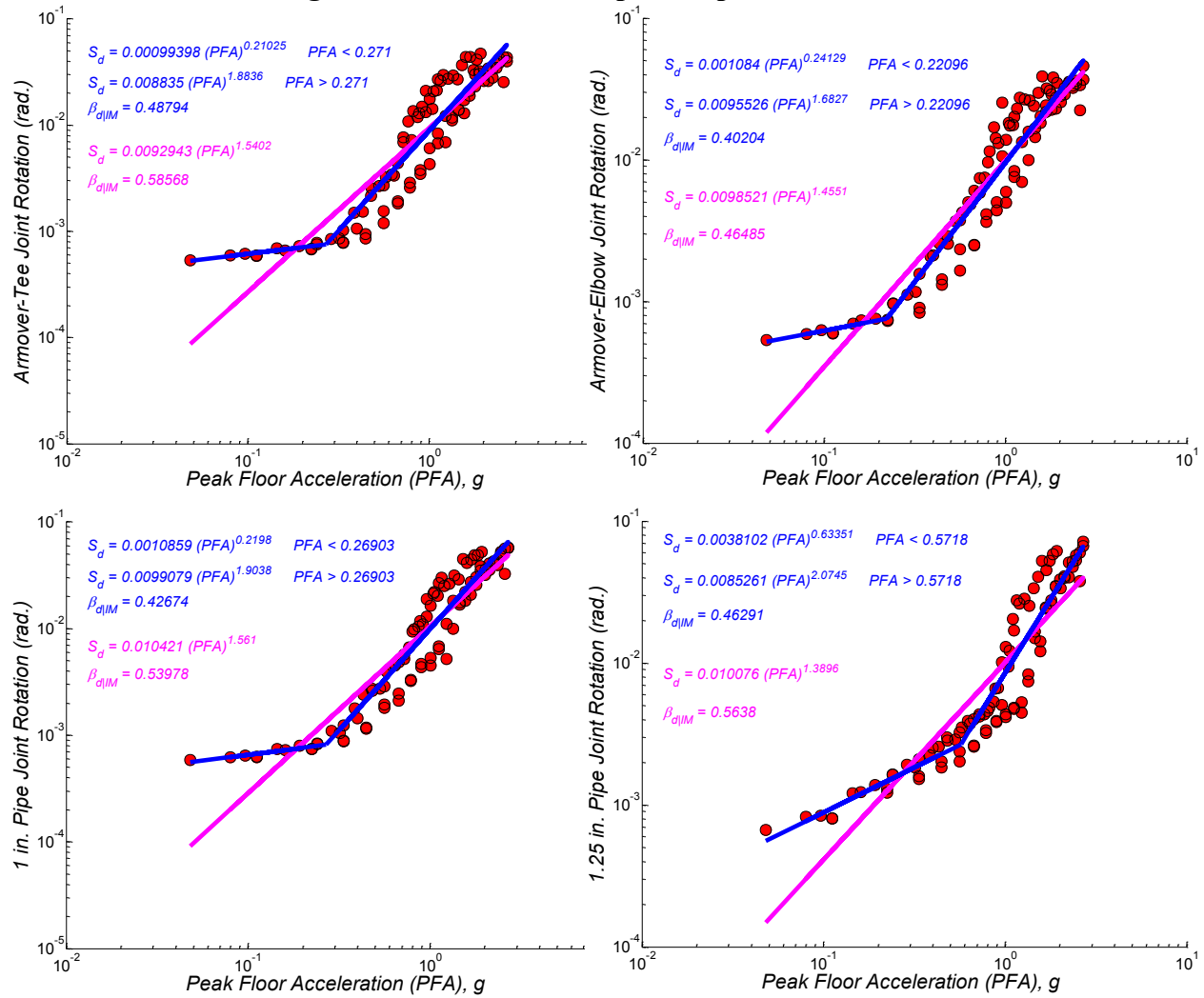


Figure C- 10 PSDMs for Pipe Components - Case 4

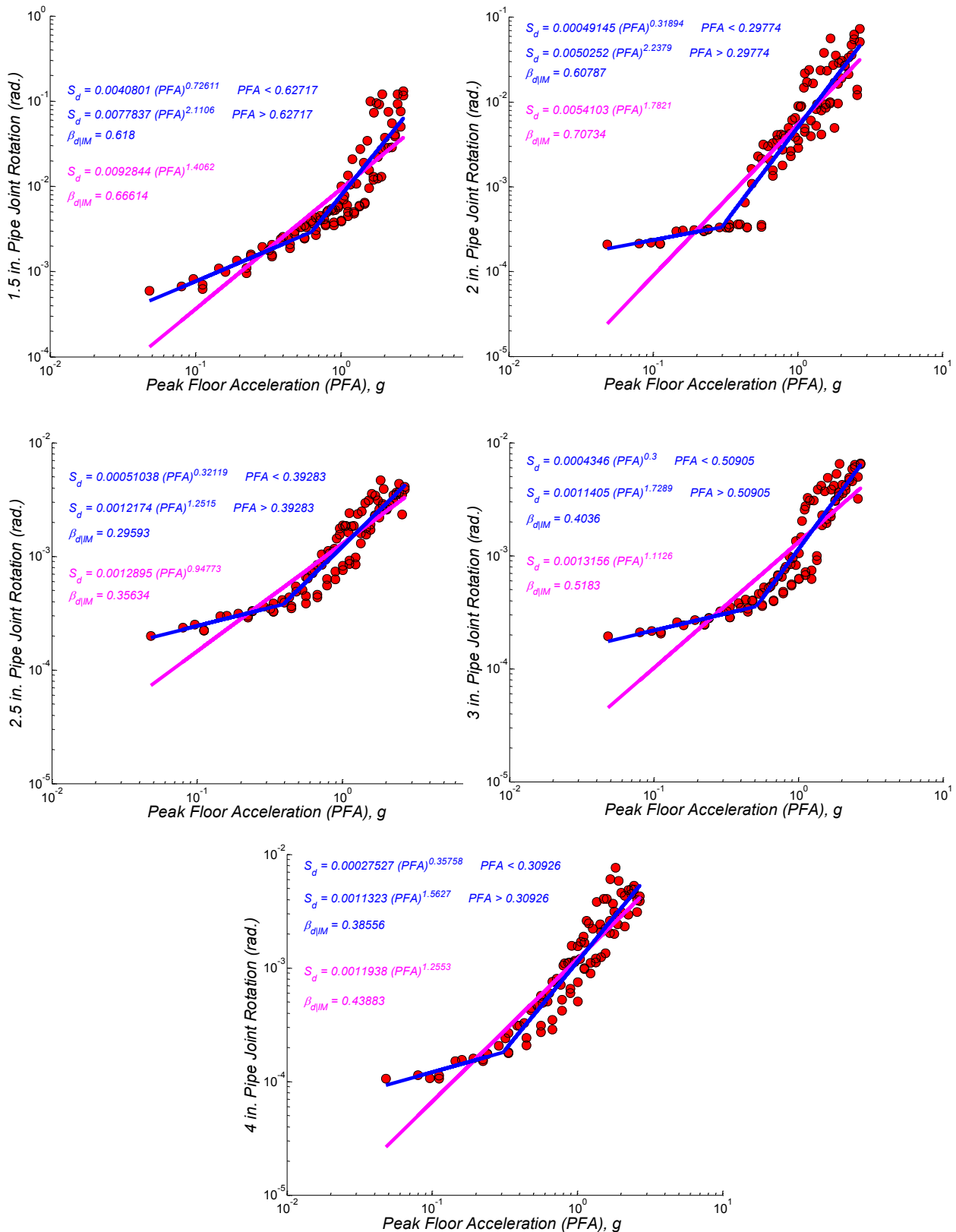
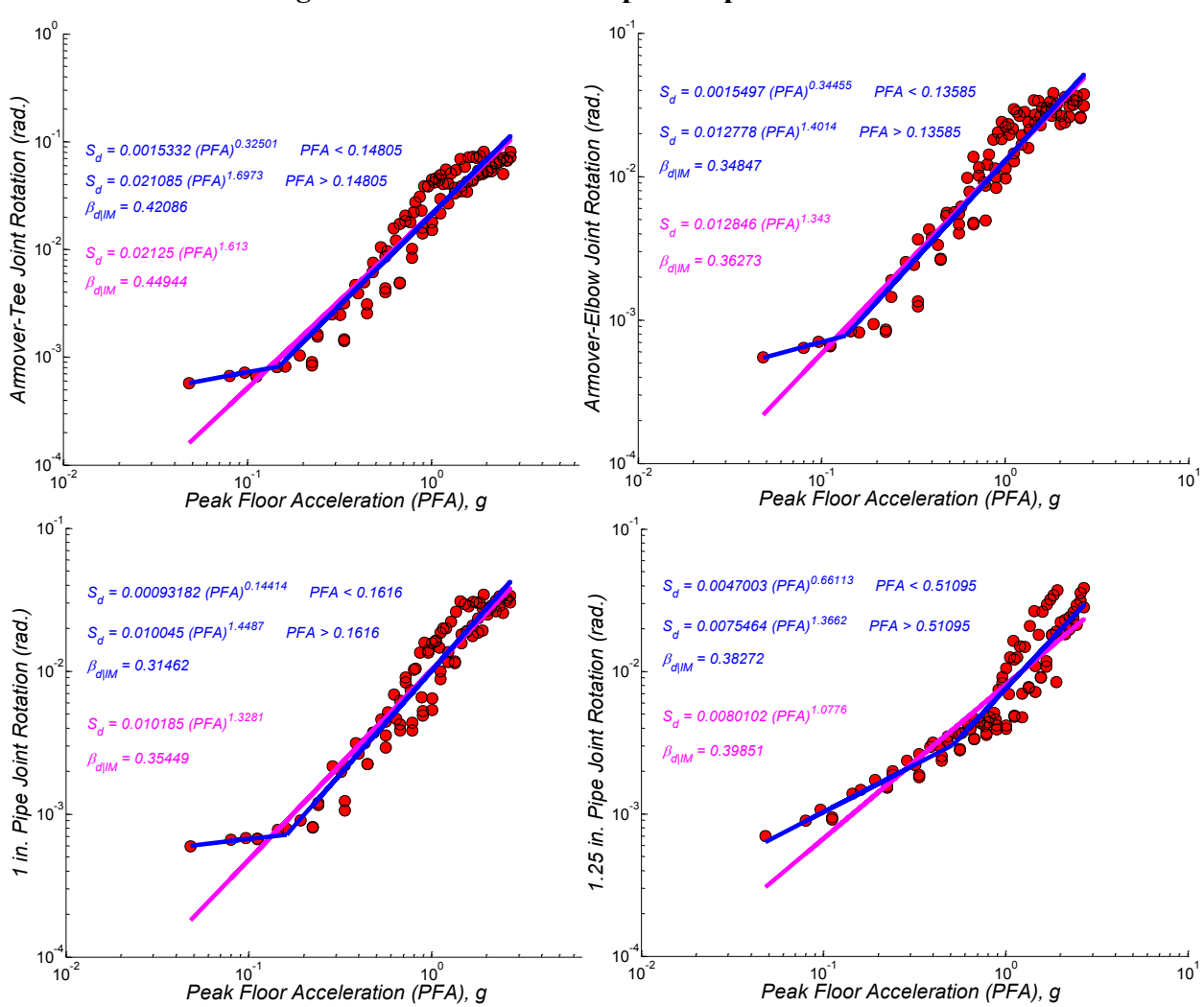
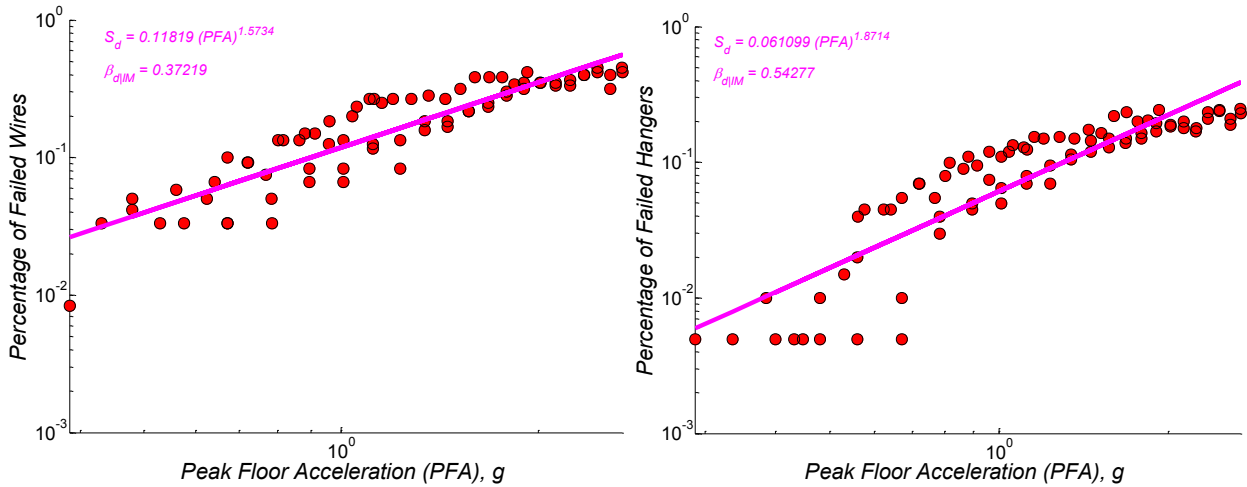


Figure C-11 PSDMs for Pipe Components - Case 4



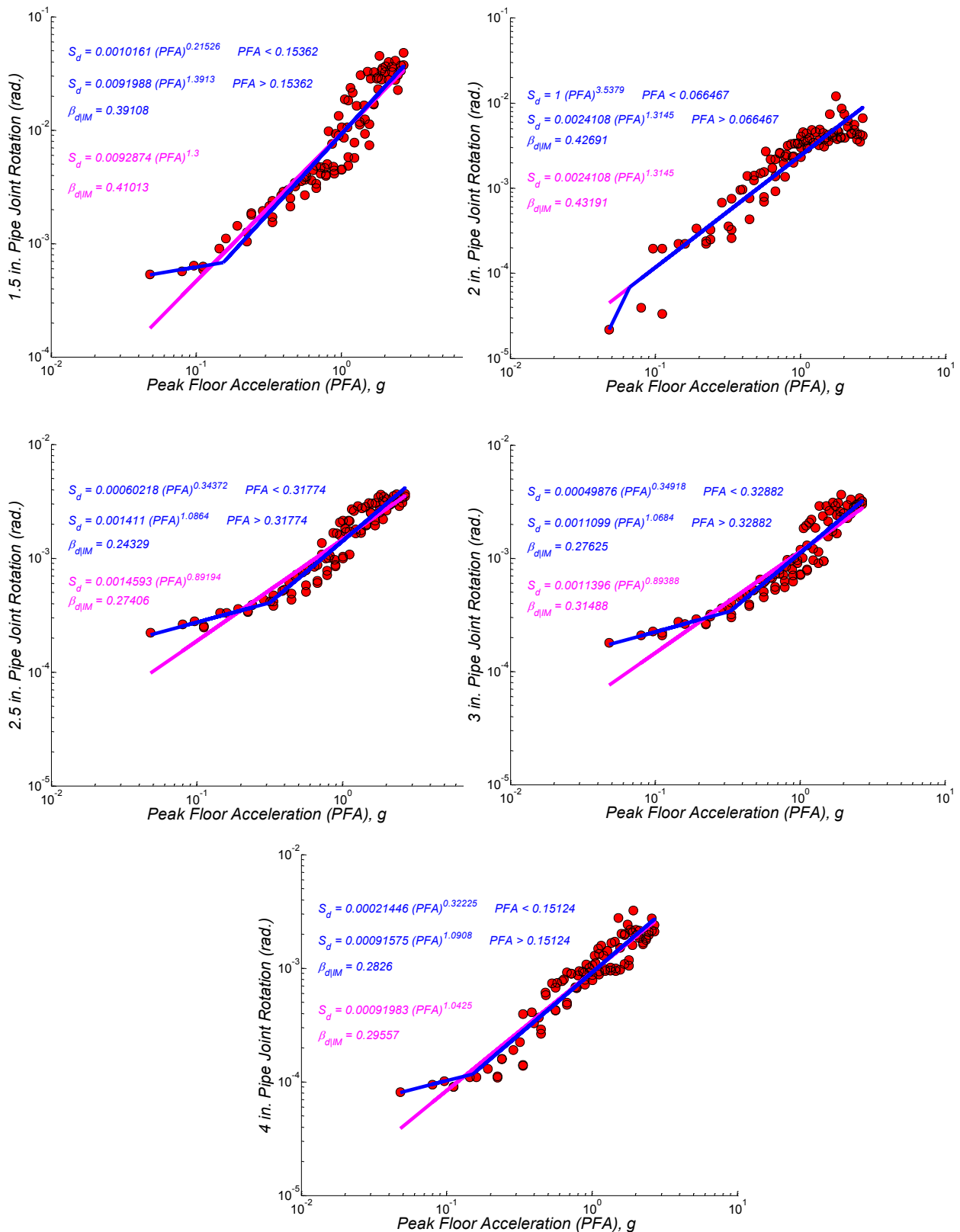


Figure C-14 PSDMs for Pipe Components - Case 5

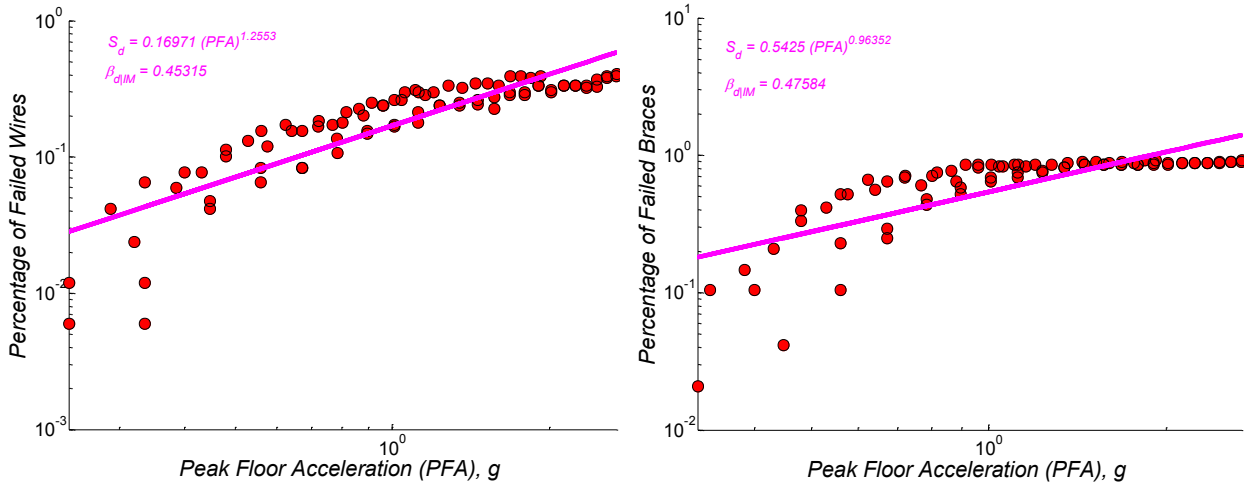


Figure C- 15 PSDMs for Pipe Components - Case 5

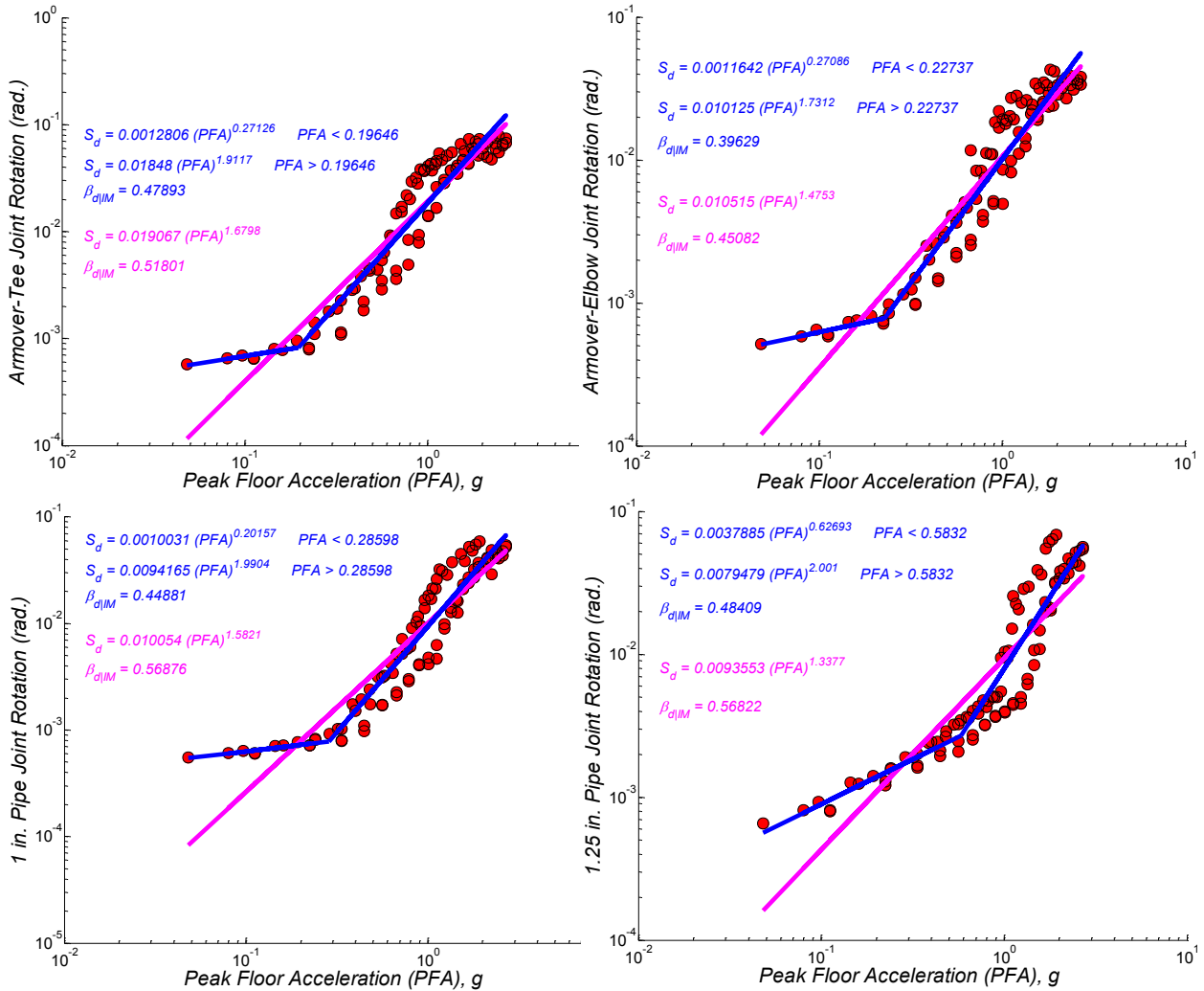


Figure C- 16 PSDMs for Pipe Components - Case 6

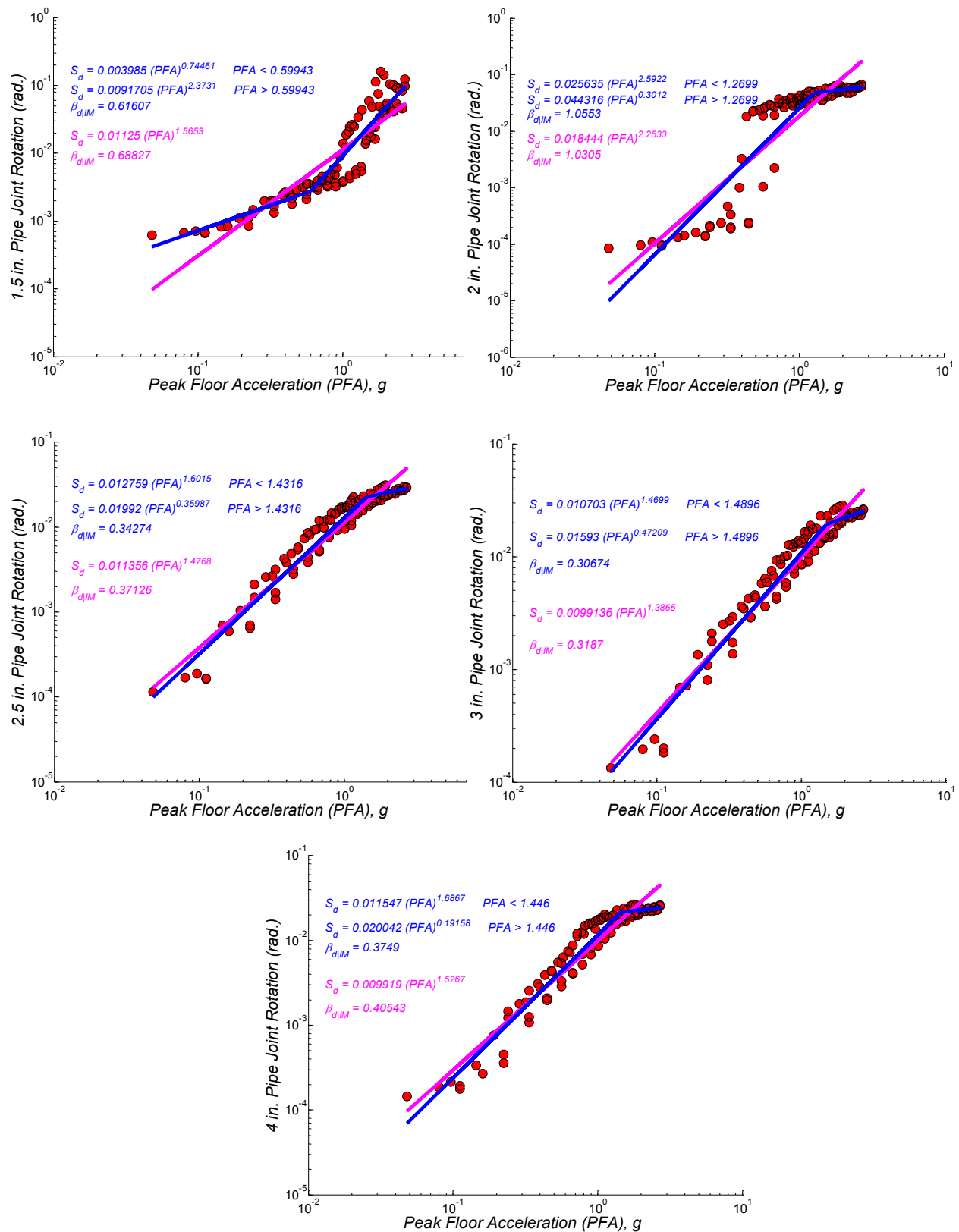


Figure C- 17 PSDMs for Pipe Components - Case 6

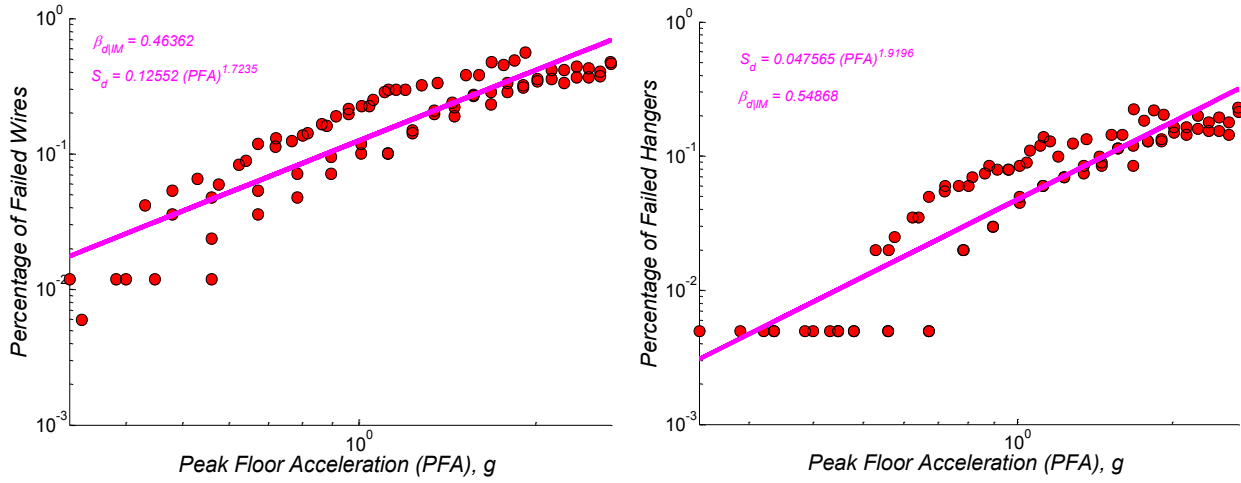


Figure C-18 PSDMs for Pipe Components - Case 6

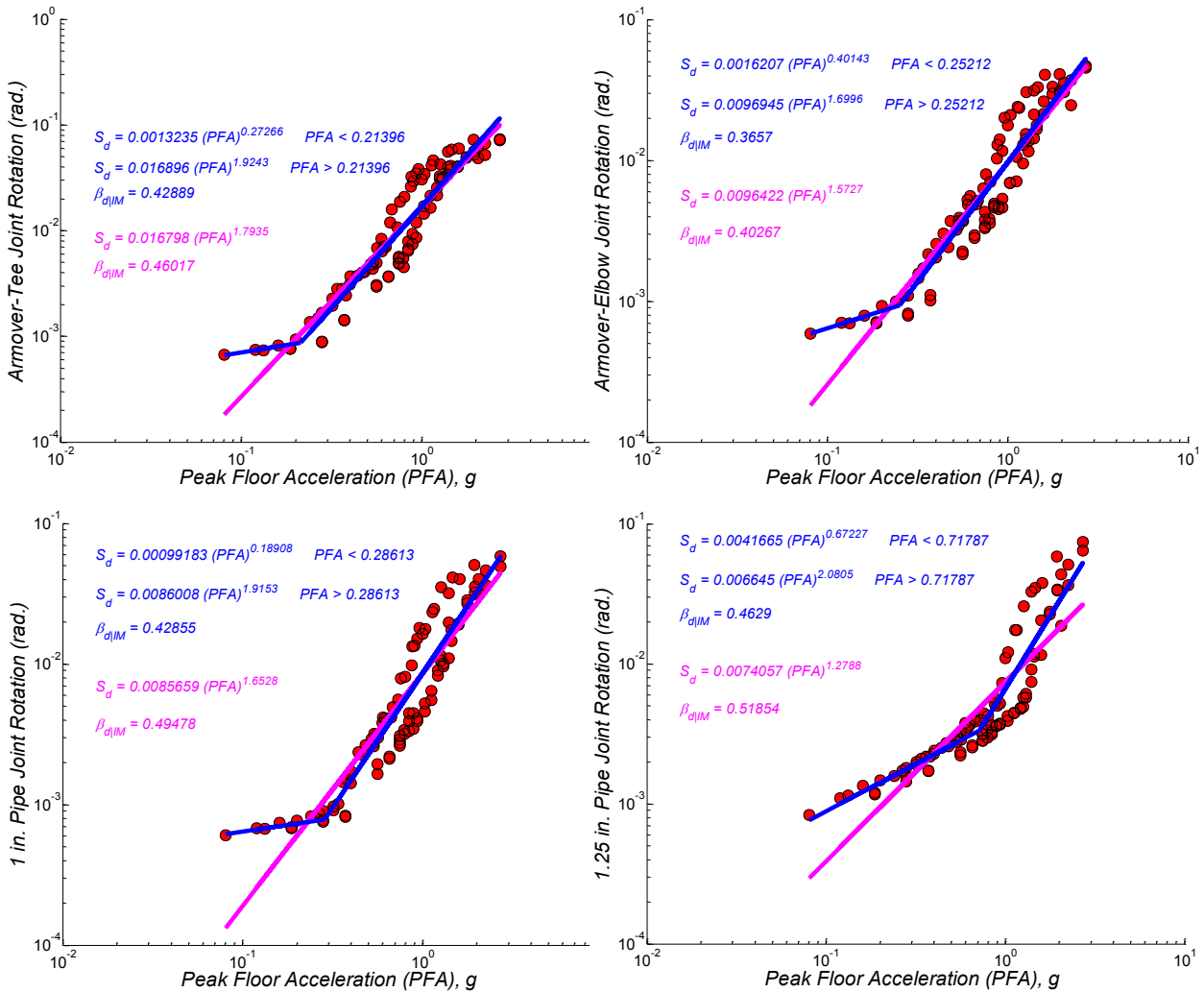


Figure C-19 PSDMs for Pipe Components - Case 7

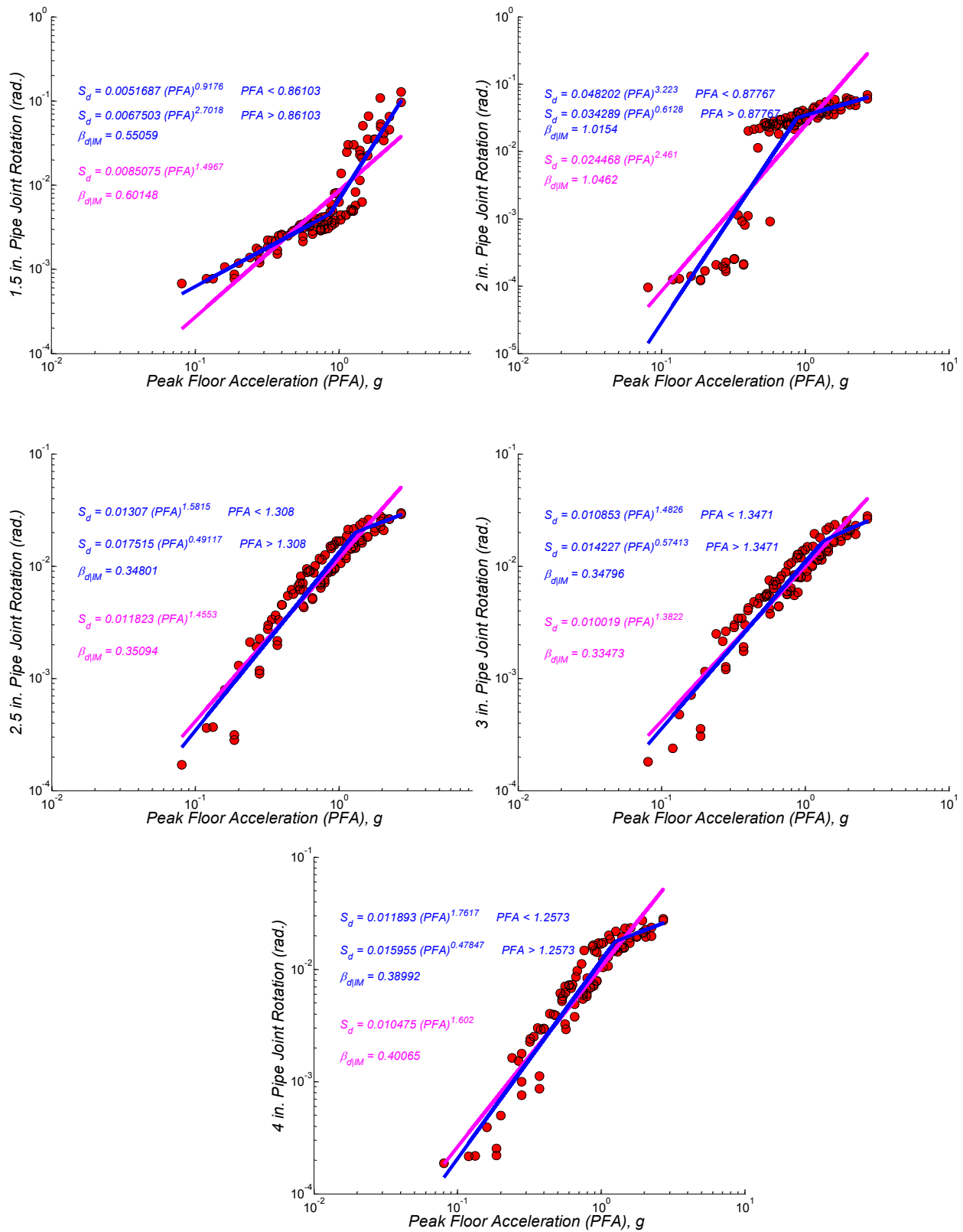


Figure C- 20 PSDMs for Pipe Components - Case 7

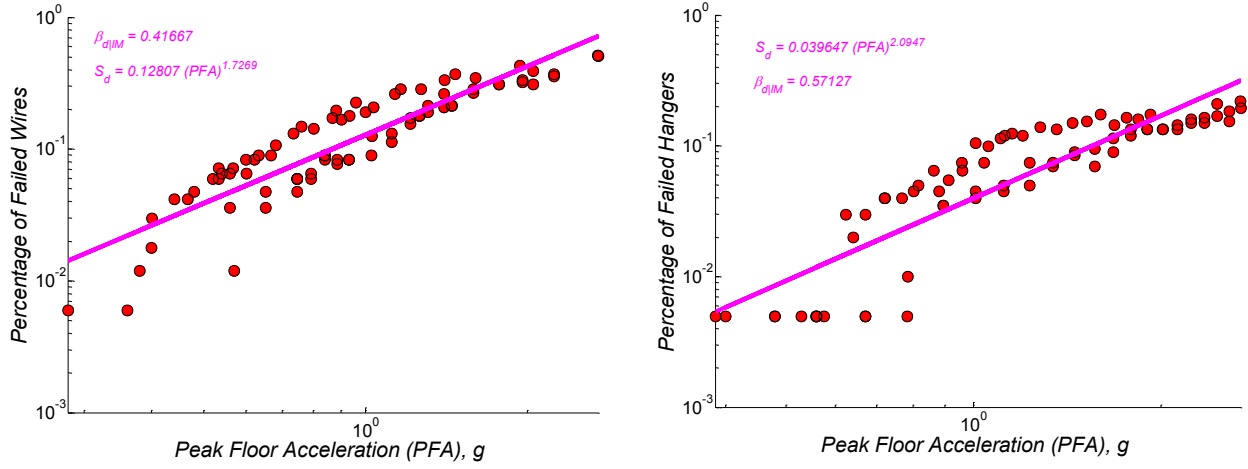


Figure C- 21 PSDMs for Pipe Components - Case 7

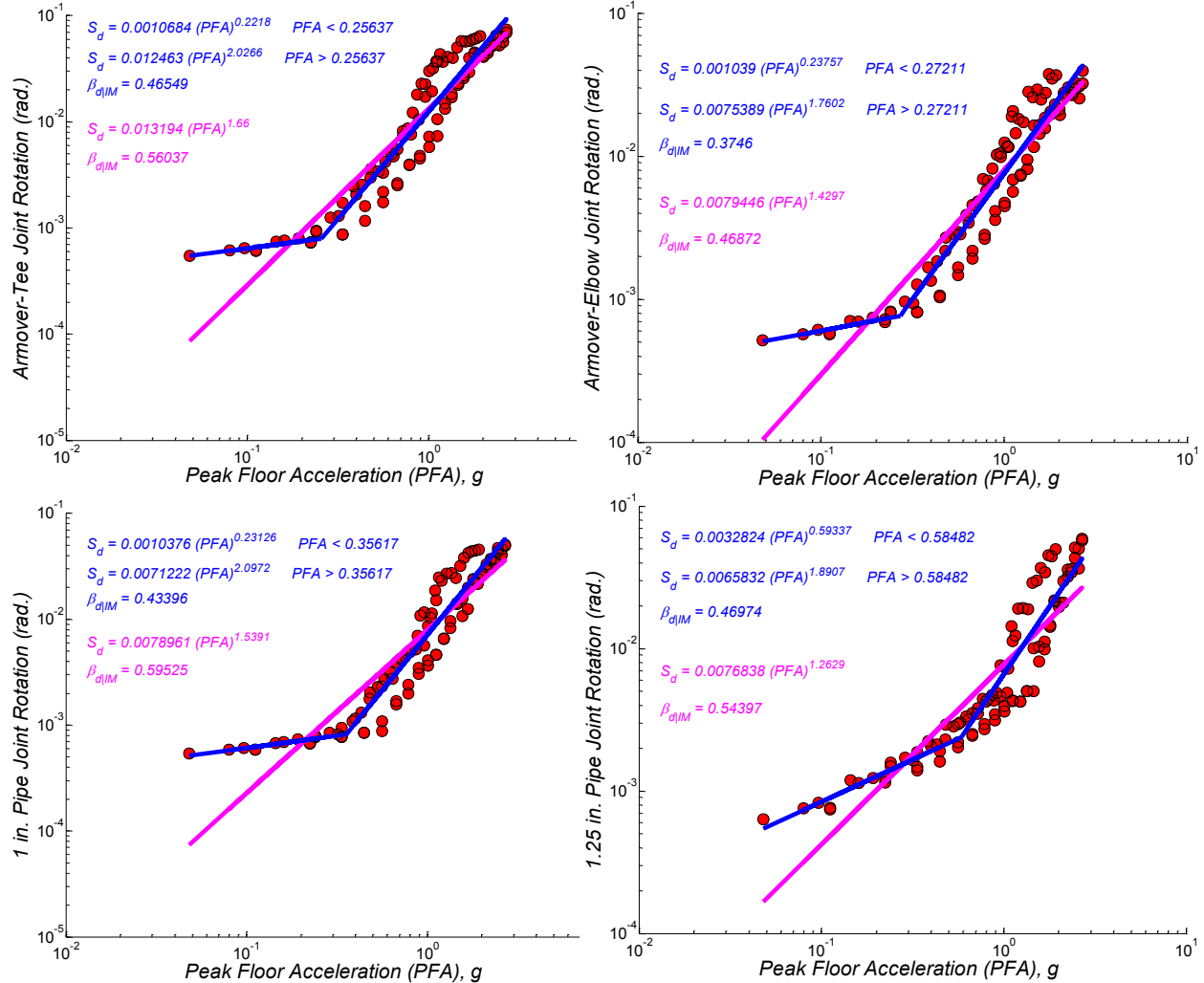


Figure C- 22 PSDMs for Pipe Components - Case 8

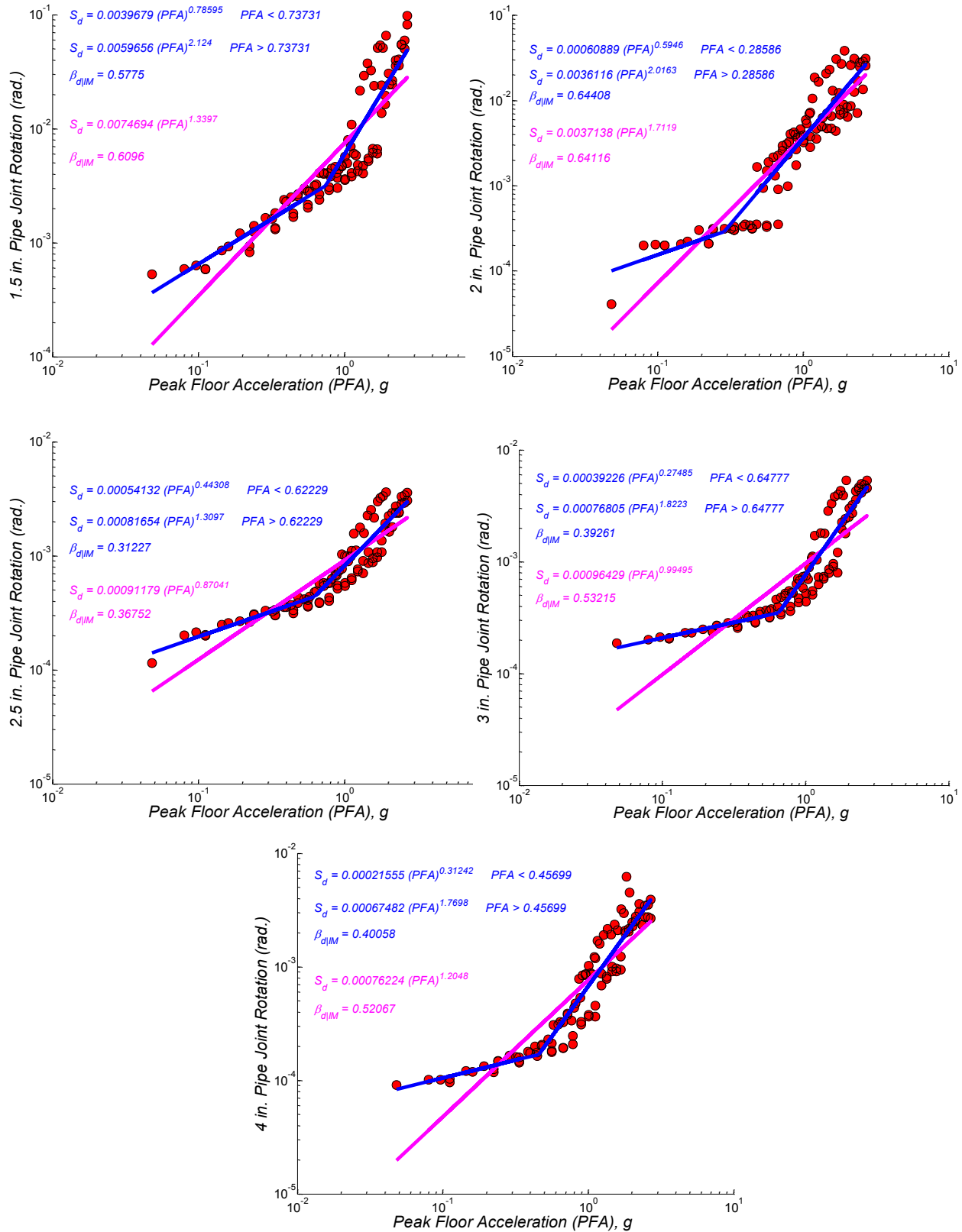
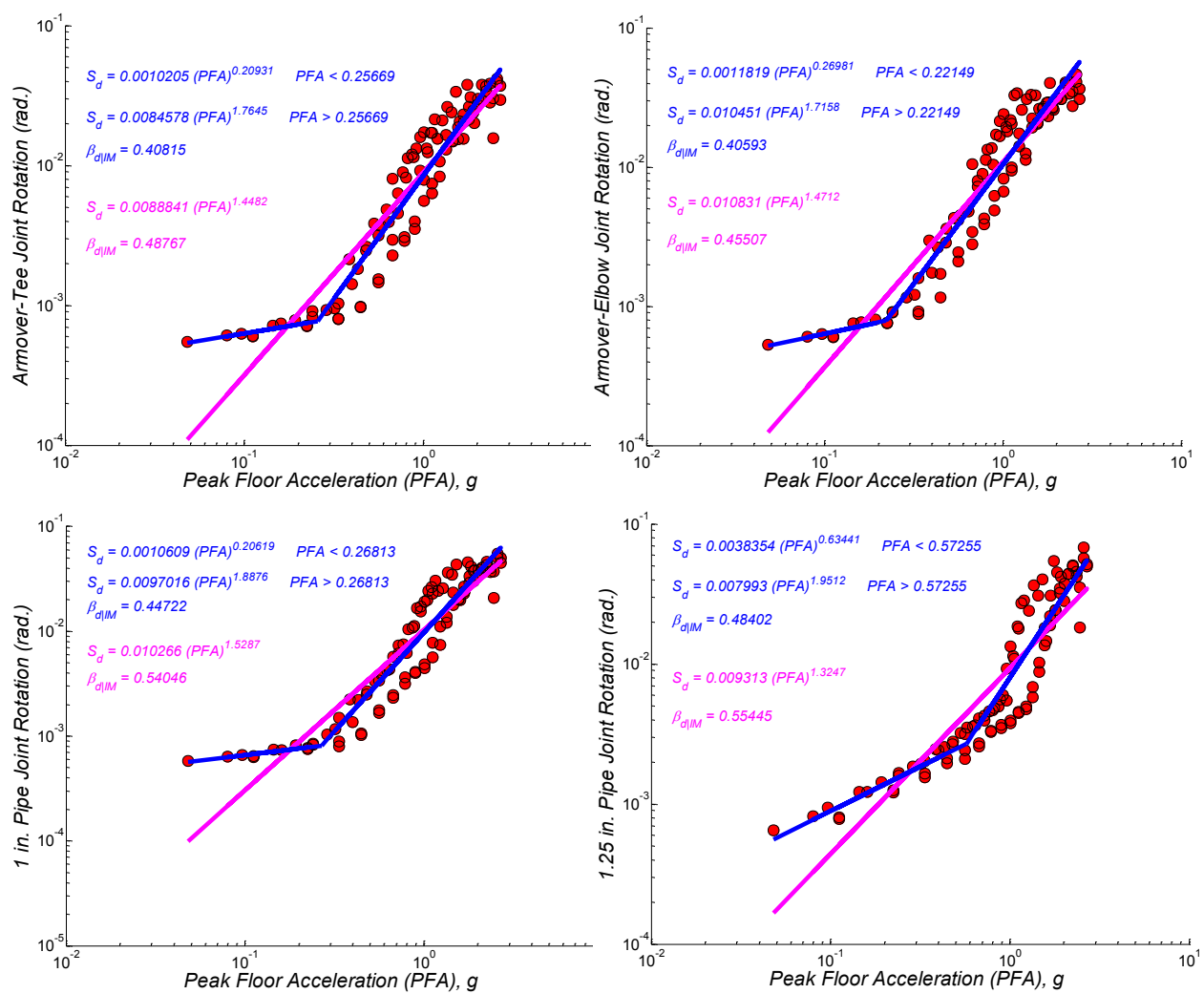
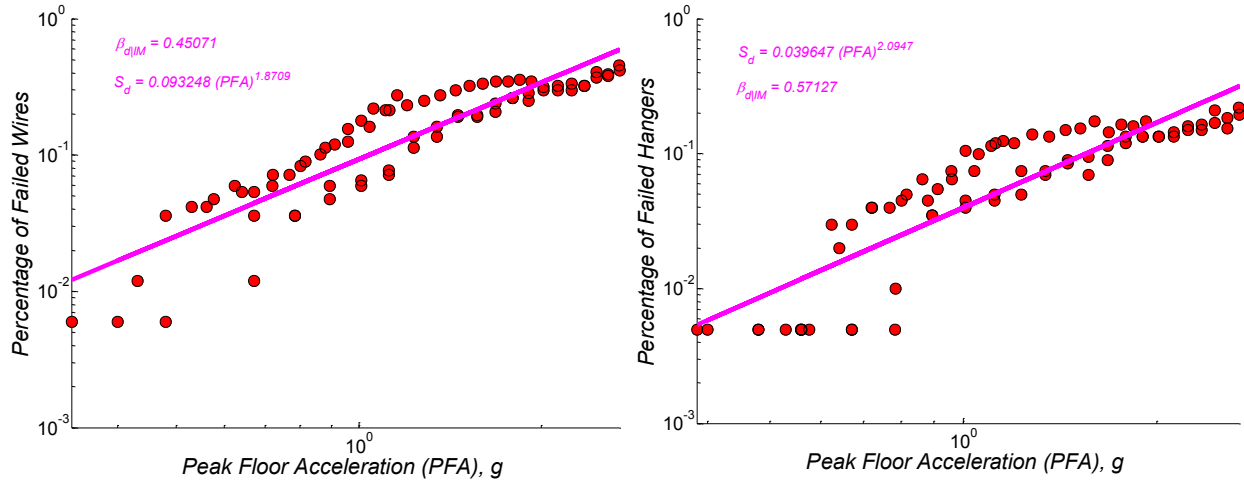


Figure C- 23 PSDMs for Pipe Components - Case 8



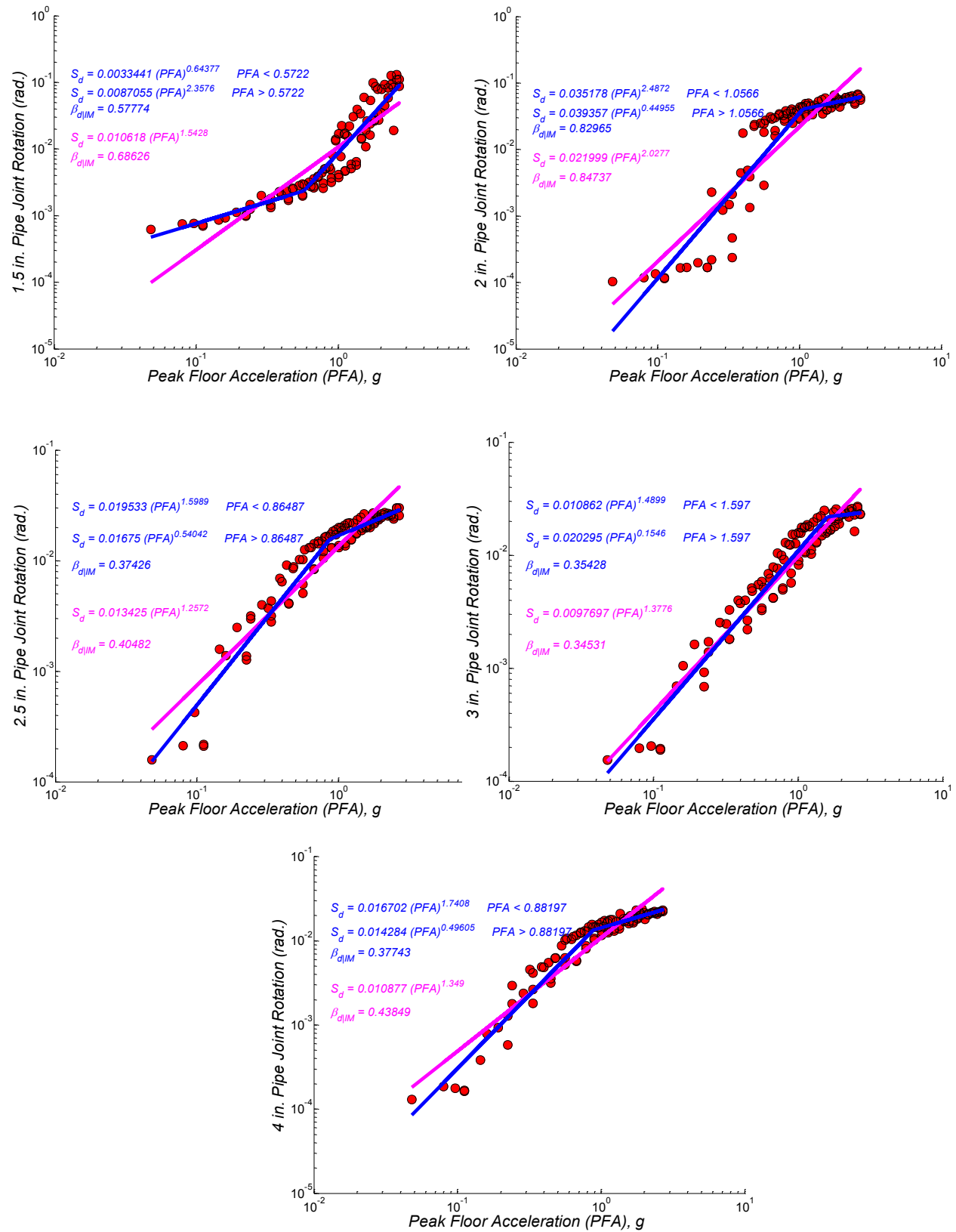


Figure C- 26 PSDMs for Pipe Components - Case 9

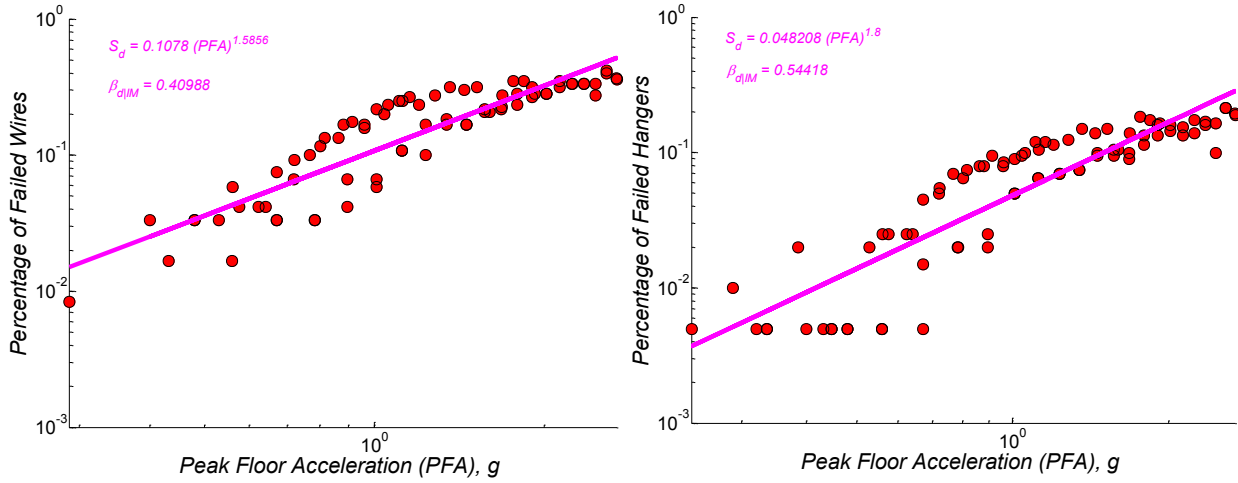


Figure C- 27 PSDMs for Pipe Components - Case 9

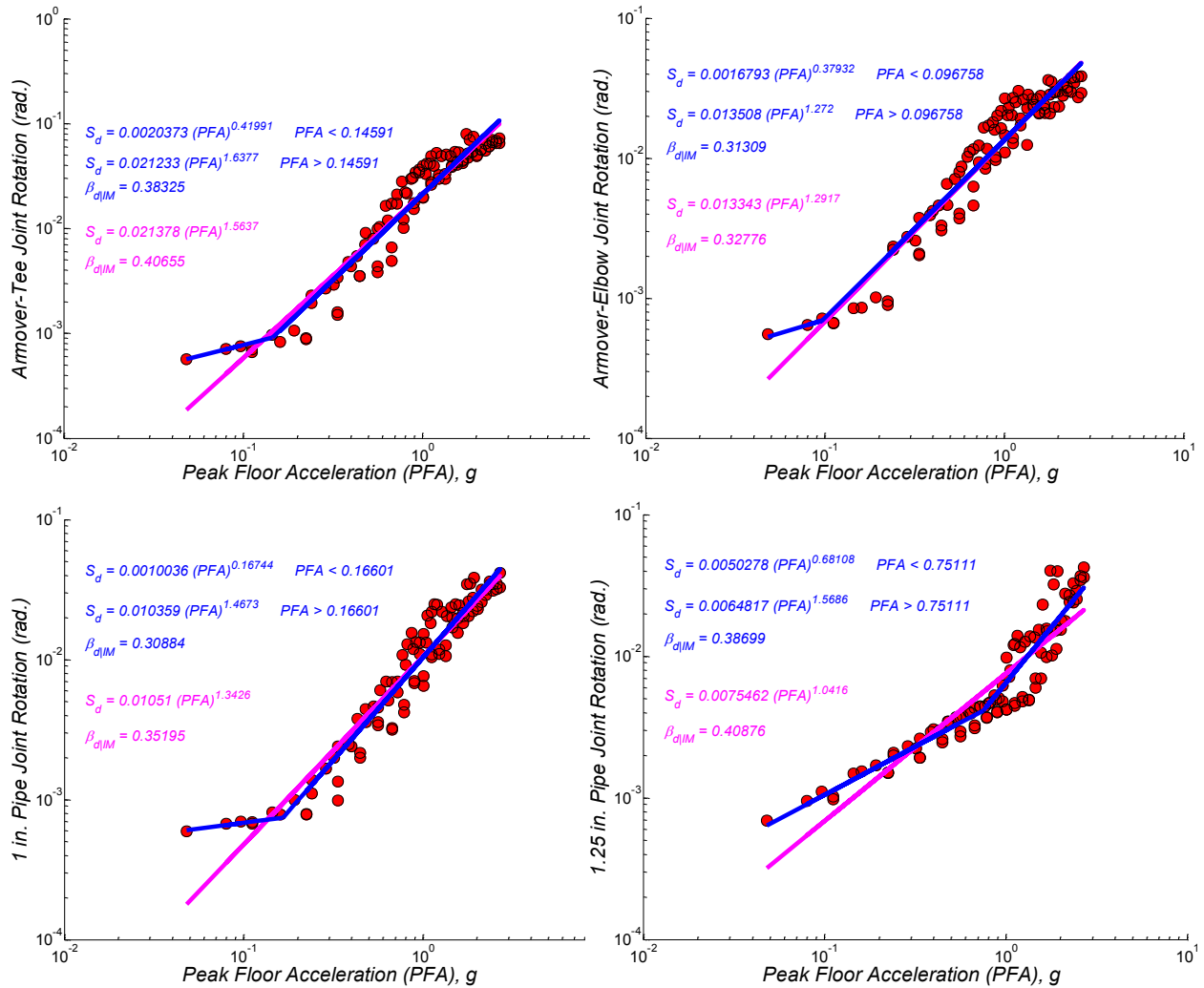


Figure C- 28 PSDMs for Pipe Components - Case 10

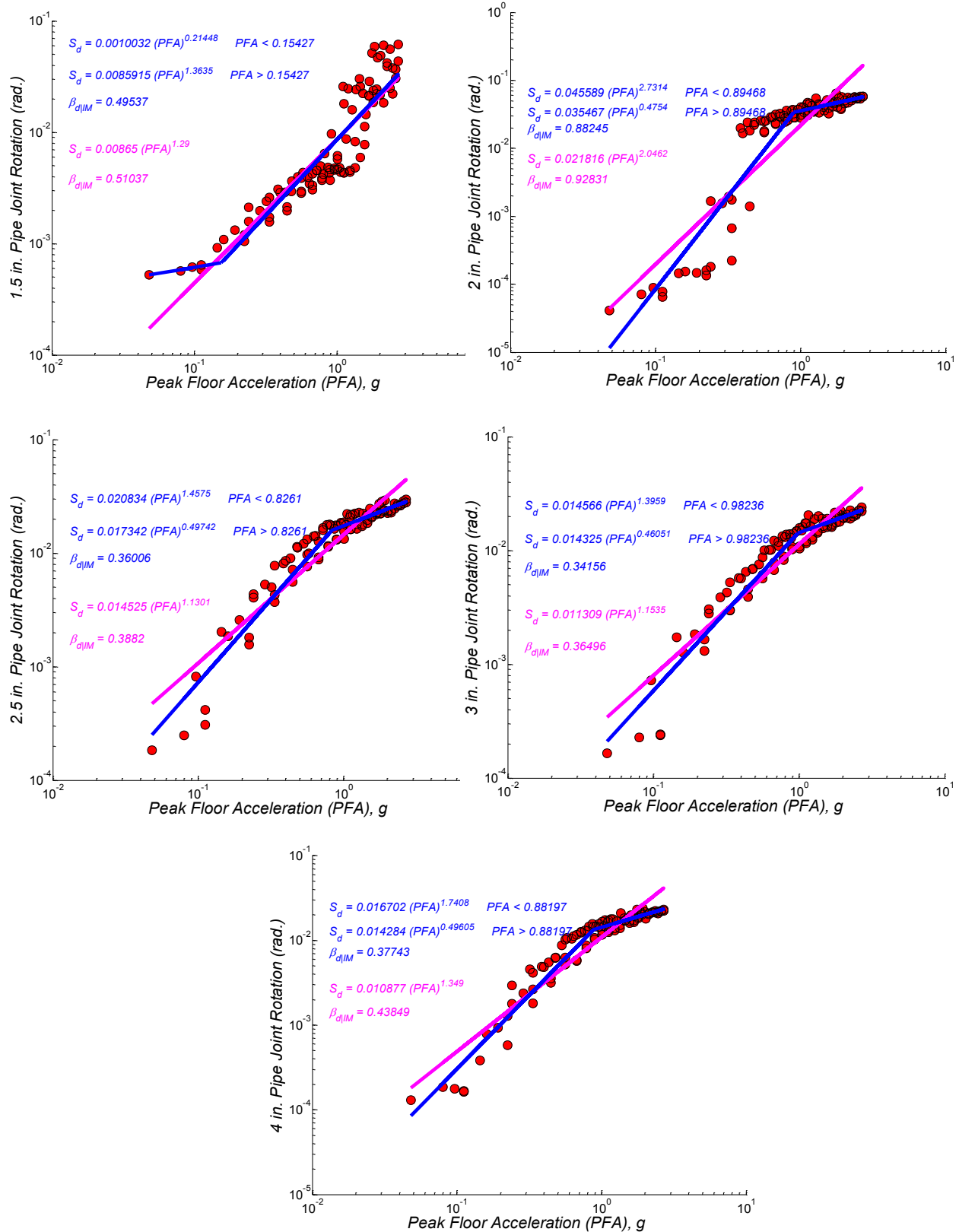


Figure C-29 PSDMs for Pipe Components - Case 10

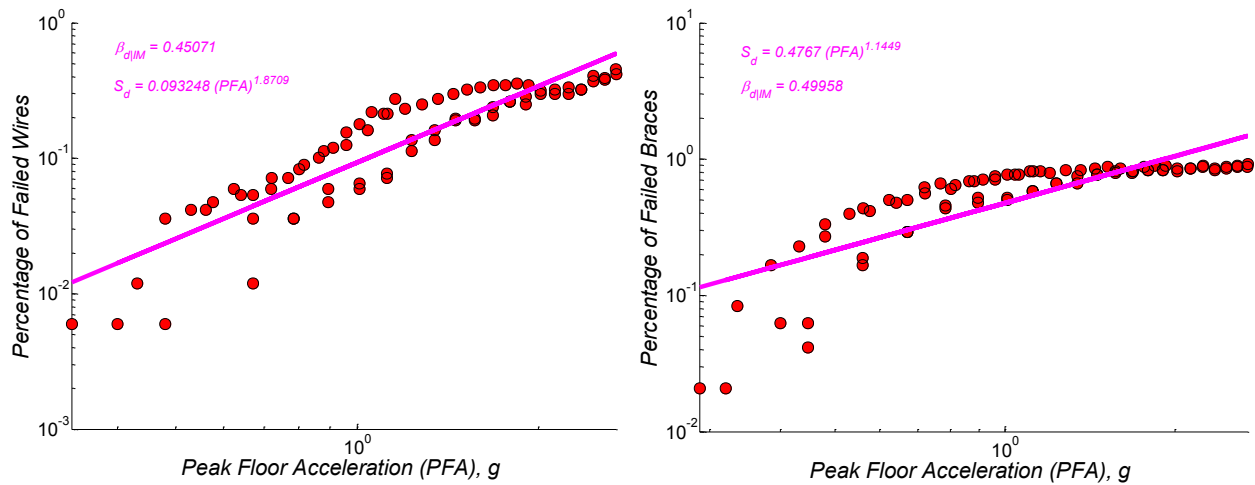


Figure C- 30 PSDMs for Pipe Components - Case 10

Appendix D

COMPONENT FRAGILITY CURVES OF PIPING SYSTEMS

Component fragility curves of piping systems were presented in Section 6. The comparisons of the remainder of the PSDMs are illustrated in this appendix. A sample comparison of linear and bilinear regression analysis was performed on component fragility curves of pipe components at the slight limit damage state for case 1. In this appendix, fragility curves for all components are presented using linear and bilinear regression analysis.

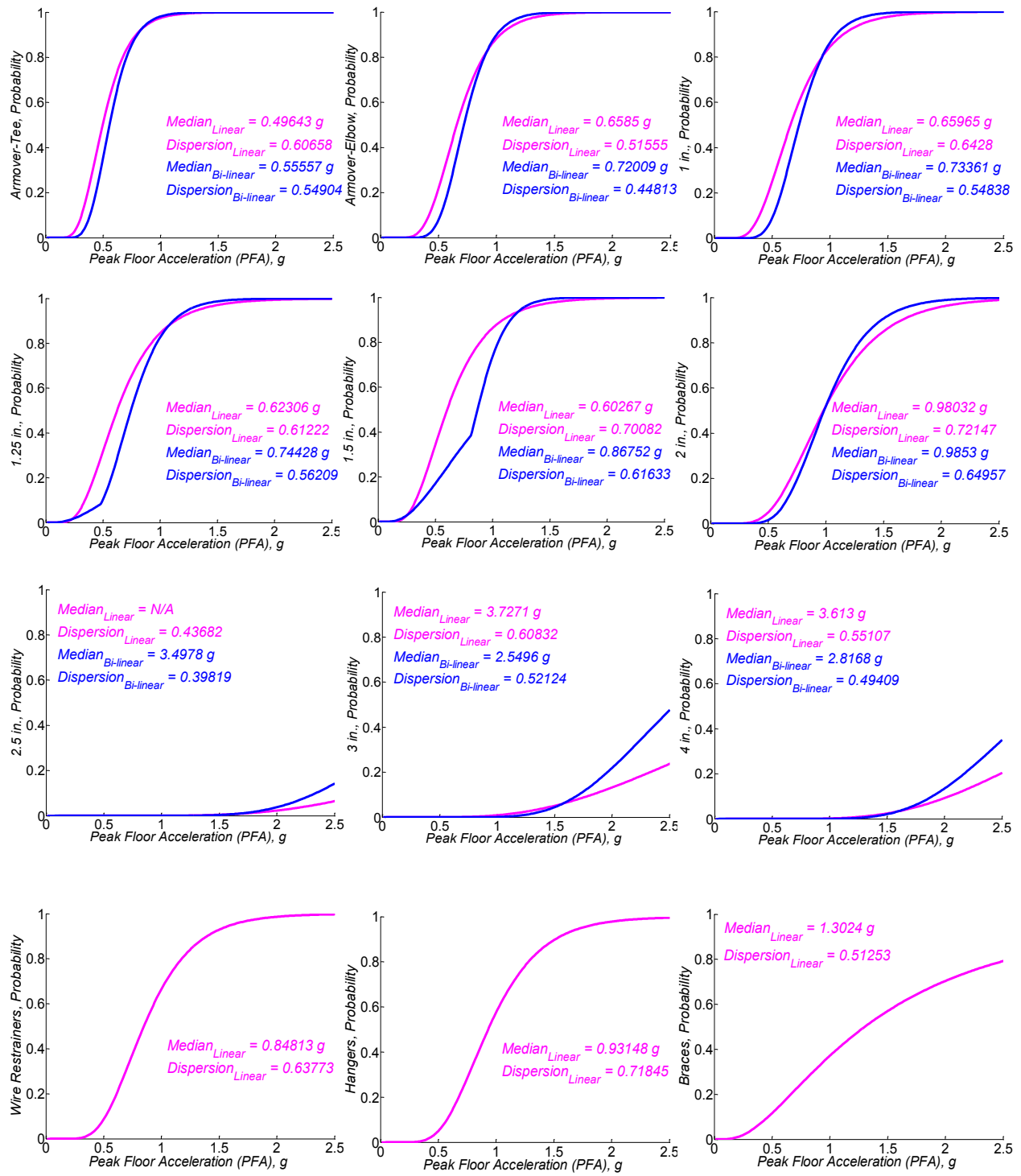


Figure D- 1 Component Fragility Curves, Slight - Case1

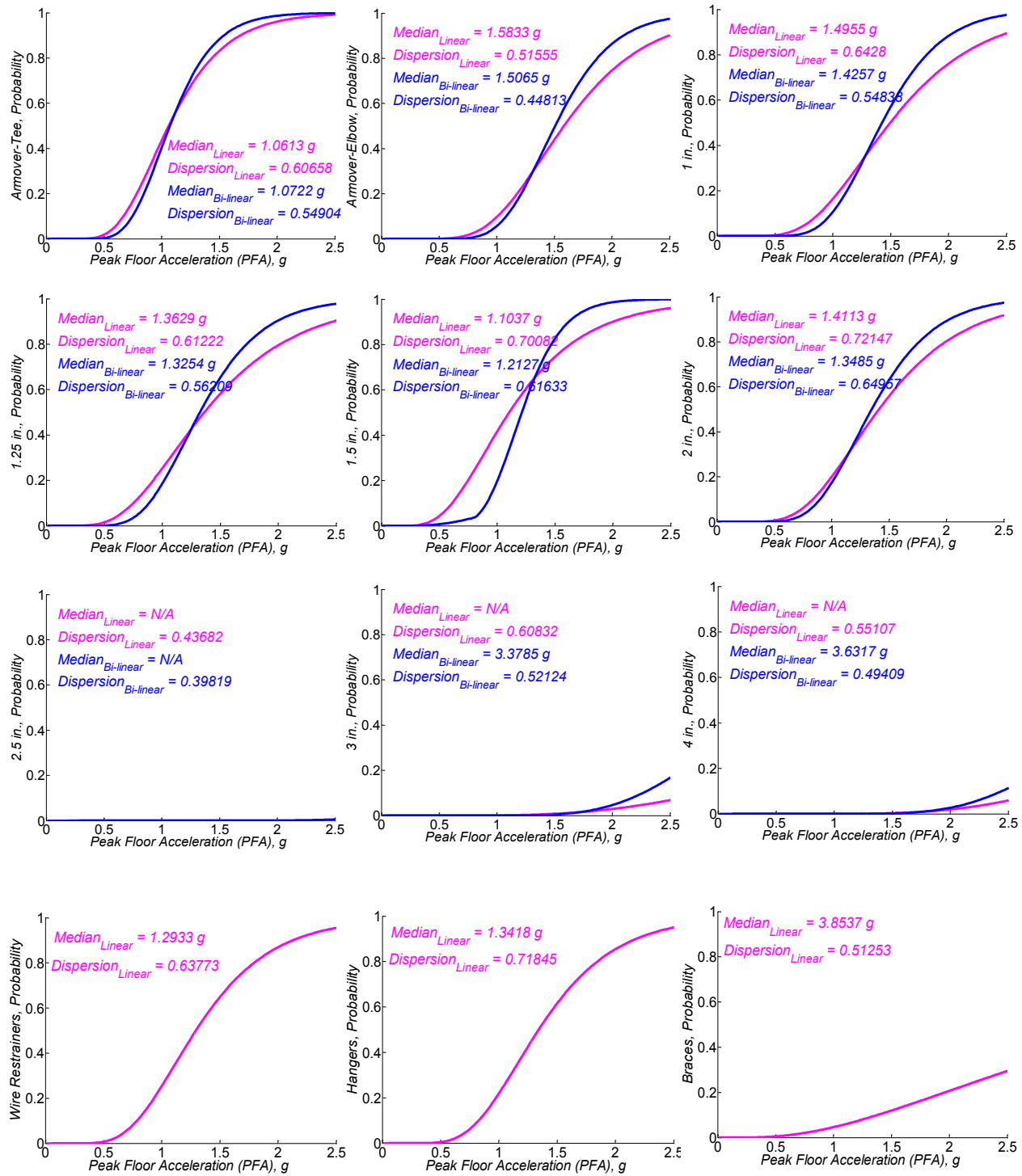


Figure D- 2 Component Fragility Curves, Moderate - Case1

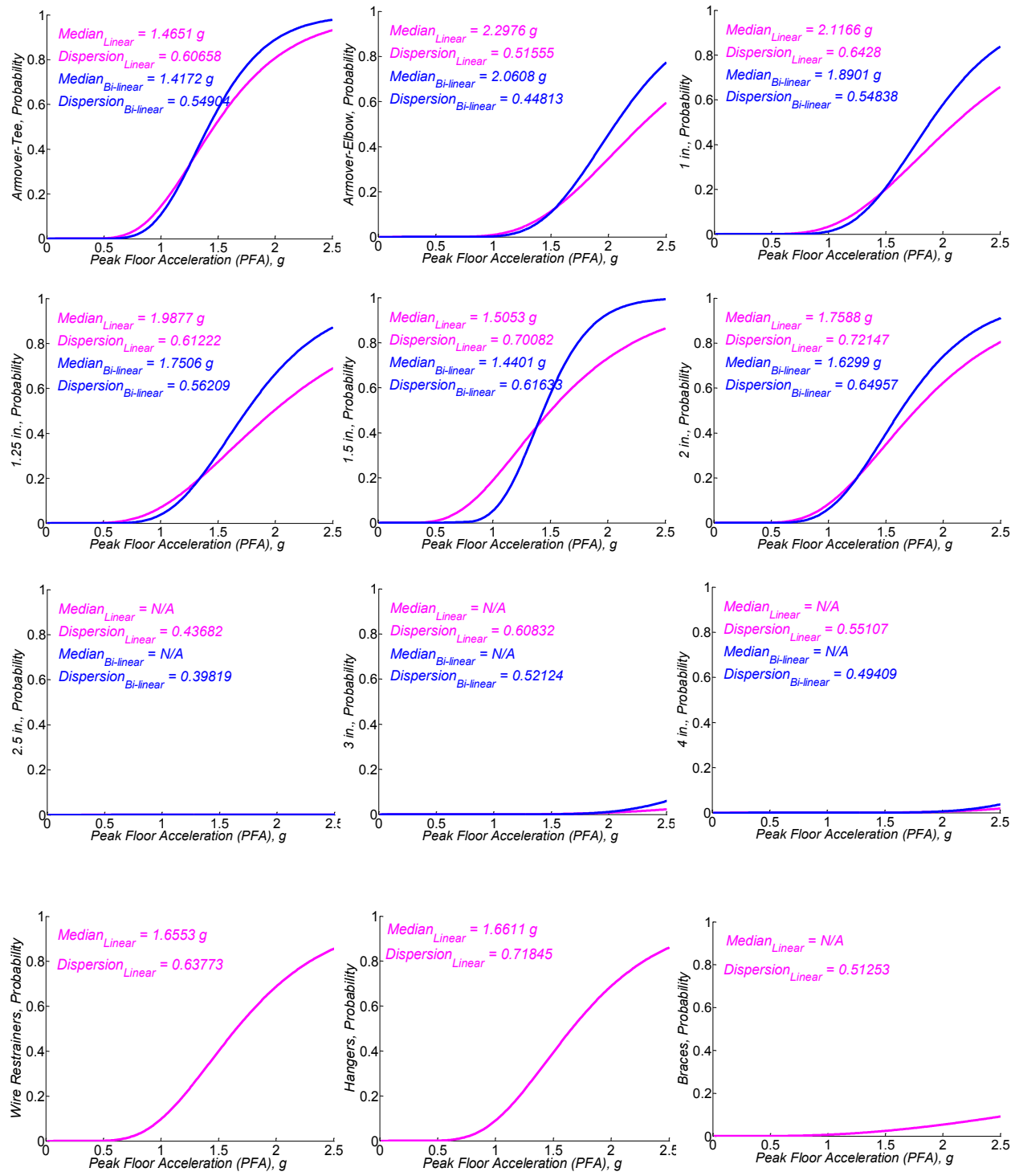


Figure D-3 Component Fragility Curves, Extensive - Case1

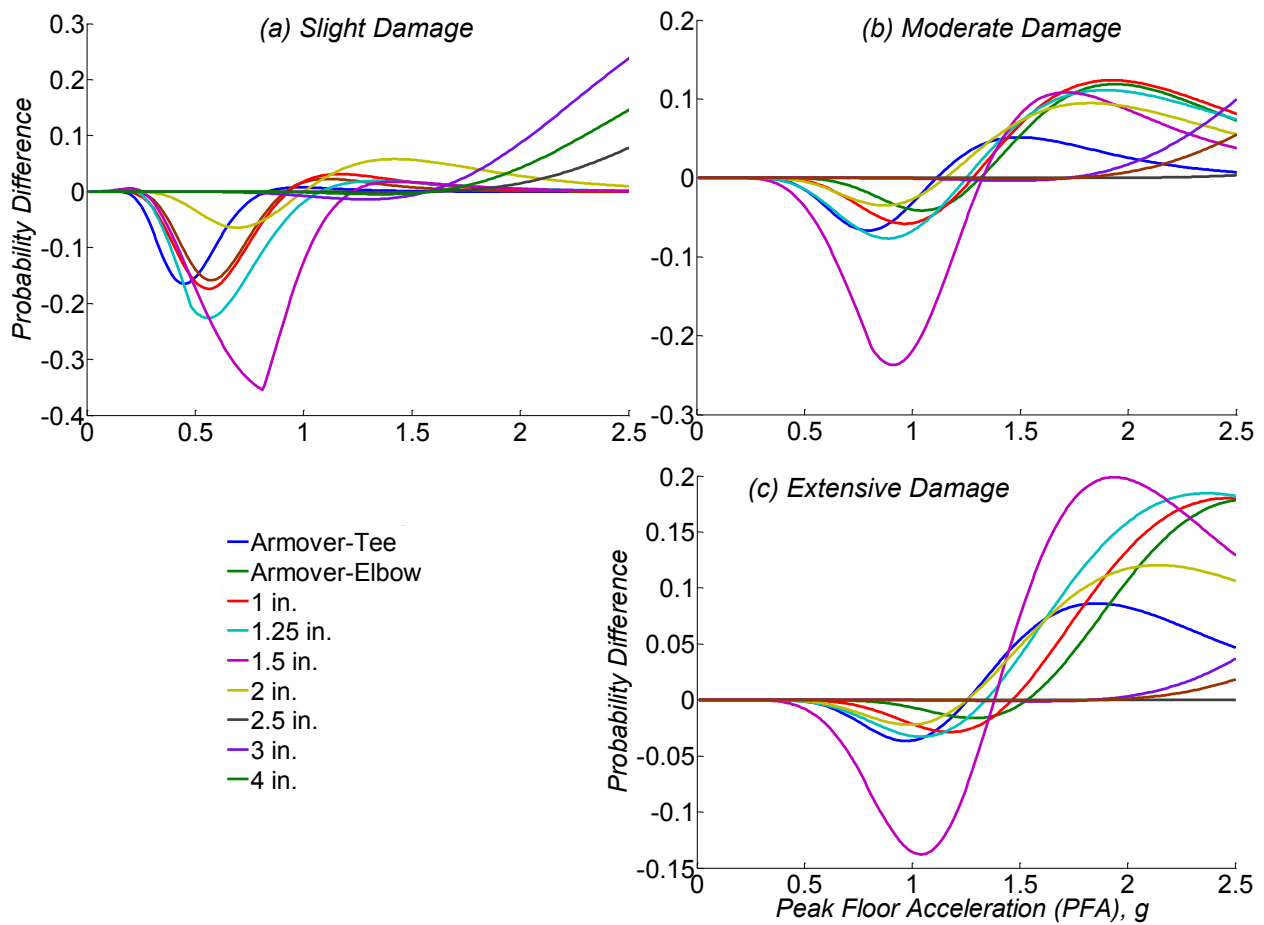


Figure D- 4 Fragility Probability Differences of Pipe Joints Using Linear and Bilinear Regression Analysis for Case1

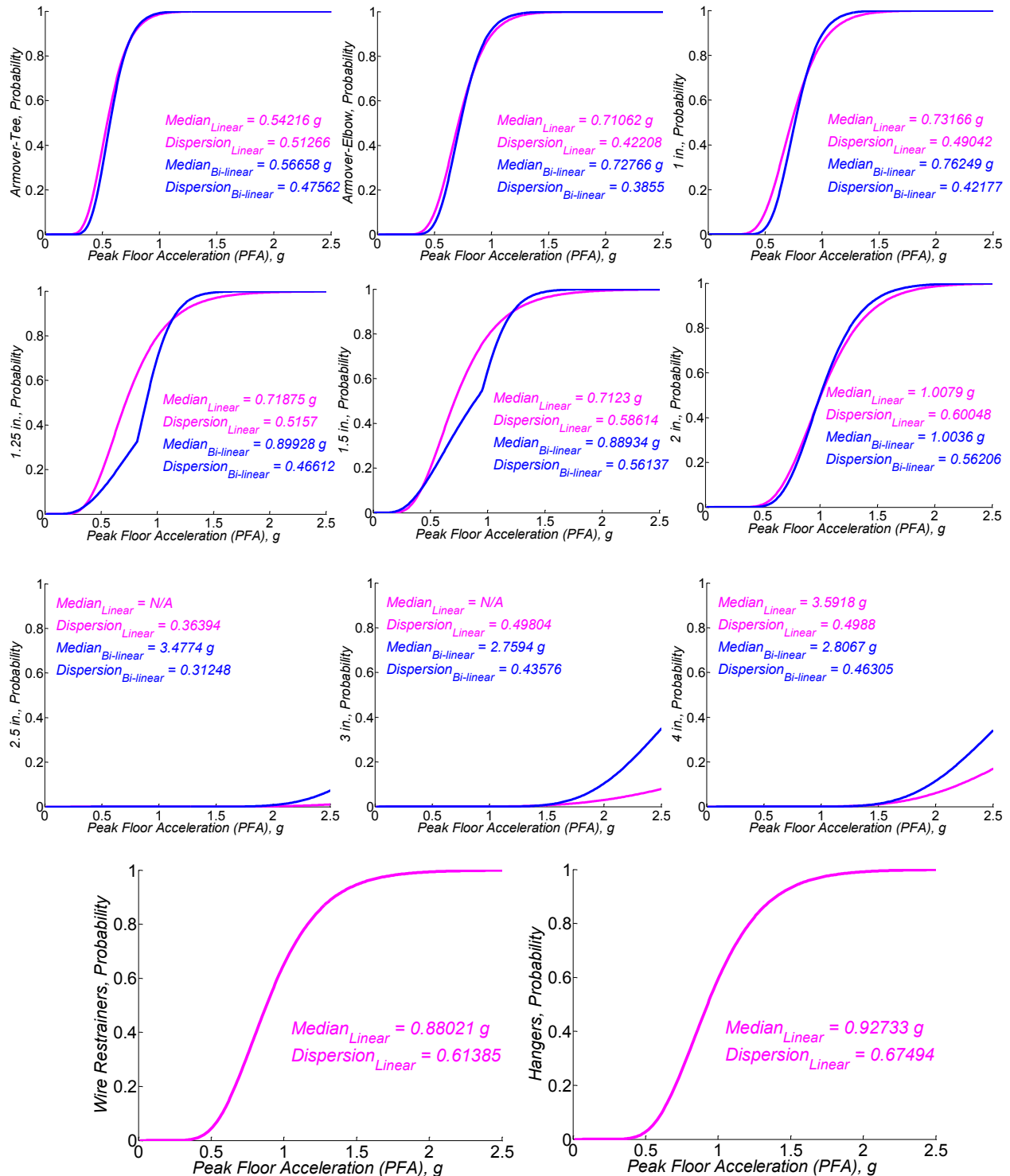


Figure D- 5 Component Fragility Curves, Slight - Case2

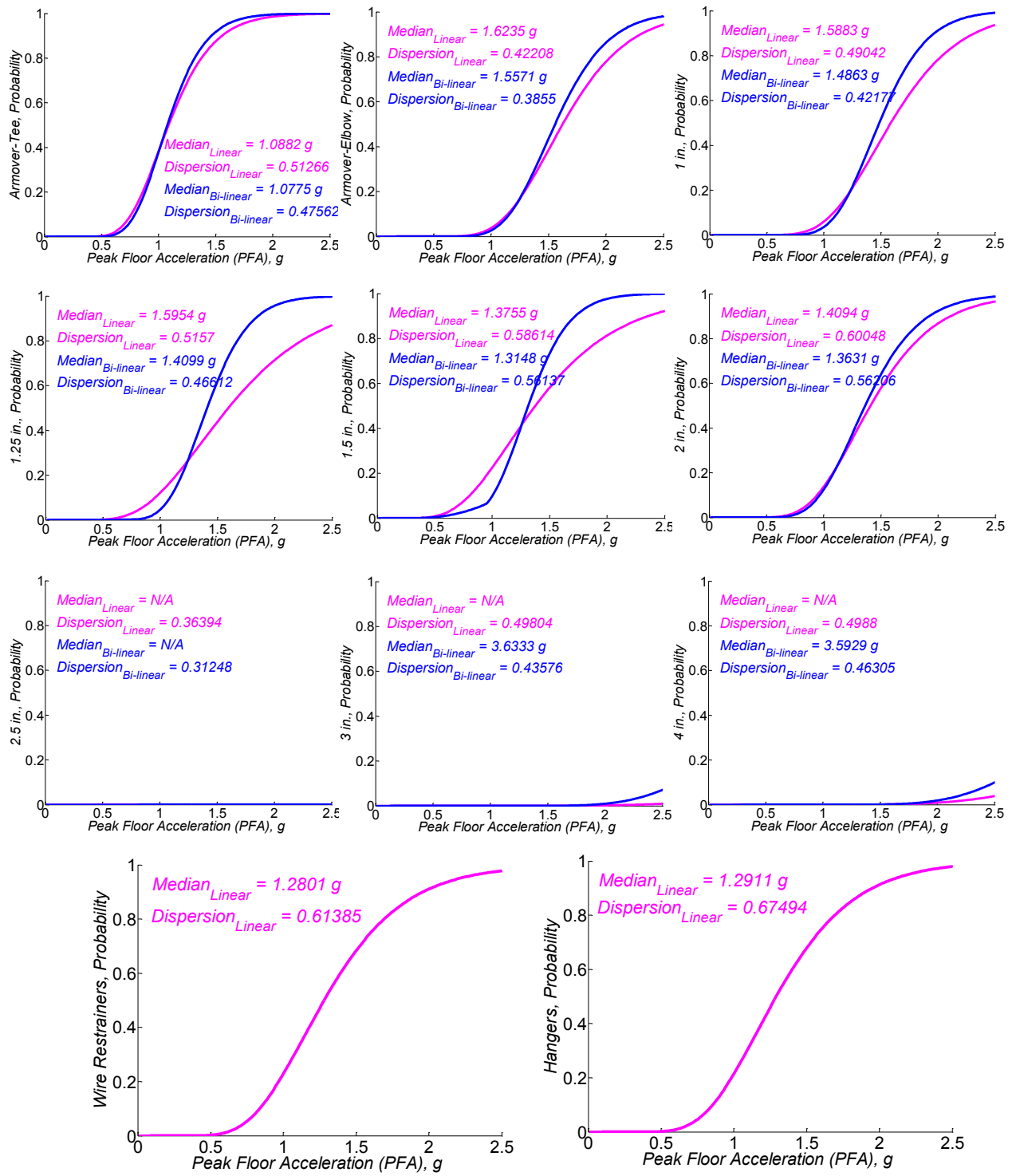


Figure D- 6 Component Fragility Curves, Moderate - Case 2

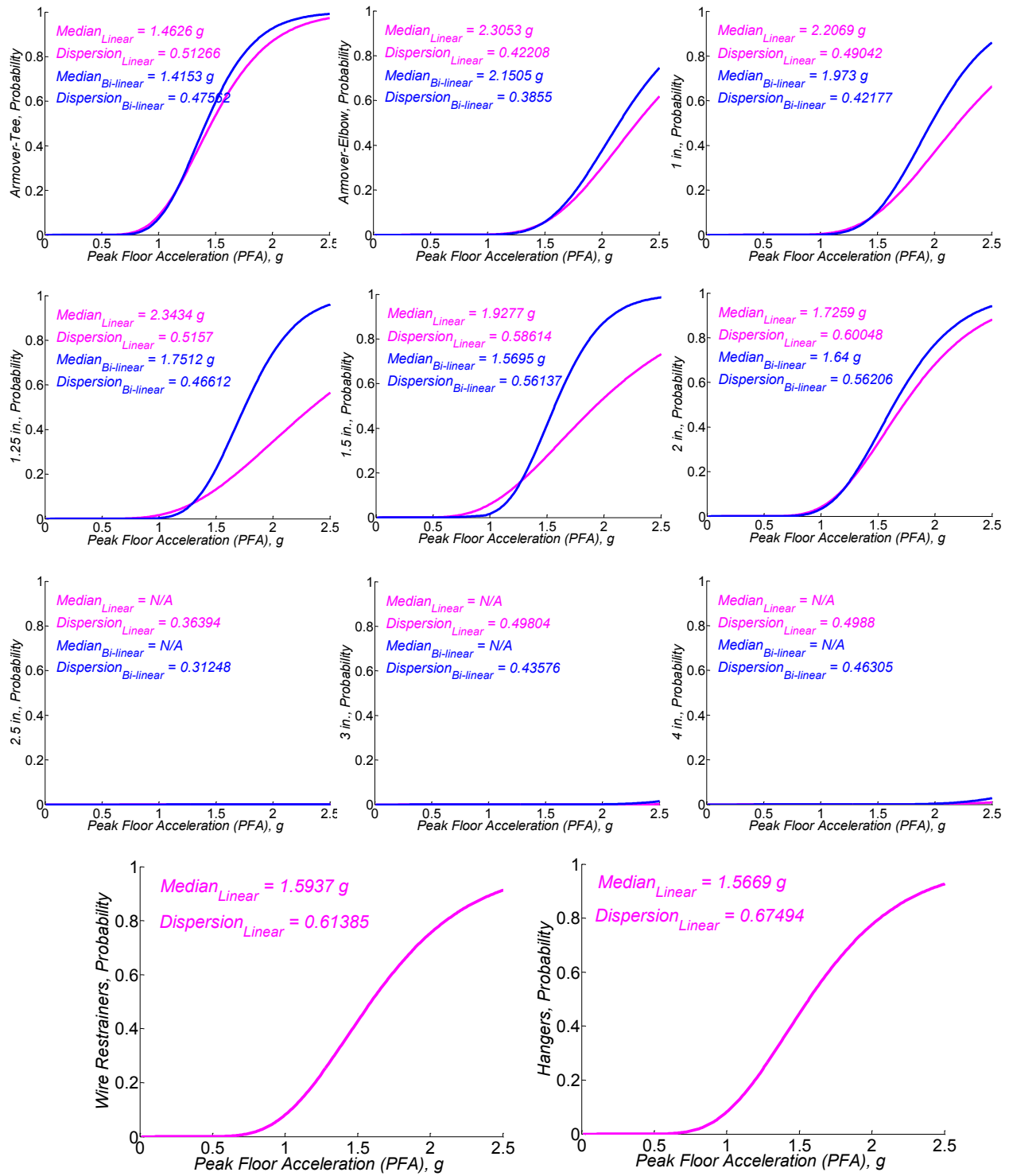


Figure D- 7 Component Fragility Curves, Extensive - Case2

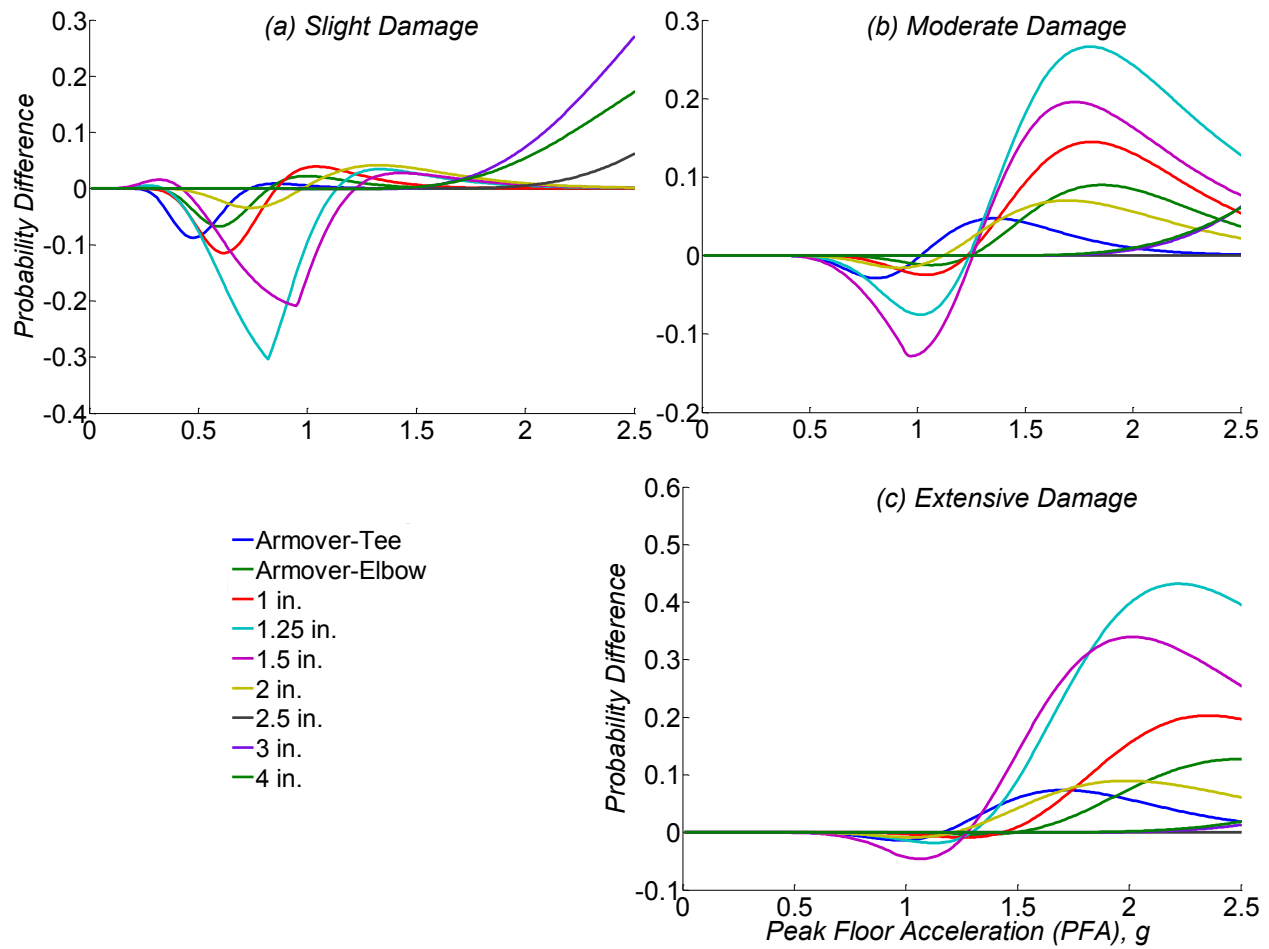


Figure D- 8 Fragility Probability Differences of Pipe Joints Using Linear and Bilinear Regression Analysis for Case2

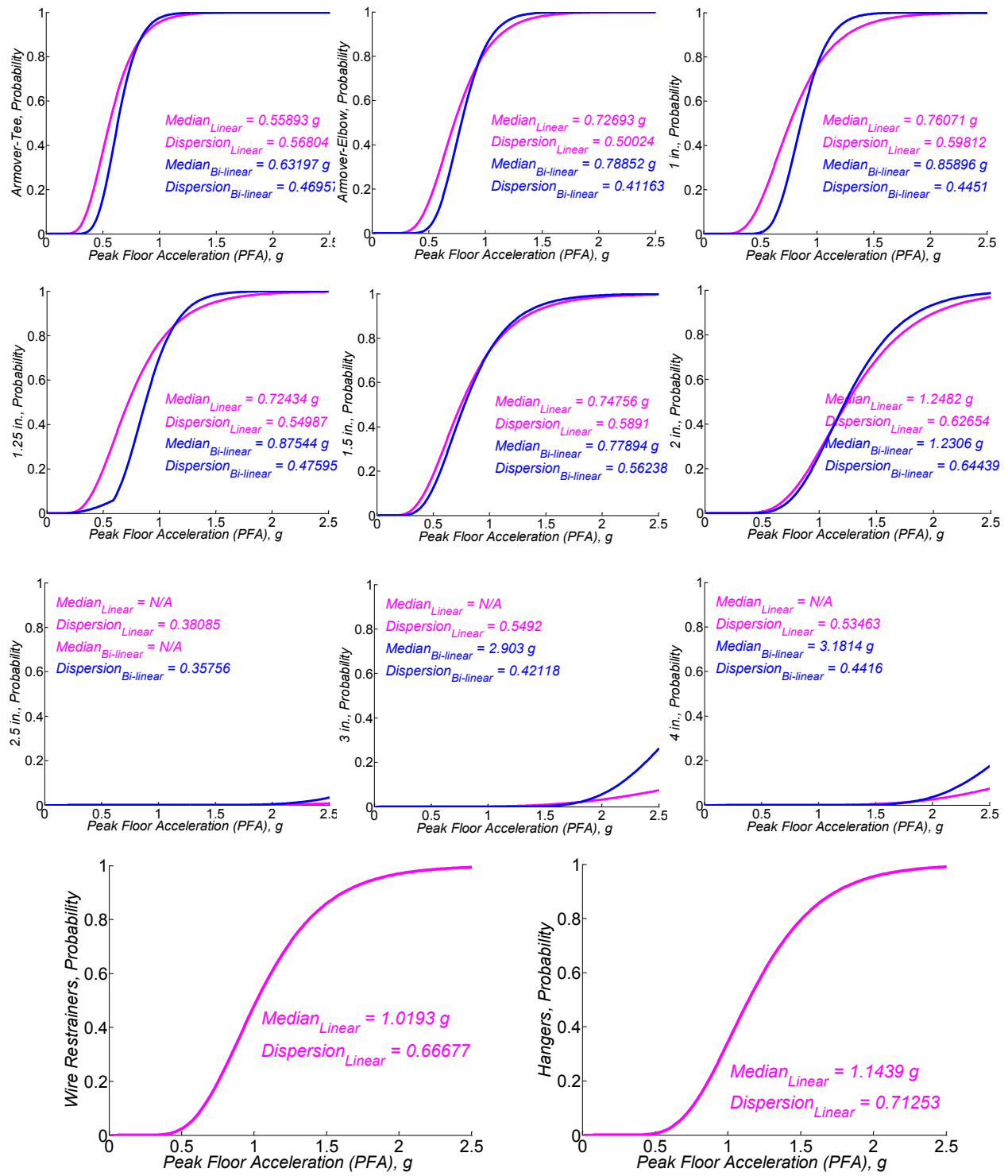


Figure D-9 Component Fragility Curves, Slight - Case 3

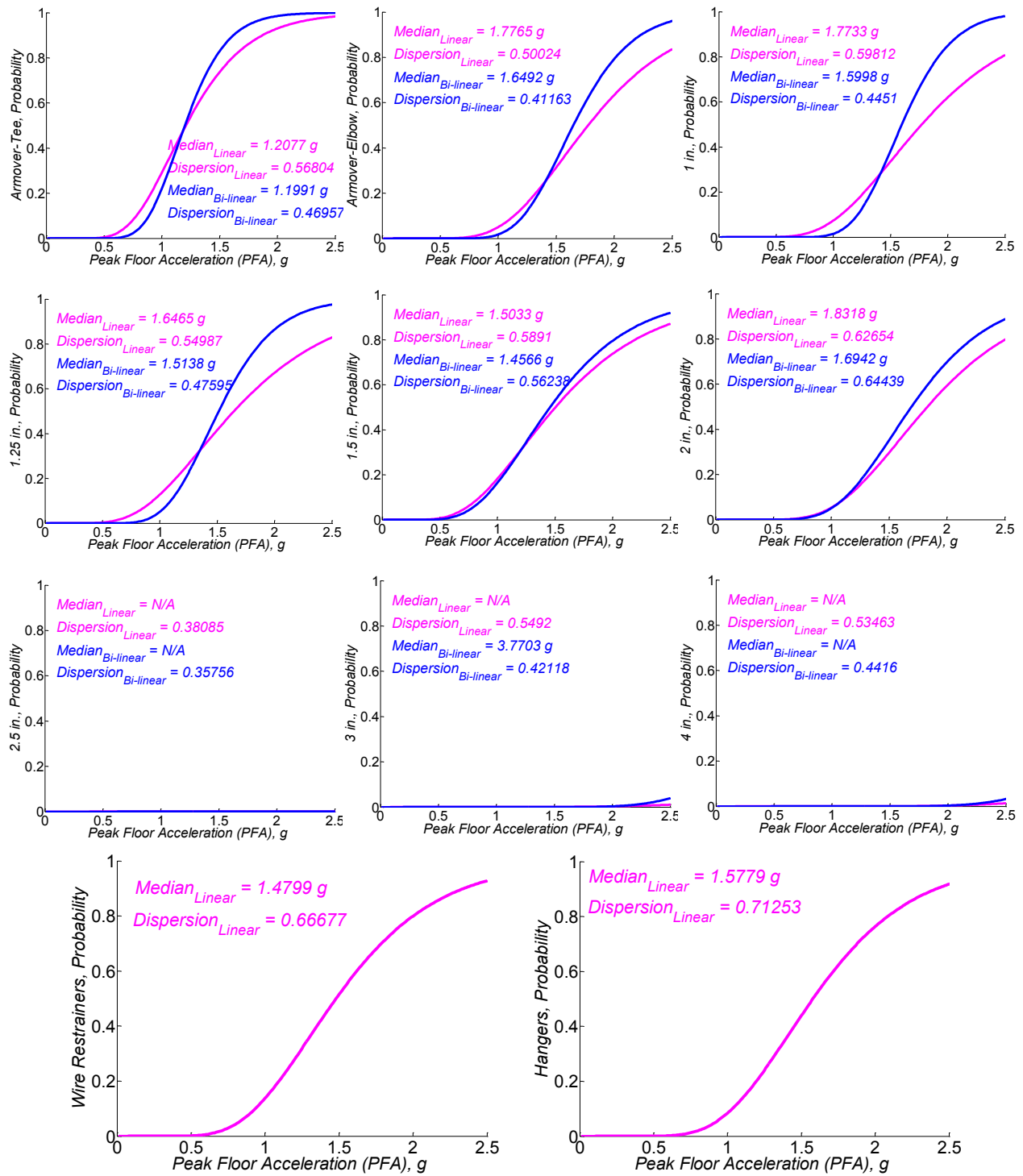


Figure D- 10 Component Fragility Curves, Moderate - Case 3

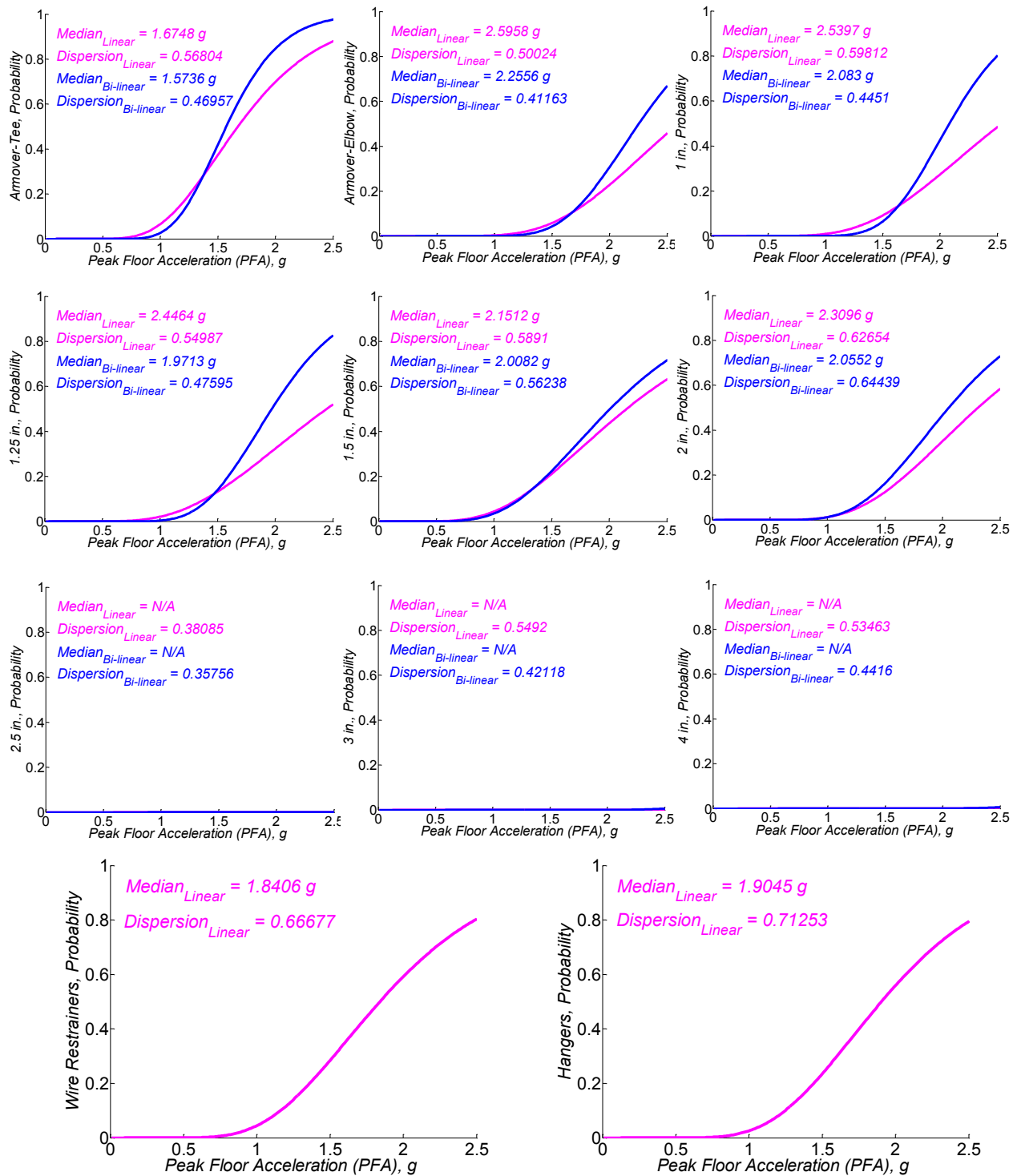


Figure D- 11 Component Fragility Curves, Extensive - Case 3

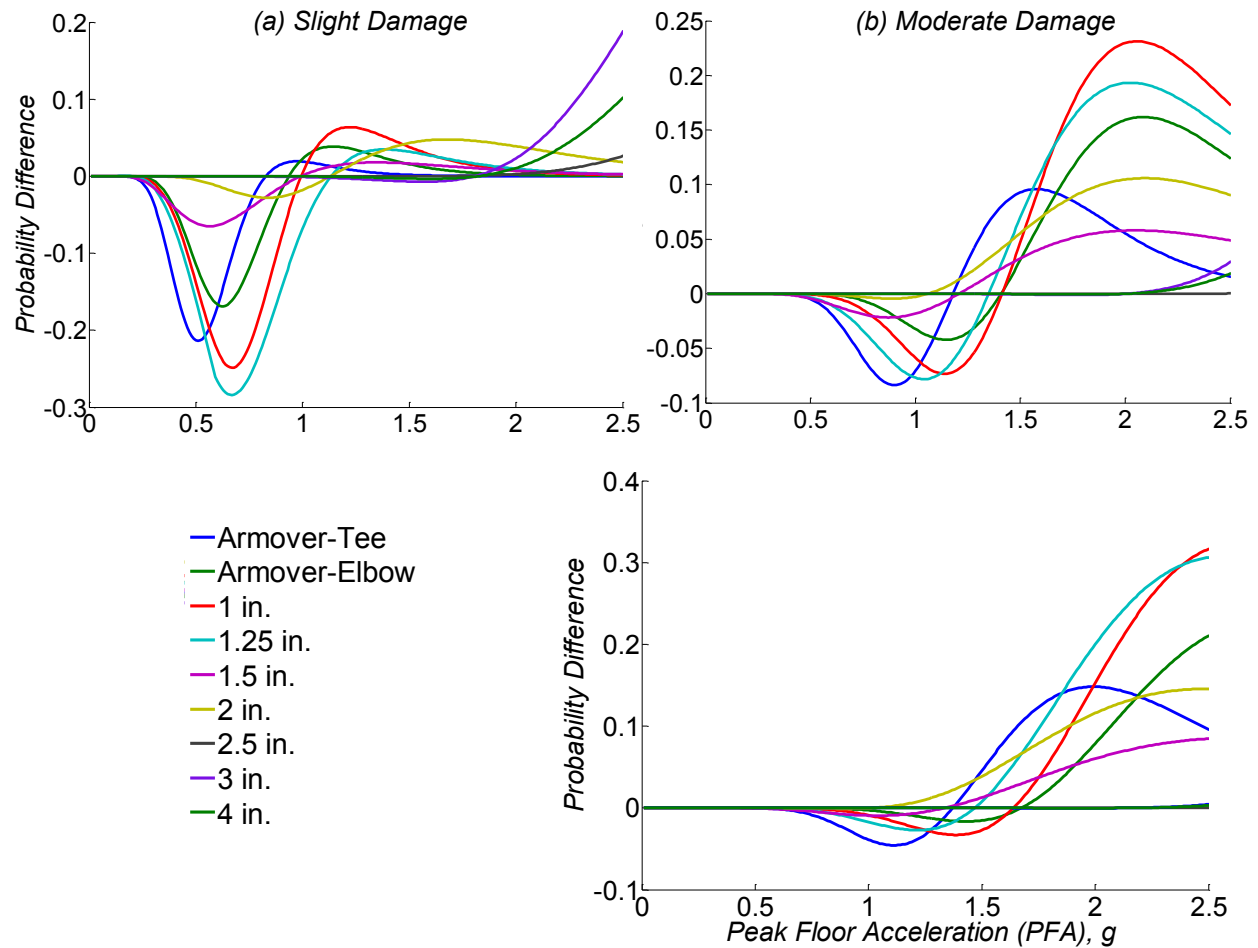


Figure D- 12 Fragility Probability Differences of Pipe Joints Using Linear and Bilinear Regression Analysis for Case 3

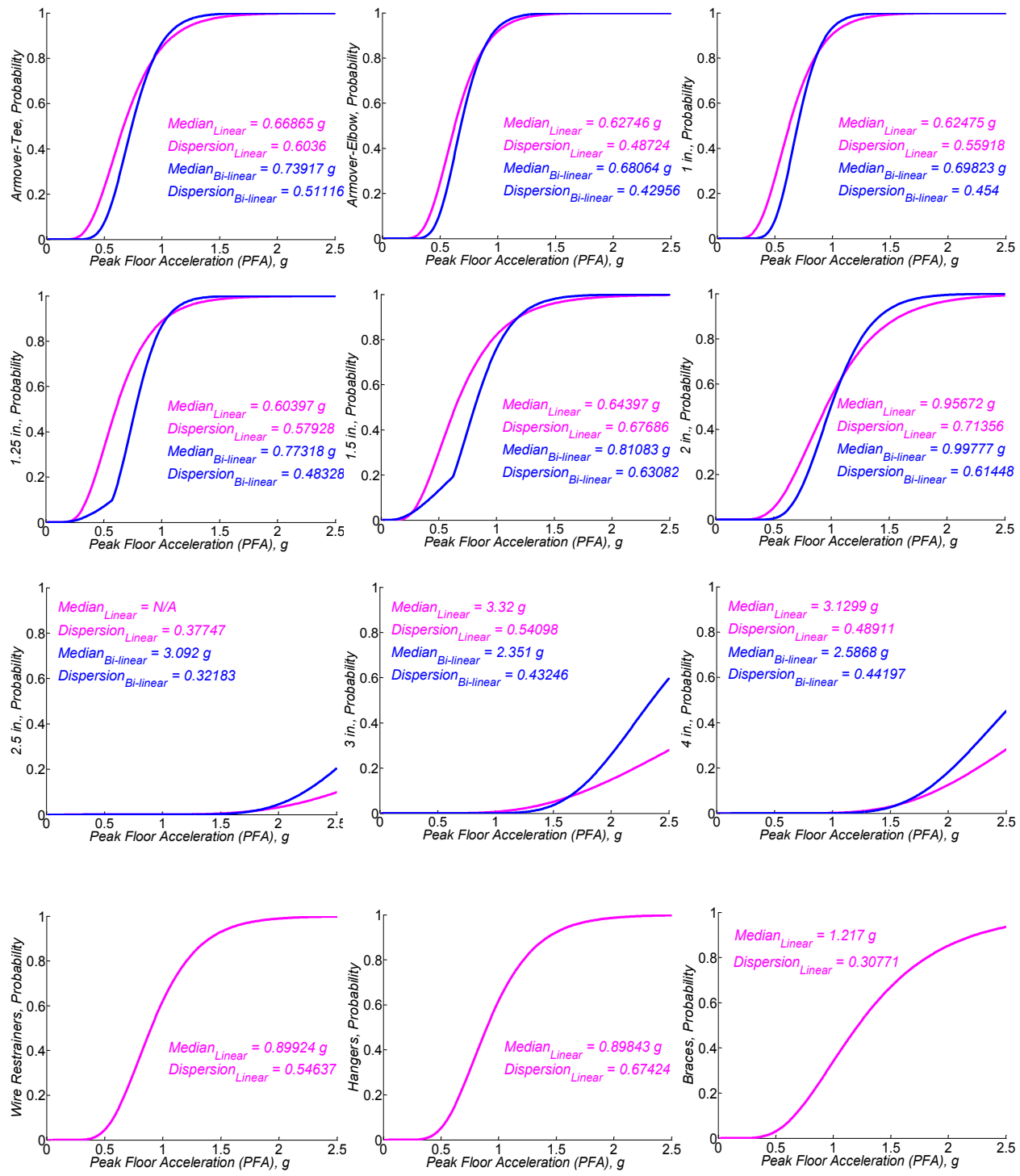


Figure D- 13 Component Fragility Curves, Slight - Case 4

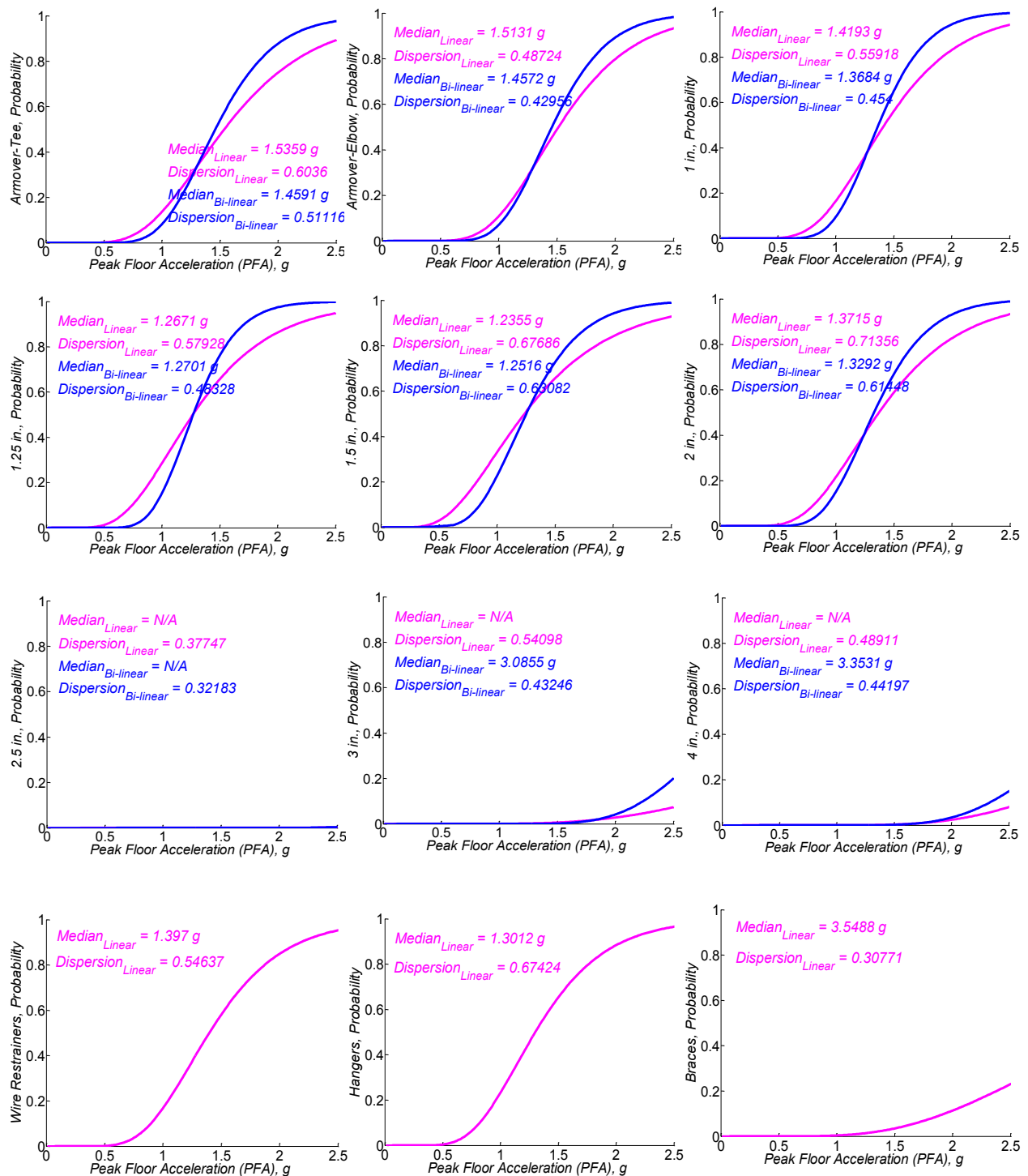


Figure D- 14 Component Fragility Curves, Moderate - Case 4

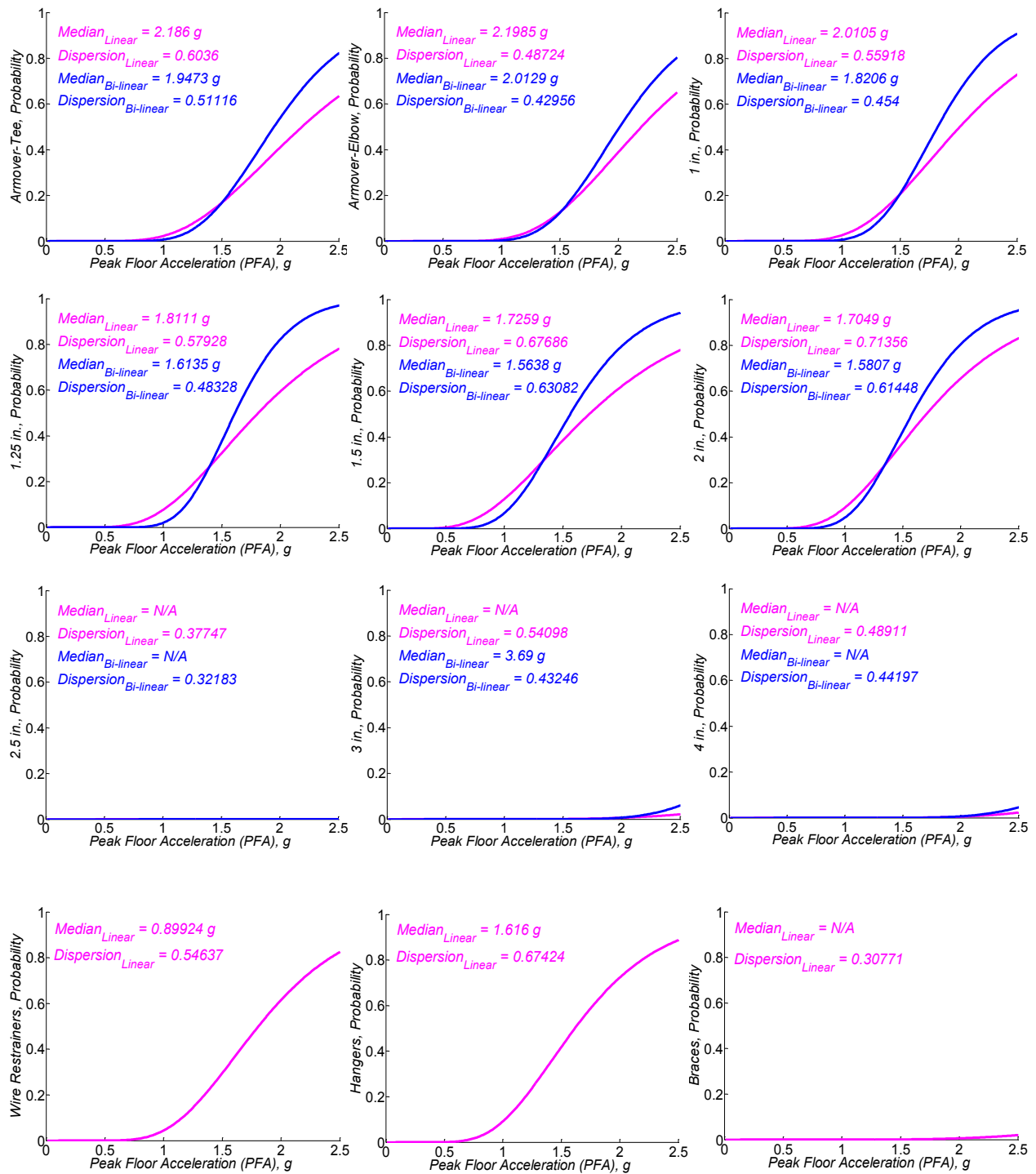


Figure D- 15 Component Fragility Curves, Extensive - Case 4

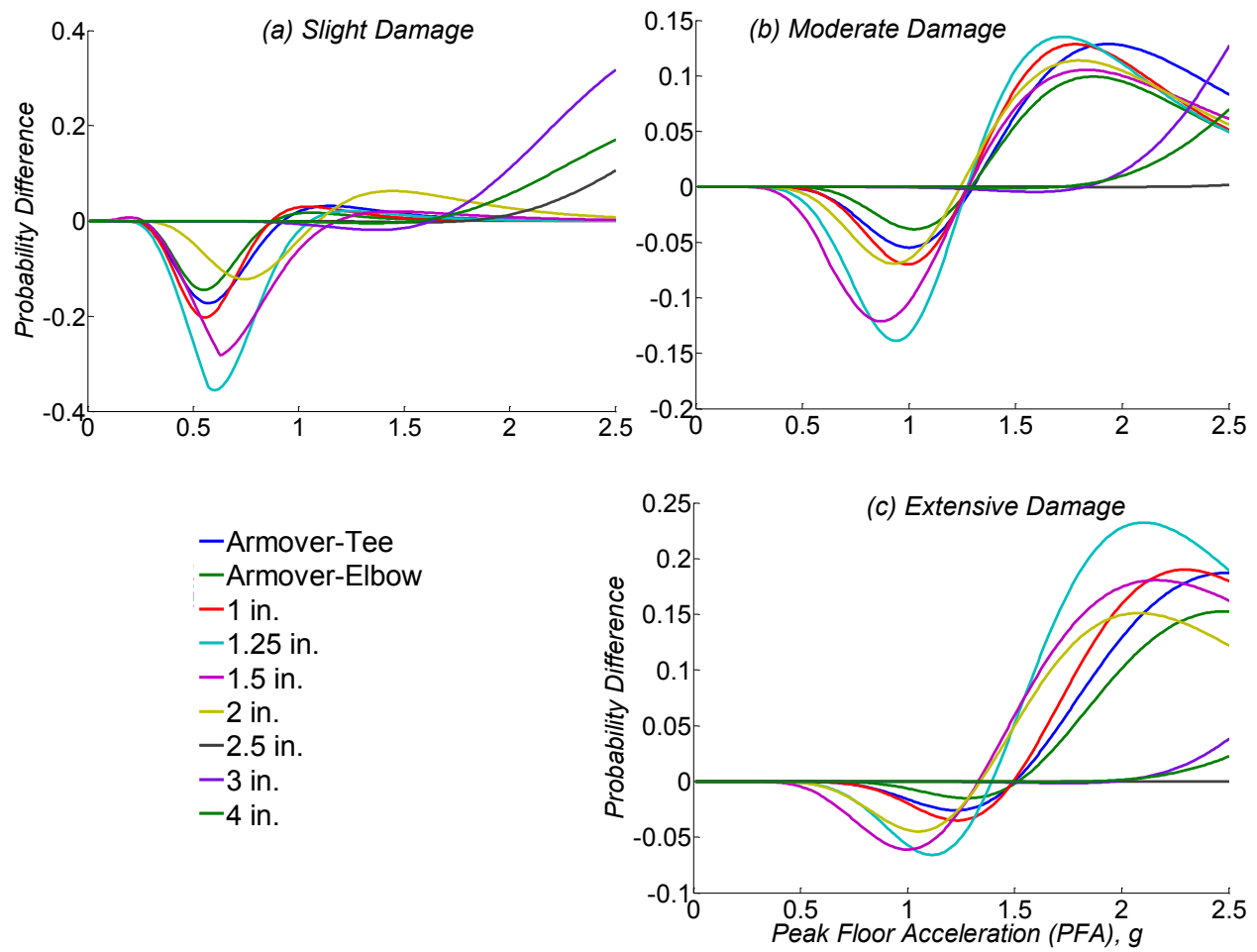


Figure D- 16 Fragility Probability Differences of Pipe Joints Using Linear and Bilinear Regression Analysis for Case 4

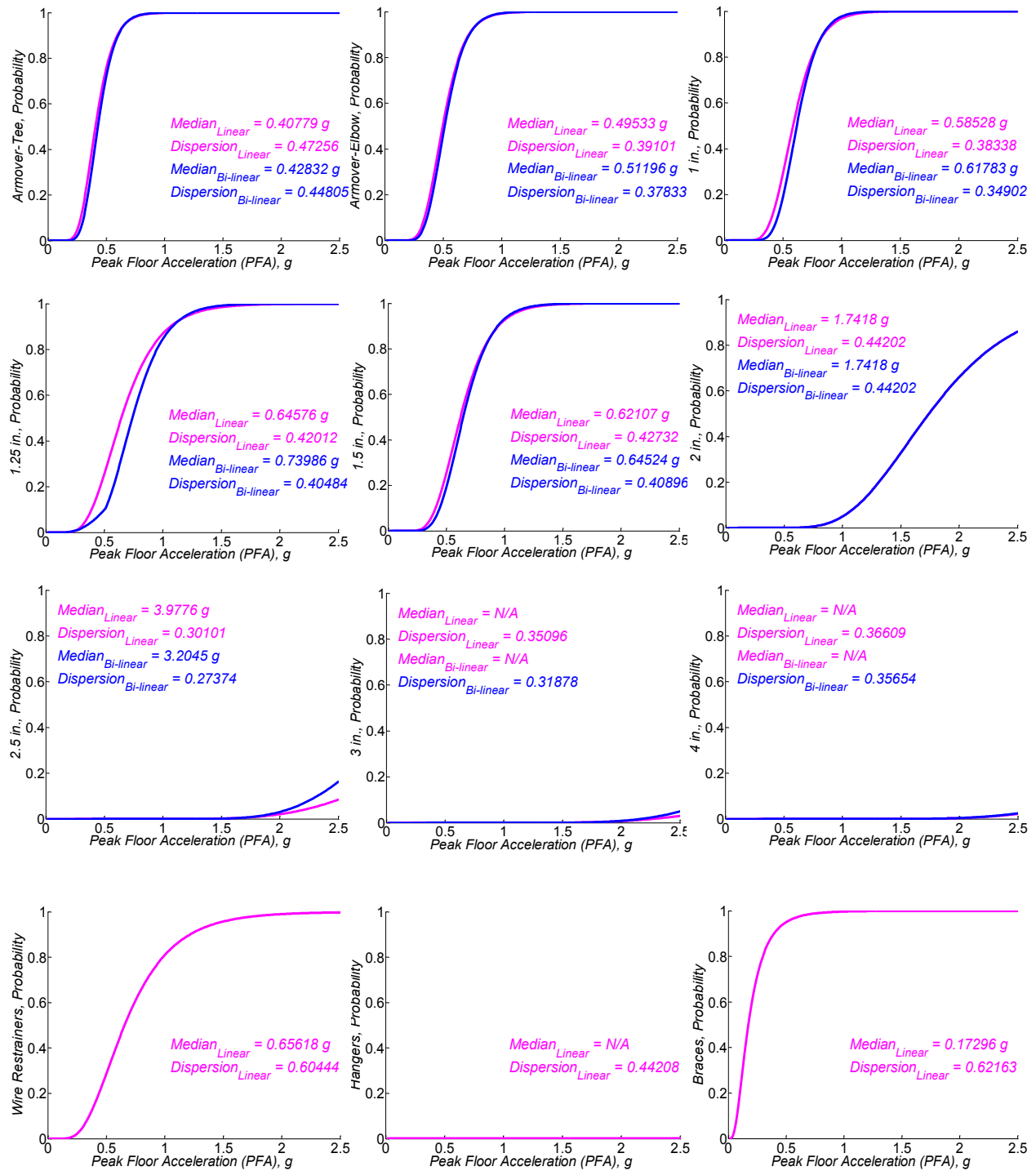


Figure D- 17 Component Fragility Curves, Slight - Case 5

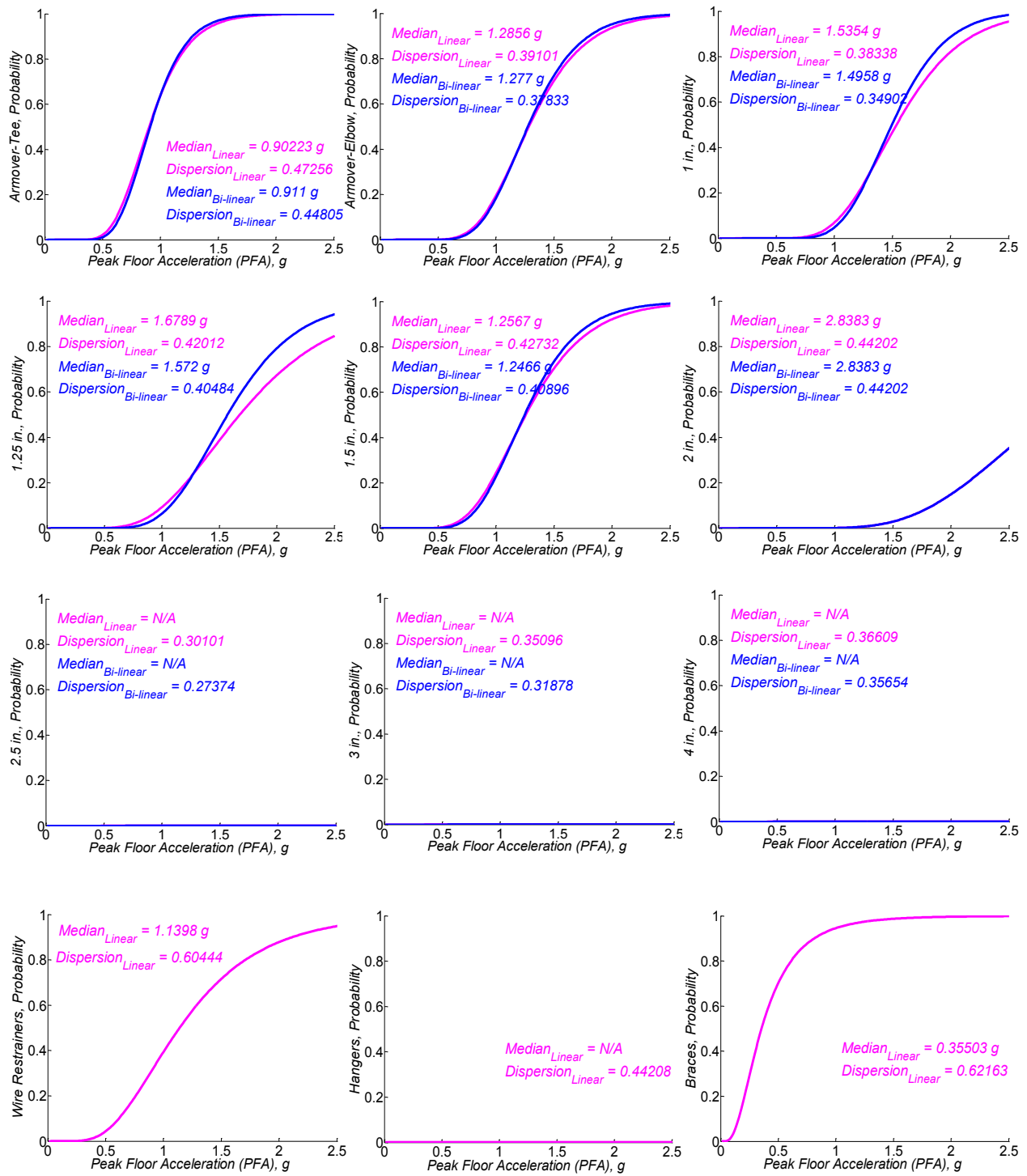


Figure D- 18 Component Fragility Curves, Moderate - Case 5

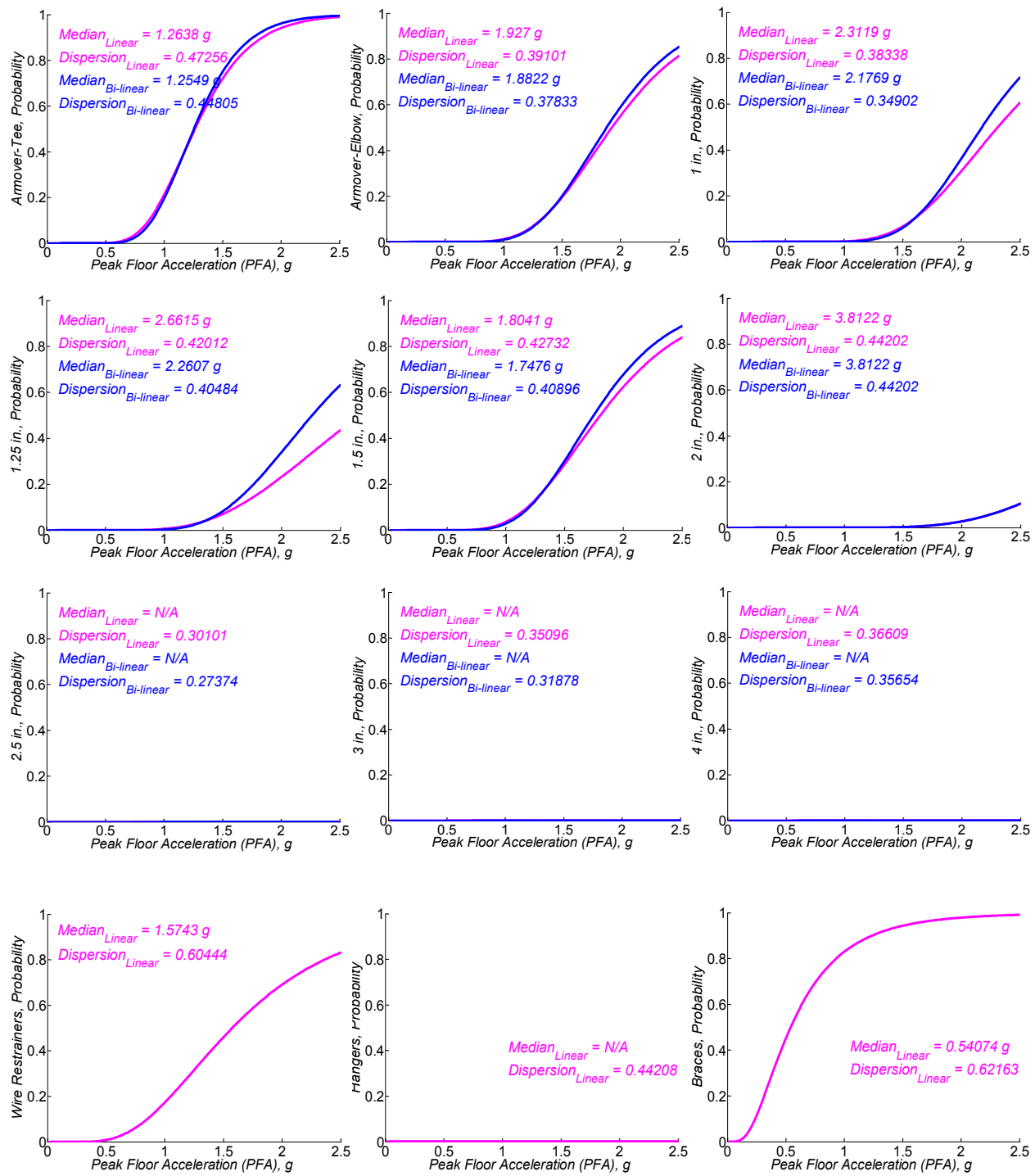


Figure D- 19 Component Fragility Curves, Extensive - Case 5

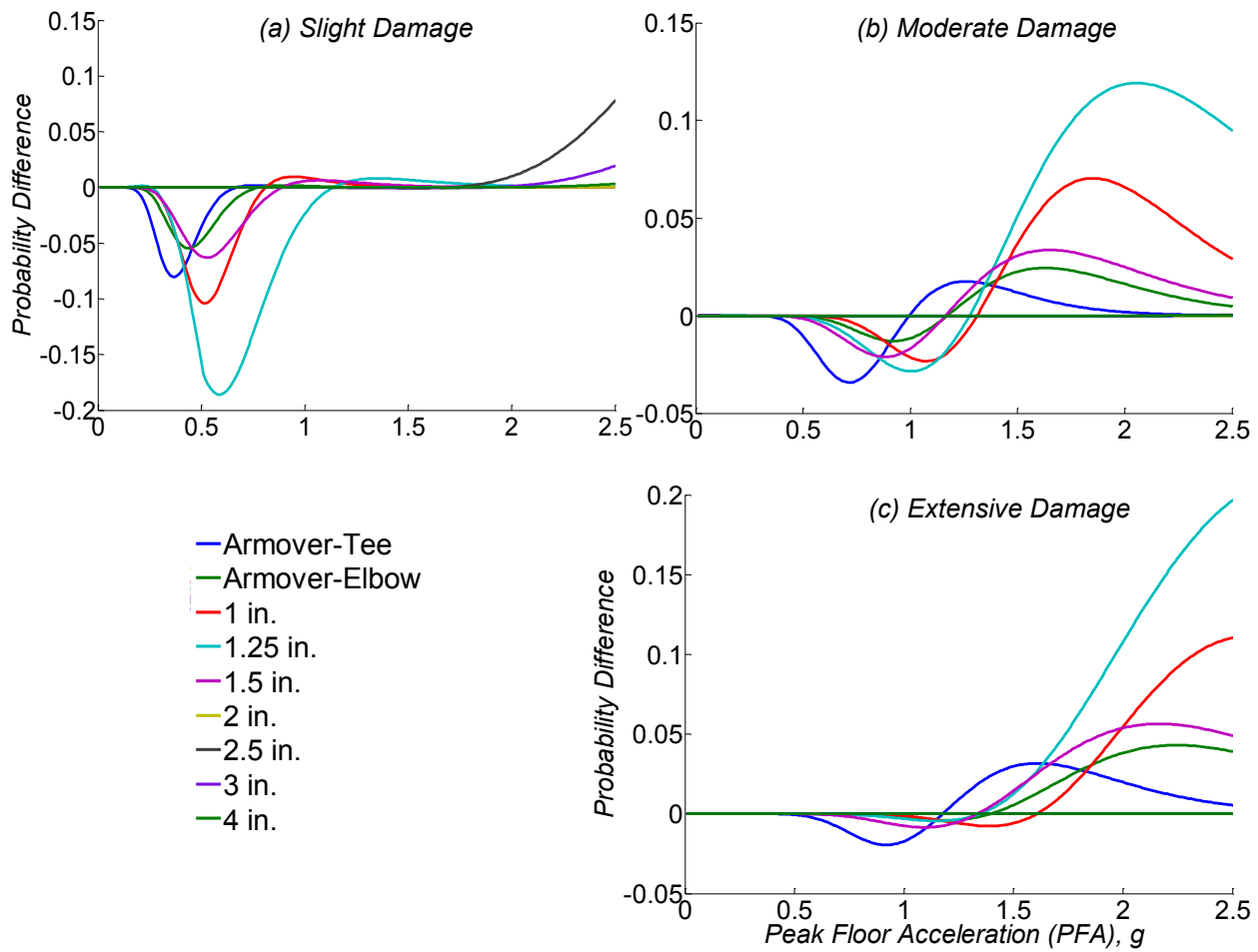


Figure D- 20 Fragility Probability Differences of Pipe Joints Using Linear and Bilinear Regression Analysis for Case 5

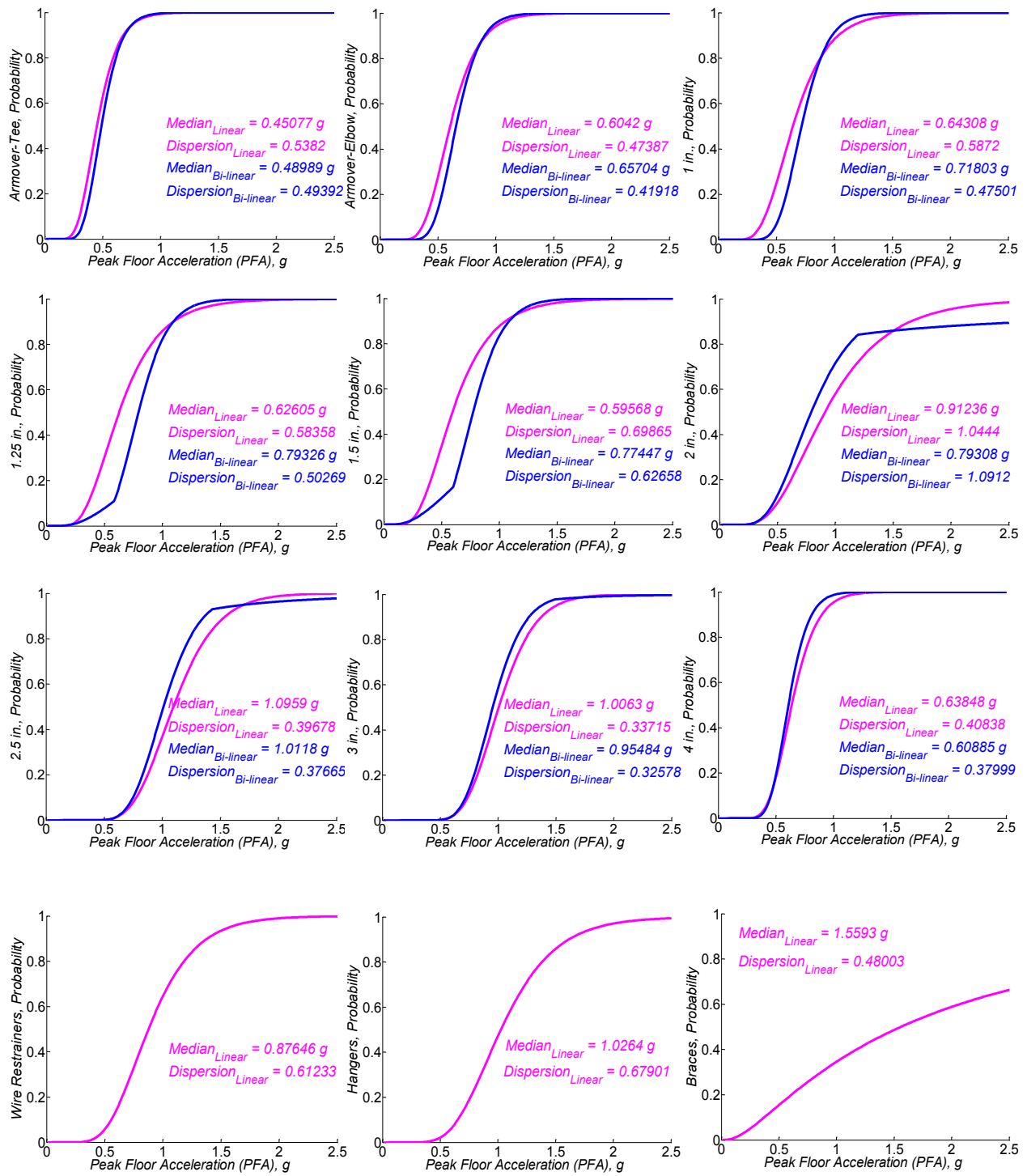


Figure D- 21 Component Fragility Curves, Slight - Case 6

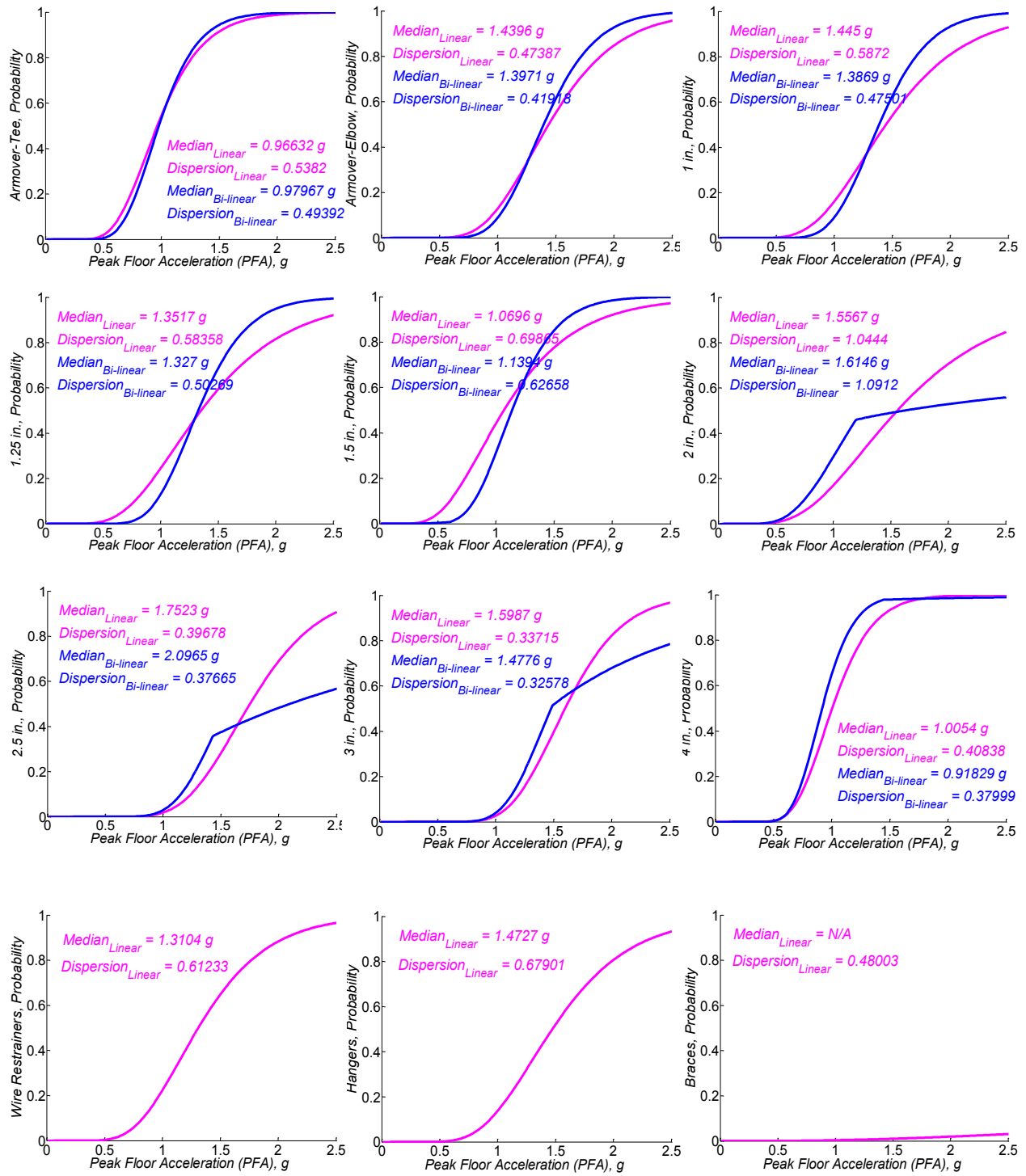


Figure D- 22 Component Fragility Curves, Moderate - Case 6

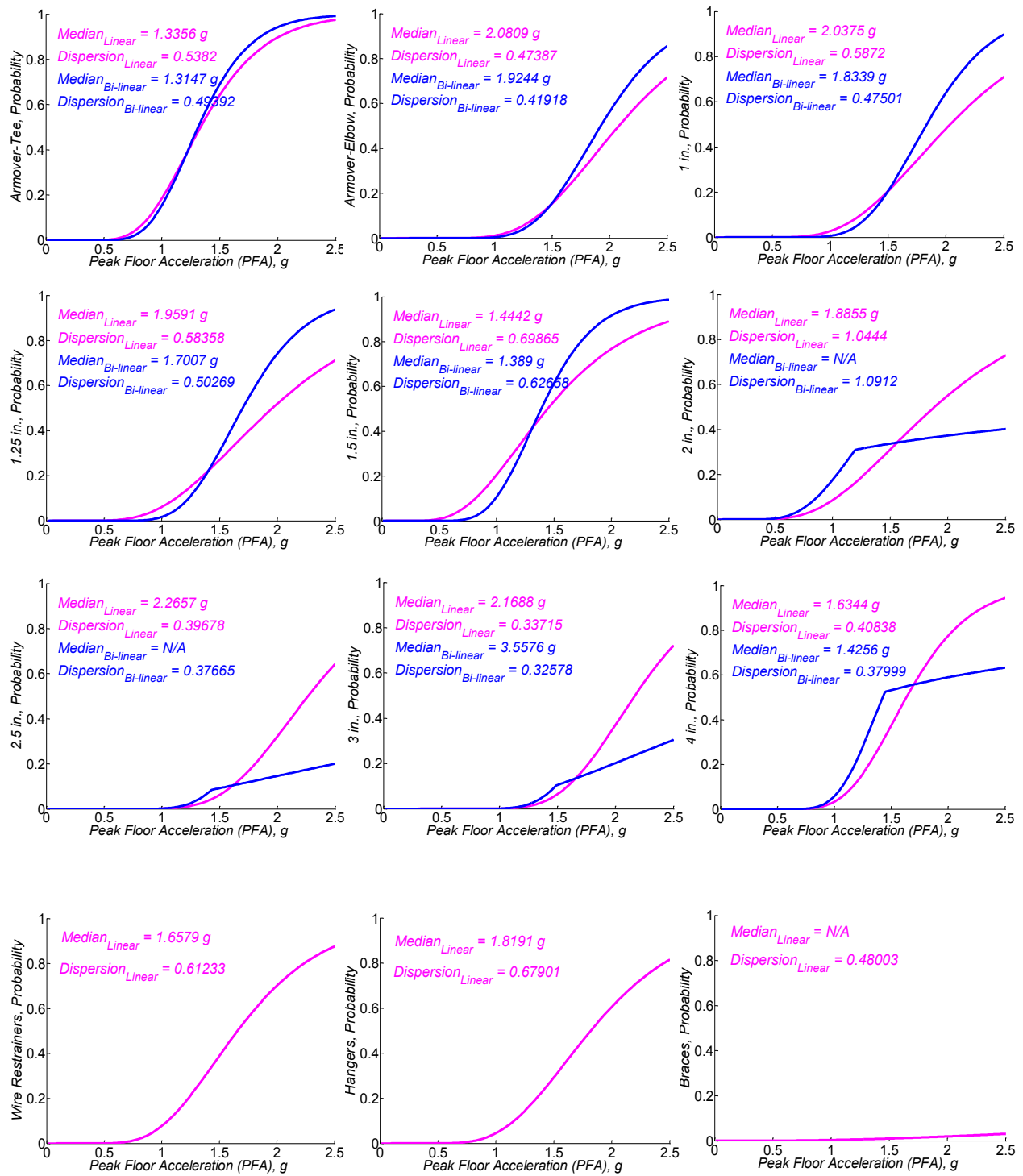


Figure D- 23 Component Fragility Curves, Extensive - Case 6

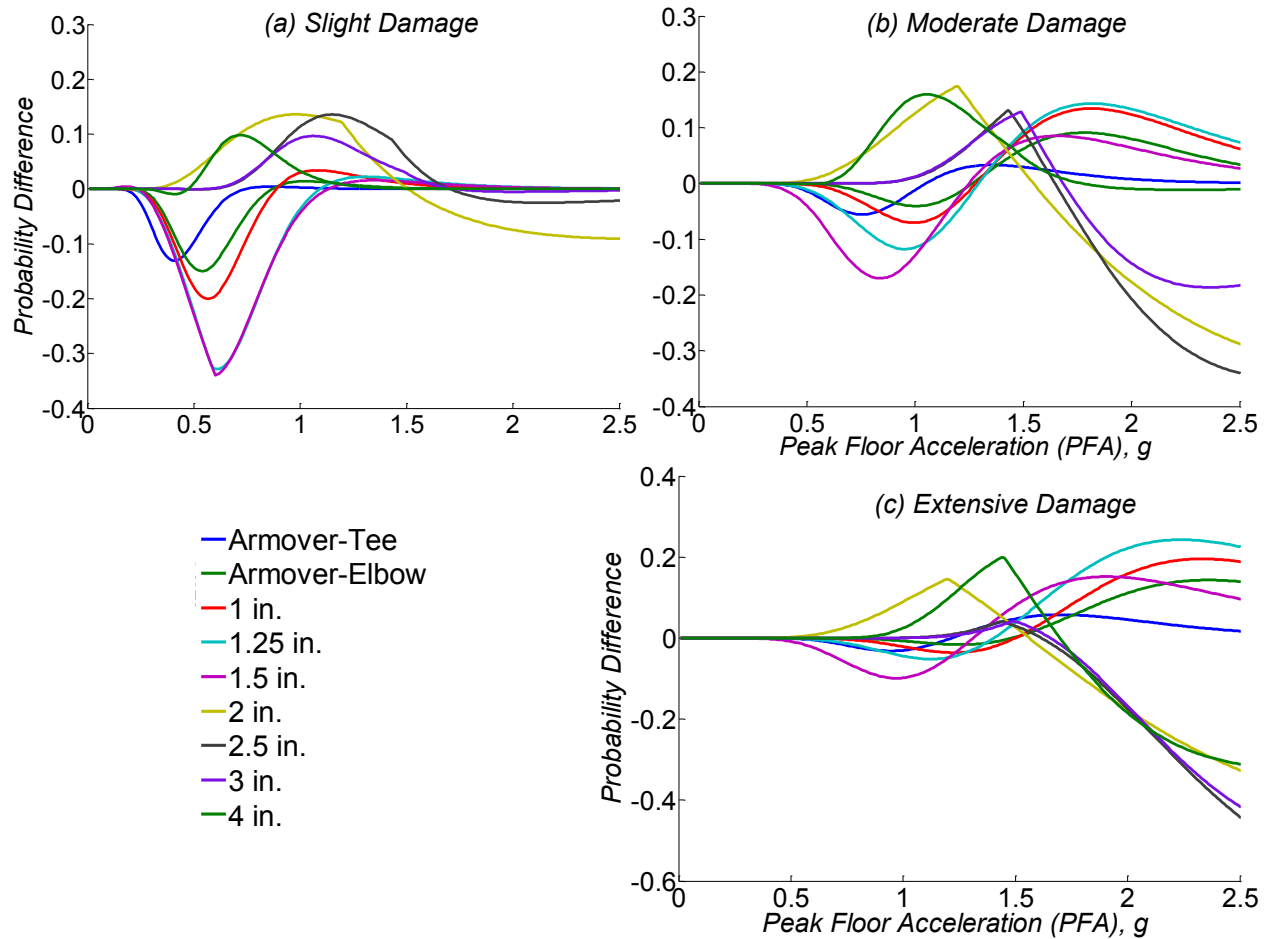


Figure D- 24 Fragility Probability Differences of Pipe Joints Using Linear and Bilinear Regression Analysis for Case 6

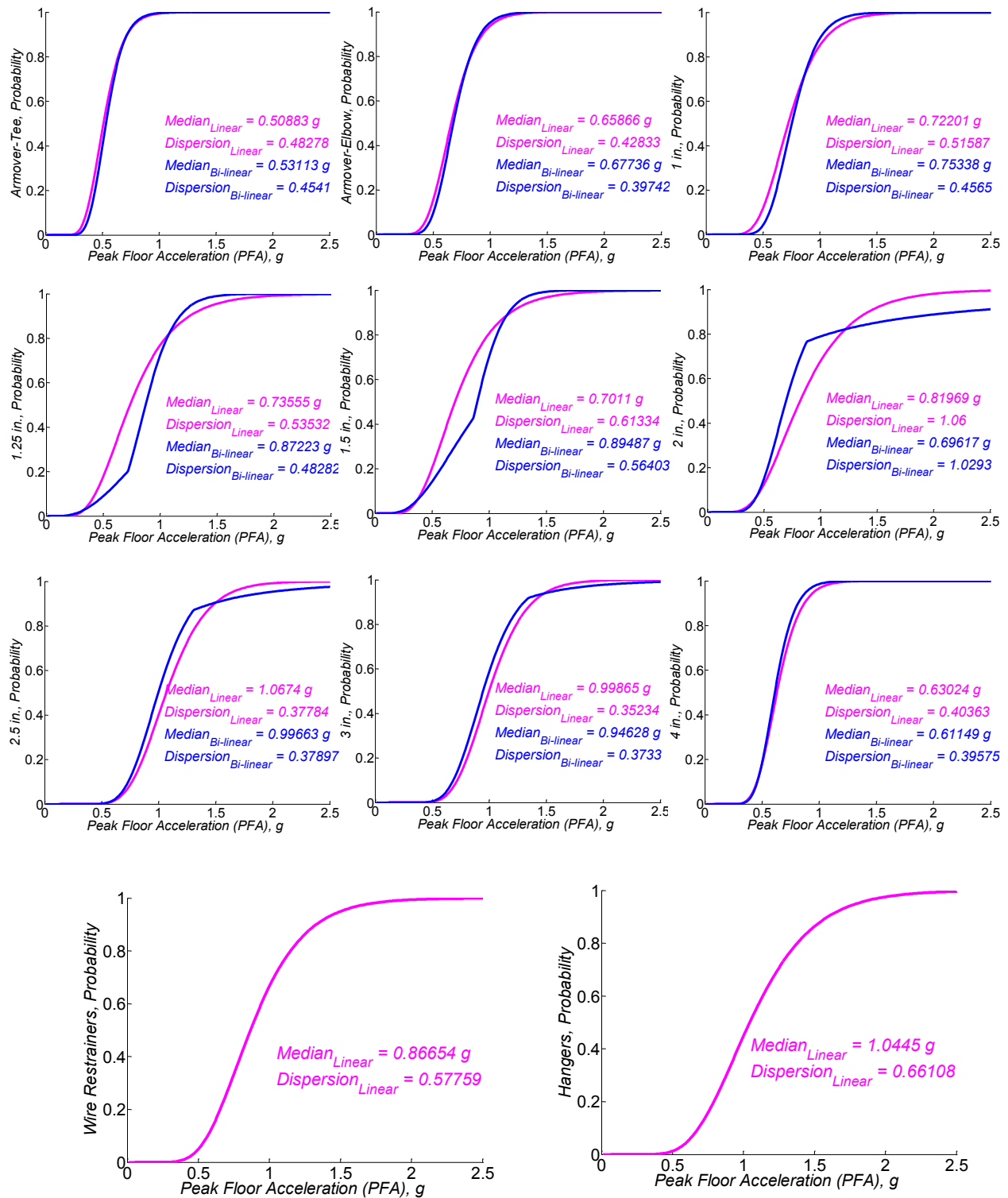


Figure D- 25 Component Fragility Curves, Slight - Case 7

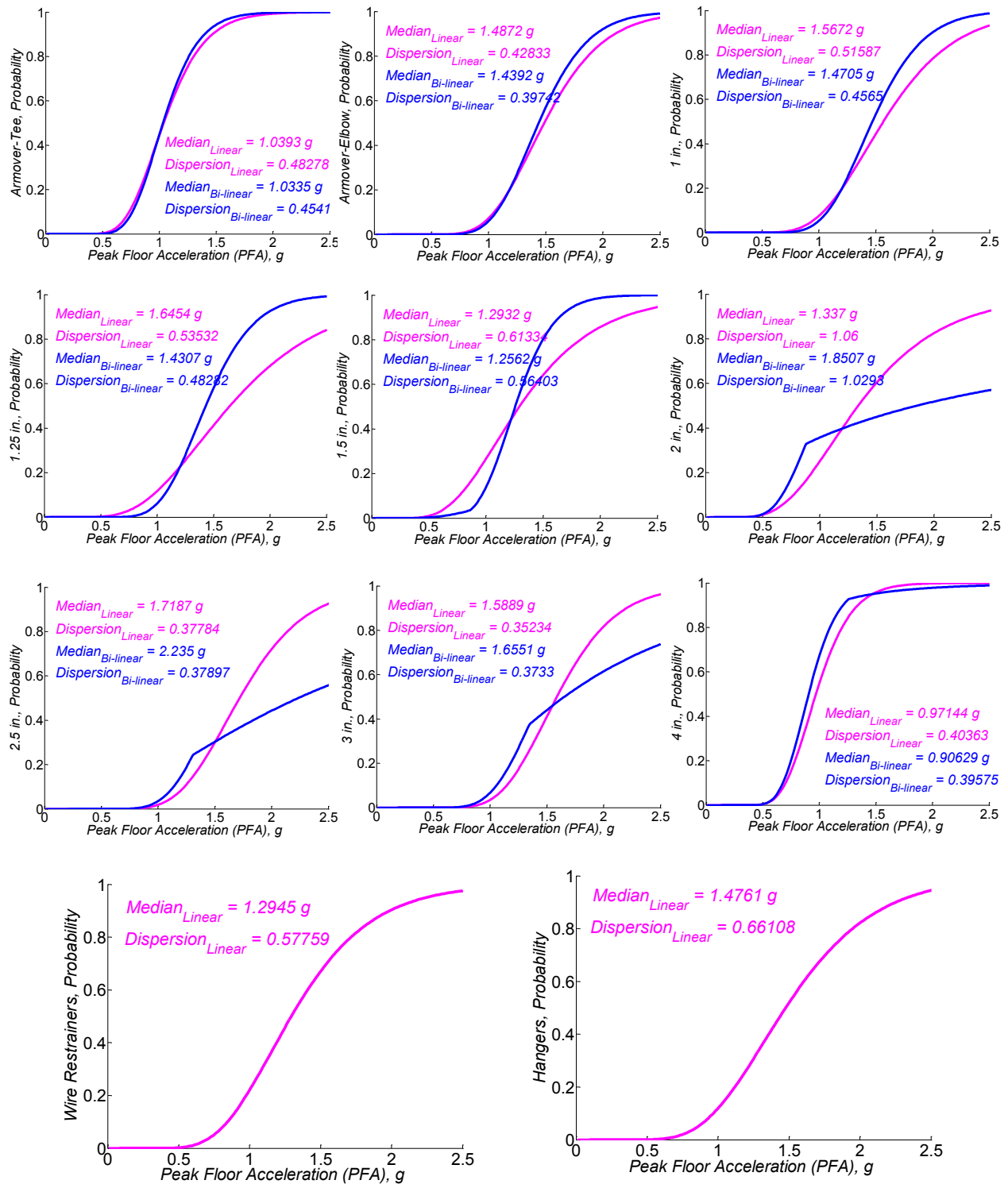


Figure D- 26 Component Fragility Curves, Moderate - Case 7

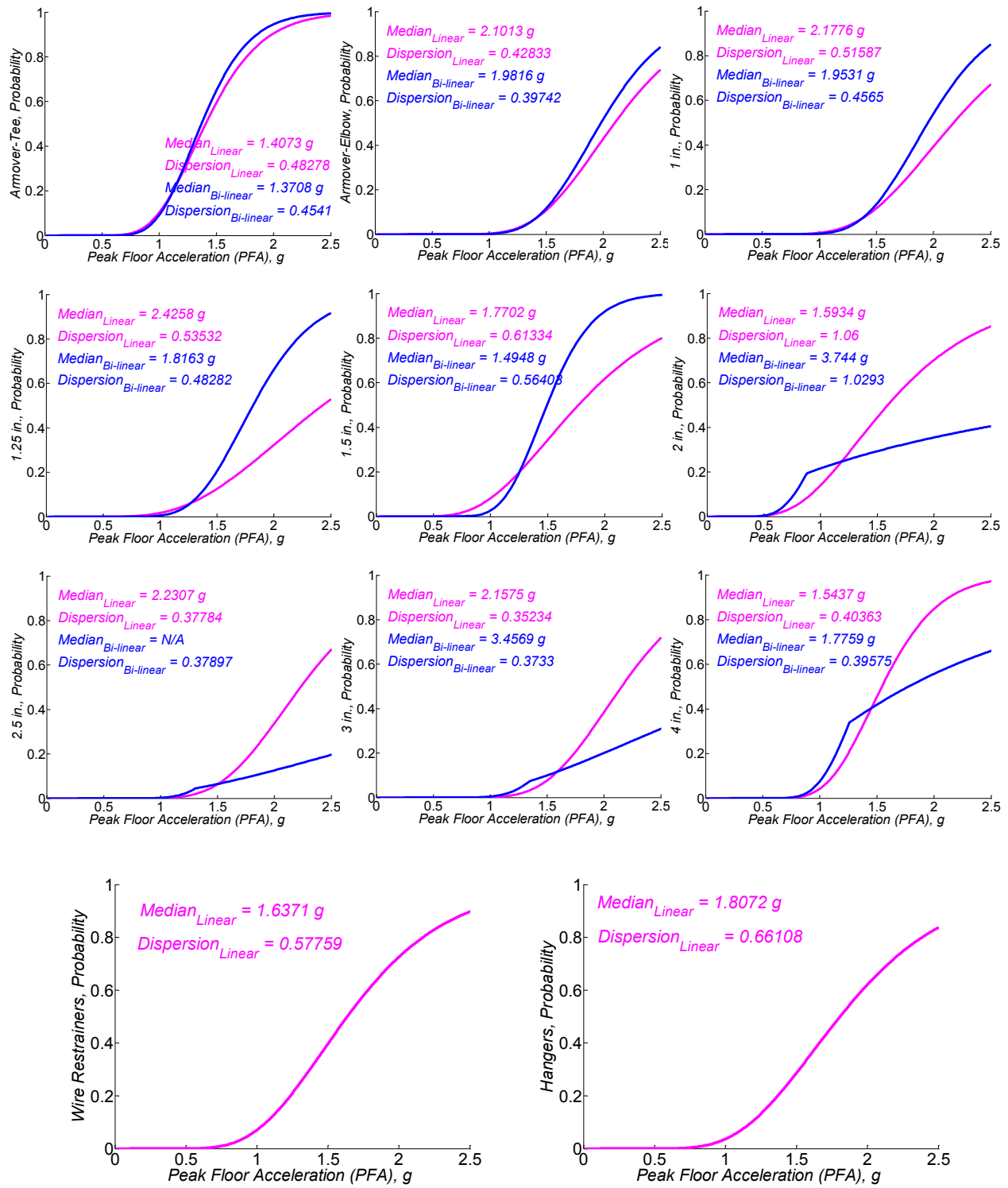


Figure D-27 Component Fragility Curves, Extensive - Case 7

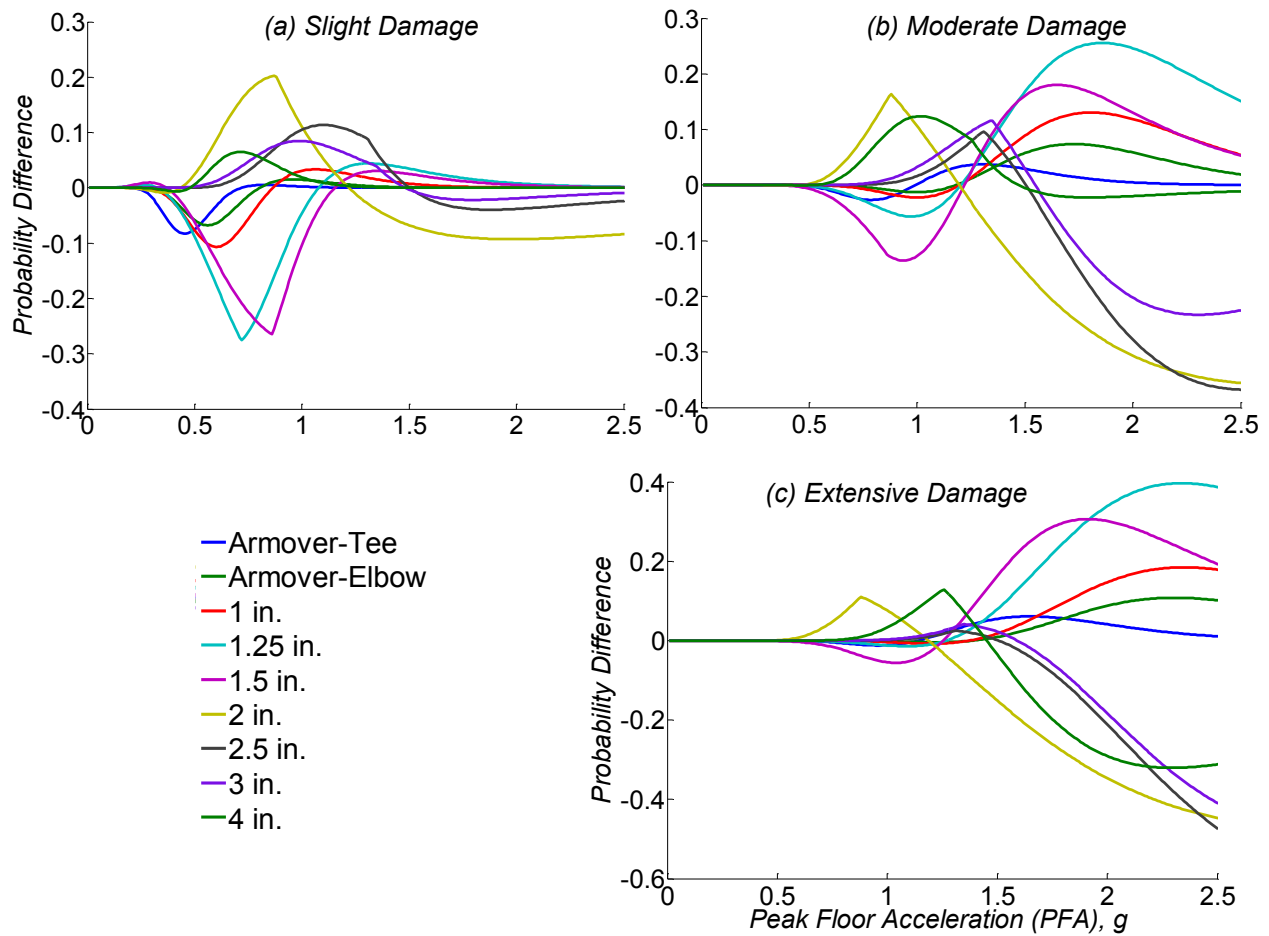


Figure D- 28 Fragility Probability Differences of Pipe Joints Using Linear and Bilinear Regression Analysis for Case 7

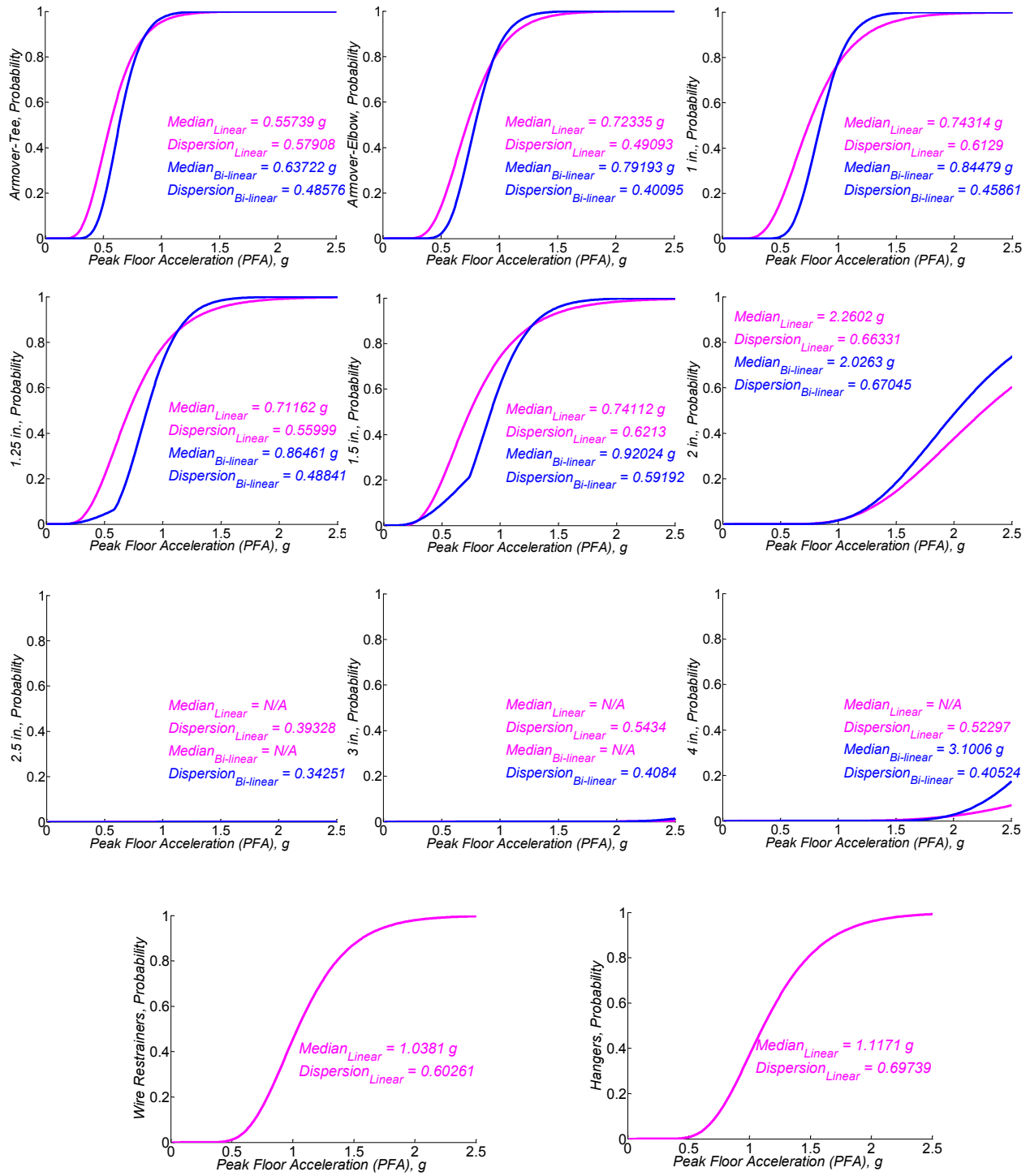


Figure D- 29 Component Fragility Curves, Slight - Case 8

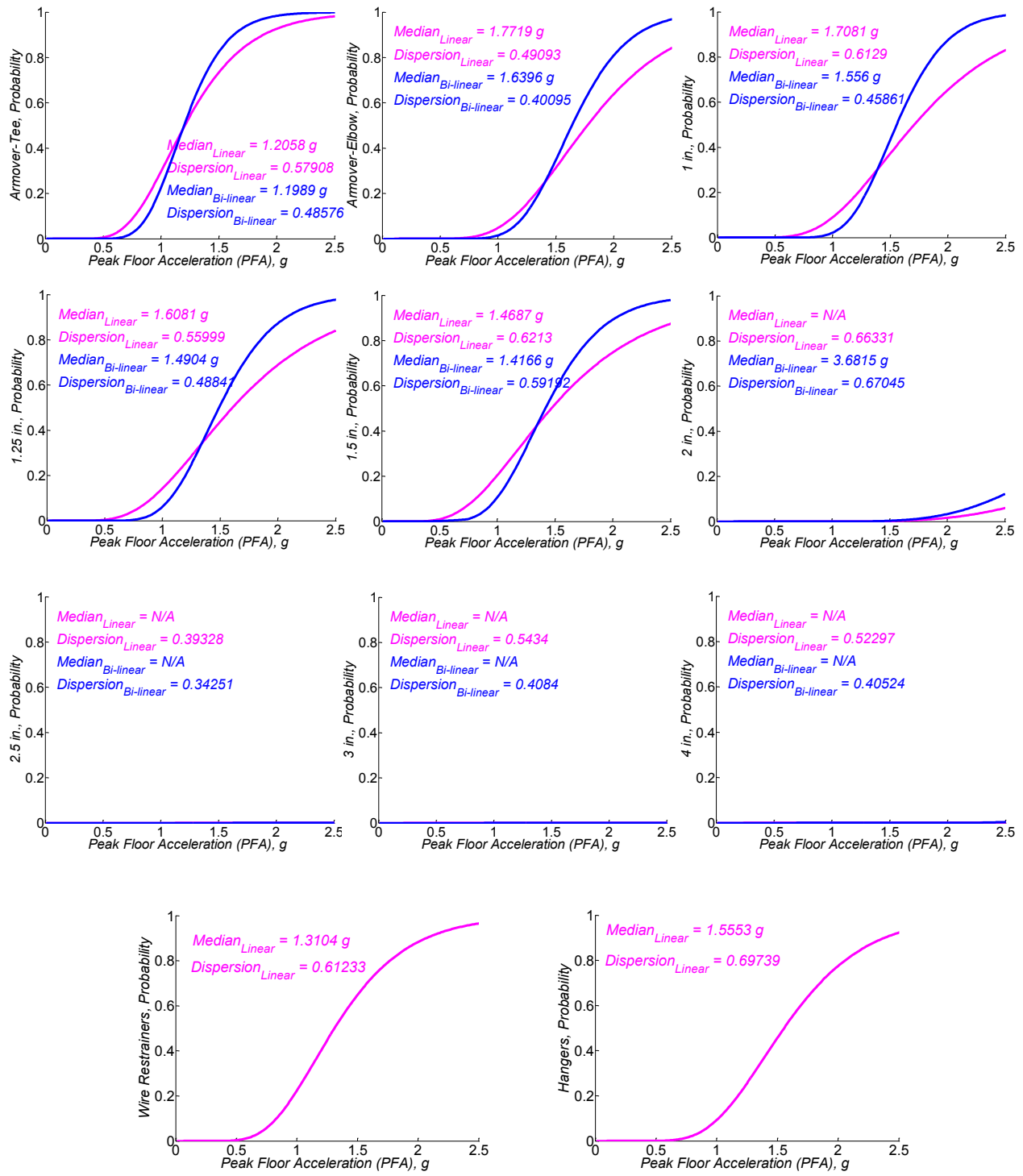


Figure D- 30 Component Fragility Curves, Moderate - Case 8

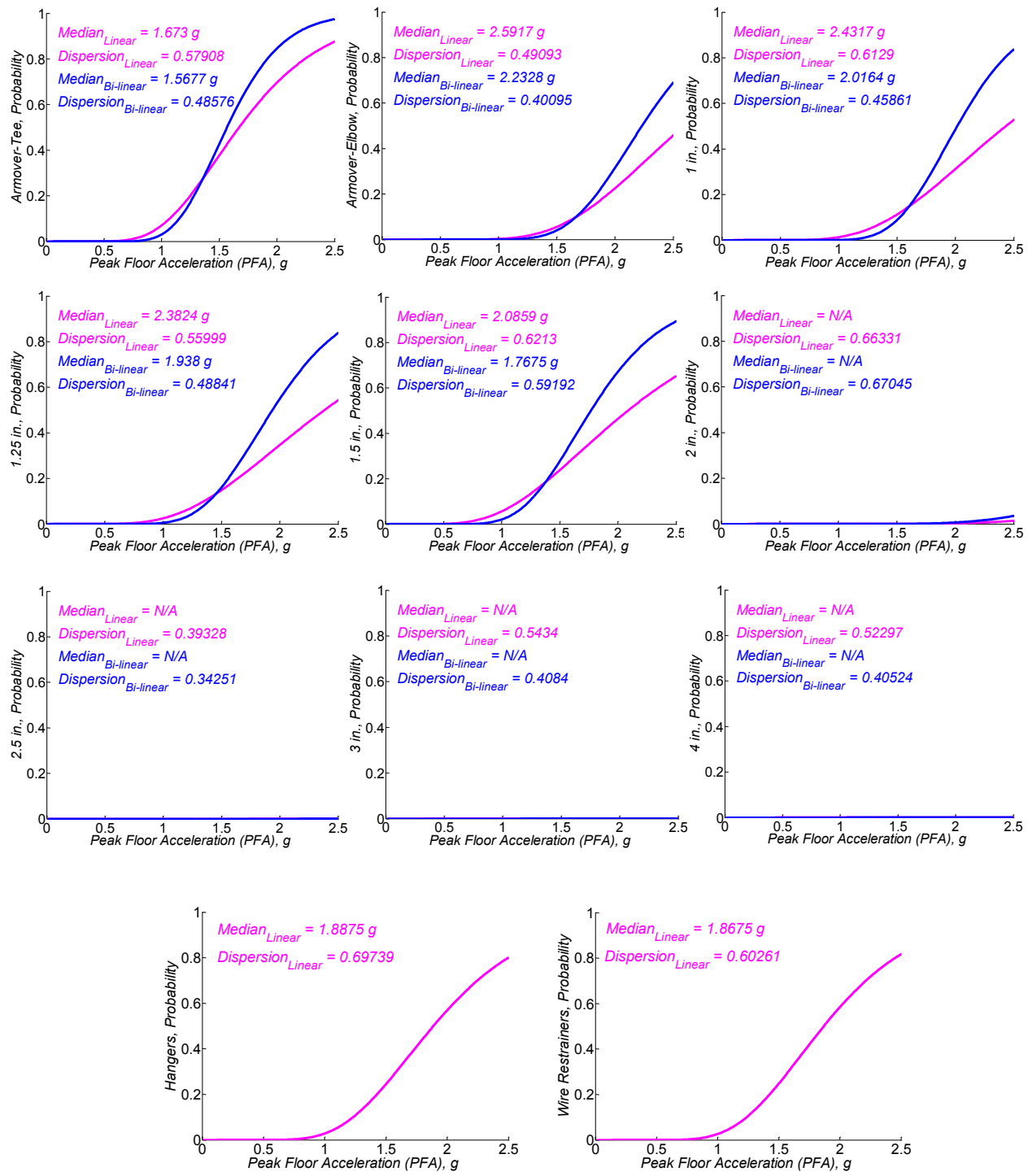


Figure D- 31 Component Fragility Curves, Extensive - Case 8

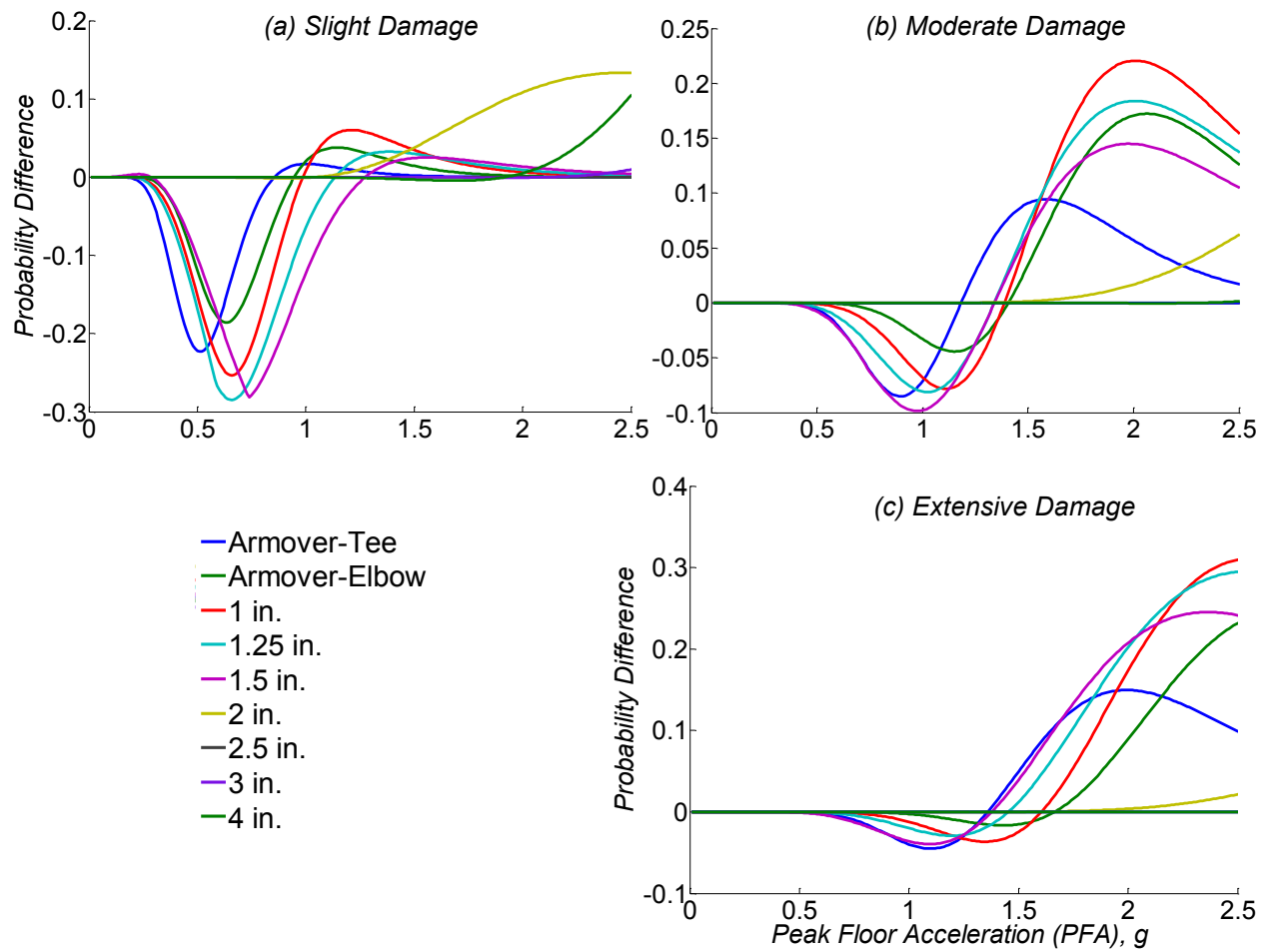


Figure D- 32 Fragility Probability Differences of Pipe Joints Using Linear and Bilinear Regression Analysis for Case 8

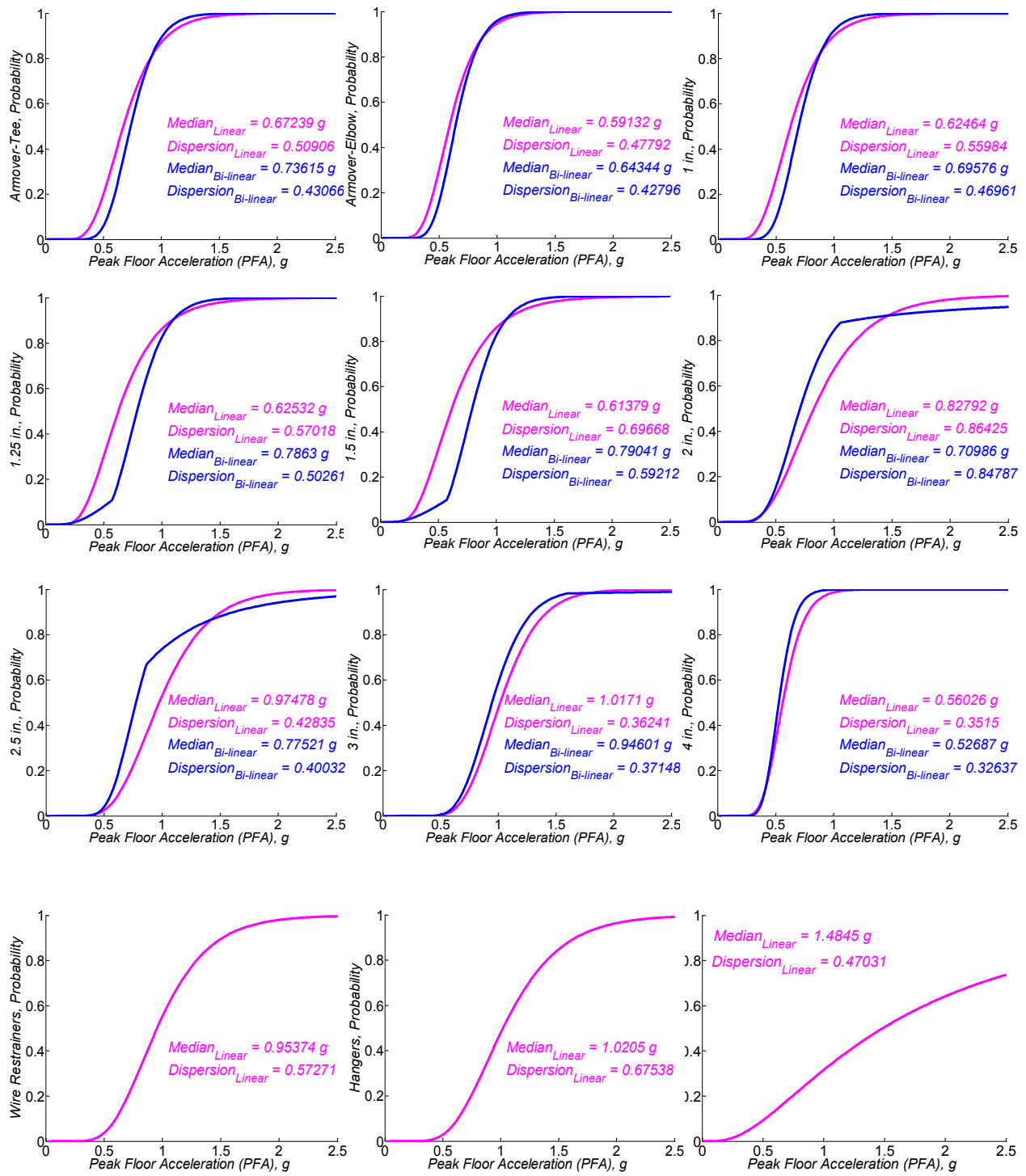


Figure D-33 Component Fragility Curves, Slight - Case 9

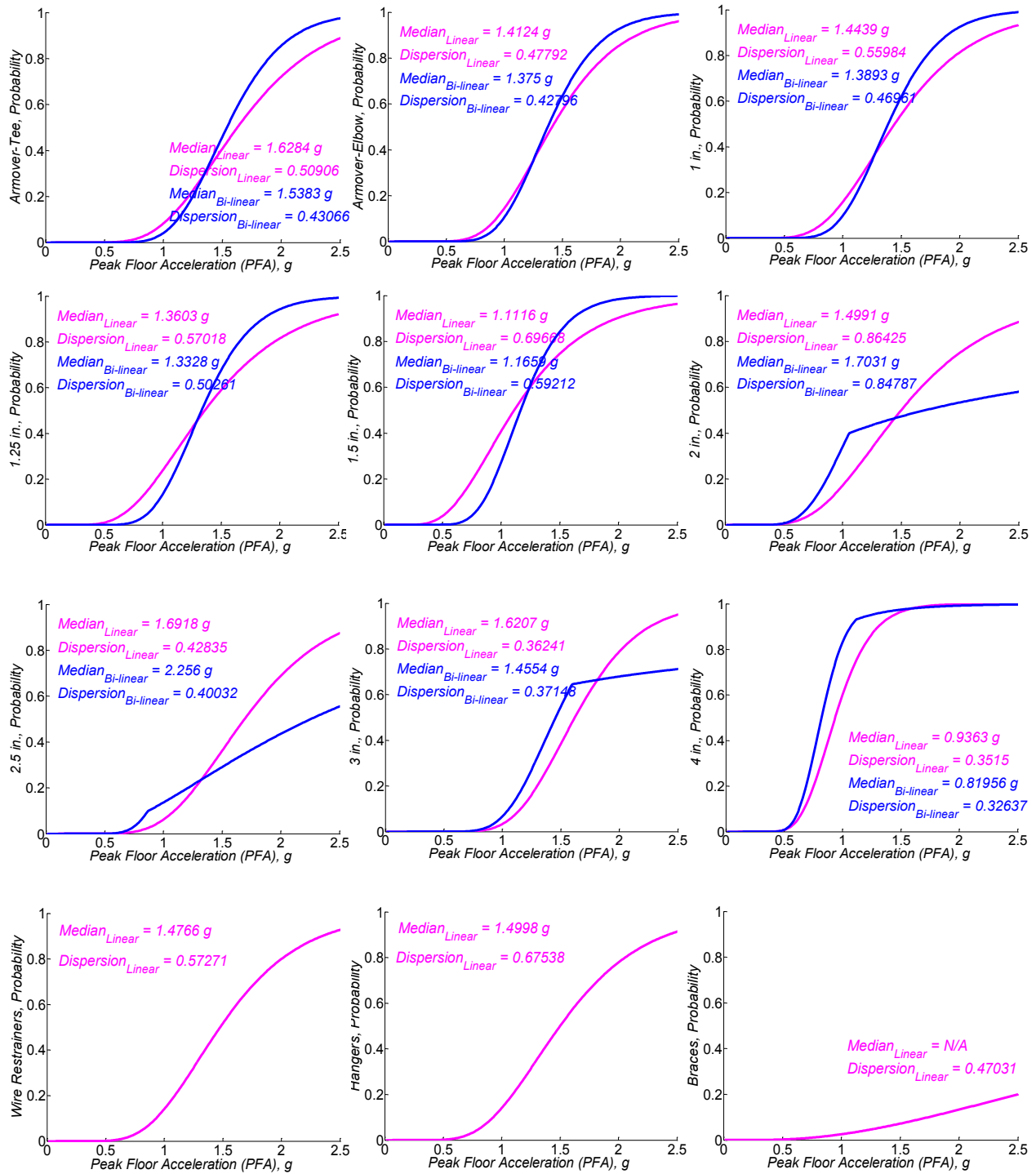
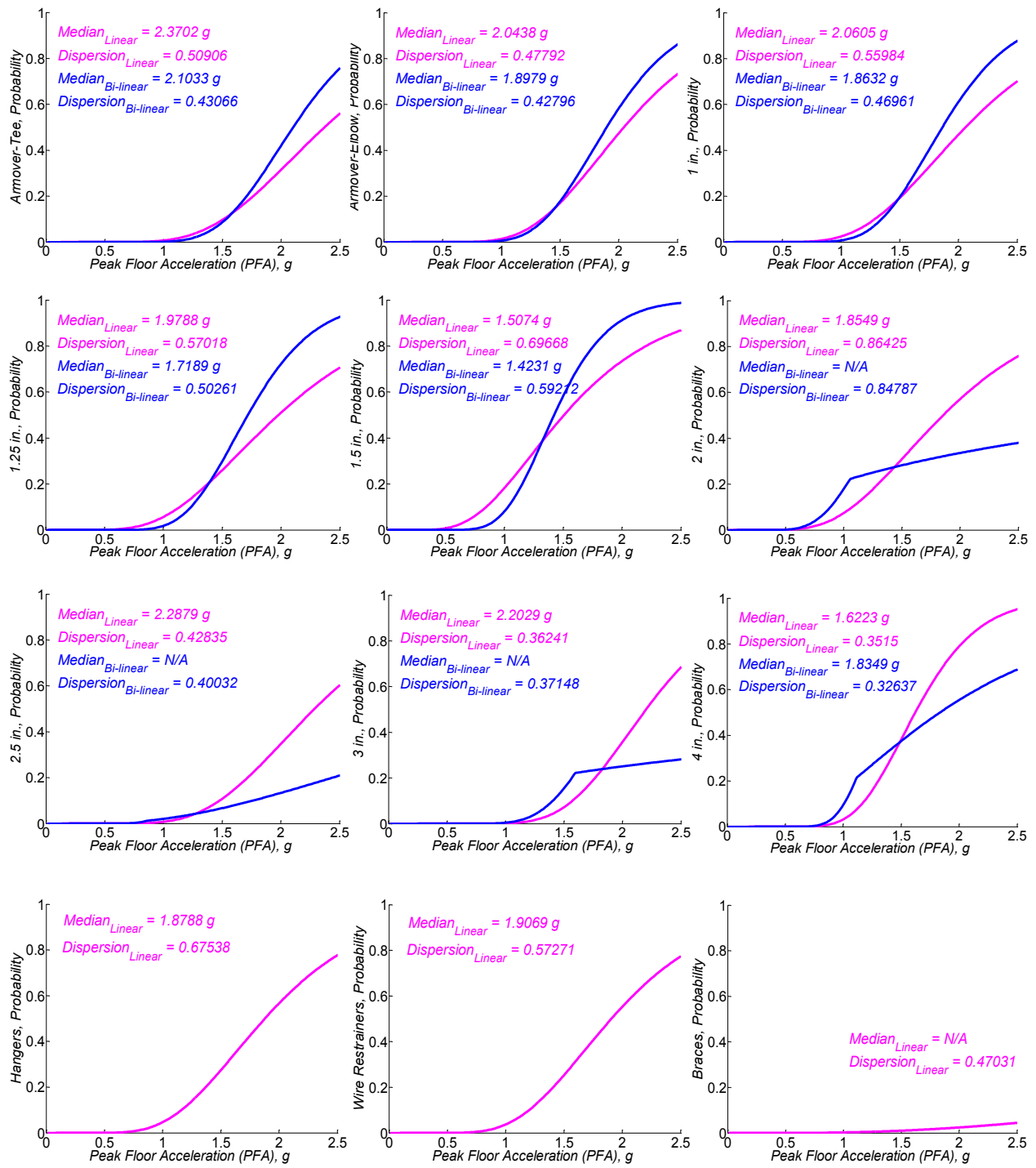


Figure D- 34 Component Fragility Curves, Moderate - Case 9



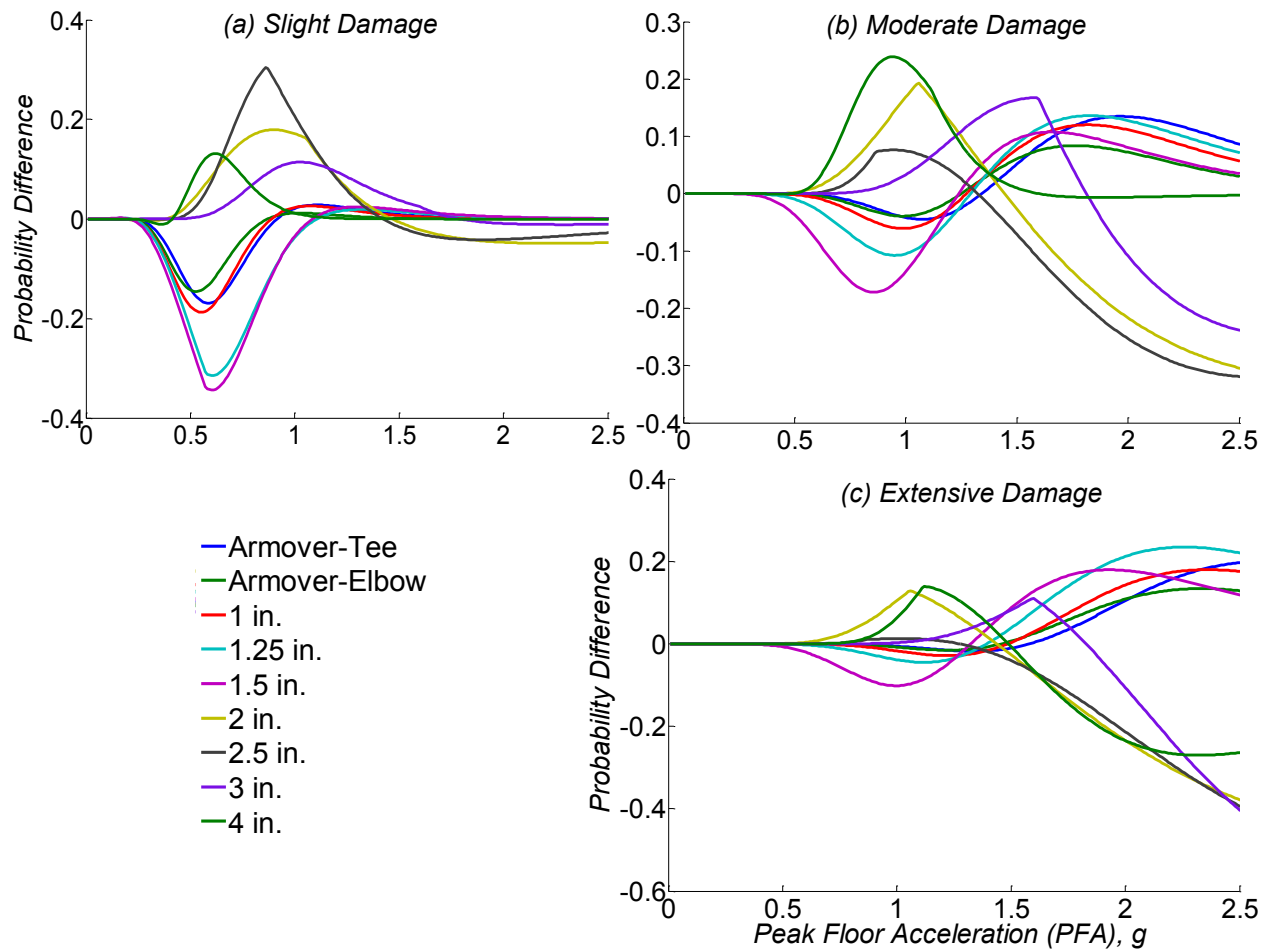


Figure D- 36 Fragility Probability Differences of Pipe Joints Using Linear and Bilinear Regression Analysis for Case 9

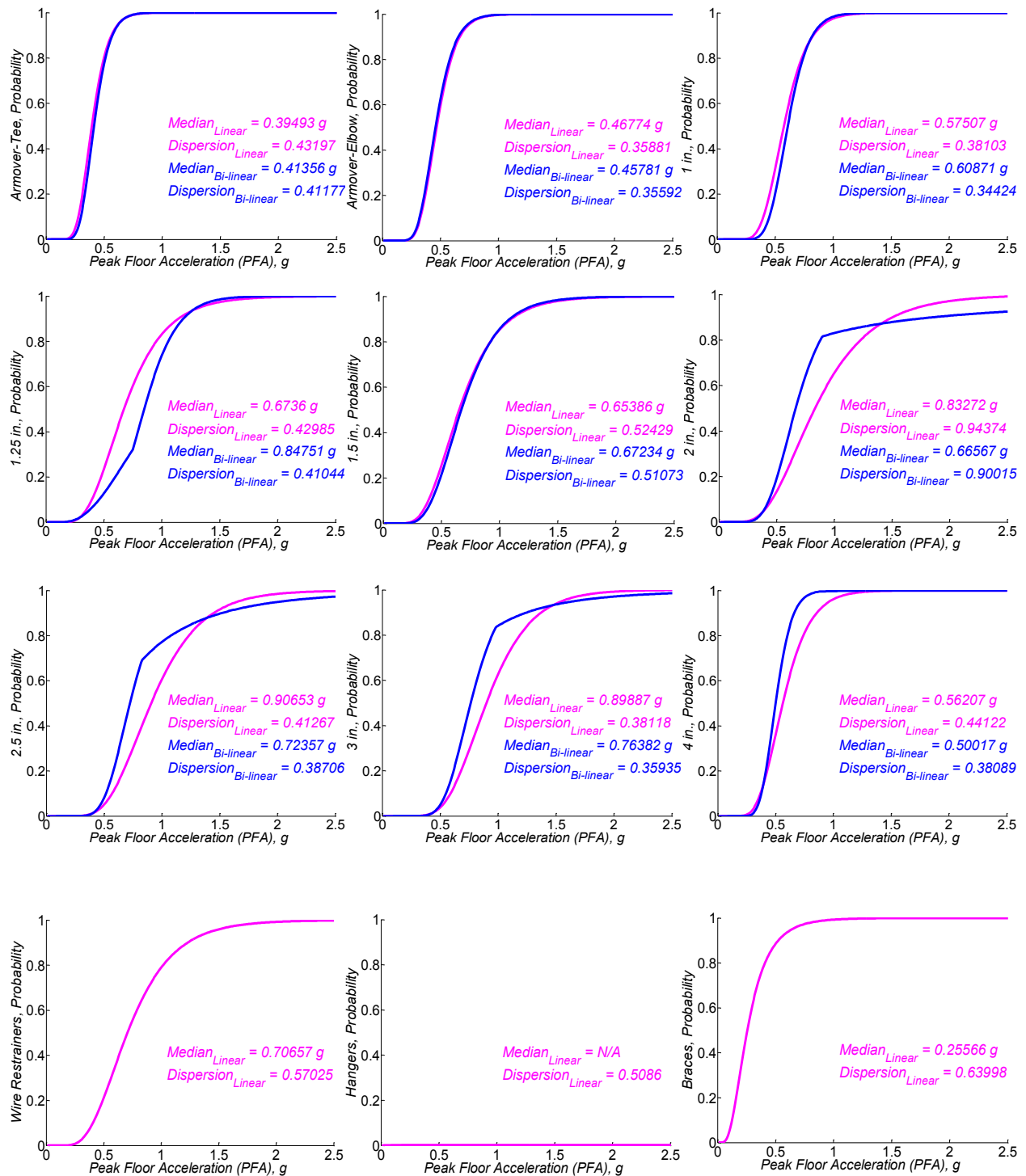


Figure D-37 Component Fragility Curves, Slight - Case 10

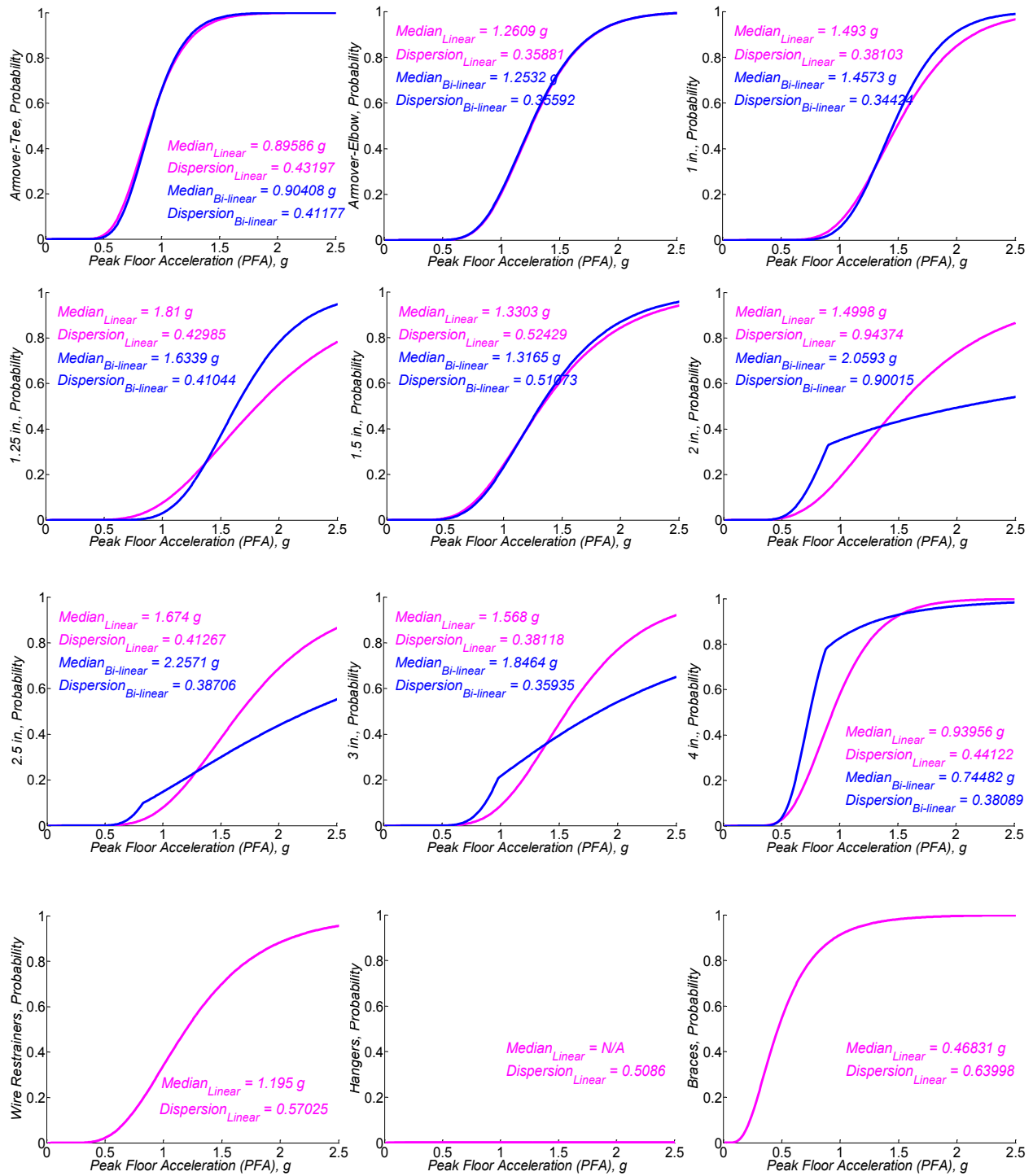


Figure D- 38 Component Fragility Curves, Moderate - Case 10

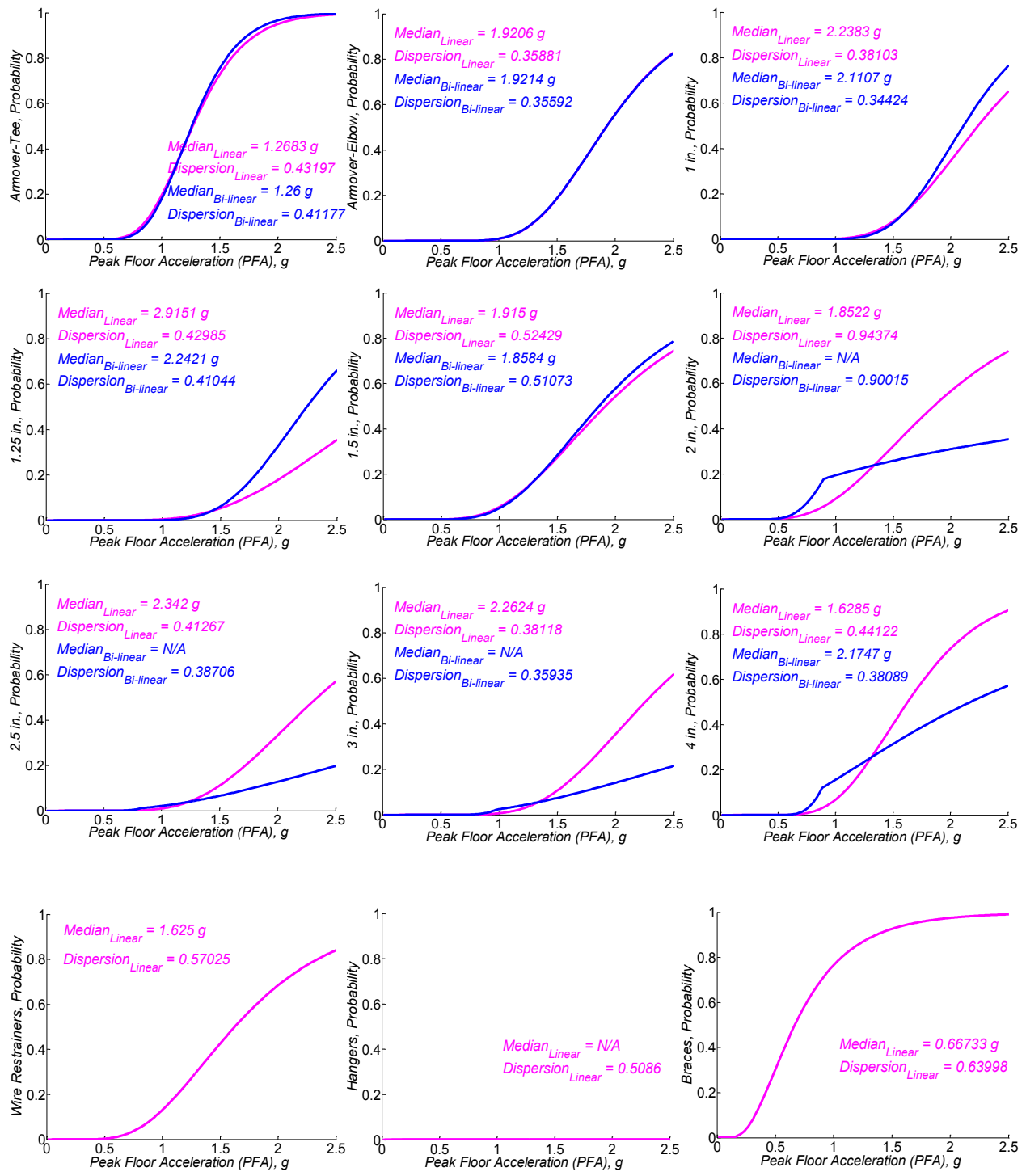


Figure D- 39 Component Fragility Curves, Extensive - Case 10

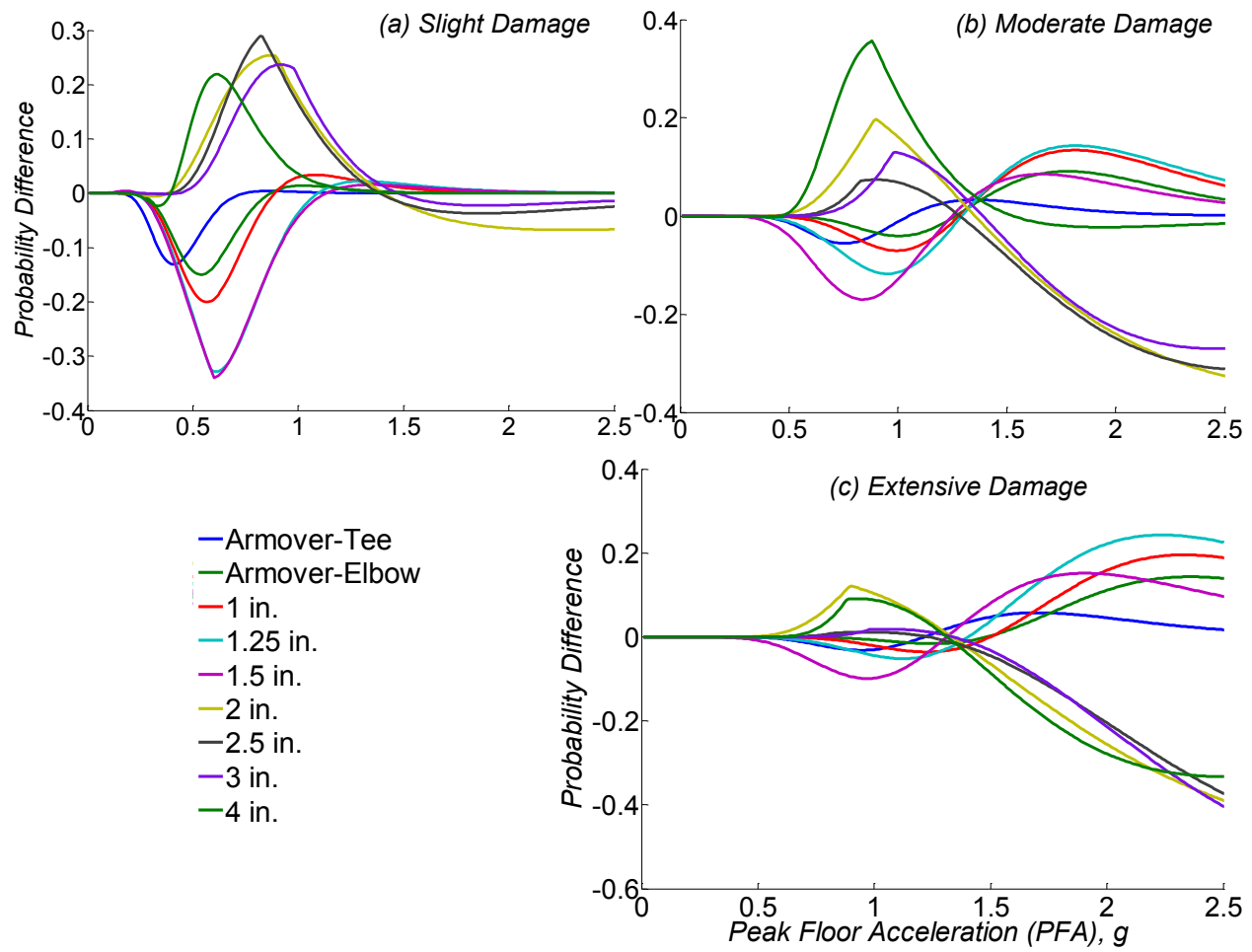


Figure D- 40 Fragility Probability Differences of Pipe Joints Using Linear and Bilinear Regression Analysis for Case 10

MCEER Technical Reports

MCEER publishes technical reports on a variety of subjects written by authors funded through MCEER. These reports are available from both MCEER Publications and the National Technical Information Service (NTIS). Requests for reports should be directed to MCEER Publications, MCEER, University at Buffalo, State University of New York, 133A Ketter Hall, Buffalo, New York 14260. Reports can also be requested through NTIS, P.O. Box 1425, Springfield, Virginia 22151. NTIS accession numbers are shown in parenthesis, if available.

NCEER-87-0001 "First-Year Program in Research, Education and Technology Transfer," 3/5/87, (PB88-134275, A04, MF-A01).

NCEER-87-0002 "Experimental Evaluation of Instantaneous Optimal Algorithms for Structural Control," by R.C. Lin, T.T. Soong and A.M. Reinhorn, 4/20/87, (PB88-134341, A04, MF-A01).

NCEER-87-0003 "Experimentation Using the Earthquake Simulation Facilities at University at Buffalo," by A.M. Reinhorn and R.L. Ketter, not available.

NCEER-87-0004 "The System Characteristics and Performance of a Shaking Table," by J.S. Hwang, K.C. Chang and G.C. Lee, 6/1/87, (PB88-134259, A03, MF-A01). This report is available only through NTIS (see address given above).

NCEER-87-0005 "A Finite Element Formulation for Nonlinear Viscoplastic Material Using a Q Model," by O. Gyebi and G. Dasgupta, 11/2/87, (PB88-213764, A08, MF-A01).

NCEER-87-0006 "Symbolic Manipulation Program (SMP) - Algebraic Codes for Two and Three Dimensional Finite Element Formulations," by X. Lee and G. Dasgupta, 11/9/87, (PB88-218522, A05, MF-A01).

NCEER-87-0007 "Instantaneous Optimal Control Laws for Tall Buildings Under Seismic Excitations," by J.N. Yang, A. Akbarpour and P. Ghaemmaghami, 6/10/87, (PB88-134333, A06, MF-A01). This report is only available through NTIS (see address given above).

NCEER-87-0008 "IDARC: Inelastic Damage Analysis of Reinforced Concrete Frame - Shear-Wall Structures," by Y.J. Park, A.M. Reinhorn and S.K. Kunmath, 7/20/87, (PB88-134325, A09, MF-A01). This report is only available through NTIS (see address given above).

NCEER-87-0009 "Liquefaction Potential for New York State: A Preliminary Report on Sites in Manhattan and Buffalo," by M. Budhu, V. Vijayakumar, R.F. Giese and L. Baumgras, 8/31/87, (PB88-163704, A03, MF-A01). This report is available only through NTIS (see address given above).

NCEER-87-0010 "Vertical and Torsional Vibration of Foundations in Inhomogeneous Media," by A.S. Veletsos and K.W. Dotson, 6/1/87, (PB88-134291, A03, MF-A01). This report is only available through NTIS (see address given above).

NCEER-87-0011 "Seismic Probabilistic Risk Assessment and Seismic Margins Studies for Nuclear Power Plants," by Howard H.M. Hwang, 6/15/87, (PB88-134267, A03, MF-A01). This report is only available through NTIS (see address given above).

NCEER-87-0012 "Parametric Studies of Frequency Response of Secondary Systems Under Ground-Acceleration Excitations," by Y. Yong and Y.K. Lin, 6/10/87, (PB88-134309, A03, MF-A01). This report is only available through NTIS (see address given above).

NCEER-87-0013 "Frequency Response of Secondary Systems Under Seismic Excitation," by J.A. HoLung, J. Cai and Y.K. Lin, 7/31/87, (PB88-134317, A05, MF-A01). This report is only available through NTIS (see address given above).

NCEER-87-0014 "Modelling Earthquake Ground Motions in Seismically Active Regions Using Parametric Time Series Methods," by G.W. Ellis and A.S. Cakmak, 8/25/87, (PB88-134283, A08, MF-A01). This report is only available through NTIS (see address given above).

NCEER-87-0015 "Detection and Assessment of Seismic Structural Damage," by E. DiPasquale and A.S. Cakmak, 8/25/87, (PB88-163712, A05, MF-A01). This report is only available through NTIS (see address given above).

NCEER-87-0016 "Pipeline Experiment at Parkfield, California," by J. Isenberg and E. Richardson, 9/15/87, (PB88-163720, A03, MF-A01). This report is available only through NTIS (see address given above).

NCEER-87-0017 "Digital Simulation of Seismic Ground Motion," by M. Shinozuka, G. Deodatis and T. Harada, 8/31/87, (PB88-155197, A04, MF-A01). This report is available only through NTIS (see address given above).

NCEER-87-0018 "Practical Considerations for Structural Control: System Uncertainty, System Time Delay and Truncation of Small Control Forces," J.N. Yang and A. Akbarpour, 8/10/87, (PB88-163738, A08, MF-A01). This report is only available through NTIS (see address given above).

NCEER-87-0019 "Modal Analysis of Nonclassically Damped Structural Systems Using Canonical Transformation," by J.N. Yang, S. Sarkani and F.X. Long, 9/27/87, (PB88-187851, A04, MF-A01).

NCEER-87-0020 "A Nonstationary Solution in Random Vibration Theory," by J.R. Red-Horse and P.D. Spanos, 11/3/87, (PB88-163746, A03, MF-A01).

NCEER-87-0021 "Horizontal Impedances for Radially Inhomogeneous Viscoelastic Soil Layers," by A.S. Veletsos and K.W. Dotson, 10/15/87, (PB88-150859, A04, MF-A01).

NCEER-87-0022 "Seismic Damage Assessment of Reinforced Concrete Members," by Y.S. Chung, C. Meyer and M. Shinozuka, 10/9/87, (PB88-150867, A05, MF-A01). This report is available only through NTIS (see address given above).

NCEER-87-0023 "Active Structural Control in Civil Engineering," by T.T. Soong, 11/11/87, (PB88-187778, A03, MF-A01).

NCEER-87-0024 "Vertical and Torsional Impedances for Radially Inhomogeneous Viscoelastic Soil Layers," by K.W. Dotson and A.S. Veletsos, 12/87, (PB88-187786, A03, MF-A01).

NCEER-87-0025 "Proceedings from the Symposium on Seismic Hazards, Ground Motions, Soil-Liquefaction and Engineering Practice in Eastern North America," October 20-22, 1987, edited by K.H. Jacob, 12/87, (PB88-188115, A23, MF-A01). This report is available only through NTIS (see address given above).

NCEER-87-0026 "Report on the Whittier-Narrows, California, Earthquake of October 1, 1987," by J. Pantelic and A. Reinhorn, 11/87, (PB88-187752, A03, MF-A01). This report is available only through NTIS (see address given above).

NCEER-87-0027 "Design of a Modular Program for Transient Nonlinear Analysis of Large 3-D Building Structures," by S. Srivastav and J.F. Abel, 12/30/87, (PB88-187950, A05, MF-A01). This report is only available through NTIS (see address given above).

NCEER-87-0028 "Second-Year Program in Research, Education and Technology Transfer," 3/8/88, (PB88-219480, A04, MF-A01).

NCEER-88-0001 "Workshop on Seismic Computer Analysis and Design of Buildings With Interactive Graphics," by W. McGuire, J.F. Abel and C.H. Conley, 1/18/88, (PB88-187760, A03, MF-A01). This report is only available through NTIS (see address given above).

NCEER-88-0002 "Optimal Control of Nonlinear Flexible Structures," by J.N. Yang, F.X. Long and D. Wong, 1/22/88, (PB88-213772, A06, MF-A01).

NCEER-88-0003 "Substructuring Techniques in the Time Domain for Primary-Secondary Structural Systems," by G.D. Manolis and G. Juhn, 2/10/88, (PB88-213780, A04, MF-A01).

NCEER-88-0004 "Iterative Seismic Analysis of Primary-Secondary Systems," by A. Singhal, L.D. Lutes and P.D. Spanos, 2/23/88, (PB88-213798, A04, MF-A01).

NCEER-88-0005 "Stochastic Finite Element Expansion for Random Media," by P.D. Spanos and R. Ghanem, 3/14/88, (PB88-213806, A03, MF-A01).

NCEER-88-0006 "Combining Structural Optimization and Structural Control," by F.Y. Cheng and C.P. Pantelides, 1/10/88, (PB88-213814, A05, MF-A01).

NCEER-88-0007 "Seismic Performance Assessment of Code-Designed Structures," by H.H-M. Hwang, J-W. Jaw and H-J. Shau, 3/20/88, (PB88-219423, A04, MF-A01). This report is only available through NTIS (see address given above).

NCEER-88-0008 "Reliability Analysis of Code-Designed Structures Under Natural Hazards," by H.H-M. Hwang, H. Ushiba and M. Shinozuka, 2/29/88, (PB88-229471, A07, MF-A01). This report is only available through NTIS (see address given above).

NCEER-88-0009 "Seismic Fragility Analysis of Shear Wall Structures," by J-W Jaw and H.H-M. Hwang, 4/30/88, (PB89-102867, A04, MF-A01).

NCEER-88-0010 "Base Isolation of a Multi-Story Building Under a Harmonic Ground Motion - A Comparison of Performances of Various Systems," by F-G Fan, G. Ahmadi and I.G. Tadjbakhsh, 5/18/88, (PB89-122238, A06, MF-A01). This report is only available through NTIS (see address given above).

NCEER-88-0011 "Seismic Floor Response Spectra for a Combined System by Green's Functions," by F.M. Lavelle, L.A. Bergman and P.D. Spanos, 5/1/88, (PB89-102875, A03, MF-A01).

NCEER-88-0012 "A New Solution Technique for Randomly Excited Hysteretic Structures," by G.Q. Cai and Y.K. Lin, 5/16/88, (PB89-102883, A03, MF-A01).

NCEER-88-0013 "A Study of Radiation Damping and Soil-Structure Interaction Effects in the Centrifuge," by K. Weissman, supervised by J.H. Prevost, 5/24/88, (PB89-144703, A06, MF-A01).

NCEER-88-0014 "Parameter Identification and Implementation of a Kinematic Plasticity Model for Frictional Soils," by J.H. Prevost and D.V. Griffiths, not available.

NCEER-88-0015 "Two- and Three- Dimensional Dynamic Finite Element Analyses of the Long Valley Dam," by D.V. Griffiths and J.H. Prevost, 6/17/88, (PB89-144711, A04, MF-A01).

NCEER-88-0016 "Damage Assessment of Reinforced Concrete Structures in Eastern United States," by A.M. Reinhorn, M.J. Seidel, S.K. Kunnath and Y.J. Park, 6/15/88, (PB89-122220, A04, MF-A01). This report is only available through NTIS (see address given above).

NCEER-88-0017 "Dynamic Compliance of Vertically Loaded Strip Foundations in Multilayered Viscoelastic Soils," by S. Ahmad and A.S.M. Israil, 6/17/88, (PB89-102891, A04, MF-A01).

NCEER-88-0018 "An Experimental Study of Seismic Structural Response With Added Viscoelastic Dampers," by R.C. Lin, Z. Liang, T.T. Soong and R.H. Zhang, 6/30/88, (PB89-122212, A05, MF-A01). This report is available only through NTIS (see address given above).

NCEER-88-0019 "Experimental Investigation of Primary - Secondary System Interaction," by G.D. Manolis, G. Juhn and A.M. Reinhorn, 5/27/88, (PB89-122204, A04, MF-A01).

NCEER-88-0020 "A Response Spectrum Approach For Analysis of Nonclassically Damped Structures," by J.N. Yang, S. Sarkani and F.X. Long, 4/22/88, (PB89-102909, A04, MF-A01).

NCEER-88-0021 "Seismic Interaction of Structures and Soils: Stochastic Approach," by A.S. Veletsos and A.M. Prasad, 7/21/88, (PB89-122196, A04, MF-A01). This report is only available through NTIS (see address given above).

NCEER-88-0022 "Identification of the Serviceability Limit State and Detection of Seismic Structural Damage," by E. DiPasquale and A.S. Cakmak, 6/15/88, (PB89-122188, A05, MF-A01). This report is available only through NTIS (see address given above).

NCEER-88-0023 "Multi-Hazard Risk Analysis: Case of a Simple Offshore Structure," by B.K. Bhartia and E.H. Vanmarcke, 7/21/88, (PB89-145213, A05, MF-A01).

NCEER-88-0024 "Automated Seismic Design of Reinforced Concrete Buildings," by Y.S. Chung, C. Meyer and M. Shinozuka, 7/5/88, (PB89-122170, A06, MF-A01). This report is available only through NTIS (see address given above).

NCEER-88-0025 "Experimental Study of Active Control of MDOF Structures Under Seismic Excitations," by L.L. Chung, R.C. Lin, T.T. Soong and A.M. Reinhorn, 7/10/88, (PB89-122600, A04, MF-A01).

NCEER-88-0026 "Earthquake Simulation Tests of a Low-Rise Metal Structure," by J.S. Hwang, K.C. Chang, G.C. Lee and R.L. Ketter, 8/1/88, (PB89-102917, A04, MF-A01).

NCEER-88-0027 "Systems Study of Urban Response and Reconstruction Due to Catastrophic Earthquakes," by F. Kozin and H.K. Zhou, 9/22/88, (PB90-162348, A04, MF-A01).

NCEER-88-0028 "Seismic Fragility Analysis of Plane Frame Structures," by H.H-M. Hwang and Y.K. Low, 7/31/88, (PB89-131445, A06, MF-A01).

NCEER-88-0029 "Response Analysis of Stochastic Structures," by A. Kardara, C. Bucher and M. Shinozuka, 9/22/88, (PB89-174429, A04, MF-A01).

NCEER-88-0030 "Nonnormal Accelerations Due to Yielding in a Primary Structure," by D.C.K. Chen and L.D. Lutes, 9/19/88, (PB89-131437, A04, MF-A01).

NCEER-88-0031 "Design Approaches for Soil-Structure Interaction," by A.S. Veletsos, A.M. Prasad and Y. Tang, 12/30/88, (PB89-174437, A03, MF-A01). This report is available only through NTIS (see address given above).

NCEER-88-0032 "A Re-evaluation of Design Spectra for Seismic Damage Control," by C.J. Turkstra and A.G. Tallin, 11/7/88, (PB89-145221, A05, MF-A01).

NCEER-88-0033 "The Behavior and Design of Noncontact Lap Splices Subjected to Repeated Inelastic Tensile Loading," by V.E. Sagan, P. Gergely and R.N. White, 12/8/88, (PB89-163737, A08, MF-A01).

NCEER-88-0034 "Seismic Response of Pile Foundations," by S.M. Mamoon, P.K. Banerjee and S. Ahmad, 11/1/88, (PB89-145239, A04, MF-A01).

NCEER-88-0035 "Modeling of R/C Building Structures With Flexible Floor Diaphragms (IDARC2)," by A.M. Reinhorn, S.K. Kunzath and N. Panahshahi, 9/7/88, (PB89-207153, A07, MF-A01).

NCEER-88-0036 "Solution of the Dam-Reservoir Interaction Problem Using a Combination of FEM, BEM with Particular Integrals, Modal Analysis, and Substructuring," by C-S. Tsai, G.C. Lee and R.L. Ketter, 12/31/88, (PB89-207146, A04, MF-A01).

NCEER-88-0037 "Optimal Placement of Actuators for Structural Control," by F.Y. Cheng and C.P. Pantelides, 8/15/88, (PB89-162846, A05, MF-A01).

NCEER-88-0038 "Teflon Bearings in Aseismic Base Isolation: Experimental Studies and Mathematical Modeling," by A. Mokha, M.C. Constantinou and A.M. Reinhorn, 12/5/88, (PB89-218457, A10, MF-A01). This report is available only through NTIS (see address given above).

NCEER-88-0039 "Seismic Behavior of Flat Slab High-Rise Buildings in the New York City Area," by P. Weidlinger and M. Ettouney, 10/15/88, (PB90-145681, A04, MF-A01).

NCEER-88-0040 "Evaluation of the Earthquake Resistance of Existing Buildings in New York City," by P. Weidlinger and M. Ettouney, 10/15/88, not available.

NCEER-88-0041 "Small-Scale Modeling Techniques for Reinforced Concrete Structures Subjected to Seismic Loads," by W. Kim, A. El-Attar and R.N. White, 11/22/88, (PB89-189625, A05, MF-A01).

NCEER-88-0042 "Modeling Strong Ground Motion from Multiple Event Earthquakes," by G.W. Ellis and A.S. Cakmak, 10/15/88, (PB89-174445, A03, MF-A01).

NCEER-88-0043 "Nonstationary Models of Seismic Ground Acceleration," by M. Grigoriu, S.E. Ruiz and E. Rosenblueth, 7/15/88, (PB89-189617, A04, MF-A01).

NCEER-88-0044 "SARCF User's Guide: Seismic Analysis of Reinforced Concrete Frames," by Y.S. Chung, C. Meyer and M. Shinouzuka, 11/9/88, (PB89-174452, A08, MF-A01).

NCEER-88-0045 "First Expert Panel Meeting on Disaster Research and Planning," edited by J. Pantelic and J. Stoyle, 9/15/88, (PB89-174460, A05, MF-A01).

NCEER-88-0046 "Preliminary Studies of the Effect of Degrading Infill Walls on the Nonlinear Seismic Response of Steel Frames," by C.Z. Chrysostomou, P. Gergely and J.F. Abel, 12/19/88, (PB89-208383, A05, MF-A01).

NCEER-88-0047 "Reinforced Concrete Frame Component Testing Facility - Design, Construction, Instrumentation and Operation," by S.P. Pessiki, C. Conley, T. Bond, P. Gergely and R.N. White, 12/16/88, (PB89-174478, A04, MF-A01).

NCEER-89-0001 "Effects of Protective Cushion and Soil Compliancy on the Response of Equipment Within a Seismically Excited Building," by J.A. HoLung, 2/16/89, (PB89-207179, A04, MF-A01).

NCEER-89-0002 "Statistical Evaluation of Response Modification Factors for Reinforced Concrete Structures," by H.H-M. Hwang and J-W. Jaw, 2/17/89, (PB89-207187, A05, MF-A01).

NCEER-89-0003 "Hysteretic Columns Under Random Excitation," by G-Q. Cai and Y.K. Lin, 1/9/89, (PB89-196513, A03, MF-A01).

NCEER-89-0004 "Experimental Study of 'Elephant Foot Bulge' Instability of Thin-Walled Metal Tanks," by Z-H. Jia and R.L. Ketter, 2/22/89, (PB89-207195, A03, MF-A01).

NCEER-89-0005 "Experiment on Performance of Buried Pipelines Across San Andreas Fault," by J. Isenberg, E. Richardson and T.D. O'Rourke, 3/10/89, (PB89-218440, A04, MF-A01). This report is available only through NTIS (see address given above).

NCEER-89-0006 "A Knowledge-Based Approach to Structural Design of Earthquake-Resistant Buildings," by M. Subramani, P. Gergely, C.H. Conley, J.F. Abel and A.H. Zaghw, 1/15/89, (PB89-218465, A06, MF-A01).

NCEER-89-0007 "Liquefaction Hazards and Their Effects on Buried Pipelines," by T.D. O'Rourke and P.A. Lane, 2/1/89, (PB89-218481, A09, MF-A01).

NCEER-89-0008 "Fundamentals of System Identification in Structural Dynamics," by H. Imai, C-B. Yun, O. Maruyama and M. Shinouzuka, 1/26/89, (PB89-207211, A04, MF-A01).

NCEER-89-0009 "Effects of the 1985 Michoacan Earthquake on Water Systems and Other Buried Lifelines in Mexico," by A.G. Ayala and M.J. O'Rourke, 3/8/89, (PB89-207229, A06, MF-A01).

NCEER-89-R010 "NCEER Bibliography of Earthquake Education Materials," by K.E.K. Ross, Second Revision, 9/1/89, (PB90-125352, A05, MF-A01). This report is replaced by NCEER-92-0018.

NCEER-89-0011 "Inelastic Three-Dimensional Response Analysis of Reinforced Concrete Building Structures (IDARC-3D), Part I - Modeling," by S.K. Kunnath and A.M. Reinhorn, 4/17/89, (PB90-114612, A07, MF-A01). This report is available only through NTIS (see address given above).

NCEER-89-0012 "Recommended Modifications to ATC-14," by C.D. Poland and J.O. Malley, 4/12/89, (PB90-108648, A15, MF-A01).

NCEER-89-0013 "Repair and Strengthening of Beam-to-Column Connections Subjected to Earthquake Loading," by M. Corazao and A.J. Durrani, 2/28/89, (PB90-109885, A06, MF-A01).

NCEER-89-0014 "Program EXKAL2 for Identification of Structural Dynamic Systems," by O. Maruyama, C-B. Yun, M. Hoshiya and M. Shinouzuka, 5/19/89, (PB90-109877, A09, MF-A01).

NCEER-89-0015 "Response of Frames With Bolted Semi-Rigid Connections, Part I - Experimental Study and Analytical Predictions," by P.J. DiCorso, A.M. Reinhorn, J.R. Dickerson, J.B. Radziminski and W.L. Harper, 6/1/89, not available.

NCEER-89-0016 "ARMA Monte Carlo Simulation in Probabilistic Structural Analysis," by P.D. Spanos and M.P. Mignolet, 7/10/89, (PB90-109893, A03, MF-A01).

NCEER-89-P017 "Preliminary Proceedings from the Conference on Disaster Preparedness - The Place of Earthquake Education in Our Schools," Edited by K.E.K. Ross, 6/23/89, (PB90-108606, A03, MF-A01).

NCEER-89-0017 "Proceedings from the Conference on Disaster Preparedness - The Place of Earthquake Education in Our Schools," Edited by K.E.K. Ross, 12/31/89, (PB90-207895, A012, MF-A02). This report is available only through NTIS (see address given above).

NCEER-89-0018 "Multidimensional Models of Hysteretic Material Behavior for Vibration Analysis of Shape Memory Energy Absorbing Devices, by E.J. Graesser and F.A. Cozzarelli, 6/7/89, (PB90-164146, A04, MF-A01).

NCEER-89-0019 "Nonlinear Dynamic Analysis of Three-Dimensional Base Isolated Structures (3D-BASIS)," by S. Nagarajaiah, A.M. Reinhorn and M.C. Constantinou, 8/3/89, (PB90-161936, A06, MF-A01). This report has been replaced by NCEER-93-0011.

NCEER-89-0020 "Structural Control Considering Time-Rate of Control Forces and Control Rate Constraints," by F.Y. Cheng and C.P. Pantelides, 8/3/89, (PB90-120445, A04, MF-A01).

NCEER-89-0021 "Subsurface Conditions of Memphis and Shelby County," by K.W. Ng, T-S. Chang and H-H.M. Hwang, 7/26/89, (PB90-120437, A03, MF-A01).

NCEER-89-0022 "Seismic Wave Propagation Effects on Straight Jointed Buried Pipelines," by K. Elhmadi and M.J. O'Rourke, 8/24/89, (PB90-162322, A10, MF-A02).

NCEER-89-0023 "Workshop on Serviceability Analysis of Water Delivery Systems," edited by M. Grigoriu, 3/6/89, (PB90-127424, A03, MF-A01).

NCEER-89-0024 "Shaking Table Study of a 1/5 Scale Steel Frame Composed of Tapered Members," by K.C. Chang, J.S. Hwang and G.C. Lee, 9/18/89, (PB90-160169, A04, MF-A01).

NCEER-89-0025 "DYNA1D: A Computer Program for Nonlinear Seismic Site Response Analysis - Technical Documentation," by Jean H. Prevost, 9/14/89, (PB90-161944, A07, MF-A01). This report is available only through NTIS (see address given above).

NCEER-89-0026 "1:4 Scale Model Studies of Active Tendon Systems and Active Mass Dampers for Aseismic Protection," by A.M. Reinhorn, T.T. Soong, R.C. Lin, Y.P. Yang, Y. Fukao, H. Abe and M. Nakai, 9/15/89, (PB90-173246, A10, MF-A02). This report is available only through NTIS (see address given above).

NCEER-89-0027 "Scattering of Waves by Inclusions in a Nonhomogeneous Elastic Half Space Solved by Boundary Element Methods," by P.K. Hadley, A. Askar and A.S. Cakmak, 6/15/89, (PB90-145699, A07, MF-A01).

NCEER-89-0028 "Statistical Evaluation of Deflection Amplification Factors for Reinforced Concrete Structures," by H.H.M. Hwang, J-W. Jaw and A.L. Ch'ng, 8/31/89, (PB90-164633, A05, MF-A01).

NCEER-89-0029 "Bedrock Accelerations in Memphis Area Due to Large New Madrid Earthquakes," by H.H.M. Hwang, C.H.S. Chen and G. Yu, 11/7/89, (PB90-162330, A04, MF-A01).

NCEER-89-0030 "Seismic Behavior and Response Sensitivity of Secondary Structural Systems," by Y.Q. Chen and T.T. Soong, 10/23/89, (PB90-164658, A08, MF-A01).

NCEER-89-0031 "Random Vibration and Reliability Analysis of Primary-Secondary Structural Systems," by Y. Ibrahim, M. Grigoriu and T.T. Soong, 11/10/89, (PB90-161951, A04, MF-A01).

NCEER-89-0032 "Proceedings from the Second U.S. - Japan Workshop on Liquefaction, Large Ground Deformation and Their Effects on Lifelines, September 26-29, 1989," Edited by T.D. O'Rourke and M. Hamada, 12/1/89, (PB90-209388, A22, MF-A03).

NCEER-89-0033 "Deterministic Model for Seismic Damage Evaluation of Reinforced Concrete Structures," by J.M. Bracci, A.M. Reinhorn, J.B. Mander and S.K. Kunnath, 9/27/89, (PB91-108803, A06, MF-A01).

NCEER-89-0034 "On the Relation Between Local and Global Damage Indices," by E. DiPasquale and A.S. Cakmak, 8/15/89, (PB90-173865, A05, MF-A01).

NCEER-89-0035 "Cyclic Undrained Behavior of Nonplastic and Low Plasticity Silts," by A.J. Walker and H.E. Stewart, 7/26/89, (PB90-183518, A10, MF-A01).

NCEER-89-0036 "Liquefaction Potential of Surficial Deposits in the City of Buffalo, New York," by M. Budhu, R. Giese and L. Baumgrass, 1/17/89, (PB90-208455, A04, MF-A01).

NCEER-89-0037 "A Deterministic Assessment of Effects of Ground Motion Incoherence," by A.S. Veletsos and Y. Tang, 7/15/89, (PB90-164294, A03, MF-A01).

NCEER-89-0038 "Workshop on Ground Motion Parameters for Seismic Hazard Mapping," July 17-18, 1989, edited by R.V. Whitman, 12/1/89, (PB90-173923, A04, MF-A01).

NCEER-89-0039 "Seismic Effects on Elevated Transit Lines of the New York City Transit Authority," by C.J. Costantino, C.A. Miller and E. Heymsfield, 12/26/89, (PB90-207887, A06, MF-A01).

NCEER-89-0040 "Centrifugal Modeling of Dynamic Soil-Structure Interaction," by K. Weissman, Supervised by J.H. Prevost, 5/10/89, (PB90-207879, A07, MF-A01).

NCEER-89-0041 "Linearized Identification of Buildings With Cores for Seismic Vulnerability Assessment," by I-K. Ho and A.E. Aktan, 11/1/89, (PB90-251943, A07, MF-A01).

NCEER-90-0001 "Geotechnical and Lifeline Aspects of the October 17, 1989 Loma Prieta Earthquake in San Francisco," by T.D. O'Rourke, H.E. Stewart, F.T. Blackburn and T.S. Dickerman, 1/90, (PB90-208596, A05, MF-A01).

NCEER-90-0002 "Nonnormal Secondary Response Due to Yielding in a Primary Structure," by D.C.K. Chen and L.D. Lutes, 2/28/90, (PB90-251976, A07, MF-A01).

NCEER-90-0003 "Earthquake Education Materials for Grades K-12," by K.E.K. Ross, 4/16/90, (PB91-251984, A05, MF-A05). This report has been replaced by NCEER-92-0018.

NCEER-90-0004 "Catalog of Strong Motion Stations in Eastern North America," by R.W. Busby, 4/3/90, (PB90-251984, A05, MF-A01).

NCEER-90-0005 "NCEER Strong-Motion Data Base: A User Manual for the GeoBase Release (Version 1.0 for the Sun3)," by P. Friberg and K. Jacob, 3/31/90 (PB90-258062, A04, MF-A01).

NCEER-90-0006 "Seismic Hazard Along a Crude Oil Pipeline in the Event of an 1811-1812 Type New Madrid Earthquake," by H.H.M. Hwang and C-H.S. Chen, 4/16/90, (PB90-258054, A04, MF-A01).

NCEER-90-0007 "Site-Specific Response Spectra for Memphis Sheahan Pumping Station," by H.H.M. Hwang and C.S. Lee, 5/15/90, (PB91-108811, A05, MF-A01).

NCEER-90-0008 "Pilot Study on Seismic Vulnerability of Crude Oil Transmission Systems," by T. Ariman, R. Dobry, M. Grigoriu, F. Kozin, M. O'Rourke, T. O'Rourke and M. Shinozuka, 5/25/90, (PB91-108837, A06, MF-A01).

NCEER-90-0009 "A Program to Generate Site Dependent Time Histories: EQGEN," by G.W. Ellis, M. Srinivasan and A.S. Cakmak, 1/30/90, (PB91-108829, A04, MF-A01).

NCEER-90-0010 "Active Isolation for Seismic Protection of Operating Rooms," by M.E. Talbott, Supervised by M. Shinozuka, 6/8/91, (PB91-110205, A05, MF-A01).

NCEER-90-0011 "Program LINEARID for Identification of Linear Structural Dynamic Systems," by C-B. Yun and M. Shinozuka, 6/25/90, (PB91-110312, A08, MF-A01).

NCEER-90-0012 "Two-Dimensional Two-Phase Elasto-Plastic Seismic Response of Earth Dams," by A.N. Yiagos, Supervised by J.H. Prevost, 6/20/90, (PB91-110197, A13, MF-A02).

NCEER-90-0013 "Secondary Systems in Base-Isolated Structures: Experimental Investigation, Stochastic Response and Stochastic Sensitivity," by G.D. Manolis, G. Juhn, M.C. Constantinou and A.M. Reinhorn, 7/1/90, (PB91-110320, A08, MF-A01).

NCEER-90-0014 "Seismic Behavior of Lightly-Reinforced Concrete Column and Beam-Column Joint Details," by S.P. Pessiki, C.H. Conley, P. Gergely and R.N. White, 8/22/90, (PB91-108795, A11, MF-A02).

NCEER-90-0015 "Two Hybrid Control Systems for Building Structures Under Strong Earthquakes," by J.N. Yang and A. Danielians, 6/29/90, (PB91-125393, A04, MF-A01).

NCEER-90-0016 "Instantaneous Optimal Control with Acceleration and Velocity Feedback," by J.N. Yang and Z. Li, 6/29/90, (PB91-125401, A03, MF-A01).

NCEER-90-0017 "Reconnaissance Report on the Northern Iran Earthquake of June 21, 1990," by M. Mehrain, 10/4/90, (PB91-125377, A03, MF-A01).

NCEER-90-0018 "Evaluation of Liquefaction Potential in Memphis and Shelby County," by T.S. Chang, P.S. Tang, C.S. Lee and H. Hwang, 8/10/90, (PB91-125427, A09, MF-A01).

NCEER-90-0019 "Experimental and Analytical Study of a Combined Sliding Disc Bearing and Helical Steel Spring Isolation System," by M.C. Constantinou, A.S. Mokha and A.M. Reinhorn, 10/4/90, (PB91-125385, A06, MF-A01). This report is available only through NTIS (see address given above).

NCEER-90-0020 "Experimental Study and Analytical Prediction of Earthquake Response of a Sliding Isolation System with a Spherical Surface," by A.S. Mokha, M.C. Constantinou and A.M. Reinhorn, 10/11/90, (PB91-125419, A05, MF-A01).

NCEER-90-0021 "Dynamic Interaction Factors for Floating Pile Groups," by G. Gazetas, K. Fan, A. Kaynia and E. Kausel, 9/10/90, (PB91-170381, A05, MF-A01).

NCEER-90-0022 "Evaluation of Seismic Damage Indices for Reinforced Concrete Structures," by S. Rodriguez-Gomez and A.S. Cakmak, 9/30/90, PB91-171322, A06, MF-A01).

NCEER-90-0023 "Study of Site Response at a Selected Memphis Site," by H. Desai, S. Ahmad, E.S. Gazetas and M.R. Oh, 10/11/90, (PB91-196857, A03, MF-A01).

NCEER-90-0024 "A User's Guide to Strongmo: Version 1.0 of NCEER's Strong-Motion Data Access Tool for PCs and Terminals," by P.A. Friberg and C.A.T. Susch, 11/15/90, (PB91-171272, A03, MF-A01).

NCEER-90-0025 "A Three-Dimensional Analytical Study of Spatial Variability of Seismic Ground Motions," by L-L. Hong and A.H.-S. Ang, 10/30/90, (PB91-170399, A09, MF-A01).

NCEER-90-0026 "MUMOID User's Guide - A Program for the Identification of Modal Parameters," by S. Rodriguez-Gomez and E. DiPasquale, 9/30/90, (PB91-171298, A04, MF-A01).

NCEER-90-0027 "SARCF-II User's Guide - Seismic Analysis of Reinforced Concrete Frames," by S. Rodriguez-Gomez, Y.S. Chung and C. Meyer, 9/30/90, (PB91-171280, A05, MF-A01).

NCEER-90-0028 "Viscous Dampers: Testing, Modeling and Application in Vibration and Seismic Isolation," by N. Makris and M.C. Constantinou, 12/20/90 (PB91-190561, A06, MF-A01).

NCEER-90-0029 "Soil Effects on Earthquake Ground Motions in the Memphis Area," by H. Hwang, C.S. Lee, K.W. Ng and T.S. Chang, 8/2/90, (PB91-190751, A05, MF-A01).

NCEER-91-0001 "Proceedings from the Third Japan-U.S. Workshop on Earthquake Resistant Design of Lifeline Facilities and Countermeasures for Soil Liquefaction, December 17-19, 1990," edited by T.D. O'Rourke and M. Hamada, 2/1/91, (PB91-179259, A99, MF-A04).

NCEER-91-0002 "Physical Space Solutions of Non-Proportionally Damped Systems," by M. Tong, Z. Liang and G.C. Lee, 1/15/91, (PB91-179242, A04, MF-A01).

NCEER-91-0003 "Seismic Response of Single Piles and Pile Groups," by K. Fan and G. Gazetas, 1/10/91, (PB92-174994, A04, MF-A01).

NCEER-91-0004 "Damping of Structures: Part 1 - Theory of Complex Damping," by Z. Liang and G. Lee, 10/10/91, (PB92-197235, A12, MF-A03).

NCEER-91-0005 "3D-BASIS - Nonlinear Dynamic Analysis of Three Dimensional Base Isolated Structures: Part II," by S. Nagarajaiah, A.M. Reinhorn and M.C. Constantinou, 2/28/91, (PB91-190553, A07, MF-A01). This report has been replaced by NCEER-93-0011.

NCEER-91-0006 "A Multidimensional Hysteretic Model for Plasticity Deforming Metals in Energy Absorbing Devices," by E.J. Graesser and F.A. Cozzarelli, 4/9/91, (PB92-108364, A04, MF-A01).

NCEER-91-0007 "A Framework for Customizable Knowledge-Based Expert Systems with an Application to a KBES for Evaluating the Seismic Resistance of Existing Buildings," by E.G. Ibarra-Anaya and S.J. Fenves, 4/9/91, (PB91-210930, A08, MF-A01).

NCEER-91-0008 "Nonlinear Analysis of Steel Frames with Semi-Rigid Connections Using the Capacity Spectrum Method," by G.G. Deierlein, S-H. Hsieh, Y-J. Shen and J.F. Abel, 7/2/91, (PB92-113828, A05, MF-A01).

NCEER-91-0009 "Earthquake Education Materials for Grades K-12," by K.E.K. Ross, 4/30/91, (PB91-212142, A06, MF-A01). This report has been replaced by NCEER-92-0018.

NCEER-91-0010 "Phase Wave Velocities and Displacement Phase Differences in a Harmonically Oscillating Pile," by N. Makris and G. Gazetas, 7/8/91, (PB92-108356, A04, MF-A01).

NCEER-91-0011 "Dynamic Characteristics of a Full-Size Five-Story Steel Structure and a 2/5 Scale Model," by K.C. Chang, G.C. Yao, G.C. Lee, D.S. Hao and Y.C. Yeh, 7/2/91, (PB93-116648, A06, MF-A02).

NCEER-91-0012 "Seismic Response of a 2/5 Scale Steel Structure with Added Viscoelastic Dampers," by K.C. Chang, T.T. Soong, S-T. Oh and M.L. Lai, 5/17/91, (PB92-110816, A05, MF-A01).

NCEER-91-0013 "Earthquake Response of Retaining Walls; Full-Scale Testing and Computational Modeling," by S. Alampalli and A-W.M. Elgamal, 6/20/91, not available.

NCEER-91-0014 "3D-BASIS-M: Nonlinear Dynamic Analysis of Multiple Building Base Isolated Structures," by P.C. Tsopelas, S. Nagarajaiah, M.C. Constantinou and A.M. Reinhorn, 5/28/91, (PB92-113885, A09, MF-A02).

NCEER-91-0015 "Evaluation of SEAOC Design Requirements for Sliding Isolated Structures," by D. Theodossiou and M.C. Constantinou, 6/10/91, (PB92-114602, A11, MF-A03).

NCEER-91-0016 "Closed-Loop Modal Testing of a 27-Story Reinforced Concrete Flat Plate-Core Building," by H.R. Somaprasad, T. Toksoy, H. Yoshiyuki and A.E. Aktan, 7/15/91, (PB92-129980, A07, MF-A02).

NCEER-91-0017 "Shake Table Test of a 1/6 Scale Two-Story Lightly Reinforced Concrete Building," by A.G. El-Attar, R.N. White and P. Gergely, 2/28/91, (PB92-222447, A06, MF-A02).

NCEER-91-0018 "Shake Table Test of a 1/8 Scale Three-Story Lightly Reinforced Concrete Building," by A.G. El-Attar, R.N. White and P. Gergely, 2/28/91, (PB93-116630, A08, MF-A02).

NCEER-91-0019 "Transfer Functions for Rigid Rectangular Foundations," by A.S. Veletsos, A.M. Prasad and W.H. Wu, 7/31/91, not available.

NCEER-91-0020 "Hybrid Control of Seismic-Excited Nonlinear and Inelastic Structural Systems," by J.N. Yang, Z. Li and A. Danielians, 8/1/91, (PB92-143171, A06, MF-A02).

NCEER-91-0021 "The NCEER-91 Earthquake Catalog: Improved Intensity-Based Magnitudes and Recurrence Relations for U.S. Earthquakes East of New Madrid," by L. Seeber and J.G. Armbruster, 8/28/91, (PB92-176742, A06, MF-A02).

NCEER-91-0022 "Proceedings from the Implementation of Earthquake Planning and Education in Schools: The Need for Change - The Roles of the Changemakers," by K.E.K. Ross and F. Winslow, 7/23/91, (PB92-129998, A12, MF-A03).

NCEER-91-0023 "A Study of Reliability-Based Criteria for Seismic Design of Reinforced Concrete Frame Buildings," by H.H.M. Hwang and H-M. Hsu, 8/10/91, (PB92-140235, A09, MF-A02).

NCEER-91-0024 "Experimental Verification of a Number of Structural System Identification Algorithms," by R.G. Ghanem, H. Gavin and M. Shinozuka, 9/18/91, (PB92-176577, A18, MF-A04).

NCEER-91-0025 "Probabilistic Evaluation of Liquefaction Potential," by H.H.M. Hwang and C.S. Lee," 11/25/91, (PB92-143429, A05, MF-A01).

NCEER-91-0026 "Instantaneous Optimal Control for Linear, Nonlinear and Hysteretic Structures - Stable Controllers," by J.N. Yang and Z. Li, 11/15/91, (PB92-163807, A04, MF-A01).

NCEER-91-0027 "Experimental and Theoretical Study of a Sliding Isolation System for Bridges," by M.C. Constantinou, A. Kartoum, A.M. Reinhorn and P. Bradford, 11/15/91, (PB92-176973, A10, MF-A03).

NCEER-92-0001 "Case Studies of Liquefaction and Lifeline Performance During Past Earthquakes, Volume 1: Japanese Case Studies," Edited by M. Hamada and T. O'Rourke, 2/17/92, (PB92-197243, A18, MF-A04).

NCEER-92-0002 "Case Studies of Liquefaction and Lifeline Performance During Past Earthquakes, Volume 2: United States Case Studies," Edited by T. O'Rourke and M. Hamada, 2/17/92, (PB92-197250, A20, MF-A04).

NCEER-92-0003 "Issues in Earthquake Education," Edited by K. Ross, 2/3/92, (PB92-222389, A07, MF-A02).

NCEER-92-0004 "Proceedings from the First U.S. - Japan Workshop on Earthquake Protective Systems for Bridges," Edited by I.G. Buckle, 2/4/92, (PB94-142239, A99, MF-A06).

NCEER-92-0005 "Seismic Ground Motion from a Haskell-Type Source in a Multiple-Layered Half-Space," A.P. Theoharis, G. Deodatis and M. Shinozuka, 1/2/92, not available.

NCEER-92-0006 "Proceedings from the Site Effects Workshop," Edited by R. Whitman, 2/29/92, (PB92-197201, A04, MF-A01).

NCEER-92-0007 "Engineering Evaluation of Permanent Ground Deformations Due to Seismically-Induced Liquefaction," by M.H. Baziar, R. Dobry and A-W.M. Elgamal, 3/24/92, (PB92-222421, A13, MF-A03).

NCEER-92-0008 "A Procedure for the Seismic Evaluation of Buildings in the Central and Eastern United States," by C.D. Poland and J.O. Malley, 4/2/92, (PB92-222439, A20, MF-A04).

NCEER-92-0009 "Experimental and Analytical Study of a Hybrid Isolation System Using Friction Controllable Sliding Bearings," by M.Q. Feng, S. Fujii and M. Shinozuka, 5/15/92, (PB93-150282, A06, MF-A02).

NCEER-92-0010 "Seismic Resistance of Slab-Column Connections in Existing Non-Ductile Flat-Plate Buildings," by A.J. Durrani and Y. Du, 5/18/92, (PB93-116812, A06, MF-A02).

NCEER-92-0011 "The Hysteretic and Dynamic Behavior of Brick Masonry Walls Upgraded by Ferrocement Coatings Under Cyclic Loading and Strong Simulated Ground Motion," by H. Lee and S.P. Prawel, 5/11/92, not available.

NCEER-92-0012 "Study of Wire Rope Systems for Seismic Protection of Equipment in Buildings," by G.F. Demetriades, M.C. Constantinou and A.M. Reinhorn, 5/20/92, (PB93-116655, A08, MF-A02).

NCEER-92-0013 "Shape Memory Structural Dampers: Material Properties, Design and Seismic Testing," by P.R. Witting and F.A. Cozzarelli, 5/26/92, (PB93-116663, A05, MF-A01).

NCEER-92-0014 "Longitudinal Permanent Ground Deformation Effects on Buried Continuous Pipelines," by M.J. O'Rourke, and C. Nordberg, 6/15/92, (PB93-116671, A08, MF-A02).

NCEER-92-0015 "A Simulation Method for Stationary Gaussian Random Functions Based on the Sampling Theorem," by M. Grigoriu and S. Balopoulou, 6/11/92, (PB93-127496, A05, MF-A01).

NCEER-92-0016 "Gravity-Load-Designed Reinforced Concrete Buildings: Seismic Evaluation of Existing Construction and Detailing Strategies for Improved Seismic Resistance," by G.W. Hoffmann, S.K. Kunnath, A.M. Reinhorn and J.B. Mander, 7/15/92, (PB94-142007, A08, MF-A02).

NCEER-92-0017 "Observations on Water System and Pipeline Performance in the Limón Area of Costa Rica Due to the April 22, 1991 Earthquake," by M. O'Rourke and D. Ballantyne, 6/30/92, (PB93-126811, A06, MF-A02).

NCEER-92-0018 "Fourth Edition of Earthquake Education Materials for Grades K-12," Edited by K.E.K. Ross, 8/10/92, (PB93-114023, A07, MF-A02).

NCEER-92-0019 "Proceedings from the Fourth Japan-U.S. Workshop on Earthquake Resistant Design of Lifeline Facilities and Countermeasures for Soil Liquefaction," Edited by M. Hamada and T.D. O'Rourke, 8/12/92, (PB93-163939, A99, MF-E11).

NCEER-92-0020 "Active Bracing System: A Full Scale Implementation of Active Control," by A.M. Reinhorn, T.T. Soong, R.C. Lin, M.A. Riley, Y.P. Wang, S. Aizawa and M. Higashino, 8/14/92, (PB93-127512, A06, MF-A02).

NCEER-92-0021 "Empirical Analysis of Horizontal Ground Displacement Generated by Liquefaction-Induced Lateral Spreads," by S.F. Bartlett and T.L. Youd, 8/17/92, (PB93-188241, A06, MF-A02).

NCEER-92-0022 "IDARC Version 3.0: Inelastic Damage Analysis of Reinforced Concrete Structures," by S.K. Kunnath, A.M. Reinhorn and R.F. Lobo, 8/31/92, (PB93-227502, A07, MF-A02).

NCEER-92-0023 "A Semi-Empirical Analysis of Strong-Motion Peaks in Terms of Seismic Source, Propagation Path and Local Site Conditions, by M. Kamiyama, M.J. O'Rourke and R. Flores-Berrones, 9/9/92, (PB93-150266, A08, MF-A02).

NCEER-92-0024 "Seismic Behavior of Reinforced Concrete Frame Structures with Nonductile Details, Part I: Summary of Experimental Findings of Full Scale Beam-Column Joint Tests," by A. Beres, R.N. White and P. Gergely, 9/30/92, (PB93-227783, A05, MF-A01).

NCEER-92-0025 "Experimental Results of Repaired and Retrofitted Beam-Column Joint Tests in Lightly Reinforced Concrete Frame Buildings," by A. Beres, S. El-Borgi, R.N. White and P. Gergely, 10/29/92, (PB93-227791, A05, MF-A01).

NCEER-92-0026 "A Generalization of Optimal Control Theory: Linear and Nonlinear Structures," by J.N. Yang, Z. Li and S. Vongchavalitkul, 11/2/92, (PB93-188621, A05, MF-A01).

NCEER-92-0027 "Seismic Resistance of Reinforced Concrete Frame Structures Designed Only for Gravity Loads: Part I - Design and Properties of a One-Third Scale Model Structure," by J.M. Bracci, A.M. Reinhorn and J.B. Mander, 12/1/92, (PB94-104502, A08, MF-A02).

NCEER-92-0028 "Seismic Resistance of Reinforced Concrete Frame Structures Designed Only for Gravity Loads: Part II - Experimental Performance of Subassemblages," by L.E. Aycardi, J.B. Mander and A.M. Reinhorn, 12/1/92, (PB94-104510, A08, MF-A02).

NCEER-92-0029 "Seismic Resistance of Reinforced Concrete Frame Structures Designed Only for Gravity Loads: Part III - Experimental Performance and Analytical Study of a Structural Model," by J.M. Bracci, A.M. Reinhorn and J.B. Mander, 12/1/92, (PB93-227528, A09, MF-A01).

NCEER-92-0030 "Evaluation of Seismic Retrofit of Reinforced Concrete Frame Structures: Part I - Experimental Performance of Retrofitted Subassemblages," by D. Choudhuri, J.B. Mander and A.M. Reinhorn, 12/8/92, (PB93-198307, A07, MF-A02).

NCEER-92-0031 "Evaluation of Seismic Retrofit of Reinforced Concrete Frame Structures: Part II - Experimental Performance and Analytical Study of a Retrofitted Structural Model," by J.M. Bracci, A.M. Reinhorn and J.B. Mander, 12/8/92, (PB93-198315, A09, MF-A03).

NCEER-92-0032 "Experimental and Analytical Investigation of Seismic Response of Structures with Supplemental Fluid Viscous Dampers," by M.C. Constantinou and M.D. Symans, 12/21/92, (PB93-191435, A10, MF-A03). This report is available only through NTIS (see address given above).

NCEER-92-0033 "Reconnaissance Report on the Cairo, Egypt Earthquake of October 12, 1992," by M. Khater, 12/23/92, (PB93-188621, A03, MF-A01).

NCEER-92-0034 "Low-Level Dynamic Characteristics of Four Tall Flat-Plate Buildings in New York City," by H. Gavin, S. Yuan, J. Grossman, E. Pekelis and K. Jacob, 12/28/92, (PB93-188217, A07, MF-A02).

NCEER-93-0001 "An Experimental Study on the Seismic Performance of Brick-Infilled Steel Frames With and Without Retrofit," by J.B. Mander, B. Nair, K. Wojtkowski and J. Ma, 1/29/93, (PB93-227510, A07, MF-A02).

NCEER-93-0002 "Social Accounting for Disaster Preparedness and Recovery Planning," by S. Cole, E. Pantoja and V. Razak, 2/22/93, (PB94-142114, A12, MF-A03).

NCEER-93-0003 "Assessment of 1991 NEHRP Provisions for Nonstructural Components and Recommended Revisions," by T.T. Soong, G. Chen, Z. Wu, R-H. Zhang and M. Grigoriu, 3/1/93, (PB93-188639, A06, MF-A02).

NCEER-93-0004 "Evaluation of Static and Response Spectrum Analysis Procedures of SEAOC/UBC for Seismic Isolated Structures," by C.W. Winters and M.C. Constantinou, 3/23/93, (PB93-198299, A10, MF-A03).

NCEER-93-0005 "Earthquakes in the Northeast - Are We Ignoring the Hazard? A Workshop on Earthquake Science and Safety for Educators," edited by K.E.K. Ross, 4/2/93, (PB94-103066, A09, MF-A02).

NCEER-93-0006 "Inelastic Response of Reinforced Concrete Structures with Viscoelastic Braces," by R.F. Lobo, J.M. Bracci, K.L. Shen, A.M. Reinhorn and T.T. Soong, 4/5/93, (PB93-227486, A05, MF-A02).

NCEER-93-0007 "Seismic Testing of Installation Methods for Computers and Data Processing Equipment," by K. Kosar, T.T. Soong, K.L. Shen, J.A. HoLung and Y.K. Lin, 4/12/93, (PB93-198299, A07, MF-A02).

NCEER-93-0008 "Retrofit of Reinforced Concrete Frames Using Added Dampers," by A. Reinhorn, M. Constantinou and C. Li, not available.

NCEER-93-0009 "Seismic Behavior and Design Guidelines for Steel Frame Structures with Added Viscoelastic Dampers," by K.C. Chang, M.L. Lai, T.T. Soong, D.S. Hao and Y.C. Yeh, 5/1/93, (PB94-141959, A07, MF-A02).

NCEER-93-0010 "Seismic Performance of Shear-Critical Reinforced Concrete Bridge Piers," by J.B. Mander, S.M. Waheed, M.T.A. Chaudhary and S.S. Chen, 5/12/93, (PB93-227494, A08, MF-A02).

NCEER-93-0011 "3D-BASIS-TABS: Computer Program for Nonlinear Dynamic Analysis of Three Dimensional Base Isolated Structures," by S. Nagarajaiah, C. Li, A.M. Reinhorn and M.C. Constantinou, 8/2/93, (PB94-141819, A09, MF-A02).

NCEER-93-0012 "Effects of Hydrocarbon Spills from an Oil Pipeline Break on Ground Water," by O.J. Helweg and H.H.M. Hwang, 8/3/93, (PB94-141942, A06, MF-A02).

NCEER-93-0013 "Simplified Procedures for Seismic Design of Nonstructural Components and Assessment of Current Code Provisions," by M.P. Singh, L.E. Suarez, E.E. Matheu and G.O. Maldonado, 8/4/93, (PB94-141827, A09, MF-A02).

NCEER-93-0014 "An Energy Approach to Seismic Analysis and Design of Secondary Systems," by G. Chen and T.T. Soong, 8/6/93, (PB94-142767, A11, MF-A03).

NCEER-93-0015 "Proceedings from School Sites: Becoming Prepared for Earthquakes - Commemorating the Third Anniversary of the Loma Prieta Earthquake," Edited by F.E. Winslow and K.E.K. Ross, 8/16/93, (PB94-154275, A16, MF-A02).

NCEER-93-0016 "Reconnaissance Report of Damage to Historic Monuments in Cairo, Egypt Following the October 12, 1992 Dahshur Earthquake," by D. Sykora, D. Look, G. Croci, E. Karaesmen and E. Karaesmen, 8/19/93, (PB94-142221, A08, MF-A02).

NCEER-93-0017 "The Island of Guam Earthquake of August 8, 1993," by S.W. Swan and S.K. Harris, 9/30/93, (PB94-141843, A04, MF-A01).

NCEER-93-0018 "Engineering Aspects of the October 12, 1992 Egyptian Earthquake," by A.W. Elgamal, M. Amer, K. Adalier and A. Abul-Fadl, 10/7/93, (PB94-141983, A05, MF-A01).

NCEER-93-0019 "Development of an Earthquake Motion Simulator and its Application in Dynamic Centrifuge Testing," by I. Krstelj, Supervised by J.H. Prevost, 10/23/93, (PB94-181773, A-10, MF-A03).

NCEER-93-0020 "NCEER-Taisei Corporation Research Program on Sliding Seismic Isolation Systems for Bridges: Experimental and Analytical Study of a Friction Pendulum System (FPS)," by M.C. Constantinou, P. Tsopelas, Y-S. Kim and S. Okamoto, 11/1/93, (PB94-142775, A08, MF-A02).

NCEER-93-0021 "Finite Element Modeling of Elastomeric Seismic Isolation Bearings," by L.J. Billings, Supervised by R. Shepherd, 11/8/93, not available.

NCEER-93-0022 "Seismic Vulnerability of Equipment in Critical Facilities: Life-Safety and Operational Consequences," by K. Porter, G.S. Johnson, M.M. Zadeh, C. Scawthorn and S. Eder, 11/24/93, (PB94-181765, A16, MF-A03).

NCEER-93-0023 "Hokkaido Nansei-oki, Japan Earthquake of July 12, 1993, by P.I. Yanev and C.R. Scawthorn, 12/23/93, (PB94-181500, A07, MF-A01).

NCEER-94-0001 "An Evaluation of Seismic Serviceability of Water Supply Networks with Application to the San Francisco Auxiliary Water Supply System," by I. Markov, Supervised by M. Grigoriu and T. O'Rourke, 1/21/94, (PB94-204013, A07, MF-A02).

NCEER-94-0002 "NCEER-Taisei Corporation Research Program on Sliding Seismic Isolation Systems for Bridges: Experimental and Analytical Study of Systems Consisting of Sliding Bearings, Rubber Restoring Force Devices and Fluid Dampers," Volumes I and II, by P. Tsopelas, S. Okamoto, M.C. Constantinou, D. Ozaki and S. Fujii, 2/4/94, (PB94-181740, A09, MF-A02 and PB94-181757, A12, MF-A03).

NCEER-94-0003 "A Markov Model for Local and Global Damage Indices in Seismic Analysis," by S. Rahman and M. Grigoriu, 2/18/94, (PB94-206000, A12, MF-A03).

NCEER-94-0004 "Proceedings from the NCEER Workshop on Seismic Response of Masonry Infills," edited by D.P. Abrams, 3/1/94, (PB94-180783, A07, MF-A02).

NCEER-94-0005 "The Northridge, California Earthquake of January 17, 1994: General Reconnaissance Report," edited by J.D. Goltz, 3/11/94, (PB94-193943, A10, MF-A03).

NCEER-94-0006 "Seismic Energy Based Fatigue Damage Analysis of Bridge Columns: Part I - Evaluation of Seismic Capacity," by G.A. Chang and J.B. Mander, 3/14/94, (PB94-219185, A11, MF-A03).

NCEER-94-0007 "Seismic Isolation of Multi-Story Frame Structures Using Spherical Sliding Isolation Systems," by T.M. Al-Hussaini, V.A. Zayas and M.C. Constantinou, 3/17/94, (PB94-193745, A09, MF-A02).

NCEER-94-0008 "The Northridge, California Earthquake of January 17, 1994: Performance of Highway Bridges," edited by I.G. Buckle, 3/24/94, (PB94-193851, A06, MF-A02).

NCEER-94-0009 "Proceedings of the Third U.S.-Japan Workshop on Earthquake Protective Systems for Bridges," edited by I.G. Buckle and I. Friedland, 3/31/94, (PB94-195815, A99, MF-A06).

NCEER-94-0010 "3D-BASIS-ME: Computer Program for Nonlinear Dynamic Analysis of Seismically Isolated Single and Multiple Structures and Liquid Storage Tanks," by P.C. Tsopelas, M.C. Constantinou and A.M. Reinhorn, 4/12/94, (PB94-204922, A09, MF-A02).

NCEER-94-0011 "The Northridge, California Earthquake of January 17, 1994: Performance of Gas Transmission Pipelines," by T.D. O'Rourke and M.C. Palmer, 5/16/94, (PB94-204989, A05, MF-A01).

NCEER-94-0012 "Feasibility Study of Replacement Procedures and Earthquake Performance Related to Gas Transmission Pipelines," by T.D. O'Rourke and M.C. Palmer, 5/25/94, (PB94-206638, A09, MF-A02).

NCEER-94-0013 "Seismic Energy Based Fatigue Damage Analysis of Bridge Columns: Part II - Evaluation of Seismic Demand," by G.A. Chang and J.B. Mander, 6/1/94, (PB95-18106, A08, MF-A02).

NCEER-94-0014 "NCEER-Taisei Corporation Research Program on Sliding Seismic Isolation Systems for Bridges: Experimental and Analytical Study of a System Consisting of Sliding Bearings and Fluid Restoring Force/Damping Devices," by P. Tsopelas and M.C. Constantinou, 6/13/94, (PB94-219144, A10, MF-A03).

NCEER-94-0015 "Generation of Hazard-Consistent Fragility Curves for Seismic Loss Estimation Studies," by H. Hwang and J-R. Huo, 6/14/94, (PB95-181996, A09, MF-A02).

NCEER-94-0016 "Seismic Study of Building Frames with Added Energy-Absorbing Devices," by W.S. Pong, C.S. Tsai and G.C. Lee, 6/20/94, (PB94-219136, A10, A03).

NCEER-94-0017 "Sliding Mode Control for Seismic-Excited Linear and Nonlinear Civil Engineering Structures," by J. Yang, J. Wu, A. Agrawal and Z. Li, 6/21/94, (PB95-138483, A06, MF-A02).

NCEER-94-0018 "3D-BASIS-TABS Version 2.0: Computer Program for Nonlinear Dynamic Analysis of Three Dimensional Base Isolated Structures," by A.M. Reinhorn, S. Nagarajaiah, M.C. Constantinou, P. Tsopelas and R. Li, 6/22/94, (PB95-182176, A08, MF-A02).

NCEER-94-0019 "Proceedings of the International Workshop on Civil Infrastructure Systems: Application of Intelligent Systems and Advanced Materials on Bridge Systems," Edited by G.C. Lee and K.C. Chang, 7/18/94, (PB95-252474, A20, MF-A04).

NCEER-94-0020 "Study of Seismic Isolation Systems for Computer Floors," by V. Lambrou and M.C. Constantinou, 7/19/94, (PB95-138533, A10, MF-A03).

NCEER-94-0021 "Proceedings of the U.S.-Italian Workshop on Guidelines for Seismic Evaluation and Rehabilitation of Unreinforced Masonry Buildings," Edited by D.P. Abrams and G.M. Calvi, 7/20/94, (PB95-138749, A13, MF-A03).

NCEER-94-0022 "NCEER-Taisei Corporation Research Program on Sliding Seismic Isolation Systems for Bridges: Experimental and Analytical Study of a System Consisting of Lubricated PTFE Sliding Bearings and Mild Steel Dampers," by P. Tsopelas and M.C. Constantinou, 7/22/94, (PB95-182184, A08, MF-A02).

NCEER-94-0023 "Development of Reliability-Based Design Criteria for Buildings Under Seismic Load," by Y.K. Wen, H. Hwang and M. Shinozuka, 8/1/94, (PB95-211934, A08, MF-A02).

NCEER-94-0024 "Experimental Verification of Acceleration Feedback Control Strategies for an Active Tendon System," by S.J. Dyke, B.F. Spencer, Jr., P. Quast, M.K. Sain, D.C. Kaspari, Jr. and T.T. Soong, 8/29/94, (PB95-212320, A05, MF-A01).

NCEER-94-0025 "Seismic Retrofitting Manual for Highway Bridges," Edited by I.G. Buckle and I.F. Friedland, published by the Federal Highway Administration (PB95-212676, A15, MF-A03).

NCEER-94-0026 "Proceedings from the Fifth U.S.-Japan Workshop on Earthquake Resistant Design of Lifeline Facilities and Countermeasures Against Soil Liquefaction," Edited by T.D. O'Rourke and M. Hamada, 11/7/94, (PB95-220802, A99, MF-E08).

NCEER-95-0001 "Experimental and Analytical Investigation of Seismic Retrofit of Structures with Supplemental Damping: Part 1 - Fluid Viscous Damping Devices," by A.M. Reinhorn, C. Li and M.C. Constantinou, 1/3/95, (PB95-266599, A09, MF-A02).

NCEER-95-0002 "Experimental and Analytical Study of Low-Cycle Fatigue Behavior of Semi-Rigid Top-And-Seat Angle Connections," by G. Pekcan, J.B. Mander and S.S. Chen, 1/5/95, (PB95-220042, A07, MF-A02).

NCEER-95-0003 "NCEER-ATC Joint Study on Fragility of Buildings," by T. Anagnos, C. Rojahn and A.S. Kiremidjian, 1/20/95, (PB95-220026, A06, MF-A02).

NCEER-95-0004 "Nonlinear Control Algorithms for Peak Response Reduction," by Z. Wu, T.T. Soong, V. Gattulli and R.C. Lin, 2/16/95, (PB95-220349, A05, MF-A01).

NCEER-95-0005 "Pipeline Replacement Feasibility Study: A Methodology for Minimizing Seismic and Corrosion Risks to Underground Natural Gas Pipelines," by R.T. Eguchi, H.A. Seligson and D.G. Honegger, 3/2/95, (PB95-252326, A06, MF-A02).

NCEER-95-0006 "Evaluation of Seismic Performance of an 11-Story Frame Building During the 1994 Northridge Earthquake," by F. Naeim, R. DiSilio, K. Benuska, A. Reinhorn and C. Li, not available.

NCEER-95-0007 "Prioritization of Bridges for Seismic Retrofitting," by N. Basöz and A.S. Kiremidjian, 4/24/95, (PB95-252300, A08, MF-A02).

NCEER-95-0008 "Method for Developing Motion Damage Relationships for Reinforced Concrete Frames," by A. Singhal and A.S. Kiremidjian, 5/11/95, (PB95-266607, A06, MF-A02).

NCEER-95-0009 "Experimental and Analytical Investigation of Seismic Retrofit of Structures with Supplemental Damping: Part II - Friction Devices," by C. Li and A.M. Reinhorn, 7/6/95, (PB96-128087, A11, MF-A03).

NCEER-95-0010 "Experimental Performance and Analytical Study of a Non-Ductile Reinforced Concrete Frame Structure Retrofitted with Elastomeric Spring Dampers," by G. Pekcan, J.B. Mander and S.S. Chen, 7/14/95, (PB96-137161, A08, MF-A02).

NCEER-95-0011 "Development and Experimental Study of Semi-Active Fluid Damping Devices for Seismic Protection of Structures," by M.D. Symans and M.C. Constantinou, 8/3/95, (PB96-136940, A23, MF-A04).

NCEER-95-0012 "Real-Time Structural Parameter Modification (RSPM): Development of Innervated Structures," by Z. Liang, M. Tong and G.C. Lee, 4/11/95, (PB96-137153, A06, MF-A01).

NCEER-95-0013 "Experimental and Analytical Investigation of Seismic Retrofit of Structures with Supplemental Damping: Part III - Viscous Damping Walls," by A.M. Reinhorn and C. Li, 10/1/95, (PB96-176409, A11, MF-A03).

NCEER-95-0014 "Seismic Fragility Analysis of Equipment and Structures in a Memphis Electric Substation," by J-R. Huo and H.H.M. Hwang, 8/10/95, (PB96-128087, A09, MF-A02).

NCEER-95-0015 "The Hanshin-Awaji Earthquake of January 17, 1995: Performance of Lifelines," Edited by M. Shinozuka, 11/3/95, (PB96-176383, A15, MF-A03).

NCEER-95-0016 "Highway Culvert Performance During Earthquakes," by T.L. Youd and C.J. Beckman, available as NCEER-96-0015.

NCEER-95-0017 "The Hanshin-Awaji Earthquake of January 17, 1995: Performance of Highway Bridges," Edited by I.G. Buckle, 12/1/95, not available.

NCEER-95-0018 "Modeling of Masonry Infill Panels for Structural Analysis," by A.M. Reinhorn, A. Madan, R.E. Valles, Y. Reichmann and J.B. Mander, 12/8/95, (PB97-110886, MF-A01, A06).

NCEER-95-0019 "Optimal Polynomial Control for Linear and Nonlinear Structures," by A.K. Agrawal and J.N. Yang, 12/11/95, (PB96-168737, A07, MF-A02).

NCEER-95-0020 "Retrofit of Non-Ductile Reinforced Concrete Frames Using Friction Dampers," by R.S. Rao, P. Gergely and R.N. White, 12/22/95, (PB97-133508, A10, MF-A02).

NCEER-95-0021 "Parametric Results for Seismic Response of Pile-Supported Bridge Bents," by G. Mylonakis, A. Nikolaou and G. Gazetas, 12/22/95, (PB97-100242, A12, MF-A03).

NCEER-95-0022 "Kinematic Bending Moments in Seismically Stressed Piles," by A. Nikolaou, G. Mylonakis and G. Gazetas, 12/23/95, (PB97-113914, MF-A03, A13).

NCEER-96-0001 "Dynamic Response of Unreinforced Masonry Buildings with Flexible Diaphragms," by A.C. Costley and D.P. Abrams," 10/10/96, (PB97-133573, MF-A03, A15).

NCEER-96-0002 "State of the Art Review: Foundations and Retaining Structures," by I. Po Lam, not available.

NCEER-96-0003 "Ductility of Rectangular Reinforced Concrete Bridge Columns with Moderate Confinement," by N. Wehbe, M. Saidi, D. Sanders and B. Douglas, 11/7/96, (PB97-133557, A06, MF-A02).

NCEER-96-0004 "Proceedings of the Long-Span Bridge Seismic Research Workshop," edited by I.G. Buckle and I.M. Friedland, not available.

NCEER-96-0005 "Establish Representative Pier Types for Comprehensive Study: Eastern United States," by J. Kulicki and Z. Prucz, 5/28/96, (PB98-119217, A07, MF-A02).

NCEER-96-0006 "Establish Representative Pier Types for Comprehensive Study: Western United States," by R. Imbsen, R.A. Schamber and T.A. Osterkamp, 5/28/96, (PB98-118607, A07, MF-A02).

NCEER-96-0007 "Nonlinear Control Techniques for Dynamical Systems with Uncertain Parameters," by R.G. Ghanem and M.I. Bujakow, 5/27/96, (PB97-100259, A17, MF-A03).

NCEER-96-0008 "Seismic Evaluation of a 30-Year Old Non-Ductile Highway Bridge Pier and Its Retrofit," by J.B. Mander, B. Mahmoodzadegan, S. Bhadra and S.S. Chen, 5/31/96, (PB97-110902, MF-A03, A10).

NCEER-96-0009 "Seismic Performance of a Model Reinforced Concrete Bridge Pier Before and After Retrofit," by J.B. Mander, J.H. Kim and C.A. Ligozio, 5/31/96, (PB97-110910, MF-A02, A10).

NCEER-96-0010 "IDARC2D Version 4.0: A Computer Program for the Inelastic Damage Analysis of Buildings," by R.E. Valles, A.M. Reinhorn, S.K. Kunzath, C. Li and A. Madan, 6/3/96, (PB97-100234, A17, MF-A03).

NCEER-96-0011 "Estimation of the Economic Impact of Multiple Lifeline Disruption: Memphis Light, Gas and Water Division Case Study," by S.E. Chang, H.A. Seligson and R.T. Eguchi, 8/16/96, (PB97-133490, A11, MF-A03).

NCEER-96-0012 "Proceedings from the Sixth Japan-U.S. Workshop on Earthquake Resistant Design of Lifeline Facilities and Countermeasures Against Soil Liquefaction, Edited by M. Hamada and T. O'Rourke, 9/11/96, (PB97-133581, A99, MF-A06).

NCEER-96-0013 "Chemical Hazards, Mitigation and Preparedness in Areas of High Seismic Risk: A Methodology for Estimating the Risk of Post-Earthquake Hazardous Materials Release," by H.A. Seligson, R.T. Eguchi, K.J. Tierney and K. Richmond, 11/7/96, (PB97-133565, MF-A02, A08).

NCEER-96-0014 "Response of Steel Bridge Bearings to Reversed Cyclic Loading," by J.B. Mander, D-K. Kim, S.S. Chen and G.J. Premus, 11/13/96, (PB97-140735, A12, MF-A03).

NCEER-96-0015 "Highway Culvert Performance During Past Earthquakes," by T.L. Youd and C.J. Beckman, 11/25/96, (PB97-133532, A06, MF-A01).

NCEER-97-0001 "Evaluation, Prevention and Mitigation of Pounding Effects in Building Structures," by R.E. Valles and A.M. Reinhorn, 2/20/97, (PB97-159552, A14, MF-A03).

NCEER-97-0002 "Seismic Design Criteria for Bridges and Other Highway Structures," by C. Rojahn, R. Mayes, D.G. Anderson, J. Clark, J.H. Hom, R.V. Nutt and M.J. O'Rourke, 4/30/97, (PB97-194658, A06, MF-A03).

NCEER-97-0003 "Proceedings of the U.S.-Italian Workshop on Seismic Evaluation and Retrofit," Edited by D.P. Abrams and G.M. Calvi, 3/19/97, (PB97-194666, A13, MF-A03).

NCEER-97-0004 "Investigation of Seismic Response of Buildings with Linear and Nonlinear Fluid Viscous Dampers," by A.A. Seleemah and M.C. Constantinou, 5/21/97, (PB98-109002, A15, MF-A03).

NCEER-97-0005 "Proceedings of the Workshop on Earthquake Engineering Frontiers in Transportation Facilities," edited by G.C. Lee and I.M. Friedland, 8/29/97, (PB98-128911, A25, MR-A04).

NCEER-97-0006 "Cumulative Seismic Damage of Reinforced Concrete Bridge Piers," by S.K. Kunnath, A. El-Bahy, A. Taylor and W. Stone, 9/2/97, (PB98-108814, A11, MF-A03).

NCEER-97-0007 "Structural Details to Accommodate Seismic Movements of Highway Bridges and Retaining Walls," by R.A. Imbsen, R.A. Schamber, E. Thorkildsen, A. Kartoum, B.T. Martin, T.N. Rosser and J.M. Kulicki, 9/3/97, (PB98-108996, A09, MF-A02).

NCEER-97-0008 "A Method for Earthquake Motion-Damage Relationships with Application to Reinforced Concrete Frames," by A. Singhal and A.S. Kiremidjian, 9/10/97, (PB98-108988, A13, MF-A03).

NCEER-97-0009 "Seismic Analysis and Design of Bridge Abutments Considering Sliding and Rotation," by K. Fishman and R. Richards, Jr., 9/15/97, (PB98-108897, A06, MF-A02).

NCEER-97-0010 "Proceedings of the FHWA/NCEER Workshop on the National Representation of Seismic Ground Motion for New and Existing Highway Facilities," edited by I.M. Friedland, M.S. Power and R.L. Mayes, 9/22/97, (PB98-128903, A21, MF-A04).

NCEER-97-0011 "Seismic Analysis for Design or Retrofit of Gravity Bridge Abutments," by K.L. Fishman, R. Richards, Jr. and R.C. Divito, 10/2/97, (PB98-128937, A08, MF-A02).

NCEER-97-0012 "Evaluation of Simplified Methods of Analysis for Yielding Structures," by P. Tsopelas, M.C. Constantinou, C.A. Kircher and A.S. Whittaker, 10/31/97, (PB98-128929, A10, MF-A03).

NCEER-97-0013 "Seismic Design of Bridge Columns Based on Control and Repairability of Damage," by C-T. Cheng and J.B. Mander, 12/8/97, (PB98-144249, A11, MF-A03).

NCEER-97-0014 "Seismic Resistance of Bridge Piers Based on Damage Avoidance Design," by J.B. Mander and C-T. Cheng, 12/10/97, (PB98-144223, A09, MF-A02).

NCEER-97-0015 "Seismic Response of Nominally Symmetric Systems with Strength Uncertainty," by S. Balopoulou and M. Grigoriu, 12/23/97, (PB98-153422, A11, MF-A03).

NCEER-97-0016 "Evaluation of Seismic Retrofit Methods for Reinforced Concrete Bridge Columns," by T.J. Wipf, F.W. Klaiber and F.M. Russo, 12/28/97, (PB98-144215, A12, MF-A03).

NCEER-97-0017 "Seismic Fragility of Existing Conventional Reinforced Concrete Highway Bridges," by C.L. Mullen and A.S. Cakmak, 12/30/97, (PB98-153406, A08, MF-A02).

NCEER-97-0018 "Loss Assessment of Memphis Buildings," edited by D.P. Abrams and M. Shinozuka, 12/31/97, (PB98-144231, A13, MF-A03).

NCEER-97-0019 "Seismic Evaluation of Frames with Infill Walls Using Quasi-static Experiments," by K.M. Mosalam, R.N. White and P. Gergely, 12/31/97, (PB98-153455, A07, MF-A02).

NCEER-97-0020 "Seismic Evaluation of Frames with Infill Walls Using Pseudo-dynamic Experiments," by K.M. Mosalam, R.N. White and P. Gergely, 12/31/97, (PB98-153430, A07, MF-A02).

NCEER-97-0021 "Computational Strategies for Frames with Infill Walls: Discrete and Smeared Crack Analyses and Seismic Fragility," by K.M. Mosalam, R.N. White and P. Gergely, 12/31/97, (PB98-153414, A10, MF-A02).

NCEER-97-0022 "Proceedings of the NCEER Workshop on Evaluation of Liquefaction Resistance of Soils," edited by T.L. Youd and I.M. Idriss, 12/31/97, (PB98-155617, A15, MF-A03).

MCEER-98-0001 "Extraction of Nonlinear Hysteretic Properties of Seismically Isolated Bridges from Quick-Release Field Tests," by Q. Chen, B.M. Douglas, E.M. Maragakis and I.G. Buckle, 5/26/98, (PB99-118838, A06, MF-A01).

MCEER-98-0002 "Methodologies for Evaluating the Importance of Highway Bridges," by A. Thomas, S. Eshenaur and J. Kulicki, 5/29/98, (PB99-118846, A10, MF-A02).

MCEER-98-0003 "Capacity Design of Bridge Piers and the Analysis of Overstrength," by J.B. Mander, A. Dutta and P. Goel, 6/1/98, (PB99-118853, A09, MF-A02).

MCEER-98-0004 "Evaluation of Bridge Damage Data from the Loma Prieta and Northridge, California Earthquakes," by N. Basoz and A. Kiremidjian, 6/2/98, (PB99-118861, A15, MF-A03).

MCEER-98-0005 "Screening Guide for Rapid Assessment of Liquefaction Hazard at Highway Bridge Sites," by T. L. Youd, 6/16/98, (PB99-118879, A06, not available on microfiche).

MCEER-98-0006 "Structural Steel and Steel/Concrete Interface Details for Bridges," by P. Ritchie, N. Kauhl and J. Kulicki, 7/13/98, (PB99-118945, A06, MF-A01).

MCEER-98-0007 "Capacity Design and Fatigue Analysis of Confined Concrete Columns," by A. Dutta and J.B. Mander, 7/14/98, (PB99-118960, A14, MF-A03).

MCEER-98-0008 "Proceedings of the Workshop on Performance Criteria for Telecommunication Services Under Earthquake Conditions," edited by A.J. Schiff, 7/15/98, (PB99-118952, A08, MF-A02).

MCEER-98-0009 "Fatigue Analysis of Unconfined Concrete Columns," by J.B. Mander, A. Dutta and J.H. Kim, 9/12/98, (PB99-123655, A10, MF-A02).

MCEER-98-0010 "Centrifuge Modeling of Cyclic Lateral Response of Pile-Cap Systems and Seat-Type Abutments in Dry Sands," by A.D. Gadre and R. Dobry, 10/2/98, (PB99-123606, A13, MF-A03).

MCEER-98-0011 "IDARC-BRIDGE: A Computational Platform for Seismic Damage Assessment of Bridge Structures," by A.M. Reinhorn, V. Simeonov, G. Mylonakis and Y. Reichman, 10/2/98, (PB99-162919, A15, MF-A03).

MCEER-98-0012 "Experimental Investigation of the Dynamic Response of Two Bridges Before and After Retrofitting with Elastomeric Bearings," by D.A. Wendichansky, S.S. Chen and J.B. Mander, 10/2/98, (PB99-162927, A15, MF-A03).

MCEER-98-0013 "Design Procedures for Hinge Restrainers and Hinge Sear Width for Multiple-Frame Bridges," by R. Des Roches and G.L. Fenves, 11/3/98, (PB99-140477, A13, MF-A03).

MCEER-98-0014 "Response Modification Factors for Seismically Isolated Bridges," by M.C. Constantinou and J.K. Quarshie, 11/3/98, (PB99-140485, A14, MF-A03).

MCEER-98-0015 "Proceedings of the U.S.-Italy Workshop on Seismic Protective Systems for Bridges," edited by I.M. Friedland and M.C. Constantinou, 11/3/98, (PB2000-101711, A22, MF-A04).

MCEER-98-0016 "Appropriate Seismic Reliability for Critical Equipment Systems: Recommendations Based on Regional Analysis of Financial and Life Loss," by K. Porter, C. Scawthorn, C. Taylor and N. Blais, 11/10/98, (PB99-157265, A08, MF-A02).

MCEER-98-0017 "Proceedings of the U.S. Japan Joint Seminar on Civil Infrastructure Systems Research," edited by M. Shinozuka and A. Rose, 11/12/98, (PB99-156713, A16, MF-A03).

MCEER-98-0018 "Modeling of Pile Footings and Drilled Shafts for Seismic Design," by I. PoLam, M. Kapuskar and D. Chaudhuri, 12/21/98, (PB99-157257, A09, MF-A02).

MCEER-99-0001 "Seismic Evaluation of a Masonry Infilled Reinforced Concrete Frame by Pseudodynamic Testing," by S.G. Buonopane and R.N. White, 2/16/99, (PB99-162851, A09, MF-A02).

MCEER-99-0002 "Response History Analysis of Structures with Seismic Isolation and Energy Dissipation Systems: Verification Examples for Program SAP2000," by J. Scheller and M.C. Constantinou, 2/22/99, (PB99-162869, A08, MF-A02).

MCEER-99-0003 "Experimental Study on the Seismic Design and Retrofit of Bridge Columns Including Axial Load Effects," by A. Dutta, T. Kokorina and J.B. Mander, 2/22/99, (PB99-162877, A09, MF-A02).

MCEER-99-0004 "Experimental Study of Bridge Elastomeric and Other Isolation and Energy Dissipation Systems with Emphasis on Uplift Prevention and High Velocity Near-source Seismic Excitation," by A. Kasalanati and M. C. Constantinou, 2/26/99, (PB99-162885, A12, MF-A03).

MCEER-99-0005 "Truss Modeling of Reinforced Concrete Shear-flexure Behavior," by J.H. Kim and J.B. Mander, 3/8/99, (PB99-163693, A12, MF-A03).

MCEER-99-0006 "Experimental Investigation and Computational Modeling of Seismic Response of a 1:4 Scale Model Steel Structure with a Load Balancing Supplemental Damping System," by G. Pekcan, J.B. Mander and S.S. Chen, 4/2/99, (PB99-162893, A11, MF-A03).

MCEER-99-0007 "Effect of Vertical Ground Motions on the Structural Response of Highway Bridges," by M.R. Button, C.J. Cronin and R.L. Mayes, 4/10/99, (PB2000-101411, A10, MF-A03).

MCEER-99-0008 "Seismic Reliability Assessment of Critical Facilities: A Handbook, Supporting Documentation, and Model Code Provisions," by G.S. Johnson, R.E. Sheppard, M.D. Quilici, S.J. Eder and C.R. Scawthorn, 4/12/99, (PB2000-101701, A18, MF-A04).

MCEER-99-0009 "Impact Assessment of Selected MCEER Highway Project Research on the Seismic Design of Highway Structures," by C. Rojahn, R. Mayes, D.G. Anderson, J.H. Clark, D'Appolonia Engineering, S. Gloyd and R.V. Nutt, 4/14/99, (PB99-162901, A10, MF-A02).

MCEER-99-0010 "Site Factors and Site Categories in Seismic Codes," by R. Dobry, R. Ramos and M.S. Power, 7/19/99, (PB2000-101705, A08, MF-A02).

MCEER-99-0011 "Restrainer Design Procedures for Multi-Span Simply-Supported Bridges," by M.J. Randall, M. Saiidi, E. Maragakis and T. Isakovic, 7/20/99, (PB2000-101702, A10, MF-A02).

MCEER-99-0012 "Property Modification Factors for Seismic Isolation Bearings," by M.C. Constantinou, P. Tsopelas, A. Kasalanati and E. Wolff, 7/20/99, (PB2000-103387, A11, MF-A03).

MCEER-99-0013 "Critical Seismic Issues for Existing Steel Bridges," by P. Ritchie, N. Kauhl and J. Kulicki, 7/20/99, (PB2000-101697, A09, MF-A02).

MCEER-99-0014 "Nonstructural Damage Database," by A. Kao, T.T. Soong and A. Vender, 7/24/99, (PB2000-101407, A06, MF-A01).

MCEER-99-0015 "Guide to Remedial Measures for Liquefaction Mitigation at Existing Highway Bridge Sites," by H.G. Cooke and J. K. Mitchell, 7/26/99, (PB2000-101703, A11, MF-A03).

MCEER-99-0016 "Proceedings of the MCEER Workshop on Ground Motion Methodologies for the Eastern United States," edited by N. Abrahamson and A. Becker, 8/11/99, (PB2000-103385, A07, MF-A02).

MCEER-99-0017 "Quindío, Colombia Earthquake of January 25, 1999: Reconnaissance Report," by A.P. Asfura and P.J. Flores, 10/4/99, (PB2000-106893, A06, MF-A01).

MCEER-99-0018 "Hysteretic Models for Cyclic Behavior of Deteriorating Inelastic Structures," by M.V. Sivaselvan and A.M. Reinhorn, 11/5/99, (PB2000-103386, A08, MF-A02).

MCEER-99-0019 "Proceedings of the 7th U.S.- Japan Workshop on Earthquake Resistant Design of Lifeline Facilities and Countermeasures Against Soil Liquefaction," edited by T.D. O'Rourke, J.P. Bardet and M. Hamada, 11/19/99, (PB2000-103354, A99, MF-A06).

MCEER-99-0020 "Development of Measurement Capability for Micro-Vibration Evaluations with Application to Chip Fabrication Facilities," by G.C. Lee, Z. Liang, J.W. Song, J.D. Shen and W.C. Liu, 12/1/99, (PB2000-105993, A08, MF-A02).

MCEER-99-0021 "Design and Retrofit Methodology for Building Structures with Supplemental Energy Dissipating Systems," by G. Pekcan, J.B. Mander and S.S. Chen, 12/31/99, (PB2000-105994, A11, MF-A03).

MCEER-00-0001 "The Marmara, Turkey Earthquake of August 17, 1999: Reconnaissance Report," edited by C. Scawthorn; with major contributions by M. Bruneau, R. Eguchi, T. Holzer, G. Johnson, J. Mander, J. Mitchell, W. Mitchell, A. Papageorgiou, C. Scaethorn, and G. Webb, 3/23/00, (PB2000-106200, A11, MF-A03).

MCEER-00-0002 "Proceedings of the MCEER Workshop for Seismic Hazard Mitigation of Health Care Facilities," edited by G.C. Lee, M. Ettouney, M. Grigoriu, J. Hauer and J. Nigg, 3/29/00, (PB2000-106892, A08, MF-A02).

MCEER-00-0003 "The Chi-Chi, Taiwan Earthquake of September 21, 1999: Reconnaissance Report," edited by G.C. Lee and C.H. Loh, with major contributions by G.C. Lee, M. Bruneau, I.G. Buckle, S.E. Chang, P.J. Flores, T.D. O'Rourke, M. Shinozuka, T.T. Soong, C-H. Loh, K-C. Chang, Z-J. Chen, J-S. Hwang, M-L. Lin, G-Y. Liu, K-C. Tsai, G.C. Yao and C-L. Yen, 4/30/00, (PB2001-100980, A10, MF-A02).

MCEER-00-0004 "Seismic Retrofit of End-Sway Frames of Steel Deck-Truss Bridges with a Supplemental Tendon System: Experimental and Analytical Investigation," by G. Pekcan, J.B. Mander and S.S. Chen, 7/1/00, (PB2001-100982, A10, MF-A02).

MCEER-00-0005 "Sliding Fragility of Unrestrained Equipment in Critical Facilities," by W.H. Chong and T.T. Soong, 7/5/00, (PB2001-100983, A08, MF-A02).

MCEER-00-0006 "Seismic Response of Reinforced Concrete Bridge Pier Walls in the Weak Direction," by N. Abo-Shadi, M. Saiidi and D. Sanders, 7/17/00, (PB2001-100981, A17, MF-A03).

MCEER-00-0007 "Low-Cycle Fatigue Behavior of Longitudinal Reinforcement in Reinforced Concrete Bridge Columns," by J. Brown and S.K. Kunnath, 7/23/00, (PB2001-104392, A08, MF-A02).

MCEER-00-0008 "Soil Structure Interaction of Bridges for Seismic Analysis," I. PoLam and H. Law, 9/25/00, (PB2001-105397, A08, MF-A02).

MCEER-00-0009 "Proceedings of the First MCEER Workshop on Mitigation of Earthquake Disaster by Advanced Technologies (MEDAT-1), edited by M. Shinozuka, D.J. Inman and T.D. O'Rourke, 11/10/00, (PB2001-105399, A14, MF-A03).

MCEER-00-0010 "Development and Evaluation of Simplified Procedures for Analysis and Design of Buildings with Passive Energy Dissipation Systems, Revision 01," by O.M. Ramirez, M.C. Constantinou, C.A. Kircher, A.S. Whittaker, M.W. Johnson, J.D. Gomez and C. Chrysostomou, 11/16/01, (PB2001-105523, A23, MF-A04).

MCEER-00-0011 "Dynamic Soil-Foundation-Structure Interaction Analyses of Large Caissons," by C-Y. Chang, C-M. Mok, Z-L. Wang, R. Settgast, F. Waggoner, M.A. Ketchum, H.M. Gonnermann and C-C. Chin, 12/30/00, (PB2001-104373, A07, MF-A02).

MCEER-00-0012 "Experimental Evaluation of Seismic Performance of Bridge Restrainers," by A.G. Vlassis, E.M. Maragakis and M. Saiid Saiidi, 12/30/00, (PB2001-104354, A09, MF-A02).

MCEER-00-0013 "Effect of Spatial Variation of Ground Motion on Highway Structures," by M. Shinozuka, V. Saxena and G. Deodatis, 12/31/00, (PB2001-108755, A13, MF-A03).

MCEER-00-0014 "A Risk-Based Methodology for Assessing the Seismic Performance of Highway Systems," by S.D. Werner, C.E. Taylor, J.E. Moore, II, J.S. Walton and S. Cho, 12/31/00, (PB2001-108756, A14, MF-A03).

MCEER-01-0001 "Experimental Investigation of P-Delta Effects to Collapse During Earthquakes," by D. Vian and M. Bruneau, 6/25/01, (PB2002-100534, A17, MF-A03).

MCEER-01-0002 "Proceedings of the Second MCEER Workshop on Mitigation of Earthquake Disaster by Advanced Technologies (MEDAT-2)," edited by M. Bruneau and D.J. Inman, 7/23/01, (PB2002-100434, A16, MF-A03).

MCEER-01-0003 "Sensitivity Analysis of Dynamic Systems Subjected to Seismic Loads," by C. Roth and M. Grigoriu, 9/18/01, (PB2003-100884, A12, MF-A03).

MCEER-01-0004 "Overcoming Obstacles to Implementing Earthquake Hazard Mitigation Policies: Stage 1 Report," by D.J. Alesch and W.J. Petak, 12/17/01, (PB2002-107949, A07, MF-A02).

MCEER-01-0005 "Updating Real-Time Earthquake Loss Estimates: Methods, Problems and Insights," by C.E. Taylor, S.E. Chang and R.T. Eguchi, 12/17/01, (PB2002-107948, A05, MF-A01).

MCEER-01-0006 "Experimental Investigation and Retrofit of Steel Pile Foundations and Pile Bents Under Cyclic Lateral Loadings," by A. Shama, J. Mander, B. Blabac and S. Chen, 12/31/01, (PB2002-107950, A13, MF-A03).

MCEER-02-0001 "Assessment of Performance of Bolu Viaduct in the 1999 Duzce Earthquake in Turkey" by P.C. Roussis, M.C. Constantinou, M. Erdik, E. Durukal and M. Dicleli, 5/8/02, (PB2003-100883, A08, MF-A02).

MCEER-02-0002 "Seismic Behavior of Rail Counterweight Systems of Elevators in Buildings," by M.P. Singh, Rildova and L.E. Suarez, 5/27/02. (PB2003-100882, A11, MF-A03).

MCEER-02-0003 "Development of Analysis and Design Procedures for Spread Footings," by G. Mylonakis, G. Gazetas, S. Nikolaou and A. Chauncey, 10/02/02, (PB2004-101636, A13, MF-A03, CD-A13).

MCEER-02-0004 "Bare-Earth Algorithms for Use with SAR and LIDAR Digital Elevation Models," by C.K. Huyck, R.T. Eguchi and B. Houshmand, 10/16/02, (PB2004-101637, A07, CD-A07).

MCEER-02-0005 "Review of Energy Dissipation of Compression Members in Concentrically Braced Frames," by K.Lee and M. Bruneau, 10/18/02, (PB2004-101638, A10, CD-A10).

MCEER-03-0001 "Experimental Investigation of Light-Gauge Steel Plate Shear Walls for the Seismic Retrofit of Buildings" by J. Berman and M. Bruneau, 5/2/03, (PB2004-101622, A10, MF-A03, CD-A10).

MCEER-03-0002 "Statistical Analysis of Fragility Curves," by M. Shinozuka, M.Q. Feng, H. Kim, T. Uzawa and T. Ueda, 6/16/03, (PB2004-101849, A09, CD-A09).

MCEER-03-0003 "Proceedings of the Eighth U.S.-Japan Workshop on Earthquake Resistant Design f Lifeline Facilities and Countermeasures Against Liquefaction," edited by M. Hamada, J.P. Bardet and T.D. O'Rourke, 6/30/03, (PB2004-104386, A99, CD-A99).

MCEER-03-0004 "Proceedings of the PRC-US Workshop on Seismic Analysis and Design of Special Bridges," edited by L.C. Fan and G.C. Lee, 7/15/03, (PB2004-104387, A14, CD-A14).

MCEER-03-0005 "Urban Disaster Recovery: A Framework and Simulation Model," by S.B. Miles and S.E. Chang, 7/25/03, (PB2004-104388, A07, CD-A07).

MCEER-03-0006 "Behavior of Underground Piping Joints Due to Static and Dynamic Loading," by R.D. Meis, M. Maragakis and R. Siddharthan, 11/17/03, (PB2005-102194, A13, MF-A03, CD-A00).

MCEER-04-0001 "Experimental Study of Seismic Isolation Systems with Emphasis on Secondary System Response and Verification of Accuracy of Dynamic Response History Analysis Methods," by E. Wolff and M. Constantinou, 1/16/04 (PB2005-102195, A99, MF-E08, CD-A00).

MCEER-04-0002 "Tension, Compression and Cyclic Testing of Engineered Cementitious Composite Materials," by K. Kesner and S.L. Billington, 3/1/04, (PB2005-102196, A08, CD-A08).

MCEER-04-0003 "Cyclic Testing of Braces Laterally Restrained by Steel Studs to Enhance Performance During Earthquakes," by O.C. Celik, J.W. Berman and M. Bruneau, 3/16/04, (PB2005-102197, A13, MF-A03, CD-A00).

MCEER-04-0004 "Methodologies for Post Earthquake Building Damage Detection Using SAR and Optical Remote Sensing: Application to the August 17, 1999 Marmara, Turkey Earthquake," by C.K. Huyck, B.J. Adams, S. Cho, R.T. Eguchi, B. Mansouri and B. Houshmand, 6/15/04, (PB2005-104888, A10, CD-A00).

MCEER-04-0005 "Nonlinear Structural Analysis Towards Collapse Simulation: A Dynamical Systems Approach," by M.V. Sivaselvan and A.M. Reinhorn, 6/16/04, (PB2005-104889, A11, MF-A03, CD-A00).

MCEER-04-0006 "Proceedings of the Second PRC-US Workshop on Seismic Analysis and Design of Special Bridges," edited by G.C. Lee and L.C. Fan, 6/25/04, (PB2005-104890, A16, CD-A00).

MCEER-04-0007 "Seismic Vulnerability Evaluation of Axially Loaded Steel Built-up Laced Members," by K. Lee and M. Bruneau, 6/30/04, (PB2005-104891, A16, CD-A00).

MCEER-04-0008 "Evaluation of Accuracy of Simplified Methods of Analysis and Design of Buildings with Damping Systems for Near-Fault and for Soft-Soil Seismic Motions," by E.A. Pavlou and M.C. Constantinou, 8/16/04, (PB2005-104892, A08, MF-A02, CD-A00).

MCEER-04-0009 "Assessment of Geotechnical Issues in Acute Care Facilities in California," by M. Lew, T.D. O'Rourke, R. Dobry and M. Koch, 9/15/04, (PB2005-104893, A08, CD-A00).

MCEER-04-0010 "Scissor-Jack-Damper Energy Dissipation System," by A.N. Sigaher-Boyle and M.C. Constantinou, 12/1/04 (PB2005-108221).

MCEER-04-0011 "Seismic Retrofit of Bridge Steel Truss Piers Using a Controlled Rocking Approach," by M. Pollino and M. Bruneau, 12/20/04 (PB2006-105795).

MCEER-05-0001 "Experimental and Analytical Studies of Structures Seismically Isolated with an Uplift-Restraint Isolation System," by P.C. Roussis and M.C. Constantinou, 1/10/05 (PB2005-108222).

MCEER-05-0002 "A Versatile Experimentation Model for Study of Structures Near Collapse Applied to Seismic Evaluation of Irregular Structures," by D. Kusumastuti, A.M. Reinhorn and A. Rutenberg, 3/31/05 (PB2006-101523).

MCEER-05-0003 "Proceedings of the Third PRC-US Workshop on Seismic Analysis and Design of Special Bridges," edited by L.C. Fan and G.C. Lee, 4/20/05, (PB2006-105796).

MCEER-05-0004 "Approaches for the Seismic Retrofit of Braced Steel Bridge Piers and Proof-of-Concept Testing of an Eccentrically Braced Frame with Tubular Link," by J.W. Berman and M. Bruneau, 4/21/05 (PB2006-101524).

MCEER-05-0005 "Simulation of Strong Ground Motions for Seismic Fragility Evaluation of Nonstructural Components in Hospitals," by A. Wanitkorkul and A. Filiatrault, 5/26/05 (PB2006-500027).

MCEER-05-0006 "Seismic Safety in California Hospitals: Assessing an Attempt to Accelerate the Replacement or Seismic Retrofit of Older Hospital Facilities," by D.J. Alesch, L.A. Arendt and W.J. Petak, 6/6/05 (PB2006-105794).

MCEER-05-0007 "Development of Seismic Strengthening and Retrofit Strategies for Critical Facilities Using Engineered Cementitious Composite Materials," by K. Kesner and S.L. Billington, 8/29/05 (PB2006-111701).

MCEER-05-0008 "Experimental and Analytical Studies of Base Isolation Systems for Seismic Protection of Power Transformers," by N. Murota, M.Q. Feng and G-Y. Liu, 9/30/05 (PB2006-111702).

MCEER-05-0009 "3D-BASIS-ME-MB: Computer Program for Nonlinear Dynamic Analysis of Seismically Isolated Structures," by P.C. Tsopelas, P.C. Roussis, M.C. Constantinou, R. Buchanan and A.M. Reinhorn, 10/3/05 (PB2006-111703).

MCEER-05-0010 "Steel Plate Shear Walls for Seismic Design and Retrofit of Building Structures," by D. Vian and M. Bruneau, 12/15/05 (PB2006-111704).

MCEER-05-0011 "The Performance-Based Design Paradigm," by M.J. Astrella and A. Whittaker, 12/15/05 (PB2006-111705).

MCEER-06-0001 "Seismic Fragility of Suspended Ceiling Systems," H. Badillo-Almaraz, A.S. Whittaker, A.M. Reinhorn and G.P. Cimellaro, 2/4/06 (PB2006-111706).

MCEER-06-0002 "Multi-Dimensional Fragility of Structures," by G.P. Cimellaro, A.M. Reinhorn and M. Bruneau, 3/1/06 (PB2007-106974, A09, MF-A02, CD A00).

MCEER-06-0003 "Built-Up Shear Links as Energy Dissipators for Seismic Protection of Bridges," by P. Dusicka, A.M. Itani and I.G. Buckle, 3/15/06 (PB2006-111708).

MCEER-06-0004 "Analytical Investigation of the Structural Fuse Concept," by R.E. Vargas and M. Bruneau, 3/16/06 (PB2006-111709).

MCEER-06-0005 "Experimental Investigation of the Structural Fuse Concept," by R.E. Vargas and M. Bruneau, 3/17/06 (PB2006-111710).

MCEER-06-0006 "Further Development of Tubular Eccentrically Braced Frame Links for the Seismic Retrofit of Braced Steel Truss Bridge Piers," by J.W. Berman and M. Bruneau, 3/27/06 (PB2007-105147).

MCEER-06-0007 "REDARS Validation Report," by S. Cho, C.K. Huyck, S. Ghosh and R.T. Eguchi, 8/8/06 (PB2007-106983).

MCEER-06-0008 "Review of Current NDE Technologies for Post-Earthquake Assessment of Retrofitted Bridge Columns," by J.W. Song, Z. Liang and G.C. Lee, 8/21/06 (PB2007-106984).

MCEER-06-0009 "Liquefaction Remediation in Silty Soils Using Dynamic Compaction and Stone Columns," by S. Thevanayagam, G.R. Martin, R. Nashed, T. Shenthal, T. Kanagalingam and N. Ecemis, 8/28/06 (PB2007-106985).

MCEER-06-0010 "Conceptual Design and Experimental Investigation of Polymer Matrix Composite Infill Panels for Seismic Retrofitting," by W. Jung, M. Chiewanichakorn and A.J. Aref, 9/21/06 (PB2007-106986).

MCEER-06-0011 "A Study of the Coupled Horizontal-Vertical Behavior of Elastomeric and Lead-Rubber Seismic Isolation Bearings," by G.P. Warn and A.S. Whittaker, 9/22/06 (PB2007-108679).

MCEER-06-0012 "Proceedings of the Fourth PRC-US Workshop on Seismic Analysis and Design of Special Bridges: Advancing Bridge Technologies in Research, Design, Construction and Preservation," Edited by L.C. Fan, G.C. Lee and L. Ziang, 10/12/06 (PB2007-109042).

MCEER-06-0013 "Cyclic Response and Low Cycle Fatigue Characteristics of Plate Steels," by P. Dusicka, A.M. Itani and I.G. Buckle, 11/1/06 06 (PB2007-106987).

MCEER-06-0014 "Proceedings of the Second US-Taiwan Bridge Engineering Workshop," edited by W.P. Yen, J. Shen, J-Y. Chen and M. Wang, 11/15/06 (PB2008-500041).

MCEER-06-0015 "User Manual and Technical Documentation for the REDARS™ Import Wizard," by S. Cho, S. Ghosh, C.K. Huyck and S.D. Werner, 11/30/06 (PB2007-114766).

MCEER-06-0016 "Hazard Mitigation Strategy and Monitoring Technologies for Urban and Infrastructure Public Buildings: Proceedings of the China-US Workshops," edited by X.Y. Zhou, A.L. Zhang, G.C. Lee and M. Tong, 12/12/06 (PB2008-500018).

MCEER-07-0001 "Static and Kinetic Coefficients of Friction for Rigid Blocks," by C. Kafali, S. Fathali, M. Grigoriu and A.S. Whittaker, 3/20/07 (PB2007-114767).

MCEER-07-0002 "Hazard Mitigation Investment Decision Making: Organizational Response to Legislative Mandate," by L.A. Arendt, D.J. Alesch and W.J. Petak, 4/9/07 (PB2007-114768).

MCEER-07-0003 "Seismic Behavior of Bidirectional-Resistant Ductile End Diaphragms with Unbonded Braces in Straight or Skewed Steel Bridges," by O. Celik and M. Bruneau, 4/11/07 (PB2008-105141).

MCEER-07-0004 "Modeling Pile Behavior in Large Pile Groups Under Lateral Loading," by A.M. Dodds and G.R. Martin, 4/16/07 (PB2008-105142).

MCEER-07-0005 "Experimental Investigation of Blast Performance of Seismically Resistant Concrete-Filled Steel Tube Bridge Piers," by S. Fujikura, M. Bruneau and D. Lopez-Garcia, 4/20/07 (PB2008-105143).

MCEER-07-0006 "Seismic Analysis of Conventional and Isolated Liquefied Natural Gas Tanks Using Mechanical Analogs," by I.P. Christovasilis and A.S. Whittaker, 5/1/07, not available.

MCEER-07-0007 "Experimental Seismic Performance Evaluation of Isolation/Restraint Systems for Mechanical Equipment – Part 1: Heavy Equipment Study," by S. Fathali and A. Filiatral, 6/6/07 (PB2008-105144).

MCEER-07-0008 "Seismic Vulnerability of Timber Bridges and Timber Substructures," by A.A. Sharma, J.B. Mander, I.M. Friedland and D.R. Allicock, 6/7/07 (PB2008-105145).

MCEER-07-0009 "Experimental and Analytical Study of the XY-Friction Pendulum (XY-FP) Bearing for Bridge Applications," by C.C. Marin-Artieda, A.S. Whittaker and M.C. Constantinou, 6/7/07 (PB2008-105191).

MCEER-07-0010 "Proceedings of the PRC-US Earthquake Engineering Forum for Young Researchers," Edited by G.C. Lee and X.Z. Qi, 6/8/07 (PB2008-500058).

MCEER-07-0011 "Design Recommendations for Perforated Steel Plate Shear Walls," by R. Purba and M. Bruneau, 6/18/07, (PB2008-105192).

MCEER-07-0012 "Performance of Seismic Isolation Hardware Under Service and Seismic Loading," by M.C. Constantinou, A.S. Whittaker, Y. Kalpakidis, D.M. Fenz and G.P. Warn, 8/27/07, (PB2008-105193).

MCEER-07-0013 "Experimental Evaluation of the Seismic Performance of Hospital Piping Subassemblies," by E.R. Goodwin, E. Maragakis and A.M. Itani, 9/4/07, (PB2008-105194).

MCEER-07-0014 "A Simulation Model of Urban Disaster Recovery and Resilience: Implementation for the 1994 Northridge Earthquake," by S. Miles and S.E. Chang, 9/7/07, (PB2008-106426).

MCEER-07-0015 "Statistical and Mechanistic Fragility Analysis of Concrete Bridges," by M. Shinozuka, S. Banerjee and S-H. Kim, 9/10/07, (PB2008-106427).

MCEER-07-0016 "Three-Dimensional Modeling of Inelastic Buckling in Frame Structures," by M. Schachter and AM. Reinhorn, 9/13/07, (PB2008-108125).

MCEER-07-0017 "Modeling of Seismic Wave Scattering on Pile Groups and Caissons," by I. Po Lam, H. Law and C.T. Yang, 9/17/07 (PB2008-108150).

MCEER-07-0018 "Bridge Foundations: Modeling Large Pile Groups and Caissons for Seismic Design," by I. Po Lam, H. Law and G.R. Martin (Coordinating Author), 12/1/07 (PB2008-111190).

MCEER-07-0019 "Principles and Performance of Roller Seismic Isolation Bearings for Highway Bridges," by G.C. Lee, Y.C. Ou, Z. Liang, T.C. Niu and J. Song, 12/10/07 (PB2009-110466).

MCEER-07-0020 "Centrifuge Modeling of Permeability and Pinning Reinforcement Effects on Pile Response to Lateral Spreading," by L.L Gonzalez-Lagos, T. Abdoun and R. Dobry, 12/10/07 (PB2008-111191).

MCEER-07-0021 "Damage to the Highway System from the Pisco, Perú Earthquake of August 15, 2007," by J.S. O'Connor, L. Mesa and M. Nykamp, 12/10/07, (PB2008-108126).

MCEER-07-0022 "Experimental Seismic Performance Evaluation of Isolation/Restraint Systems for Mechanical Equipment – Part 2: Light Equipment Study," by S. Fathali and A. Filiatral, 12/13/07 (PB2008-111192).

MCEER-07-0023 "Fragility Considerations in Highway Bridge Design," by M. Shinozuka, S. Banerjee and S.H. Kim, 12/14/07 (PB2008-111193).

MCEER-07-0024 "Performance Estimates for Seismically Isolated Bridges," by G.P. Warn and A.S. Whittaker, 12/30/07 (PB2008-112230).

MCEER-08-0001 "Seismic Performance of Steel Girder Bridge Superstructures with Conventional Cross Frames," by L.P. Carden, A.M. Itani and I.G. Buckle, 1/7/08, (PB2008-112231).

MCEER-08-0002 "Seismic Performance of Steel Girder Bridge Superstructures with Ductile End Cross Frames with Seismic Isolators," by L.P. Carden, A.M. Itani and I.G. Buckle, 1/7/08 (PB2008-112232).

MCEER-08-0003 "Analytical and Experimental Investigation of a Controlled Rocking Approach for Seismic Protection of Bridge Steel Truss Piers," by M. Pollino and M. Bruneau, 1/21/08 (PB2008-112233).

MCEER-08-0004 "Linking Lifeline Infrastructure Performance and Community Disaster Resilience: Models and Multi-Stakeholder Processes," by S.E. Chang, C. Pasion, K. Tatebe and R. Ahmad, 3/3/08 (PB2008-112234).

MCEER-08-0005 "Modal Analysis of Generally Damped Linear Structures Subjected to Seismic Excitations," by J. Song, Y-L. Chu, Z. Liang and G.C. Lee, 3/4/08 (PB2009-102311).

MCEER-08-0006 "System Performance Under Multi-Hazard Environments," by C. Kafali and M. Grigoriu, 3/4/08 (PB2008-112235).

MCEER-08-0007 "Mechanical Behavior of Multi-Spherical Sliding Bearings," by D.M. Fenz and M.C. Constantinou, 3/6/08 (PB2008-112236).

MCEER-08-0008 "Post-Earthquake Restoration of the Los Angeles Water Supply System," by T.H.P. Tabucchi and R.A. Davidson, 3/7/08 (PB2008-112237).

MCEER-08-0009 "Fragility Analysis of Water Supply Systems," by A. Jacobson and M. Grigoriu, 3/10/08 (PB2009-105545).

MCEER-08-0010 "Experimental Investigation of Full-Scale Two-Story Steel Plate Shear Walls with Reduced Beam Section Connections," by B. Qu, M. Bruneau, C-H. Lin and K-C. Tsai, 3/17/08 (PB2009-106368).

MCEER-08-0011 "Seismic Evaluation and Rehabilitation of Critical Components of Electrical Power Systems," S. Ersoy, B. Feizi, A. Ashrafi and M. Ala Saadeghvaziri, 3/17/08 (PB2009-105546).

MCEER-08-0012 "Seismic Behavior and Design of Boundary Frame Members of Steel Plate Shear Walls," by B. Qu and M. Bruneau, 4/26/08 . (PB2009-106744).

MCEER-08-0013 "Development and Appraisal of a Numerical Cyclic Loading Protocol for Quantifying Building System Performance," by A. Filiatral, A. Wanitkorkul and M. Constantinou, 4/27/08 (PB2009-107906).

MCEER-08-0014 "Structural and Nonstructural Earthquake Design: The Challenge of Integrating Specialty Areas in Designing Complex, Critical Facilities," by W.J. Petak and D.J. Alesch, 4/30/08 (PB2009-107907).

MCEER-08-0015 "Seismic Performance Evaluation of Water Systems," by Y. Wang and T.D. O'Rourke, 5/5/08 (PB2009-107908).

MCEER-08-0016 "Seismic Response Modeling of Water Supply Systems," by P. Shi and T.D. O'Rourke, 5/5/08 (PB2009-107910).

MCEER-08-0017 "Numerical and Experimental Studies of Self-Centering Post-Tensioned Steel Frames," by D. Wang and A. Filiatral, 5/12/08 (PB2009-110479).

MCEER-08-0018 "Development, Implementation and Verification of Dynamic Analysis Models for Multi-Spherical Sliding Bearings," by D.M. Fenz and M.C. Constantinou, 8/15/08 (PB2009-107911).

MCEER-08-0019 "Performance Assessment of Conventional and Base Isolated Nuclear Power Plants for Earthquake Blast Loadings," by Y.N. Huang, A.S. Whittaker and N. Luco, 10/28/08 (PB2009-107912).

MCEER-08-0020 "Remote Sensing for Resilient Multi-Hazard Disaster Response – Volume I: Introduction to Damage Assessment Methodologies," by B.J. Adams and R.T. Eguchi, 11/17/08 (PB2010-102695).

MCEER-08-0021 "Remote Sensing for Resilient Multi-Hazard Disaster Response – Volume II: Counting the Number of Collapsed Buildings Using an Object-Oriented Analysis: Case Study of the 2003 Bam Earthquake," by L. Gusella, C.K. Huyck and B.J. Adams, 11/17/08 (PB2010-100925).

MCEER-08-0022 "Remote Sensing for Resilient Multi-Hazard Disaster Response – Volume III: Multi-Sensor Image Fusion Techniques for Robust Neighborhood-Scale Urban Damage Assessment," by B.J. Adams and A. McMillan, 11/17/08 (PB2010-100926).

MCEER-08-0023 "Remote Sensing for Resilient Multi-Hazard Disaster Response – Volume IV: A Study of Multi-Temporal and Multi-Resolution SAR Imagery for Post-Katrina Flood Monitoring in New Orleans," by A. McMillan, J.G. Morley, B.J. Adams and S. Chesworth, 11/17/08 (PB2010-100927).

MCEER-08-0024 "Remote Sensing for Resilient Multi-Hazard Disaster Response – Volume V: Integration of Remote Sensing Imagery and VIEWSTM Field Data for Post-Hurricane Charley Building Damage Assessment," by J.A. Womble, K. Mehta and B.J. Adams, 11/17/08 (PB2009-115532).

MCEER-08-0025 "Building Inventory Compilation for Disaster Management: Application of Remote Sensing and Statistical Modeling," by P. Sarabandi, A.S. Kiremidjian, R.T. Eguchi and B. J. Adams, 11/20/08 (PB2009-110484).

MCEER-08-0026 "New Experimental Capabilities and Loading Protocols for Seismic Qualification and Fragility Assessment of Nonstructural Systems," by R. Retamales, G. Mosqueda, A. Filiatral and A. Reinhorn, 11/24/08 (PB2009-110485).

MCEER-08-0027 "Effects of Heating and Load History on the Behavior of Lead-Rubber Bearings," by I.V. Kalpakidis and M.C. Constantinou, 12/1/08 (PB2009-115533).

MCEER-08-0028 "Experimental and Analytical Investigation of Blast Performance of Seismically Resistant Bridge Piers," by S. Fujikura and M. Bruneau, 12/8/08 (PB2009-115534).

MCEER-08-0029 "Evolutionary Methodology for Aseismic Decision Support," by Y. Hu and G. Dargush, 12/15/08.

MCEER-08-0030 "Development of a Steel Plate Shear Wall Bridge Pier System Conceived from a Multi-Hazard Perspective," by D. Keller and M. Bruneau, 12/19/08 (PB2010-102696).

MCEER-09-0001 "Modal Analysis of Arbitrarily Damped Three-Dimensional Linear Structures Subjected to Seismic Excitations," by Y.L. Chu, J. Song and G.C. Lee, 1/31/09 (PB2010-100922).

MCEER-09-0002 "Air-Blast Effects on Structural Shapes," by G. Ballantyne, A.S. Whittaker, A.J. Aref and G.F. Dargush, 2/2/09 (PB2010-102697).

MCEER-09-0003 "Water Supply Performance During Earthquakes and Extreme Events," by A.L. Bonneau and T.D. O'Rourke, 2/16/09 (PB2010-100923).

MCEER-09-0004 "Generalized Linear (Mixed) Models of Post-Earthquake Ignitions," by R.A. Davidson, 7/20/09 (PB2010-102698).

MCEER-09-0005 "Seismic Testing of a Full-Scale Two-Story Light-Frame Wood Building: NEESWood Benchmark Test," by I.P. Christovasilis, A. Filiatral and A. Wanitkorkul, 7/22/09 (PB2012-102401).

MCEER-09-0006 "IDARC2D Version 7.0: A Program for the Inelastic Damage Analysis of Structures," by A.M. Reinhorn, H. Roh, M. Sivaselvan, S.K. Kunnath, R.E. Valles, A. Madan, C. Li, R. Lobo and Y.J. Park, 7/28/09 (PB2010-103199).

MCEER-09-0007 "Enhancements to Hospital Resiliency: Improving Emergency Planning for and Response to Hurricanes," by D.B. Hess and L.A. Arendt, 7/30/09 (PB2010-100924).

MCEER-09-0008 "Assessment of Base-Isolated Nuclear Structures for Design and Beyond-Design Basis Earthquake Shaking," by Y.N. Huang, A.S. Whittaker, R.P. Kennedy and R.L. Mayes, 8/20/09 (PB2010-102699).

MCEER-09-0009 "Quantification of Disaster Resilience of Health Care Facilities," by G.P. Cimellaro, C. Fumo, A.M Reinhorn and M. Bruneau, 9/14/09 (PB2010-105384).

MCEER-09-0010 "Performance-Based Assessment and Design of Squat Reinforced Concrete Shear Walls," by C.K. Gulec and A.S. Whittaker, 9/15/09 (PB2010-102700).

MCEER-09-0011 "Proceedings of the Fourth US-Taiwan Bridge Engineering Workshop," edited by W.P. Yen, J.J. Shen, T.M. Lee and R.B. Zheng, 10/27/09 (PB2010-500009).

MCEER-09-0012 "Proceedings of the Special International Workshop on Seismic Connection Details for Segmental Bridge Construction," edited by W. Phillip Yen and George C. Lee, 12/21/09 (PB2012-102402).

MCEER-10-0001 "Direct Displacement Procedure for Performance-Based Seismic Design of Multistory Woodframe Structures," by W. Pang and D. Rosowsky, 4/26/10 (PB2012-102403).

MCEER-10-0002 "Simplified Direct Displacement Design of Six-Story NEESWood Capstone Building and Pre-Test Seismic Performance Assessment," by W. Pang, D. Rosowsky, J. van de Lindt and S. Pei, 5/28/10 (PB2012-102404).

MCEER-10-0003 "Integration of Seismic Protection Systems in Performance-Based Seismic Design of Woodframed Structures," by J.K. Shinde and M.D. Symans, 6/18/10 (PB2012-102405).

MCEER-10-0004 "Modeling and Seismic Evaluation of Nonstructural Components: Testing Frame for Experimental Evaluation of Suspended Ceiling Systems," by A.M. Reinhorn, K.P. Ryu and G. Maddaloni, 6/30/10 (PB2012-102406).

MCEER-10-0005 "Analytical Development and Experimental Validation of a Structural-Fuse Bridge Pier Concept," by S. El-Bahey and M. Bruneau, 10/1/10 (PB2012-102407).

MCEER-10-0006 "A Framework for Defining and Measuring Resilience at the Community Scale: The PEOPLES Resilience Framework," by C.S. Renschler, A.E. Frazier, L.A. Arendt, G.P. Cimellaro, A.M. Reinhorn and M. Bruneau, 10/8/10 (PB2012-102408).

MCEER-10-0007 "Impact of Horizontal Boundary Elements Design on Seismic Behavior of Steel Plate Shear Walls," by R. Purba and M. Bruneau, 11/14/10 (PB2012-102409).

MCEER-10-0008 "Seismic Testing of a Full-Scale Mid-Rise Building: The NEESWood Capstone Test," by S. Pei, J.W. van de Lindt, S.E. Pryor, H. Shimizu, H. Isoda and D.R. Rammer, 12/1/10 (PB2012-102410).

MCEER-10-0009 "Modeling the Effects of Detonations of High Explosives to Inform Blast-Resistant Design," by P. Sherkar, A.S. Whittaker and A.J. Aref, 12/1/10 (PB2012-102411).

MCEER-10-0010 "L'Aquila Earthquake of April 6, 2009 in Italy: Rebuilding a Resilient City to Withstand Multiple Hazards," by G.P. Cimellaro, I.P. Christovasilis, A.M. Reinhorn, A. De Stefano and T. Kirova, 12/29/10.

MCEER-11-0001 "Numerical and Experimental Investigation of the Seismic Response of Light-Frame Wood Structures," by I.P. Christovasilis and A. Filiatral, 8/8/11 (PB2012-102412).

MCEER-11-0002 "Seismic Design and Analysis of a Precast Segmental Concrete Bridge Model," by M. Anagnostopoulou, A. Filiatral and A. Aref, 9/15/11.

MCEER-11-0003 'Proceedings of the Workshop on Improving Earthquake Response of Substation Equipment,' Edited by A.M. Reinhorn, 9/19/11 (PB2012-102413).

MCEER-11-0004 "LRFD-Based Analysis and Design Procedures for Bridge Bearings and Seismic Isolators," by M.C. Constantinou, I. Kalpakidis, A. Filiatral and R.A. Ecker Lay, 9/26/11.

MCEER-11-0005 "Experimental Seismic Evaluation, Model Parameterization, and Effects of Cold-Formed Steel-Framed Gypsum Partition Walls on the Seismic Performance of an Essential Facility," by R. Davies, R. Retamales, G. Mosqueda and A. Filiatral, 10/12/11.

MCEER-11-0006 "Modeling and Seismic Performance Evaluation of High Voltage Transformers and Bushings," by A.M. Reinhorn, K. Oikonomou, H. Roh, A. Schiff and L. Kempner, Jr., 10/3/11.

MCEER-11-0007 "Extreme Load Combinations: A Survey of State Bridge Engineers," by G.C. Lee, Z. Liang, J.J. Shen and J.S. O'Connor, 10/14/11.

MCEER-12-0001 "Simplified Analysis Procedures in Support of Performance Based Seismic Design," by Y.N. Huang and A.S. Whittaker.

MCEER-12-0002 "Seismic Protection of Electrical Transformer Bushing Systems by Stiffening Techniques," by M. Koliou, A. Filiatral, A.M. Reinhorn and N. Oliveto, 6/1/12.

MCEER-12-0003 "Post-Earthquake Bridge Inspection Guidelines," by J.S. O'Connor and S. Alampalli, 6/8/12.

MCEER-12-0004 "Integrated Design Methodology for Isolated Floor Systems in Single-Degree-of-Freedom Structural Fuse Systems," by S. Cui, M. Bruneau and M.C. Constantinou, 6/13/12.

MCEER-12-0005 "Characterizing the Rotational Components of Earthquake Ground Motion," by D. Basu, A.S. Whittaker and M.C. Constantinou, 6/15/12.

MCEER-12-0006 "Bayesian Fragility for Nonstructural Systems," by C.H. Lee and M.D. Grigoriu, 9/12/12.

MCEER-12-0007 "A Numerical Model for Capturing the In-Plane Seismic Response of Interior Metal Stud Partition Walls," by R.L. Wood and T.C. Hutchinson, 9/12/12.

MCEER-12-0008 "Assessment of Floor Accelerations in Yielding Buildings," by J.D. Wieser, G. Pekcan, A.E. Zaghi, A.M. Itani and E. Maragakis, 10/5/12.

MCEER-13-0001 "Experimental Seismic Study of Pressurized Fire Sprinkler Piping Systems," by Y. Tian, A. Filiatral and G. Mosqueda, 4/8/13.

MCEER-13-0002 "Enhancing Resource Coordination for Multi-Modal Evacuation Planning," by D.B. Hess, B.W. Conley and C.M. Farrell, 2/8/13.

MCEER-13-0003 "Seismic Response of Base Isolated Buildings Considering Pounding to Moat Walls," by A. Masroor and G. Mosqueda, 2/26/13.

MCEER-13-0004 "Seismic Response Control of Structures Using a Novel Adaptive Passive Negative Stiffness Device," by D.T.R. Pasala, A.A. Sarlis, S. Nagarajaiah, A.M. Reinhorn, M.C. Constantinou and D.P. Taylor, 6/10/13.

MCEER-13-0005 "Negative Stiffness Device for Seismic Protection of Structures," by A.A. Sarlis, D.T.R. Pasala, M.C. Constantinou, A.M. Reinhorn, S. Nagarajaiah and D.P. Taylor, 6/12/13.

MCEER-13-0006 "Emilia Earthquake of May 20, 2012 in Northern Italy: Rebuilding a Resilient Community to Withstand Multiple Hazards," by G.P. Cimellaro, M. Chiriaci, A.M. Reinhorn and L. Tirca, June 30, 2013.

MCEER-13-0007 "Precast Concrete Segmental Components and Systems for Accelerated Bridge Construction in Seismic Regions," by A.J. Aref, G.C. Lee, Y.C. Ou and P. Sideris, with contributions from K.C. Chang, S. Chen, A. Filiatral and Y. Zhou, June 13, 2013.

MCEER-13-0008 "A Study of U.S. Bridge Failures (1980-2012)," by G.C. Lee, S.B. Mohan, C. Huang and B.N. Fard, June 15, 2013.

MCEER-13-0009 "Development of a Database Framework for Modeling Damaged Bridges," by G.C. Lee, J.C. Qi and C. Huang, June 16, 2013.

MCEER-13-0010 "Model of Triple Friction Pendulum Bearing for General Geometric and Frictional Parameters and for Uplift Conditions," by A.A. Sarlis and M.C. Constantinou, July 1, 2013.

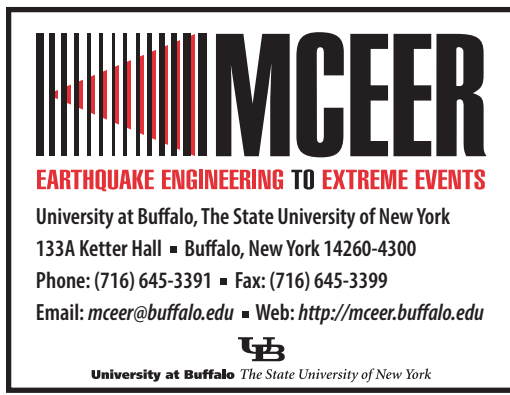
MCEER-13-0011 "Shake Table Testing of Triple Friction Pendulum Isolators under Extreme Conditions," by A.A. Sarlis, M.C. Constantinou and A.M. Reinhorn, July 2, 2013.

MCEER-13-0012 "Theoretical Framework for the Development of MH-LRFD," by G.C. Lee (coordinating author), H.A Capers, Jr., C. Huang, J.M. Kulicki, Z. Liang, T. Murphy, J.J.D. Shen, M. Shinotzuka and P.W.H. Yen, July 31, 2013.

MCEER-13-0013 "Seismic Protection of Highway Bridges with Negative Stiffness Devices," by N.K. Attary, M.D. Symans, S. Nagarajaiah, A.M. Reinhorn, M.C. Constantinou, A.A. Sarlis, D.T.R. Pasala, and D.P. Taylor, July 31, 2013.

MCEER-14-0001 "Simplified Seismic Collapse Capacity-Based Evaluation and Design of Frame Buildings with and without Supplemental Damping Systems," by M. Hamidia, A. Filiatral, and A. Aref, May 19, 2014.

MCEER-14-0002 "Comprehensive Analytical Seismic Fragility of Fire Sprinkler Piping Systems," by Siavash Soroushian, Emmanuel "Manos" Maragakis, Arash E. Zaghi, Alicia Echevarria, Yuan Tian and Andre Filiatral, August 26, 2014.



ISSN 1520-295X